

AD-A047 955

FRANK J SEILER RESEARCH LAB UNITED STATES AIR FORCE --ETC F/O 13/8  
EXPLOSIVE IMPULSE WELDING. VOLUME I.(U)  
JUL 77 D H MERKLE, G E CANNON

**UNCLASSIFIED**

NL

1 OF 5  
AD  
A047955



AD A047955



AD NO  
JDC FILE COPY

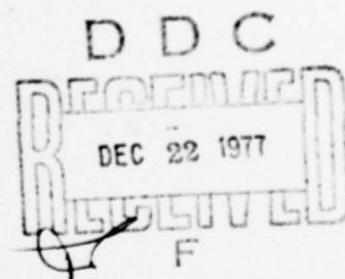
12

FRANK J. SEILER RESEARCH LABORATORY

SRL-TR-77-0012

JULY 1977

EXPLOSIVE IMPULSE WELDING  
(VOLUME 1)



FINAL REPORT

APPROVED FOR PUBLIC RELEASE;  
DISTRIBUTION UNLIMITED.

AIR FORCE SYSTEMS COMMAND  
UNITED STATES AIR FORCE



UNCLASSIFIED

SECURITY CLASSIFICATION OF THIS PAGE (When Data Entered)

REPORT DOCUMENTATION PAGE		READ INSTRUCTIONS BEFORE COMPLETING FORM
1. REPORT NUMBER <b>14</b> FJSRL-TR-77-0012-VOL-1	2. GOVT ACCESSION NO.	3. RECIPIENT'S CATALOG NUMBER
4. TITLE (and Subtitle) <b>6</b> Explosive Impulse Welding. <b>Volume I.</b> <b>9</b>	5. TYPE OF REPORT & PERIOD COVERED Final Report. Jan 1967-Jul 1977.	
7. AUTHOR(s) <b>10</b> Douglas H. Merkle George E. Cannon, Jr.	6. PERFORMING ORG. REPORT NUMBER	
8. PERFORMING ORGANIZATION NAME AND ADDRESS Department of Civil Engineering, Engineering Mechanics and Materials (DFCEM) USAF Academy, CO 80840	9. CONTRACT OR GRANT NUMBER(s)	
11. CONTROLLING OFFICE NAME AND ADDRESS <b>16</b> 7904	10. PROGRAM ELEMENT, PROJECT, TASK AREA & WORK UNIT NUMBERS PE 61102F WU FJSRL 7904-01-46	
14. MONITORING AGENCY NAME & ADDRESS (if different from Controlling Office) Dean of the Faculty <b>17</b> 01 USAF Academy, CO 80840	12. REPORT DATE July 1977	
	13. NUMBER OF PAGES <b>12</b> 448 p.	
	15. SECURITY CLASS. (of this report) UNCLASSIFIED	
16. DISTRIBUTION STATEMENT (of this Report) Approved for public release; distribution unlimited.		15a. DECLASSIFICATION/DOWNGRADING SCHEDULE
17. DISTRIBUTION STATEMENT (of the abstract entered in Block 20, if different from Report) <b>DDC</b> <b>RECEIVED</b> DEC 22 1977 <b>RECEIVED</b> <b>F</b>		
18. SUPPLEMENTARY NOTES		
19. KEY WORDS (Continue on reverse side if necessary and identify by block number) Explosive Welding, Welding, Aluminum, Steel, Bonding, Strength, Finite Elements		
20. ABSTRACT (Continue on reverse side if necessary and identify by block number) Explosive welds were conducted with various combinations of aluminum and steel varying plate thicknesses, different configurations, several explosives at various concentrations and atmospheres of various types. Framing camera, flash x-ray, collapsable velocity probes and manganin wire pressure gages were used to record position-time data, velocities and pressures. Welded specimens were tested destructively and nondestructively to measure weld tensile and shear strength, metallographic data, and ultrasonic character- istics. Test results were correlated with welding variables. Data were		

DD FORM 1473 EDITION OF 1 NOV 65 IS OBSOLETE

SECURITY CLASSIFICATION OF THIS PAGE (When Data Entered)

319920

Block 20 cont.

analyzed for correlation with parameters. Models were developed to predict flyer plate response and weld interface response during welding. Weld quality (tensile strength) for a given material was found to be primarily a function of collision point velocity, collision angle and flyer plate thickness. These parameters can be optimized to consistently achieve weld tensile strength in excess of parent metal strength by considering four criteria: (1) The critical collision angle for jet formation, (2) The critical impact velocity (or pressure) for jet formation in the subsonic regime, (3) The critical collision point transition velocity, and (4) The kinetic energy of the flyer plate versus the heat dissipation characteristics of the collision region.

## PREFACE

The work reported herein was conducted under the supervision of the Department of Civil Engineering, (now the Department of Civil Engineering, Engineering Mechanics and Materials), of the USAF Academy between 1969 and 1977 under the sponsorship of the Air Force Systems Command through the Air Force Weapons Laboratory, the Frank J. Seiler Research Laboratory, and the Air Force Civil Engineering Center. Many investigators were involved in the research program, as shown in Table 1, and their efforts resulted in numerous published and unpublished papers. The authors of this report have included edited portions of those papers in an effort to present a comprehensive summary of the work accomplished in the Explosive Impulse Welding program. Therefore, this report represents the combined efforts of all the researchers, not merely the authors listed on the cover. Consequently, terms and symbols are defined in each section of the report to avoid possible confusion over inconsistencies in usage between contributors.

ACCESSION for	White Section <input checked="" type="checkbox"/>
NTIS	Buff Section <input type="checkbox"/>
DOC	
UNCLASSIFIED	
CLASSIFICATION	
DISTRIBUTION/AVAILABILITY CODES	
SPECIAL	
A	

TABLE 1  
RESEARCH CONTRIBUTORS \*

Principal Investigators

Major George E. Cannon, Jr.  
Major Charles Lindbergh  
Major Douglas H. Merkle

Department of Civil Engineering,  
Engineering Mechanics and Materials,  
USAF Academy, Colorado

Research Associates

Mr. Robert H. Wittman  
Dr. Jim Workman  
Dr. Richard D. Potter  
Dr. Winfred O. Carter

Experimental &  
Applications  
Analytical &  
Applications  
Experimental  
(Spot Welding)  
Applications  
Denver Research Institute  
Denver, Colorado  
Agabian-Jacobsen Associates  
Los Angeles, California  
General Dynamics Corporation  
Fort Worth, Texas  
Department of Civil Engineering  
Utah State University  
Logan, Utah

\* The grades, titles and organizational affiliations of individuals listed in this table are the most recent information for each individual while actively involved in ELW research. The information is not intended to be current as of publication of this report.



TABLE 1 (CONTINUED)

Research Participants (All of USAF Academy, Colorado)

Colonel Wallace E. Fluhr	General Consultant	Dept of Civil Engineering, Engineering Mechanics and Materials (DFCEM)
Major Jack F. Hilbing	Computer Analysis	Dept of Astronautics and Computer Science (DFACS)
Major J. Snide	Metallurgy	DFCEM
Captain M. Gyauch	Computer Science	DFACS
Captain Cleat Simmons	Metallurgy	DFCEM
Lt Lanny J. Larson	Fracture Mechanics	DFCEM
ClC J. Burg	Armor Concepts	DFCEM
ClC G. J. Butson	Armor Concepts	DFCEM
ClC M. P. Cannon	Fatigue	DFCEM
ClC M. Cosby	Ultrasonic Testing	DFCEM
ClC B. E. Crimin	Ultrasonic Testing	DFCEM
ClC J. D. Dustin	Symmetrical Impulse Methods	DFCEM



TABLE 1 (CONTINUED)

Research Participants (All of USAF Academy, Colorado)		
CIC M. Ewing	Heat Treatment of EIW	DFCEM
CIC C. M. Kline	Inclined Steel Plate Welds	DFCEM
CIC D. J. Meister	Fatigue Testing of Welds	DFCEM
CIC J. B. Norman	AN2 Bomb Damage Repair	DFCEM
CIC P. U. Sutton	Vacuum Effects	DFCEM
C2C J. D. Thompson	Ultrasonic Testing	DFCEM
CIC W. S. Vinal	Vacuum Effects	DFCEM
CIC L. J. Willadsen	Nondestructive Evaluation of Bond Strengths	DFCEM
CIC J. Young	Mandrel Design	DFCEM
CIC K. F. Zickrick	Steel-to-Aluminum Welds	DFCEM

# TABLE OF CONTENTS

	PAGE
Preface	i
List of Figures	vii
List of Tables	xiii
I. INTRODUCTION	1
A. Objectives of this Study	1
B. Summary of Work Accomplished	2
C. Fundamentals of Explosive Impulse Welding	4
D. Brief History of Explosive Impulse Welding	8
II. EXPERIMENTAL PROGRAM	21
A. Tests Conducted at Denver Research Institute	21
B. Tests Conducted at Los Alamos Scientific Laboratory	39
1. Atmospheric Tests	39
2. Helium Tests	53
3. Vacuum Tests	56
4. Resolved Technique	65
C. Tests Conducted at United States Air Force Academy	69
D. Spot Welding Tests	69
E. Weld Evaluation	98
1. Ultrasonic Testing	98
2. Wavelength Variations with Selected Welding Parameters	103
3. Destructive Mechanical Tests for Weld Strength Evaluation	106
III. ANALYSES	119
A. Strength Variation with Position Along Weld and Explosive Loading	119
B. Shear Strength as Related to Direction of Shear Application	122
C. Variation of Wavelength	126
D. Finite Element Model	126
1. Basic Model	126
2. Constitutive Equations for Aluminum	133
E. Analytical Simulation of Flyer Plate Dynamic Response	138
1. Dynamic Equilibrium Model (by C. Lindbergh)	138
2. Analysis of LASL Framing Camera Velocity Data	149
3. Analysis of Flash X-Ray Data, LASL, DRI and USAFA	284
F. The Influence of Collision Parameters on the Strength and Microstructure of an Explosion Welded Aluminum Alloy (by R. H. Wittman)	381
1. Introduction	381
2. Experimental Details	382
3. Analysis and Discussion of Results	386

# TABLE OF CONTENTS (cont)

	PAGE
4. Explosion Weldability	403
5. Conclusions	405
IV. APPLICATIONS	407
A. Introduction	407
B. Spot Welding	407
C. Explosive Impulse Welding of Tubular Aluminum Joints	407
D. Connections Formed Using Symmetrical Impulse Techniques	416
V. CONCLUSIONS AND RECOMMENDATIONS	424
REFERENCES	427
APPENDICES	
A. Least Squares Fit of a Nonlinear Curve	A-1
B. Mathematical Description of Flyer Plate Motion	B-1
C. USAFA EIW Test Site Instrumentation System	C-1
D. Characteristics of Explosives	D-1
E. WELD2 Computer Program	E-1

# LIST OF FIGURES

FIGURE		PAGE
1	Explosive Impulse Welding Configurations	6
2	Cross Section of the Head of a U.S. Army Bazooka, Showing Conical Steel Liner in the Shaped Charge	11
3	Formation of Jet and Slug From a Cone or Wedge-Shaped Liner Whose Sides Collapse with Constant Velocity $V_o$ as a Result of the Explosion of a Charge that was in Contact with the Outer Surface	11
4	Formation of Jet Slug by a Cone or Wedge-Shaped Liner Shown in Figure 2 from the Point of View of an Observer Stationed at the Moving Junction 0	12
5	Penetration of A Thin Oblique Target by a Flat Nosed Bullet	14
6	Asymmetric Collision Treated by Abrahamson (1961) Showing Deformation of Target	14
7	Formation of Waves (After Bahrani, 1967)	17
8	Relationship of the Important Process Variables for Explosive Bonding with a Low-Detonation-Velocity Explosive	18
9	Component Configuration for Parallel Geometry Welding	26
10	Component Configuration for Preset Angle Geometry Welding	35
11	Initial LASL Experimental Arrangement (Atmospheric Conditions)	43
12	Initial LASL Specimen Assembly (Atmospheric Conditions)	44
13	LASL Explosive Loading Arrangement	46
14	Argon Flash Box	46
15	Typical Framing Camera Record (Atmospheric Conditions)	50
16	Experimental Arrangement Using Helium	55
17	Vacuum Welding Apparatus	57
18	Components of Vacuum Welding Apparatus	59
19	Typical Framing Camera Record (Vacuum)	63
20	Superimposed Framing Camera and Radiograph Records	66
21	Typical Radiograph	67
22	Component Arrangement of Resolved Technique	68
23	"T" Weld Specimen Mount	87
24	Spot Welding Configurations	88
25	Ultrasonic Test System	99
26	Ultrasonic Trace-Bond Strength Correlation	100
27	Plate Weld Ultrasonic Examination	101
28	Photomicrograph of Weld Interface Waves	103
29	Interface Wavelength Variations with Mass Ratio	105
30	Pattern for Destructive Test Specimens	107

# LIST OF FIGURES (cont)

FIGURE		PAGE
31	Early Shear Test Specimen Design	108
32	Lug Shear Test Device	110
33	Final Shear Test Specimen Design	111
34	Final Shear Test Specimen and Specimen Mount	112
35	Early Tensile Test Specimen and Specimen Mount	113
36	Final Tensile Test Specimen Mount	115
37	Final Tensile Test Specimen	116
38	Tensile Test Specimen Mount	117
39	Tensile Test Specimen and Specimen Mount	118
40	Length of Weld Test Specimen Arrangements	120
41a	Variations of Strength with Length of Weld	121
41b	Variations of Strength with Length of Weld	121a
42	Variations of Strength with Length of Weld: Inclined Aluminum Plates	123
43	Tensile Strength Versus Explosive Loading	124
44	Shear Strength Variation with Shear Direction	128
45	Variation of Wavelength with Length of Weld	129
46	Interface Wavelength Variations with Tensile Strength	130
47	Vanishing Element Technique	132
48	Model Hydrostat and Bulk Modulus for 24 ST Aluminum	137
49	Flyer Plate Bottom Pressure by WELD2 Analysis	139
50	Base Plate Top Pressure by WELD2 Analysis	140
51	Interface Position by WELD2 Analysis	141
52	Model of Flyer Plate Response	143
53	Dynamic Equilibrium of Plate Element	144
54	Accuracy of Dynamic Equilibrium Model	145
54a	Calculated Deformation Response: Case A Detonation Velocity Variation	146
54b	Calculated Deformation Response: Case B Detonation Velocity Variation	147
54c	Calculated Deformation Response: Case C Detonation Velocity Variation	148
55	LASL Test Configuration	151
56	Framing Camera Projection LASL 1268	154
57	Framing Camera Projection LASL 1269	155
58	Framing Camera Projection LASL 1270	156
59	Framing Camera Projection LASL 1271	157
60	Framing Camera Projection LASL 1273	157
61	Framing Camera Projection LASL 1274	158
62	Framing Camera Projection LASL 1277	158
63	Framing Camera Projection LASL 1278	159
64	Framing Camera Projection LASL 1279	160
65	Framing Camera Projection LASL 1280	160
66	Framing Camera Projection LASL 1281	161
67	Framing Camera Projection LASL 1282	162
68	Framing Camera Projection LASL 1283	163



# LIST OF FIGURES (cont)

FIGURE		PAGE
69	Framing Camera Projection LASL 1284	164
70	Framing Camera Projection LASL 1285	165
71	Framing Camera Projection LASL 1286	166
72	Framing Camera Projection LASL 1312	167
73	Framing Camera Projection LASL 1317	168
74	Framing Camera Projection LASL 1320	169
75	Framing Camera Projection LASL 1321	170
76	Framing Camera Projection LASL 1321	171
77	Framing Camera Projection LASL 1322	172
78	Framing Camera Projection LASL 1322	173
79	Framing Camera Projection LASL 1323	174
80	Framing Camera Projection LASL 1323	175
81	Framing Camera Projection LASL 1324	176
82	Framing Camera Projection LASL 1325	177
83	Framing Camera Projection LASL 1328	178
84	Framing Camera Projection LASL 1362	179
85	LASL 1268 Detonation Position	232
86	LASL 1268 Flyer Plate Position	233
87	LASL 1269 Detonation Position	234
88	LASL 1269 Flyer Plate Position	235
89	LASL 1270 Detonation Position	236
90	LASL 1271 Detonation Position	237
91	LASL 1271 Flyer Plate Position	238
92	LASL 1273 Detonation Position	239
93	LASL 1273 Flyer Plate Position	240
94	LASL 1274 Detonation Position	241
95	LASL 1277 Detonation Position	242
96	LASL 1277 Flyer Plate Position	243
97	LASL 1278 Detonation Position	244
98	LASL 1278 Flyer Plate Position	245
99	LASL 1279 Detonation Position	246
100	LASL 1279 Flyer Plate Position	247
101	LASL 1280 Detonation Position	248
102	LASL 1280 Flyer Plate Position	249
103	LASL 1281 Detonation Position	250
104	LASL 1281 Flyer Plate Position	251
105	LASL 1282 Detonation Position	252
106	LASL 1282 Flyer Plate Position	253
107	LASL 1283 Detonation Position	254
108	LASL 1283 Flyer Plate Position	255
109	LASL 1284 Detonation Position	256
110	LASL 1284 Flyer Plate Position	257
111	LASL 1285 Detonation Position	258
112	LASL 1285 Flyer Plate Position	259
113	LASL 1286 Detonation Position	260
114	LASL 1286 Flyer Plate Position	261
115	LASL 1312 Detonation Position	262

# LIST OF FIGURES (cont)

FIGURE		PAGE
116	LASL 1312 Flyer Plate Position	263
117	LASL 1317 Detonation Position	264
118	LASL 1317 Flyer Plate Position	265
119	LASL 1320 Detonation Position	266
120	LASL 1320 Flyer Plate Position	267
121	LASL 1321 Detonation Position	268
122	LASL 1321 Flyer Plate Position	269
123	LASL 1322 Detonation Position	270
124	LASL 1322 Flyer Plate Position	271
125	LASL 1323 Detonation Position	272
126	LASL 1323 Flyer Plate Position	273
127	LASL 1324 Detonation Position	274
128	LASL 1324 Flyer Plate Position	275
129	LASL 1325 Detonation Position	276
130	LASL 1325 Flyer Plate Position	277
131	LASL 1328 Detonation Position	278
132	LASL 1328 Flyer Plate Position	279
133	LASL 1362 Detonation Position	280
134	LASL 1362 Flyer Plate Position	281
135	LASL Shots	283
136	Basic Steady State Geometry of Parallel Plate Explosive Impulse Welding	285
137	Calculation of Detonation Velocity from Continuous Writing Velocity Probe Oscilloscope Trace	288
138	Test No. LASL 1311	336
139	Test No. LASL 1312	337
140	Test No. LASL 1317	338
141	Test No. LASL 1321	339
142	Test No. LASL 1322	340
143	Test No. LASL 1324	341
144	Test No. LASL 1325	342
145	Test No. LASL 1362	343
146	Test No. DRI 3	344
147	Test No. DRI 4	345
148	Test No. DRI 5	346
149	Test No. DRI 6	347
150	Test No. DRI 7	348
151	Test No. DRI 8	349
152	Test No. DRI 9	350
153	Test No. DRI 11	351
154	Test No. DRI 13	352
155	Test No. DRI 14	353
156	Test No. DRI 15	354
157	Test No. DRI 16	355
158	Test No. DRI 22	356
159	Test No. DRI 24	357
160	Test No. DRI 28	358

# LIST OF FIGURES (cont)

FIGURE		PAGE
161	Test No. USAFA 45	359
162	Test No. USAFA 46	360
163	Test No. USAFA 48	361
164	Test No. USAFA 51	362
165	Test No. USAFA 54	363
166	Test No. USAFA 55	364
167	Test No. USAFA 57	365
168	Test No. USAFA 59	366
169	Test No. USAFA 60	367
170	Test No. USAFA 62A	368
171	Test No. USAFA 72	369
172	Test No. USAFA 73	370
173	Test No. USAFA 79	371
174	Test No. USAFA 82	372
175	Test No. USAFA 89	373
176	Test No. USAFA 94	374
177	Test No. USAFA 96	375
178	Test No. USAFA 97	376
179	Test No. USAFA 98	377
180	Test No. USAFA 110	378
181	The Generalized Explosion Welding Configuration and Definition of Parameters	385
182	Continuous Writing Velocity Probe	385
183	Arrange of Velocity Probes in Flyer and Base Plates of Explosion Welding Experiment	387
184	Block Circuit Diagram of Velocity Measuring System	387
185	Typical Oscilloscope Record of Detonation Frtton and Collision Point Distance-Time Profiles	387
186	Detonation Velocity as a Function of Explosive Loading	388
187	Weld Tensile Test Configuration	388
188	Four Conditions Bounding the Optimum Welding Range Represented Schematically as Functions of $V_c$ and $\alpha$	390
189	Weld Tensile Strength Data as a Function of $V_c$ and $\alpha$	391
190	Weld Microstructure as a Function of $V_c$ and $\alpha$	392
191	Effect of Flyer Plate Thickness on the Range of Optimum Collision Parameters	402
192	External Collar Welding Configuration	409
193	External Collars	410
194	Internal Collar Weld Configuration	411
195	Internal Collar Weld Configuration and Welded Specimen	412
196	Symmetrical Pipe Flange Joint Configuration	413
197	Symmetrical Pipe Flange Joint Test Specimen	414
198	Symmetrical Explosive Load Configurations	418

# LIST OF FIGURES (cont)

FIGURE		PAGE
199	Application of Symmetrical Explosive Impulse Welding Configuration; Shear Connector	419
200	Flat Laminite Formed Using the Symmetrical Impulse Technique	421
201	Longitudinal Seam Weld Made Using the Symmetrical Impulse Technique	422
202	Structural Decking Formed Using the "T" Weld Configuration	423
B-1	N <sup>th</sup> Order Hyperbolic Curve	B-7
C-1	Trigger Details	C-2
C-2	Specimen Instrumentation Details	C-6
C-3	Instrumentation Apparatus at USAFA Test Site	C-7
C-4	Complete Instrumentation System	C-8
C-5a	X-Ray Console & Gas Bottle Details	C-9
C-5b	X-Ray Console Details	C-10
C-5c	X-Ray Console Details	C-11
C-6a	Wiring Details	C-12
C-6b	Specimen Wiring and Polarity Details	C-13
C-6c	Specimen Wiring and Polarity Details	C-14
C-7a	Specimen Placement Details	C-16
C-7b	Specimen Placement Details	C-17
C-7c	Specimen Anvil Configuration Details	C-18
C-7d	Specimen Terminal Strip Details	C-19
C-8	Explosive Details	C-21
C-9	Oscilloscope #1	C-22
C-10a	Set Up for Bottom Trace	C-25
C-10b	Set Up for Top Trace	C-25
C-10c	Detonation Pressure Pulse Photo	C-26
C-10d	Interface Pressure Pulse Photo	C-26
C-11	Final Checklist for Quadruple Instrument Shot	C-27
C-12	Oscilloscope #3	C-34
C-13	Capping Up Details	C-37
C-14a	Detonation Velocity Trace	C-41
C-14b	Detonation Velocity Trace	C-41
C-15a	Detonation Velocity Probe	C-42
C-15b	Detonation Velocity Probe	C-43

# LIST OF TABLES

TABLE		PAGE
1	Research Contributors	ii
2	Parallel Geometry Aluminum EIW Parametric Schedule	22
3	Summary of Later Tests at DRI	23
4	Ultimate Shear Strengths for Parallel Geometry Aluminum Welding	27
5	Ultimate Tensile Strengths for Parallel Geometry Aluminum Welding	34
6	Preset Angle Geometry Aluminum EIW Parametric Schedule	34
7	Preset Angle Geometry Aluminum Plate Weld Strengths	36
8	Specimen Schedule for LASL Tests	41
9	LASL Experimental Technique Evaluation	54
10	LASL Atmospheric Welding Series	60
11	LASL Vacuum Welding Series	70
12	USAFA Plate Welding Series	72
13	Spot Welding Results	90
14	Shear Strength Variation with Shear Direction	127
15	LASL Series Summary	150
16	LASL 1268 - Detonation Front Position	180
17	LASL 1268 - Flyer Plate Position	181
18	LASL 1269 - Detonation Front	182
19	LASL 1269 - Flyer Plate	183
20	LASL 1270 - Detonation Front	184
21	LASL 1270 - Flyer Plate	185
22	LASL 1271 - Detonation Front	186
23	LASL 1271 - Flyer Plate	187
24	LASL 1273 - Detonation Front	188
25	LASL 1273 - Flyer Plate	189
26	LASL 1274 - Detonation Front	190
27	LASL 1274 - Flyer Plate	191
28	LASL 1277 - Detonation Front	192
29	LASL 1277 - Flyer Plate	193
30	LASL 1278 - Detonation Front	194
31	LASL 1278 - Flyer Plate	195
32	LASL 1279 - Detonation Front	196
33	LASL 1279 - Flyer Plate	197
34	LASL 1280 - Detonation Front	198
35	LASL 1280 - Flyer Plate	199
36	LASL 1281 - Detonation Front	200
37	LASL 1281 - Flyer Plate	201
38	LASL 1282 - Detonation Front	202
39	LASL 1282 - Flyer Plate	203
40	LASL 1283 - Detonation Front	204
41	LASL 1283 - Flyer Plate	205
42	LASL 1284 - Detonation Front	206
43	LASL 1284 - Flyer Plate	207
44	LASL 1285 - Detonation Front	208



# LIST OF TABLES (cont)

TABLE		PAGE
45	LASL 1285 - Flyer Plate	209
46	LASL 1286 - Detonation Front	210
47	LASL 1286 - Flyer Plate	211
48	LASL 1312 - Detonation Front	212
49	LASL 1312 - Flyer Plate	213
50	LASL 1317 - Detonation Front	214
51	LASL 1317 - Flyer Plate	215
52	LASL 1320 - Detonation Front	216
53	LASL 1320 - Flyer Plate	217
54	LASL 1321 - Detonation Front	218
55	LASL 1321 - Flyer Plates Projection by WEF	219
56	LASL 1322 - Detonation Front	220
57	LASL 1322 - Flyer Plate	221
58	LASL 1323 - Detonation Front	222
59	LASL 1323 - Flyer Plate	223
60	LASL 1324 - Detonation Front	224
61	LASL 1324 - Flyer Plate	225
62	LASL 1325 - Detonation Front	226
63	LASL 1325 - Flyer Plate	227
64	LASL 1328 - Detonation Front	228
65	LASL 1328 - Flyer Plate	229
66	LASL 1362 - Detonation Front	230
67	LASL 1362 - Flyer Plate	231
68	LASL Detonation and Collision Point Velocities	282
69	DRI Series Summary	286
70	USAFA Series Summary	287
71	Detonation Velocity for DRI and USAFA Series	290
72	Digitized Flash X-Ray Data - LASL 1311	293
73	Digitized Flash X-Ray Data - LASL 1312	294
74	Digitized Flash X-Ray Data - LASL 1317	295
75	Digitized Flash X-Ray Data - LASL 1321	296
76	Digitized Flash X-Ray Data - LASL 1322	297
77	Digitized Flash X-Ray Data - LASL 1324	298
78	Digitized Flash X-Ray Data - LASL 1325	299
79	Digitized Flash X-Ray Data - LASL 1362	300
80	Digitized Flash X-Ray Data - DRI 3	301
81	Digitized Flash X-Ray Data - DRI 4	302
82	Digitized Flash X-Ray Data - DRI 5	303
83	Digitized Flash X-Ray Data - DRI 6	304
84	Digitized Flash X-Ray Data - DRI 7	305
85	Digitized Flash X-Ray Data - DRI 8	306
86	Digitized Flash X-Ray Data - DRI 9	307
87	Digitized Flash X-Ray Data - DRI 11	308
88	Digitized Flash X-Ray Data - DRI 13	309
89	Digitized Flash X-Ray Data - DRI 14	310
90	Digitized Flash X-Ray Data - DRI 15	311
91	Digitized Flash X-Ray Data - DRI 16	312

# LIST OF TABLES (cont)

TABLE		PAGE
92	Digitized Flash X-Ray Data - DRI 22	313
93	Digitized Flash X-Ray Data - DRI 24	314
94	Digitized Flash X-Ray Data - DRI 28	315
95	Digitized Flash X-Ray Data - USAFA 45	136
96	Digitized Flash X-Ray Data - USAFA 46	317
97	Digitized Flash X-Ray Data - USAFA 48	318
98	Digitized Flash X-Ray Data - USAFA 51	319
99	Digitized Flash X-Ray Data - USAFA 54	320
100	Digitized Flash X-Ray Data - USAFA 55	321
101	Digitized Flash X-Ray Data - USAFA 57	322
102	Digitized Flash X-Ray Data - USAFA 59	323
103	Digitized Flash X-Ray Data - USAFA 60	324
104	Digitized Flash X-Ray Data - USAFA 62A	325
105	Digitized Flash X-Ray Data - USAFA 72	326
106	Digitized Flash X-Ray Data - USAFA 73	327
107	Digitized Flash X-Ray Data - USAFA 79	328
108	Digitized Flash X-Ray Data - USAFA 82	329
109	Digitized Flash X-Ray Data - USAFA 89	330
110	Digitized Flash X-Ray Data - USAFA 94	331
111	Digitized Flash X-Ray Data - USAFA 96	332
112	Digitized Flash X-Ray Data - USAFA 97	333
113	Digitized Flash X-Ray Data - USAFA 98	334
114	Digitized Flash X-Ray Data - USAFA 110	335
115	Flyer Plate Position-Time Parameters	379
116	Flyer Plate Collision Parameters	380
117	Mechanical-Physical Properties of Selected Metals and Alloys and Their Weldability Rating	401
D-1	Characteristics of Explosives	D-7

## I. INTRODUCTION

### A. Objectives of this Study

The objectives of the EIW research conducted in this study were the collection of data on important parameters affecting the quality and characteristics of explosive welds, the evaluation of weld quality, the analysis of data using models developed for that purpose, and the determination of possible applications for the EIW process. Explosive weld design has tended to be a very pragmatic trial-and-expensive-error process. If EIW is to become a useful technique in field applications, it is necessary that a firm theoretical basis be established to permit design of welds and accurate prediction of results. The purpose of this study, then, has been to advance the understanding of the EIW phenomenon toward that point where weld characteristics can be accurately forecast and the necessary parameters for high quality welding can be reliably established by the designer.

Additionally, EIW offers the capability to accomplish feats impossible with conventional welding techniques, such as: welding highly dissimilar metals, achieving quality welds in aluminum and other metals usually difficult to weld, bonding large interface areas, achieving weld strengths which equal the strength of the parent metal, and cladding multiple layers of metal plate together simultaneously. Because these additional capabilities exist, new applications of welding are possible. This study identifies a representative sampling of new applications for EIW in an effort to illustrate its versatility and expanded capabilities.

### 3. Summary of Work Accomplished

In pursuit of the objectives discussed in the preceding section a large number of highly instrumented welds were made at three sites: Los Alamos Scientific Laboratory (LASL), Denver Research Institute (DRI), and the United States Air Force Academy (USAFA). These tests were conducted over a three-year period and involved various combinations of aluminum and steel, varying plate thicknesses, different weld configurations, several different explosives and explosive concentrations and atmospheres of various types. While the above parameters were varied, measurements were made of detonation velocities, collision point velocities, detonation pressure and impact pressure. The measurements were made by means of high speed framing camera, flash x-ray, collapsable velocity probes recorded by oscilloscope cameras and manganin wire pressure gages also recorded by oscilloscope cameras. The result was a series of over one hundred fifty extremely well instrumented tests.

The welded specimens were then subjected to a wide variety of destructive and non-destructive tests to determine the quality and strength of the welds, so that these characteristics could be compared with the corresponding welding record to obtain an understanding of their possible correlation. The tests included weld tensile strength, weld shear strength, limited fatigue and ultrasonic testing, metallographic examination and photomicroscopy. Tests were correlated with location within the welded specimen as well as with the other parameters previously discussed.

Analysis of the data consisted in part of determining the correlation between various combinations of weld strength/quality and the controlled parameters in accomplishing the weld. The second major portion of the analysis effort was the development of several models for predicting behavior of the flyer plate and the weld interface during weld formation. Two of these models are intended solely for prediction of flyer plate response under explosive loading. The model developed by Lindbergh (1973), and reported herein, is based on a series of disjointed mass elements, each acted upon by the explosive load. The resulting differential equations are computerized and used to predict flyer plate deflection, velocity and acceleration. The flyer plate model developed by Merkle as a portion of this report relates instantaneous flyer plate deformation to the motion-time history of a typical flyer plate element, using a least squares fit to evaluate the parameters in the equations. The final model, developed by Agbabian Associates, is a finite element study of the flyer plate, base plate and the air space between them. The air space is modeled as a series of elements with very low stiffness. The model is programmed for use on a large computer and used to predict the response of the flyer and base plates, including deformation stress and interface pressure. The computer program includes a plotting routine, and plots of displacements, pressures and plate stresses are developed.

Based on an extensive analysis of test data, plus theoretical considerations, Wittman of DRI describes four bounding criteria for the regime in which successful welds can be accomplished. He utilizes kinetic energy and heat transfer calculations to predict the upper



velocity limit for welds above which melt of the plates occurs with resulting reduction in weld strength for aluminum.

In an effort to demonstrate various applications for which EIW is particularly well suited, a limited number of welds was performed purely to illustrate a concept. These included tubular welds, symmetrically loaded welds and spot welds. Two applications were investigated in more detail. These were the repair of bomb-damaged aluminum airfield matting and the fabrication of multi-layered armor.

All of the items of work mentioned above are reported in this report. If the work has been previously published, it is summarized herein with appropriate references. In all other cases, detailed discussion is included.

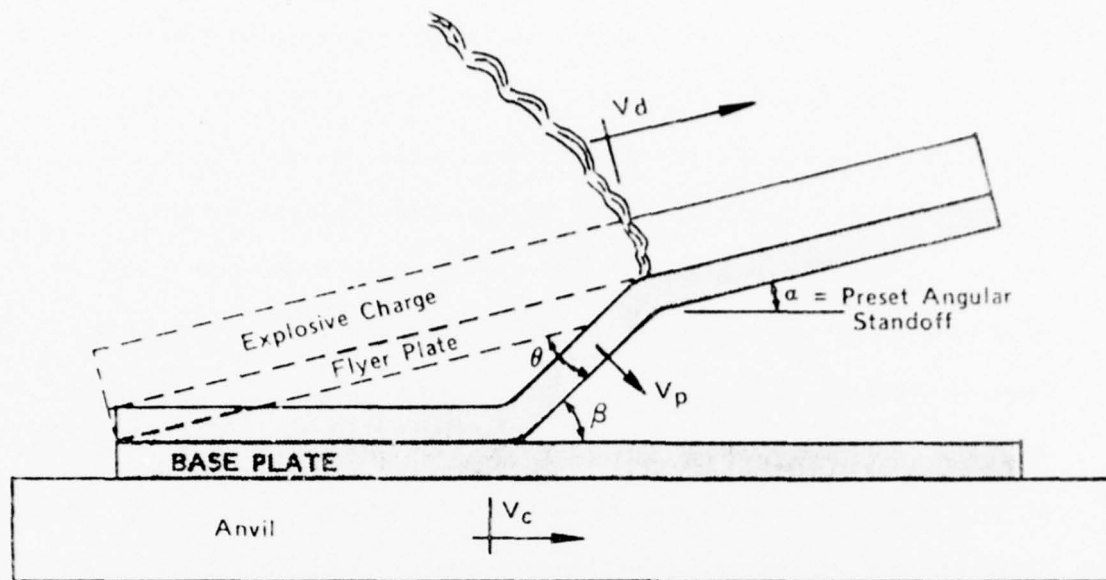
C. Fundamentals of Explosive Impulse Welding (EIW) (Lindbergh, 1973)

Explosive impulse welding is basically a solid-state welding process. At excessive input energy levels, temperatures resulting at the interface can be intense enough to cause phase changes and areas of fusion bonding. However, assuming the energy levels experienced upon impact are optimum relative to produced bond strengths, little phase change occurs and the welding process occurs in the solid state.

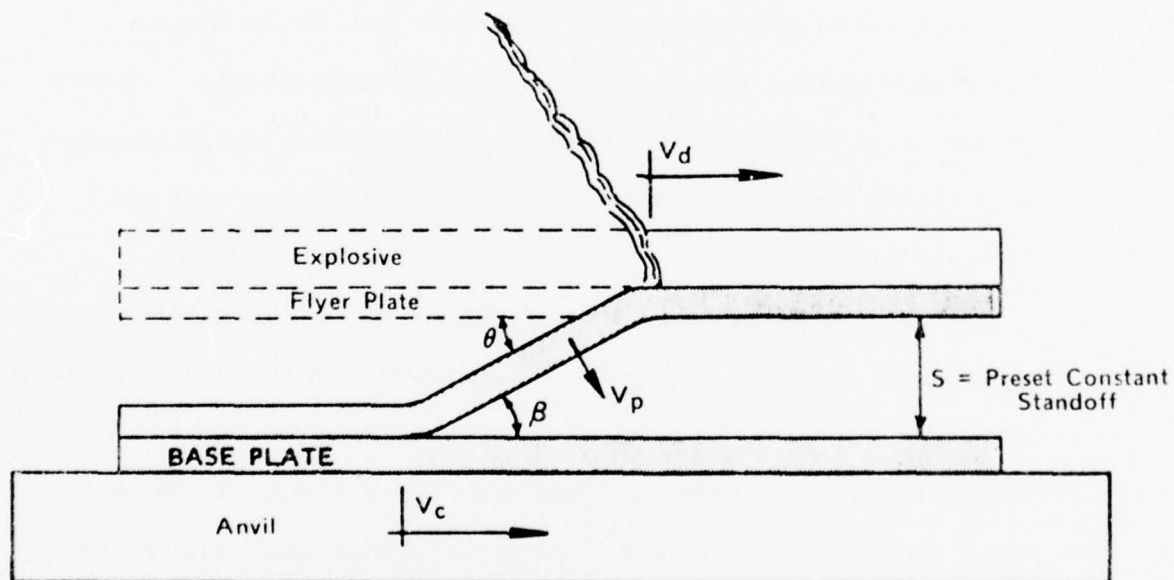
As is the case for other solid-state welding techniques, there is no comprehensive theory available to explain the EIW phenomenon on a quantitative basis. Milner and Rowe (1962) have presented an excellent assessment of evidence contributed by each technique exclusive of EIW towards an understanding of the mechanism of bonding. The accumulated evidence reflects many factors shown to influence bond formation. These are: the amount and type of deformation;

the metal(s) being bonded: lattice structure, relative motion at the weld interface, metal purity, surface preparation, solubility of oxygen in the metal, the temperature, pressure, and time of welding and high strain-rate effects. Based upon this assessment, Milner and Rowe presented an energy-barrier hypothesis that is very consistent with the results of previous investigations of explosive impulse welding. Basically, the hypothesis considers the redistribution of surface atoms to form a grain boundary as the criterion of weld formation. With an optimum redistribution, the valence electrons are shared by the metal as a whole. That is, if two metallic surfaces are brought into sufficiently close proximity, the electrons will effectively belong to both and a full interatomic bonding of the metals will occur. The hypothesis states that a certain level of applied energy is required in order to achieve this redistribution and, consequently, solid-state bonding. If this hypothesis is modified to account for the additional energy necessary to initially disperse surface contaminants, it relates well to explosive impulse welding.

Explosive impulse welding is produced through the controlled oblique collision of two metal surfaces. The two most common process geometrics, the preset angle and the parallel plate, are shown in Fig. 1. As is indicated, the basic components include a flyer plate, an explosive charge used to accelerate the flyer plate, a stationary base plate and a supporting anvil. The initial system configurations and simplified intermediate deformation are also shown.



a) PRESET ANGLE GEOMETRY



b) PARALLEL GEOMETRY

Figure 1. Explosive Impulse Welding  
Initial and Intermediate  
Configurations

In response to the impulse provided by the detonating explosive layer, the flyer plate gains velocity as it traverses the standoff distance originally separating the two plates. Upon impact, an intense, unsymmetrical pressure state is generated in the region of the collision point. If compatible with welding, the impact will establish several characteristic conditions.

First, the collision point velocity,  $V_c$ , will be subseismic. That is, it will be subseismic relative to the sonic velocities of the flyer or base plate material. In the parallel plate configuration, this requires the explosive detonation velocity to be relatively subseismic also since it equals the collision point velocity. This assumes a constant detonation velocity. If the detonation velocity is superseismic, the preset angle plate geometry must be used to insure a subseismic collision point velocity. The oblique direction of the detonation relative to the direction in which the collision point is progressing accounts for this adjustment. A comparison of calculated stress distributions along the interfaces for the cases of super- and subseismic collision velocities highlights the essential qualitative difference between these two conditions. For the superseismic collision, the disturbance is confined to the region behind the contact point. In the subseismic collision, however, the disturbance moves ahead of the collision point.

Second, the developed stress will be sufficiently intense to produce the plastic flow of plate metals in the surface regions behind the advancing shock fronts and, assuming the necessary subseismic collision velocity, ahead of the collision point.

If these conditions are met, the high energy shocked material seeks relief by plastically flowing into the interface region immediately ahead of the collision point. Such a gross local deformation is common to explosive impulse welds. As a product of this disruption, surface contaminants are loosened and expelled from the collision region in a spray of metallic particles originating in the collision region. Thus, disrupted atomically clean metal surfaces are left to be brought together under an intense stress state to within interatomic distances. The forces of atomic attraction become effective, locking the surfaces in a metallic bond.

#### D. Brief History of Explosive Impulse Welding

Explosive Impulse Welding (EIW) offers many advantages in metal joining and adds a new dimension in fabrication innovation potential. This relatively new process involves the bonding of metal elements as a direct result of a carefully controlled oblique high-velocity impact of the elements. The most significant aspect of EIW is that the bond is not a result of fusion or melting. Instead, the impact conditions force the common metal surfaces close enough for them to acquire a balance of interatomic attractive forces or cohesive energy. There are many apparent advantages to this bonding process. For example, most bimetal combinations can be bonded. High bond strengths at least equal to the parent metal strength of the weaker of the metals to be joined can be consistently obtained.

During the past 10 years, a considerable amount has been published regarding the EIW phenomenon and its applications. Despite this



impressive effort, a sufficient quantitative description and explanation of the bonding process does not now exist. These are essential to the derivation of an adequate engineering design approach. Perhaps these deficiencies are due to the many different disciplines involved and the complexity of their involvements. As a result, application developments are normally approached on the basis of an experimental parametric investigation. Such an approach is expensive in terms of time as well as money, and cannot feasibly lead to an adequate understanding of the phenomenon.

The Air Force has already tested EIW for possible use in meeting operational requirements. In September 1971, an AM2 airfield bomb damage repair method using EIW was successfully demonstrated (AFWL-TR-70-160). This application proved its compatibility with austere field conditions and semi-skilled technicians. More importantly, it suggested numerous possible areas of application such as equipment repair, pipeline fabrication, building erection and fuel storage tank fabrication. Aircraft fabrication is still another potential beneficiary.

The development of explosive impulse welding as a commercially applicable metal joining technique is a relatively recent event. The only widely known commercial application is the production of explosively clad plate which was not initiated until 1964 (Stone, 1969). Knowledge of the basic process--the development of metallurgical bonds during impact--however, can be traced back to considerably earlier times, having been reported as an interesting sidelight in studies of armor and armor-piercing projectiles, as an unwanted side effect of explosive forming and, more recently, as an adjunct to hypervelocity impact

experiments (Rolsten, 1967). Little evidence of attempts to understand the processor to harness it appeared before the late 1950's and early 1960's. When theoretical investigations of explosive impulse welding were finally undertaken, attention was focused on two associated phenomena--(1) jetting and (2) surface wave formation.

Early studies of jetting were undertaken to support the development of shaped charge armor-piercing weapons such as the bazooka shown in Figure 2. An early report of the theory of jet formation with conical and wedge-shaped liners is given by Birkhoff (1948). If one considers the steady collapse of the wedge-shaped liner shown in Figure 3, an observer moving with the collision point 0 would see material flowing past as indicated in Figure 4. Since, in the hydrodynamic model the forces acting can only deflect the stream, the velocities,  $V_F$ ,  $V_S$ , and  $V_J$  are equal. Conservation of mass and of momentum require that

$$m_s + m_j = m$$

$$m_s - m_j = m \cos \beta$$

so that

$$m_j = \frac{m}{2} (1 - \cos \beta)$$

$$m_s = \frac{m}{2} (1 + \cos \beta)$$

The incompressible hydrodynamic model thus predicts jet formation in symmetric impacts for all wedge angles. The basic assumption that the liner material can be adequately described as an incompressible fluid requires that the plate velocity exceed a value which produces impact pressures considerably above the shear strength of the liner material and precludes the consideration of shock waves (collision point velocities must not be greater than the sonic velocity of the plate material).

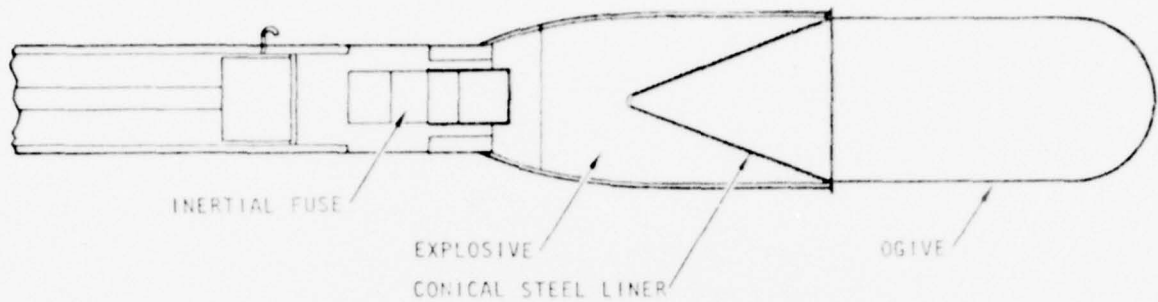


Figure 2. Cross Section of the Head of a U.S. Army Bazooka, Showing Conical Steel Liner in the Shaped Charge

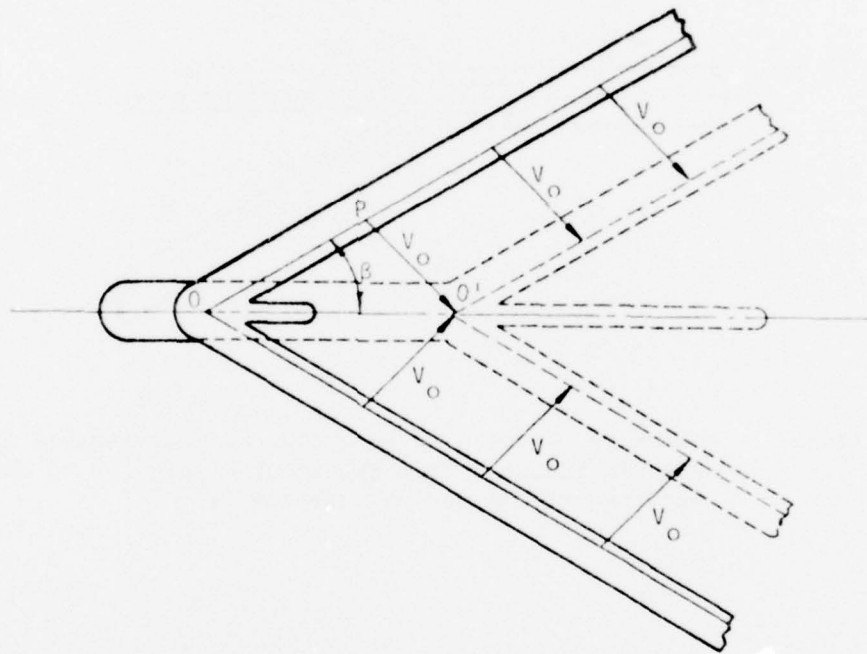


Figure 3. Formation of jet and slug from a cone or wedge-shaped liner whose sides collapse with constant velocity  $V_0$  as a result of the explosion of a charge that was in contact with the outer surface. The solid lines show conditions at an early instant of time, and the dotted lines show conditions after the walls have moved a distance equal to the velocity  $V_0$ .

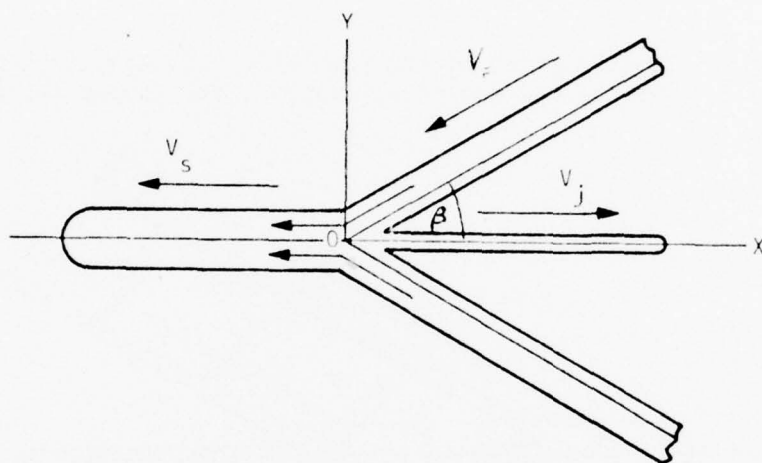


Figure 4. Formation of jet slug by a cone or wedge-shaped liner shown in Figure 2 from the point of view of an observer stationed at the moving junction  $O$ .

Walsh, Shreffler, and Willing treated high velocity collisions as problems in compressible hydrodynamics, allowing the consideration of shock waves. A theoretical velocity-dependent wedge angle which separated conditions for jetting and jetless collisions was predicted and experimental confirmation of the theory was obtained. The theory is applicable only to high velocity impacts where the collision point velocity exceeds the sonic velocity in the plates, i.e., velocities above those considered by Rolsten (1967). Again, only steady flows were considered; bond development was not of interest, and no attempt was made to relate jet formation and bonding phenomena.

The occurrence of wavelike deformations on the surface of projectiles shot obliquely at thin metal targets (See Figure 5) was first reported by Allen, Mapes, and Wilson (Allen, 1954). Abrahamson (1961) proposed a mechanism of wave formation based on a rather vague hydrodynamic instability. Starting from the theory describing jetting and jetless collisions by Birkhoff (1948) and Walsh and an examination of the surface deformation caused by a moving load, Abrahamson used heuristic arguments to describe the wave-producing process for the asymmetric collision shown in Figure 6. The basic theory requires an incoming stream of material, a deformable translating target, and instabilities (fluctuations) in the stream. Experimental verification that surface waves could be developed was obtained by subjecting beds of grease or silicone putty to jets of air or water. Evidence from the bullet and other impact experiments reported by Allen (1954) indicated that wave formation and jetting are associated phenomena occurring



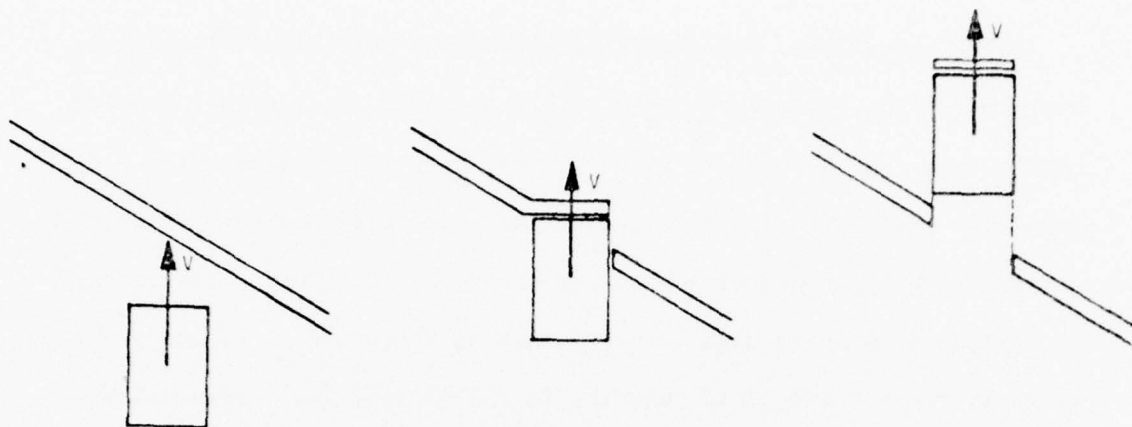


Figure 5. Penetration of a Thin Oblique Target by a Flat Nosed Bullet

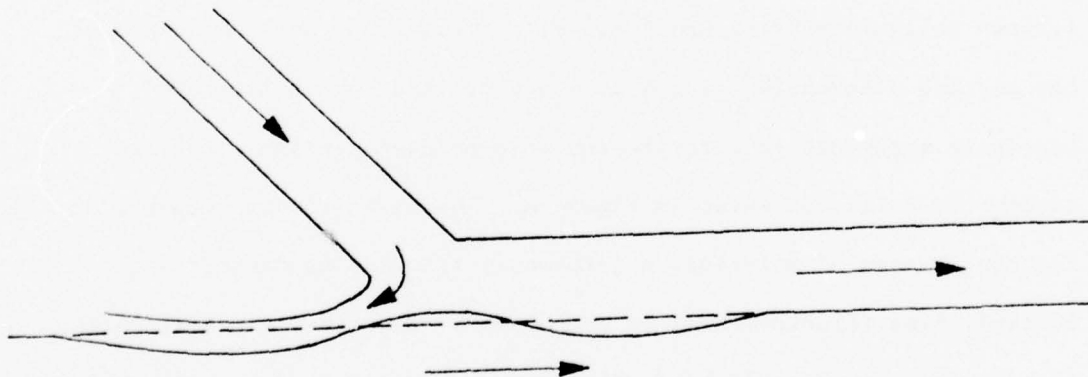


Figure 6. Asymmetric Collision Treated by Abrahamson (1961) Showing Deformation of Target

under effectively the same conditions. Although "explosive welding" is mentioned and conditions for obtaining good bonds are described in general terms, no correlation between bond formation and jetting or wave formation was proposed. A study by Cowan and Holtzman combined the work of Birkhoff (1948) and Walsh, correcting some errors in the description of asymmetric collision, with the work of Abrahamson (1961) and examined experimental evidence from explosively welded specimens to determine conditions necessary for bonding. It was determined that jetting was a necessary part of the welding process and that three basic types of bonds occurred: (1) a direct bond exhibiting a smooth interface, (2) a fusion bond exhibiting a uniform layer of solidified melt, and (3) an alternating bond showing surface waviness and alternating regions of direct bond and solidified melt. Heuristic arguments were proposed to account for viscosity, elasticity and plasticity of the metals, and an oblique reference was made to the Kármán vortex street as the wave-forming mechanism.

A later study by Hunt (1968) extended the hydrodynamic models of Rolsten (1968) and Birkhoff (1948) and treated the development of waves at the interface as a manifestation of Helmholtz instability at a fluid interface. The wavelength of the resulting waves should be proportional to the flyer plate thickness but independent of the plate velocity. No experimental verification was obtained. Hunt's investigation dealt specifically with deformation of the interface between explosively welded metal plates, but emphasis was placed on explaining wave formation, not bond development.

The wave formation process hypothesized by Bahrani, Black, and Crossland (Bahrani, 1967 and Crossland, 1967) appears to be the most satisfactory model proposed to date. Shown schematically in Figure 7 it accounts for the experimentally observed deposition of flyer plate surface material behind the wave crest and parent plate surface material ahead of the crest. However, it must be pointed out that what has been proposed is an interpretation of post-test evidence. Although the evidence is the result of a very thorough and carefully executed program of experiments, there has been no parallel development of theoretical evidence to support the hypothesis or to relate the process to the physical properties of the plates and the collision.

Keller (1968) has also examined the problem associated with the development of waves at the interface and has proposed that the change in the character of waves along the interface represents a change in the flow conditions--laminar flow occurring at the initiation end of the weld, a transition region with regular vortices in the intermediate region, and a turbulent flow region.

Although the theoretical investigations have provided only a descriptive picture of jetting and surface rippling as phenomena associated with bond development in explosive impulse welding, sufficient experimental data have been amassed to establish empirical rules satisfactory for some commercial applications, including the preparation of sandwich coinage stock and clad plate. For a particular explosive, the empirical rule describing conditions for welding may be of the form shown in Figure 8. This particular one is common in that it is

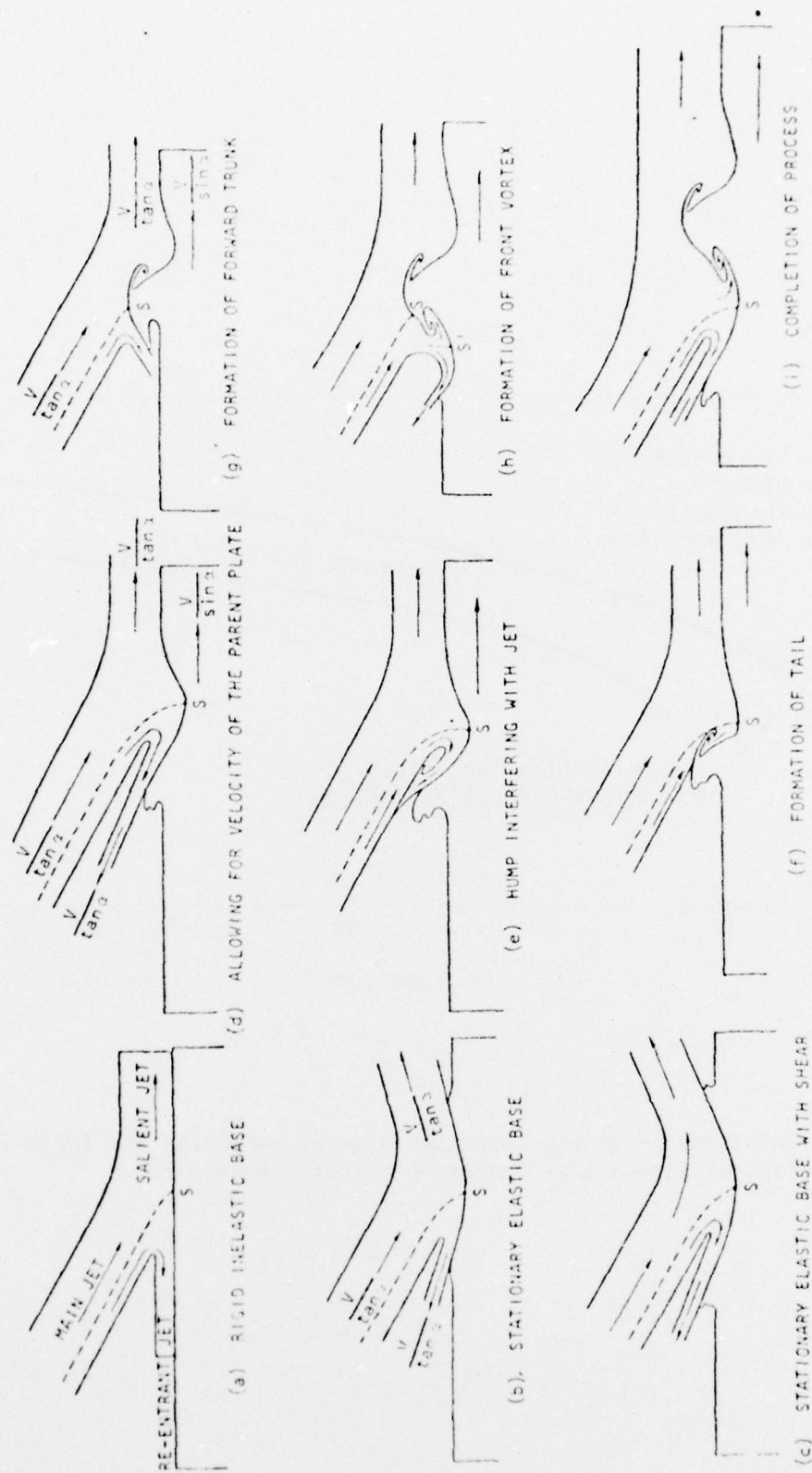


Figure 7. Formation of Waves (After Bahrani, 1967)

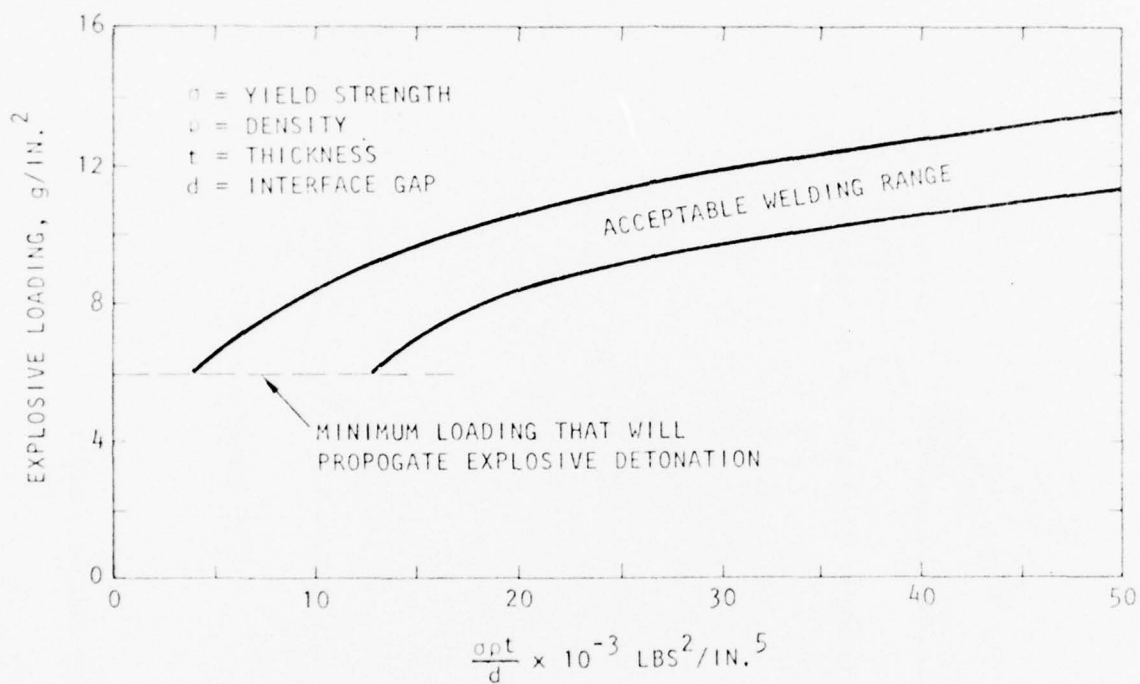


Figure 8. Relationship of the Important Process Variables for Explosive Bonding with a Low-Detonation-Velocity Explosive



intended to yield only a rough approximation of explosive load requirements for welding.

The same body of data has also provided evidence that, in some cases, even when surface waves were developed, the plates could be easily separated to allow examination of the interface (Deribas, 1967). Similar observations have been made during this research with indications that such cases indicate either a good but brittle weld fractured by elastic recovery activity or the existence of conditions at the upper transition from weld to no-weld. Otto (1964) reports instances of welding without jet formation which tend to discredit the hydrodynamic descriptions. He proposes a shear mechanism as the cause of interface waves. His proposal fails, however, to account for all aspects of the observed deformation patterns. Attempts by Crossland and Bahrani (1967) to reproduce Otto's results, however, were unsuccessful.

## II. EXPERIMENTAL PROGRAM

### A. Tests Conducted at Denver Research Institute (DRI)

The parametric investigation began with the explosion welding of aluminum using the parallel standoff configuration. The explosive chosen for that investigation was a 40% extra nitroglycerine dynamite manufactured by du Pont. The explosive has a medium detonation velocity (approximately 3,300 m/sec), is inexpensive, readily available, and had been successfully used for other explosion welding applications at the University of Denver. See Appendix D for a discussion of explosive characteristics. The aluminum parallel geometry parametric welding study was completed in September 1969 using the 40% extra dynamite. A summary of the parallel plate aluminum tests conducted is shown in Tables 2 and 3. Note that a precise tabulation of earlier shot results (Table 2) is not available.

As shown in Table 2, three trials were made for each combination of welding of parameters, and, in most instances, the three trials were performed simultaneously.

Except for the 1/2- and 3/8-inch thick specimens which were 5x12 inch, all plate coupons were 5 in x 6 in. The plate coupons were sheared from 6061-T6 aluminum alloy.

No surface preparation was used prior to explosion welding. The plates were used as sheared; the surface often contained scratches, mill identification marks, and dust.

Table 2. PARALLEL GEOMETRY ALUMINUM EIW PARAMETRIC SCHEDULE

Explosive Loading	Stand-Off	Number of Weld Trials				
		Base and Flyer Plate Thickness, T (inches)				
		1/8	3/16	1/4	3/8	1/2
6 g. /in. <sup>2</sup>	T/2	3	3	3	3	
	T	3	3	3	3	
	2T	3	3	3	3	
8 g. /in. <sup>2</sup>	T/2	3	3	3	3	3
	T	3	3	3	3	3
	2T	3	3	3	3	3
10 g. /in. <sup>2</sup>	T/2	3	3	3	3	3
	T	3	3	3	3	3
	2T	3	3	3	3	3
12 g. /in. <sup>2</sup>	T/2	3	3	3	3	3
	T	3	3	3	3	3
	2T	3	3	3	3	3
14 g. /in. <sup>2</sup>	T/2		3	3	3	3
	T		3	3	3	3
	2T		3	3	3	3
16 g. /in. <sup>2</sup>	T/2		3	3	3	3
	T		3	3	3	3
	2T					3
18 g. /in. <sup>2</sup>	T/2					3
	T					3
20 g. /in. <sup>2</sup>	T/2					3
	T					3
Welds, each T		36	51	51	51	57

Total Welding Trials - 246

TABLE 3

## Summary of Later Tests at DRI\*

DRI #	Plate Thickness (in)	Detonation Velocity (m/sec)	Explosive Loading (g/in <sup>2</sup> )	Standoff Distance (T=Plate Thickness)	Impact Velocity (m/sec)	Position from Initial	Tensile Test Strength (psi)
2	1/4	3060	12	T/2	373	3/4	43,500
3	1/4	2940	12	2T	586	1/2	20,800
4	1/4	2350	8	2T	443	1/2	44,350
5	1/4	2500	8	2T	407	1/2	49,500
6	1/4	2600	8	T	452	1/2	38,300
7	1/4	3000	8	T/2	417	1/2	47,000
8	1/4	2520	8	T/2	263	1/2	49,000
9	1/4	2920	8	T	457	1/2	41,000
10	1/4	3420	12.8	T/2	682	1/2	30,800
11	1/4	3140	12	T/2	437	3/4	30,000
12	1/4	3230	12	T	505	3/4	21,800
13	1/4	3350	12	T	525	3/4	23,600
14	1/4	3100	12	2T	618	1/2	32,350
15	1/4	3140	12	2T	600	1/2	29,850
16	1/4	3030	12	T/2	264		58,000
17	1/2	2960	10	T/2	361	3/4	50,600
18	1/2	3100	10	T/2	351	1/2	49,300
19	1/2	3030	10	T	396	3/4	38,700
20	1/2	2850	10	T	323	3/4	47,300

\*All tests were parallel plate, 6061-T6 aluminum, 40% Red Cross Extra Dynamite

TABLE 3 (Contd)

## Summary of Later Tests at DRI\*

DRI #	Plate Thickness (in)	Detonation Velocity (m/sec)	Explosive Loading (g/in <sup>2</sup> )	Standoff Distance (T=Plate Thickness)	Velocity (m/sec)	Tensile Test Position from Initial	Strength (psi)
21	1/2						
22	1/2	3040	14	T	423	3/4	31,000
23	1/2	2640	10	2T	366	no weld	
24	1/2	2920	10	T	369	3/4	60,600
25	1/2	3280	14	T	455	3/4	14,000
26	1/2	3390	14	2/T	443	3/4	29,700
27	1/2	2920	10	2T	431	no weld	
28	1/2	3280	14	2/T	456	1/2	25,600
29	1/2	3280	14	2T	598	3/4	11,000
30	1/2	2850	14	2T	495	3/4	6,800

\*All tests were parallel plate, 6061-T6 aluminum, 40% Red Cross Extra Dynamite



Granular 40% extra du Pont dynamite was packed into a posterboard box to the desired loading. The correct amount of explosive was pre-weighed and used to fill a box having a specific volume, thus developing the required loading (in grams/in<sup>2</sup>) at the correct packing density. A du Pont Detasheet explosive line wave generator was attached to the end of the box and used to initiate the dynamite charge.

Pieces of balsa of proper thicknesses were placed at the corners of the aluminum plates to maintain the desired standoff. The open edges of the plates were taped shut to keep out debris and to help prevent the explosive detonation products from entering the standoff region before plate collision.

The aluminum plates and explosive box were placed on a 1-inch thick steel anvil which in turn was resting on a thick slab of concrete. The general configuration of components for the parallel standoff aluminum welding experiments is shown in Figure 9.

The ultimate shear and tensile weld strength evaluation tests were conducted as described in a later section on weld testing. Ultimate shear strengths are shown in Table 4, and the ultimate tensile strength values in Table 5.

The schedule of preset angle aluminum welds performed is listed in Table 6. Both the number of welding trials and the number of welds (without regard to extent or quality) obtained for each combination of parameters are indicated.

Aluminum alloy 6061-T6 plate stock was sheared to size for the welding experiments. All plate coupons were 5 inches wide. The 1/8-,

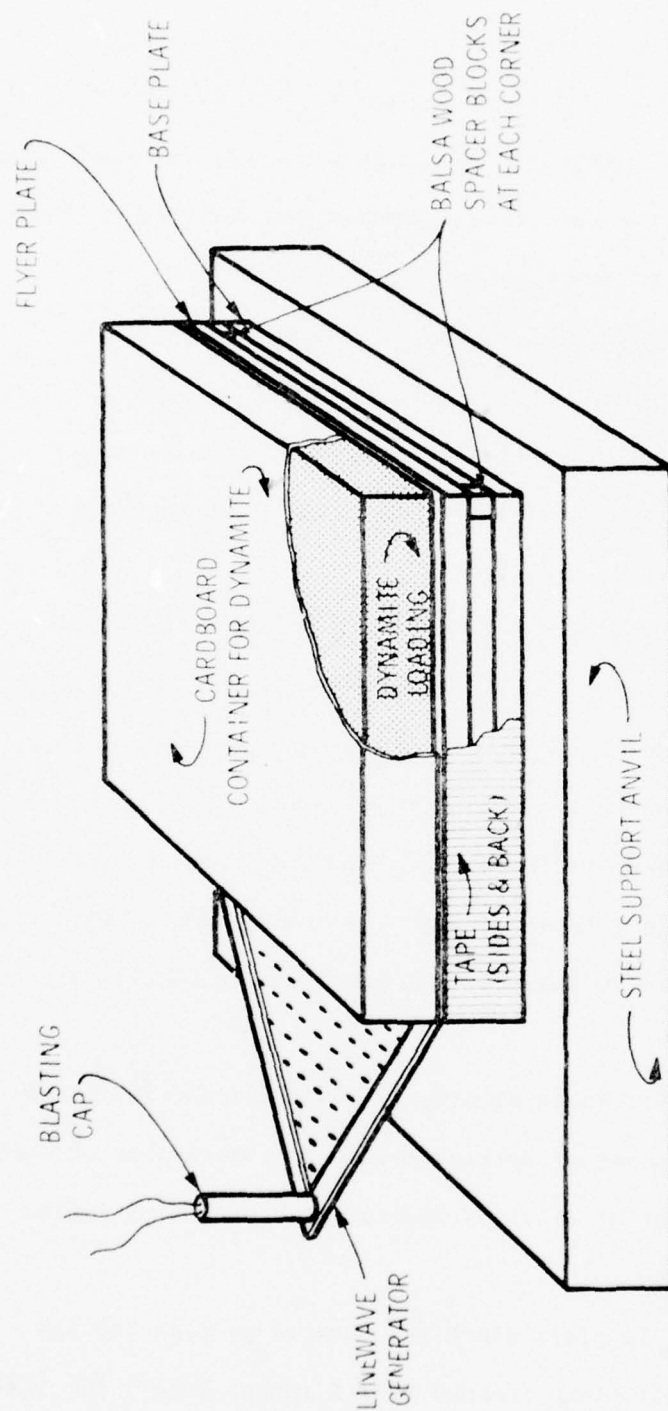


Figure 9. Component Configuration for Parallel Geometry Welding

Table 4. ULTIMATE SHEAR STRENGTHS FOR PARALLEL  
GEOMETRY ALUMINUM WELDING

Explosive Loadings (grams/cm <sup>2</sup> )	Plate Thickness, t (in.)	Ultimate Shear Strength, psi			
		Standoff = t/2		Standoff = t	
0.930	3/16	0 0 0	0	22,515 19,630 20,625	20,923
	1/4	7,609 6,340 8,978	7,642	2,850 2,000 0	1,617
	3/8	0 0 0	0	0 0 0	0
	1/2	0 0 0	0	0 0 0	0
1.240	3/16	26,515 26,970	26,743	27,700 28,150 26,108	27,319
	1/4	23,843 26,600 24,558	25,000	20,000 22,016 20,040	20,685
	3/8	22,200 20,900 20,029	21,043	29,069 26,357	27,713
	1/2	0 0 0	0	0 0 0	0

Table 4 (continued)

Explosive Loadings (grams/cm <sup>2</sup> )	Plate Thickness, t (in)	Ultimate Shear Strength, psi	
		Standoff = t/2	Standoff = t
1.550	3/16	26,288 } 25,152 } 26,339 27,576 }	24,589 } 26,850 } 24,946 23,400 }
	1/4	27,100 } 27,273 } 26,869 26,234 }	20,718 } 21,366 } 21,186 21,474 }
	3/8	19,450 } 9,259 } 15,460 17,672 }	9,788 } 12,793 } 10,836 9,929 }
	1/2	17,090 } 22,800 } 19,945 0 }	0 } 0 } 0 0 }
1.860	3/16	22,121 } 22,500 } 25,682 27,424 }	23,413 } 24,691 } 23,506 22,414 }
	1/4	24,445 } 24,800 } 25,381 26,900 }	19,643 } 20,990 } 20,092 19,643 }
	3/8	18,151 } 14,350 } 16,341 16,522 }	10,833 } 10,680 } 10,737 10,700 }
	1/2	26,852 } 22,600 } 25,090 25,817 }	3,354 } 500 } 1,927 0 }

Table 4 (continued)

Explosive Loadings (grams/cm <sup>2</sup> )	Plate Thickness, t (in.)	Ultimate Shear Strength, psi	
		Standoff = t/2	Standoff = t
2.175	3/16	28,561 24,849 27,273 } 26,895	
	1/4	20,200 26,200 20,700 } 22,366	22,161 19,044 21,562 } 20,922
	3/8		22,500 20,602 23,265 } 22,122
	1/2	24,008 22,792 22,917 } 23,239	16,150 9 0 } 16,159
2.480	3/16	25,378 26,894 21,515 } 24,596	
	1/4		21,700 23,900 22,400 } 22,666
	3/8		31,008 26,357 26,938 } 28,098
	1/2	21,561 21,087 21,014 } 21,220	12,804 8,842 12,107 } 11,251
2.790	1/2	24,391 } 24,391	0 0 } 0
3.100	1/2	21,341 } 21,341	28,353 } 28,353



Table 5. ULTIMATE TENSILE STRENGTHS FOR PARALLEL  
GEOMETRY ALUMINUM WELDING

Explosive Loadings (grams/cm <sup>2</sup> )	Plate Thickness, t (in.)	Ultimate Tensile Strength, psi			
		Standoff = t/2		Standoff = t	
0.930 (6 G/in <sup>2</sup> )	3/16	0		48,092	
		0	0	52,464	49,885
		0		49,100	
	1/4	44,600		17,300	
		42,857	41,940	19,900	18,500
		41,364		18,300	
	3/8	0		0	
		0	0	0	0
		0		0	
	1/2	0		0	
		0	0	0	0
		0		0	
1.240 (8 G/in <sup>2</sup> )	3/16	26,448		48,639	
		15,301	20,874	53,010	50,096
				48,639	
	1/4	61,321		47,272	
		57,383	61,790	43,636	47,335
		66,667		51,098	
	3/8	52,800		65,600	
		58,511	51,301	59,800	62,700
		42,593			
	1/2	0		0	
		0	0	0	0
		0		0	

Table 5 (continued)

Explosive Loadings (grams/cm <sup>2</sup> )	Plate Thickness, t (in.)	Ultimate Strength, psi			
		Standoff = t/2		Standoff = t	
1.550  (10 G/in <sup>2</sup> )	3/16	50,383 50,219 48,120	49,574	37,225 35,500 28,302	33,676
	1/4	62,847 45,094 56,604	54,848	40,179 38,233 35,600	38,004
	3/8	25,800 16,275 15,969	19,015	8,400 2,186 19,947	10,178
	1/2	60,377 59,040	59,709	40,100 43,800 0	41,950
1.860 (12 G/in <sup>2</sup> )	3/16	56,066 39,978 44,098	46,714	30,604 39,621 44,266	38,164
	1/4	29,200 34,976 27,250	30,475	38,528 20,767 28,372	29,222
	3/8	27,500 31,424 14,209	24,378	18,400 17,350 18,308	18,019
	1/2	42,375 43,080 44,960	43,472	32,200 36,400	34,300

Table 5 (continued)

Explosive Loadings (grams/cm <sup>2</sup> )	Plate Thickness, t (in.)	Ultimate Shear Strength, psi			
		Standoff = t/2		Standoff = t	
2.170 (14 G/in <sup>2</sup> )	3/16	38,798 56,175 56,066	50,346	48,000	48,000
	1/4	37,200 45,800 39,100	40,700	38,801 41,261 42,627	40,896
	3/8	26,550	26,550	32,000 33,500 31,400	32,300
	1/2	31,200 27,325 33,337	30,621	31,700 23,800	27,750
2.480 (16 G/in <sup>2</sup> )	3/16	55,191 56,284 57,924	56,466		
	1/4			27,600 33,000 27,800	29,467
	3/8			35,500 38,800 41,200	38,500
	1/2	41,400 34,200	37,800	28,200 31,300	29,750
2.790 (18 G/in <sup>2</sup> )	1/2	46,200	46,200	27,200 32,800	30,000
3.100 (20 G/in <sup>2</sup> )	1/2	30,600	30,600	33,400	33,400

3/16-, and 1/4-inch thick plates were 9 inches long, while the 3/8- and 1/2-inch plates were 12 inches long. The flyer and base plates were the same thickness in all cases.

Surface preparation for the explosive impulse welding consisted only of degreasing the sheared aluminum plates using an alkaline cleaner followed by a water rinse and air blast dry. Surface scratches and printed mill identification were not removed prior to welding.

The aluminum base plate of the explosion welding assembly was supported by a 1-inch thick steel anvil plate. The steel anvil was supported by a thick slab of concrete at ground level.

The IRECO 4000 m/sec explosive was used exclusively for the preset angle aluminum parametric welding. The explosive was sliced to proper thickness using the modified meat saw device described in Appendix D. It is believed that explosive thickness was controlled within  $-1/32 + 1/16$  inch. In most cases the thickness of explosive was slightly greater than the specified thickness.

Balsa supports were used to maintain the proper angular separation, while fabric tape was used to hinge the apex of the angle and enclose the sides of the angular standoff. The general configuration of components for the aluminum preset angle welding experiments is shown in Figure 10.

Strength tests were conducted as described in the section of this report dealing with weld testing. The results are shown in Table 7.

Table 6 PRESET ANGLE GEOMETRY ALUMINUM EIW PARAMETRIC SCHEDULE

Explosive Loading	Preset Angle	Number of Welds/Weld Trials				
		Base and Flyer Plate Thickness, T (inches)				
		1/8	3/16	1/4	3/8	1/2
5 g. /in. <sup>2</sup>	5°	3/3	3/3	3/3		
	10°	3/3	3/3	3/3		
	15°	3/3	3/3	3/3		
7-1/2 g. /in. <sup>2</sup>	5°	3/3	3/3	3/3	3/3	3/3
	10°	3/3	3/3	3/3	3/3	3/3
	15°	3/3	3/3	3/3	0/3	0/3
10 g. /in. <sup>2</sup>	5°	3/3	3/3	3/3	3/3	3/3
	10°	3/3	3/3	3/3	3/3	2/3
	15°	3/3	2/3	2/3	1/3	0/3
12-1/2 g. /in. <sup>2</sup>	5°			3/3	3/3	3/3
	10°			1/3	3/3	3/3
	15°			2/3	3/3	1/3
15 g. /in. <sup>2</sup>	5°				3/3	3/3
	10°				3/3	3/3
	15°				3/3	1/3

Total Welding Trials - 162



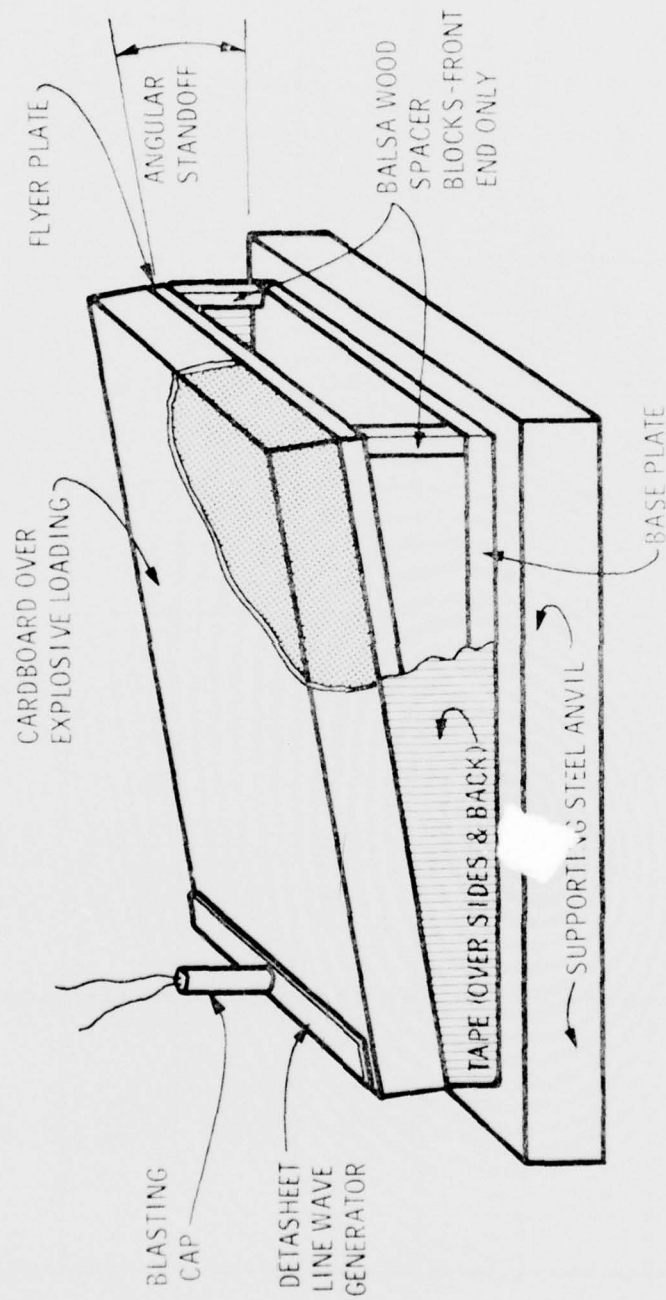


Figure 10. Component Configuration for Preset Angle Geometry Welding

Table 7 PRESET ANGLE GEOMETRY ALUMINUM PLATE WELD STRENGTHS\*

Explosive Loading (grams/in <sup>2</sup> )	Plate Thickness (in.)	Preset Angle		
		5°	10°	15°
5	1/8	43,700 / 30,750	23,400 / 12,400	7,425 / 32,000
		47,500 / 20,400	22,500 / 29,450	28,300 / 18,250
		40,900 / 34,000	37,400 / 6,620	0 / 0
	3/16	18,400 / 34,100	2,600 / 0	25,500 / 0
		63,000 / 31,000	6,600 / 0	0 / 0
		58,200 / 34,350	2,120 / 0	0 / 0
7 1/2	1/4	48,200 / 17,600	15,200 / 0	0 / 0
		61,000 / 34,300	20,800 / 29,800	0 / 0
		15,333 / 24,900	0 / 0	0 / 0
	1/8	47,300 / 25,400	25,000 / 16,000	19,900 / 0
		47,700 / 34,600	42,100 / 34,400	14,300 / 16,650
		44,400 / 33,400	50,900 / 32,900	23,250 / 20,500
	3/16	52,600 / 29,400	15,800 / 15,700	13,000 / 0
		27,000 / 25,800	19,800 / 19,400	15,020 / 0
		57,600 / 31,300	15,800 / 17,600	4,800 / 0
	1/4	46,200 / 30,600	43,700 / 32,400	6,200 / 0
		31,200 / 26,600	24,000 / 28,000	0 / 0
		47,300 / 32,100	31,200 / 0	0 / 0
	3/8	61,200 / 21,900	0 / 0	0
		57,600 / 12,100	6,400 / 37,000	0
		59,700 / 30,300	0 / 0	0

\*Given as, Ultimate Tensile Strength (psi)/Ultimate Shear Strength (psi)

Table 7 (continued)

Explosive Loading (grams/in <sup>2</sup> )	Plate Thickness (in.)	Preset Angle		
		5°	10°	15°
7 1/2	1/2	24,096 / 28,100	40,900 / 29,000	
		18,900 / 29,500	0 / 0	
		40,000 / 29,800	0 / 0	
10	1/8	17,050 / 30,500	32,600 / 31,400	31,000 / 22,500
		41,100 / 0	36,000 / 33,000	33,000 / 26,500
		41,600 / 28,200	39,700 / 32,200	33,900 / 33,900
	3/16	36,900 / 29,300	16,300 / 30,350	7,400 / 0
		26,800 / 25,000	12,000 / 19,550	18,000 / 0
		31,800 / 29,600	22,800 / 22,100	
	1/4	32,000 / 24,760	7,200 / 0	25,500 / 22,400
		23,000 / 16,900	19,200 / 21,100	3,000 / 0
		20,400 / 26,900	0 / 0	
	3/8	48,000 / 14,150	48,000 / 0	0 / 0
		47,020 / 30,100	14,000 / 0	
		43,200 / 25,500	49,200 / 0	
	1/2	24,096 / 28,400	40,900 / 29,000	
		18,900 / 29,500	0 / 0	
		40,000 / 29,800	0 / 0	

Table 7 (continued)

Explosive Loading (grams/in <sup>2</sup> )	Plate Thickness (in.)	Preset Angle		
		5°	10°	15°
12 1/2	1/4	9,300 / 13,750	24,400 / 0	0 / 0
		18,800 / 24,450		0 / 0
		29,000 / 34,400		
	3/8	44,200 / 23,960	23,400 / 0	0 / 0
		24,000 / 30,000	6,500 / 0	0 / 0
		18,800 / 21,000	13,942 / 0	0 / 0
15	1/2	33,400 / 26,900	59,100 / 28,900	0 / 0
		63,300 / 24,500	12,300 / 0	
		59,980 / 23,700	44,000 / 8,410	
	3/8	24,000 / 19,400	0 / 0	0 / 0
		23,300 / 18,800	0 / 0	0 / 0
		25,500 / 21,100	0 / 0	0 / 0
	1/2	25,400 / 9,350	0 / 0	0 / 0
		35,200 / 6,930	25,133 / 0	
		11,600 / 5,000	0 / 0	

B. Tests Conducted at Los Alamos Scientific Laboratory (LASL)

1. Atmospheric Tests

Thirty flyer plate experiments were conducted at the facilities of the GMX-6 Division of the Los Alamos Scientific Laboratory. The test facility consisted of a buried concrete control room with the firing table located overhead on the ground surface. The control room housed the flash X-ray equipment exclusive of the remote tube head, the framing camera, associated electronic and mechanical equipment, the time delay trigger generator for sequencing the multiple detonations of each event, and pulsing circuitry for detonating the charges. The firing table consisted of a steel plate 4' x 4' x 6". A line of sight between the framing camera and specimen was established using a periscope arrangement. The periscope consisted of an expendable tilt mirror positioned at the upper end of a vertical tube which penetrated the bunker's roof and overburden. All explosive detonations were electronically initiated.

The event was recorded using a LASL fabricated framing camera sequenced in operation with a 600 KV flash X-ray system manufactured by the Field Emission Corporation.

The framing camera used 25 separate optical trains to provide an equal number of frames per strip of film. The camera consisted essentially of an objective and a field lens, a gas driven turbine mirror and the 25 optical trains mentioned above. The revolving mirror, on which the object was imaged, reflected the light in turn to the optics for each individual frame. The time interval between each frame was determined by the rotational speed of the camera turbine.



A time interval of 4 microseconds per frame was used in this study.

The camera was capable of time intervals as low as 1 microsecond.

Of those methods reviewed, the framing camera seemed most appropriate for the proposed study. Each experiment yielded a framing camera record and a welded specimen. The framing camera recorded the explosive detonation and the flyer plate deformation responses as they progressed with time. By superimposing the images of all frames, a historical record of flyer plate dynamic deformation and explosive detonation was obtained. This allowed measured weld strengths to be positively related to dynamic parameters such as collision point velocity, impact velocity and flyer plate velocity. Several earlier observations had emphasized the importance of such complete event coverage. First, the uniformity of the dynamite explosive to be used was highly questionable. Thus, only a complete record of the deformation time history could insure representative measurements. Second, boundary effects were of interest. Using the parallel welding geometry, defective or no bonding was always experienced within the first few inches of interface length. This was thought to be caused by a lack of confinement of the explosive's perimeter. Third, it was desired to record the jetting activity occurring within the interface region. The usual radiograph resolution does not provide such evidence.

A single 600 KV flash X-ray system was also available. This unit provided an X-ray pulse of 18 nanosecond duration and was fired by a signal from a time delayed trigger generator. The system was equipped with a remote tube head. The radiographs were formed on high-speed X-ray film. The resolution was improved through the use of

calcium tungstate intensifying screens. The film/screen laminate was inserted in a cardboard envelope and placed within an aluminum cassette holder for protection from blast damage.

A total of 12 different parallel plate welding events were selected for the flyer plate study. These included two plate thickness, 1/4 and 1/2 inch. The base and flyer plates were of equal thickness in each event. Three standoff distances and two explosive load levels were used with each plate thickness. These are indicated in the specimen schedule given in Table 8.

Thickness, in.	1/4			1/2		
Standoff, in.	1/8	1/4	1/2	1/4	1/2	2/2
M/C = 2.17	-	-	-	X	X	X
M/C = 1.37	X	X	X	X	X	X
M/C = 1.82	X	X	X	-	-	-

Table 8  
Specimen Schedule for LASL Tests

The explosive quantities are specified in terms of the ratio, M/C. This factor is the mass of the flyer plate per unit area divided by the mass of explosive associated with that unit surface area. The mass density of the explosive used is 1.25 grams/cc. Du Pont 40% Red Cross Extra Dynamite from the same batch as the DRI tests was used to permit close control and comparison of results.

The experimental technique evolved through the investigation of several possible alternate approaches. These varied primarily in the environment in which welding was achieved. Specifically, the first attempts to resolve an experimental technique involved welding under normal atmospheric conditions. The technique development phase progressed through considerations of inert and vacuum interface environments respectively, until the adopted technique was resolved. Basically, the atmospheric welding technique complemented with select radiographic coverage proved to be satisfactory. These candidates and the selected experimental techniques will be discussed in the following paragraphs.

The first attempt to resolve an experimental welding technique involved the arrangement illustrated in Figure 11. As the plan view and section show, the entire welding event occurred under standard atmospheric conditions.

The specimen assembly consisted of the flyer and base plates, detonation gas shield, explosive loading and calibration side panel. The final assembly is illustrated in Figure 12.

Flyer and base plates were sheared from commercial 6061-T6 aluminum plate stock. Both the 1/4 and 1/2 inch specimens were 6 inches wide and 12 inches long. Prior to welding each plate was degreased using a commercial solvent.

The experiments were conducted using the 40% Red Cross extra granular dynamite manufactured by Du Pont. It is of a nitroglycerine-sensitized, ammonium nitrate based composition. The explosive charge was prepared

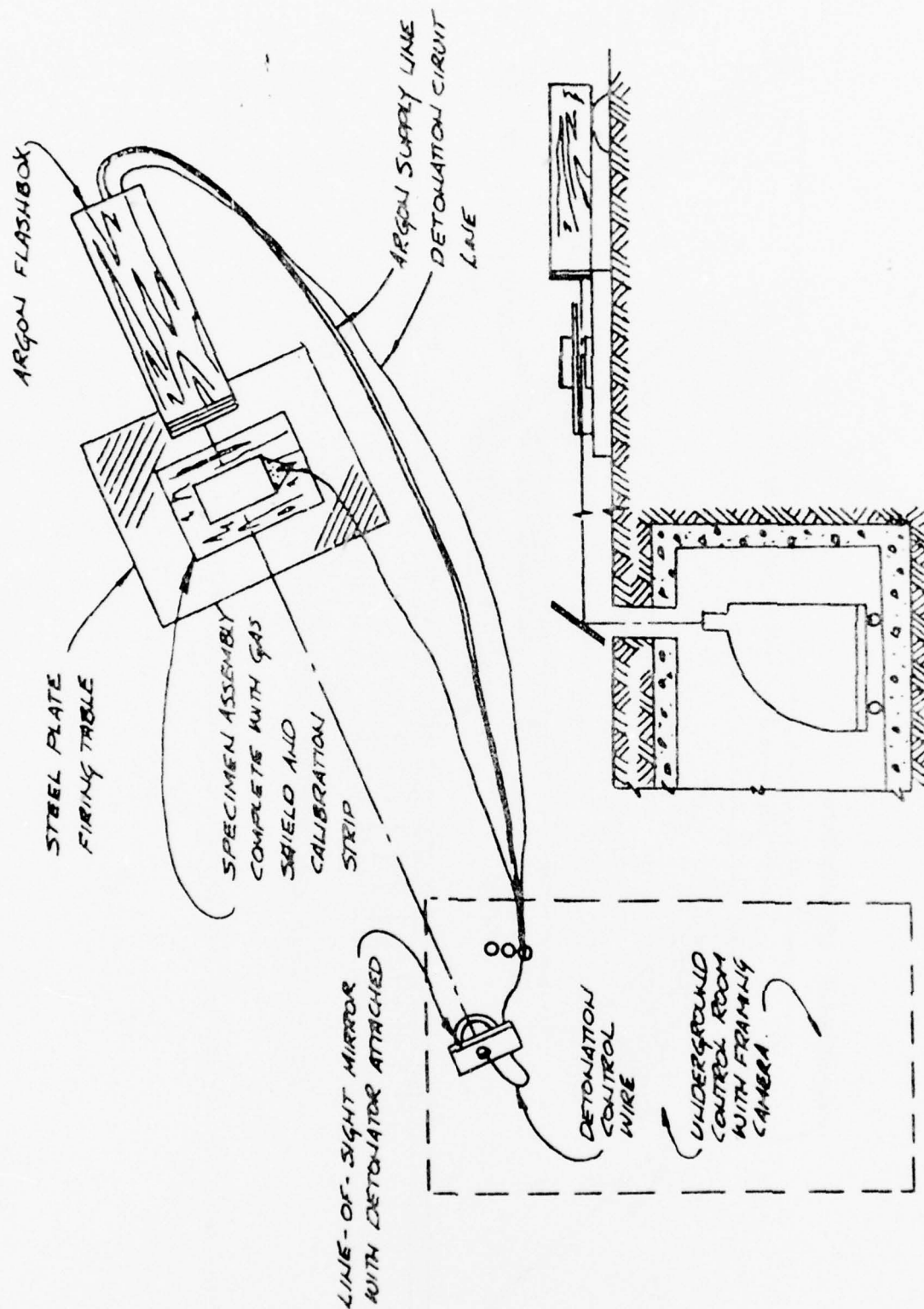


Figure 11. Initial LASL Experimental Arrangement (Atmospheric Conditions)

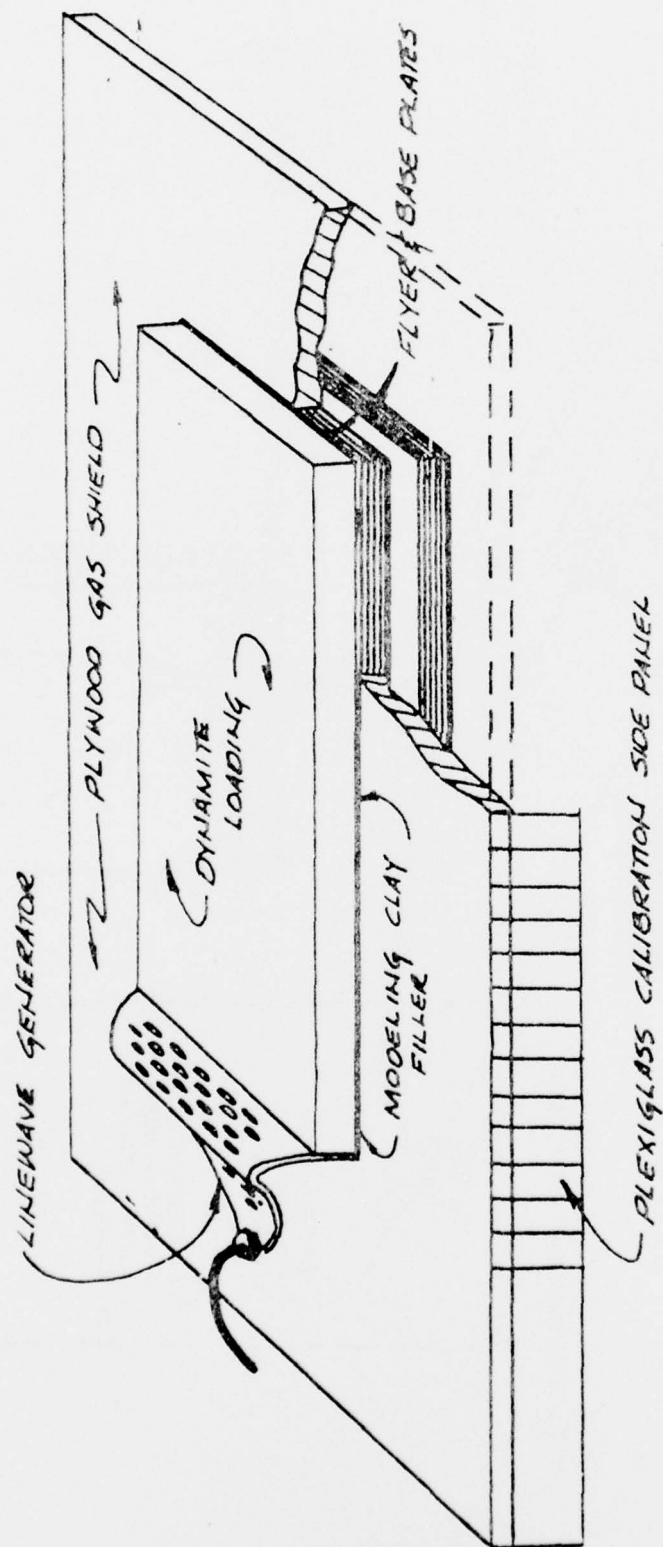


Figure 12. Initial LASL Specimen Assembly (Atmospheric Conditions)



by manually loading the granular dynamite into a cardboard box with lateral dimensions of 6 and 12 inches to conform to the adjacent surface area of the flyer plate. Loss of nitroglycerine to the absorptive cardboard was minimized by thinly coating the inner surfaces of the box with enamel paint. The height of the box was dictated by the volume of explosive to be accommodated. As it was deposited, the explosive was spread and lightly tamped with a wood stick in a manner to promote a uniform packing density. The preparation of the charge was completed by attaching a linewave generating sheet explosive (Dupont EL506C Detasheet) to one end of the explosive charge. The resulting explosive arrangement is shown in Figure 13. Prior to its use, the line wave generator was inclined so it initiated the dynamite charge's end surface from top to bottom. The line wave generator transitions the curved detonation pattern produced at its apex by the initiator to the linear configuration desired for the dynamite. The explosive quantities used for each event have been previously specified in Table 8.

The flyer plate was recessed in a 1/4 inch plywood detonation gas shield as Figure 12 illustrates. The plates were flush-mounted relative to the bottom surface of the shield. Although careful fabrication provided a fairly close fit, modeling clay was carefully packed into the space between the shield and flyer plate. Earlier trial experiments had proved these measures were necessary to prevent detonation gases from obstructing the view of the standoff region. The calibration strip was formed by painting vertical lines at 1/2 inch intervals along the length of a plexiglass sheet. It

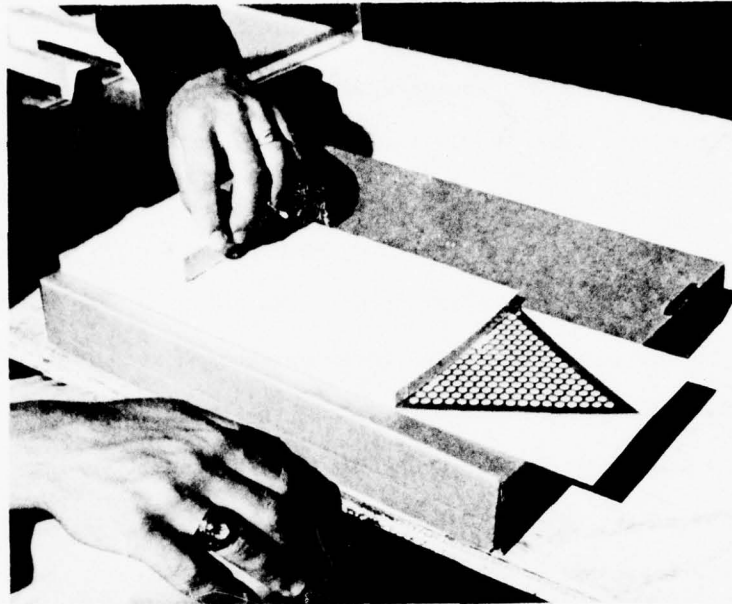


Figure 13. LASL Explosive Loading Arrangement

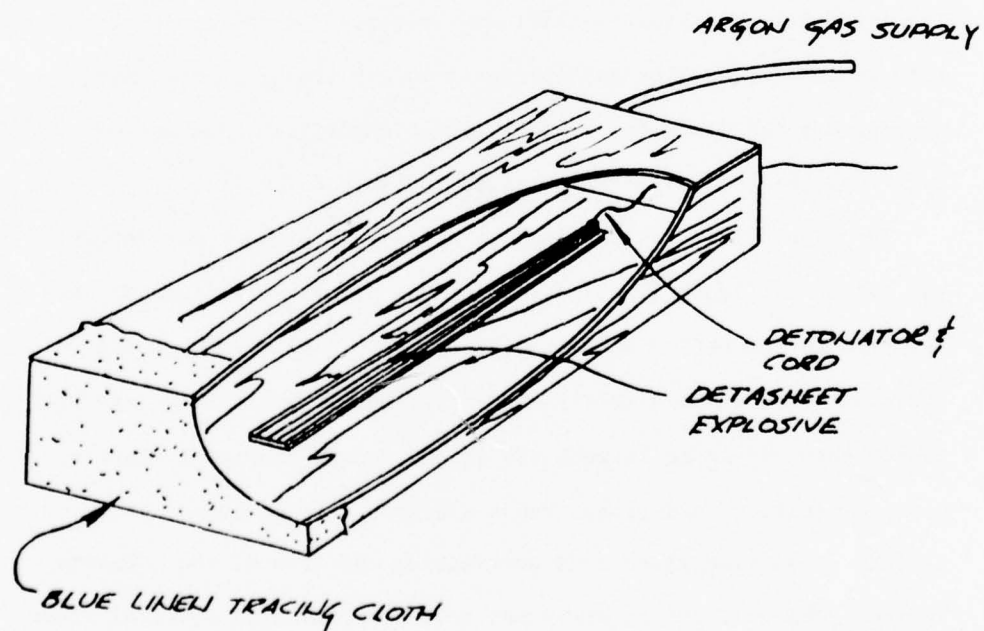


Figure 14. Argon Flash Box

was taped in position along the outer edge of the gas shield. Earlier attempts to fix the strip immediately adjacent to the plate edges were unsuccessful as the plexiglass became translucent as it experienced shock pressures.

Backlighting provided by an explosively-driven, argon-filled flash box was used to illuminate the profile of the welding specimen for photographic purposes. Figure 14 illustrates the design. Argon gas becomes highly luminous under shock conditions such as those produced by explosive. The box was 14 x 48 x 6 inches in dimensions and constructed of 1/4 inch plywood. A 4 x 33 inch strip of sheet explosive (Dupont Detasheet) was placed on the inner bottom surface of the box along its centerline. Its length was calculated considering its detonation velocity and the time duration of the photographic sequence. While one end of the flash box was covered with plywood, the other end was covered with two layers of commercial blue tracing linen. The linen allowed the lighting intensity to be suitably adjusted. During its use, the box was kept flooded with argon gas.

The explosively loaded specimen assembly was centered on the steel plate firing table as shown in Figure 11. The entire assembly was carefully aligned relative to the line of sight established by the framing camera mirror. This required the length of the aluminum plates to be perpendicular to the line of sight. In addition, the assembly had to be elevated and leveled so that the line of sight would bisect the standoff region running

parallel to the plate surface. Adjustments in the elevation and inclination of the tilt mirror were useful in achieving proper alignment. Otherwise, the recorded flyer plate profile would be distorted and non-representative. Following the alignment, the argon flash box was positioned. As the final act of preparation, initiators were positioned to initiate the linewave generator of the specimen assembly and the strip of sheet explosive within the flash box. A third detonator was used to destroy the tilt mirror at the appropriate time to prevent double exposure of the framing camera's strip film.

In conducting the event, flooding of the flash box with argon gas was the first step. As the proper velocity of the rotating mirror within the framing camera was achieved, the pulser unit was manually fired, detonating the specimen and flash box initiators and activating the time delay generator to sequentially open the framing camera lens's shutters and destroy the tilt mirror. The delay times were 20 and 120 microseconds respectively.

Three technique resolution experiments were conducted using a common specimen assembly design. In all cases, a 10 grams/in.<sup>2</sup> explosive loading was applied to a 1/2 inch thick flyer plate of 6061-T6 aluminum. The first experiment, LASL 1268, failed due to a visual obstruction of the interface region. There were two causes. First, the plexiglass calibration strip, located immediately adjacent to the flyer plate, was shocked and, consequently, became opaque. Secondly, the close fit between the flyer plate and gas shield proved to be inadequate as detonation gases rapidly moved

into the interface region. As a consequence, experiments LASL 1269 and 1270 were conducted with the calibration strip along the outer edge of the gas shield and various means of sealing the juncture between the flyer plate and gas shield. LASL 1269 continued to use a plywood gas shield, sealed with modeling clay. LASL 1270 used an aluminum plate gas shield, sealed with a commercial epoxy sealing compound.

Both experiments successfully avoided the obstruction problems mentioned above. However, another problem became evident; viz. luminosity generated within the interface region. Figure 15 shows several early frames taken from the LASL 1270 framing camera record. They reveal a luminous cloud originating within the collision region upon initial impact. This luminosity is due to freed surface particles encountering air resistance as they were ejected at a high velocity from the collision region. The resulting friction generated intense light as well as a quantity of heat. Subsequent research has indicated this heat is insignificant under optimum conditions. As the process continues, the luminosity steadily grows in size obscuring more of the interface region.

Despite this problem, the film records were most revealing. First, a significant part of the flyer plate segment in motion is evident. Secondly, the detonation fronts did not progress by equal amounts each frame. Thus, detonation velocities were not constant. Third, during the first several time intervals, the flyer plate segment in motion had considerable curvature in the direction of detonation. This results from the explosive in





Figure 15. Typical Framing Camera Record: Atmospheric Conditions

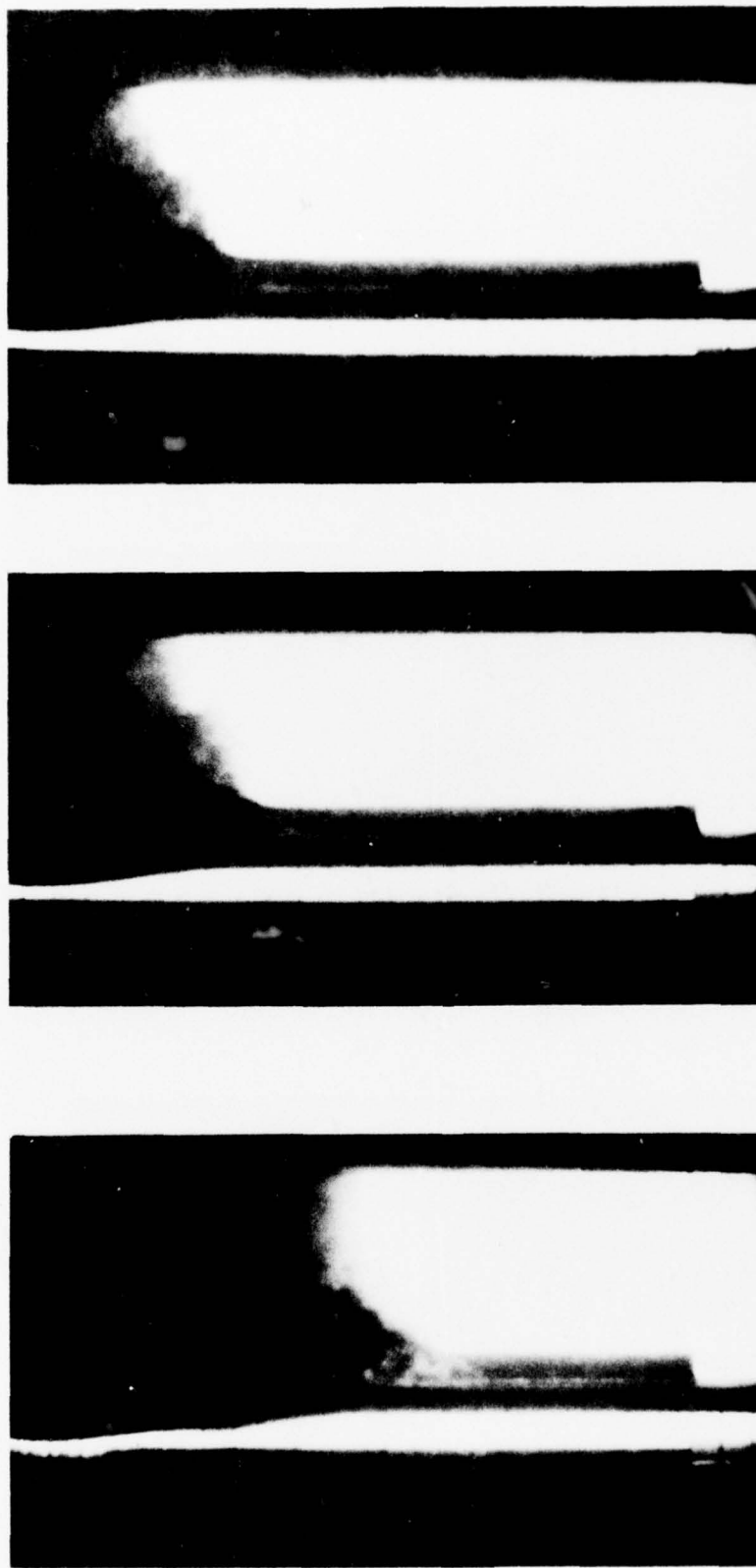


Figure 15. (Cont'd) Typical Framing Camera Record: Atmospheric Conditions

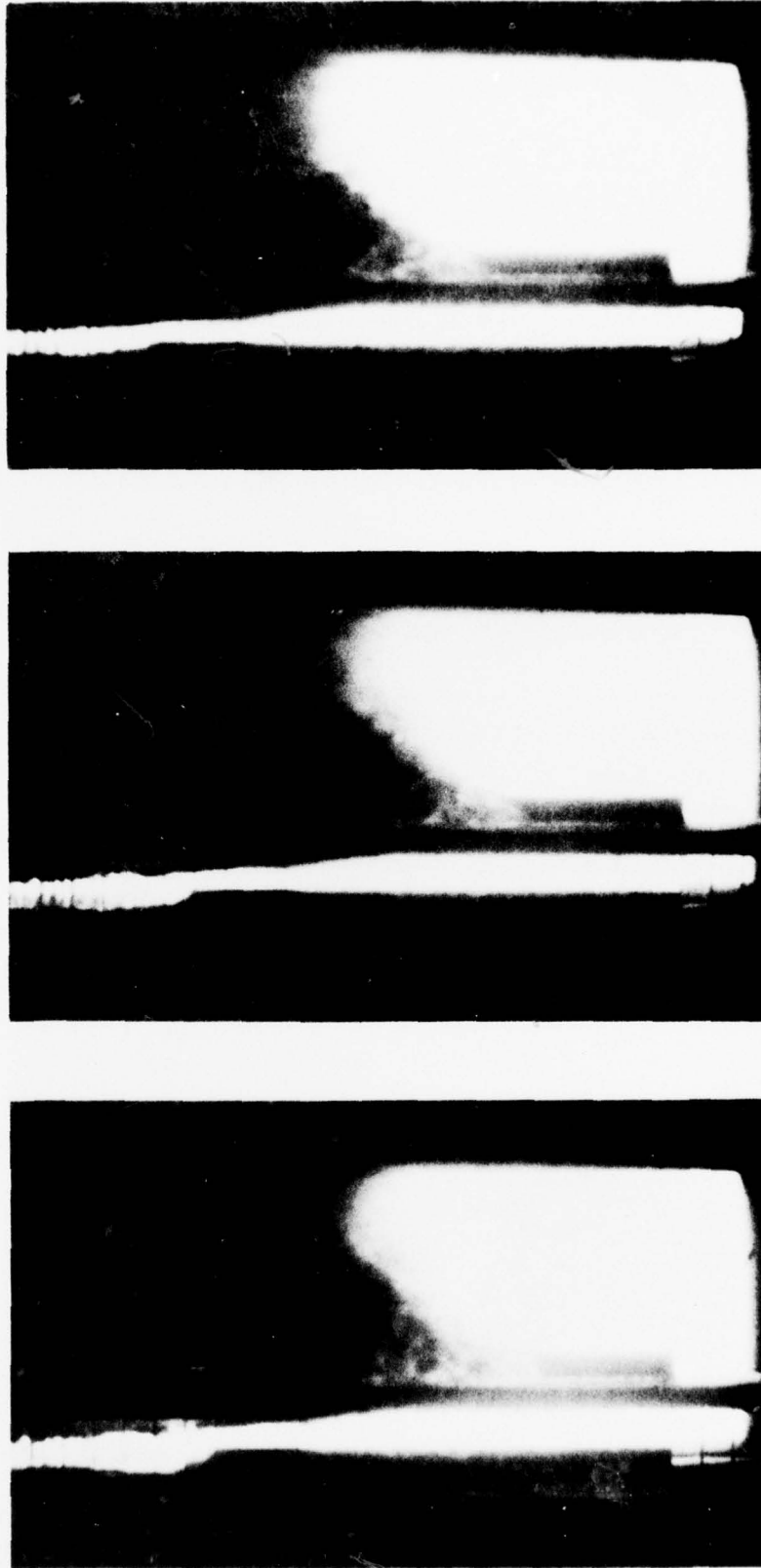


Figure 15. (Cont'd) Typical Framing Camera Record: Atmospheric Conditions

the boundary region not being as confined as that in the inner areas. The curvature indicates that the impairment is greatest at the explosive's edge and progressively decreases to zero over the first two inches of plate length. Consequently, bonding results in this early region are inconsistent with those obtained further along the plate. Due to such boundary effects, the plate material along the longitudinal edges also accelerates at a lower rate than does the center region material. As a result some of the luminous formation advances in a direction inclined toward the camera. Specific data reduction for the shots used in establishing an experimental technique is included in Table 9.

## 2. Helium Tests

In an attempt to reduce the extent of obstruction caused by the luminosity, an experiment was conducted using an inert gas flooding of the interface region. Designated as LASL 1271, the experimental configuration is shown in Figure 16. A plexiglass gas shield served as the top of a gas containment box constructed of the same material. The base plate was situated on a thick steel anvil plate to reduce damage to the firing table. A steady supply of helium gas was maintained until after the event. Helium was chosen because it does not ionize unless extremely high temperatures are realized.

Despite this provision, the obstruction was not eliminated. In fact, the area of ionization within the interface increased. This was due apparently to the less dense helium offering less obstruction to particle passage. In this case, the ionized

TABLE 9  
LASL EXPERIMENTAL TECHNIQUE EVALUATION

Experiment Identification	Specimen Description	Measured Collision Velocity	Bond Tensile Strength	Remarks
LASL 1268	10D-1/2T-1/2S	UNK	3.0* / 0 9.0 / 40,540 psi	Shocked Calibration Grid Strip
LASL 1269	10D-1/2T-1/2S		3.0 / 0 9.0 / 31,216 psi	Developed Luminous Obstruction
LASL 1270	10D-1/2T-1/2S	2.0* / .010 7.0 / 9.0 / .0145	3.0 / 19,256 9.0 / 59,187	Developed Luminous Obstruction
LASL 1271	10D-1/2T-1/2S	-	-	Helium in interface region. Conducted to determine influence of helium.

\* Distance along weld interface from initiation end in inches.



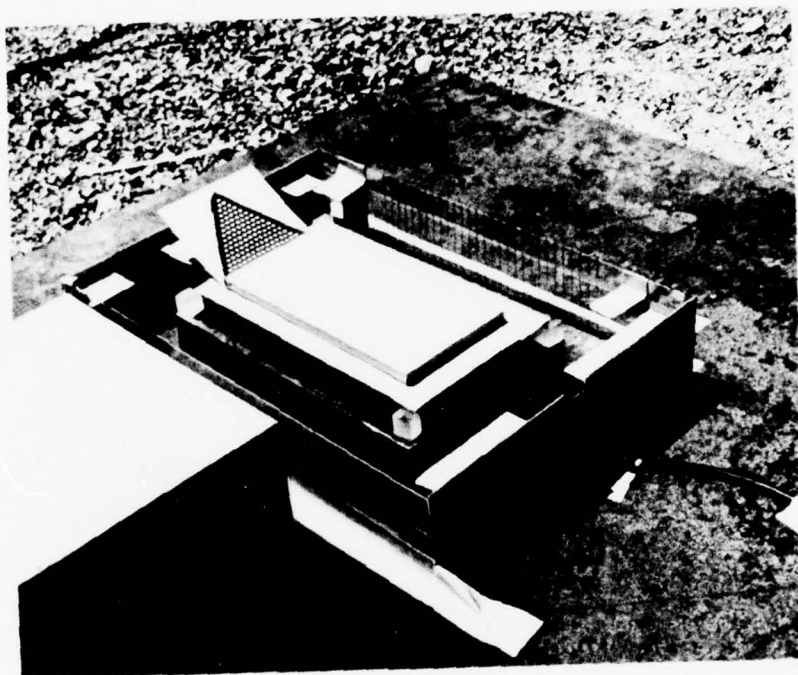


Figure 16. Experimental Arrangement Using Helium

region exhibited a bluish color.

The only apparent possibility left for improvement was to exclude all air from the interface region during the welding.

### 3. Vacuum Tests

In order to accommodate vacuum welding experiments, an expendable plexiglass vacuum chamber was developed. Due to the indefinite nature of the vacuum series, the fabrication of a more permanent steel or concrete vacuum chamber could not be justified. Several designs were tested in welding events LASL 1273 through LASL 1279 until the final vacuum welding configuration was resolved.

The resolved vacuum chamber design and the integration of the total specimen/chamber system are shown in Figures 17 and 18. Figure 18 identifies each component and illustrates its use. Three of these components require special comment: the gas shield, the detonation gas deflector and the explosive environmental bag. The detonation gas shield was of plexiglass to avoid the potential outgassing problem associated with plywood in a vacuum. Second, the explosive environment bag was used to prevent a similar situation from occurring with the dynamite. The high nitroglycerine content of this explosive demanded special precautions be taken to preclude its outgassing. The adopted solution involved the plastic environment bag to preserve the atmospheric surroundings of the explosive. The detonation gas deflector was necessary to prevent the bag from assuming a high degree of curvature as the

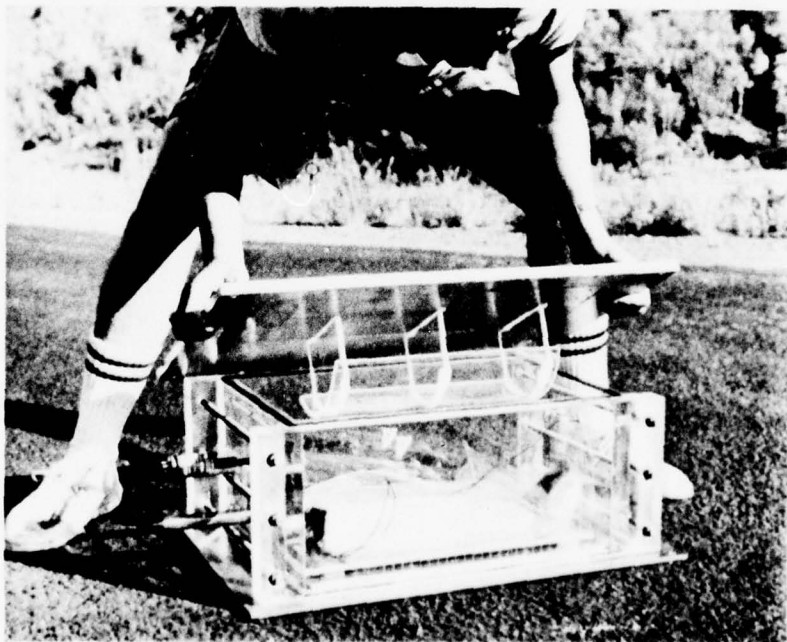
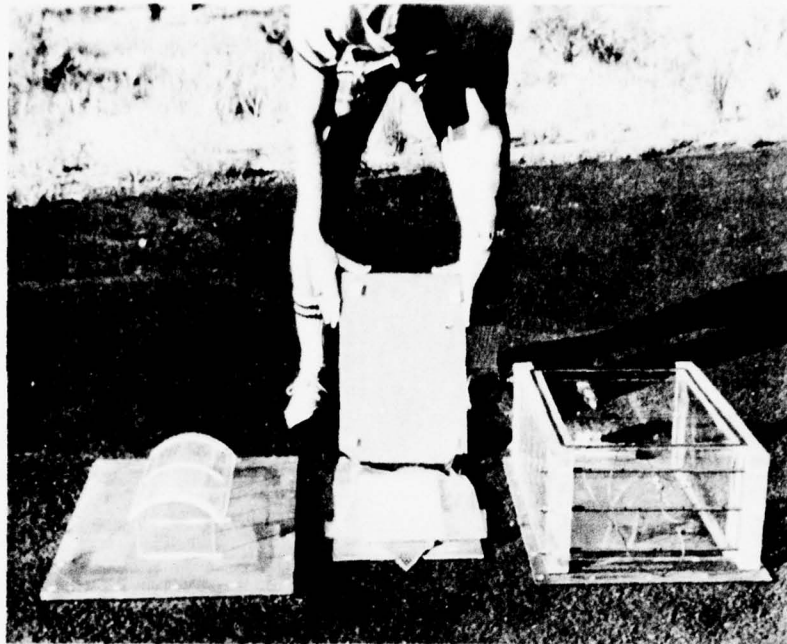


Figure 17. Vacuum Welding Apparatus

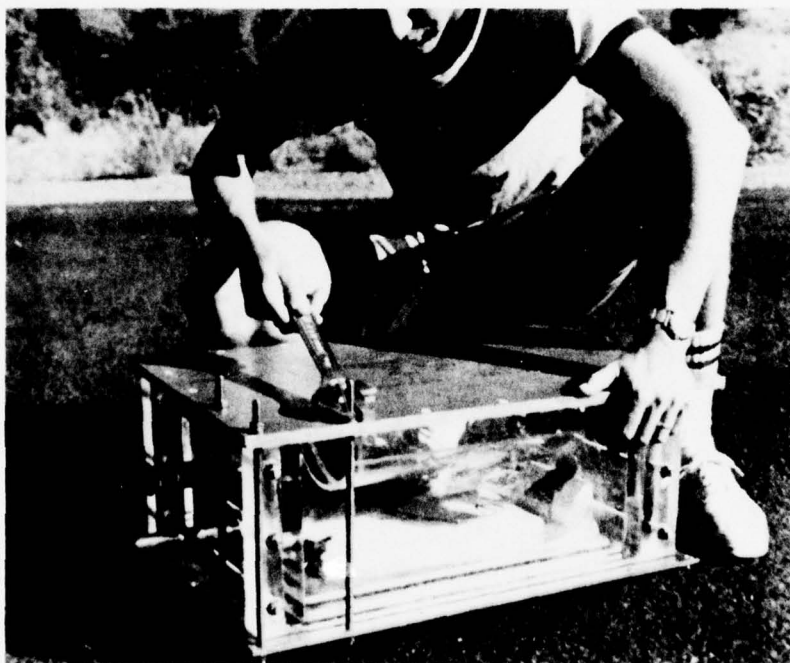
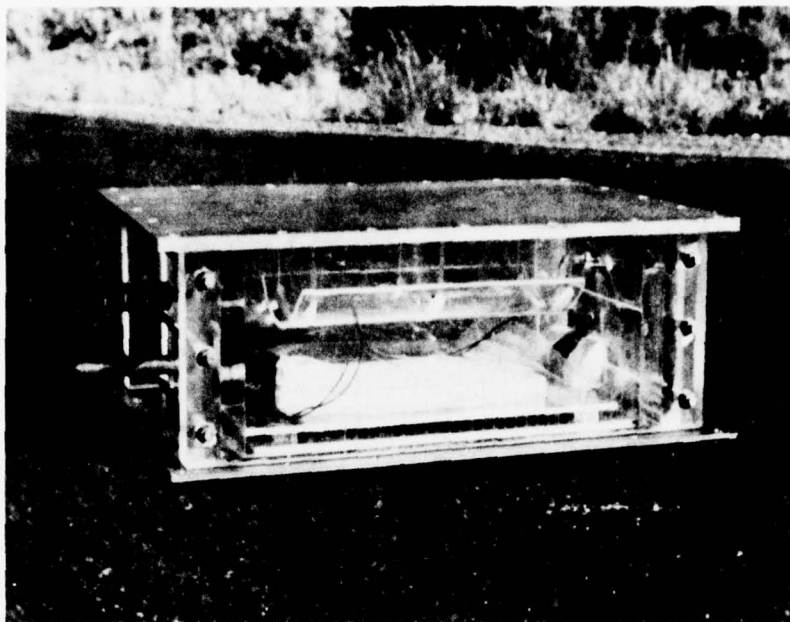
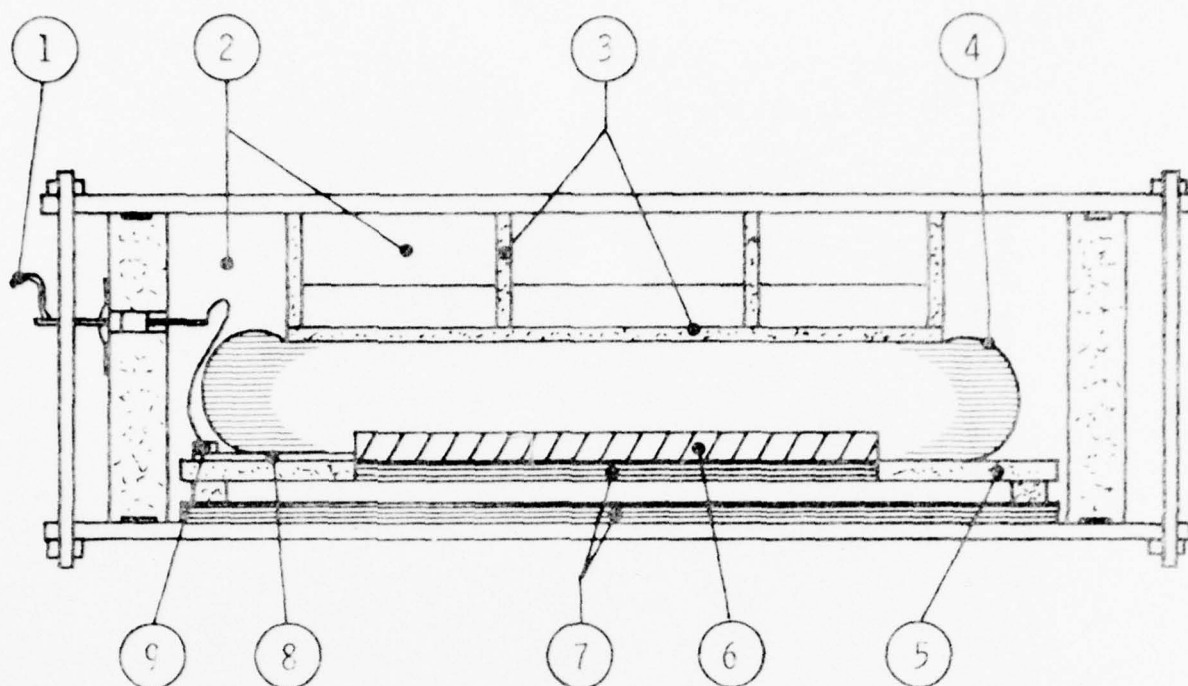


Figure 17 (cont). Arrangement for Vacuum Welding Experiments



- ① DETONATOR LEAD-IN WIRES
- ② VACUUM
- ③ PLEXIGLASS GAS DEFLECTOR AND EXPLOSIVE SYSTEM ENVIRONMENT BAG CONSTRAINT. PRECLUDES BAG FROM CONFORMING TO SPHERICAL CONFIGURATION IN VACUUM AND CONSEQUENTLY LIFTING EXPLOSIVE LOAD OFF OF FLYER PLATE.
- ④ EXPLOSIVE ENVIRONMENT BAG TO PRECLUDE OUTGASSING OF DYNAMITE DUE TO VACUUM STATE.
- ⑤ PLEXIGLASS DETONATION GAS SHIELD, PREVENTS INTERFACE CONTAMINATION.
- ⑥ CARDBOARD BOX LOADED WITH DYNAMITE.
- ⑦ FLYER AND BASE PLATES.
- ⑧ LINE WAVE GENERATOR
- ⑨ DETONATOR

Figure 18. Components of Vacuum Welding Apparatus



TABLE 10  
LASL ATMOSPHERIC WELDING SERIES

Experiment Identification	Specimen Configuration	Local Detonation Velocity*	Collision Angle	Plate Calculated	Flyer Velocity** Measured	Bond Tensile Strength***
LASL 1311	8D-1/4T-1/4S		9°			
LASL 1312	10D-1/2T-1/2S		6°30'		7.5/.016 8.0/.0165 9.0/.0147	
LASL 1317	10D-1/4T-1/2S	.115	9°45'	.019		6.0/27,900 9.0
LASL 1318	10D-1/4T-1/8S	.130				6.0/40,000 9.0
LASL 1319	12D-1/4T-1/8S	.120	7°	.0146		3.0/56,247 6.0/34,000 9.0/56,198
LASL 1320	12D-1/4T-1/4S	.115	9°	.0180		3.0/21,074 6.0/23,200 9.0/28,099
LASL 1321	14D-1/2T-1/2S	.125	8°45'	.0178	.017	3.0/0 6.0/17,100 9.0/58,539
LASL 1322	10D-1/2T-1/4S	.145	6°15'	.0158		6.0/0 9.0/

Table 10 (cont)

Experiment Identification	Specimen Configuration	Local Detonation Velocity*	Collision Angle	Plate Velocity** Calculated	Flyer Velocity** Measured	Bond Tensile Strength***
LASL 1323	14D-1/2T-1/4S	.125	7°30'	.016	/.022	6.0/0 9.0/
LASL 1324	10D-1/2T-1S	.105	8°	.0146	/.013	6.0/0 9.0/
LASL 1325	14D-1/2T-1S	.125	9°	.020	/.021	3.0/0 6.0/1,100 9.0/12,058
LASL 1326	8D-1/4T-1/8S	.1075- .0325X	10°	.0165		3.0/36,880 6.0/21,100 9.0/59,125
LASL 1327	8D-1/4T-1/8S	.115	9°	.018	/.0165	6.0/39,400 9.0/
LASL 1328	12D-1/4T-1/4S	.150	10°	.0265		3.0/8,196 6.0/32,800 9.0/35,124
LASL 1362	12D-1/4T-1/2S	.110	12°30'	.024		4.0/14,270 8.0/28,538
LASL 1363	8D-1/4T-1/8S	-	6°45'			4.0/40,926 8.0/35,271
LASL 1364	12D-1/4T-1/2S	.125	8°30'	.018		8.0/44,645

\*Velocity (inch/microsecond)

\*\*Position of measurement (inches from initiation end) and velocity (inch/micro/sec.)

\*\*\*Position of measurement (inches from initiation end) and measured tensile strength (lbs/sq inch)

vacuum was applied and, consequently, lifting the explosive loading off the flyer plate. By being curved in one direction, the deflector prevented significant shock pressures from being reflected back onto the flyer plate. Using this system design, vacuum states of less than 50 microns were achieved.

One interesting problem was encountered during the early experiments conducted with this system. Specifically, the linewave generator had been included within the environment bag in such a position that energy generated by the detonating detasheet was reflected from the inner surface of the bag. In reflecting, the energy caused a secondary dynamite initiation about 2 inches ahead of the normal detonation front. This condition was corrected by moving the detasheet outside the environment bag as shown in the figures.

Nine experiments were conducted using the developed vacuum welding configuration. These are summarized in Table 10. Figure 19 contains a sequence of frames taken from LASL 1281. The luminosity had been replaced by a formation of plasma. Since the vacuum offers essentially no resistance, the plasma formation more quickly flooded the interface region than did the luminosity. The plasma formation was opaque though not of a high density. Consequently, the vacuum condition resulted in a higher percentage of the flyer plate profile being obscured.

As the photograph sequence also illustrates, a continuous record of detonation velocity is not always possible. The detonation products travel faster in the vacuum environment than within the

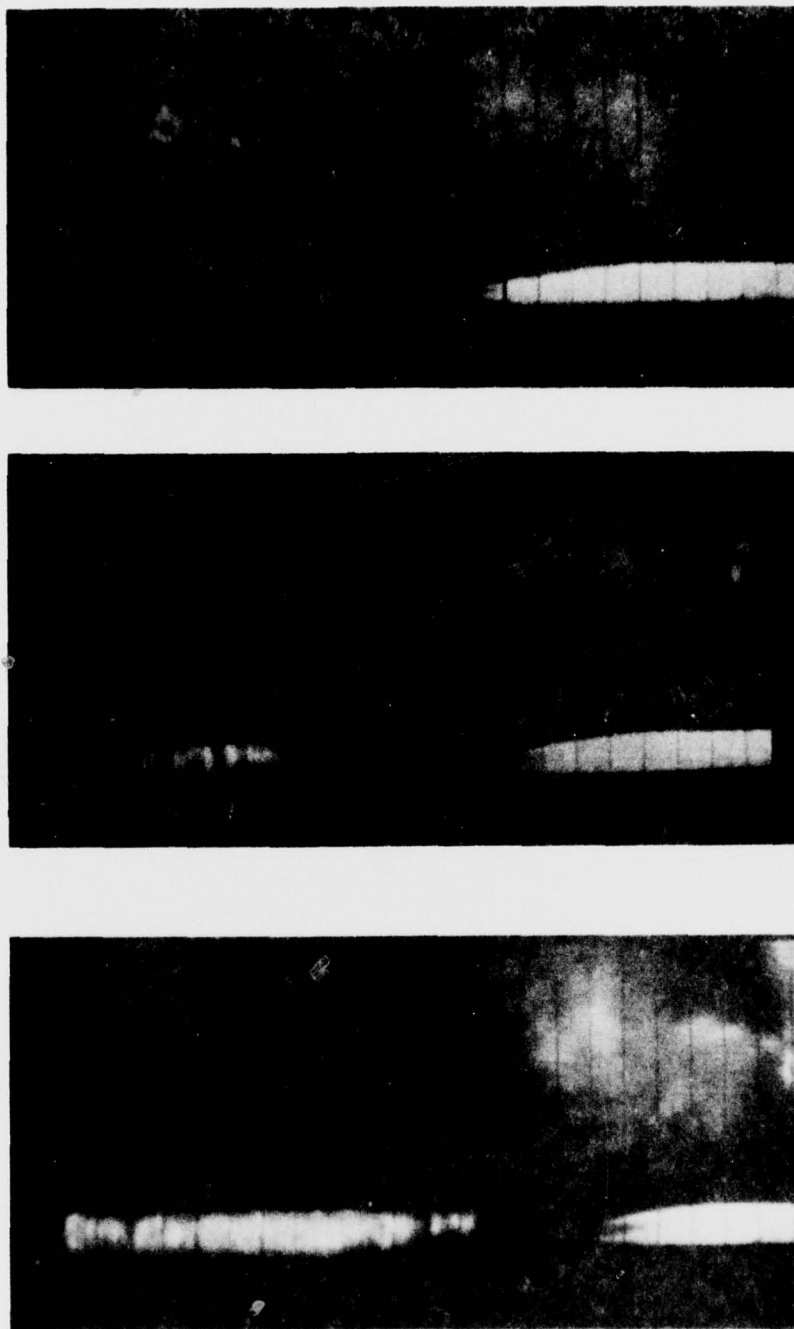


Figure 19. Typical Framing Camera Record:  
Vacuum Conditions

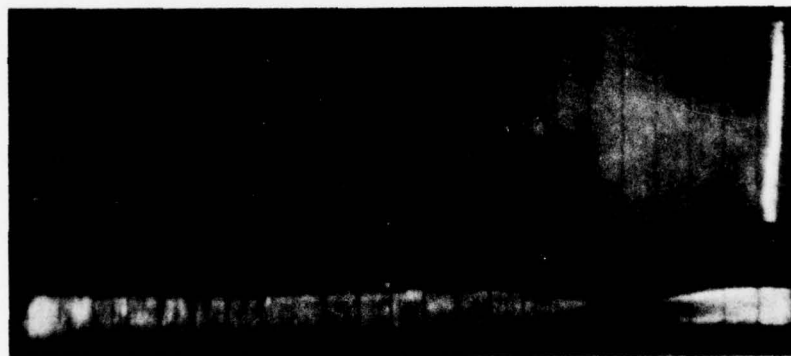
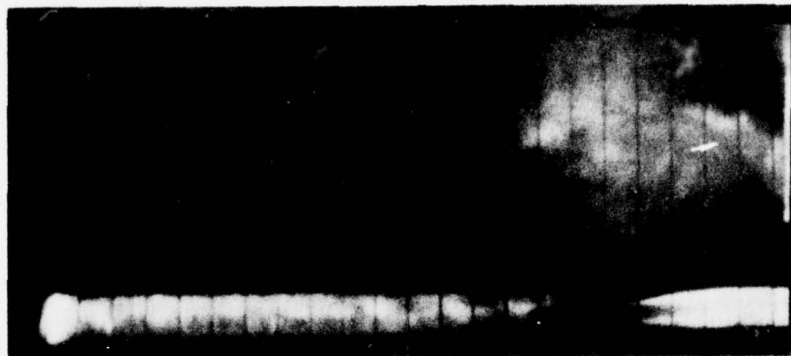


Figure 19. (Cont'd) Typical Framing  
Camera Record: Vacuum  
Conditions



air-filled environment bag. Consequently, the detonation front position becomes obscured as it advances.

This experimental technique was most constructive, although not suited for the general flyer plate experiments. The framing camera photos provided a unique record of the jetting phenomenon.

#### 4. Resolved Technique

As previously stated, the resolved experimental technique consisted of the atmospheric welding technique complemented by radiography. Despite luminosity, which hampered framing camera photos, a sequenced flash X-Ray would provide a complete flyer plate profile at a predetermined time. Using this record, the associated framing camera representation could be extended beyond the time when luminosity obscured camera records as shown in Figure 20. Figure 21 shows a typical radiograph.

The experimental arrangement is shown in Figure 22. The addition of the flash X-Ray film cassette approximately 12 inches behind the specimen required a new position for the flash box. The mirror placed between the film cassette and the specimen assembly proved quite adequate in establishing the required interface illumination.

The experimental procedure varied little from that used in the atmospheric welding experiments previously discussed. The firing sequence was modified to include the operation of the flash X-Ray unit. The time delay generator was used to sequentially open the framing camera shutters, fire the flash X-Ray unit and, finally, destroy the tilt mirror. The delay

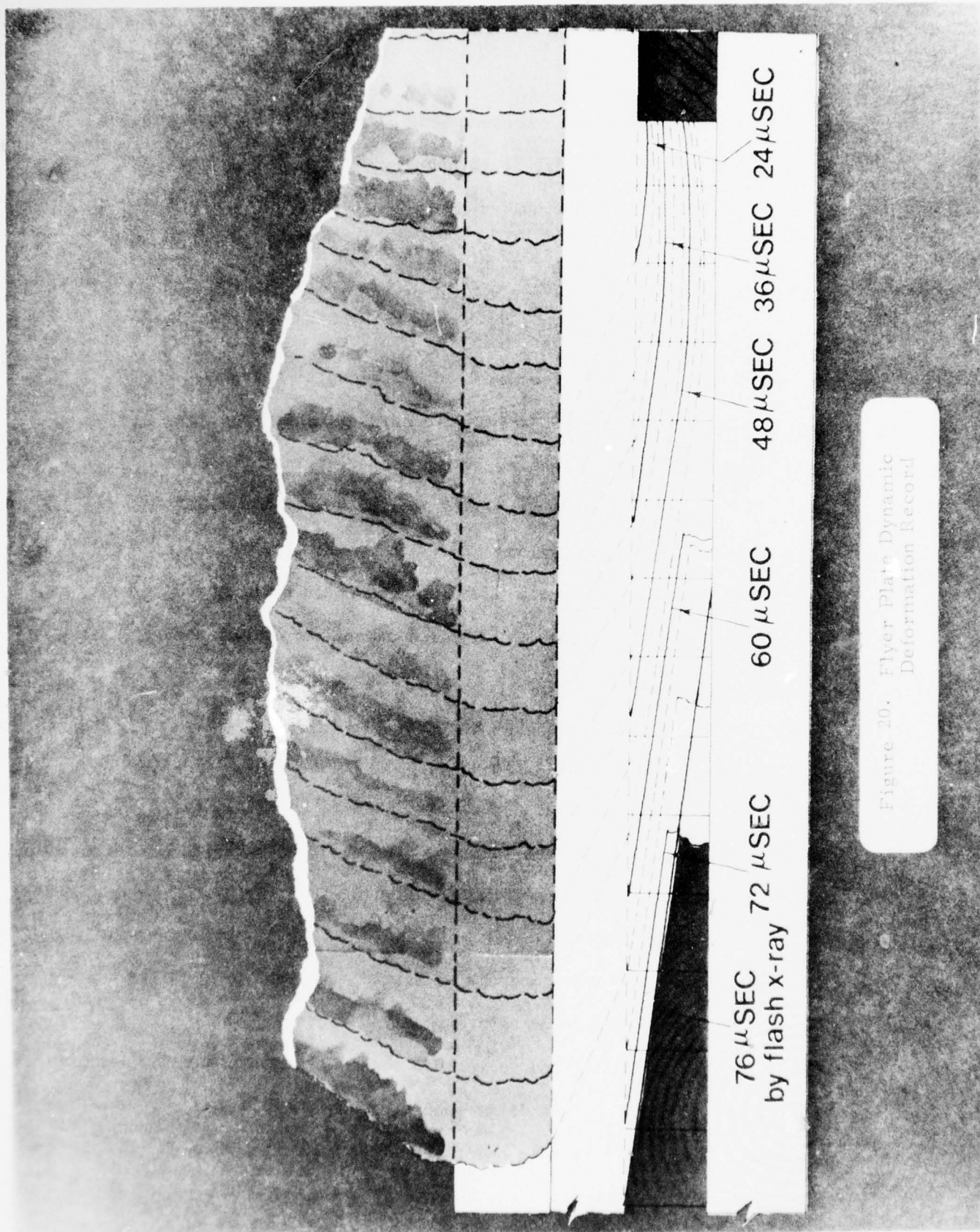


Figure 20. Flyer Plate Dynamic  
Deformation Record



Figure 21. Typical Radiograph

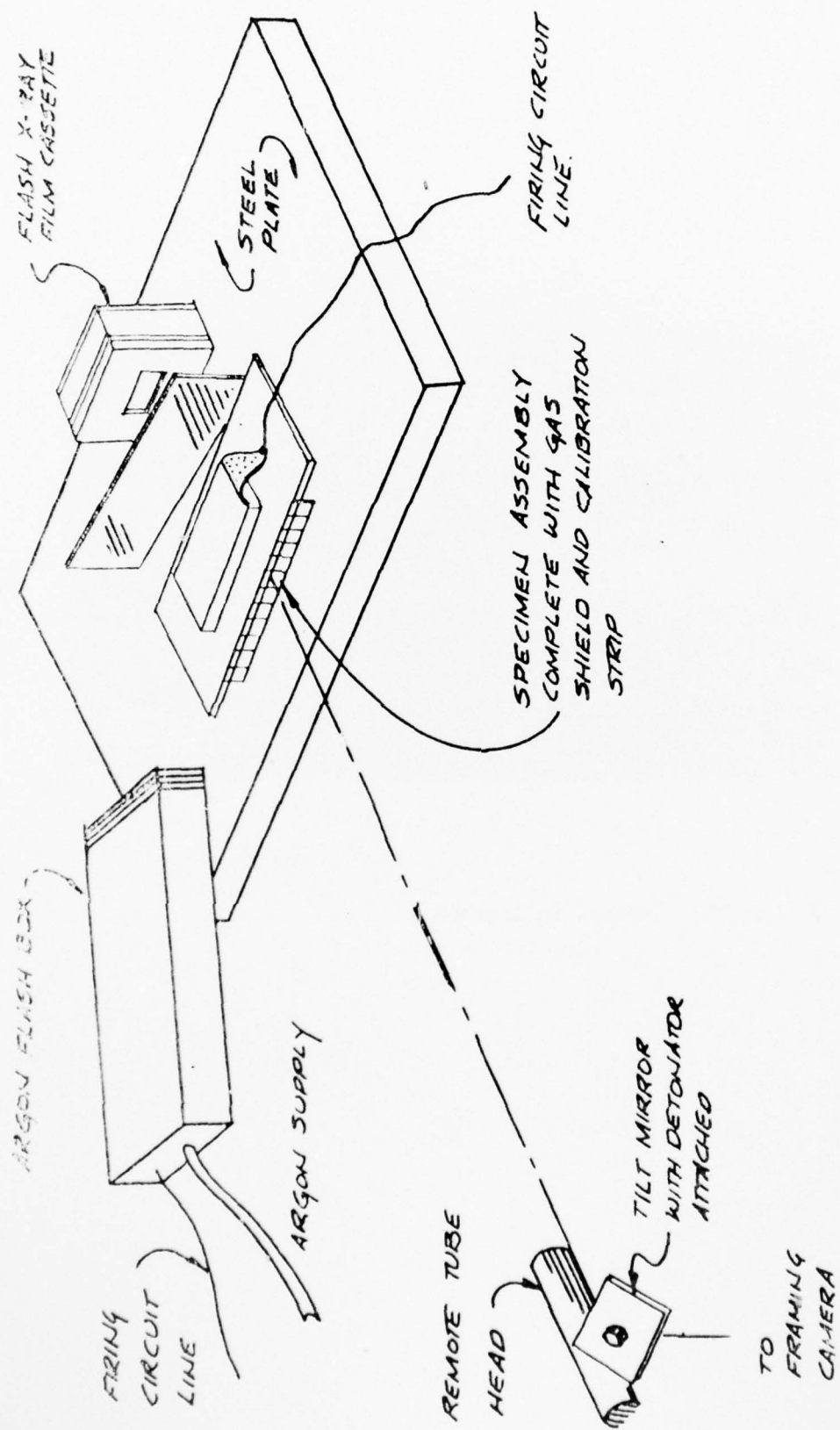


Figure 22. Component Arrangement of Resolved Technique

times were 40, 102, and 140 microseconds respectively. The pulsing of the flash X-ray unit also detonated an indicial cap located on the front side of the plate assembly. This served to mark the particular framing camera frame common to the radiograph record.

The results of the tests run using the resolved technique are summarized in Table 11.

#### C. Tests Conducted at United States Air Force Academy (USAFA)

##### 1. Plate Welds

The plate welding techniques utilized for tests conducted at USAFA were very similar to those described in the previous section on LASL tests. The specific details of the test configurations and instrumentation arrangements are given in Appendix C.

A total of 127 plate tests were made at the USAFA test site during the period covered by this report. These tests are summarized in Table 12. The data, consisting of flash X-rays and oscilloscope photographs, are on file in the Department of Civil Engineering, Engineering Mechanics, and Materials at the USAF Academy. The digitized data from many of these tests are included in the analyses in the following chapter.

#### D. Spot Welding Tests

Using specimens provided by the USAF Academy, spot welding was attempted at the Forth Worth Division of General Dynamics, using various kinds and amounts of explosives, and weld set-up conditions such as explosive placement and detonation described below.

##### a. Spot Welding Investigation



TABLE 11  
LASL VACUUM WELDING SERIES

Experiment Identification	Specimen Description	Measured Collision Velocity*	Bond Tensile Strength**	Remarks
LASL 1280	10D-1/2T-1/4S	2.0/.0136 3.5/.0136	6.0/0 9.0/	
LASL 1281	10D-1/2T-1/2S	3.5/.015 5.5/.0133 8.5/.0136	6.0/0 9.0/	
LASL 1282	10D-1/2T-1S	4.0/.0144 6.0/.0136	6.0/42,400 9.0/	
LASL 1283	14D-1/2T-1S	2.0/.018 3.0/.017 5.0/.017 8.0/.017	6.0/13,450 9.0/	
LASL 1284	8D-1/4T-1/4S	2.0/.016	2.0/61,081 6.0/48,000 9.8/67,635	
LASL 1285	14D-1/2T-1/2S	2.5/.019 3.5/.018 4.0/.017	3.0/3,716 6.0/25,800 9.7/37,837	
LASL 1286	14D-1/2T-1/4S	/ .018	2.9/6,351 6.0/16,300 9.7/31,081	Framing camera record blurred.

Table 11 (cont)

Experiment Identification	Specimen Description	Measured Collision Velocity*	Bond Tensile Strength**	Remarks
LASL 1287	14D-1/4T-1/4S	UNK	6.0/31,600	Total obstruction of interface region.
LASL 1298	10D-1/4T-1/2S			

\* Data entered as position of measurement (inches from initiation end) and measured velocity (inch/microsecond).

\*\* Data entered as position of measurement (inches from initiation end) and measured tensile strength (lbs/square inch).

Table 12. USAFA Plate Welding Series

<u>Experiment #</u>	<u>Date</u>	<u>Research Task Plan and/or Objective</u>	<u>Explosive Loading</u>	<u>Metal Configuration</u>	<u>Instrumentation</u>
USAFA 1	3/17/72	RTP 1072 Test Mang. Gage Det. Press. Recording. Computer Corr.	14 G DY 40%	1/2" 6061-T6 AL (Single)	Det. Pressure
USAFA 2	3/21/72	RTP1-72 Proof Det. Pressure Test Mang. Gage. Computer Corr.	10 G DY 40%	1/2" 6061-T6 AL (Single)	Det. Pressure
USAFA 3	3/22/72	RTP 1-72 Proof Det. Press. Test. Weld 2 Code Corr.	10 G DY 40%	1/2" 6061-T6 AL (Single)	Det. Pressure
USAFA 4	3/22/72	RTP 1-72 Proof Det Press. Test. Weld 2 Code Corr.	10 G DY 40%	1/2" 6061-T6 AL (Single)	Det. Pressure
USAFA 5		No Record			
USAFA 6	4/3/72	AL to Steel Series	.6"x6"x12" IRECO	3/8 6061-T6 ALTO 3/8 Steel T/2 Standoff	None
USAFA 7	4/3/72	AL to Steel Series	.6"x6"x12" IRECO	3/8 6061-T6 AL to 3/8 Steel w/.015" Steel Shim 1/8" & 1/16" Standoff	None
USAFA 8	4/3/72	AL to Steel Series	.7 IRECO	Same as USAFA #7	None
USAFA 9	4/4/72	AL to Steel Series	.7 IRECO	3/8" 6061-T6 AL to 3/8 steel T/2 Standoff	None

Table 12 (cont)

Experiment #	Date	Research Task Plan and/or Objective	Explosive Loading	Metal Configuration	Instrumentation
USAFA 10	4/5/72	REP 1-72 Proof Test Mang. Gage Interface Press. Measurement-Code Corr.	10 G DY 40%	1/2" AL to 1/2" AL. Both 6061-T6 AL, w/inter-face Press. Gage & T Standoff	Interface
USAFA 11	4/5/72	RTP 1-72-Confirmation of Interface Press. Scheme. Weld 2 Code Corr.	10 G DY 40%	Same as USAFA 10	Interface Press.
USAFA 13	4/7/72	AL to Steel Series	.7" IRECO	3/8" 6061-T6 AL to 3/8" Steel 2/.001" steel shim 1/8" & 1/16" Standoffs, Resp.	None
USAFA 14		No Record			
USAFA 15	4/10/72	AL to Steel Series	.7" IRECO	3/8" 6061-T6AL to 3/8" steel w/.008" steel Shim 1/8" & 1/16" Standoffs, Resp.	None
USAFA 16	4/10/72	AL to Steel Series	.7" IRECO	3/8" 6061-T6 AL to 3/8", Steel 2/.006 steel Shim 1/8" & 1/16" Standoffs, Resp.	None



Table 12 (cont)

<u>Experiment #</u>	<u>Date</u>	<u>Research Task Plan and/or Objective</u>	<u>Explosive Loading</u>	<u>Metal Configuration</u>	<u>Instrumentation</u>
USAF 17	4/11/72	AL to Steel Series	.7" IRECO	3/8" 6061-T6 AL to 3/8" steel w/.003" steel Shim, 1/8" & 1/16" Standoffs, Resp.	None
USAF 18	4/11/72	AL to Steel Series	.7" IRECO	3/8" 6061-T6 AL to 3/8" steel w/.002" steel Shim, 1/8" & 1/16" Standoffs Resp.	
USAF 19	4/13/72	Vacuum Effects (Cadet Vinal)	2 layers 1/4" orn. Thiokol	(2) 1/4" 6061-T6 AL Plates T/2 Standoff (Atmosphere)	Det. Vel. + Flash X-Ray
USAF 20	4/13/72	Vacuum Effects (Cadet Vinal)	2 layers 1/4" orn. Thiokol	(2) 1/4" 6061-T6 AL Plates T/2 Standoff (100 ucrons VAC.)	Det. Vel. + Flash X-Ray
USAF 21	4/14/72	AL-to-Steel Series	.5" IRECO	1/4" steel to 1/4" AL w/ T/2 S.O.	None
USAF 22	4/14/72	AL to Steel Series	.6" IRECO	1/4" steel to 1/4" AL w/T/2 S.O. & .001" Steel Shim on AL.	None



Table 12 (cont)

<u>Experiment #</u>	<u>Date</u>	<u>Research Task Plan and/or Objective</u>	<u>Explosive Loading</u>	<u>Metal Configuration</u>	<u>Instrumentation</u>
USAF 23	4/14/72	AL to Steel Series	.6" IRECO (03)	3/8" AL to 1/2" Maraging Steel w/.006 Steel Shim & 1/8" & 1/16" Standoffs, Resp.	None
USAF 24	4/14/72	AL to Steel Series	.6" IRECO (04)	3/8" AL to 3/8" Steel w/.006" Steel Shim, & 1/8" & 1/16" S.O., Resp.	None
USAF 25	4/17/72	AL to Steel Series	DY 40%	3/8" AL to 3/8" steel w/ steel shim & 1/8" & 1/16" Standoffs, Resp.	None
USAF 26	4/17/72	AL to Steel Series	DY 40%	3/8" AL to 3/8" steel w/ steel Shim & S.O. Resp.	None
USAF 27	4/18/72	Weld 2 Code Corr. Confirmation of Complete Meas. System	10 G DY 40%	(2) 1/4" 6061-T6 AL w/T/2 Standoff	Det. Vel. + Det. Press. + Interface Press. + Flash X-Ray
USAF 28	4/18/72	Weld 2 Code Corr. Confirmation of Complete Meas. System	10 G DY 40%	Same as for USAFA 27	Same as for USAFA 27
USAF 29	4/19/72	Weld 2 Code Corr. Confirmation of Complete Meas. System	DY 40%	Same as for USAFA 27	Det. Vel. + Det. Press. + Interface Press. + X-Ray

Table 12 (cont)

<u>Experiment #</u>	<u>Date</u>	<u>Research Task Plan and/or Objective</u>	<u>Explosive Loading</u>	<u>Metal Configuration</u>	<u>Instrumentation</u>
USAFA 30	4/19/72	X-Ray System Test	None	3/8" AL Flyer-- 3/8" Steel Base	X-Ray Only
USAFA 31		No Record			
USAFA 32		No Record			
USAFA 33		No Record			
USAFA 34		No Record			
USAFA 35	4/21/72	Fracture Toughness Series	.6" DY 40%	(2) 1/4" T1 64 Plates w/ Standoff	None
USAFA 36	4/21/72	Fracture Toughness Series	.7" DY 40%	Same as for USAFA 35	None
USAFA 37	4/21/72	Vacuum Effects	1 Sht Orn Thiokol (232 G)	(2) 1/4" AL Plates T/2 Standoff (Atmosphere)	Det. Vel. + Flash X-Ray
USAFA 38	4/21/72	Vacuum Effects	1 Sht Orn Thiokol (232 G)	(37 + 38 Both 6061- T6 AL)	
USAFA 39	4/21/72	Vacuum Effects	1 Sht Orn Thiokol (238 G)	(2) 1/4" 6061-T6AL Plates w/T/2 S.O. (Atmosphere)	Det. Vel. + Flash X-Ray
USAFA 40	4/25/72	Weld 2 Code Correlation	576 G 40% DY (.4"x6" x12")	2 1/4" AL Plates w/T/2 Standoff	Det. Vel. + Det. Press. + Interface Press. + X-Ray

Table 12 (cont)

<u>Experiment #</u>	<u>Date</u>	<u>Research Task Plan and/or Objective</u>	<u>Explosive Loading</u>	<u>Metal Configuration</u>	<u>Instrumentation</u>
USAF 41	4/27/72	Aluminum-to-Steel Series	864G 40% DY (.6" x 6" x 12") (12 G/in <sup>2</sup> )	3/8" AL Flyer to 3/8" St Base .007" steel Shim 1/8" Flyer to Shim 1/16" Shim to Base	None
USAF 42	4/27/72	Aluminum-to-Steel Series	864G 40% DY (.6" x 6" x 12") (12 G/in <sup>2</sup> )	Same as USAF 41 except 1/16" rubber between explosive & flyer	None
USAF 43	4/28/72	Weld 2 Code Correlation System Test	N A (DY)	N A	Full Inst. (Test Only for System Check)
USAF 44	4/28/72	Weld 2 Code Correlation System Test	40% DY	N A	Det. Vel. Only
USAF 45	5/1/72	Vacuum Effects	230G Orn. Thiokol	(2) 1/4" AL Plates w/2T Standoff (Atmosphere)	Det. Vel. & Flash X-Ray
USAF 46	5/1/72	Vacuum Effects	230G Orn. Thiokol	(2) 1/4" AL Plates w/2T Standoff (Vacuum=150 ucrs)	Det. Vel. & Flash X-Ray
USAF 47	5/2/72	Vacuum Effects	225G Orn Thiokol	(2) 1/4" AL Plates w/T Standoff (Vacuum=150 ucrs)	Det. Vel. & Flash X-Ray
USAF 48	5/2/72	Vacuum Effects	230G Orn Thiokol (pieced together)	(2) 1/4" AL Plates w/T Standoff. Atmosphere	Det. Vel. & Flash X-Ray

Table 12 (cont)

<u>Experiment #</u>	<u>Date</u>	<u>Research Task Plan and/or Objective</u>	<u>Explosive Loading</u>	<u>Metal Configuration</u>	<u>Instrumentation</u>
USAFA 49	5/3/72	Instrumentation System Test	Orn. Thiokol (1/4"x1"x11")	N A	Full; for System Test Only
USAFA 50	5/3/72	Instrumentation System Test	Orn. Thiokol (1/4"x1"x11")	N A	Full; for System Test Only
USAFA 51	5/4/72	Weld 2 Code Correlation	40% DY 576 G	(2) 1/4" AL Plates w/T/2 S.O.	Det. Vel. + Det. Press. + Interf Press. + X-Ray
USAFA 52	5/4/72	Weld 2 Code Correlation			
USAFA 53	5/5/72	Aluminum-to-Steel Series			
USAFA 54	5/8/72	Vacuum Effects	460 G Orn Thiokol	(2) 1/4" AL Plates, w/T/2 S.O. Atmosphere	Det. Vel. + Flash X-Ray
USAFA 55	5/8/72	Vacuum Effects	460G Orn Thiokol	(2) 1/4" AL Plates, w/T/2 S.O. Vacuum (100 ucrons)	Det. Vel. + Flash X-Ray
USAFA 56	5/9/72	Vacuum Effects	460G Orn Thiokol	(2) 1/4" AL Plates w/T S.O. Atmosphere	Det. Vel. + Flash X-Ray
USAFA 57	5/10/72	Vacuum Effects	460G Orn Thiokol	(2) 1/4" AL Plates w/T S.O. Atmosphere	Det. Vel. + Flash X-Ray
USAFA 58	5/11/72	Armor Plate Series			
USAFA 59	5/16/72	Vacuum Effects	560G Orn Thiokol	(2) 1/4" Plates w/2 T S.O. Vacuum= 100 ucrons	Det. Vel. + Flash X-Ray



Table 12 (cont)

Experiment #	Date	Research Task Plan and/or Objective	Explosive Loading	Metal Configuration	Instrumentation
USAFA 60	5/16/72	Vacuum Effects	460G Orn Thiokol	(2) 1/4" Plates w/2T S.O. Atmosphere	Det. Vel. + Flash X-Ray
USAFA 61	5/18/72	Armor Plate Series	Orn Thiokol (1/4"x6"x12")	1/8" Flyer to 1/2" None Base w/.04 wire mesh + .06 Balsa Wood S.O. All 6061-T6 AL	
USAFA 62	5/19/72	Weld 2 Code Correlation	40% DY 864G	(2) 1/4" AL Plates w/T2 S.O.	Det. Vel. + Det. Press + Interf Press + X-Ray
USAFA 62A	5/22/72	Weld 2 Code Correlation	40% DY 720G	(2) 1/2" AL Plates w/T/2 Standoff	
USAFA 63	5/24/72	Aluminum-to-Steel Series	40% DY 1008G	1/2" AL Flyer to None 3/8" Steel base w/ Spall rails by Steel & 3/16" S.O.	
USAFA 64	5/29/72	Aluminum-to-Steel Series	40% DY 1008G	1/2" AL Flyer to None 3/8" steel base w/ .006 annealed steel shim, (S.O.) 1/16" AL to Shim-1/8" Shim to Steel	
USAFA 65	5/30/72	Aluminum-to-Steel Series	40% DY 1008G	Same as USAFA 64 but with 2 circular areas in shim w/holes drilled close together.	



AD-A047 955

FRANK J SEILER RESEARCH LAB UNITED STATES AIR FORCE --ETC F/6 13/8  
EXPLOSIVE IMPULSE WELDING. VOLUME I.(U)  
JUL 77 D H MERKLE, G E CANNON

UNCLASSIFIED

FJSRL-TR-77-0012-VOL-1

NL

2 OF 5

AD  
A047955

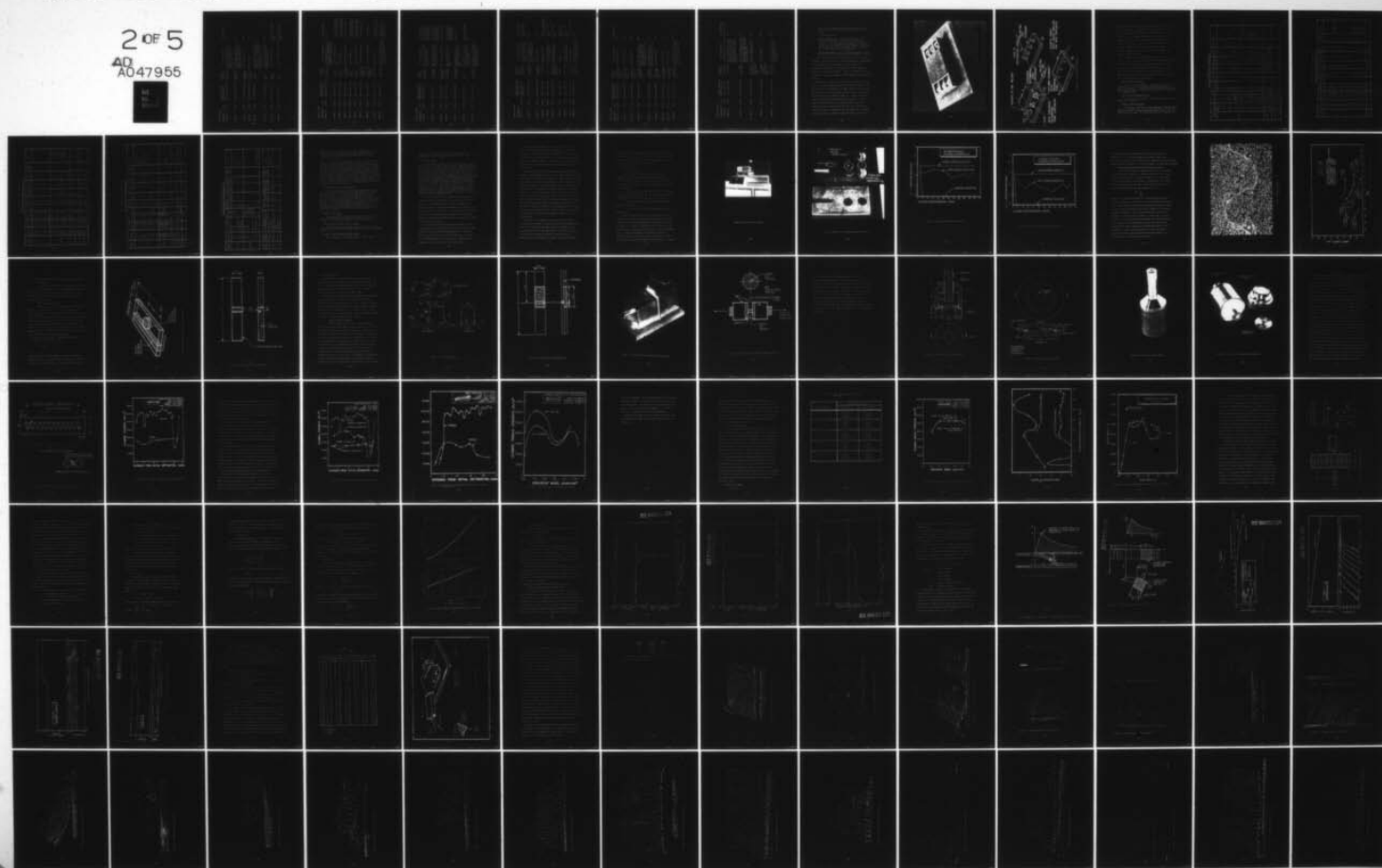


Table 12 (cont)

<u>Experiment #</u>	<u>Date</u>	<u>Research Task Plan and/or Objective</u>	<u>Explosive Loading</u>	<u>Metal Configuration</u>	<u>Instrumentation</u>
USAFA 66	6/2/72	Artillery Shell Series	Blk Thiokol 4G/in <sup>2</sup>	1/4" Gilding Metal to 3/8" Maraging steel base w/5° angle, & 1/4" Rubber buffer between flyer & exp.	None
USAFA 67	6/2/72	Artillery Shell Series	Blk Thiokol 8 G/in <sup>2</sup>	1/4" Gilding Metal Flyer to 3/8" Maraging Steel Base w/5° Angle, & 1/4" rubber buffer between flyer and exp.	None
USAFA 68	6/2/72	Artillery Shell Series	6 shts C-1 Detasheet	Same as USAFA 67	None
USAFA 69	6/2/72	Artillery Shell Series	4 shts C-1 Detasheet	Same as USAFA 67	None
USAFA 70	6/6/72	AL to Steel Series	40% DY 1008G	3/8" 7075-W AL Flyer to 3/8" Maraging steel base w/.006 steel shim. S.O. 1/8" between AL & shim, & 1/16" between shim & steel	None
USAFA 71	6/6/72	AL to Steel Series	40% DY 864G	Same as USAFA 70, except 1/4" between AL & shim & 1/16" between shim & steel	None
USAFA 72	6/8/72	Weld 2 Code Corr.	40% DY 1008G	(2) 1/2" AL Plates w/T/2 S.O.	Det. Press + Interf Press. + Det. Vel. + X-Ray
USAFA 73	6/9/72	Weld 2 Code Corr.	40% DY 432 G	(2) 1/4" AL Plates w/T/2 S.O.	Det. Press + Interf Press + Det Vel + X-Ray

Table 12 (cont)

Experiment #	Date	Research Task Plan and/or Objective	Explosive Loading	Metal Configuration	Instrumentation
USAF 74	6/12/72	Artillery Shell Series	8 G/in <sup>2</sup> Blk Thiokol	1/4" Gilding Metal Collar w/50° Angle to Maraging steel cylinder & (2) 1/4" layers rubber betw collar and exp.	None
USAF 75	6/13/72	Weld 2 Code Corr.	40% DY 576 G	(2) 1/2" AL Plates w/T/2 S.O.	Det. Vel + Det Press + Interf Press + X-Ray
USAF 76	6/14/72	Weld 2 Code Corr.	40% DY 576 G	Same as USAFA 75	Det Vel + Det Press + Interf Press + X-Ray
USAF 77	6/16/72	Weld 2 Code Corr.	(2) 2"x12"C-1 Detasheet	1/2 AL Base Plate Only	Det Vel Test Only
USAF 78	6/16/72	Weld 2 Code Corr.	40% DY 1008 G	Same as USAFA 75	Det Vel + Det Press + Interf Press + X-Ray
USAF 79	6/19/72	Weld 2 Code Corr.	40% DY 864 G	(2) 1/4" AL Plates w/T/2 S.O.	Det Vel + Det Press + Interf Press + X-Ray
USAF 80	6/20/72	Weld 2 Code Corr.	40% DY 576G +4"x6" C-1 Detasheet	1/4" AL Base Plate Only	Det Vel Test Only
USAF 81	6/20/72	Weld 2 Code Corr.	40% DY 576G +4"x6" C-1 Detasheet	1/4" AL Base Plate Only	Det Vel Test Only
USAF 82	6/20/72	Weld 2 Code Corr.	40% DY 576G	Same as USAFA 75	Det Vel + Det Press + Interf Press + X-Ray
USAF 83	6/21/72	Weld 2 Code Corr.	Orn Thiokol 1/4"x2"x12"	(2) 1/4" AL Plates w/exp on top on one side over probe at interface - gage in interface on other size T/2 S.O.	Interf Vel Probe + Gage in Interf to Determine Gage Proximity Effects

Table 12 (cont)

<u>Experiment #</u>	<u>Date</u>	<u>Research Task Plan and/or Objective</u>	<u>Explosive Loading</u>	<u>Metal Configuration</u>	<u>Instrumentation</u>
USAF 84	6/21/72	Weld 2 Code Corr.	Orn Thiokol 1/4"x2"x12"	Same as USAFA 83, but with steel shim over probe & insulated from same	Interf Vel Probe + Gage in Interf to Determine Gage Proximity Effects
USAF 85	6/21/72	Weld 2 Code Corr.	Orn Thiokol 1/4"x2"x12"	Same as USAFA 84, but with steel shim also over gage, & insulated from same.	Interf Vel Probe + Gage in Interf to Determine Gage Proximity Effects
USAF 86	6/22/72	Weld 2 Code Corr.	Orn Thiokol 1/4"x2"x12"	1/4" AL Base Plate Only	Det Vel Test Only
USAF 87	6/22/72	Weld 2 Code Corr.	Orn Thiokol 1/4"x2"x12"	Same as USAFA 83, but with probe grounded to base plate.	Interf Vel Probe + Gage in Interf to Determine Gage Proximity Effects
USAF 88	6/22/72	Weld 2 Code Corr.	Orn Thiokol 1/4"x2"x12"	AL Base Plate only, w/ implanted gage; shim over gage; & vel probe on top of shim	Det Vel + Det Press
USAF 89	6/26/72	Weld 2 Code Corr.	40% DY 720G	(2) 1/2"x8"x12" AL Plates w/T/2 S.O. w/interf probe & gage shielded w/AL shim - Gage floating	Det Vel + Interface Press + Det Press + X-Ray
USAF 90	6/27/72	Armor Plate Series	GRY Thiokol 8G/in <sup>2</sup> (2shts)	1/8" Flyer to 1/2" base w/ 1/8" screen wire in between all 6061-T6 AL w/rubber between Flyer & Exp.	None



Table 12 (cont)

Experiment #	Date	Research Task Plan and/or Objective	Explosive Loading	Metal Configuration	Instrumentation
USAF 91	6/26/72	Weld 2 Code Corr. System Test	Orn Thiokol 1/4"x2"x12"	1/4" AL Base plate only w/ probe att. to shim-shim shielding probe from gage	Det Vel + Det Press Proximity Test
USAF 92	6/28/72	Armor Plate Series	Orn Thiokol 3/8"x6"x12"	1/8" AL Flyer to 1/2" AL base, w/screen wire betw & 1/8" rubber betw flyer & exp.	None
USAF 93	6/28/72	Armor Plate Series	Orn Thiokol 5/8"x6"x12"	Same as USAFA 92	None
USAF 94	6/29/72	Weld 2 Code Corr.	40% DY 576G	(2) 1/2" AL Plates w/T/2 S.O.	Det Vel + Det Press + Interf Press + X-Ray
USAF 95	6/29/72	Weld 2 Code Corr.	40% DY 576G	1/4" AL Base Plate Only, w 1" S.O. from Anvil	Det Vel + Det Press
USAF 96	7/3/72	Weld 2 Code Corr.	8 G/in <sup>2</sup> -8 in old DY-4 in new DY-40%	1/4" AL Base Plate only w/1" S.O. from Anvil	Det Vel + Det Press
USAF 97	7/3/72	Weld 2 Code Corr.	Unknown	Unknown	Det Vel + Det Press
USAF 98	7/4/72	Weld 2 Code Corr.	40% DY-720G	1/4"x12" AL Flyer to 1/4"x6" base (AL)w/1" S.O.	Det Vel + Det Press
USAF 99	7/4/72	Weld 2 Code Corr.	40% DY-864G	Same as USAFA 98	Det Vel + Det Press
USAF 100	7/10/72	Armor Plate Series	Orn Thiokol 270G (2) 1/4 Layers	1/8" AL Flyer to 1/2" base (AL) w/screen wire betw & 1/8" rubber betw flyer & exp.	None



Table 12 (cont)

<u>Experiment #</u>	<u>Date</u>	<u>Research Task Plan and/or Objective</u>	<u>Explosive Loading</u>	<u>Metal Configuration</u>	<u>Instrumentation</u>
USAFA 101	7/10/72	Armor Plate Series	Orn Thiokol 540 G(2) 1/4 Layers	Same as USAFA 100	None
USAFA 102	7/10/72	Armor Plate Series	Orn Thiokol 270G (1 1/4" Layer)	Same as USAFA 100	None
USAFA 103	7/11/72	Armor Plate Series	Orn Thiokol 270G (1 1/4" Layer)	Same as USAFA 100	None
USAFA 104	7/11/72	Armor Plate Series	Orn Thiokol 416G(3/8") (2) Layers	(2) 1/16" Flyer Plates to (1) 1/2" base plate, w/(2) layers screen wire inter- leaved betw flyers. 1/8" rubber betw top flyer, & exp.	None
USAFA 105	7/17/72	Armor Plate Series	Orn Thiokol 986G(2) 1/4" shts	1/8" AL Flyer to 1/2" AL base w/screen wire betw & 1/8" rubber betw flyer & exp.	None
USAFA 106	7/17/72	Armor Plate Series	Orn Thiokol 1038G(2) 1/4" shts	Same as USAFA 105	None
USAFA 107	7/17/72	Armor Plate Series	Orn Thiokol 578G(1/4"sht)	Same as USAFA 105	None
USAFA 108	7/17/72	Armor Plate Series	Orn Thiokol 508G(1/4"sht)	Same as USAFA 105	None
USAFA 109	7/18/72	Armor Plate Series	Orn Thiokol 850G(3/8"shts (2))	(2) 1/8" 12"x12" AL Flyer plates w/2 screen wire inter- leaved, to 1/2" AL base plate, w 1/8" rubber betw top flyer & exp.	None

Table 12 (cont)

Experiment #	Date	Research Task Plan and/or Objective	Explosive Loading	Metal Configuration	Instrumentation
USAFA 110	7/19/72	Weld 2 Code Corr.	40% DY-576G	1/8" AL Flyer to 3/8" AL base	Det Vel + X-Ray
USAFA 111	7/20/72	AL to Steel Series	40% DY-720G	3/8" AL flyer to 3/8" steel base w .007 steel shim betw 1/8" betw AL & shim & .0207" betw shim & steel. (15) .0207" long wires soldered to shim	None
USAFA 112	7/31/72	Armor Plate Series	Orn Thiokol 5.52 G/in <sup>2</sup>	(5) 1/8" AL plates w (4) shts screen wire interleaved exp on both ends welded vertically w/1/8" rubber betw exp & 1st plate on both ends	None
USAFA 113	7/31/72	Armor Plate Series	Orn Thiokol 6.19 G/in <sup>2</sup> one side--6.29 G/in <sup>2</sup> other side	Same as USAFA 112, except 12"x12" instead of 6"x12"	None
USAFA 114	8/2/72	Armor Plate Series	Orn Thiokol 5.46 G/in <sup>2</sup> one side--5.41 G/in <sup>2</sup> other side	Same as USAFA 113	None
USAFA 115	8/3/72	Armor Plate Series	Orn Thiokol 7.24 G/in <sup>2</sup>	1/8" AL flyer to 1/2" AL base w/screen wire betw & 1/8" rubber betw flyer & exp. 12"x12"	None

Spot welds were attempted using 6 plate thickness (1/16, 1/8, 3/16, 1/4, 3/8, 1/2-inches) and 5 impulse intensity levels.

b. "T" Weld Investigation

Various attempts to weld a plate (flange) to the top of a stem section were made. The weld plate thickness was 0.250 inches, and the stem was initially 0.375 inches in thickness. This arrangement was intended as a transition specimen with the ultimate specimen configuration being that of the AM2 aluminum airfield matting repair kit described in a separate technical report (USAF, 1971).

The specimen mount for the "T" welding experiments was also designed, fabricated and provided by the Academy. (Figure 23)

A total of 149 parallel plate welds and 54 "T" type welds were attempted. Evaluation of most of the weld specimens was accomplished at the Fort Worth Division instead of at the Academy. This procedure was adopted as the work progressed to allow immediate feedback on weld set-up variables. A final set of the welded plate specimens was sent to the Academy in the as-welded condition for final testing.

The explosive set-up used in these studies consisted of a short (1/2 to 1 1/4 inches long) length of Detonating Cord explosive (the "spot explosive") set upright on the upper surface of the top plate. The explosive core of the Detonating Cord was set in direct contact with the metal plate as shown in Figure 24. A mound of modeling clay was used to hold the Detonating Cord in place. A second length of Detonating Cord, the stringer or lead-in explosive (Figure 24a), was strung across the top of the spot explosive and served as the means for detonating the spot explosive. A modified set-up consisted of a separate stringer and lead-in (Figure 24b).



Figure 23 "T" field Specimen Mount

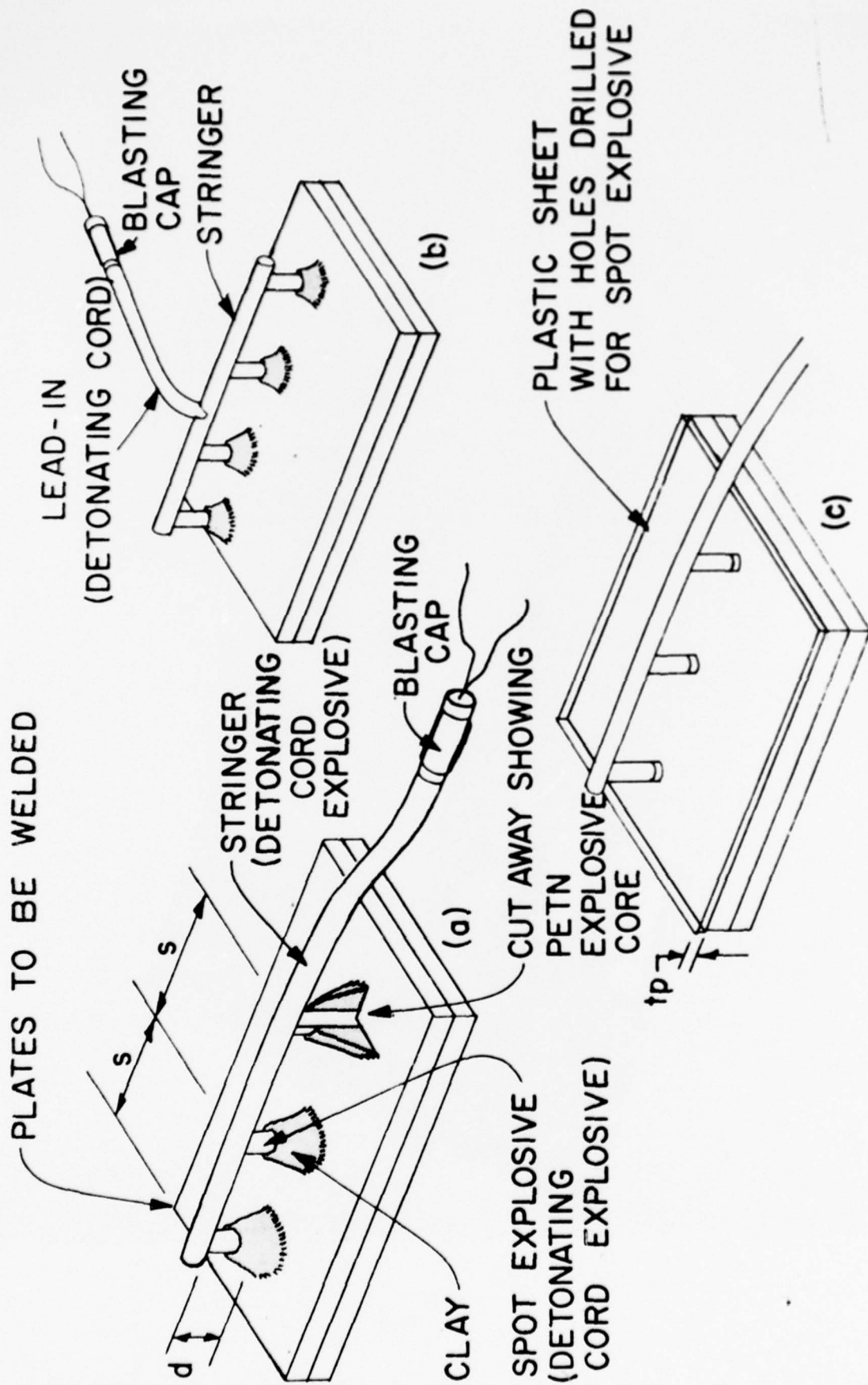


Figure 24 Spot Welding Configurations



An electric blasting cap was attached to the far end of the lead-in (or to the stringer if a separate lead-in was not used). The electric blasting cap initiated the explosion which then followed the lead-in to the stringer and then to the spot explosive. The detonation of the lead-in, stringer and spot explosive (and electric blasting cap, if too close) all have an effect on the explosive welding action. Figure 24c illustrates another variation in which a plastic sheet, drilled to accommodate spot explosive charges, was used.

The overall results of the parametric study are summarized in Table 13. Each table presents the results of both the parallel plate and "T" weld investigations for a single plate thickness. The "T" welds are listed according to the top plate thickness and are identified by specimen number starting with the number "2". The nomenclature used in the tables and additional details relative to the spot welding set-ups are given below.

#### Column 1, Welding Grouping

Entry indicates the number of spot welds simultaneously attempted (i.e., a single or multiple spot weld arrangement). The number in parenthesis ( ) following the multi-spot numbers represents the interspot distance; if the spot spacing varied, it is described in the REMARKS column.

#### Column 2, Specimen Identification

The entry is the specimens' unique numerical identification marked on the specimen.

#### Column 3, Explosive System

These entries describe the three components of the particular explosive arrangement used; the spot explosive, the stringer and the lead-in (if used). The first subcolumn, labeled "Spot", codes the spot explosive element. The first number gives the length of spot

Table 13 Spot Welding Results  
SPOT WELD STUDY USING 1/16-INCH PLATE

Weld Grouping	Specimen Identification	Explosive System			Preliminary Weld Evaluation	Bond Region		Outer Diameter Surface Cleaning	Outer Diameter "Sunburst" Effect	Remarks
		Spot	Stranger	Lead-in		Inner Diameter	Outer Diameter			
One Spot	11-26-1	1 1/4 / 50	2 / 50		NW	3/16	1/2	1 1/4		
	11-28-1	1 1/4 / 50	2 / 50		NW	1/2				
	11-26-2	1 1/4 / 60	2 / 60		NW	3/8	5/8	1 3/4	Some	
	11-28-2	1 1/4 / 60	2 / 60		W	1/4	1/2			
	12-29-1	1/2 / 200	5 / 200		W	3/8	1 3/16	2	Some	2nd ring 1/32
	11-26-3	1 1/4 / 200	2 / 200		W	1/4	1/2			
	11-28-3	1 1/4 / 200	2 / 200		W	7/16	13/16	1 1/2	2 1/2	
	2-2-1	1/2 / 400	14 / 60		W	9/16	15/16	1 15/16	4 m	2nd ring OD 1 1/4
	2-2-2	1/2 / 400	14 / 60		W	9/16	1	1 3/4	2 1/2	
	2-2-3	1/2 / 400	14 / 60		W	9/16	1	1 3/4	3	
	2-4-1	1/2 / 200	14 / 60		S1 W	7/16	3/4	1 1/2	S1 1 1/2 P	Cold - reg. clay
	2-4-2	1/2 / 200	14 / 60		W	3/8	7/8	1 3/8	3 m	Warmer - 1/2 clay
	2-4-3	1/2 / 200	14 / 60		W1	1/4	3/4	1 1/4	4 h	Warmer - 1/3 clay
	2-4-4	1/2 / 200	14 / 60		NW	Indent	3/8	1/2		0 clay
	2-5-1	3/8 / 200	14 / 60		S1 W	1/2	13/16	1 1/2		Soft anvil
	2-5-2	1/2 / 200	14 / 60		PW	3/8	13/16	1 5/8	1 3/4	Soft anvil
	2-5-3	3/4 / 200	14 / 60		PW	3/8	13/16	1 3/4	2	Hard anvil
	2-5-4	1 1/4 / 200	14 / 60		W2	3/8	13/16	1 3/4	3 1/2 m	Hard anvil
	2-5-5	1 1/4 / 200	14 / 60		W1	3/8	13/16	1 7/8	2 1/2 l	Hard anvil
Two Spot (1 3/4")	2-6-1	3/4 / 50	8 / 200		S1 W	3/16	7/16	1 3/8	S1 1	
	2-6-2	3/4 / 60	8 / 200		S1 W1	1/8	7/16	1 5/16	S1 1 3/4	
	2-6-3	3/4 / 200	8 / 200		S1 W	3/8	7/8	1 3/4	2 m	
	2-6-4	3/4 / 400	8 / 200		S1 W	5/8	1 1/4	2	1/2	
Three Spot (1 1/2")	11-29-3	1 1/4 / 50	3 / 60		NW	1/4 - 1/8	1/2 - 3/8	1		
	11-29-2	1 1/4 / 60	3 / 60		NW	3/16 - 1/4	1/4 - 1/2	1 1/8 - 1 1/8	3/4	
	11-29-1	1 1/4 / 200	3 / 200		PW	3/8 - 5/16	1/2 - 3/4	1 3/4 - 1 5/8	2	
	12-30-1	1/2 / 200	12 / 200		PW	5/16 - 7/16	5/8 - 3/4	1 3/4 - 1 3/4		
Three Spot (1 1/2")	12-1-1	1 1/4 / 50	4 / 50		NW	1				
	12-1-2	1 1/4 / 50	4 / 60		NW	1				
	12-1-3	1 1/4 / 200	4 / 200		S1 W	1				
	12-2-2	1 1/4 / 200	12 / 200		PW	7/16 - 7/16	3/4	1 1/6	2	
	12-30-2	1/2 / 200	8 / 200		PW	5/16 - 3/8	1	1 7/8		

Table 13 (Contd) Spot Welding Results

## SPOT WELD STUDY USING 1/8-INCH PLATE

Weld Grouping	Specimen Identification	Explosive System			Preliminary Weld Evaluation	Bond Region		Outer Diameter Surface Cleaning	Outer Diameter "Sunburst" Effect	Remarks
		Spot	Stringer	Lead-In		Inner Diameter	Outer Diameter			
One Spot	12-9-1	1 1/4 / 400	2 / 400		W	1 1/16	1 1/4	1 7/8	3 1/4	
	12-9-2	1 1/4 / 200	2 / 200		NW	5/8	1 1/16	1 3/4	-	
	2-3-1	1/2 / 400	8 / 400		S1 W	3/4	1 1/4	1 3/4	S1 3	
	2-3-2	1/2 / 400	8 / 200		W2	1/2	1 1/4	1 3/4	3 1/4 in	
	2-3-3	1/2 / 400	8 / 200		NW	5/8	1 5/16	1 7/8	-	
	2-3-4	3/4 / 400	8 / 200		PW	5/8	1 1/8	1 11/16	2 3/4	.030" plastic - NC*
	2-3-5	3/4 / 400	8 / 200		W2	3/8	1	1 1/2	6	w/o plastic - NC*
	2-5-6	3/4 / 400	8 / 200		W3	3/8	1 5/16	1 11/16	6	w/o plastic - NC*
	2-9-1	3/4 / 400	8 / 60		W3	1/2	1 1/4	1 11/16	6	
	2-9-2	3/4 / 400	8 / 200		W2	3/8	1 1/4	1 5/8	6	
	2-9-4	3/4 / 400	8 / 400		W	1/2	1 1/8	1 3/4	4	
	2-12-1	1/2 / 400	8 / 200		W3	5/16	1	1 1/2	4 1/2	
	2-12-2	3/4 / 400	8 / 200		W2	5/8	1 1/4	2	2 1/2	
	2-12-4	1 1/4 / 400	8 / 200		W	1/2	1 1/4	2	3 in	
	2-16-2	3/4 / 400	8 / 400		WX					Not Cleaned
	2-16-4	3/4 / 400	8 / 400		WX					Not Cleaned
	2-17-1	3/4 / 400	8 / 400		WX					Not Cleaned
	2-17-4	3/4 / 400	8 / 400		WX					Not Cleaned
	2-17-5	3/4 / 400	8 / 400		NWX					Not Cleaned
	2-18-1	3/4 / 400	8 / 400		WX					Not Cleaned
	2-18-3	3/4 / 400	8 / 400		WX					Not Cleaned
	2-18-4	3/4 / 400	8 / 400		WX					Not Cleaned
	2-18-5	3/4 / 400	8 / 400		WX					Not Cleaned
Two Spots (2 1/2")	12-9-3	1 1/4 / 400	6 / 400		W2	9/16-9/16	1 1/4-1 1/8	1 3/4-2 1/16	4-2 1/2	
	12-9-4	1 1/4 / 200	6 / 200		NW	5/8-5/8	1 1/8-1 1/8	1 5/8-1 5/8	-	

\* NC = Not Cleaned

Table 13 (Contd) Spot Welding Results

## SPOT WELD STUDY USING 3/16-INCH PLATE

Weld Grouping	Specimen Identification	Explosive System			Preliminary Weld Evaluation	Bond Region		Outer Diameter Surface Cleaning	Outer Diameter "Sunburst" Effect	Remarks
		Spot	Stringer	Lead-in		Inner Diameter	Outer Diameter			
One Spot	12-10-3	1 1/4 /60	2 1/2 /60		NW	5/8	1 7/16	3/4	1 3/4	Wax
	12-17-4	1/2 /400	2 1/2 /400		W			2		"
	12-17-1	1/2 /400	12 /400		NW			2 1/4		"
	12-17-2	1/2 /400	2 1/2 /400		NW	13/16	1 3/8	2 1/8		"
	12-10-1	1 1/4 /400	2 1/2 /400		NW	7/8	1 1/2	2		"
	12-10-2	1 1/4 /400	2 1/2 /400		NW	f	f	1 7/8		"
Two Spots (See Remarks)	2-13-1	3/4 /400	8 /400		NW	3/4	1 1/2	2		"
	2-13-3	3/4 /400	8 /200		S1 W	3/4	1 5/16			"
	2-13-5	Rolled Detasheet			WX					
	12-15-3	1 1/4 /60	5 /60		NW	f 3/4	f 1 1/4	f 1 1/4		" 3-in. spacing " 1 1/2 in."
	12-11-3	1 1/4 /60	2 1/2 /60		NW			f 1 1/4		"
	12-15-2	1 1/4 /200	5 /200		NW	f 7/8	f 1 5/16	f 1 3/4		" 3-in. spacing " 1 1/2 in."
Three Spots (See Remarks)	12-11-2	1 1/4 /200	2 1/2 /200		NW	(Can see faint outline of 3 to 5 rings)				"
	12-16-1	1/2 /400	12 /400		PW	3/4 7/8	13/8 13/8	2 1/8 2 1/4	f	" 3-in. spacing " 3-in. spacing
	12-16-2	1 1/4 /400	12 /400		NW	3/4 15/16	13/8 13/8	17/8 2		" 3-in. spacing " 3-in. spacing
	12-15-1	1 1/4 /400	5 /400		NW	f 7/8	f 1 1/4	f 1 3/4		" 3-in. spacing " 1 1/2 in."
	12-11-1	1 1/4 /400	2 1/2 /400		NW	f 1	f 2 1/4			" 3-in. spacing " 1 1/2 in."
	12-11-4	Rolled Detasheet			NW	5/8 3/4	7/8 1	13/8 15/8		" 3-in. spacing " 1 1/2 in."
Four Spots (1 1/4")	12-12-3	1/4 /60	4 /60		NW	Vf	f 3/4	1 3/8		" 1 1/4 in."
	12-12-2	1 1/4 /200	4 /200		NW	Vf		1 7/8		"
	12-12-1	1 1/4 /400	4 /400		PW	3/4	1 3/8	1 7/8		"
	12-18-1	1/2 /400	6 /400		NW			2		" 2-in. spacing " 2-in. spacing
	12-18-2	1/2 /400	12 /400		NW	7/8 7/8	1 1/2 1 1/2	2 1/8		"
Four Spots (1 1/4")	12-13-3	1 1/4 /60	10 /60		NW		Vf	1 3/4		Wax
	12-13-2	1 1/4 /200	10 /200		NW			1 15/16		"
	12-13-1	1 1/4 /400	10 /400		S1 W			1 7/16	f	"
	12-18-3	1/2 /400	8 /400	12 /50	NW			2 1/8		"

Table 13 (Contd) Spot Welding Results

## SPOT WELD STUDY USING 1/4-INCH PLATE

Weld Grouping	Specimen Identification	Explosive System			Preliminary Weld Evaluation	Bond Region		Outer Diameter Surface Cleaning	Outer Diameter "Sunburst" Effect	Remarks
		Spot	Stringer	Lead-in		Inner Diameter	Outer Diameter			
One spot	12-6-3	1 1/4 / 60	2 / 60		NW	1/4	7/8			Old Ts/redeposit Multi rings
	12-6-5	1 1/4 / 200	2 / 200		NW		f			
	12-6-2	1 1/4 / 200	2 / 200		NW	7/16	1 1/16	1 3/8		
	12-4-2	1 1/4 / 400	2 / 400		NW					Uncleaned Old Ts + lava Ts Old Ts/redeposit
	12-4-1	1 1/4 / 400	2 / 400		NW					
	12-6-1	1 1/4 / 400	2 / 400		NW	3/4	1 3/4	2nd order f		
	12-3-3	1 1/4 / 400	2 / 400		NW					
	12-15-4	1/2 / 400	cap		W	3/8	1 1/8H	1 3/4		
	12-16-3	1/2 / 400	12 / 400		W	3/8	1 3/8	1 3/4	1 1/2	
	12-19-1	1/2 / 400	4 / 400		W	5/16	1 1/4	2	f	
Two spots (2 1/2")	2-13-6	Rolled Detasheet			WX	(Bounced)				Collision wave center by V lead. Bounced
	2-16-1	3/4 / 400	8 / 400		NW					
	12-19-4	1/2 / 400	12 / 400		NW	7/8-1	1 1/4-1 1/2	2		
	12-22-7	1/2 / 400dbble	6 / 400		NW		Vf	2 1/4		
	12-20-1	1/2 / 400	6 / 400		NW			2		
	12-19-2	1/2 / 400	6 / 400	12 / 400 V	NW	(Vf 1)	(Vf 1 1/2)	2 1/8		
	12-22-6	2/4 / 400	6 / 400	12 / 50 V	NW			2 2 1/2		
	12-21-1	1 / 400dbble	4 / 400		NW	7/8	1 1/4	2 1/8		
	12-20-2	3/4 / 400	dynamite		NW					
	12-23-1	1/2 / 400	18 / 400		NW					
Three spots (2")	12-23-4	1/2 / 400dbble	6 / 400		NW	1/2	1 1/4	1 7/8		3 holes in plastic sheet
	12-19-3	3/4 / 400	Detasheet		NW		Vf			
Four spots (1 1/4")	12-20-3	3/4 / 400	dynamite 6"	6 / 400- detasheet	S1 W					Slight weld at one end
Five spots (1")	12-5-1	1 1/4 / 400	9 / 400		NW	7/8-1	1 1/8-1 7/8			



Table 13 (Contd) Spot Welding Results  
SPOT WELD STUDY USING 3/8-INCH PLATE

Weld Grouping	Specimen Identification	Explosive System		Preliminary Weld Evaluation	Bond Region		Outer Diameter Surface Cleaning	Outer Diameter "Sunburst" Effect	Remarks
		Spot	Stringer		Inner Diameter	Outer Diameter			
One Spot	12-16-4	1/2 /400	12 /400	NW	5/8 (1 1/4)	15/16 (1 1/2)	1 11/16 2 x 3 1/2		Old Top- of 2nd Order Effects  Heavy Indent Large Indent
	12-26-3	1/2 /400	dbie 2 /400	NW					
	12-27-2	(1/2 RDX + 1/2 /400)	12 /400	NW	1 7/16	2	2 5/8		
	12-31-2	(3/8 RDX + Dynamite)		NW	1 13/4	2 1/4	2 1/2		
	12-31-3	(1x 2 D Dynamite)		NW					
Four Spots (1 1/4")	12-5-3	(1 /400 + Detasheet)	2 /400	NW		Vf			4 Hole Plastic    Very Little Interface Action - Specimen burned
	12-24-1	1/2 /400	18/400 + 3-6/400	NW		Vf	2 3/4		
	12-20-4	3/4 /400	6" Dynamite + Strip Deta sheet + 6/400	NW			2 1/4		
	12-24-2	RDX Seam + 4 Hole	Detasheet + 12/400	W					
	12-23-3	3 Rows 400 over 5 hole		NW					

Weld Grouping	Specimen Identification	Explosive System		Preliminary Weld Evaluation	Bond Region		Outer Diameter Surface Cleaning	Outer Diameter "Sunburst" Effect	Remarks
		Spot	Stringer		Inner Diameter	Outer Diameter			
One Spot	12-16-5	1/2 /400 + dbie 2 1/2 /400		NW	Vf 7/8	Vf 2 1/4			Not Cleaned Burned Indent
	12-27-4	5/8 RDX 1 1/4 high		NW	1 3/4	2 3/8	1	2 3/4	
Four Spot	12-29-2	1/2 /400 + 6 /400 Detasheet spot x 3 spots		NW	Vf 3/8	Vf 1/2	2		
	12-19-5	One spot of 1/2 /400 + DC + 2 /400 + 12 /400		NW	Vf 1/2		2 1/4		

explosive used (1/2, 3/4, 1, or 1 1/4 inches); then follows a slash line (/) with the next number indicating the explosive strength in grains-per-foot of PETN explosive Detonating Cord for the spot explosive (where something other than Primacord was used, it is specifically called out).

The middle and third subcolumns describe the lead-in/stringer elements. In most cases, Primacord Detonating Cord was used for stringers and lead-ins; deviations from this practice are indicated and the substitute identified. In the thicker plate shots (1/4 inch and greater) there were some complicated set-ups, but, since most of these failed to produce suitable results, little description of them is given. In the stringer code the first number indicates the length of Detonating Cord (2 inches up to 18 inches), while the second number indicates the Detonating Cord explosive strength in grains-per-foot. For stringer lengths of 6 inches or less, the electric blasting cap was centered in the stringer. The longer stringer lengths indicate a combined stringer + lead-in with the electric blasting cap set at the far end of the lead-in. A stringer marked dble means that the stringer was double (two lengths).

#### Column 4, Preliminary Weld Evaluation

This third column gives the welding action observed; "NW" is no weld, "W" indicates that the pieces stuck together and had to be pried apart. Welded parts that were mildly difficult to pry apart are merely marked "W". "W1" means they came apart with great difficulty and "W2", "W3" with extreme difficulty (torn metal). "S1 W" means only slight welding took place and the parts came apart easily or if on a "W1", that welding occurred only a small part of potential weld area. "PW" means that welding was only partially complete -- incomplete ring or incomplete series in multiple spot shots. "X" in conjunction with "W" and "NW" indicates test specimens which were sent to the Academy for final testing (no attempt was made to pry these specimens apart)

#### Column 5, Bond Region

The extent of the bond region is described in terms of the inner and outer diameters in inches of the weld ring (halo). The letters f, Vf indicate that the effect was faint or very faint.

#### Column 6, Outer Diameter Surface Cleaning

This column gives the maximum diameter of affected (polished, cleaned) interface area which usually extends beyond the actual welding zone.

#### Column 7, Outer Diameter "Sunburst" Effect

This column gives the maximum diameter in inches of any

sunburst ray extending out from the weld action area; "h" indicates the rays were heavy, "m" medium heavy, "Sl" slight, "p" partial (one side), "f" faint.

Column 8, Remarks

Other pertinent conditions are described in this column. Some of these are: "Cold - warmer - warmest" indicating a series where the weld specimen was heated above the outside air temperature on a cold day prior to welding; warmest was hot to touch but tolerable. "Reg clay -- 1/2 clay - 0 clay" indicates a variation in the amount of clay around the spot explosive. "W / o plastic" was without the .030" thick plastic used on the 1st shot in the series. "NC" indicates that the aluminum plates were not specially deoxidized or cleaned in acid. "Tsi" was the deoxidizing solution (Tsi Rust and Carbon Remover) used in preparing cleaned plates. Old Tsi solution tended to "redeposit" material on the aluminum plates which remained in the solution for more than 3 - 4 hours; redeposit was sometimes removed with "lava" soap. "Three holes in plastic" refers to a shot where the spot explosive was placed in holes drilled in a plastic sheet. "Bounced" indicates that a sample knocked off its anvil by the response of the anvil base. "Burned" designates a sample seriously burned on the top surface by excessive or improper explosive action.

The results indicate that the unclad 6061-T6 aluminum alloy as received (without deoxidizing), can be explosively welded at thicknesses up through about 1/8 inch with the commercially available explosives such as PETN Detonating Cord (Primacord) and PETN sheet explosive (Detasheet). It was quite apparent throughout the study that commercially available explosives lack uniform detonation characteristics when used in the small quantities needed for explosive spot welding.

The 1/16 inch and 1/8 inch thick 6061-T6 aluminum could be satisfactorily welded using the normal solid-state explosive spot welding techniques with the Primacord explosive. The thicker plates, particularly the 3/16 inch thick material, as received, were contaminated with a wax-like preservative which could be removed only with difficulty in a hot-vapor-degreaser.

Another pertinent result of the plate and "T" weld studies is that presently available commercial explosives are not available in adequate strengths or with sufficient uniformity to accomplish good solid-state welds at plate thicknesses of 3/16 inch or greater when using zero standoff techniques. The solution to this part of the problem requires the identification or development of new explosives or techniques.

The parallel plate and "T" weld studies indicate that the spot welding of 6061 aluminum alloy plates to "T" stems (as might occur in fabricating the structural "H" connectors for AM2 landing mats) would require some special design considerations. This is apparent in that the outside diameters of the weld regions which were obtained are bigger than the "T" stem widths previously considered for the mat connectors. This would mean that in using a stem narrower than the weld area diameters the welded joint would consist of a series of nearly parallel weld band zones spaced along the length of the stem. Although this weld effect would not necessarily be unsatisfactory for the purpose intended, the parallel plate welding approach was judged to produce a more desirable result. This was the reason for emphasis on the parallel plate approach throughout the remainder of this investigation.

In addition to the single spot weld attempts, some multiple spot welds were attempted. This was done to allow preliminary information to be obtained on interspot effects which might occur in field repair and construction applications. Shock fronts from two or more explosion origins may interact, either reinforcing or nullifying the effects which lead to solid state bond development.



Results from the study indicate that spot welds (at the explosive load levels used) should be at least 3 to 5 inches apart. More exact limitations would have to be determined when actual field spot welding applications are investigated.

E. Weld Evaluation

1. Ultrasonic Testing

Various parallel aluminum plate specimens were examined prior to destructive testing using the ultrasonic test system shown in Figure 25. This system consisted of the latest commercially available ultrasonic equipment which included the following:

a. Automatic Research Tank and C-Scan Recorder System, Automation Industries Model SR-451. This system was equipped with a type 57A2786 search unit (5.0 MHz, FM, 0.375" diameter).

b. Reflectoscope Display Unit, Automation Industries Model 721 Type 50B721.

c. 10N Pulser/Receiver Module, Automation Industries Model 50E533.

The only correlation found to exist between the resulting ultrasonic C-scan traces and subsequent destructive tensile test results was the anticipated agreement in identification of bond-disbond areas. Figure 26 illustrates such a correlation using a welded specimen formed with two 3/8 inch thick 6061-T6 aluminum plates. Detailed examinations of variations of ultrasonic interface and back surface echo signals with tensile strengths have yielded no additional insight into bond conditions. Figure 27



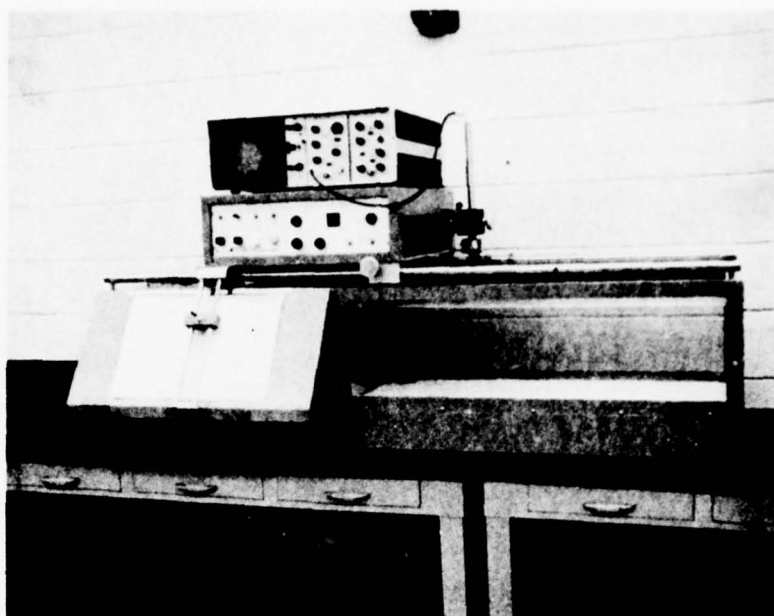


Figure 25 Ultrasonic Test System

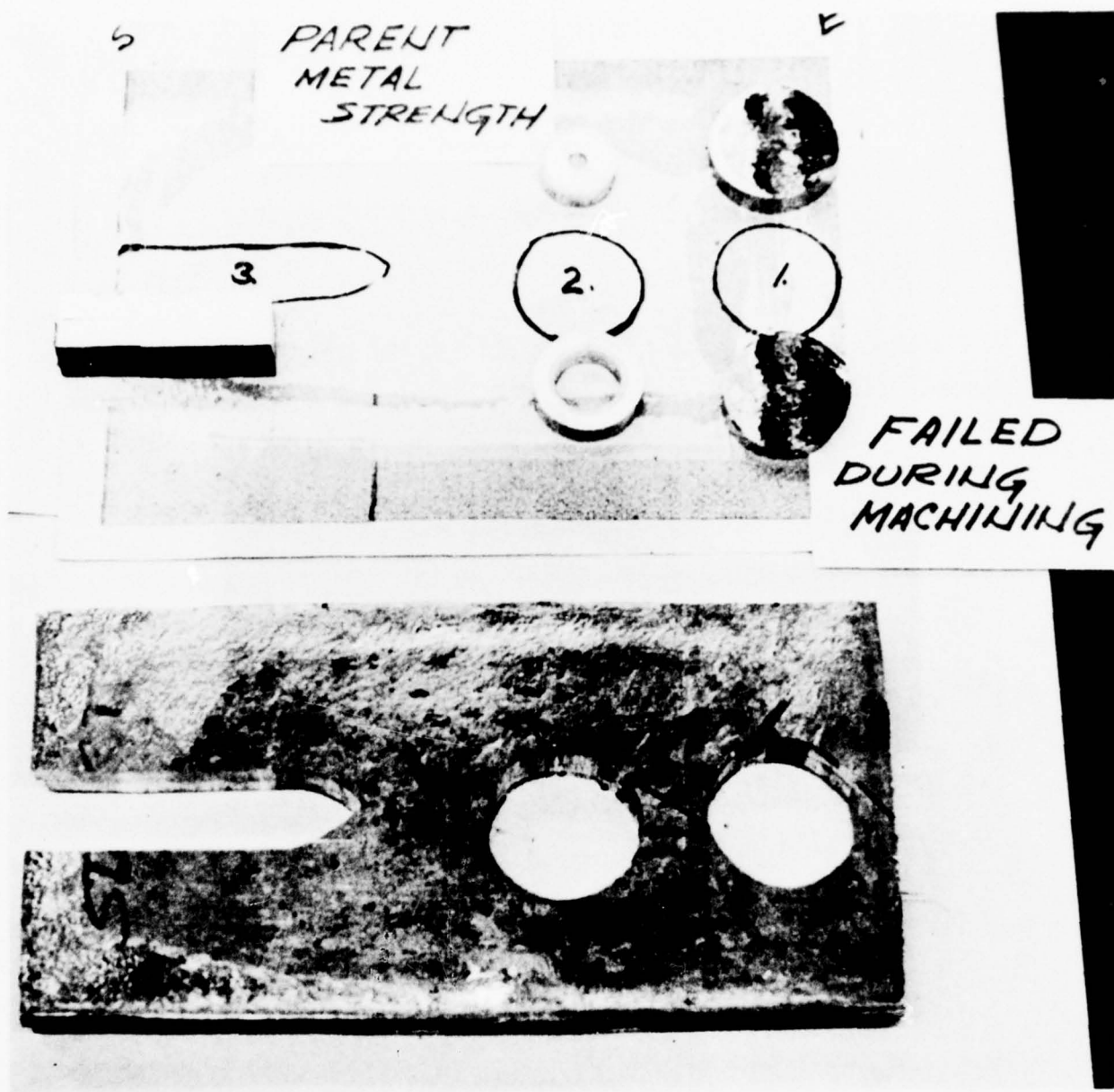


Figure 26 Ultrasonic Trace-Bond Strength Correlation

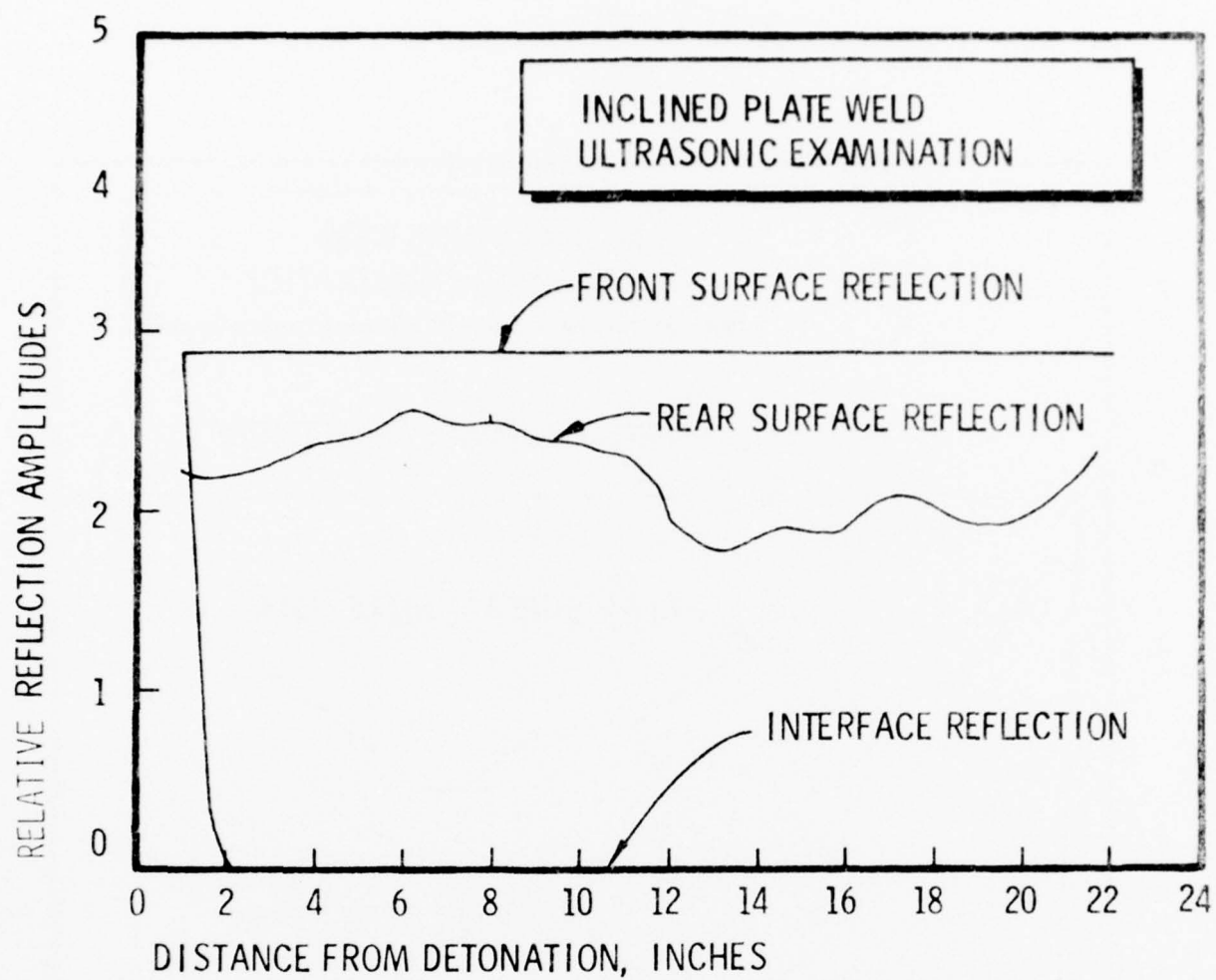


Figure 27 Plate Weld Ultrasonic Examination

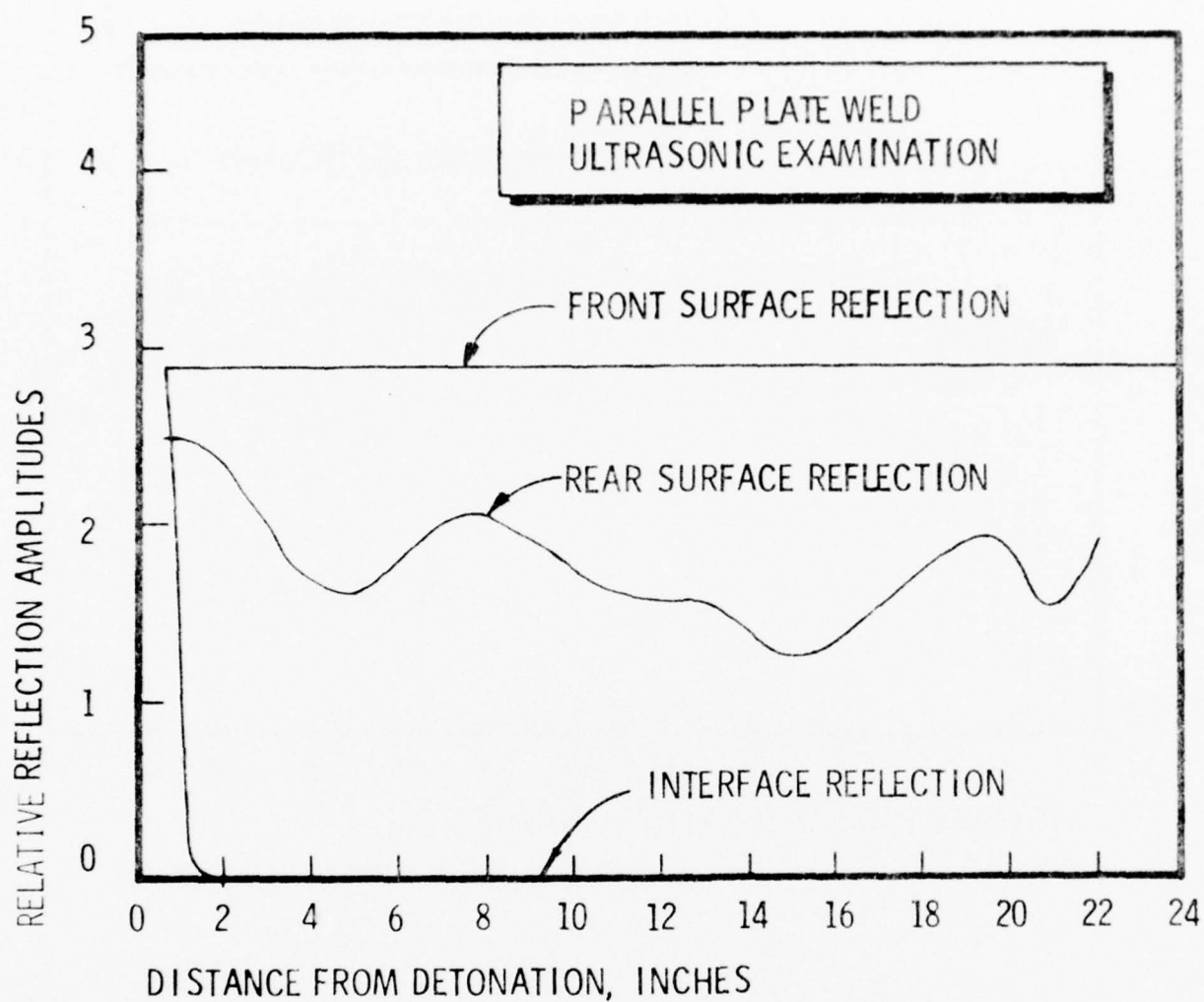


Figure 27 (Contd) Plate Weld Ultrasonic Examination

shows relative reflection amplitudes plotted versus distance from detonation end for the angular standoff and parallel plate welds. These cases are typical in that they reveal no apparent relationship between signal frequency, amplitude of the reflected signal, and bond tensile strength.

## 2. Wavelength Variations with Selected Welding Parameters

Several impact parameters commonly associated with wavelength variations include the explosive's detonation velocity,  $D$ , the initial linear standoff distances,  $S$ , between the plates, the initial angle of relative inclination,  $\alpha$ , and finally, a dimensionless ratio of the mass,  $M$ , of the flyer plate per unit surface area to the mass,  $C$ , of explosive associated with the same surface area, i.e.,

$$\frac{M}{C} = \frac{\rho_1 t}{\rho_o h}$$

where  $\rho_1$  and  $\rho_o$  are the densities of the flyer plate metal and the explosive, respectively, and  $t$  and  $h$  are the corresponding thicknesses. In this study, data from the parallel aluminum plate parametric study was used; explosive detonation velocity was assumed to be independent of explosive thickness. Thus, the impact parameters of interest reduced to the constant linear standoff,  $S$ , and the mass to charge ratio  $M/C$ . Interface deformation wavelengths were obtained from the center region of the specimen either by direct measurement using failed tensile strength specimens or from photomicrographs of the wave profiles (Figure 28) and were plotted as shown in Figure 29. Analysis of the wave length variation with welding parameters is included in the following chapter on analyses.



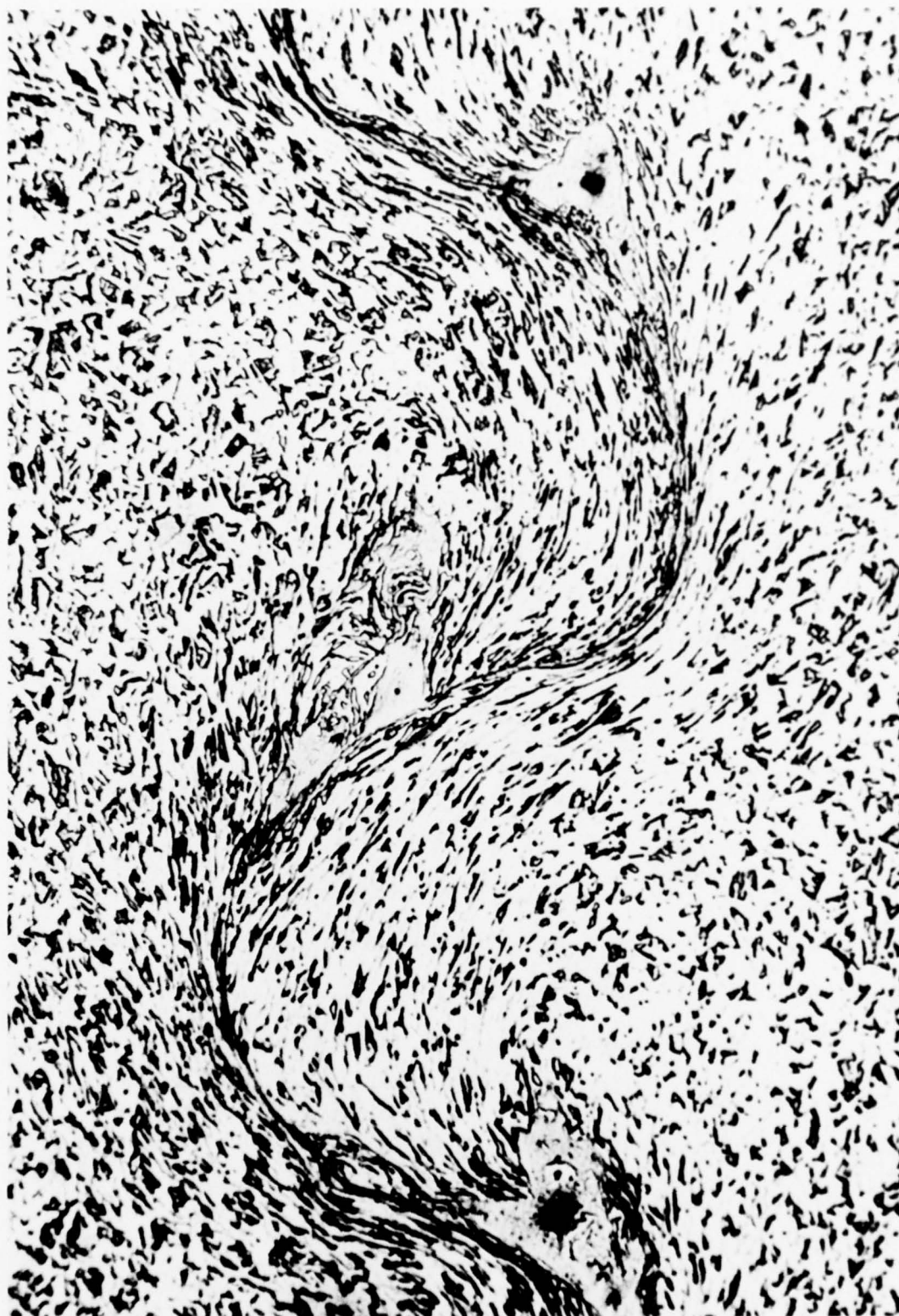


Figure 28 Photomicrograph of Weld  
Interface Waves

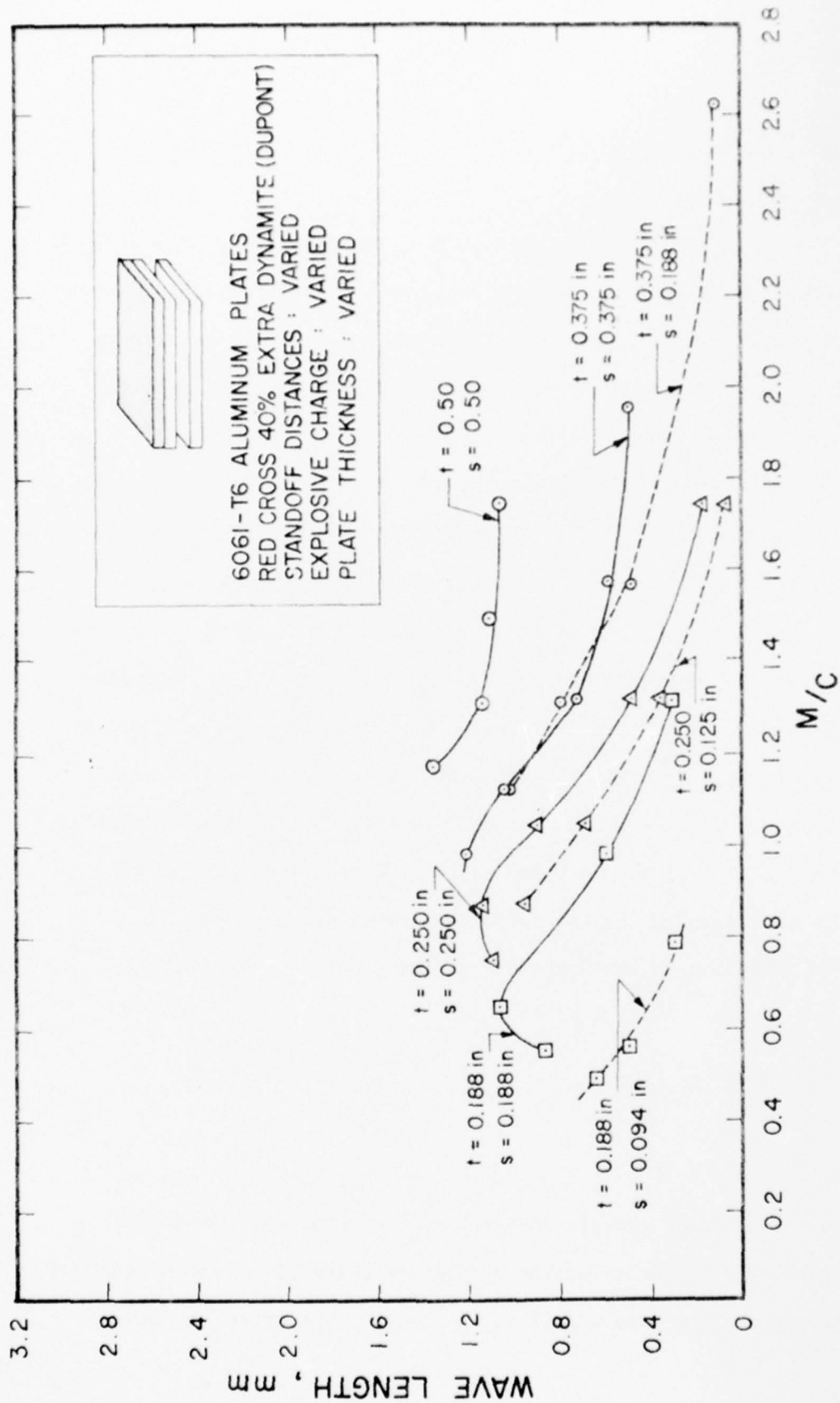


Figure 29 Interface Wavelength Variations with Mass Ratio

### 3. Destructive Mechanical Tests for Weld Strength Evaluation

#### a. Introduction

In the following paragraphs, the specimen welding schedules and the welding strengths associated with each of the explosive load-specimen assembly configurations are presented. The various destructive test methods used in the evaluation of these weld strengths are also described.

#### b. Shear Strength Evaluation

Specimens for shear tests were saw cut from the welded composite as shown in Figure 30. In the early stages of the study, the practice of previous investigators influenced the use of the shear test specimen design shown in Figure 31. This arrangement is commonly called a tension-shear specimen as shear is produced across the weld interface section through an application of axial tension force. This design was used in testing most of the parallel aluminum plate welds. In these cases, the interface failure length,  $d$ , was calculated using the following reasoning.

FAILURE LOAD ON SHEAR PLANE < FAILURE LOAD IN TENSION

$$\left[ (.9") \times d \right] \tau_u < \left[ (.9") \times t \right] \sigma_u$$
$$d < t \frac{\sigma_u}{\tau_u}$$

or  $d < 2 t$

since the ultimate tensile strength ( $\sigma_u$ ) of 6061-T6 aluminum is approximately twice its ultimate shear strength ( $\tau_u$ ). Using a factor of safety of 2 to insure failure in shear, a cut offset distance

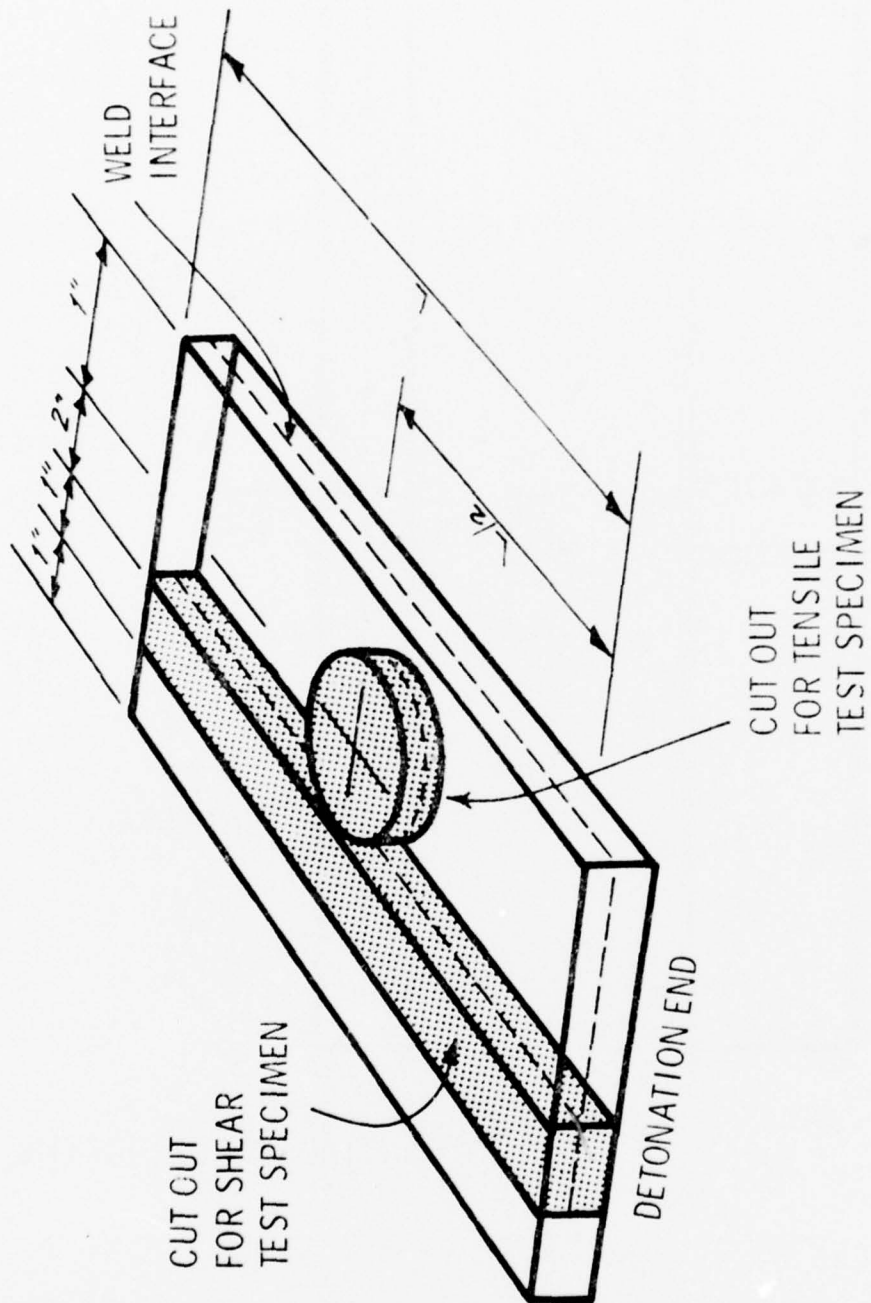
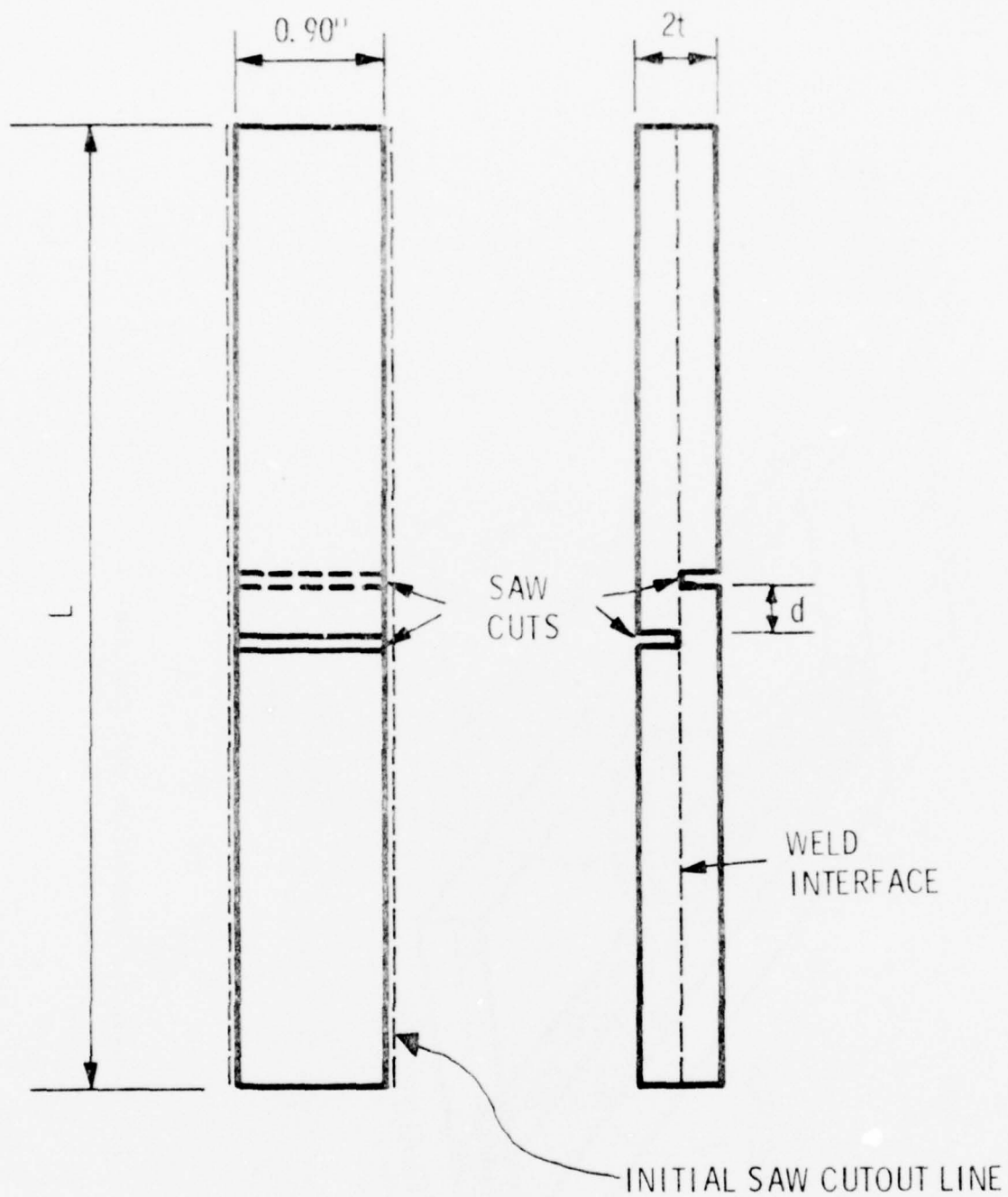


Figure 30. Pattern for Destructive Test Specimens



-108-

Figure 31 Early Shear Test Specimen Design

-108-



$d = t$  was normally used.

During the initial shear testing of steel specimens, however, it became obvious that an alternate test technique was necessary. The steel specimens were cocking considerably prior to failure due to the unwanted presence of major bending stresses. Such a condition invalidated the test failure as one in shear alone.

A search of related ASTM publications resulted in the replacement of the tension-shear test with the lug shear test described in ASTM-A264-44T. Using the guidance given in this standard, the shear test specimen mount and specimen designs shown in Figures 32 through 34 were conceived and adopted for use. These were most successful. In practically every case, the machinist could easily detect the interface position as the lug depth was being developed.

c. Tensile Strength Evaluation

At the beginning of this study, little reference to tensile bond strength (force applied normal to interface) or the means of measuring it could be found in the literature. Instead, great dependence was placed upon tension-shear test results. Following the suggestions contained in the literature (Wittman, 1967), the tensile test arrangement shown in Figure 35 was adopted and used in testing a considerable part of the parallel aluminum plate weld test sequence. As the test program progressed, however, several test deficiencies became obvious. First, the tensile stresses being transmitted through the adhesive were not uniform. Consequently, even though the adhesive used had an unusually high tensile strength ( $\approx 12,500$  psi) many adhesive failures occurred, which initiated in the center region

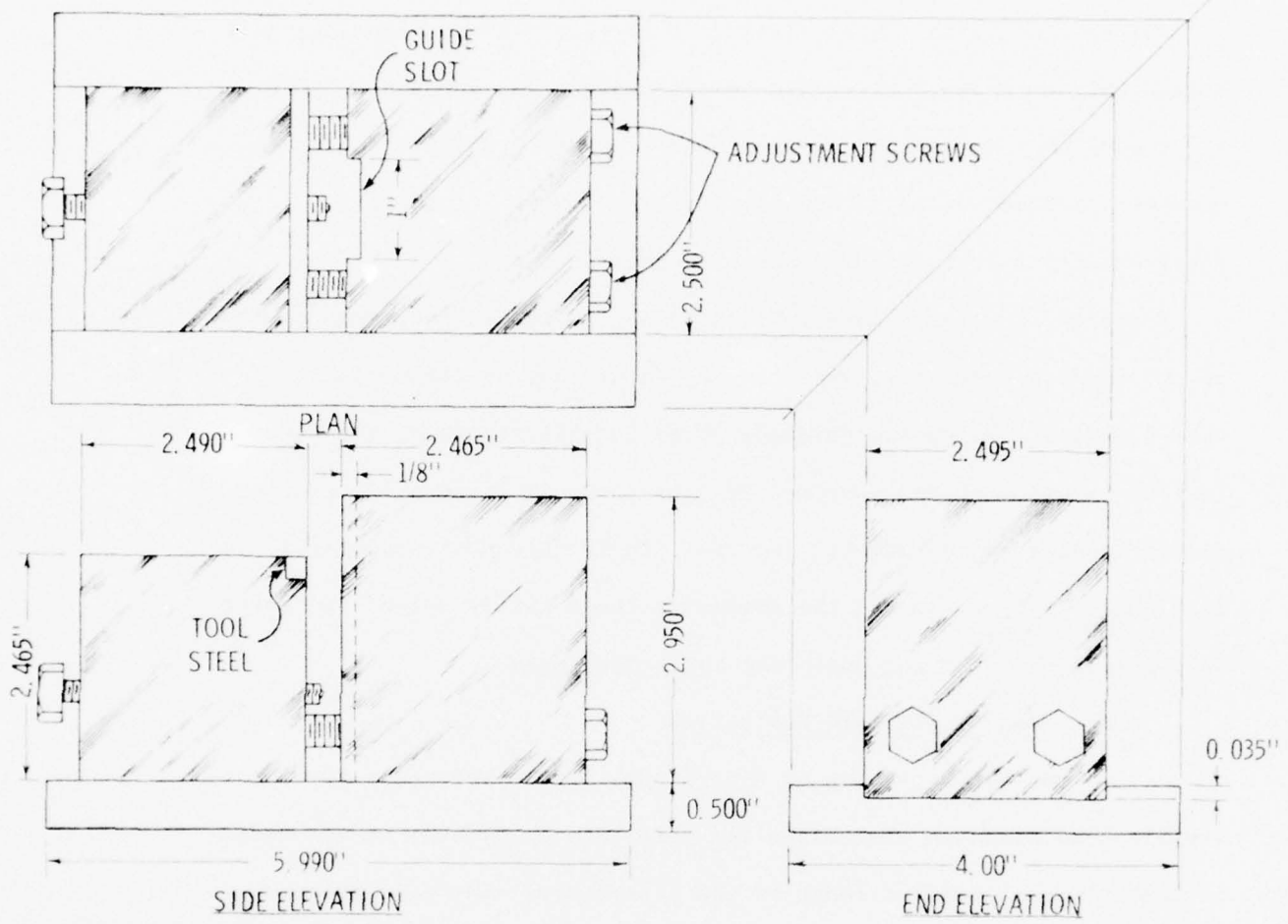


Figure 32 Lug Shear Test Device

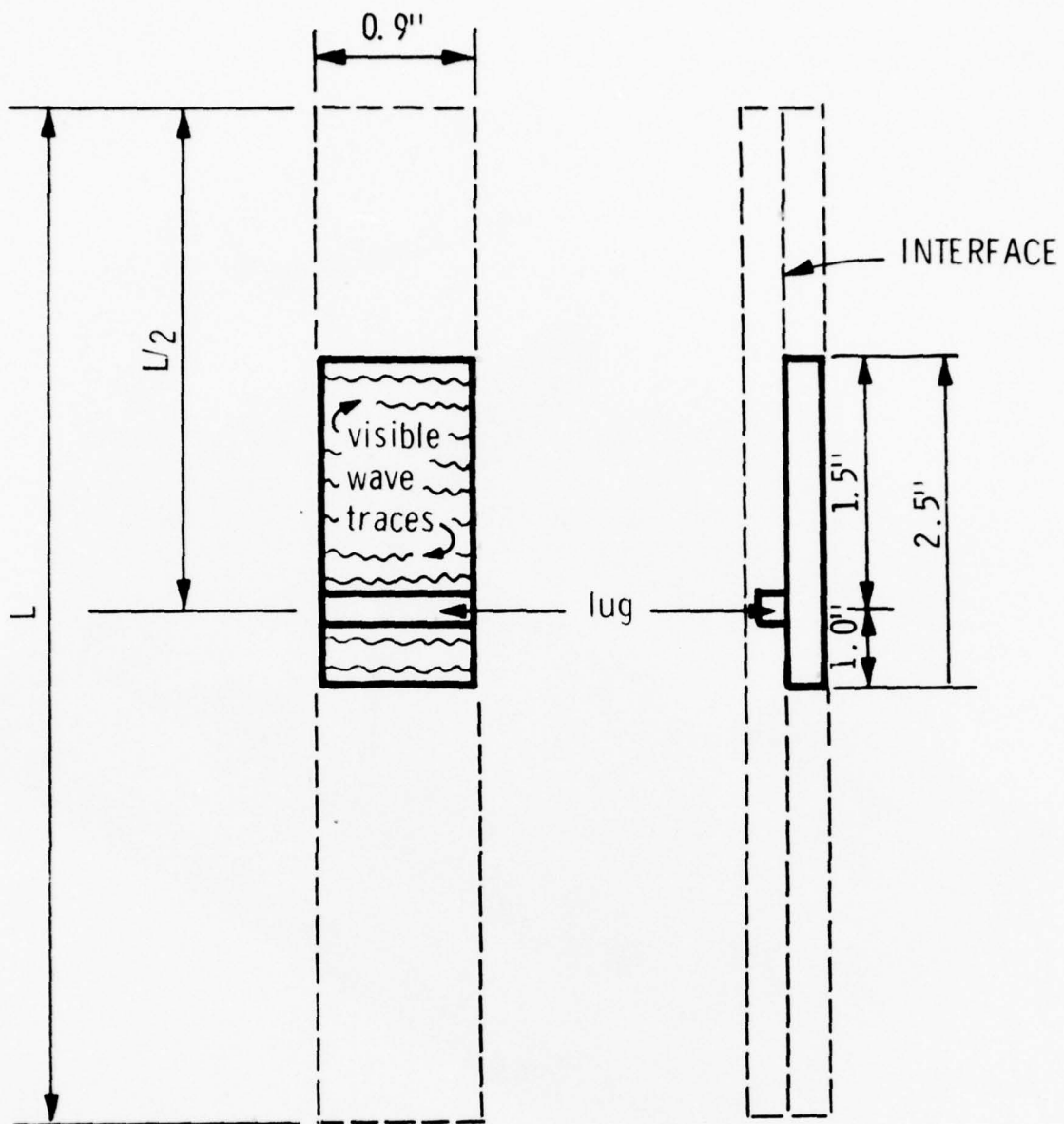


Figure 33 Final Shear Test Specimen Design

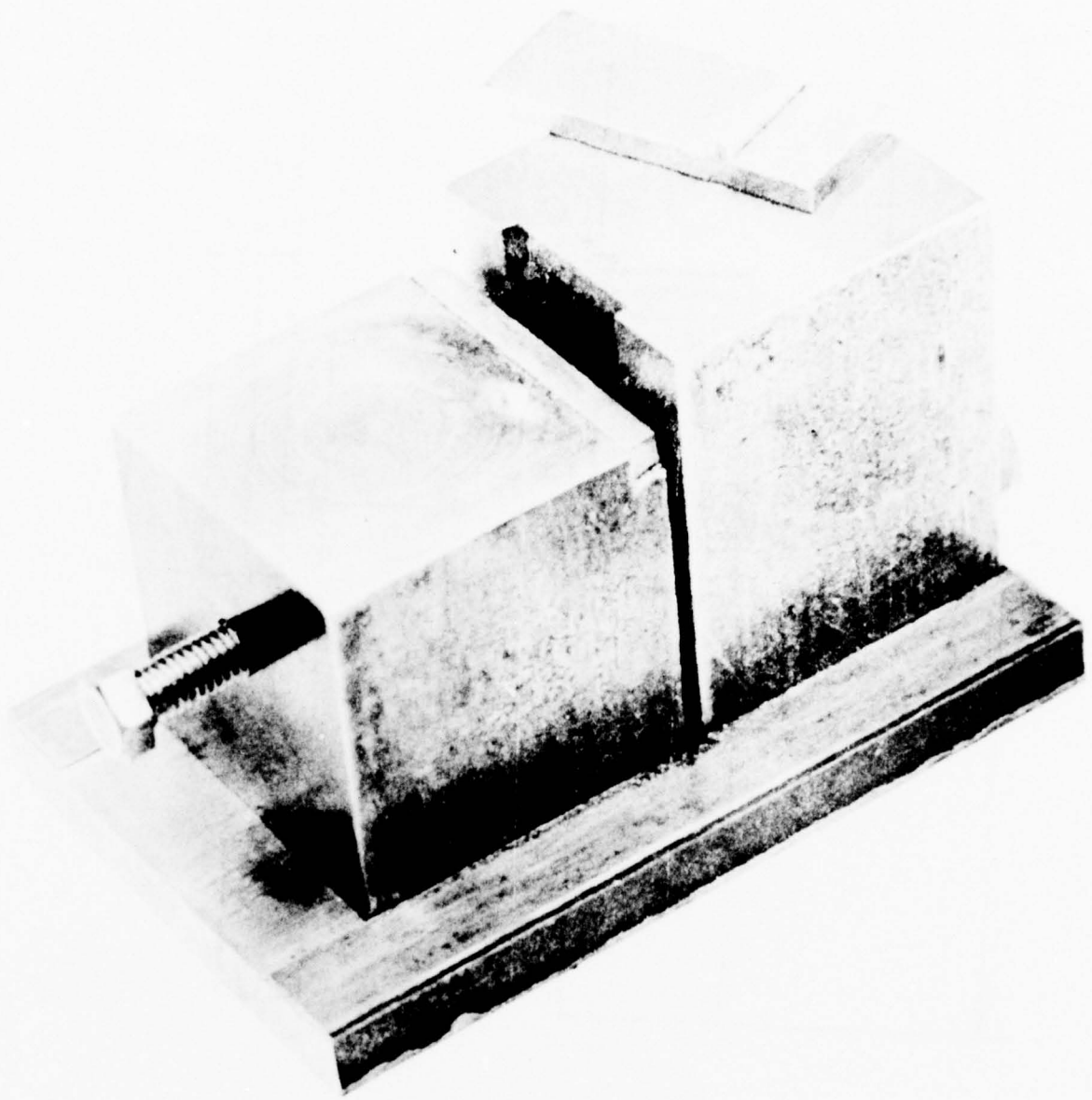


Figure 34 Final Shear Test Specimen and Specimen Mount

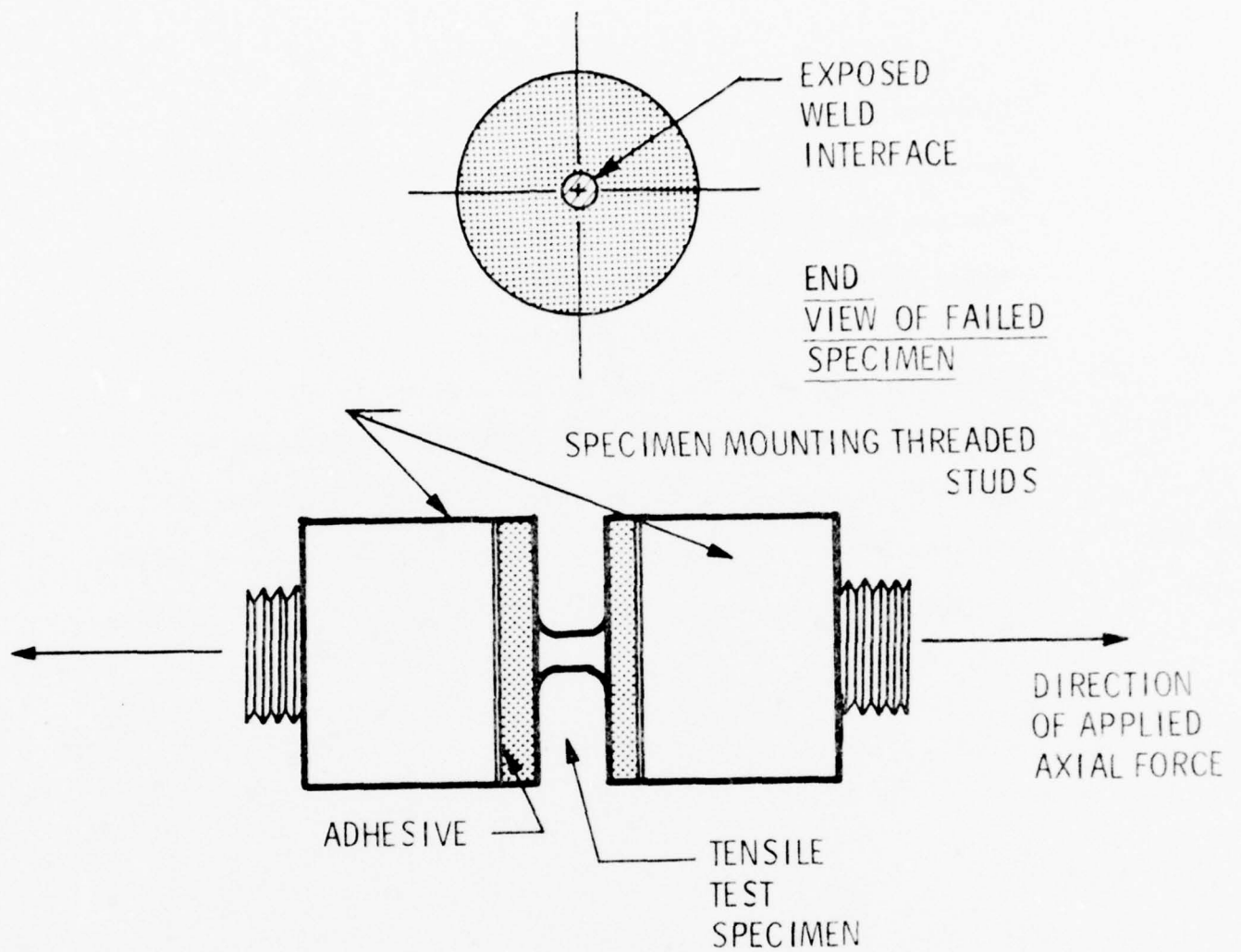


Figure 35 Early Tensile Test Specimen and Specimen Mount



in a tensile mode, transitioning to subsequent peeling out to the test coupon's perimeter. Second, the weld interface failure area was very small allowing small occasional bond imperfections to unduly influence test results. Third, force alignment was critical. As a result of this unfavorable evaluation, a tensile test arrangement first used at Du Pont was investigated and found to be outstanding for weld tensile strength evaluation. The design of specimen and specimen mount are shown in Figures 36 through 39. The tensile test specimen mount can accommodate specimens of various interface areas and outer diameters through the use of a transition ring insert.

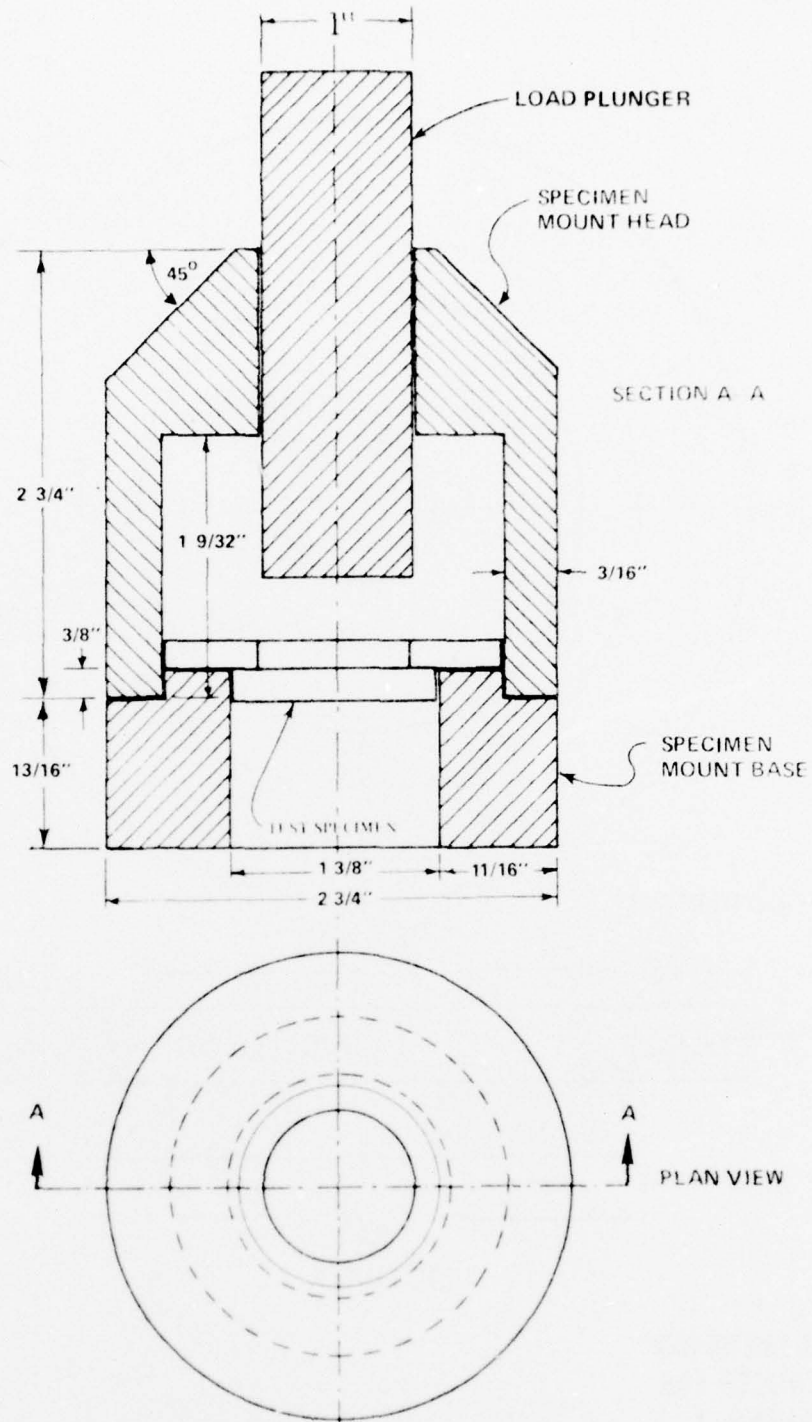
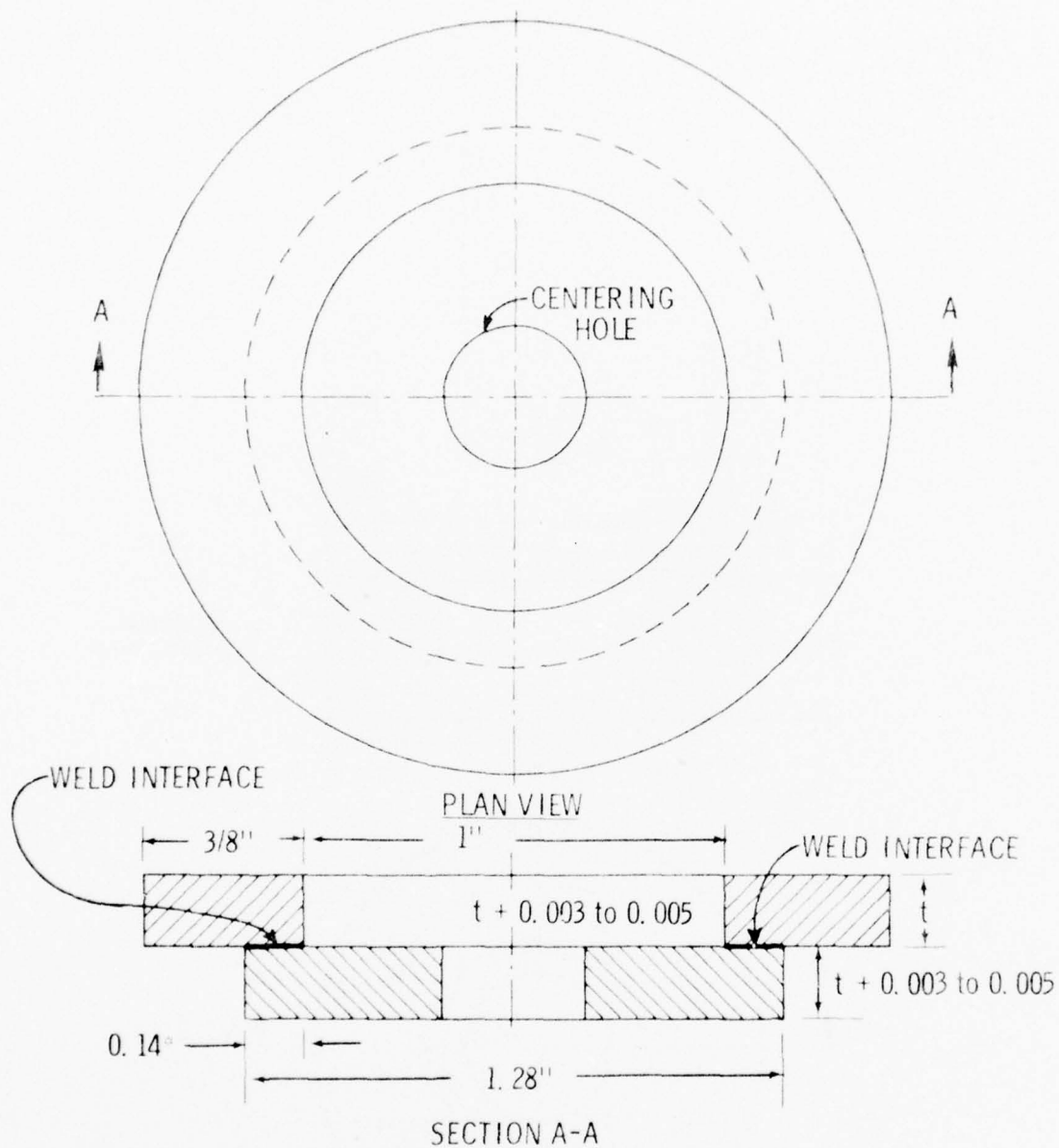


Figure 36 Final Tensile Test Specimen Mount



\* THIS DIMENSION  
IS REDUCED FOR  
THICKNESS,  $t$ ,  
LESS THAN  $3/16"$ .

Figure 37. Final Tensile Test Specimen

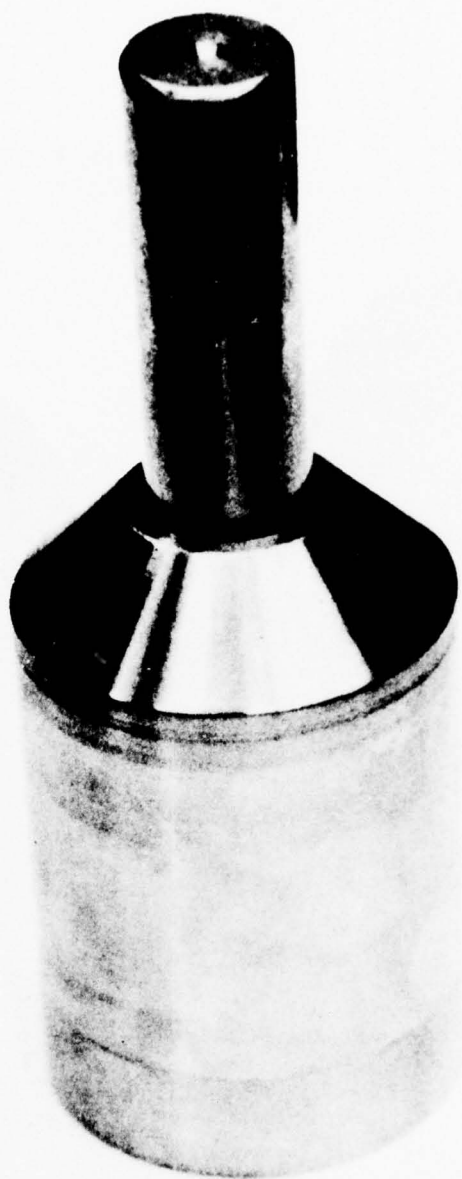
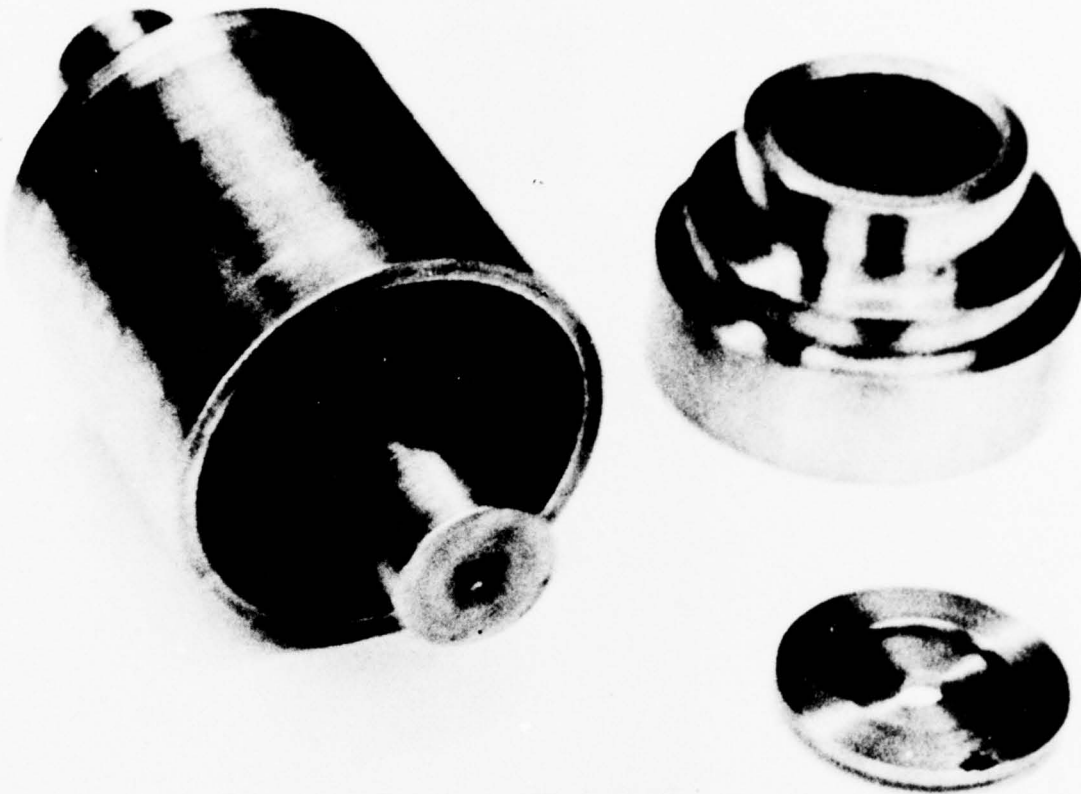


Figure 38 Tensile Test Specimen Mount

SPECIMEN MOUNT  
HEAD

SPECIMEN MOUNT  
BASE



TENSILE TEST  
SPECIMEN

Figure 39 Tensile Test Specimen and Specimen Mount



### III. ANALYSES

#### A. Strength Variation with Position Along Weld and Explosive Loading

There has been a recurring reliance on theoretical models limited to considerations of steady fluid flow which do not permit proper consideration of several aspects of the welding process including starting transients and boundary conditions. In order to demonstrate that these latter two aspects significantly influence the welding response, a parallel plate specimen 24 inches long was prepared using 1/4-inch thick, 6061-T6 aluminum plate stock. Both plates, the flyer and the base plates, were 6 inches wide and positioned with a constant 0.125 inch ( $t/2$ ) standoff. Using earlier aluminum parallel plate parametric data, an optimum explosive loading of  $1.2 \text{ grams/cm}^2$  of dynamite was selected for use. Subsequent to welding, tensile test specimens were taken at stations 1 inch on center along the length of weld (Figure 40). Shear specimens were taken from the plate area immediately adjacent to the line of tensile test specimens. Metallographic specimens were taken from the regions between the tensile test specimens as shown in the same figure. The results of the destructive tensile and shear tests are shown in Figure 41a. As shown, the indicated strengths were fairly uniform except for two significant differences. These were the two strength reductions occurring approximately 6 and 21 inches from the detonation end. Conceivably these variations were due to differences in the local states of stress as influenced by material properties, specimen boundary conditions, and location. The necessity for optimizing welding parameters is shown in

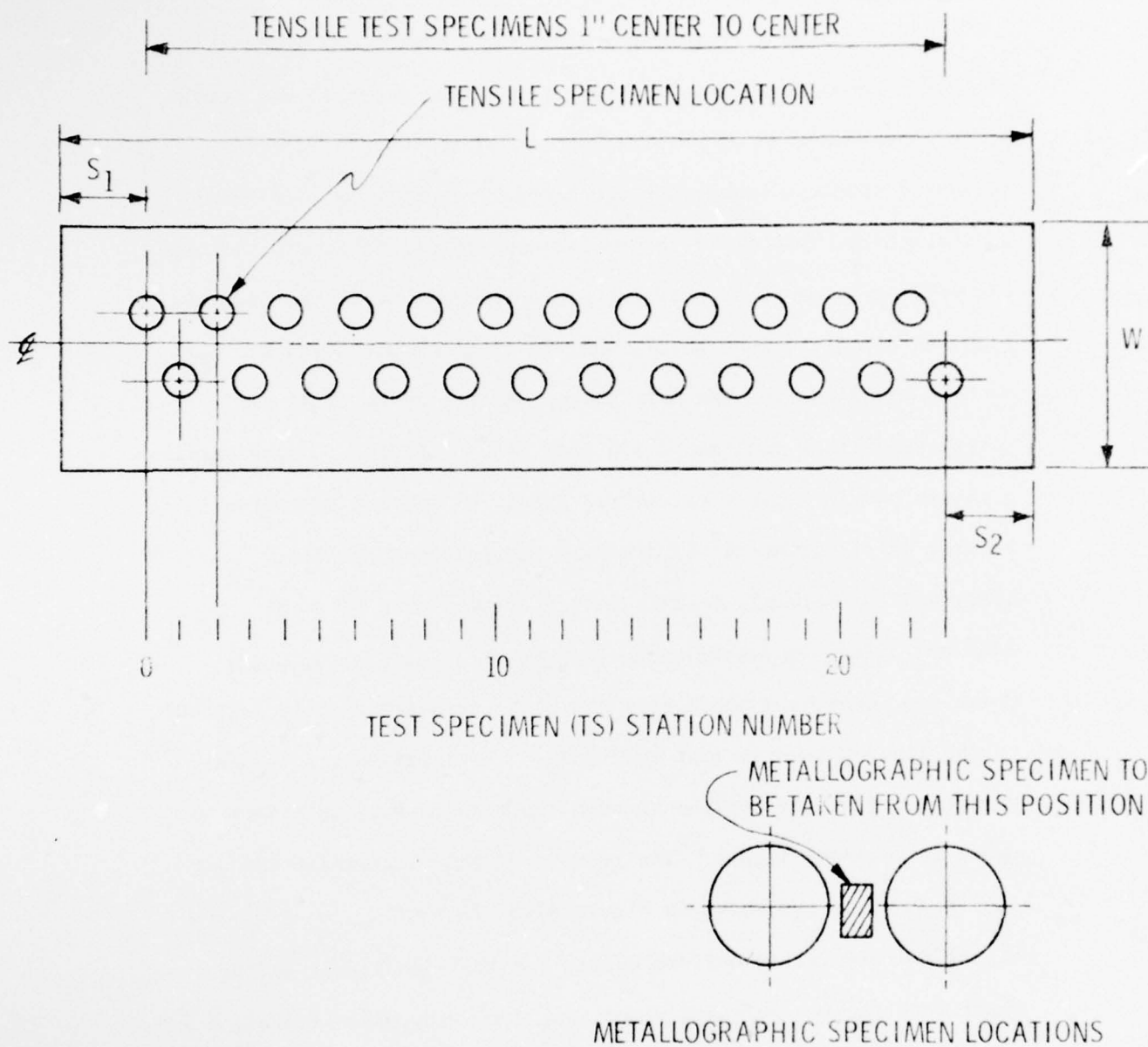


Figure 40 Length of Weld Test Specimen Arrangements

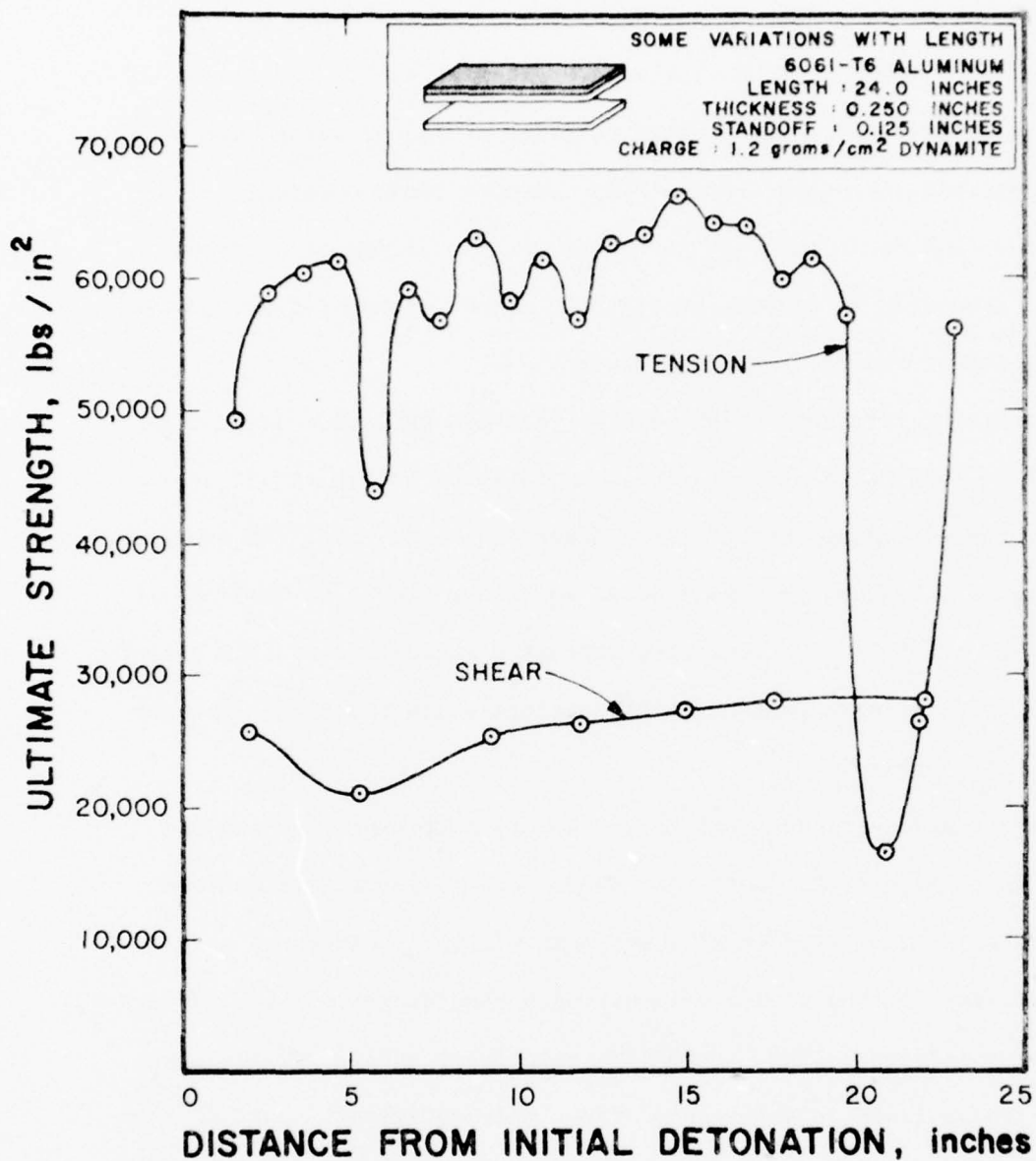


Figure 41a. Variations of Strength with Length of Weld

Figure 41b. The only input parameter variation was in the choice of explosive load level; the greater quantity of  $1.5 \text{ grams/cm}^2$  was used. The resulting strengths are superimposed upon those obtained in the previous case for comparison purposes. As the figure illustrates, a marked reduction in tensile strength occurred accompanied by, however, a very slight change in shear strength.

A related illustration of welding response variation using a 24 inch long inclined plate weld specimen is shown in Figure 42. As noted, the same plate material and dimensions were used. An explosive loading of  $1.2 \text{ grams/cm}^2$  was applied while the plate was inclined at an angle of  $1^{\circ}50'$ . The resulting strengths follow a different pattern; the tensile strength remains fairly uniform while the shear strength varies noticeably.

Weld tensile strength was found to vary with explosive loading as shown in Figure 43. Note that there is a rapid transition from no weld to optimum weld tensile strength within a very short range of explosive loadings. The weld strength then decreases with increased explosive loading. Thus, there is a relatively narrow optimum range of explosive loads in which weld strength is optimized. This phenomenon is discussed in detail in Section F of this chapter (Chapter III).

#### B. Shear Strength as Related to Direction of Shear Application

In mathematically formulating a description of the welding phenomenon, it was necessary to know whether the direction of applied shear influenced the apparent shear strength. In particular, it was desired to determine if the resistance to relative motion of the bonded plates was greater when the motion was attempted across the ridges

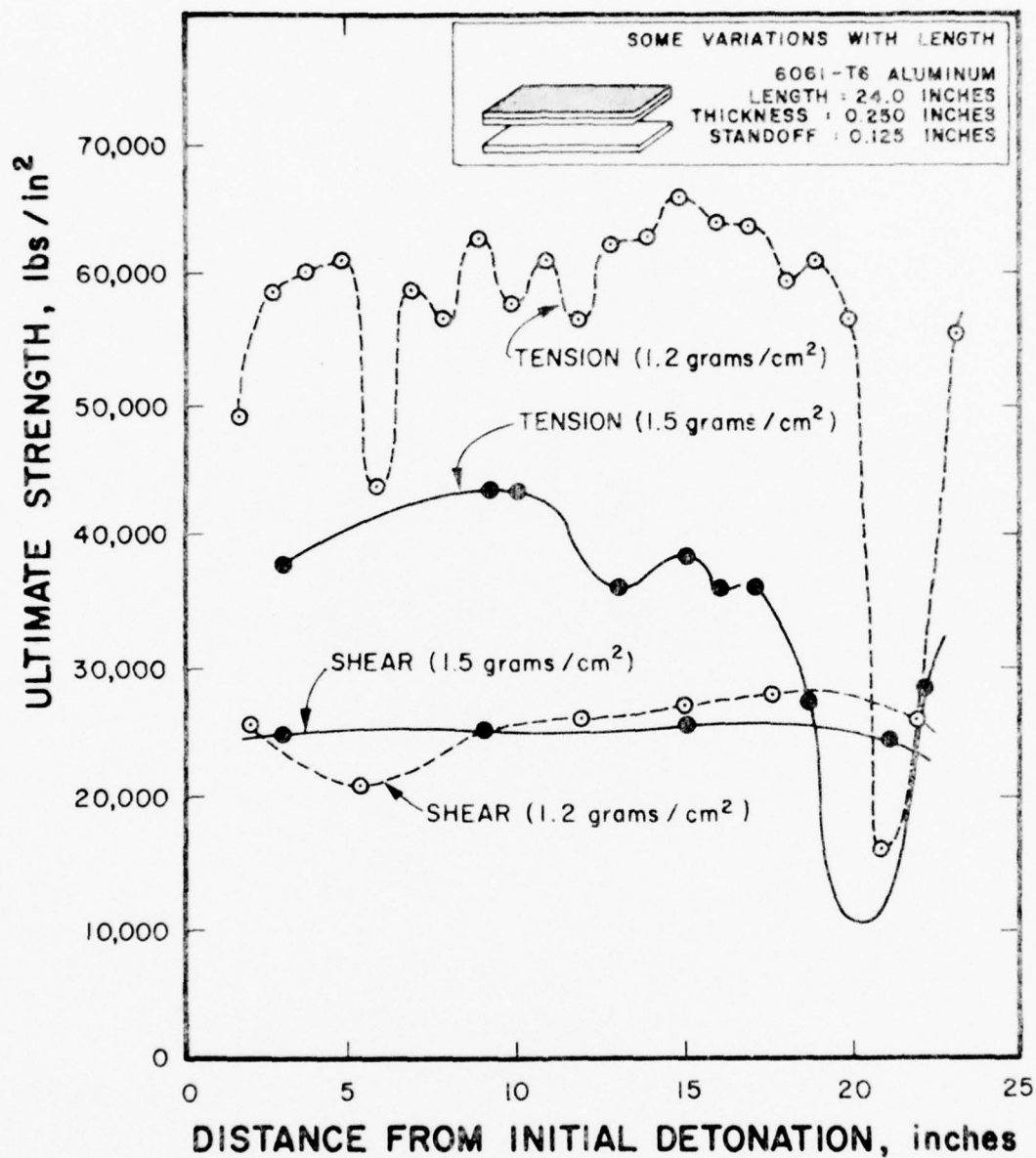


Figure 41b. Variations of Strength with Length of Weld



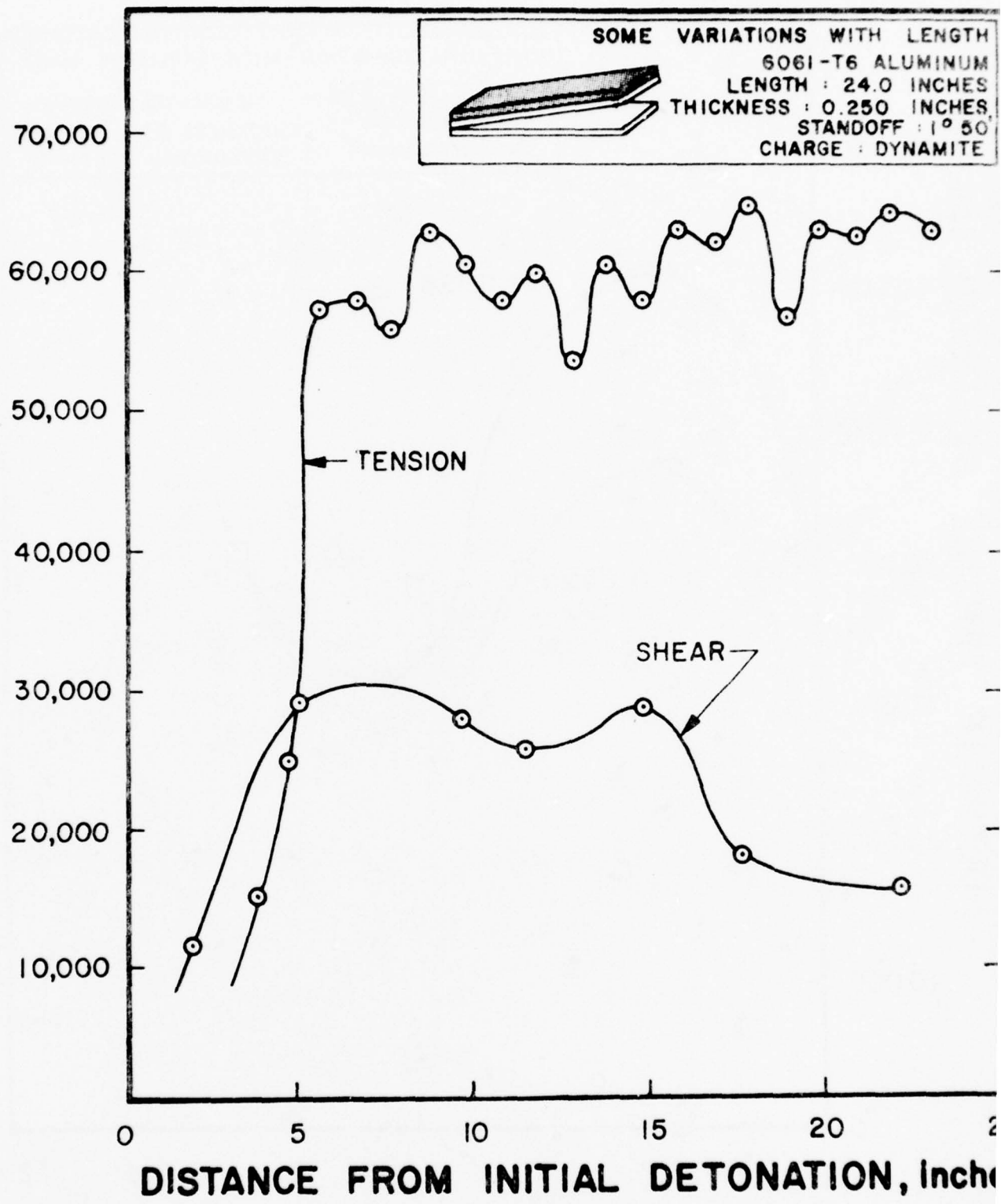


Figure 42. Variations of Strength with Length of Weld: Inclined Aluminum Plates

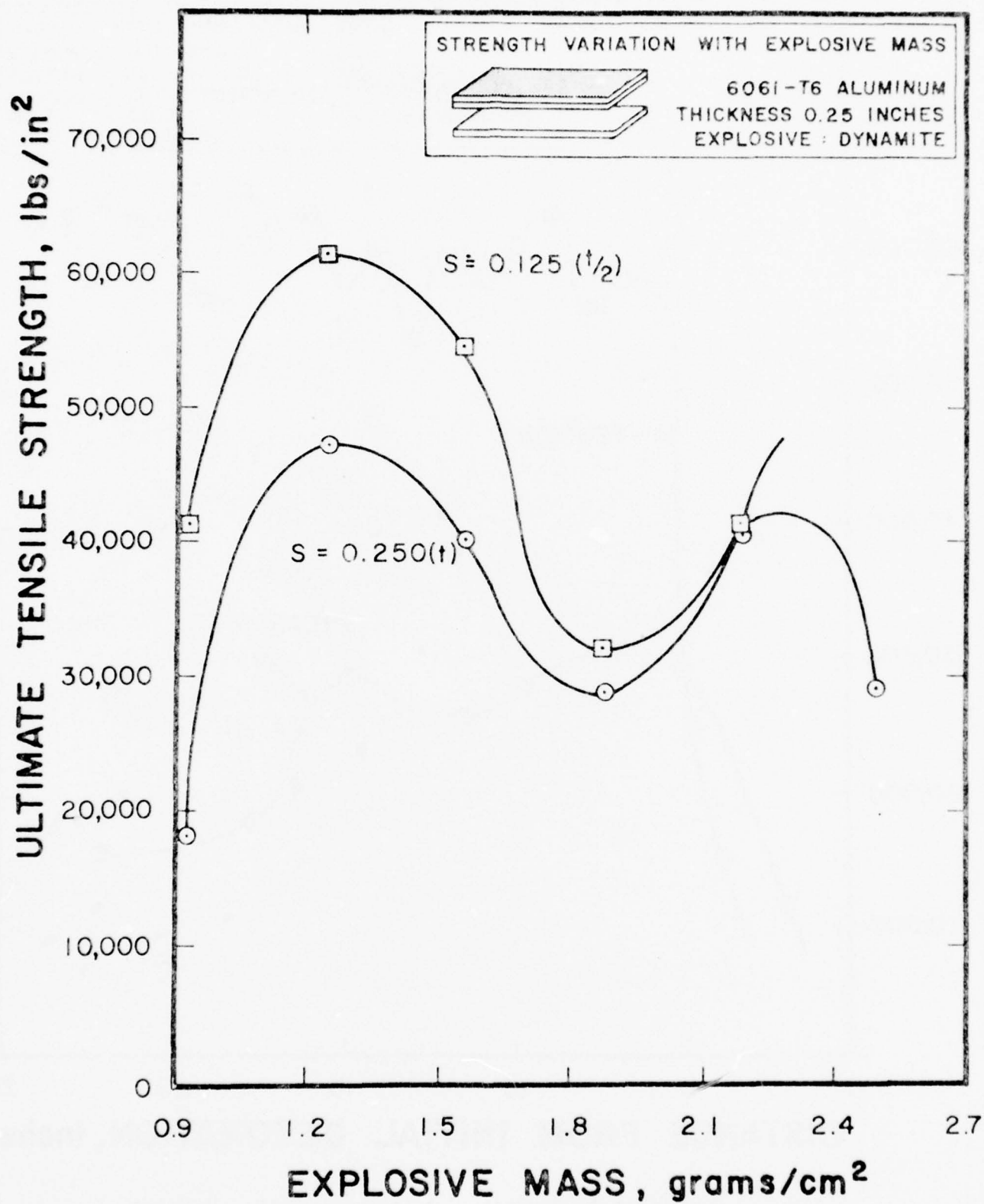


Figure 43. Tensile Strength Versus Explosive Loading

of the wave formation. The resulting experimental investigation involved the welding of aluminum parallel plate weld specimens 0.188 inches thick. Three identical specimen arrangements were welded for each of five explosive loadings: 1.55, 1.86, 2.17, 2.48, and 2.79 grams/cm<sup>2</sup> of Red Cross Extra dynamite.

Subsequent to welding, a pair of mutually orthogonal shear test specimens were taken from the center region of the plate specimens.

One was oriented so that the shearing force would be applied in the direction of wave formation. The ultimate shear strengths measured in subsequent tests are recorded in Table 14 and their average values plotted in Figure 44. According to these results, the shear strengths do not differ in these two orthogonal directions. This observation strongly suggests that the weld shear strength in the plane of the interface is independent of direction.

#### C. Variation of Wavelength

The wavelength variation with position along the weld for the two parallel plate cases is shown in Figure 45. These quantities were scaled from the numerous photomicrographs of the metallographic specimens. Two notable features are apparent. First, wavelengths are greater for the higher explosive loading. Second, as the figure shows, a deformation wave apparently does not exist in the 5 to 7 inch distance range for the  $1.2 \text{ gram/cm}^2$  explosive loading case. However, a substantial degree of bond was developed in this region.

The large accumulation of aluminum parallel plate data was used to investigate relationships between wavelength and strength. By combining the explosive mass versus strength data and the wavelength variation data presented in Figure 29, the relationship between wavelength and bond strength shown in Figure 46 was obtained. This analysis indicates that there is no apparent functional relationship between wavelength and bond strength, but the data show appreciable scatter.

#### D. Finite Element Model

##### 1. Basic Model

Table 14 Shear Strength Variation with Shear Direction

Explosive Loading Grams/CM <sup>2</sup>	Shear Strength (Lb/In <sup>2</sup> )	
	Parallel to Wave Direction	Transverse to Wave Direction
1.55	26,515 7,727 <u>26,970</u> 20,404 Ave.	23,359 9,160 <u>27,480</u> 20,000 Ave.
1.86	23,300 23,939 30,303 <u>25,837</u> Ave.	26,288 25,152 27,576 <u>26,339</u> Ave.
2.17	27,121 22,500 27,424 <u>25,682</u> Ave.	28,485 25,909 26,515 <u>26,970</u> Ave.
2.48	28,561 24,849 27,273 <u>26,894</u> Ave.	27,955 25,758 25,379 <u>26,364</u> Ave.
2.79	25,378 26,894 21,515 <u>24,596</u> Ave.	27,803 26,742 26,970 <u>27,172</u> Ave.



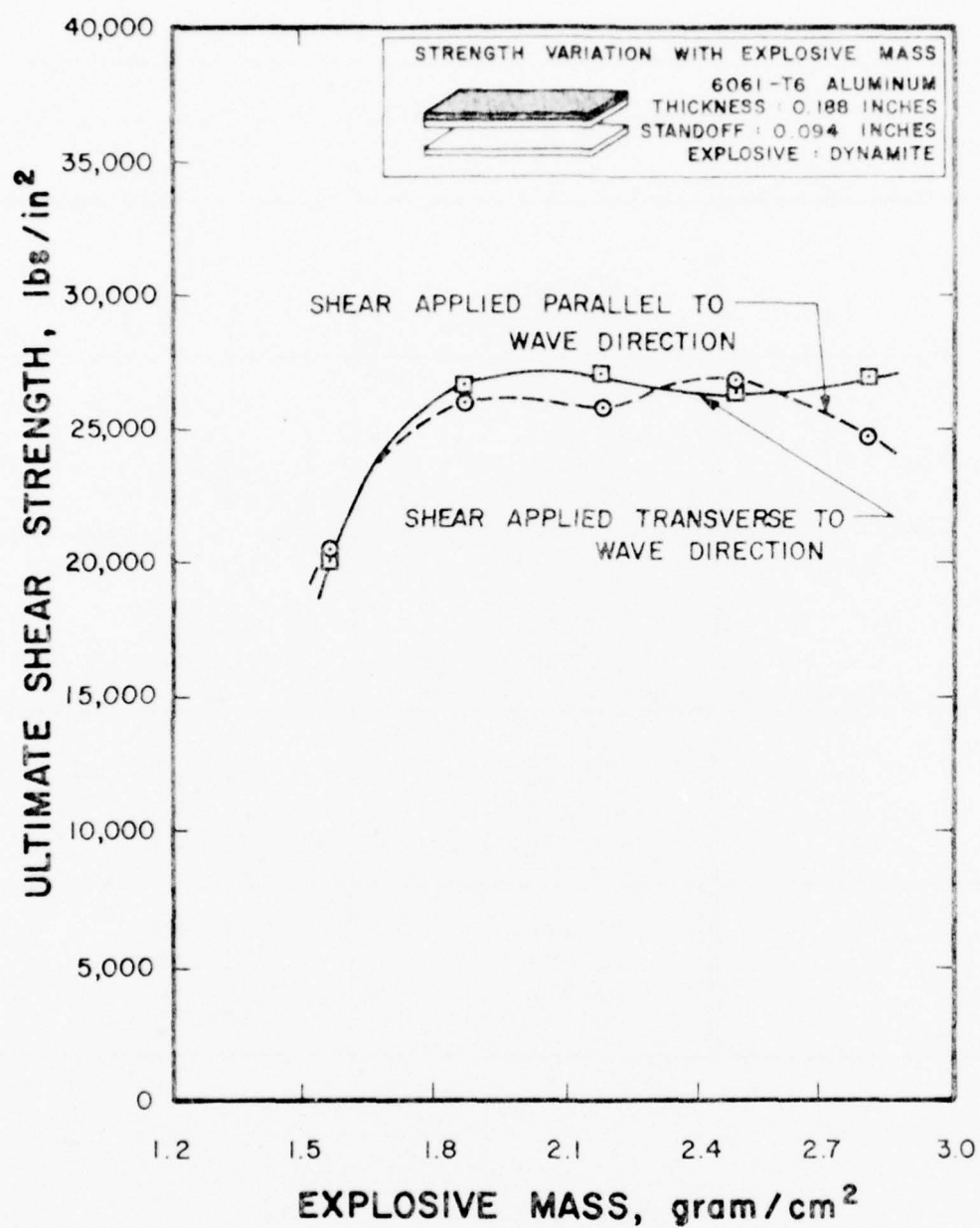


Figure 44 Shear Strength Variation with Shear Direction

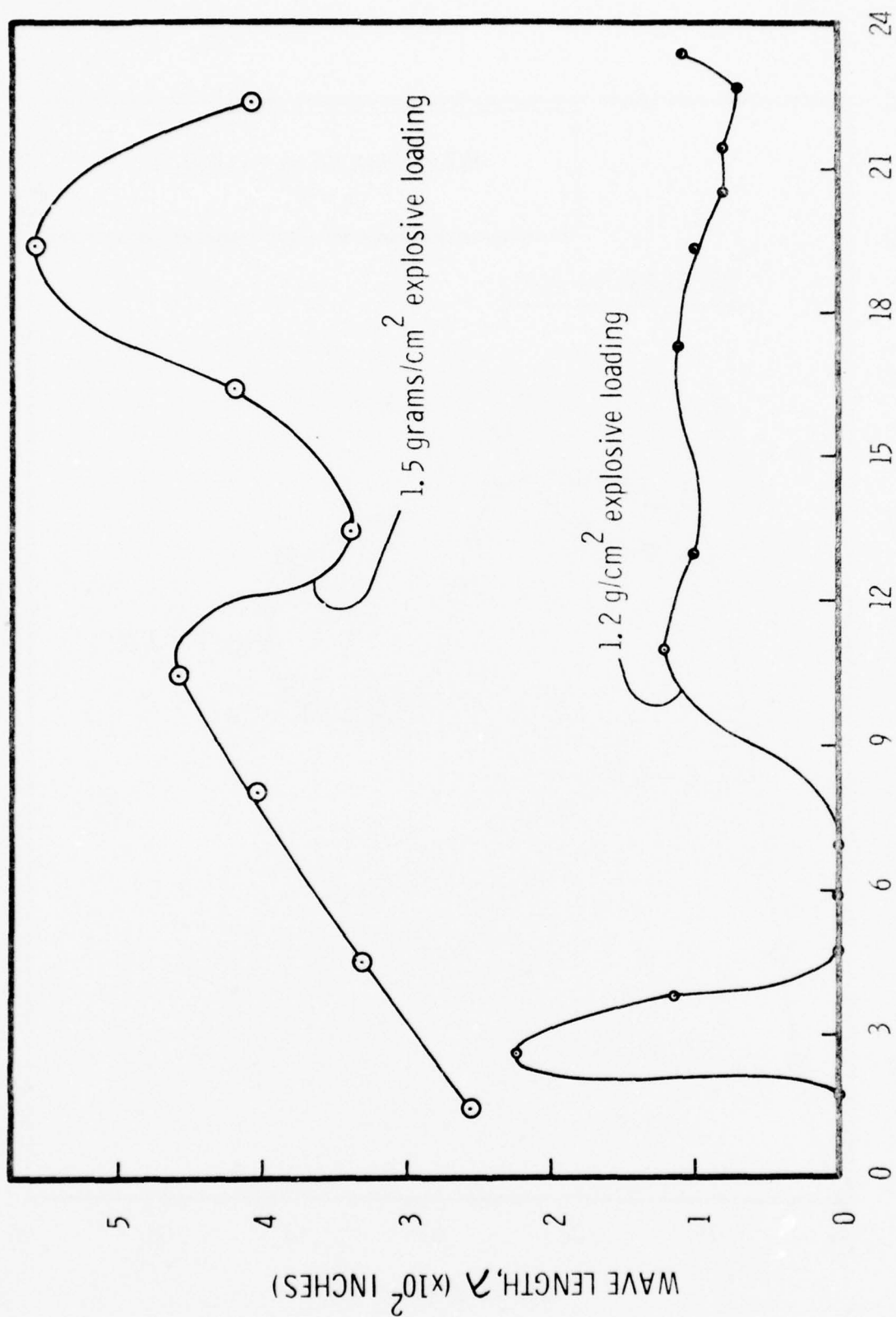


Figure 45 Variation of Wavelength with Length of Weld

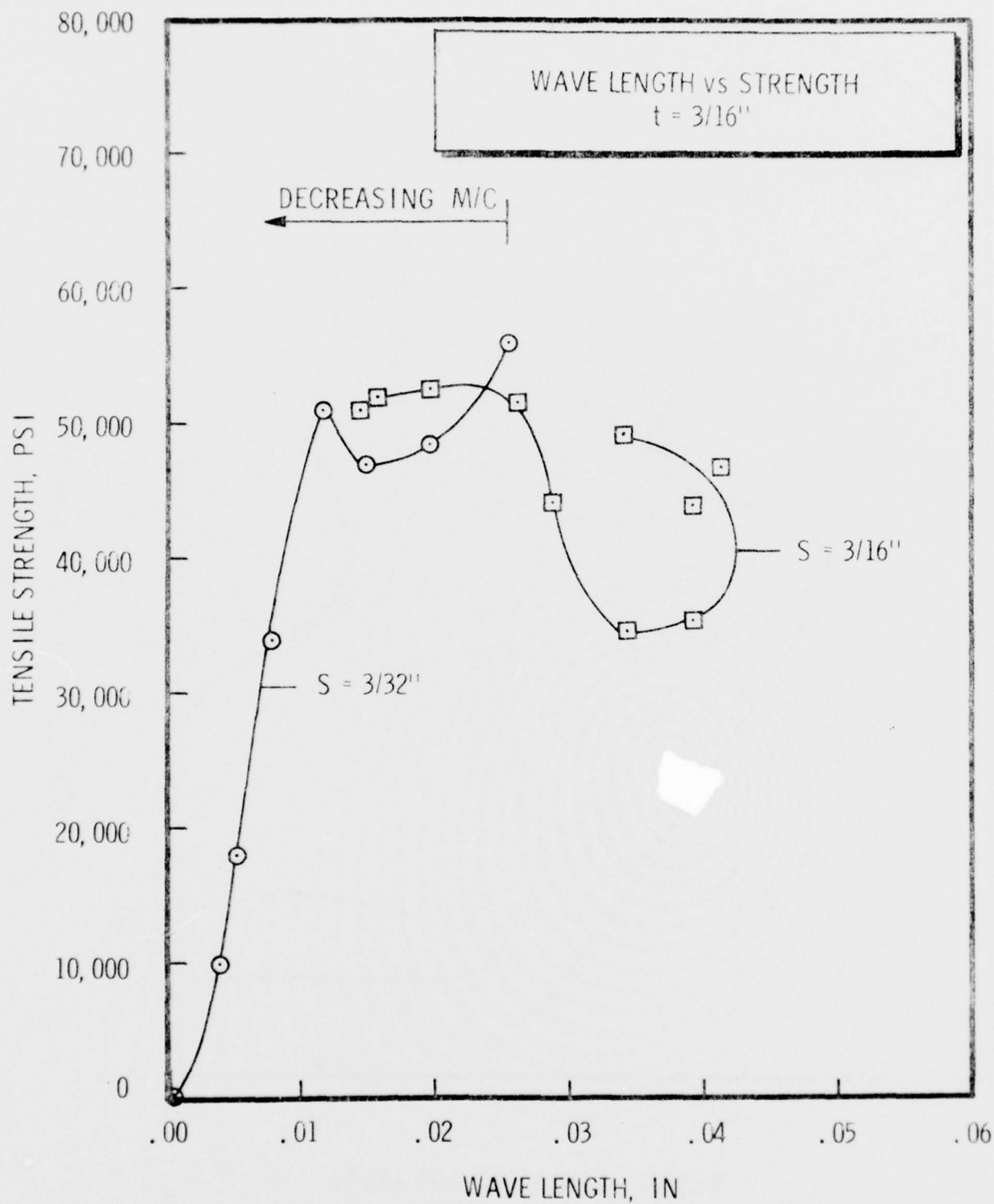


Figure 46 Interface Wavelength Variations with Tensile Strength

A finite element model of the impact of the two plates was developed under contract by Agbabian Associates. Since transient behavior was felt to be important, initially separated plates were considered. Although bond development was of primary concern, the details of bonding at the scale of the metallic lattice were ignored; instead, adhesion was assumed to develop upon contact and to persist thereafter. Under these assumptions, stress and strain histories in the vicinity of the interface could be obtained and compared with experimental evidence of bond development and bond strength. Details of the explosive acceleration of the plate were also simplified so that both parallel and inclined plate welding were represented by an inclined plate with uniform velocity. Representative plate velocities and inclinations were then obtained from experimental data.

The Vanishing Element Technique (VET) developed from the model requirements allowed use of the finite element technique to examine plate impact problems. As its name implies, the VET is based on the physical picture that air is expelled as the plates come together and the element representing the air thus "vanishes". The manner in which this is achieved is outlined in Figure 47. This subroutine was then combined with an existing inelastic step-by-step plane strain finite element program developed by AJA, to produce EXWELD, a program applicable to the study of plate impact and explosive impulse welding. The program was then improved to include dynamic material properties and flyer plate acceleration. The final program, known as WELD2, is included in Appendix E. In the main integration loop, the lengths of the one-dimensional air elements are examined after

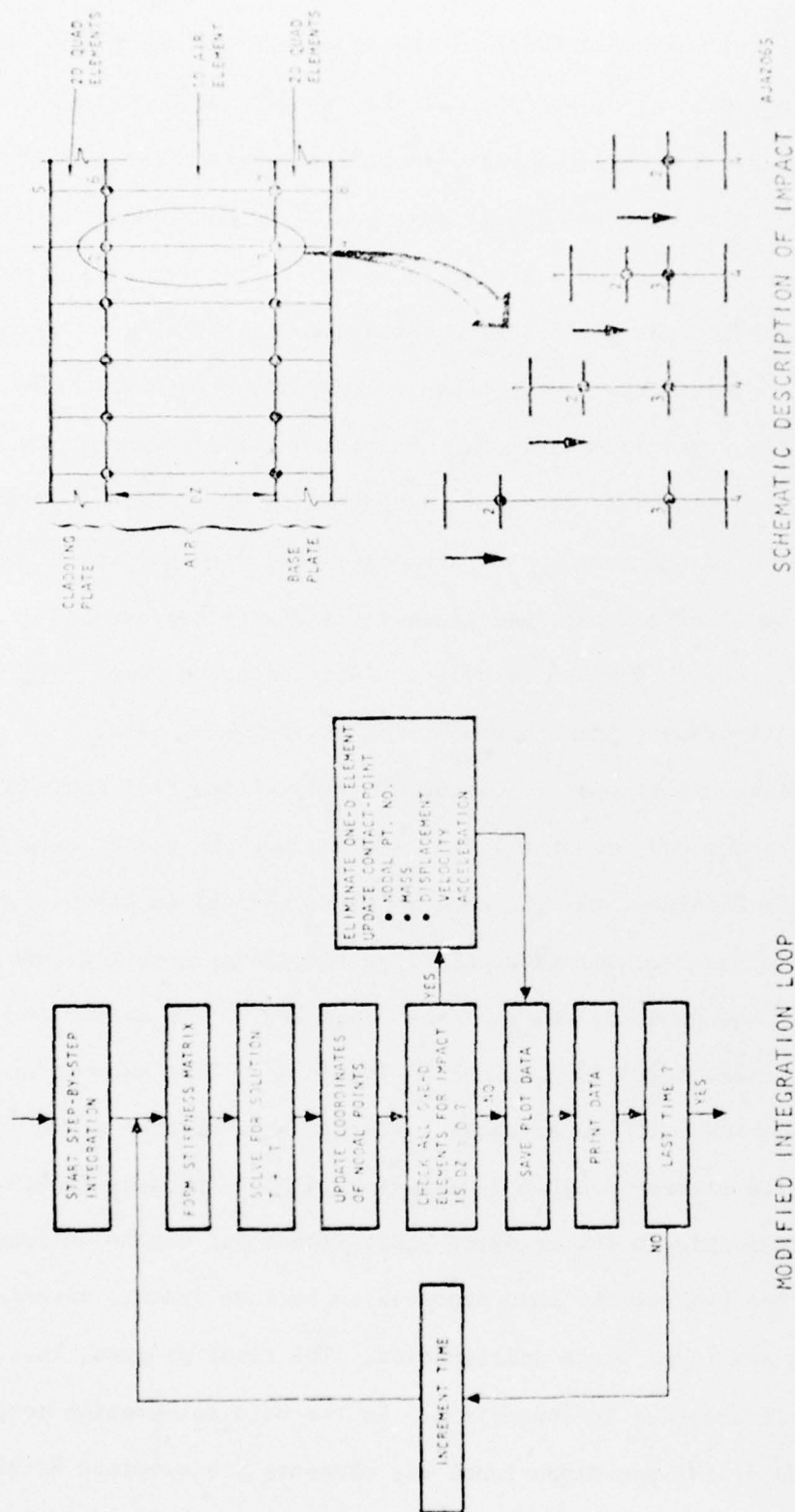


Figure 47. Vanishing Element Technique



each integration cycle (advance in time) to check for the occurrence of impact. (Impact is defined here to occur at the instant when the calculated length of the one-dimensional element first becomes negative or zero. When impact occurs, the nodal points defining the uppermost element in the bottom plate are renumbered in such a way that at the point of contact the lower plate shares a nodal point with the top plate (Point 2 in Figure 47, for example) after impact. The top and bottom plate elements are then connected and the impact force is transmitted directly to the lower plate element. The air element has, in this sense, vanished. Renumbering nodal points and elements in this manner changes the bandwidth of the system of equations, usually resulting in an increase. This disadvantage, however, can be minimized by a judicious choice of the original numbering system and can be eliminated altogether in most cases.

## 2. Constitutive Equations for Aluminum

After demonstrating that the finite element code with VET was capable of treating impact problems, efforts were directed toward modeling the mechanical properties of aluminum. The material property routines already incorporated in the basic finite element computer program allowed:

1. The bulk modulus to be defined as a function of the excess volumetric compression  $\mu = \rho/\rho_0 - 1$  where  $\rho$  = current density and  $\rho_0$  = initial density.
2. The shear modulus to be defined as a function of the current state of stress.

3. A yield criterion to be defined as a function of the first stress invariant ( $J_1$ ) and of the second invariant of deviator stress ( $J'_2$ ).
4. Work- or strain-hardening rules to be incorporated.
5. Use of either the Prandtl-Reuss or plastic potential flow rules to relate stress and plastic strain when the yield criterion is satisfied.

Thermodynamic and strain rate effects were not accounted for:

The mechanical behavior attributed to aluminum is analogous to that of conventional models of elastic-plastic media. In the present model, however, the bulk modulus is a function of the excess compression  $\mu$ . The descriptions of the bulk modulus, shear modulus, yield criterion and flow rule for aluminum are detailed below.

#### Bulk Modulus:

The model bulk modulus is based on Bergmann's (1966A) hydrostatic compression data for pressures between 0 and 100 kb and on shock wave experiments for pressures up to 1 Mb (Bergmann, 1966B). The empirical fit to data for 24 ST Aluminum (Bergmann, 1966B)

$$P = A\mu + B\mu^2 + C\mu^3$$

$$= 765\mu + 1659\mu^2 + 428\mu^3 \text{ kb}^*$$

has been adopted and differentiated to obtain the bulk modulus

$$B(\mu) = \frac{dP}{d\mu} = 765 + 3318\mu + 1284\mu^2 \text{ kb}$$

$$* 1 \text{ bar} = 1 \frac{\text{dyne}}{\text{cm}^2} = 0.1 \text{ Pascal}$$

The hydrostat and bulk modulus are illustrated in Figure 48 for compression. They are considered valid for both loading and unloading in tension ( $\mu < 0$ ) or compression ( $\mu > 0$ ). An initial density of  $2.7 \text{ gm/cm}^3$  was assigned.

Shear Modulus:

Although some dependence of the shear modulus on pressure has been observed (Bergmann, 1966A), a constant shear modulus based on the zero stress values of the bulk modulus  $B_0$  and Poisson's ratio  $\nu_0$  and the linear theory of elasticity has been adopted. Thus

$$G = B_0 \left[ \frac{3(1 - 2\nu_0)}{2(1 + \nu_0)} \right] \quad (3)$$

with  $\nu_0 = 0.33$  and  $B_0 = 765 \text{ kb}$ , the shear modulus has the value

$$G = 287 \text{ kb} \quad (4)$$

By assuming a constant value of the shear modulus, a variable Poisson's ratio is introduced, which is related to excess compression or pressure through the bulk modulus:

$$\nu = \frac{1}{2} \left\{ 1 - \left[ \frac{3G}{3B(\mu) + G} \right] \right\} \quad (5)$$

and on shock wave experiments for pressures up to 1 Mb (Bergmann, 1966B).

The empirical fit to data for 24 ST Aluminum (Bergmann, 1966B).

$$P = A\mu + B\mu^2 + C\mu^3$$

$$= 765\mu + 1659\mu^2 + 428\mu^3 \text{ kb} \quad (1)$$

has been adopted and differentiated to obtain the bulk modulus

$$B(\mu) = \frac{dP}{d\mu} = 765 + 3318 |\mu| + 1284\mu^2 \text{ kb} \quad (2)$$

The hydrostat and bulk modulus are illustrated in Figure 48 for compression. They are considered valid for both loading and unloading in tension ( $\mu < 0$ ) or compression ( $\mu > 0$ ). An initial density of  $2.7 \text{ gm/cm}^3$  was assigned.

Shear Modulus:

Although some dependence of the shear modulus on pressure has been observed (Bergmann, 1966A), a constant shear modulus based on the zero stress values of the bulk modulus  $B_0$  and Poisson's ratio  $\nu_0$  and the linear theory of elasticity has been adopted. Thus

$$G = B_0 \cdot \frac{3(1 - 2\nu_0)}{2(1 + \nu_0)} \quad (3)$$

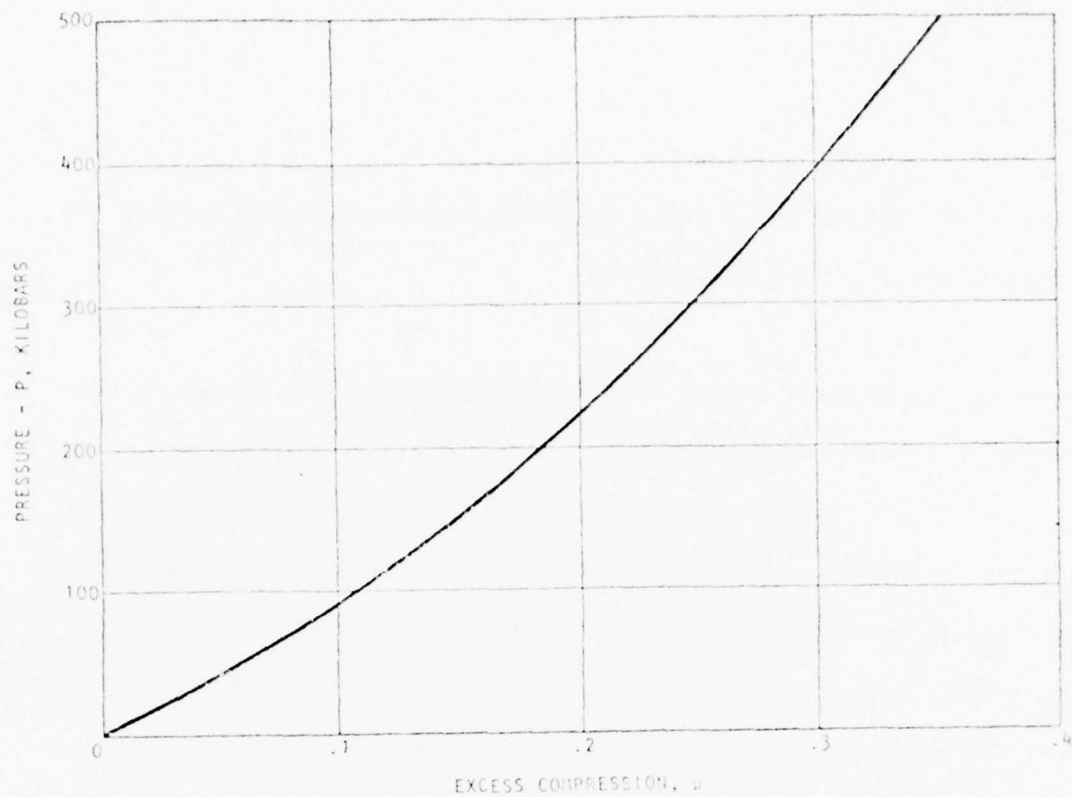
with  $\nu_0 = 0.33$  and  $B_0 = 765 \text{ kb}$ , the shear modulus has the value

$$G = 287 \text{ kb} \quad (4)$$

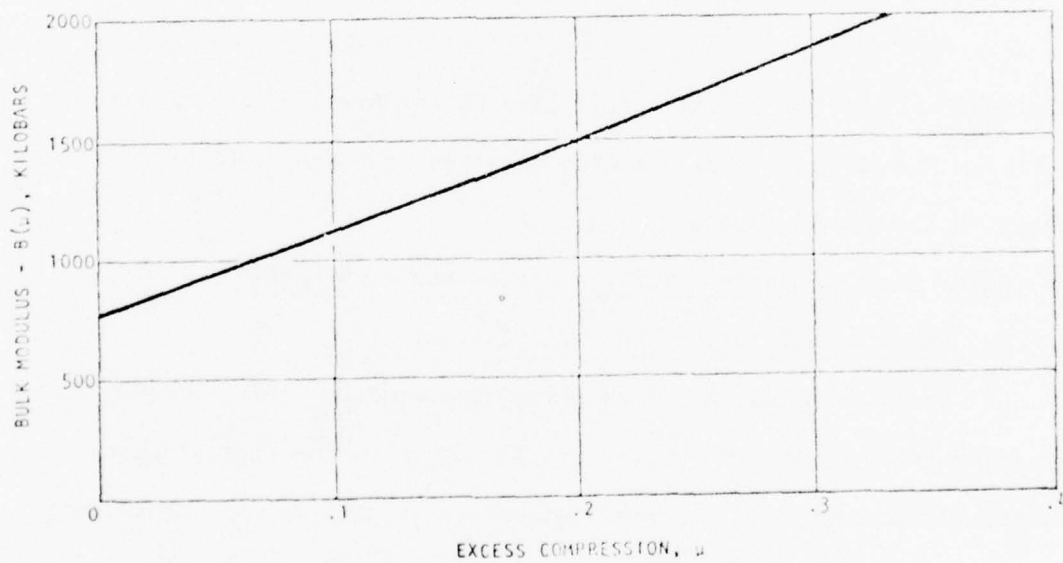
By assuming a constant value of the shear modulus, a variable Poisson's ratio is introduced whose dependence on excess compression or pressure indicated by that of the bulk modulus:

$$\nu = \frac{1}{2} \left[ 1 - \frac{3G}{3B(\mu) + G} \right] \quad (5)$$





(a) MODEL HYDROSTAT



(b) MODEL BULK MODULUS

Figure 48. Model Hydrostat and Bulk Modulus for 24 ST Aluminum



#### Yield Criterion:

The von Mises yield criterion has been adopted for the aluminum model and takes the form

$$f = J'_2 - \frac{\sigma_y^2}{3} > 0 \quad (6)$$

where  $\sigma_y$  is the yield stress in simple tension (and the assumed yield stress in simple compression).

Temperature and strain rate effects on the yield stress are not considered. The yield stress value obtained from static room temperature measurements for 24 ST aluminum,  $\sigma_y = 2.9 \text{ kb}$ , is used and the formulation of the plastic potential flow rule is used, although when the von Mises yield criterion is used the same results are obtained with the Prandtl-Reuss formulation.

Several runs of the WELD2 program were made using experimental data to determine appropriate flyer plate velocities and acceleration. Representative plots of the flyer plate bottom pressure, base plate top pressure and interface position obtained from WELD2 analyses are shown in Figures 49 through 51.

#### E. Analytical Simulation of Flyer Plate Dynamic Response

##### 1. Dynamic Equilibrium Model (Lindbergh, 1973)

Description of the flyer plate acceleration, velocity and position under explosive loading are essential to the understanding of the EIW process. As described elsewhere in this report, there is considerable evidence that bond strength is related to collision velocity. It is therefore desirable to be able to predict collision velocity for a given plate and explosive loading so that proper conditions may be selected for welding. One model which predicts acceleration,

BEST AVAILABLE COPY

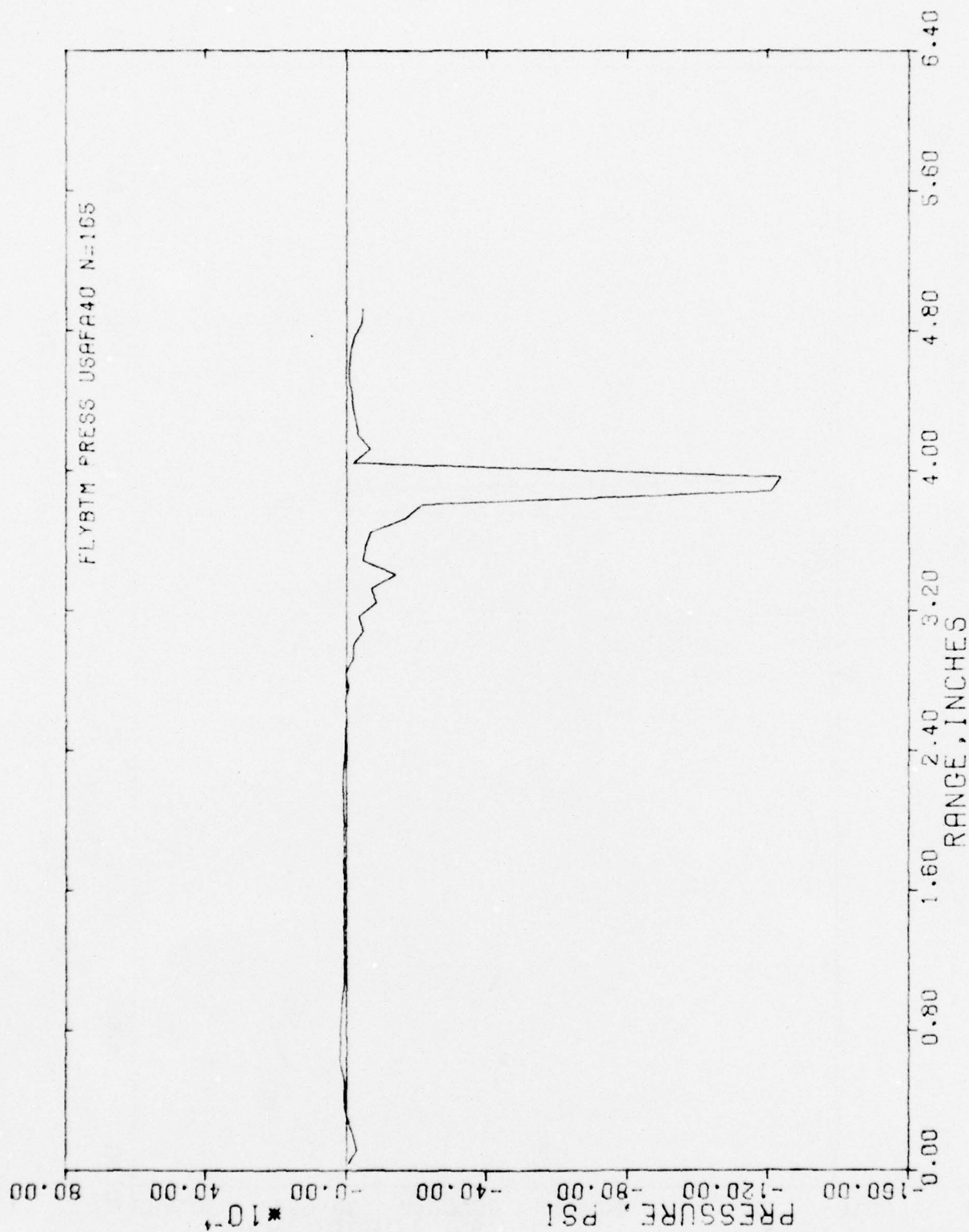


Figure 49 Flyer Plate Bottom Pressure by WELD2 Analysis

BEST AVAILABLE COPY

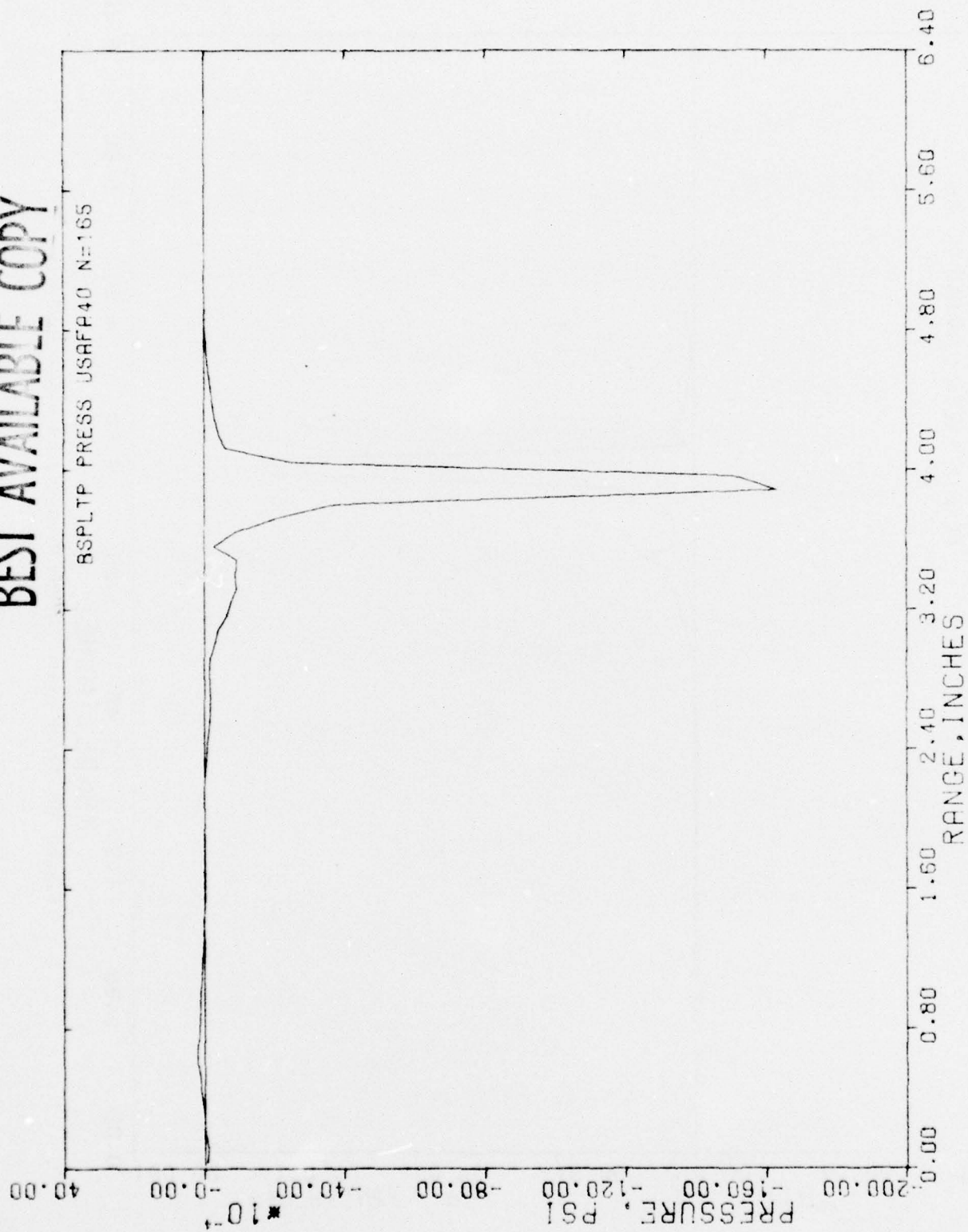


Figure 50 Base Plate Top Pressure by WELD2 Analysis

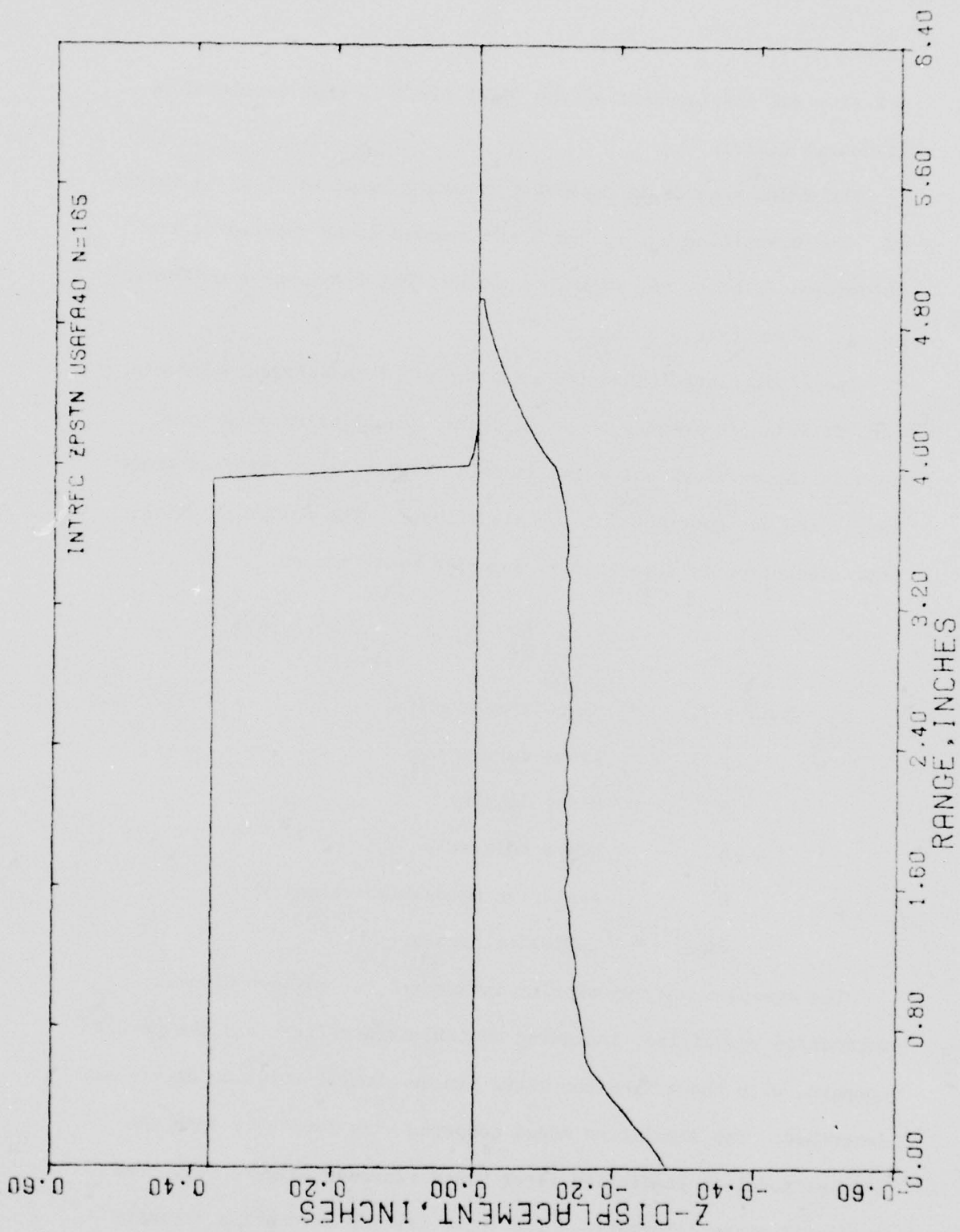


Figure 51 Interface Position by WELD2 Analysis



velocity and displacement of the flyer plate is that developed by Lindbergh (1973).

The model assumes an explosive pressure pulse as shown in Figure 52. The quantities  $p_0$ ,  $t_r$  and  $\Theta$  are assumed to be related to the detonation velocity,  $D$ , in such a manner that the impulse delivered to each element is a constant.

The flyer plate is modeled as a series of independent elements, each of which is assumed to be in dynamic equilibrium when acted upon by the pressure pulse and inertia (Figure 53). Internal plate forces are not considered to be significant. The following differential equation is developed to describe plate motion:

$$\ddot{y}(t) = \frac{1}{\rho h} \left( 1 - \frac{1}{2D^2} \dot{y}^2 \right) P(t)$$

where  $\ddot{y}(t)$  = plate acceleration

$\dot{y}$  = plate velocity

$\rho$  = plate density

$h$  = plate thickness

$D$  = explosive detonation velocity

$P(t)$  = explosive pressure

The equation was numerically integrated for various assumed detonation velocities, including variable velocities, and the results compared with those from the WELD2 finite element solution previously described. The simplified model compared very favorably with the complex model in predicting flyer plate response (Figure 54). The predicted plate deformations for three assumed detonation velocity profiles are shown in Figures 55 a, b and c.





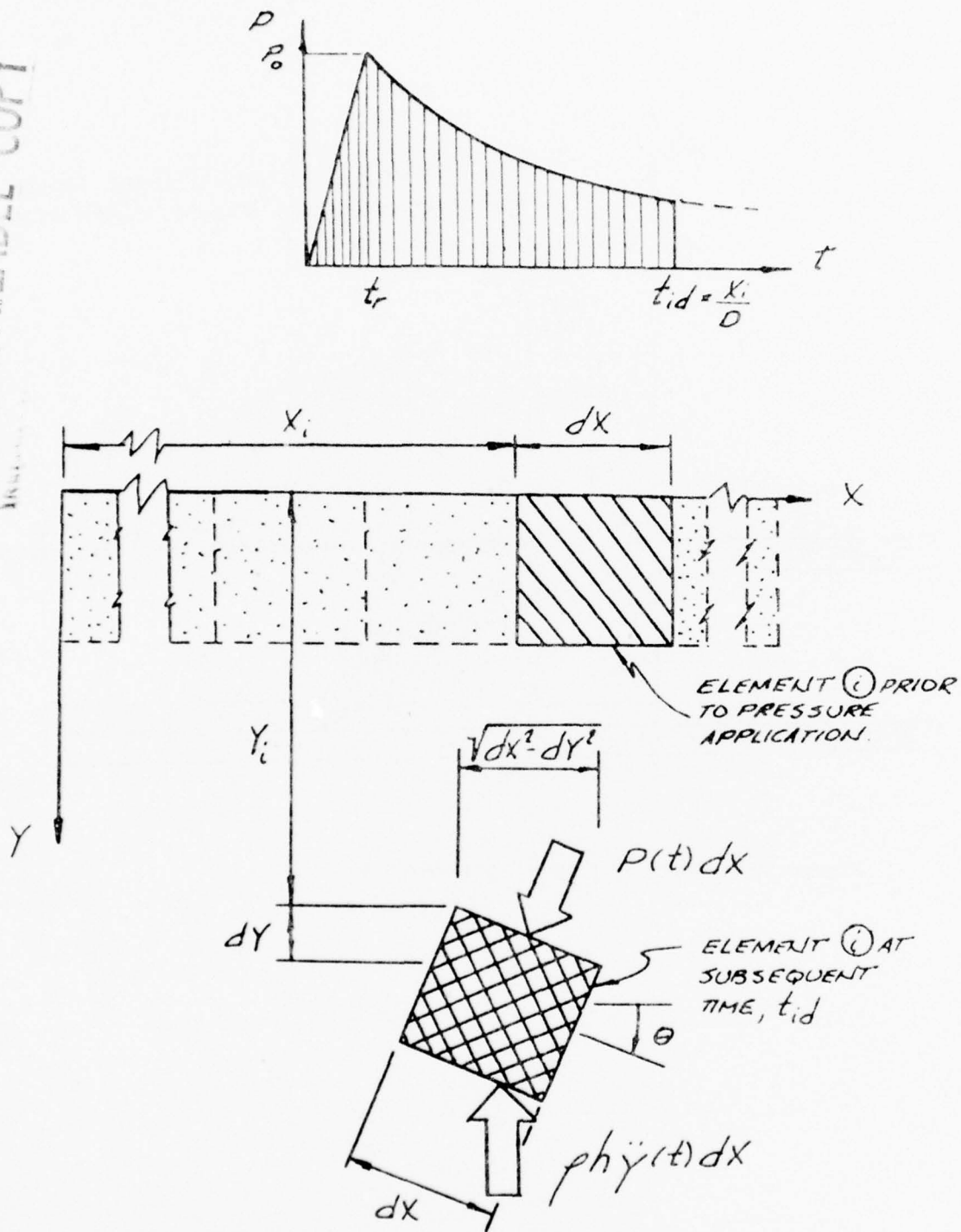
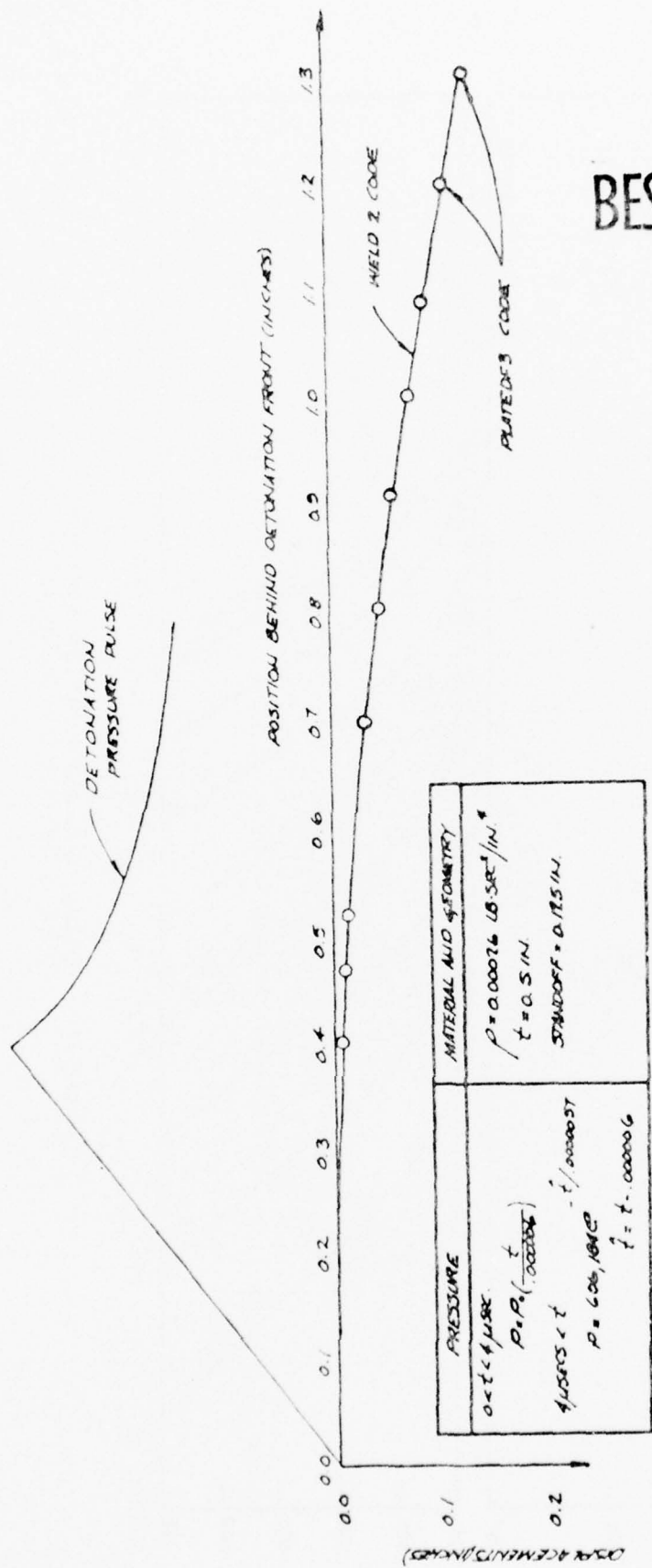


Figure 53. Dynamic Equilibrium of Plate Element



BEST AVAILABLE COPY

Figure 54. Accuracy of Dynamic Equilibrium Model

BEST AVAILABLE COPY

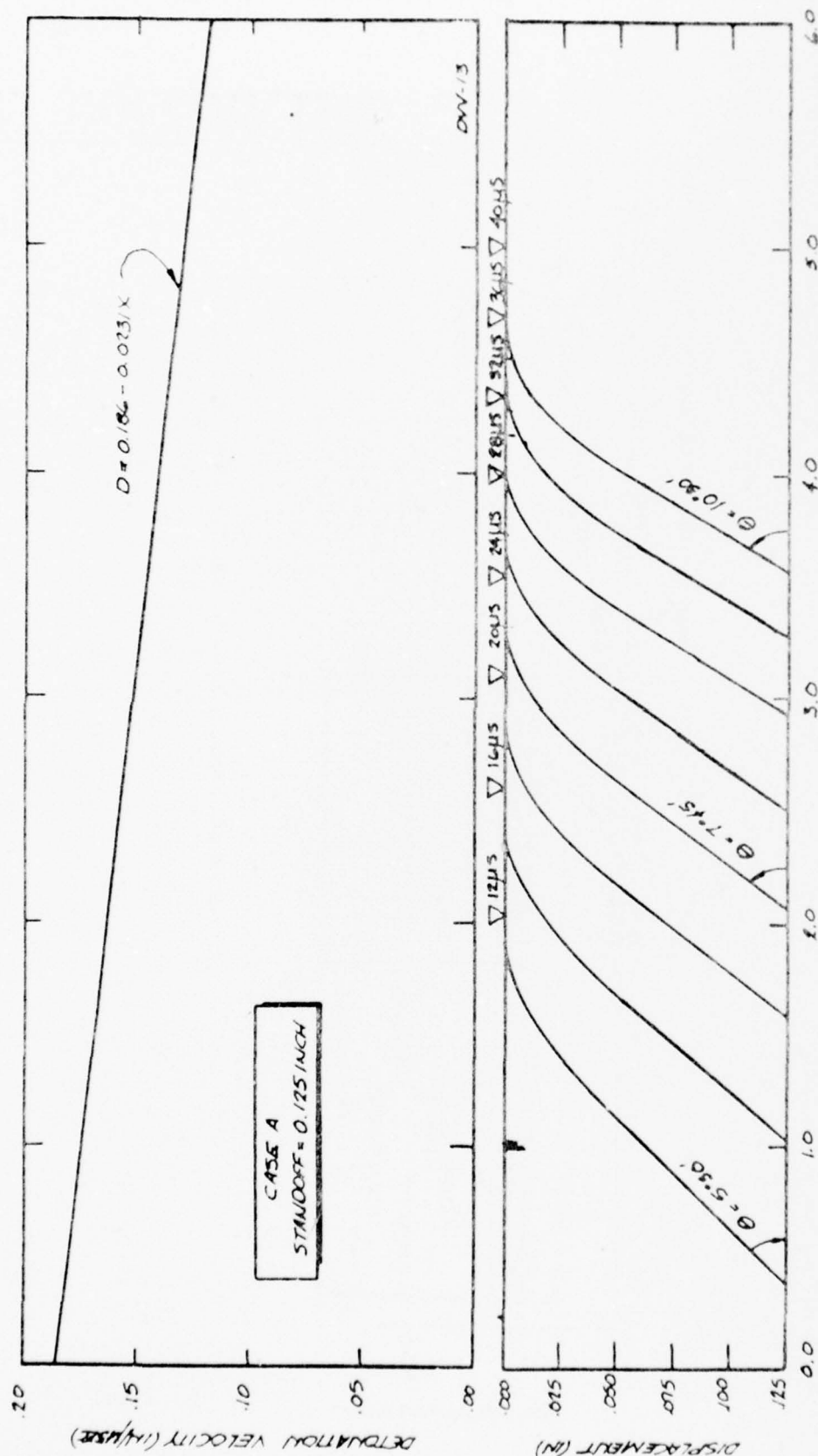


Figure 54. Calculated Deformation Response:  
a. Case A Detonation Velocity Variation

BEST AVAILABLE COPY

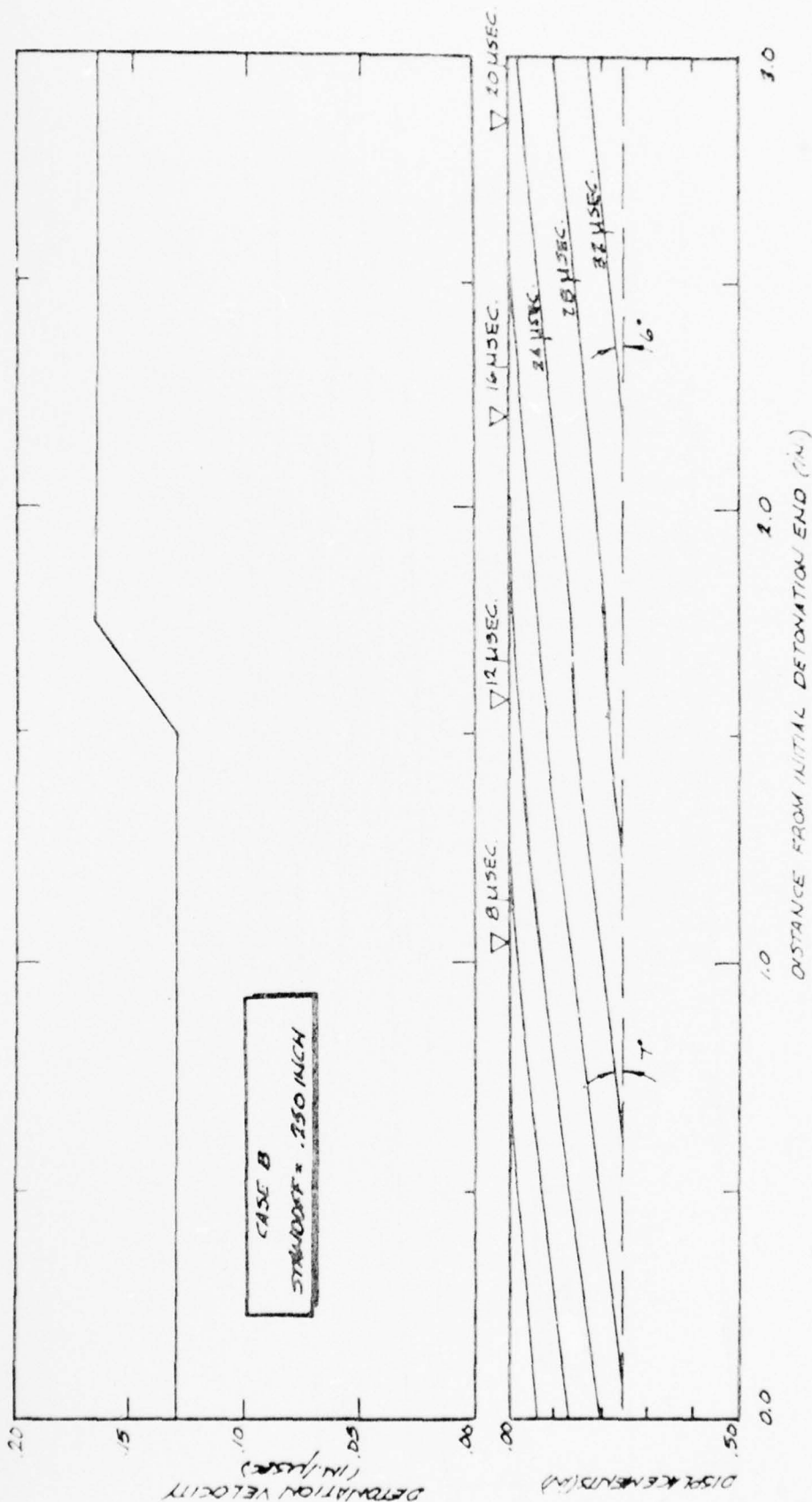


Figure 54. Calculated Deformation Response: (Cont)  
b. Case B Detonation Velocity Variation



BEST AVAILABLE COPY

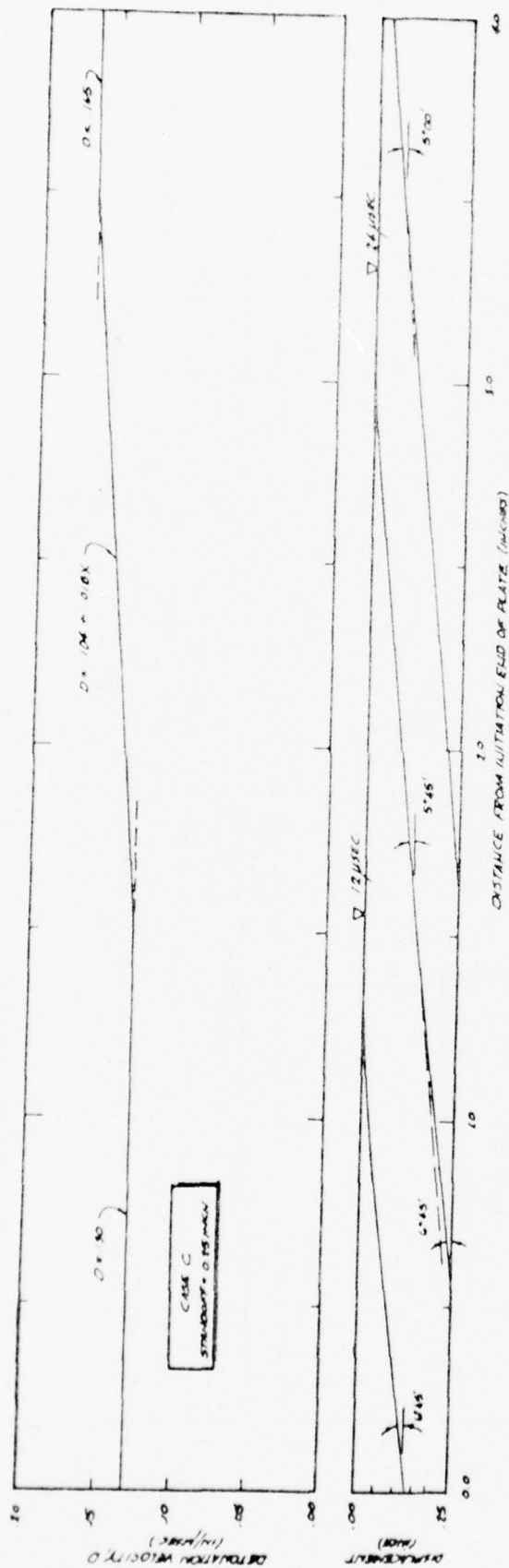


Figure 54. Calculated Deformation Response: (cont)  
c. Case C Detonation Velocity Variation

## 2. Analysis of LASL Framing Camera Velocity Data

During the summer of 1971 explosive welding tests using 6061-T6 aluminum and Dupont 40% Red Cross Extra Granular Dynamite were conducted at the GMX-6 Division of the Los Alamos Scientific Laboratory, New Mexico (LASL), under a cooperative arrangement between USAFA and LASL. These tests have been described in detail by [SUTTON (1971)] and [LINDBERGH (1973)].

The purpose of the LASL tests was to:

- (1) obtain flyer plate impact velocity data for correlation with bond tensile strength data, and
- (2) obtain flyer plate configuration data for use in an analytical description of flyer plate response.

Table 15 summarizes the LASL tests, which were conducted in three environments: atmospheric, inert gas (helium) and vacuum. Flyer and base plates were all 6 IN wide and 12 IN long, and the dynamite packing density was 1.25 G/CC. The density of 6061-T6 aluminum is 2.71 G/CC. Figure 55 shows the test setup for the final atmospheric series, which proved to be the most satisfactory.

Since a framing camera was used throughout the LASL tests, an ideal opportunity presented itself to investigate whether the steady state assumption of equal detonation and collision point velocities [LINDBERGH (1973,9)] is accurate. The investigation was begun by projecting the 35MM framing camera slides obtained at 4  $\mu$  SEC intervals during each shot [LINDBERGH (1973, 28)] on a sheet of white paper 27IN x 32IN, and tracing successive outlines of the detonation front and flyer plate bottom surface configurations. The projections are shown in Figures 56 through 84. The

TABLE 15  
LASL SERIES SUMMARY

Test Number	Explosive Loading	Flyer Thickness	Standoff Distance	Environment*	Framing Camera	Flash X-Ray
	G/in <sup>2</sup>	in	in			
1268	10	1/2	1/2	A	yes	no
1269	10	1/2	1/2	A	yes	no
1270	10	1/2	1/2	A	yes	no
1271	10	1/2	1/2	H	yes	no
1273	10	1/2	1/2	V	yes	no
1274	10	1/2	1/2	V	yes	no
1275	10	1/2	1/2	V	no	no
1277	10	1/2	1/2	V	yes	no
1278	10	1/2	1/2	V	yes	no
1279	10	1/2	1/4	V	yes	no
1280	10	1/2	1/4	V	yes	no
1281	10	1/2	1/2	V	yes	no
1282	10	1/2	1	V	yes	no
1283	14	1/2	1	V	yes	no
1284	8	1/4	1/4	V	yes	no
1285	14	1/2	1/2	V	yes	no
1286	14	1/2	1/4	V	yes	no
1287	14	1/4	1/4	V	yes	no
1298	10	1/4	1/2	V	yes	no
1311	8	1/4	1/4	A	yes	yes
1312	10	1/2	1/2	A	yes	yes
1317	10	1/4	1/2	A	yes	yes
1318	10	1/4	1/8	A	yes	yes
1319	12	1/4	1/8	A	yes	yes
1320	12	1/4	1/4	A	yes	yes
1321	14	1/2	1/2	A	yes	yes
1322	10	1/2	1/4	A	yes	yes
1323	14	1/2	1/4	A	yes	yes
1324	10	1/2	1	A	yes	yes
1325	14	1/2	1	A	yes	yes
1326	8	1/4	1/8	A	yes	yes
1327	8	1/4	1/8	A	yes	yes
1328	12	1/4	1/4	A	yes	yes
1362	12	1/4	1/2	A	yes	yes
1363	8	1/4	1/8	A	yes	yes
1364	12	1/4	1/8	A	yes	yes

\* A = atmosphere  
H = helium  
V = vacuum

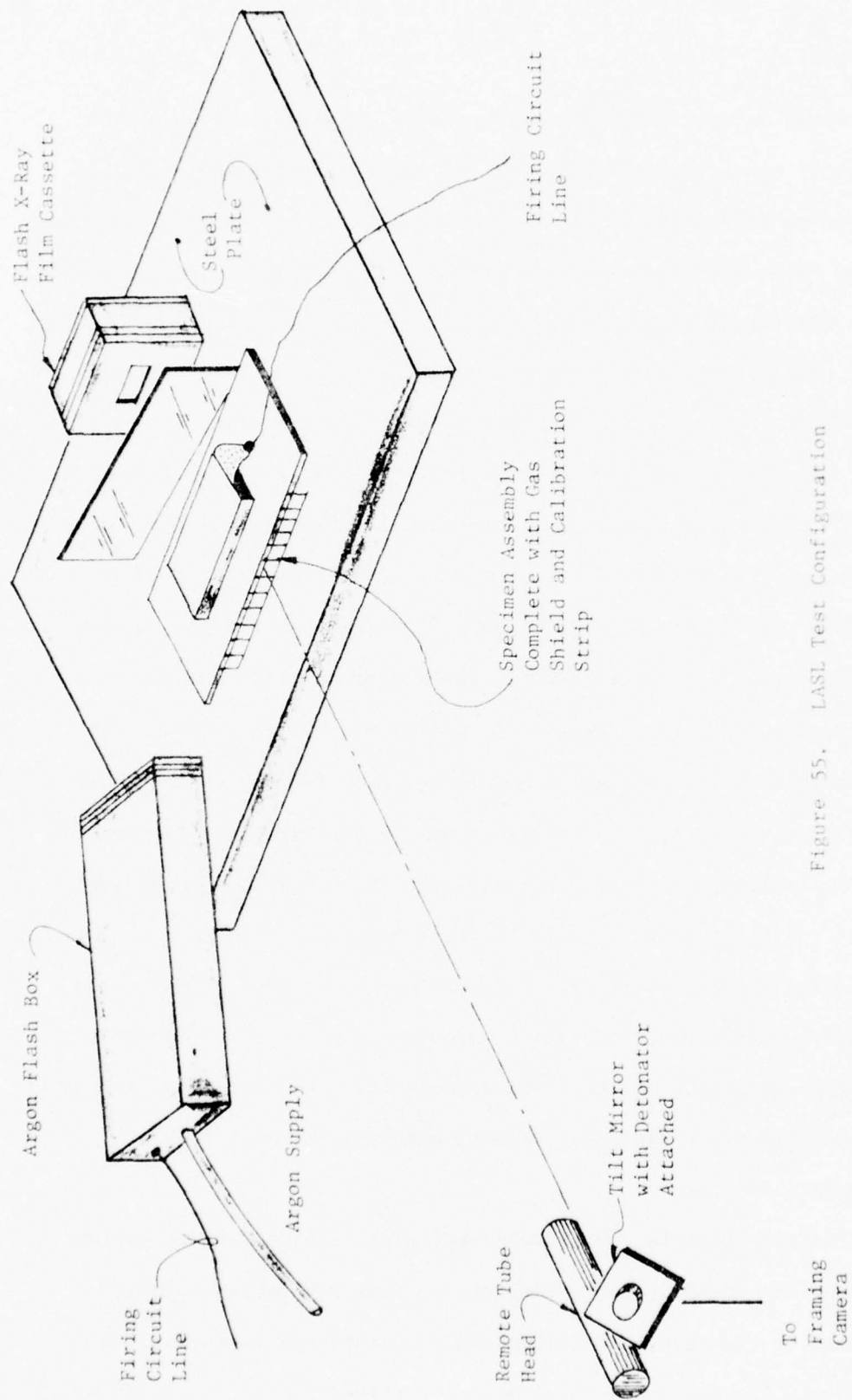


Figure 55. LASL Test Configuration

grid lines on a stationary plastic strip, located in front of the stand-off space, were also traced and used for reference and scale. Convenient elevations were selected at which to determine the detonation front and flyer plate positions. The detonation and collision point velocities were then calculated using linear regression [HOEL (1954, 126)], [BENJAMIN & CORNELL (1970, 428)]. Tables 16 through 67 contain the tabulated detonation front and flyer plate position data, and Figures 85 through 134 contain plots of the same raw data and the fitted straight lines. The associated velocities are shown in both the tables and figures, and are summarized in Table 68.

After excluding shots 1270 and 1274 because collision velocity was not measured, and shots 1282, 1283, 1284 and 1285 because of poor quality data (see Figures 67, 68, 69 and 70), a linear regression analysis was performed on the data for the remaining 20 shots. The purpose of the analysis was to determine whether detonation and collision point velocities were about equal. The average of the collision point velocities differed from the average of the detonation velocities by only 0.59 percent. The plot of collision point velocity VERSUS detonation velocity in Figure 135 indicates that the assumption of equal collision point and detonation velocities for parallel plate explosive welding configurations is indeed reasonably accurate.

Finally, the relation between explosive loading and detonation velocity was investigated, using the average detonation velocity for each of the three explosive loadings employed. Referring to Table 68, the following results were obtained:



Explosive Loading G/IN <sup>2</sup>	Detonation Velocity IN/μSEC	Number of Shots
10	0.11793	13
12	0.12169	3
14	0.12017	4

In general, the detonation velocity appears to have increased slightly with explosive loading.

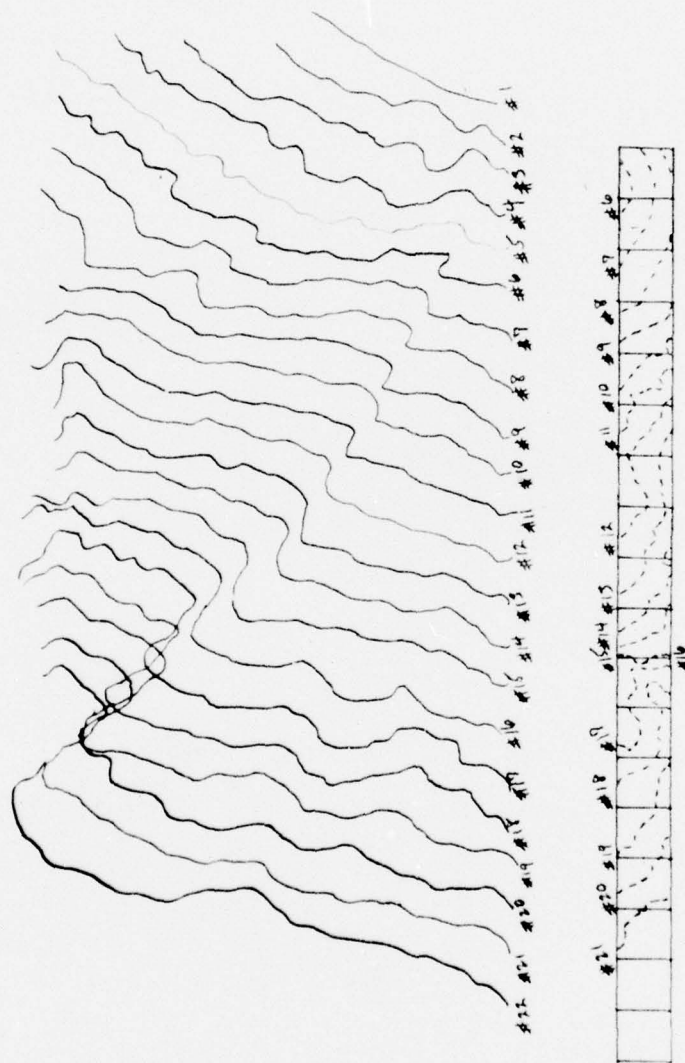


Figure 56. Framing Camera Projection LASL 1268



Figure 57. Framing Camera Projection LASL 1269

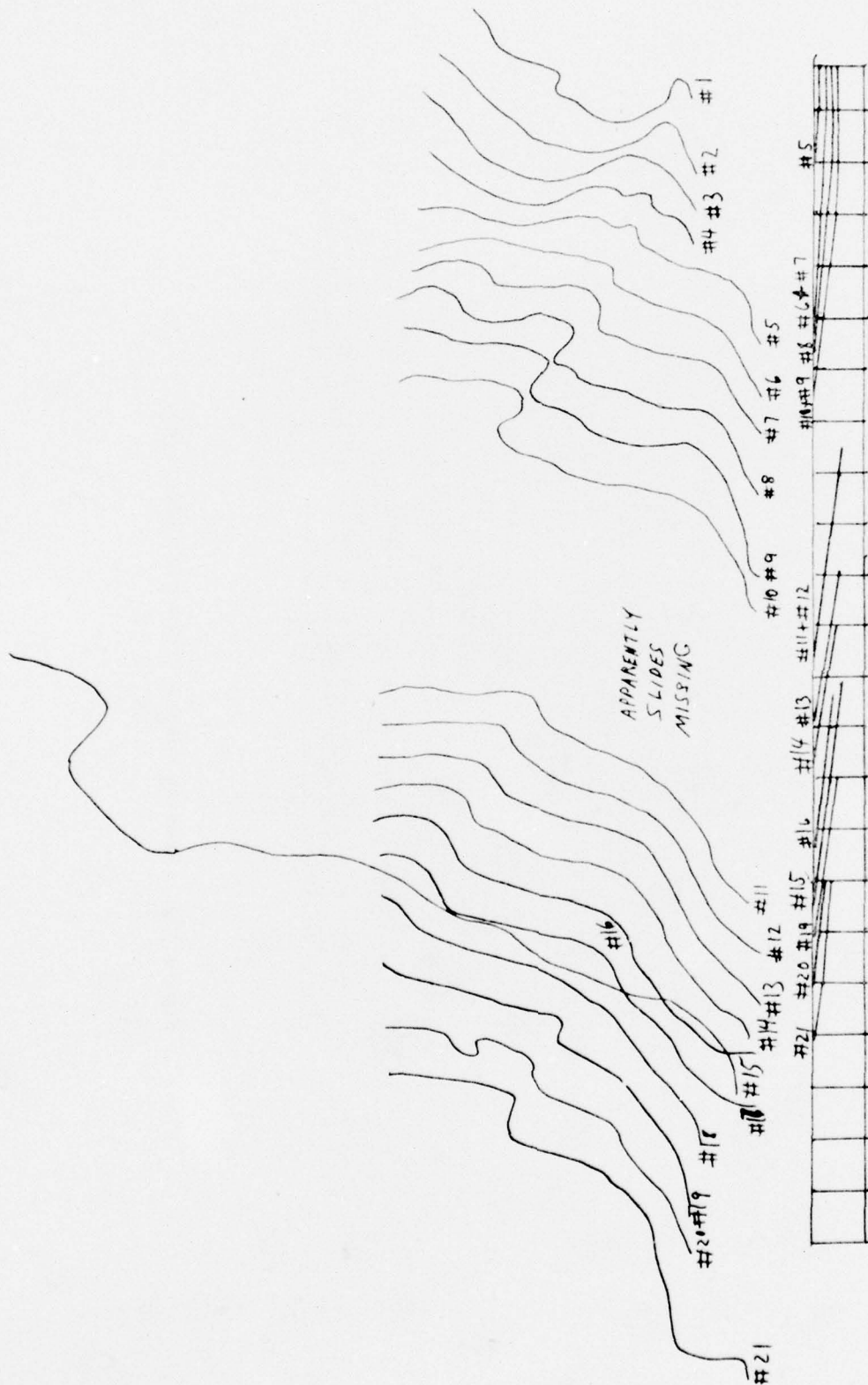


Figure 58. Framing Camera Projection LASL 1270



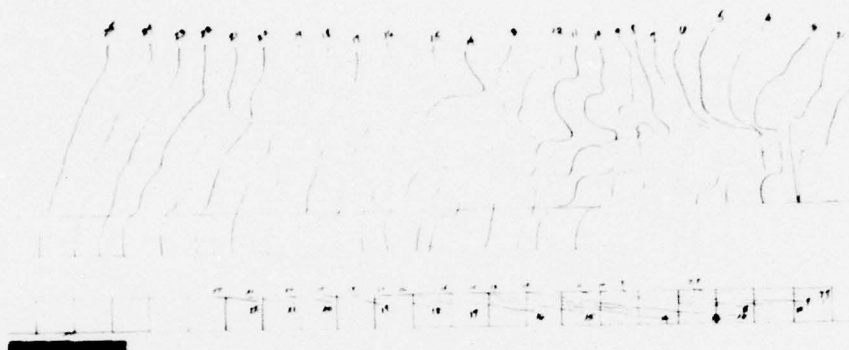


Figure 59. Framing Camera Projection LASL 1271

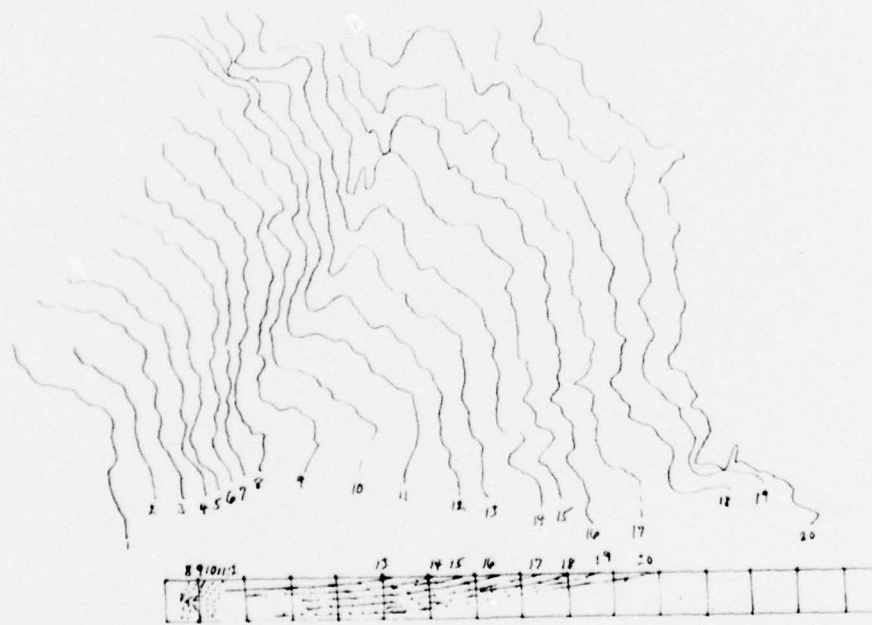


Figure 60. Framing Camera Projection LASL 1273





Figure 61. Framing Camera Projection LASL 1274

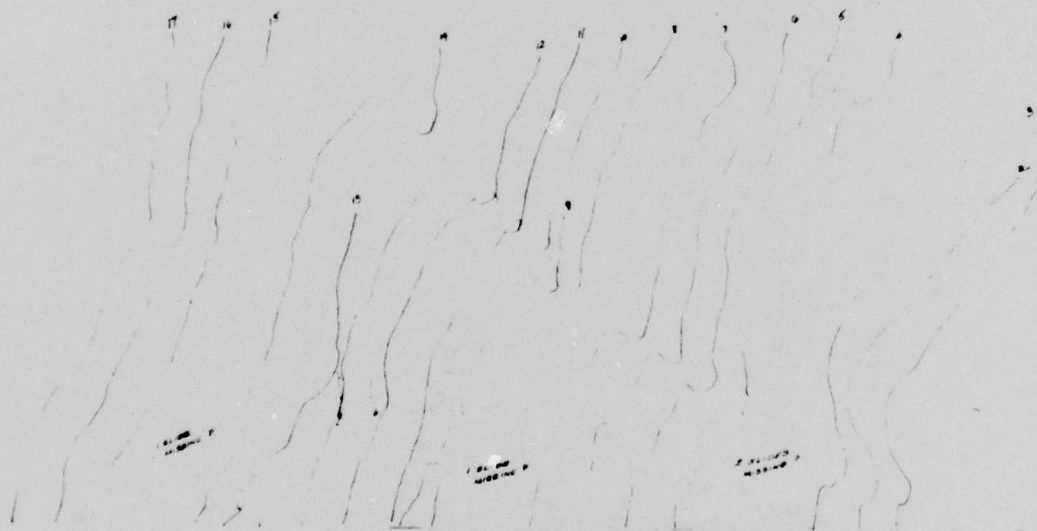


Figure 62. Framing Camera Projection LASL 1277

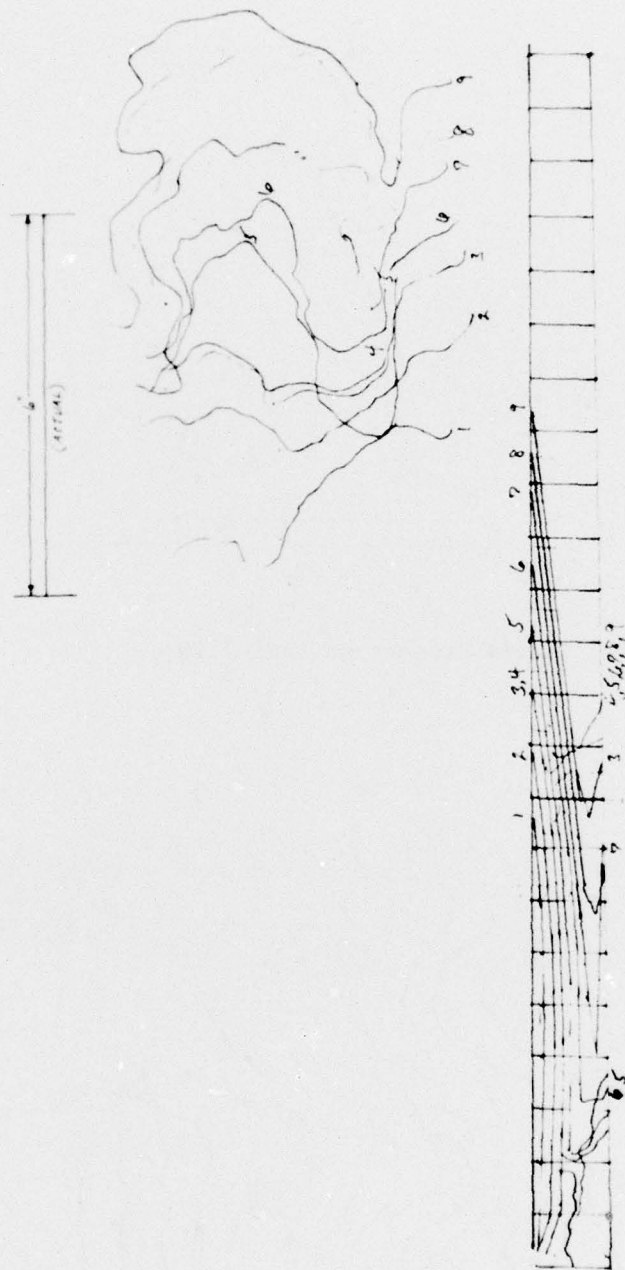


Figure 63. Framing Camera Projection LASL 1278

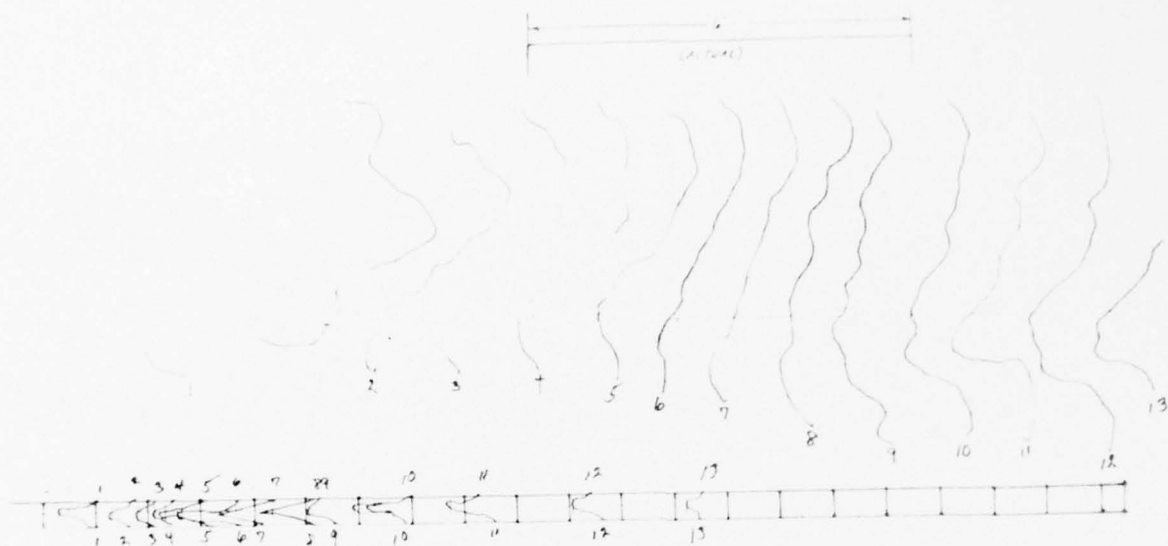


Figure 64. Framing Camera Projection LASL 1279

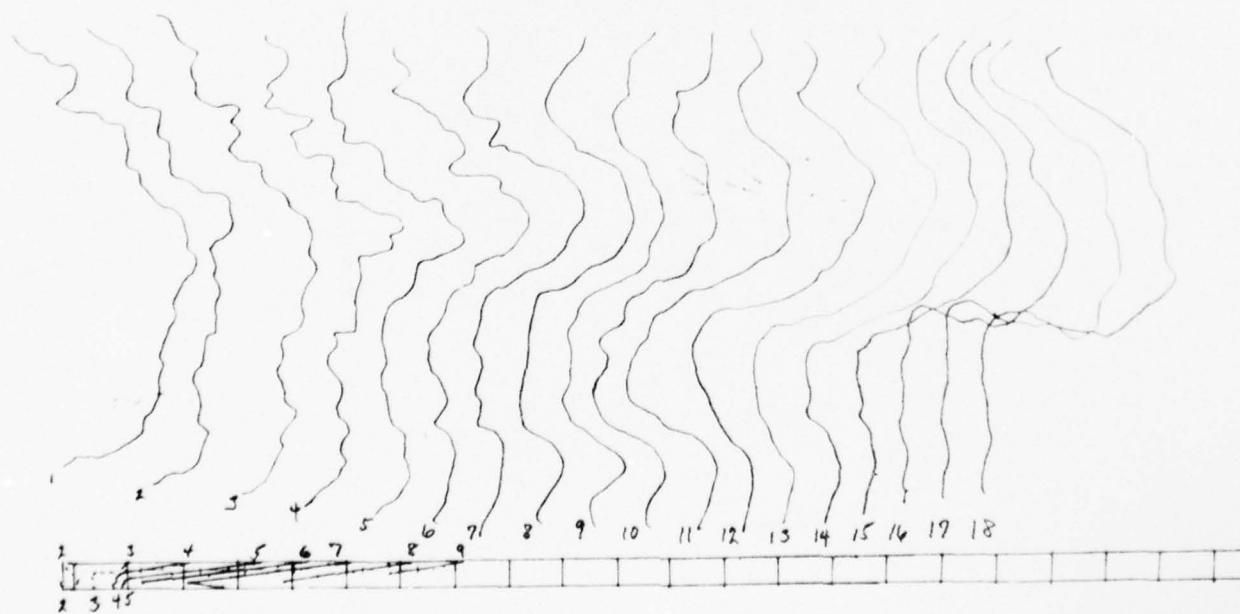


Figure 65. Framing Camera Projection LASL 1280

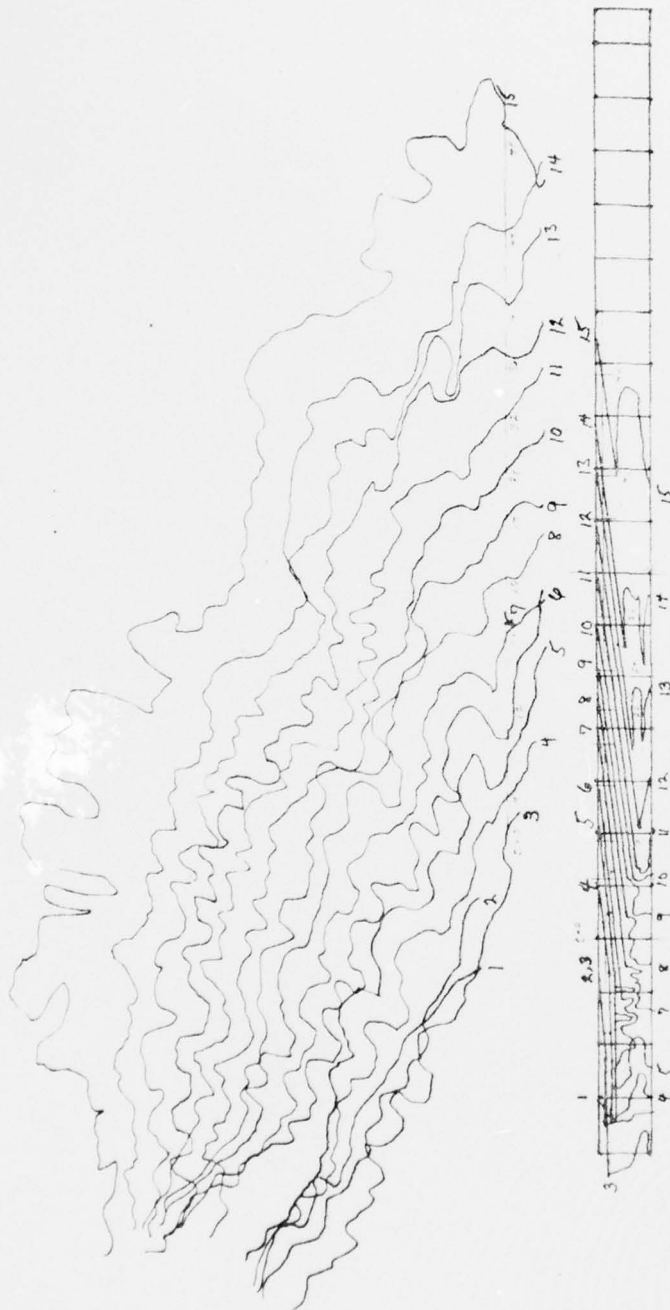


Figure 66. Framing Camera Projection LASL 1281

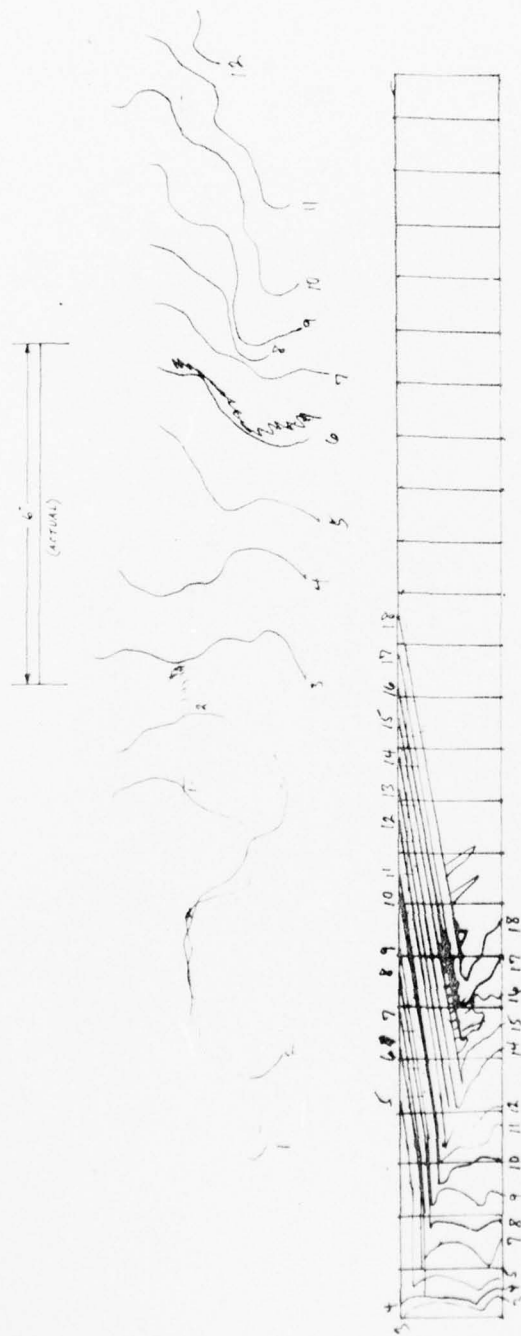


Figure 67. Framing Camera Projection LASL 1282



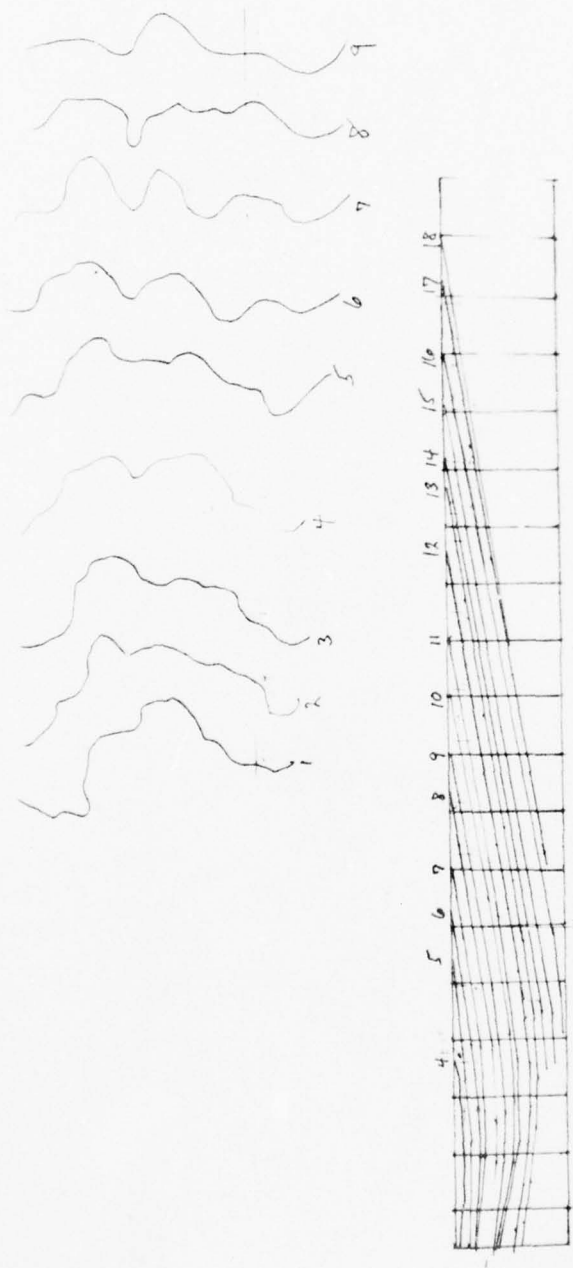


Figure 68. Framing Camera Projection LASL 1283

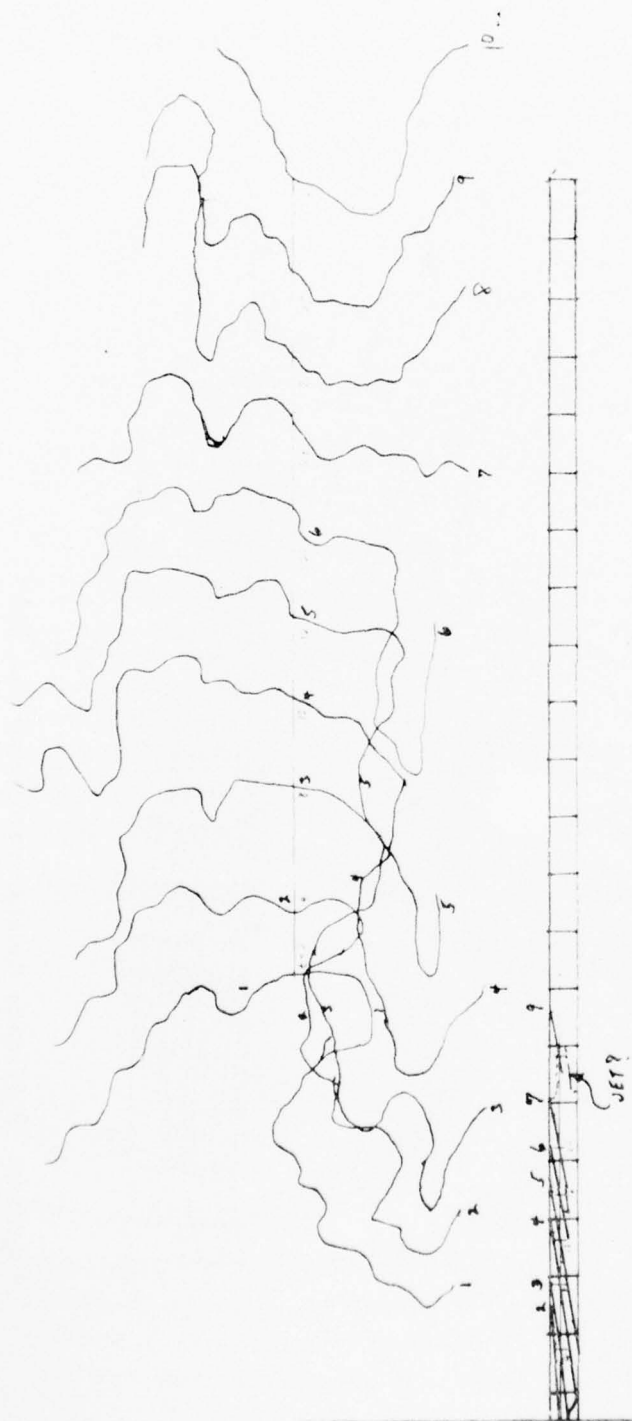


Figure 69. Framing Camera Projection LASL 1284



Figure 70. Framing Camera Projection LASL 1285

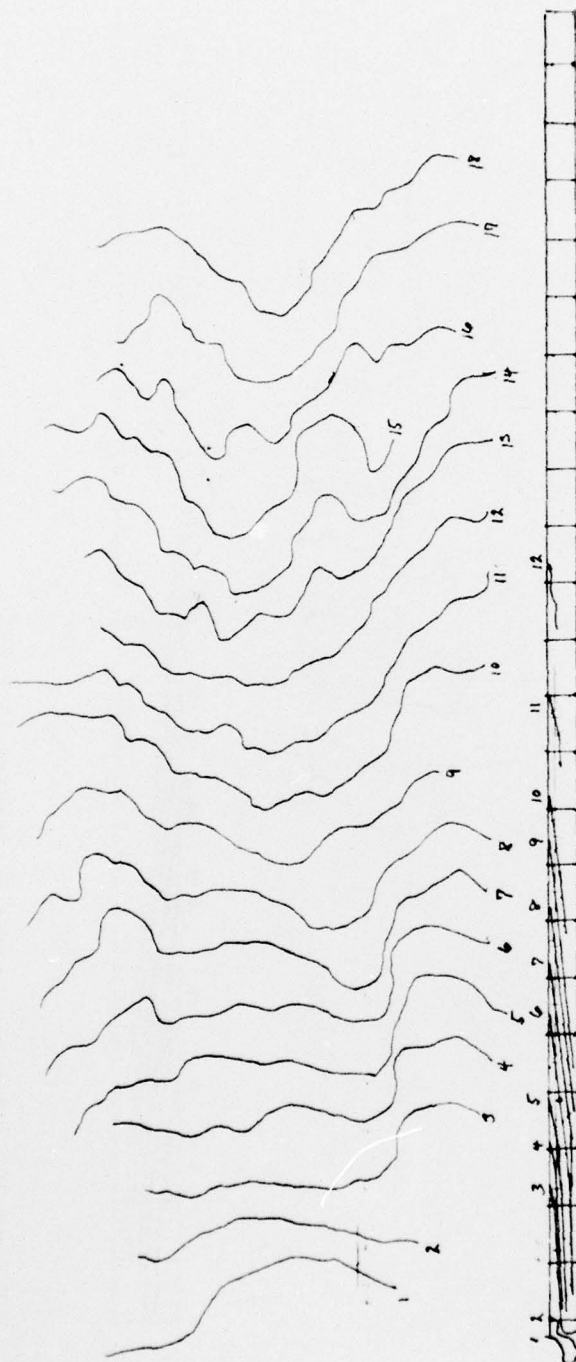


Figure 71. Framing Camera Projection LASL 1286

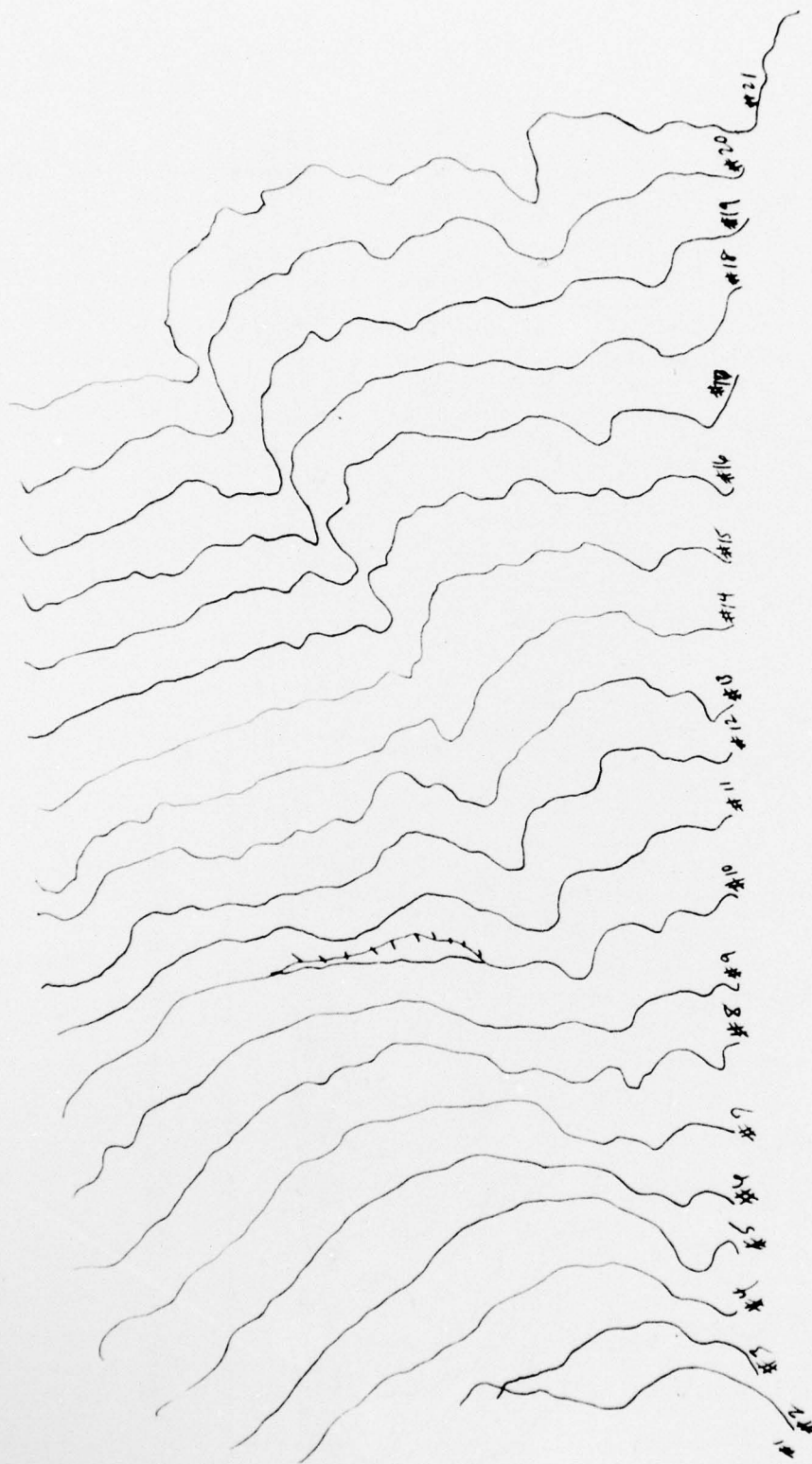


Figure 72. Framing Camera Projection LASL 1312



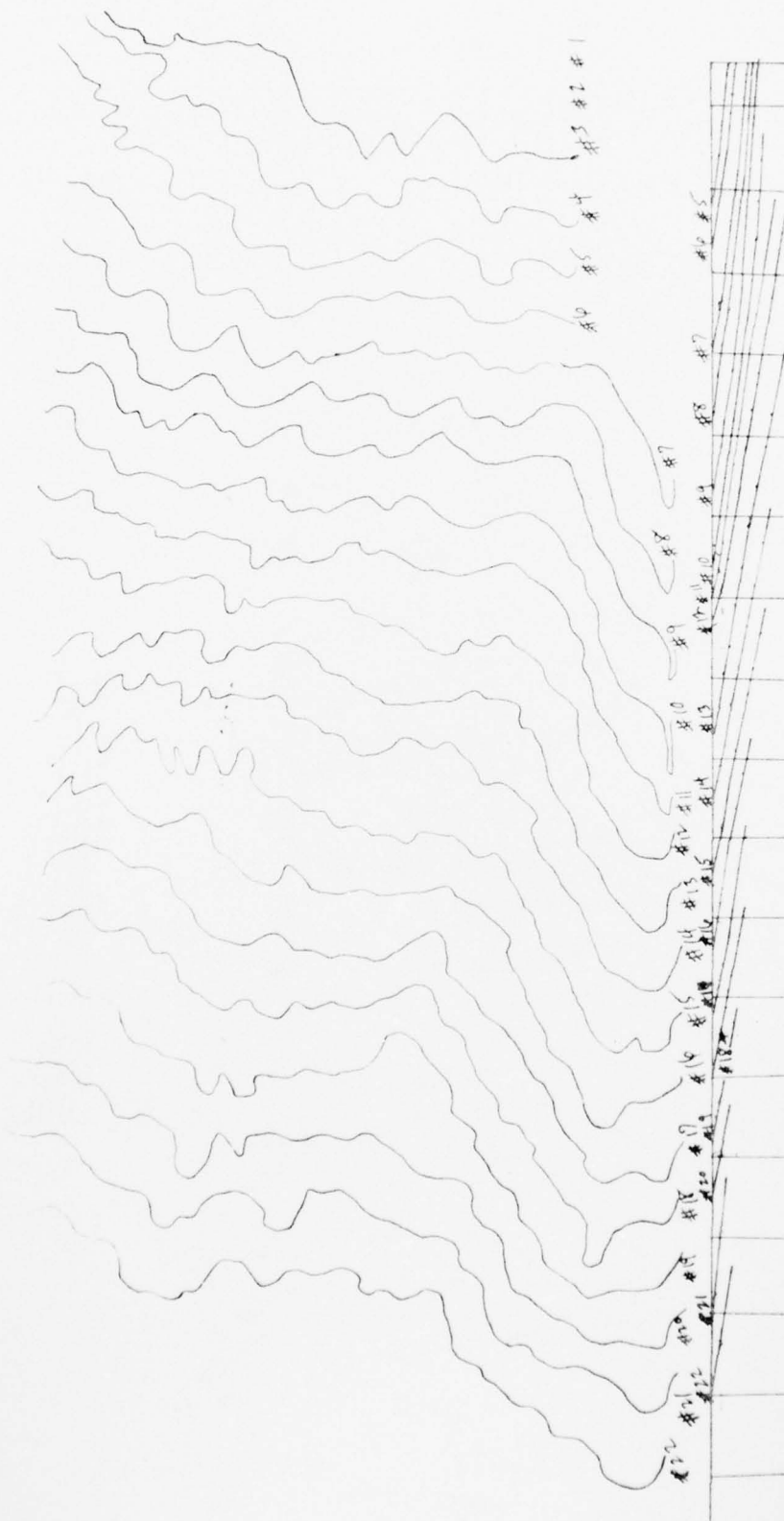


Figure 73. Framing Camera Projection LASL 1317



Figure 74. Framing Camera Projection LASL 1320

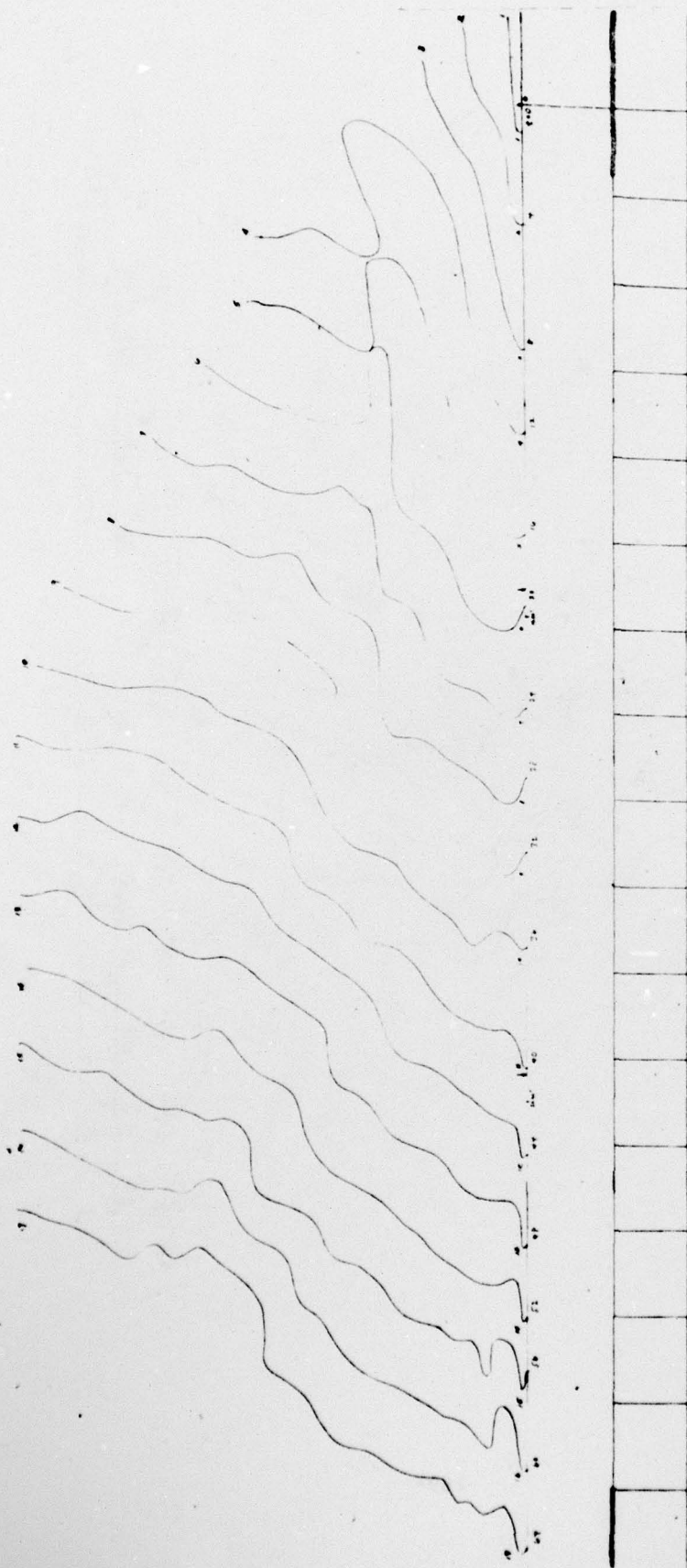


Figure 75. Framing Camera Projection LASL 1321

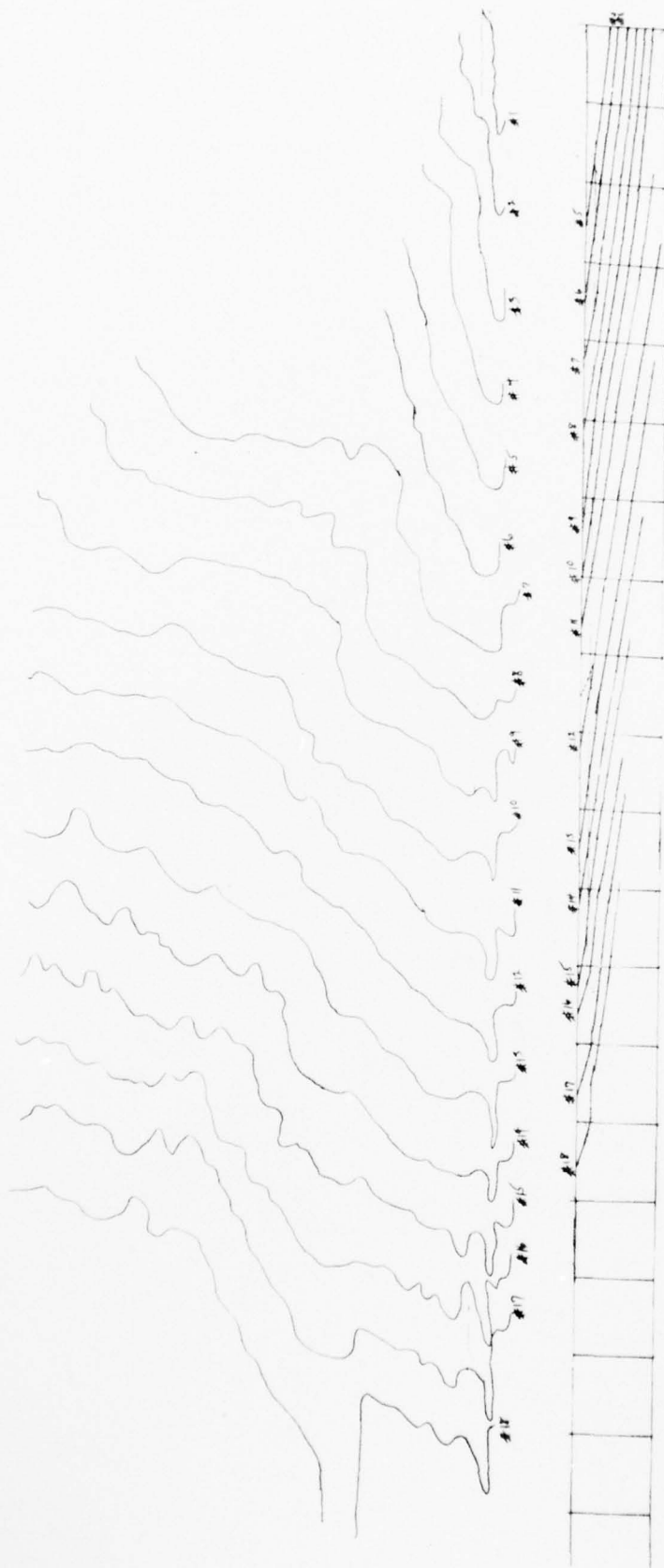


Figure 76. Framing Camera Projection LASL 1321



Figure 77. Framing Camera Projection LASL 1322



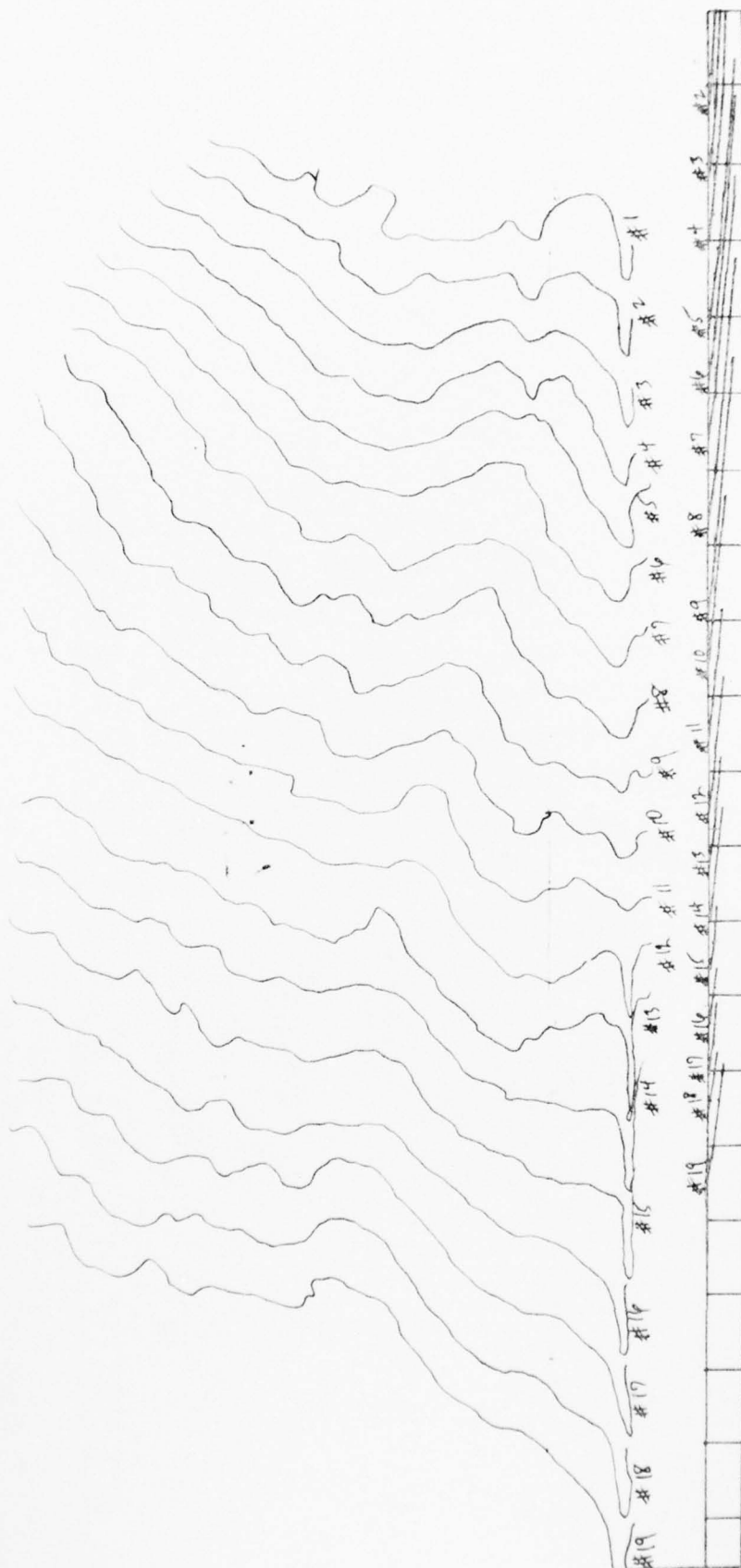


Figure 78. Framing Camera Projection LASL 1322

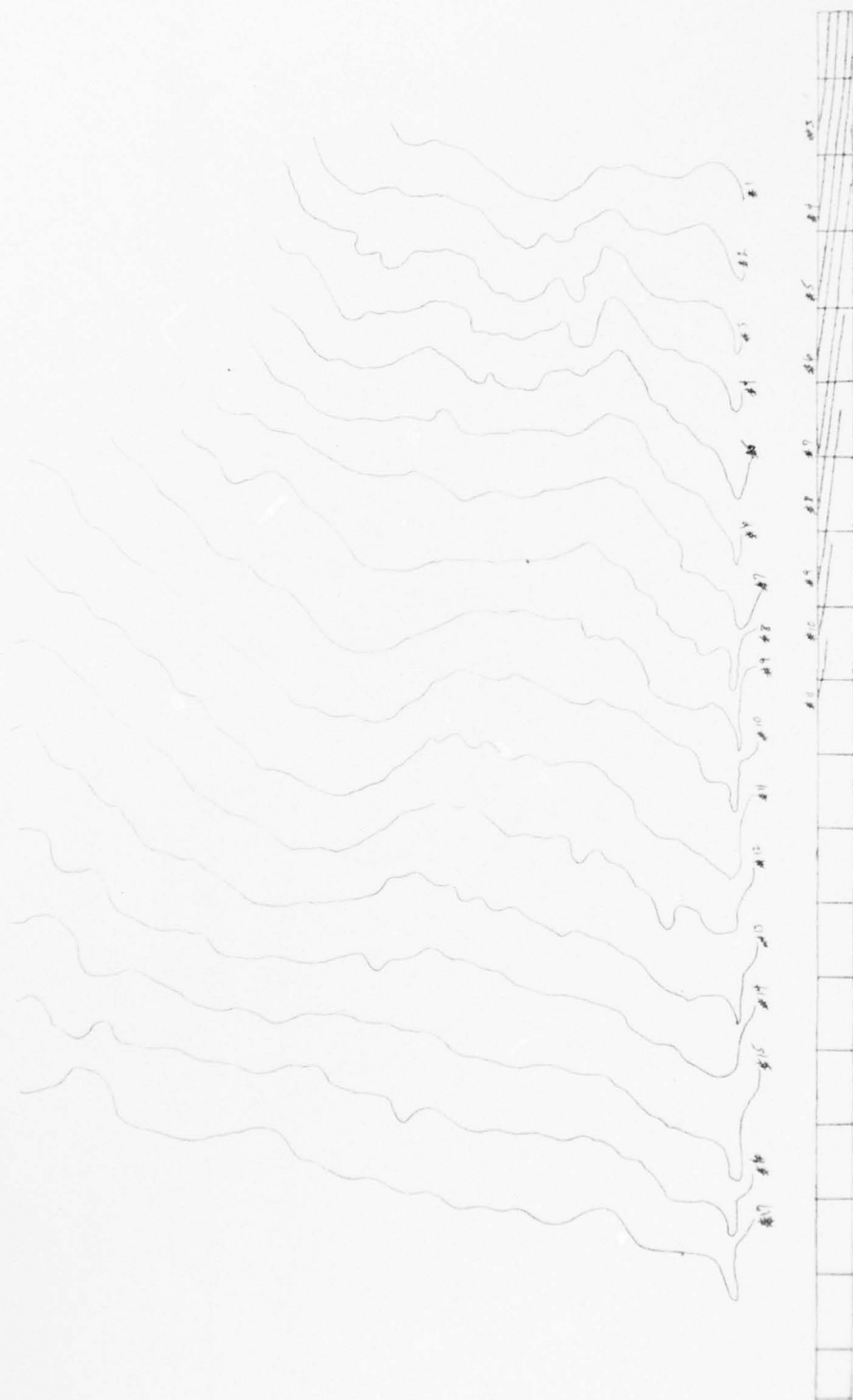


Figure 79. Framing Camera Projection LASL 1323

AD-A047 955

FRANK J SEILER RESEARCH LAB UNITED STATES AIR FORCE --ETC F/6 13/8  
EXPLOSIVE IMPULSE WELDING. VOLUME I.(U)

JUL 77 D H MERKLE, G E CANNON

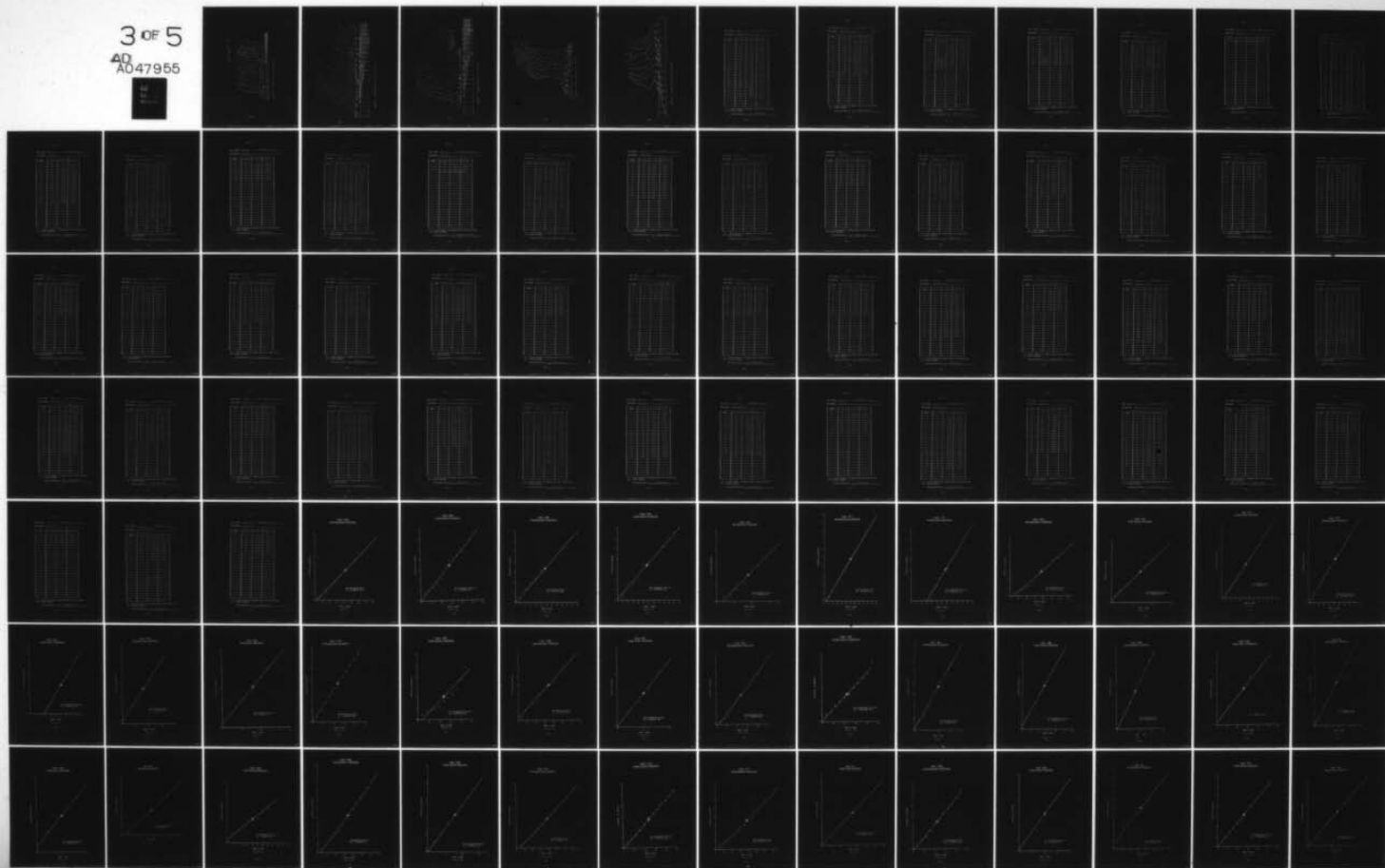
UNCLASSIFIED

FJSRL-TR-77-0012-VOL-1

NL

3 OF 5

AD  
A047955



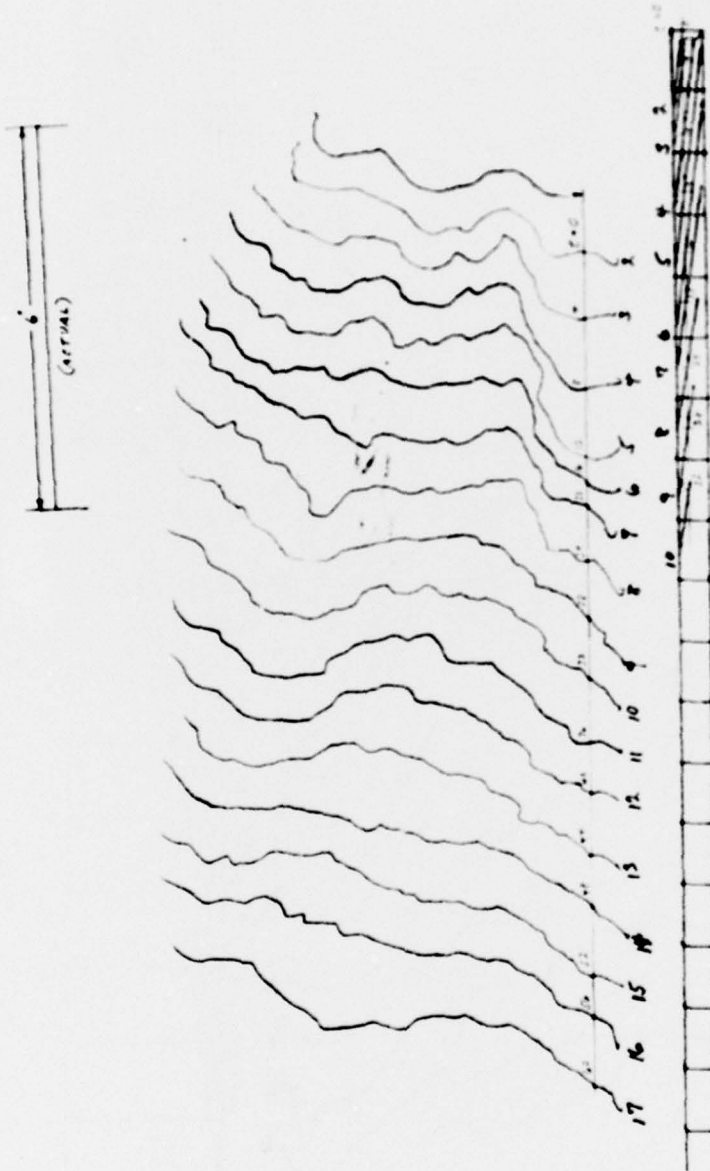


Figure 80. Framing Camera Projection LASL 1323



Figure 81. Framing Camera Projection LASL 1324



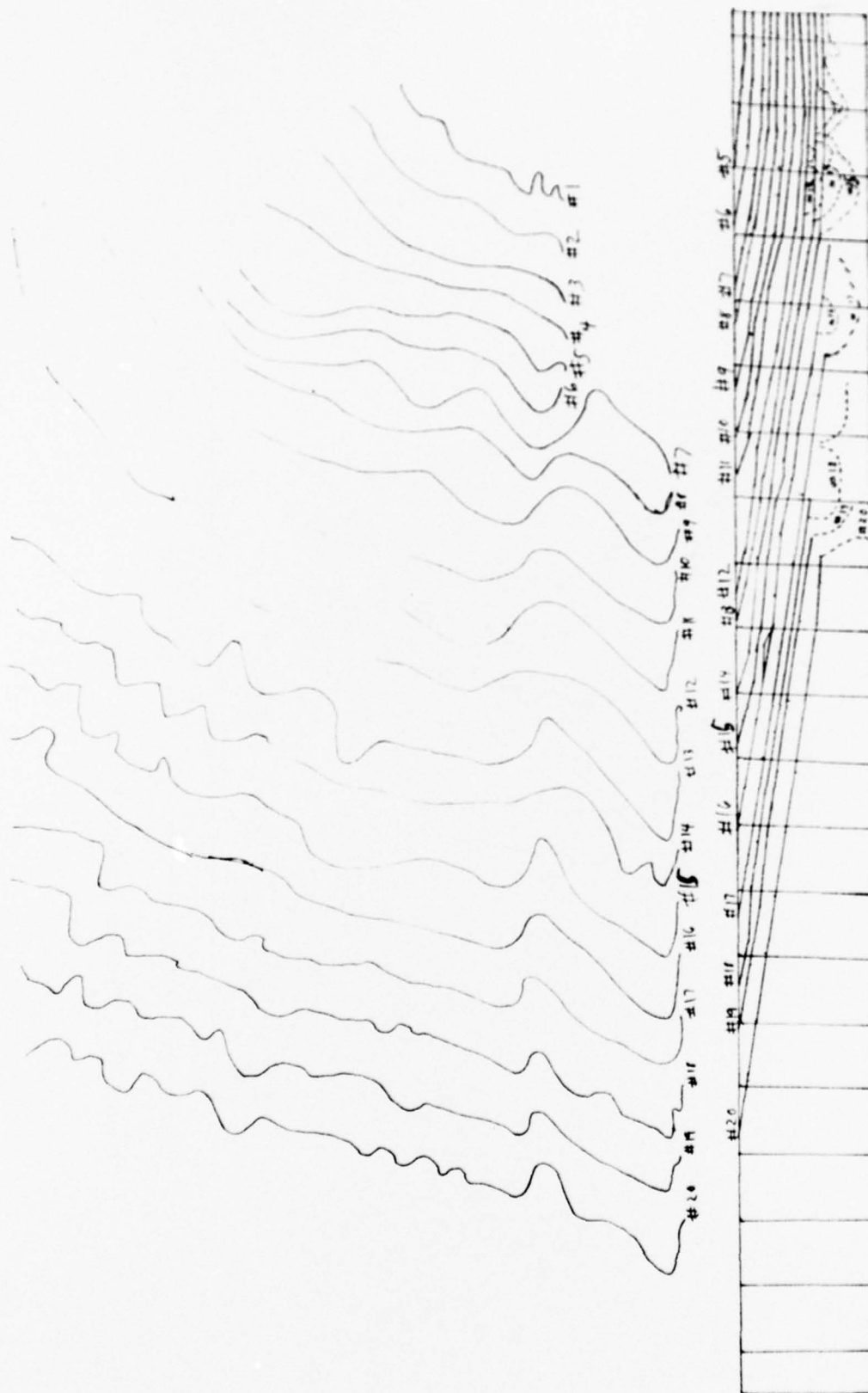


Figure 82. Framing Camera Projection LASL 1325

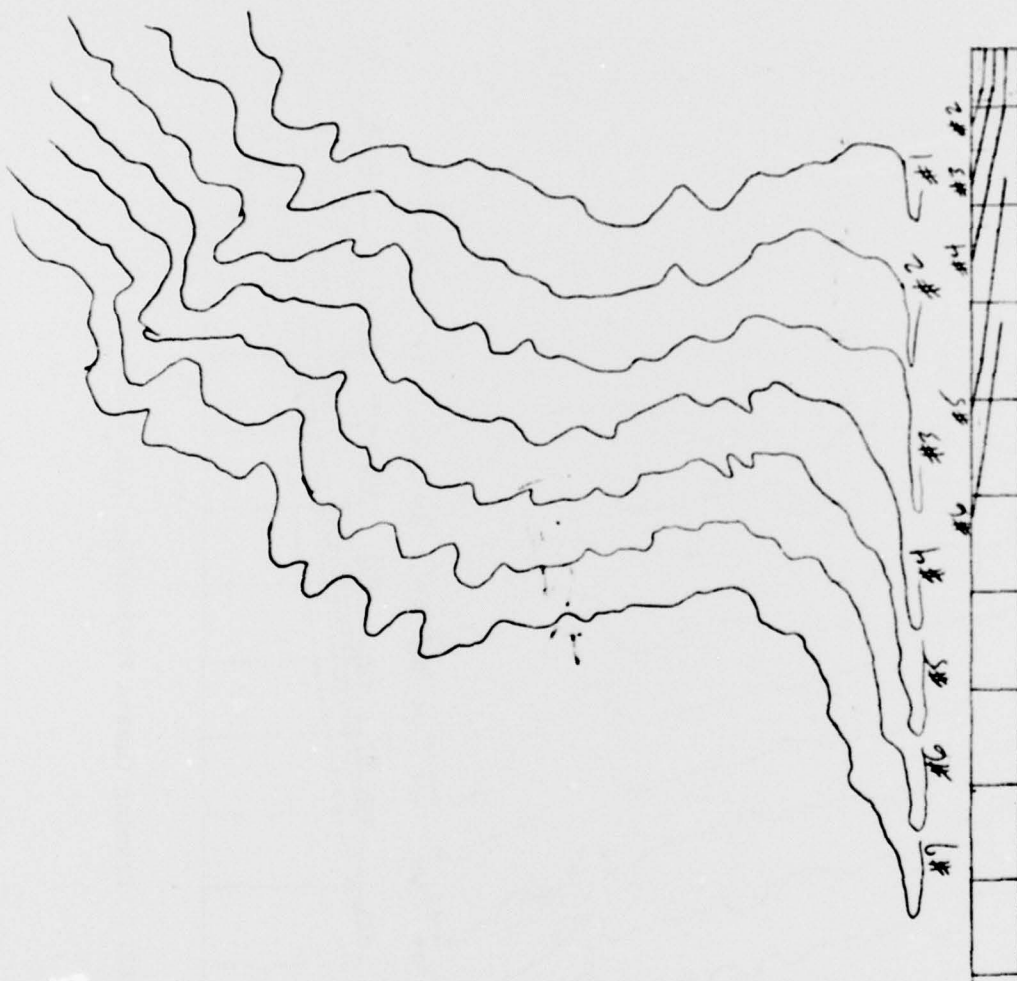


Figure 83. Framing Camera Projection LASL 1328

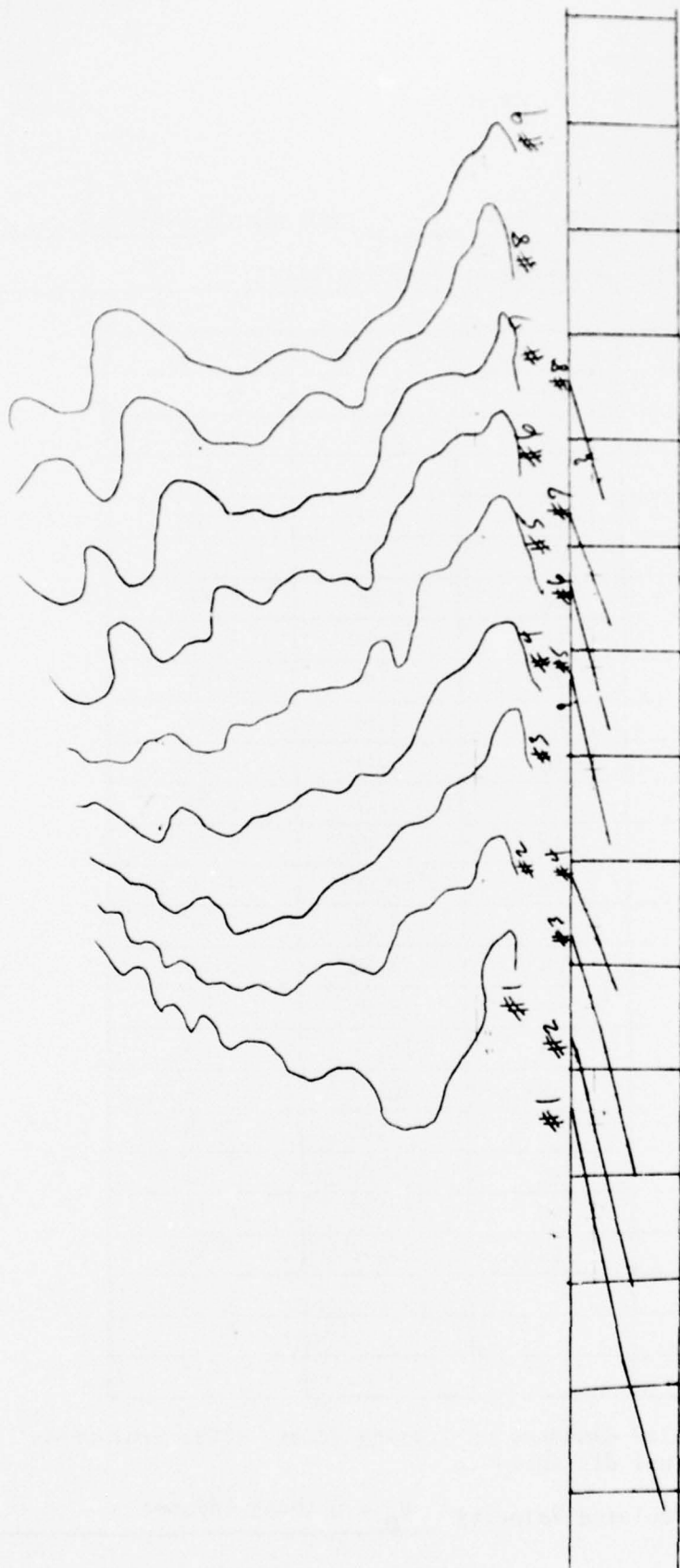


Figure 84. Framing Camera Projection LASL 1362

TABLE 16

SHOT NUMBER LASL 1268 SCALE FACTOR 1.6/1.0MEASUREMENT Detonation Front Position

FRAME	t ( $\mu$ sec)	z* (in)	y** (in)
1	0	0	0
2	4	0.55	0.34
3	8	1.00	0.63
4	12	1.50	0.94
5	16	2.05	1.28
6	20	2.90	1.81
7	24	3.50	2.19
8	28	4.05	2.53
9	32	4.85	3.03
10	36	5.50	3.44
11	40	6.30	3.94
12	44	7.05	4.41
13	48	7.60	4.75
14	52	8.15	5.09
15	56	8.85	5.53
16	60	9.80	6.13
17	64	10.20	6.38
18	68	10.95	6.84
19	72	11.80	7.38
20	76	12.50	7.81
21	80	13.05	8.16
22	84	13.75	8.59

\*z = scaled distance on framing camera slide projection  
 \*\*y = actual distance

Calculated Velocity  $V_D = 0.10465$  in/ $\mu$ sec

TABLE 17

SHOT NUMBER IASL 1268 SCALE FACTOR 1.6/1.0

MEASUREMENT Flyer Plate Position

[illegible]

\*z = scaled distance on framing camera slide projection  
 \*\*y = actual distance

Calculated Velocity  $V_C = 0.12160 \text{ in}/\mu\text{sec}$



MEASUREMENT Detonation Front

[illegible]

Calculated Velocity  $V_D = 0.14275 \text{ in}/\mu\text{sec}$

TABLE 19

SHOT NUMBER	LASL 1269	SCALE FACTOR	0.70/0.50
MEASUREMENT	Flyer Plate		

[illegible]

\*z = scaled distance on framing camera slide projection  
 \*\*y = actual distance

Calculated Velocity  $V_C = 0.14492 \text{ in}/\mu\text{sec}$

MEASUREMENT	Detonation Front
-------------	------------------

[illegible]

**\*\*y** = actual distance

Calculated Velocity  $V_D = 0.10070$  in/μsec

TABLE 21

SHOT NUMBER LASL 1270 SCALE FACTOR 1.6/1.0

MEASUREMENT Flyer Plate

[illegible]

\*z = scaled distance on framing camera slide projection  
\*\*y = actual distance

Calculated Velocity \_\_\_\_\_

TABLE 22

SHOT NUMBER LASL 1271 SCALE FACTOR 0.60/0.50MEASUREMENT Detonation Front

FRAME	t ( $\mu$ sec)	z* (in)	y** (in)
1	0	0	0
2	4	0.03	0.03
3	8	0.58	0.48
4	12	1.15	0.96
5	16	1.63	1.36
6	20	2.13	1.78
7	24	2.79	2.33
8	28	3.20	2.67
9	32	3.84	3.20
10	36	4.19	3.49
11	40	4.81	4.01
12	44	5.37	4.48
13	48	5.89	4.91
14	52	6.40	5.33
15	56	6.85	5.71
16	60	7.25	6.04
17	64	7.75	6.46
18	68	8.34	6.95
19	72	8.85	7.38
20	76	9.40	7.83
21	80	9.95	8.29
22	84	10.51	8.76
23	88	10.86	9.05
24	92	11.30	9.42
25	96	11.84	9.87

\*z = scaled distance on framing camera slide projection

\*\*y = actual distance

Calculated Velocity  $V_D = 0.10617$  in/ $\mu$ sec



TABLE 23

SHOT NUMBER LASL 1271 SCALE FACTOR 0.60/0.50MEASUREMENT Flyer Plate

FRAME	t ( $\mu$ sec)	z* (in)	y** (in)
7	24	0	0
8	28	0	0
9	32	1.10	0.92
10	36	1.47	1.23
11	40	1.79	1.49
12	44	2.62	2.18
13	48	3.15	2.63
14	52	3.48	2.90
15	56	3.91	3.26
16	60	4.55	3.79
17	64	4.91	4.09
18	68	5.38	4.48
19	72	5.80	4.83
20	76	6.35	5.29
21	80	6.98	5.82
22	84	7.50	6.25

\*z = scaled distance on framing camera slide projection  
 \*\*y = actual distance

Calculated Velocity  $V_c = 0.10449$  in/ $\mu$ sec

TABLE 24

SHOT NUMBER LASL 1275 SCALE FACTOR 1.8/1.0  
 MEASUREMENT Detonation Front

FRAME	t ( $\mu$ sec)	z* (in)	y** (in)
1	0	0	0
2	4	0.45	0.25
3	8	0.90	0.50
4	12	1.25	0.69
5	16	1.50	0.83
6	20	1.85	1.03
7	24	2.20	1.22
8	28	2.80	1.55
9	32	3.85	2.14
10	36	4.80	2.66
11	40	5.70	3.17
12	44	6.20	3.44
13	48	6.85	3.81
14	52	7.70	4.28
15	56	8.25	4.58
16	60	8.65	4.81
17	64	9.05	5.03
18	68	10.30	5.72
19	72	10.95	6.08
20	76	11.15	6.19

\*z = scaled distance on framing camera slide projection

\*\*y = actual distance

Calculated Velocity  $V_D = 0.08727$  in/ $\mu$ sec

TABLE 25

SHOT NUMBER	LASL 1273	SCALE FACTOR	1.8/1.0
MEASUREMENT	Flyer Plate		

[illegible]

\*z = scaled distance on framing camera slide projection  
 \*\*y = actual distance

Calculated Velocity  $V_C = 0.09890 \text{ in}/\mu\text{sec}$

TABLE 26

SHOT NUMBER LASL 1274 SCALE FACTOR 1.20/0.75MEASUREMENT Detonation Front

FRAME	t ( $\mu$ sec)	z* (in)	y** (in)
4	0	0	0
5	4	0.30	0.19
6	8	0.70	0.44
7	12	1.38	0.86
8	16	1.84	1.15
9	20	2.39	1.49
10	24	2.83	1.77
11	28	3.33	2.08
12	32	3.95	2.47
13	36	4.32	2.70
14	40	5.06	3.16
15	44	6.09	3.81
16	48	6.49	4.06
17	52	6.96	4.35
18	56	7.44	4.65
19	60	8.20	5.13
20	64	9.00	5.63
21	68	9.65	6.03
22	72	10.30	6.44
23	76	11.10	6.94
24	80	11.75	7.34
25	84	12.53	7.83

\*z = scaled distance on framing camera slide projection

\*\*y = actual distance

Calculated Velocity  $V_D = 0.09399$  in/ $\mu$ sec

TABLE 27

SHOT NUMBER LASL 1274 SCALE FACTOR 1.20/0.75

MEASUREMENT Flyer Plate

[illegible]

\*z = scaled distance on framing camera slide projection

\*\*y = actual distance

Calculated Velocity  $V_C = 0.13625 \text{ in}/\mu\text{sec (est)}$



TABLE 28

SHOT NUMBER LASL 1277 SCALE FACTOR 0.85/0.50MEASUREMENT Detonation Front

FRAME	t ( $\mu$ sec)	z* (in)	y** (in)
1	0	0	0
2	4	0.59	0.35
3	8	1.30	0.76
4	20	3.48	2.05
5	24	4.25	2.50
6	28	4.96	2.92
7	32	5.78	3.40
8	40	7.30	4.29
9	44	7.80	4.59
10	48	7.95	4.68
11	52	8.70	5.12
12	56	9.35	5.50
13	60	10.58	6.22
14	64	11.03	6.49
15	72	12.40	7.29
16	76	13.20	7.76
17	80	13.89	8.17

\*z = scaled distance on framing camera slide projection  
 \*\*y = actual distance

Calculated Velocity  $V_D = 0.10144$  in/ $\mu$ sec

TABLE 29

SHOT NUMBER LASL 1277 SCALE FACTOR 0.85/0.50

MEASUREMENT Flyer Plate

[illegible]

\*z = scaled distance on framing camera slide projection  
 \*\*y = actual distance

Calculated Velocity  $V_C = 0.10120 \text{ in}/\mu\text{sec}$

SHOT NUMBER      LASL 1278                      SCALE FACTOR   1.7/1.0

MEASUREMENT	Detonation Front
Pressure	1000-1500 atm
Temperature	2000-2500°C
Velocity	1500-2000 m/s
Reaction Time	10 <sup>-6</sup> -10 <sup>-5</sup> s
Reaction Zone Thickness	0.1-0.5 mm
Reaction Zone Structure	Cellular
Reaction Zone Orientation	Random
Reaction Zone Frequency	10 <sup>3</sup> -10 <sup>4</sup> Hz
Reaction Zone Wavelength	0.1-0.5 mm
Reaction Zone Amplitude	0.1-0.5 mm
Reaction Zone Phase	0-360°
Reaction Zone Velocity	1500-2000 m/s
Reaction Zone Acceleration	10 <sup>3</sup> -10 <sup>4</sup> m/s <sup>2</sup>
Reaction Zone Density	1.5-2.0 g/cm <sup>3</sup>
Reaction Zone Composition	CO <sub>2</sub> , H <sub>2</sub> O, CH <sub>4</sub> , C <sub>2</sub> H <sub>6</sub> , C <sub>3</sub> H <sub>8</sub> , C <sub>4</sub> H <sub>10</sub> , C <sub>5</sub> H <sub>12</sub> , C <sub>6</sub> H <sub>14</sub> , C <sub>7</sub> H <sub>16</sub> , C <sub>8</sub> H <sub>18</sub> , C <sub>9</sub> H <sub>20</sub> , C <sub>10</sub> H <sub>22</sub> , C <sub>11</sub> H <sub>24</sub> , C <sub>12</sub> H <sub>26</sub> , C <sub>13</sub> H <sub>28</sub> , C <sub>14</sub> H <sub>30</sub> , C <sub>15</sub> H <sub>32</sub> , C <sub>16</sub> H <sub>34</sub> , C <sub>17</sub> H <sub>36</sub> , C <sub>18</sub> H <sub>38</sub> , C <sub>19</sub> H <sub>40</sub> , C <sub>20</sub> H <sub>42</sub> , C <sub>21</sub> H <sub>44</sub> , C <sub>22</sub> H <sub>46</sub> , C <sub>23</sub> H <sub>48</sub> , C <sub>24</sub> H <sub>50</sub> , C <sub>25</sub> H <sub>52</sub> , C <sub>26</sub> H <sub>54</sub> , C <sub>27</sub> H <sub>56</sub> , C <sub>28</sub> H <sub>58</sub> , C <sub>29</sub> H <sub>60</sub> , C <sub>30</sub> H <sub>62</sub> , C <sub>31</sub> H <sub>64</sub> , C <sub>32</sub> H <sub>66</sub> , C <sub>33</sub> H <sub>68</sub> , C <sub>34</sub> H <sub>70</sub> , C <sub>35</sub> H <sub>72</sub> , C <sub>36</sub> H <sub>74</sub> , C <sub>37</sub> H <sub>76</sub> , C <sub>38</sub> H <sub>78</sub> , C <sub>39</sub> H <sub>80</sub> , C <sub>40</sub> H <sub>82</sub> , C <sub>41</sub> H <sub>84</sub> , C <sub>42</sub> H <sub>86</sub> , C <sub>43</sub> H <sub>88</sub> , C <sub>44</sub> H <sub>90</sub> , C <sub>45</sub> H <sub>92</sub> , C <sub>46</sub> H <sub>94</sub> , C <sub>47</sub> H <sub>96</sub> , C <sub>48</sub> H <sub>98</sub> , C <sub>49</sub> H <sub>100</sub> , C <sub>50</sub> H <sub>102</sub> , C <sub>51</sub> H <sub>104</sub> , C <sub>52</sub> H <sub>106</sub> , C <sub>53</sub> H <sub>108</sub> , C <sub>54</sub> H <sub>110</sub> , C <sub>55</sub> H <sub>112</sub> , C <sub>56</sub> H <sub>114</sub> , C <sub>57</sub> H <sub>116</sub> , C <sub>58</sub> H <sub>118</sub> , C <sub>59</sub> H <sub>120</sub> , C <sub>60</sub> H <sub>122</sub> , C <sub>61</sub> H <sub>124</sub> , C <sub>62</sub> H <sub>126</sub> , C <sub>63</sub> H <sub>128</sub> , C <sub>64</sub> H <sub>130</sub> , C <sub>65</sub> H <sub>132</sub> , C <sub>66</sub> H <sub>134</sub> , C <sub>67</sub> H <sub>136</sub> , C <sub>68</sub> H <sub>138</sub> , C <sub>69</sub> H <sub>140</sub> , C <sub>70</sub> H <sub>142</sub> , C <sub>71</sub> H <sub>144</sub> , C <sub>72</sub> H <sub>146</sub> , C <sub>73</sub> H <sub>148</sub> , C <sub>74</sub> H <sub>150</sub> , C <sub>75</sub> H <sub>152</sub> , C <sub>76</sub> H <sub>154</sub> , C <sub>77</sub> H <sub>156</sub> , C <sub>78</sub> H <sub>158</sub> , C <sub>79</sub> H <sub>160</sub> , C <sub>80</sub> H <sub>162</sub> , C <sub>81</sub> H <sub>164</sub> , C <sub>82</sub> H <sub>166</sub> , C <sub>83</sub> H <sub>168</sub> , C <sub>84</sub> H <sub>170</sub> , C <sub>85</sub> H <sub>172</sub> , C <sub>86</sub> H <sub>174</sub> , C <sub>87</sub> H <sub>176</sub> , C <sub>88</sub> H <sub>178</sub> , C <sub>89</sub> H <sub>180</sub> , C <sub>90</sub> H <sub>182</sub> , C <sub>91</sub> H <sub>184</sub> , C <sub>92</sub> H <sub>186</sub> , C <sub>93</sub> H <sub>188</sub> , C <sub>94</sub> H <sub>190</sub> , C <sub>95</sub> H <sub>192</sub> , C <sub>96</sub> H <sub>194</sub> , C <sub>97</sub> H <sub>196</sub> , C <sub>98</sub> H <sub>198</sub> , C <sub>99</sub> H <sub>200</sub> , C <sub>100</sub> H <sub>202</sub> , C <sub>101</sub> H <sub>204</sub> , C <sub>102</sub> H <sub>206</sub> , C <sub>103</sub> H <sub>208</sub> , C <sub>104</sub> H <sub>210</sub> , C <sub>105</sub> H <sub>212</sub> , C <sub>106</sub> H <sub>214</sub> , C <sub>107</sub> H <sub>216</sub> , C <sub>108</sub> H <sub>218</sub> , C <sub>109</sub> H <sub>220</sub> , C <sub>110</sub> H <sub>222</sub> , C <sub>111</sub> H <sub>224</sub> , C <sub>112</sub> H <sub>226</sub> , C <sub>113</sub> H <sub>228</sub> , C <sub>114</sub> H <sub>230</sub> , C <sub>115</sub> H <sub>232</sub> , C <sub>116</sub> H <sub>234</sub> , C <sub>117</sub> H <sub>236</sub> , C <sub>118</sub> H <sub>238</sub> , C <sub>119</sub> H <sub>240</sub> , C <sub>120</sub> H <sub>242</sub> , C <sub>121</sub> H <sub>244</sub> , C <sub>122</sub> H <sub>246</sub> , C <sub>123</sub> H <sub>248</sub> , C <sub>124</sub> H <sub>250</sub> , C <sub>125</sub> H <sub>252</sub> , C <sub>126</sub> H <sub>254</sub> , C <sub>127</sub> H <sub>256</sub> , C <sub>128</sub> H <sub>258</sub> , C <sub>129</sub> H <sub>260</sub> , C <sub>130</sub> H <sub>262</sub> , C <sub>131</sub> H <sub>264</sub> , C <sub>132</sub> H <sub>266</sub> , C <sub>133</sub> H <sub>268</sub> , C <sub>134</sub> H <sub>270</sub> , C <sub>135</sub> H <sub>272</sub> , C <sub>136</sub> H <sub>274</sub> , C <sub>137</sub> H <sub>276</sub> , C <sub>138</sub> H <sub>278</sub> , C <sub>139</sub> H <sub>280</sub> , C <sub>140</sub> H <sub>282</sub> , C <sub>141</sub> H <sub>284</sub> , C <sub>142</sub> H <sub>286</sub> , C <sub>143</sub> H <sub>288</sub> , C <sub>144</sub> H <sub>290</sub> , C <sub>145</sub> H <sub>292</sub> , C <sub>146</sub> H <sub>294</sub> , C <sub>147</sub> H <sub>296</sub> , C <sub>148</sub> H <sub>298</sub> , C <sub>149</sub> H <sub>300</sub> , C <sub>150</sub> H <sub>302</sub> , C <sub>151</sub> H <sub>304</sub> , C <sub>152</sub> H <sub>306</sub> , C <sub>153</sub> H <sub>308</sub> , C <sub>154</sub> H <sub>310</sub> , C <sub>155</sub> H <sub>312</sub> , C <sub>156</sub> H <sub>314</sub> , C <sub>157</sub> H <sub>316</sub> , C <sub>158</sub> H <sub>318</sub> , C <sub>159</sub> H <sub>320</sub> , C <sub>160</sub> H <sub>322</sub> , C <sub>161</sub> H <sub>324</sub> , C <sub>162</sub> H <sub>326</sub> , C <sub>163</sub> H <sub>328</sub> , C <sub>164</sub> H <sub>330</sub> , C <sub>165</sub> H <sub>332</sub> , C <sub>166</sub> H <sub>334</sub> , C <sub>167</sub> H <sub>336</sub> , C <sub>168</sub> H <sub>338</sub> , C <sub>169</sub> H <sub>340</sub> , C <sub>170</sub> H <sub>342</sub> , C <sub>171</sub> H <sub>344</sub> , C <sub>172</sub> H <sub>346</sub> , C <sub>173</sub> H <sub>348</sub> , C <sub>174</sub> H <sub>350</sub> , C <sub>175</sub> H <sub>352</sub> , C <sub>176</sub> H <sub>354</sub> , C <sub>177</sub> H <sub>356</sub> , C <sub>178</sub> H <sub>358</sub> , C <sub>179</sub> H <sub>360</sub> , C <sub>180</sub> H <sub>362</sub> , C <sub>181</sub> H <sub>364</sub> , C <sub>182</sub> H <sub>366</sub> , C <sub>183</sub> H <sub>368</sub> , C <sub>184</sub> H <sub>370</sub> , C <sub>185</sub> H <sub>372</sub> , C <sub>186</sub> H <sub>374</sub> , C <sub>187</sub> H <sub>376</sub> , C <sub>188</sub> H <sub>378</sub> , C <sub>189</sub> H <sub>380</sub> , C <sub>190</sub> H <sub>382</sub> , C <sub>191</sub> H <sub>384</sub> , C <sub>192</sub> H <sub>386</sub> , C <sub>193</sub> H <sub>388</sub> , C <sub>194</sub> H <sub>390</sub> , C <sub>195</sub> H <sub>392</sub> , C <sub>196</sub> H <sub>394</sub> , C <sub>197&lt;/</sub>

```
*z = scaled distance on framing camera slide projection
**y = actual distance
```

Calculated Velocity  $V_D = 0.15275 \text{ in}/\mu\text{sec}$

TABLE 31

SHOT NUMBER	LASL 1278	SCALE FACTOR	1.7/1.0
MEASUREMENT	Flyer Plate		

[illegible]

\*z = scaled distance on framing camera slide projection  
 \*\*y = actual distance

Calculated Velocity  $V_C = 0.11946 \text{ in}/\mu\text{sec}$

MEASUREMENT	Detonation Front
Pressure	1000-1500 atm
Temperature	2000-3000 K
Velocity	1500-2500 m/s
Acceleration	10 <sup>5</sup> -10 <sup>6</sup> g
Time	10 <sup>-6</sup> -10 <sup>-5</sup> s
Length	10 <sup>-3</sup> -10 <sup>-2</sup> m
Area	10 <sup>-4</sup> -10 <sup>-3</sup> m <sup>2</sup>
Volume	10 <sup>-6</sup> -10 <sup>-5</sup> m <sup>3</sup>
Mass	10 <sup>-9</sup> -10 <sup>-8</sup> kg
Energy	10 <sup>-10</sup> -10 <sup>-9</sup> J
Power	10 <sup>-10</sup> -10 <sup>-9</sup> W
Frequency	10 <sup>10</sup> -10 <sup>11</sup> Hz
Wavelength	10 <sup>-10</sup> -10 <sup>-9</sup> m
Amplitude	10 <sup>-10</sup> -10 <sup>-9</sup> m
Phase	0-2π
Period	10 <sup>-10</sup> -10 <sup>-9</sup> s
Wave Number	10 <sup>10</sup> -10 <sup>11</sup> m <sup>-1</sup>
Angular Frequency	10 <sup>10</sup> -10 <sup>11</sup> rad/s
Angular Velocity	10 <sup>10</sup> -10 <sup>11</sup> rad/s
Angular Acceleration	10 <sup>10</sup> -10 <sup>11</sup> rad/s <sup>2</sup>
Angular Displacement	10 <sup>-10</sup> -10 <sup>-9</sup> rad
Angular Momentum	10 <sup>-10</sup> -10 <sup>-9</sup> kg m <sup>2</sup> /s
Angular Impulse	10 <sup>-10</sup> -10 <sup>-9</sup> kg m <sup>2</sup> /s
Angular Force	10 <sup>-10</sup> -10 <sup>-9</sup> N
Angular Torque	10 <sup>-10</sup> -10 <sup>-9</sup> N m
Angular Power	10 <sup>-10</sup> -10 <sup>-9</sup> W
Angular Energy	10 <sup>-10</sup> -10 <sup>-9</sup> J
Angular Mass	10 <sup>-10</sup> -10 <sup>-9</sup> kg
Angular Length	10 <sup>-10</sup> -10 <sup>-9</sup> m
Angular Area	10 <sup>-10</sup> -10 <sup>-9</sup> m <sup>2</sup>
Angular Volume	10 <sup>-10</sup> -10 <sup>-9</sup> m <sup>3</sup>
Angular Density	10 <sup>-10</sup> -10 <sup>-9</sup> kg/m <sup>3</sup>
Angular Pressure	10 <sup>-10</sup> -10 <sup>-9</sup> atm
Angular Temperature	10 <sup>-10</sup> -10 <sup>-9</sup> K
Angular Velocity	10 <sup>-10</sup> -10 <sup>-9</sup> m/s
Angular Acceleration	10 <sup>-10</sup> -10 <sup>-9</sup> m/s <sup>2</sup>
Angular Displacement	10 <sup>-10</sup> -10 <sup>-9</sup> m
Angular Momentum	10 <sup>-10</sup> -10 <sup>-9</sup> kg m <sup>2</sup> /s
Angular Impulse	10 <sup>-10</sup> -10 <sup>-9</sup> kg m <sup>2</sup> /s
Angular Force	10 <sup>-10</sup> -10 <sup>-9</sup> N
Angular Torque	10 <sup>-10</sup> -10 <sup>-9</sup> N m
Angular Power	10 <sup>-10</sup> -10 <sup>-9</sup> W
Angular Energy	10 <sup>-10</sup> -10 <sup>-9</sup> J
Angular Mass	10 <sup>-10</sup> -10 <sup>-9</sup> kg
Angular Length	10 <sup>-10</sup> -10 <sup>-9</sup> m
Angular Area	10 <sup>-10</sup> -10 <sup>-9</sup> m <sup>2</sup>
Angular Volume	10 <sup>-10</sup> -10 <sup>-9</sup> m <sup>3</sup>
Angular Density	10 <sup>-10</sup> -10 <sup>-9</sup> kg/m <sup>3</sup>
Angular Pressure	10 <sup>-10</sup> -10 <sup>-9</sup> atm
Angular Temperature	10 <sup>-10</sup> -10 <sup>-9</sup> K
Angular Velocity	10 <sup>-10</sup> -10 <sup>-9</sup> m/s
Angular Acceleration	10 <sup>-10</sup> -10 <sup>-9</sup> m/s <sup>2</sup>
Angular Displacement	10 <sup>-10</sup> -10 <sup>-9</sup> m
Angular Momentum	10 <sup>-10</sup> -10 <sup>-9</sup> kg m <sup>2</sup> /s
Angular Impulse	10 <sup>-10</sup> -10 <sup>-9</sup> kg m <sup>2</sup> /s
Angular Force	10 <sup>-10</sup> -10 <sup>-9</sup> N
Angular Torque	10 <sup>-10</sup> -10 <sup>-9</sup> N m
Angular Power	10 <sup>-10</sup> -10 <sup>-9</sup> W
Angular Energy	10 <sup>-10</sup> -10 <sup>-9</sup> J
Angular Mass	10 <sup>-10</sup> -10 <sup>-9</sup> kg
Angular Length	10 <sup>-10</sup> -10 <sup>-9</sup> m
Angular Area	10 <sup>-10</sup> -10 <sup>-9</sup> m <sup>2</sup>
Angular Volume	10 <sup>-10</sup> -10 <sup>-9</sup> m <sup>3</sup>
Angular Density	10 <sup>-10</sup> -10 <sup>-9</sup> kg/m <sup>3</sup>
Angular Pressure	10 <sup>-10</sup> -10 <sup>-9</sup> atm
Angular Temperature	10 <sup>-10</sup> -10 <sup>-9</sup> K
Angular Velocity	10 <sup>-10</sup> -10 <sup>-9</sup> m/s
Angular Acceleration	10 <sup>-10</sup> -10 <sup>-9</sup> m/s <sup>2</sup>
Angular Displacement	10 <sup>-10</sup> -10 <sup>-9</sup> m
Angular Momentum	10 <sup>-10</sup> -10 <sup>-9</sup> kg m <sup>2</sup> /s
Angular Impulse	10 <sup>-10</sup> -10 <sup>-9</sup> kg m <sup>2</sup> /s
Angular Force	10 <sup>-10</sup> -10 <sup>-9</sup> N
Angular Torque	10 <sup>-10</sup> -10 <sup>-9</sup> N m
Angular Power	10 <sup>-10</sup> -10 <sup>-9</sup> W
Angular Energy	10 <sup>-10</sup> -10 <sup>-9</sup> J
Angular Mass	10 <sup>-10</sup> -10 <sup>-9</sup> kg
Angular Length	10 <sup>-10</sup> -10 <sup>-9</sup> m
Angular Area	10 <sup>-10</sup> -10 <sup>-9</sup> m <sup>2</sup>
Angular Volume	10 <sup>-10</sup> -10 <sup>-9</sup> m <sup>3</sup>
Angular Density	10 <sup>-10</sup> -10 <sup>-9</sup> kg/m <sup>3</sup>
Angular Pressure	10 <sup>-10</sup> -10 <sup>-9</sup> atm
Angular Temperature	10 <sup>-10</sup> -10 <sup>-9</sup> K
Angular Velocity	10 <sup>-10</sup> -10 <sup>-9</sup> m/s
Angular Acceleration	10 <sup>-10</sup> -10 <sup>-9</sup> m/s <sup>2</sup>
Angular Displacement	10 <sup>-10</sup> -10 <sup>-9</sup> m
Angular Momentum	10 <sup>-10</sup> -10 <sup>-9</sup> kg m <sup>2</sup> /s
Angular Impulse	10 <sup>-10</sup> -10 <sup>-9</sup> kg m <sup>2</sup> /s
Angular Force	10 <sup>-10</sup> -10 <sup>-9</sup> N
Angular Torque	10 <sup>-10</sup> -10 <sup>-9</sup> N m
Angular Power	10 <sup>-10</sup> -10 <sup>-9</sup> W
Angular Energy	10 <sup>-10</sup> -10 <sup>-9</sup> J
Angular Mass	10 <sup>-10</sup> -10 <sup>-9</sup> kg
Angular Length	10 <sup>-10</sup> -10 <sup>-9</sup> m
Angular Area	10 <sup>-10</sup> -10 <sup>-9</sup> m <sup>2</sup>

**\*\*y = actual distance**

Calculated Velocity  $V_D = 0.15012 \text{ in}/\mu\text{sec}$



TABLE 33

SHOT NUMBER LASL 1279 SCALE FACTOR 1.7/1.0

MEASUREMENT Flyer Plate

[illegible]

\*z = scaled distance on framing camera slide projection  
 \*\*y = actual distance

Calculated Velocity  $V_C = 0.10537 \text{ in/usec}$

TABLE 34

SHOT NUMBER LASL 1280 SCALE FACTOR 1.6/1.0  
 MEASUREMENT Detonation Front

FRAME	t ( $\mu$ sec)	z* (in)	y** (in)
1	0	0	0
2	4	0.60	0.38
3	8	1.85	1.16
4	12	2.70	1.69
5	16	3.35	2.10
6	20	4.25	2.66
7	24	4.70	2.94
8	28	5.40	3.38
9	32	6.05	3.78
10	36	6.45	4.03
11	40	6.95	4.34
12	44	8.10	5.06
13	48	8.85	5.53
14	52	9.65	6.03
15	56	10.40	6.50
16	60	11.05	6.91
17	64	11.70	7.31
18	68	12.25	7.66

\*z = scaled distance on framing camera slide projection  
 \*\*y = actual distance

Calculated Velocity  $V_D = 0.11120$  in/ $\mu$ sec

TABLE 35

SHOT NUMBER LASL 1280 SCALE FACTOR 1.6/1.0

MEASUREMENT Flyer Plate[illegible]

\*z = scaled distance on framing camera slide projection  
 \*\*y = actual distance

Calculated Velocity  $V_C = 0.12693 \text{ in}/\mu\text{sec}$

SHOT NUMBER	<u>LASL 1281</u>	SCALE FACTOR	<u>1.7/1.0</u>
MEASUREMENT	Detonation Front		

[illegible]

```
*z = scaled distance on framing camera slide projection
**y = actual distance
```

Calculated Velocity  $V_D = 0.13434 \text{ in/usec}$

TABLE 37

SHOT NUMBER LASL 1281 SCALE FACTOR 1.7/1.0

MEASUREMENT Flyer Plate

[illegible]

\*z = scaled distance on framing camera slide projection  
 \*\*y = actual distance

Calculated Velocity  $V_C = 0.10915 \text{ in}/\mu\text{sec}$



0

0

TABLE 39

SHOT NUMBER LASL 1282 SCALE FACTOR 1.8/1.0

MEASUREMENT      Flyer Plate

[illegible]

\*z = scaled distance on framing camera slide projection

**\*\*y** = actual distance

Calculated Velocity  $V_G = 0.09214 \text{ in}/\mu\text{sec}$

TABLE 40

SHOT NUMBER LASL 1283 SCALE FACTOR 1.8/1.0

MEASUREMENT Detonation Front

[illegible]

\*z = scaled distance on framing camera slide projection  
 \*\*y = actual distance

Calculated Velocity  $V_D = 0.20396 \text{ in}/\mu\text{sec}$

TABLE 41

SHOT NUMBER      LASL 1283      SCALE FACTOR      1.8/1.0

MEASUREMENT Flyer Plate[illegible]

\*z = scaled distance on framing camera slide projection  
 \*\*y = actual distance

Calculated Velocity  $V_C = 0.12691 \text{ in}/\mu\text{sec}$

MEASUREMENT	Detonation Front
Pressure	1000-1500 atm
Temperature	2000-3000 K
Velocity	1500-2500 m/s
Acceleration	10 <sup>5</sup> -10 <sup>6</sup> g
Time	10 <sup>-6</sup> -10 <sup>-5</sup> s
Length	10 <sup>-3</sup> -10 <sup>-2</sup> m
Mass	10 <sup>-6</sup> -10 <sup>-4</sup> g
Energy	10 <sup>-3</sup> -10 <sup>-1</sup> J
Power	10 <sup>3</sup> -10 <sup>5</sup> W
Force	10 <sup>2</sup> -10 <sup>4</sup> N
Stress	10 <sup>8</sup> -10 <sup>10</sup> Pa
Strain	10 <sup>-2</sup> -10 <sup>0</sup>
Displacement	10 <sup>-3</sup> -10 <sup>-1</sup> m
Angular displacement	10 <sup>-1</sup> -10 <sup>1</sup> rad
Angular velocity	10 <sup>3</sup> -10 <sup>5</sup> rad/s
Angular acceleration	10 <sup>5</sup> -10 <sup>7</sup> rad/s <sup>2</sup>
Frequency	10 <sup>3</sup> -10 <sup>5</sup> Hz
Wavelength	10 <sup>-3</sup> -10 <sup>-1</sup> m
Wave number	10 <sup>3</sup> -10 <sup>5</sup> m <sup>-1</sup>
Wave velocity	10 <sup>3</sup> -10 <sup>5</sup> m/s
Wave acceleration	10 <sup>5</sup> -10 <sup>7</sup> m/s <sup>2</sup>
Wave force	10 <sup>2</sup> -10 <sup>4</sup> N
Wave stress	10 <sup>8</sup> -10 <sup>10</sup> Pa
Wave strain	10 <sup>-2</sup> -10 <sup>0</sup>
Wave displacement	10 <sup>-3</sup> -10 <sup>-1</sup> m
Wave angular displacement	10 <sup>-1</sup> -10 <sup>1</sup> rad
Wave angular velocity	10 <sup>3</sup> -10 <sup>5</sup> rad/s
Wave angular acceleration	10 <sup>5</sup> -10 <sup>7</sup> rad/s <sup>2</sup>
Wave frequency	10 <sup>3</sup> -10 <sup>5</sup> Hz
Wave wavelength	10 <sup>-3</sup> -10 <sup>-1</sup> m
Wave wave number	10 <sup>3</sup> -10 <sup>5</sup> m <sup>-1</sup>
Wave wave velocity	10 <sup>3</sup> -10 <sup>5</sup> m/s
Wave wave acceleration	10 <sup>5</sup> -10 <sup>7</sup> m/s <sup>2</sup>
Wave wave force	10 <sup>2</sup> -10 <sup>4</sup> N
Wave wave stress	10 <sup>8</sup> -10 <sup>10</sup> Pa
Wave wave strain	10 <sup>-2</sup> -10 <sup>0</sup>
Wave wave displacement	10 <sup>-3</sup> -10 <sup>-1</sup> m
Wave wave angular displacement	10 <sup>-1</sup> -10 <sup>1</sup> rad
Wave wave angular velocity	10 <sup>3</sup> -10 <sup>5</sup> rad/s
Wave wave angular acceleration	10 <sup>5</sup> -10 <sup>7</sup> rad/s <sup>2</sup>
Wave wave frequency	10 <sup>3</sup> -10 <sup>5</sup> Hz
Wave wave wavelength	10 <sup>-3</sup> -10 <sup>-1</sup> m
Wave wave wave number	10 <sup>3</sup> -10 <sup>5</sup> m <sup>-1</sup>
Wave wave wave velocity	10 <sup>3</sup> -10 <sup>5</sup> m/s
Wave wave wave acceleration	10 <sup>5</sup> -10 <sup>7</sup> m/s <sup>2</sup>
Wave wave wave force	10 <sup>2</sup> -10 <sup>4</sup> N
Wave wave wave stress	10 <sup>8</sup> -10 <sup>10</sup> Pa
Wave wave wave strain	10 <sup>-2</sup> -10 <sup>0</sup>
Wave wave wave displacement	10 <sup>-3</sup> -10 <sup>-1</sup> m
Wave wave wave angular displacement	10 <sup>-1</sup> -10 <sup>1</sup> rad
Wave wave wave angular velocity	10 <sup>3</sup> -10 <sup>5</sup> rad/s
Wave wave wave angular acceleration	10 <sup>5</sup> -10 <sup>7</sup> rad/s <sup>2</sup>
Wave wave wave frequency	10 <sup>3</sup> -10 <sup>5</sup> Hz
Wave wave wave wavelength	10 <sup>-3</sup> -10 <sup>-1</sup> m
Wave wave wave wave number	10 <sup>3</sup> -10 <sup>5</sup> m <sup>-1</sup>
Wave wave wave wave velocity	10 <sup>3</sup> -10 <sup>5</sup> m/s
Wave wave wave wave acceleration	10 <sup>5</sup> -10 <sup>7</sup> m/s <sup>2</sup>
Wave wave wave wave force	10 <sup>2</sup> -10 <sup>4</sup> N
Wave wave wave wave stress	10 <sup>8</sup> -10 <sup>10</sup> Pa
Wave wave wave wave strain	10 <sup>-2</sup> -10 <sup>0</sup>
Wave wave wave wave displacement	10 <sup>-3</sup> -10 <sup>-1</sup> m
Wave wave wave wave angular displacement	10 <sup>-1</sup> -10 <sup>1</sup> rad
Wave wave wave wave angular velocity	10 <sup>3</sup> -10 <sup>5</sup> rad/s
Wave wave wave wave angular acceleration	10 <sup>5</sup> -10 <sup>7</sup> rad/s <sup>2</sup>
Wave wave wave wave frequency	10 <sup>3</sup> -10 <sup>5</sup> Hz
Wave wave wave wave wavelength	10 <sup>-3</sup> -10 <sup>-1</sup> m
Wave wave wave wave wave number	10 <sup>3</sup> -10 <sup>5</sup> m <sup>-1</sup>
Wave wave wave wave wave velocity	10 <sup>3</sup> -10 <sup>5</sup> m/s
Wave wave wave wave wave acceleration	10 <sup>5</sup> -10 <sup>7</sup> m/s <sup>2</sup>
Wave wave wave wave wave force	10 <sup>2</sup> -10 <sup>4</sup> N
Wave wave wave wave wave stress	10 <sup>8</sup> -10 <sup>10</sup> Pa
Wave wave wave wave wave strain	10 <sup>-2</sup> -10 <sup>0</sup>
Wave wave wave wave wave displacement	10 <sup>-3</sup> -10 <sup>-1</sup> m
Wave wave wave wave wave angular displacement	10 <sup>-1</sup> -10 <sup>1</sup> rad
Wave wave wave wave wave angular velocity	10 <sup>3</sup> -10 <sup>5</sup> rad/s
Wave wave wave wave wave angular acceleration	10 <sup>5</sup> -10 <sup>7</sup> rad/s <sup>2</sup>
Wave wave wave wave wave frequency	10 <sup>3</sup> -10 <sup>5</sup> Hz
Wave wave wave wave wave wavelength	10 <sup>-3</sup> -10 <sup>-1</sup> m
Wave wave wave wave wave wave number	10 <sup>3</sup> -10 <sup>5</sup> m <sup>-1</sup>
Wave wave wave wave wave wave velocity	10 <sup>3</sup> -10 <sup>5</sup> m/s
Wave wave wave wave wave wave acceleration	10 <sup>5</sup> -10 <sup>7</sup> m/s <sup>2</sup>
Wave wave wave wave wave wave force	10 <sup>2</sup> -10 <sup>4</sup> N
Wave wave wave wave wave wave stress	10 <sup>8</sup> -10 <sup>10</sup> Pa
Wave wave wave wave wave wave strain	10 <sup>-2</sup> -10 <sup>0</sup>
Wave wave wave wave wave wave displacement	10 <sup>-3</sup> -10 <sup>-1</sup> m
Wave wave wave wave wave wave angular displacement	10 <sup>-1</sup> -10 <sup>1</sup> rad
Wave wave wave wave wave wave angular velocity	10 <sup>3</sup> -10 <sup>5</sup> rad/s
Wave wave wave wave wave wave angular acceleration	10 <sup>5</sup> -10 <sup>7</sup> rad/s <sup>2</sup>
Wave wave wave wave wave wave frequency	10 <sup>3</sup> -10 <sup>5</sup> Hz
Wave wave wave wave wave wave wavelength	10 <sup>-3</sup> -10 <sup>-1</sup> m
Wave wave wave wave wave wave wave number	10 <sup>3</sup> -10 <sup>5</sup> m <sup>-1</sup>
Wave wave wave wave wave wave wave velocity	10 <sup>3</sup> -10 <sup>5</sup> m/s
Wave wave wave wave wave wave wave acceleration	10 <sup>5</sup> -10 <sup>7</sup> m/s <sup>2</sup>
Wave wave wave wave	



TABLE 43

SHOT NUMBER LASL 1284 SCALE FACTOR 1.8/1.0

MEASUREMENT      Flyer Plate

[illegible]

\*z = scaled distance on framing camera slide projection  
 \*\*y = actual distance

Calculated Velocity  $V_C = 0.12271 \text{ in}/\mu\text{sec}$

MEASUREMENT Detonation Front

[illegible]

TABLE 45

SHOT NUMBER      LASL 1285                      SCALE FACTOR      1.8/1.0

MEASUREMENT    Flyer Plate

[illegible]

\*z = scaled distance on framing camera slide projection  
\*\*y = actual distance

Calculated Velocity  $V_c = 0.10264 \text{ in}/\mu\text{sec}$

TABLE 46

SHOT NUMBER LASL 1286 SCALE FACTOR 1.8/1.0  
 MEASUREMENT Detonation Front

FRAME	t ( $\mu$ sec)	z* (in)	y** (in)
1	0	0	0
2	4	0.60	0.33
3	8	1.45	0.81
4	12	2.35	1.31
5	16	3.10	1.72
6	20	3.90	2.17
7	24	4.45	2.47
8	28	5.50	3.10
9	32	7.00	3.88
10	36	7.80	4.33
11	40	8.80	4.88
12	44	10.00	5.55
13	48	11.00	6.11
14	52	11.80	6.55
15	56	13.25	7.36
16	60	14.55	8.08
17	64	15.40	8.55
18	68	16.60	9.22

\*z = scaled distance on framing camera slide projection  
 \*\*y = actual distance

Calculated Velocity  $V_D = 0.13760$  in/ $\mu$ sec

TABLE 47

SHOT NUMBER      LASL 1286      SCALE FACTOR      1.8/1.0

MEASUREMENT Flyer Plate[illegible]

\*z = scaled distance on framing camera slide projection  
 \*\*y = actual distance

Calculated Velocity  $V_C = 0.13808$  in/psec



TABLE 48

SHOT NUMBER LASL 1312 SCALE FACTOR 3.2/1.0MEASUREMENT Detonation Front

FRAME	t ( $\mu$ sec)	z* (in)	y** (in)
2	0	0	0
3	4	1.00	0.31
4	8	1.55	0.48
5	12	2.55	0.80
6	16	3.45	1.08
7	20	4.70	1.47
8	24	6.40	2.00
9	28	7.55	2.36
10	32	9.15	2.86
11	36	10.85	3.39
12	40	12.25	3.83
13	44	13.50	4.22
14	48	14.75	4.61
15	52	16.40	5.13
16	56	17.90	5.59
17	60	19.15	5.98
18	64	20.30	6.34
19	68	22.20	6.94
20	72	23.95	7.48
21	76	24.95	7.80

\*z = scaled distance on framing camera slide projection

\*\*y = actual distance

Calculated Velocity  $V_D = 0.10670$  in/ $\mu$ sec

TABLE 49

SHOT NUMBER IASL 1312 SCALE FACTOR 3.2/1.0

MEASUREMENT Flyer Plate[illegible]

\*z = scaled distance on framing camera slide projection  
\*\*y = actual distance

Calculated Velocity  $V_c = 0.11102 \text{ in}/\mu\text{sec}$

TABLE 50

SHOT NUMBER LASL 1317 SCALE FACTOR 3.2/1.0  
 MEASUREMENT Detonation Front

FRAME	t ( $\mu$ sec)	z* (in)	y** (in)
3	0	0	0
4	4	1.05	0.33
5	8	2.50	0.78
6	12	3.25	1.02
7	16	4.15	1.30
8	20	5.50	1.66
9	24	6.05	1.89
10	28	7.10	2.22
11	32	8.00	2.50
12	36	9.45	2.95
13	40	10.70	3.34
14	44	12.40	3.87
15	48	14.05	4.39
16	52	15.30	4.78
17	56	17.25	5.39
18	60	19.00	5.94
19	64	20.30	6.34
20	68	22.05	6.89
21	72	23.40	7.31
22	76	24.40	7.63

\*z = scaled distance on framing camera slide projection  
 \*\*y = actual distance

Calculated Velocity  $V_D = 0.10237$  in/ $\mu$ sec

TABLE 51

SHOT NUMBER LASL 1317 SCALE FACTOR 3.2/1.0MEASUREMENT Flyer Plate

FRAME	t ( $\mu$ sec)	z* (in)	y** (in)
5	0	0	0
6	4	1.05	0.33
7	8	3.20	1.00
8	12	4.25	1.33
9	16	6.05	1.89
10	20	7.30	2.28
11	24	8.15	2.55
12	28	8.95	2.80
13	32	11.00	3.44
14	36	12.30	3.84
15	40	13.70	4.28
16	44	15.00	4.69
17	48	16.55	5.17
18	52	17.60	5.50
19	56	18.95	5.92
20	60	19.95	6.23
21	64	21.50	6.72
22	68	23.60	7.38

\*z = scaled distance on framing camera slide projection

\*\*y = actual distance

Calculated Velocity  $V_c = 0.10528$  in/ $\mu$ sec

MEASUREMENT Detonation Front

[illegible]

Calculated Velocity  $V_D = 0.12148 \text{ in}/\mu\text{sec}$



TABLE 53

SHOT NUMBER	LASL 1320	SCALE FACTOR	3.0/1.0
-------------	-----------	--------------	---------

MEASUREMENT      Flyer Plate

[illegible]

\*z = scaled distance on framing camera slide projection  
 \*\*y = actual distance

Calculated Velocity  $V_c = 0.13759 \text{ in}/\mu\text{sec}$

TABLE 54

SHOT NUMBER LASL 1321 SCALE FACTOR 4.5/1.0MEASUREMENT Detonation Front

FRAME	t ( $\mu$ sec)	z* (in)	y** (in)
1	0	0	0
2	4	3.10	0.69
3	8	6.95	1.54
4	12	10.75	2.39
5	16	13.25	2.94
6	20	16.25	3.61
7	24	18.30	4.07
8	28	20.35	4.52
9	32	22.55	5.01
10	36	24.25	5.39
11	40	26.65	5.92
12	44	29.25	6.50
13	48	31.15	6.92
14	52	33.50	7.44
15	56	35.30	7.84
16	60	36.65	8.14
17	64	39.10	8.69
18	68	41.15	9.14

\*z = scaled distance on framing camera slide projection  
 \*\*y = actual distance

Calculated Velocity  $V_D = 0.12939$  in/ $\mu$ sec

TABLE 55

SHOT NUMBER LASL 1321 SCALE FACTOR 4.5/1.0

MEASUREMENT      Flyer Plates Projection by WEF

[illegible]

\*z = scaled distance on framing camera slide projection  
 \*\*y = actual distance

Calculated Velocity  $V_c = 0.12253 \text{ in/psec}$

TABLE 56

SHOT NUMBER LASL 1322 SCALE FACTOR 2.9/1.0MEASUREMENT Detonation Front

FRAME	t (u sec)	z* (in)	y** (in)
1	0	0	0
2	4	1.30	0.45
3	8	2.30	0.79
4	12	3.20	1.10
5	16	4.05	1.40
6	20	6.20	2.14
7	24	7.35	2.53
8	28	9.15	3.16
9	32	10.50	3.62
10	36	11.45	3.95
11	40	12.90	4.45
12	44	14.70	5.07
13	48	15.55	5.36
14	52	17.00	5.86
15	56	18.45	6.36
16	60	19.65	6.78
17	64	21.05	7.26
18	68	22.40	7.72
19	72	23.65	8.16

\*z = scaled distance on framing camera slide projection  
 \*\*y = actual distance

Calculated Velocity  $v_p = 0.11570$  in/usec

TABLE 57

SHOT NUMBER LASL 1322 SCALE FACTOR 2.9/1.0MEASUREMENT Flyer Plate

FRAME	t ( $\mu$ sec)	z* (in)	y** (in)
2	0	0	0
3	4	1.70	0.59
4	8	2.95	1.02
5	12	4.75	1.64
6	16	5.75	1.98
7	20	6.90	2.38
8	24	8.40	2.90
9	28	10.00	3.45
10	32	10.80	3.72
11	36	12.35	4.26
12	40	13.80	4.76
13	44	15.10	5.21
14	48	16.15	5.57
15	52	17.25	5.95
16	56	18.05	6.22
17	60	18.85	6.50
18	64	19.80	6.83
19	68	21.05	7.26

\*z = scaled distance on framing camera slide projection  
 \*\*y = actual distance

Calculated Velocity  $V_c = 0.10648$  in/ $\mu$ sec



MEASUREMENT Detonation Front

[illegible]

\*\*y = actual distance

Calculated Velocity  $v_p = 0.11145 \text{ in/usec}$

TABLE 59

SHOT NUMBER LASL 1323 SCALE FACTOR 1.9/1.0

MEASUREMENT Flyer Plate[illegible]

\*z = scaled distance on framing camera slide projection  
 \*\*y = actual distance

Calculated Velocity  $V_c = 0.12042 \text{ in}/\mu\text{sec}$

TABLE 60

SHOT NUMBER LASL 1324 SCALE FACTOR 2.8/1.0  
 MEASUREMENT Detonation Front

FRAME	t ( $\mu$ sec)	z* (in)	y** (in)
1	0	0	0
2	4	1.15	0.41
3	8	2.05	0.73
4	12	3.05	1.09
5	16	4.05	1.45
6	20	5.20	1.86
7	24	6.65	2.37
8	28	7.75	2.77
9	32	9.50	3.39
10	36	11.45	4.09
11	40	12.70	4.54
12	44	14.10	5.03
13	48	15.65	5.59
14	52	16.80	6.00
15	56	18.15	6.48
16	60	19.40	6.93
17	64	20.50	7.32
18	68	21.80	7.78
19	72	22.85	8.16
20	76	24.25	8.66
21	80	25.10	8.96

\*z = scaled distance on framing camera slide projection  
 \*\*y = actual distance

Calculated Velocity  $V_D = 0.11758$  in/ $\mu$ sec

TABLE 61

SHOT NUMBER      LASL 1324                      SCALE FACTOR      2.8/1.0

MEASUREMENT Flyer Plate

[illegible]

\*z = scaled distance on framing camera slide projection

$$**y = \text{actual distance}$$

Calculated Velocity  $V_C = 0.11866 \text{ in}/\mu\text{sec}$

TABLE 62

SHOT NUMBER LASL 1325 SCALE FACTOR 2.9/1.0MEASUREMENT Detonation Front

FRAME	t ( $\mu$ sec)	z* (in)	y** (in)
1	0	0	0
2	4	1.30	0.45
3	8	2.15	0.74
4	12	2.75	0.95
5	16	3.55	1.22
6	20	4.50	1.55
7	24	5.50	1.90
8	28	6.30	2.17
9	32	7.75	2.67
10	36	8.90	3.07
11	40	10.15	3.50
12	44	11.10	3.83
13	48	12.95	4.46
14	52	13.90	4.79
15	56	15.70	5.41
16	60	17.00	5.86
17	64	18.30	6.31
18	68	19.70	6.79
19	72	21.00	7.24
20	76	22.40	7.72

\*z = scaled distance on framing camera slide projection

\*\*y = actual distance

Calculated Velocity  $V_D = 0.10224$  in/ $\mu$ sec



TABLE 63

SHOT NUMBER LASL 1325 SCALE FACTOR 2.9/1.0

MEASUREMENT Flyer Plate

[illegible]

\*z = scaled distance on framing camera slide projection  
 \*\*y = actual distance

Calculated Velocity  $V_c = 0.12011 \text{ in}/\mu\text{sec}$

TABLE 64

SHOT NUMBER LASL 1328 SCALE FACTOR 2.9/1.0

MEASUREMENT Detonation Front

[illegible]

\*z = scaled distance on framing camera slide projection  
 \*\*y = actual distance

Calculated Velocity  $\frac{V}{D} = 0.11670 \text{ in}/\mu\text{sec}$

TABLE 65

SHOT NUMBER LASL 1328 SCALE FACTOR 2.9/1.0

MEASUREMENT Flyer Plate[illegible]

\*z = scaled distance on framing camera slide projection  
 \*\*y = actual distance

Calculated Velocity  $V_c = 0.12500 \text{ in}/\mu\text{sec}$

TABLE 66

SHOT NUMBER LASL 1362 SCALE FACTOR 3.4/1.0

MEASUREMENT Detonation Front

[illegible]

\*z = scaled distance on framing camera slide projection  
 \*\*y = actual distance

Calculated Velocity  $V_D = 0.12688 \text{ in}/\mu\text{sec}$

TABLE 67

SHOT NUMBER LASL 1362 SCALE FACTOR 3.4/1.0

MEASUREMENT Flyer Plate[illegible]

\*z = scaled distance on framing camera slide projection

**\*\*y** = actual distance

Calculated Velocity  $V_G = 0.12759 \text{ in}/\mu\text{sec}$



LASL 1268  
DETONATION POSITION

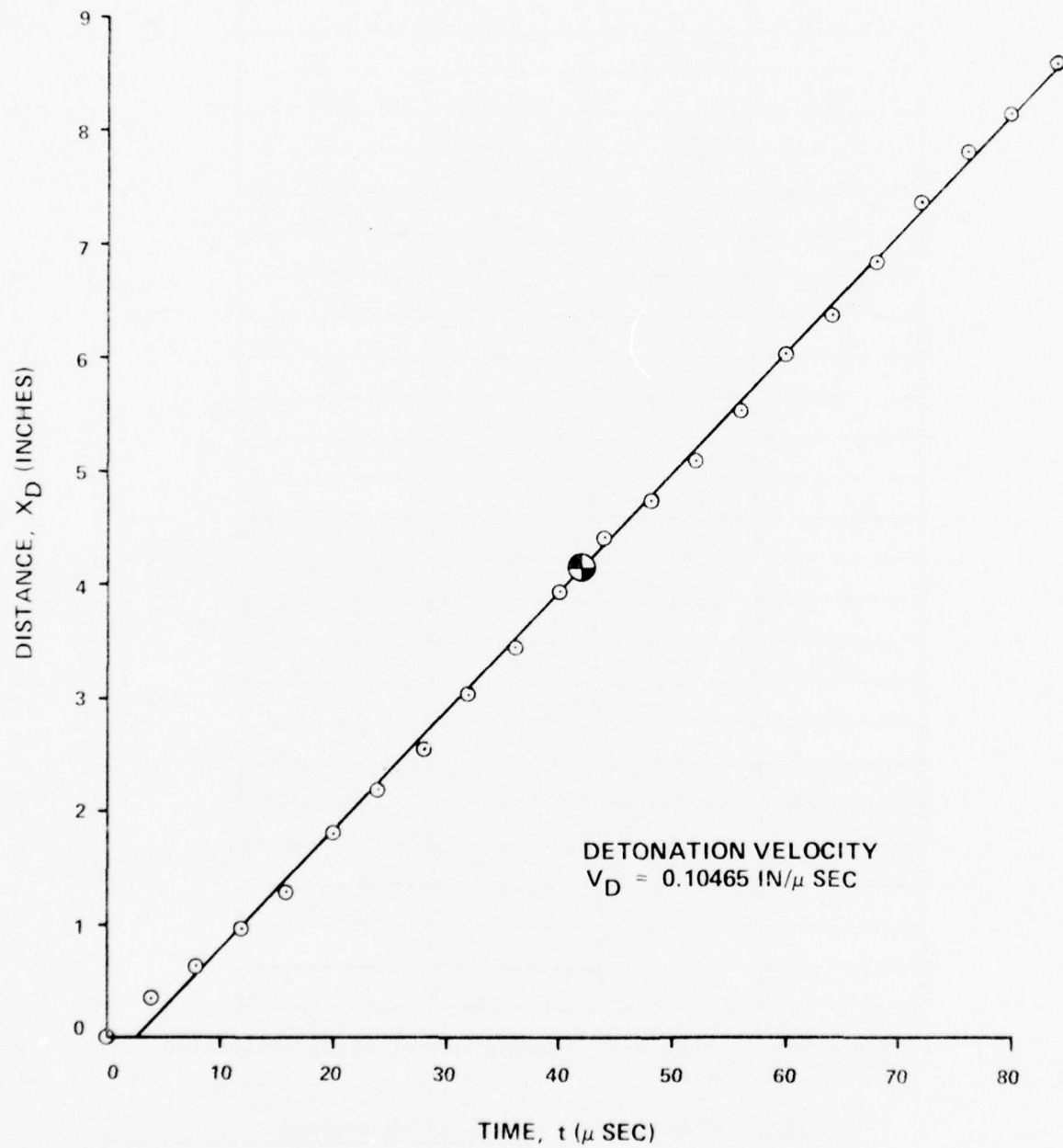


Figure 85

LASL 1268  
FLYER PLATE POSITION

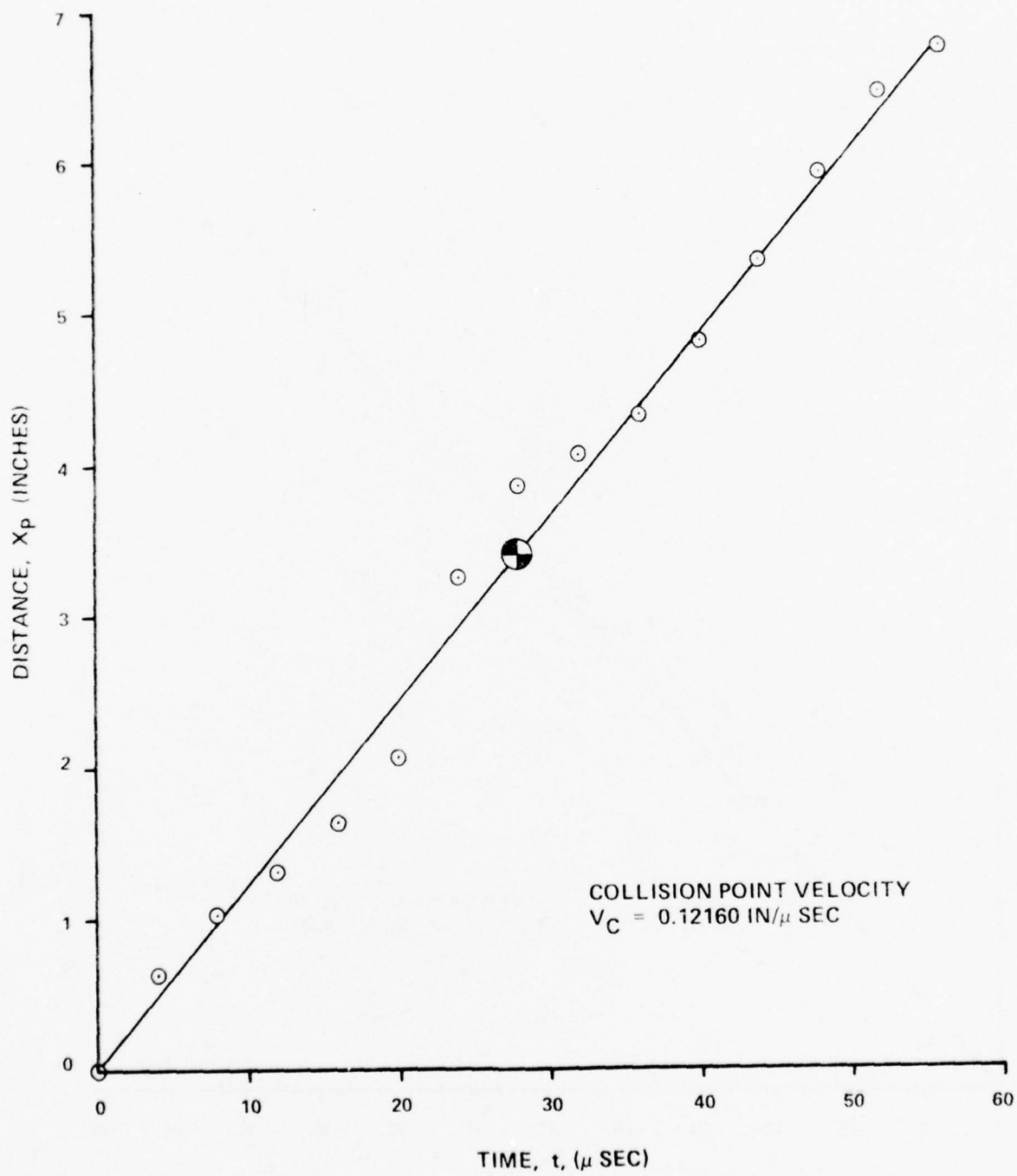


Figure 86

LASL 1269  
DETONATION POSITION

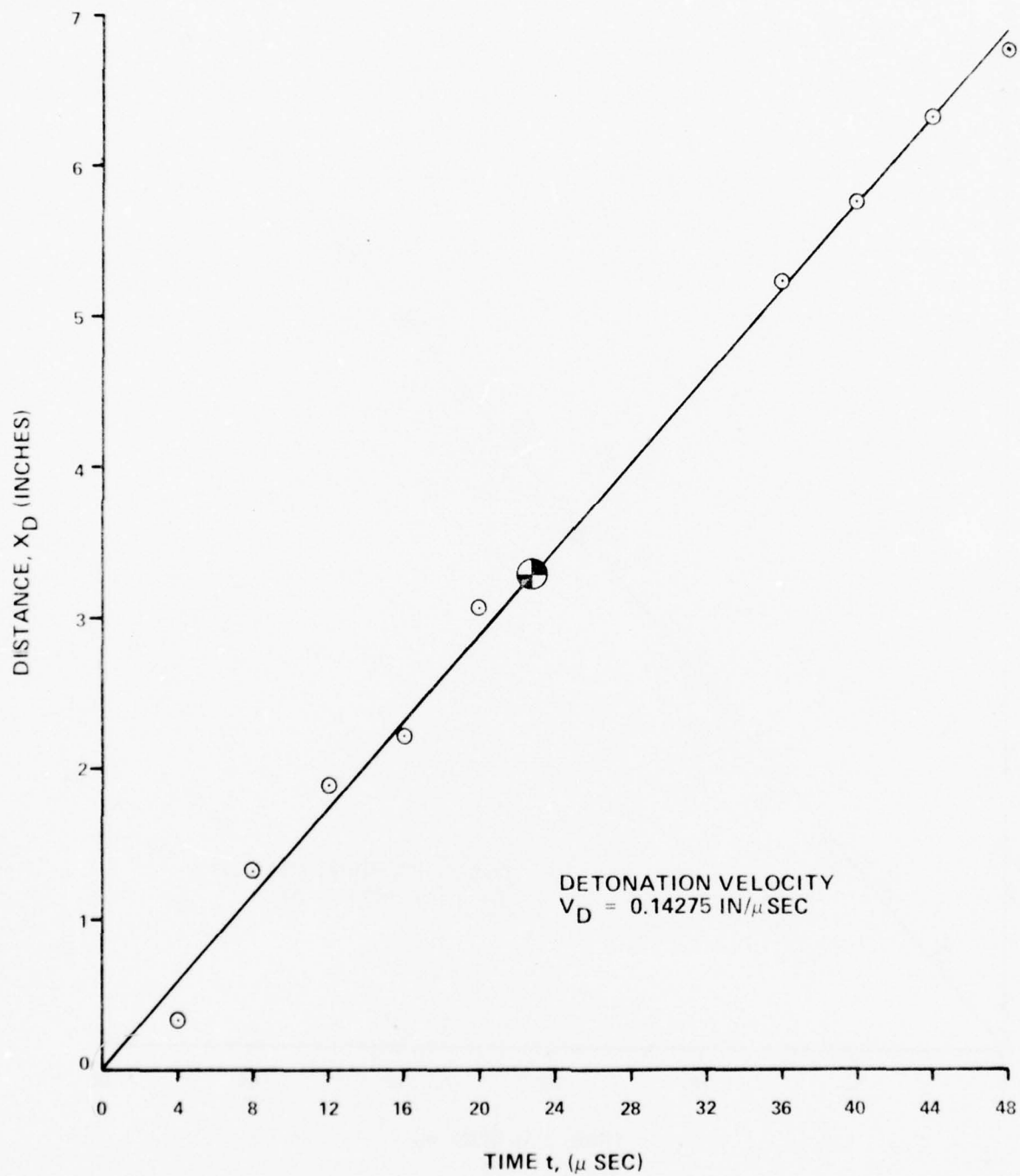


Figure 87

LASL 1269  
FLYER PLATE POSITION

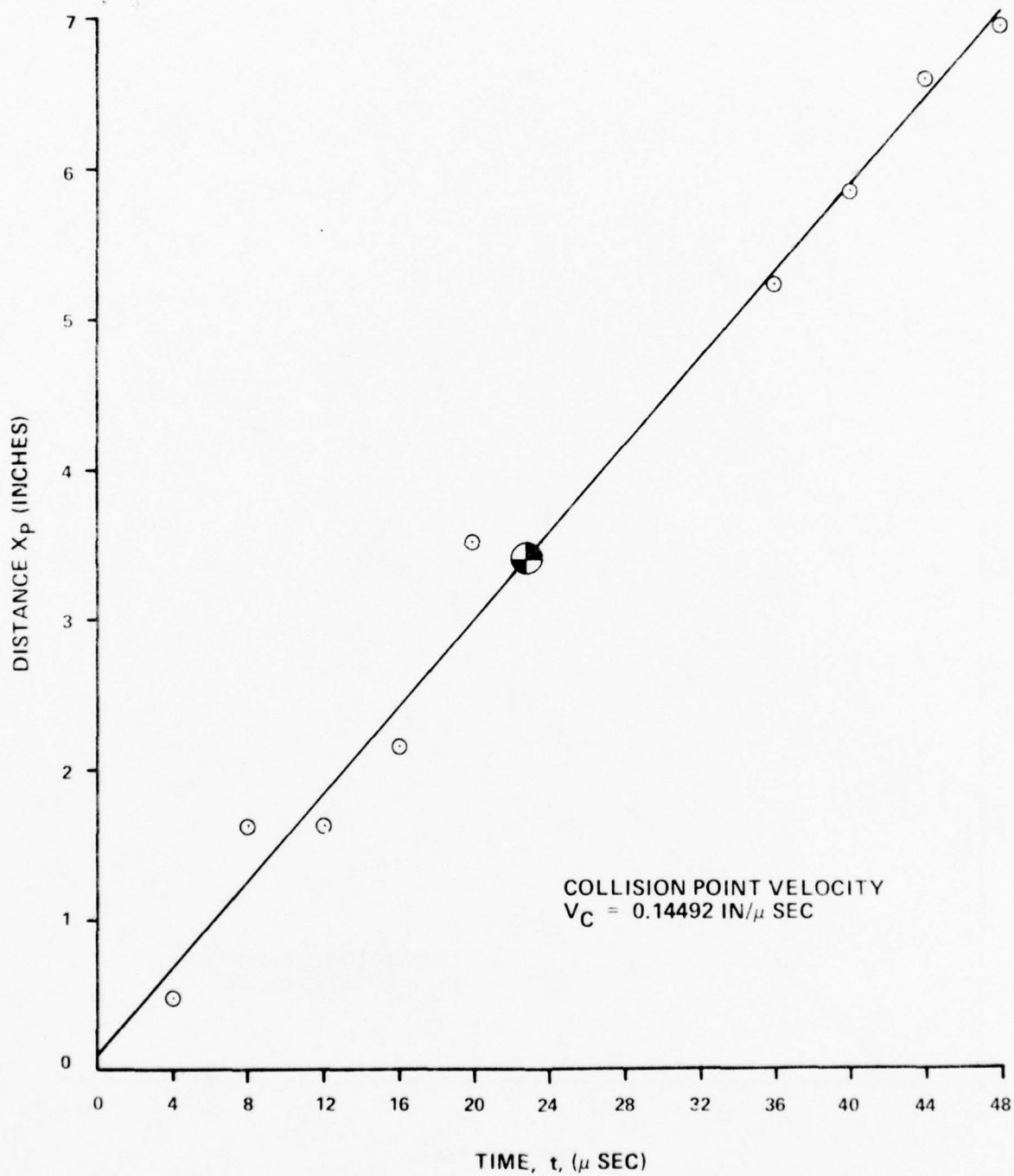


Figure 88

LASL 1270  
DETONATION POSITION

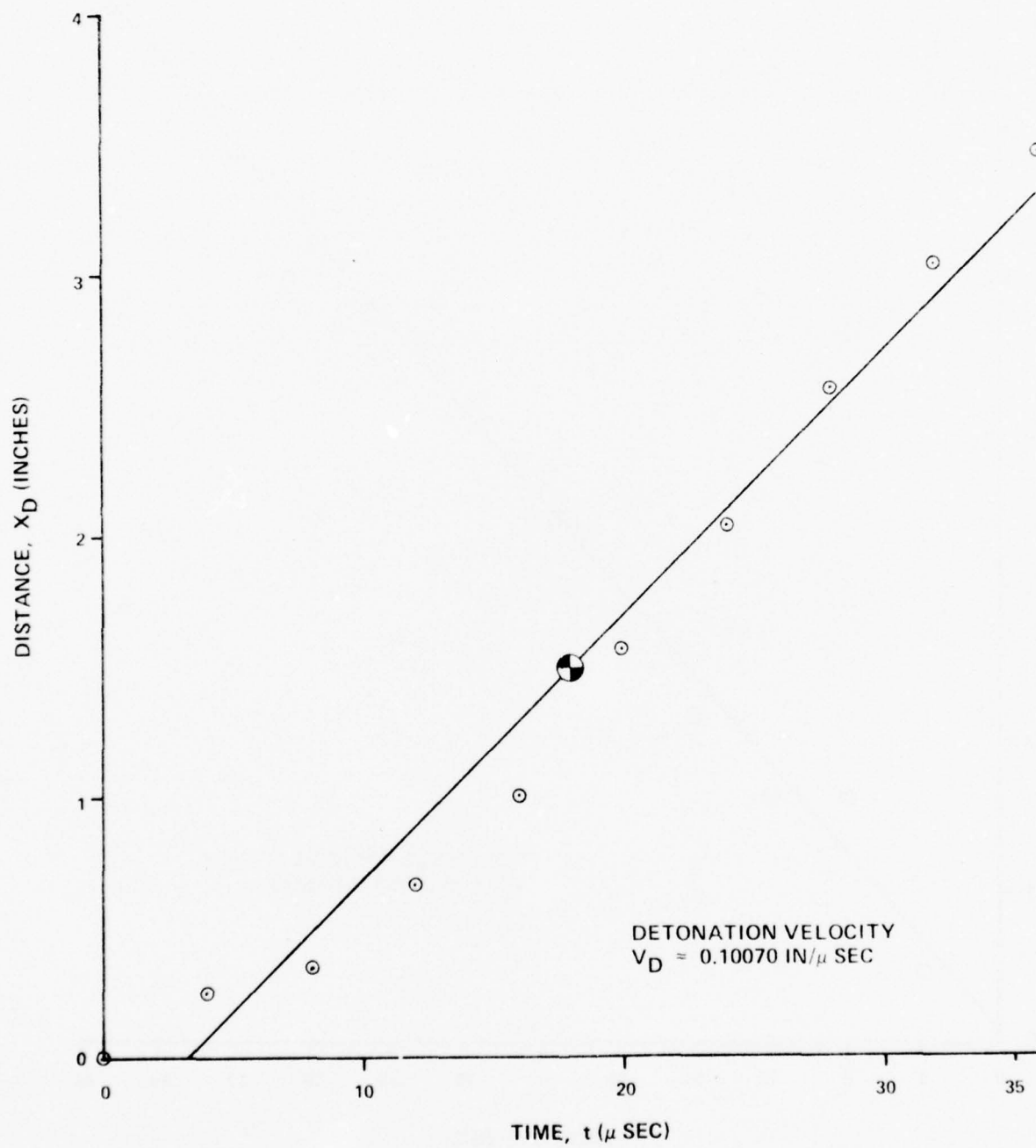


Figure 89



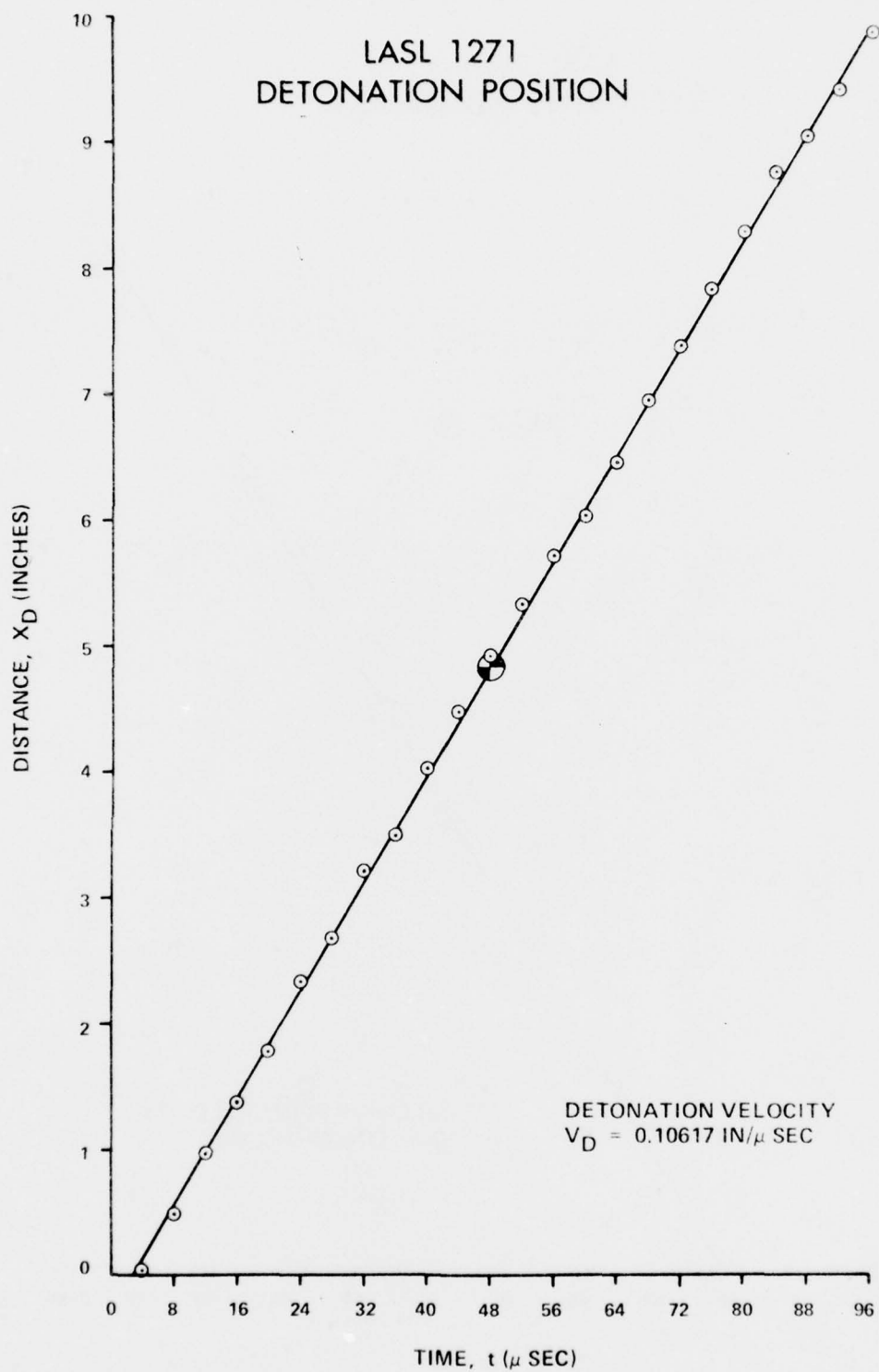


Figure 90

LASL 1271  
FLYER PLATE POSITION

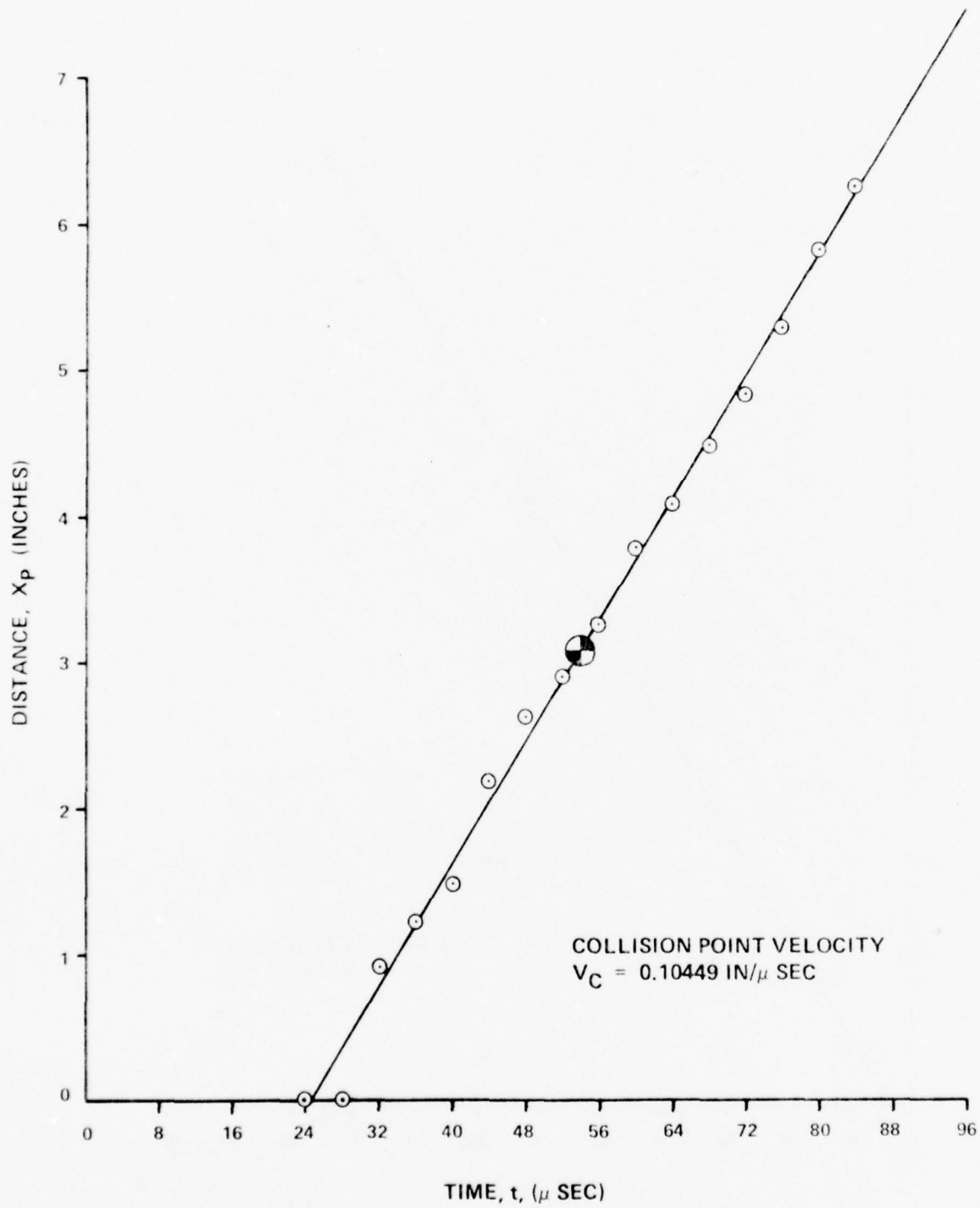


Figure 91

LASL 1273  
DETONATION POSITION

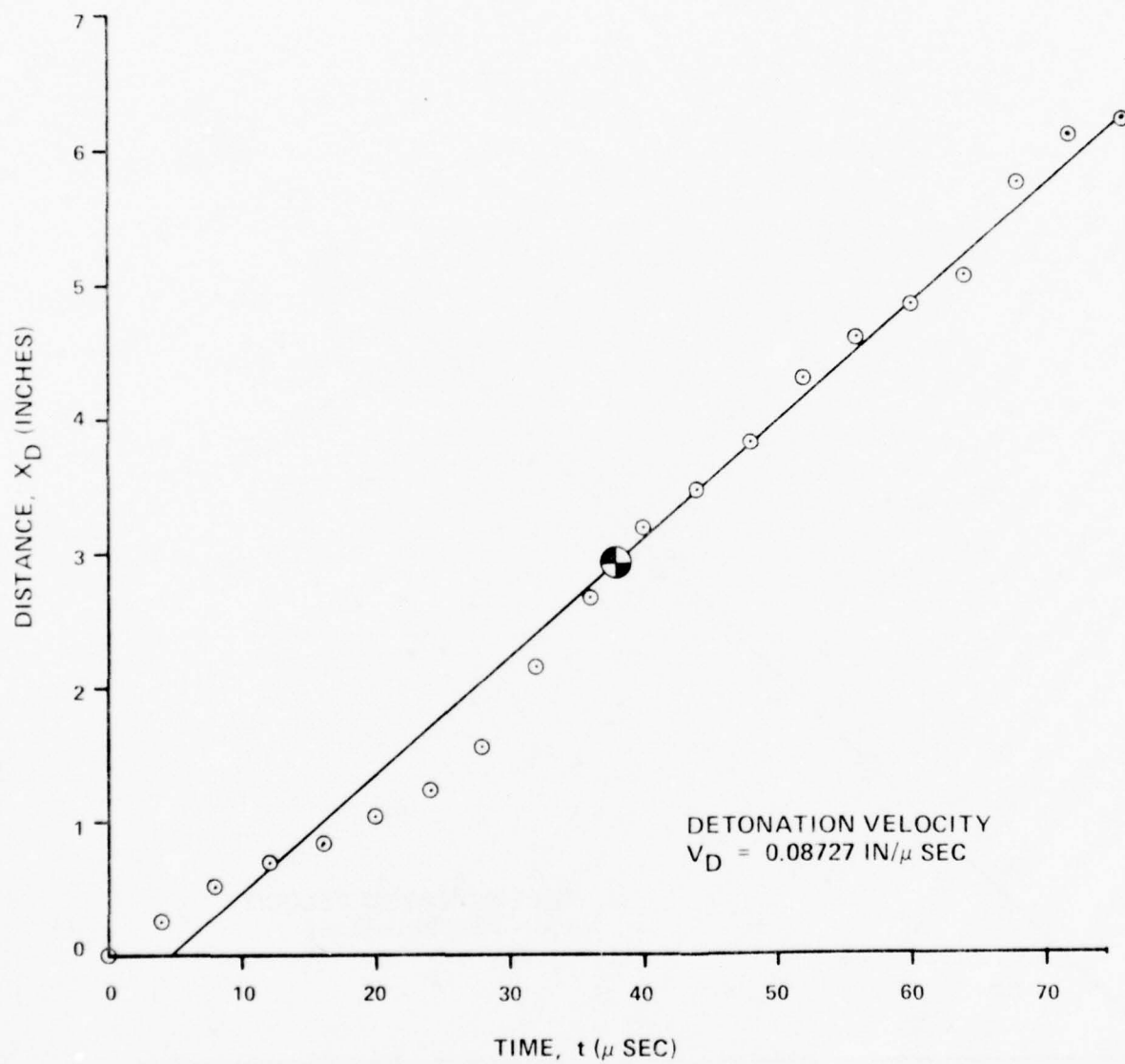


Figure 92

LASL 1273  
FLYER PLATE POSITION

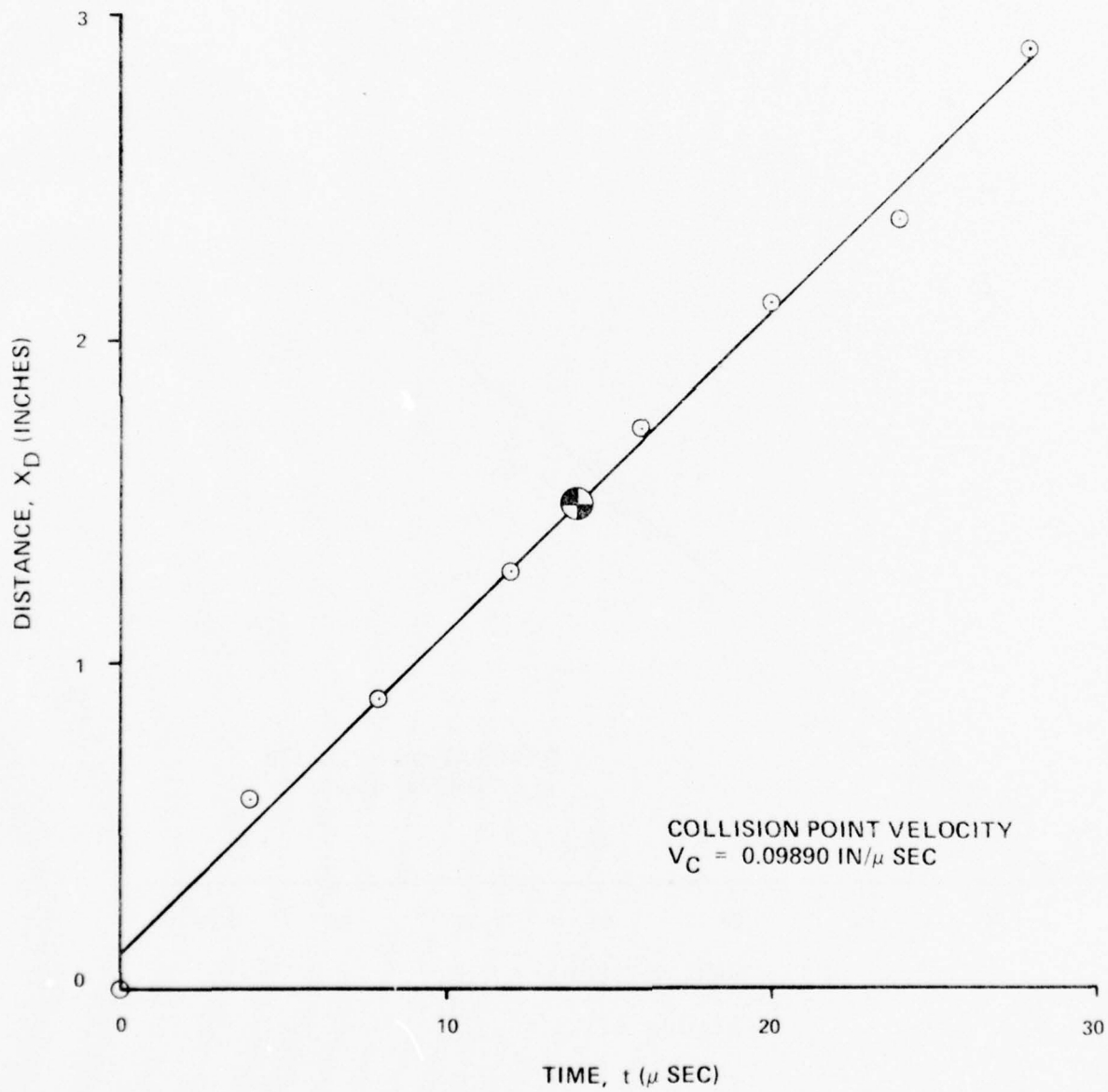


Figure 93

LASL 1274  
DETONATION POSITION

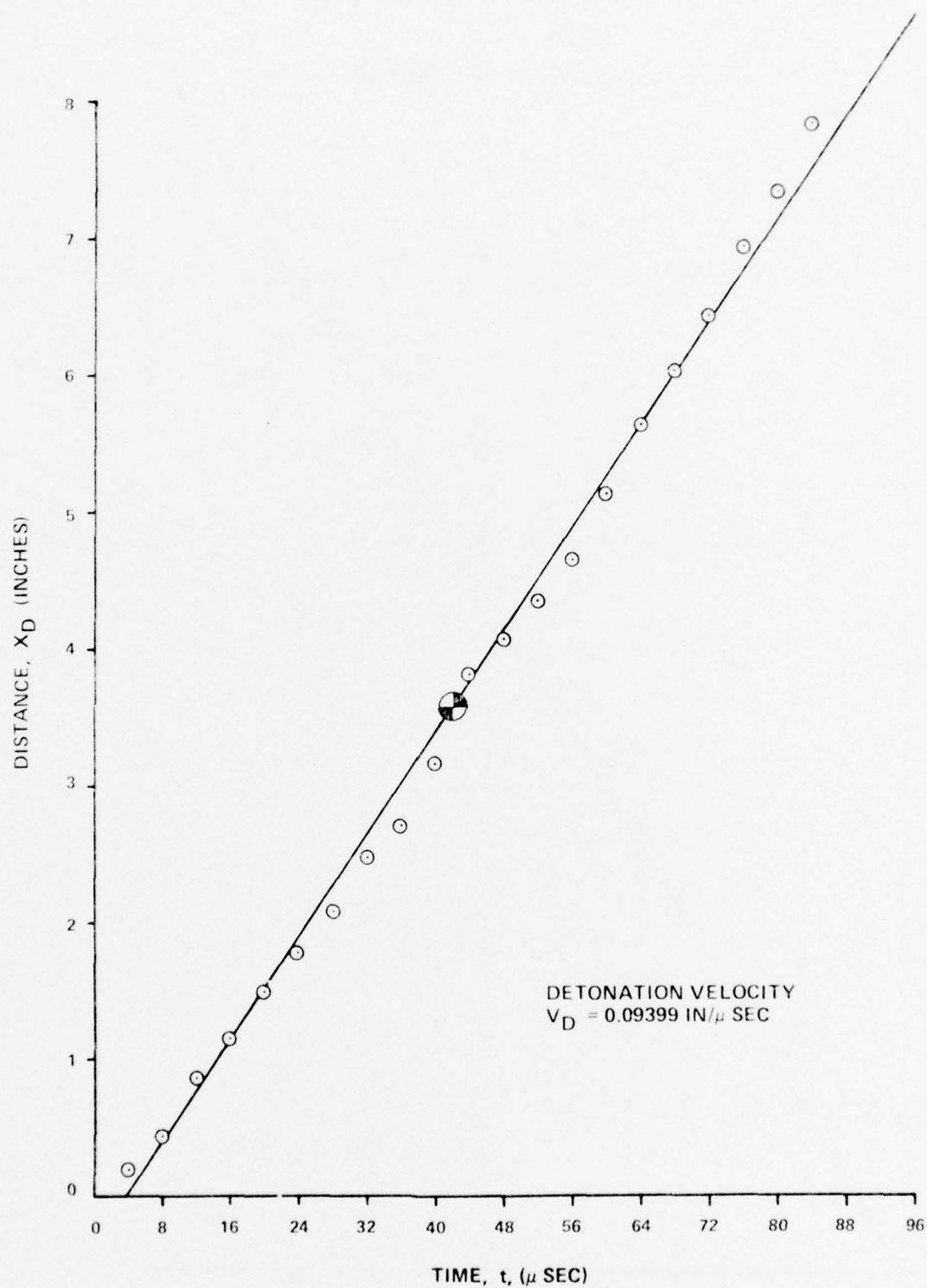


Figure 94



LASL 1277  
DETONATION POSITION

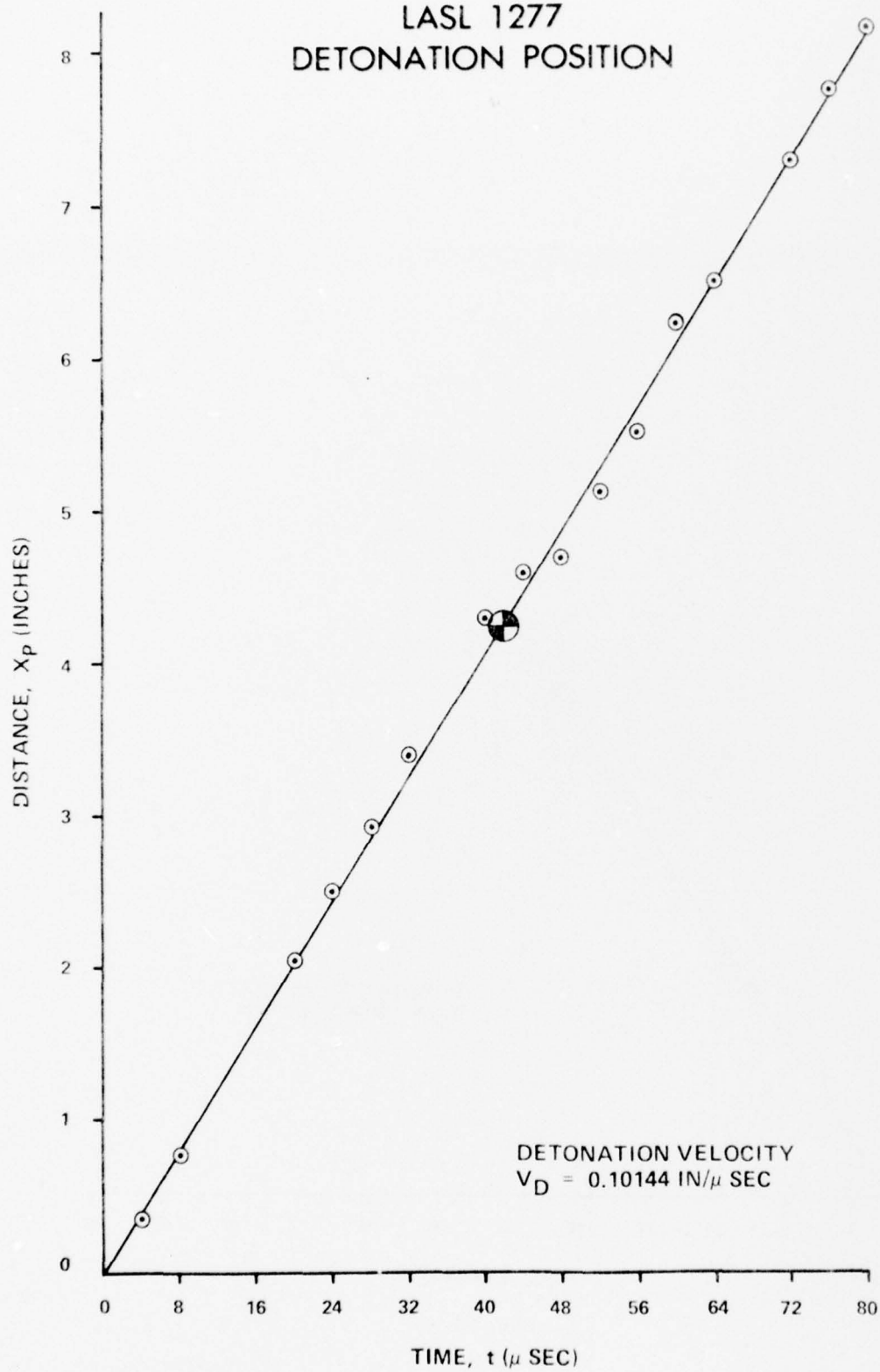
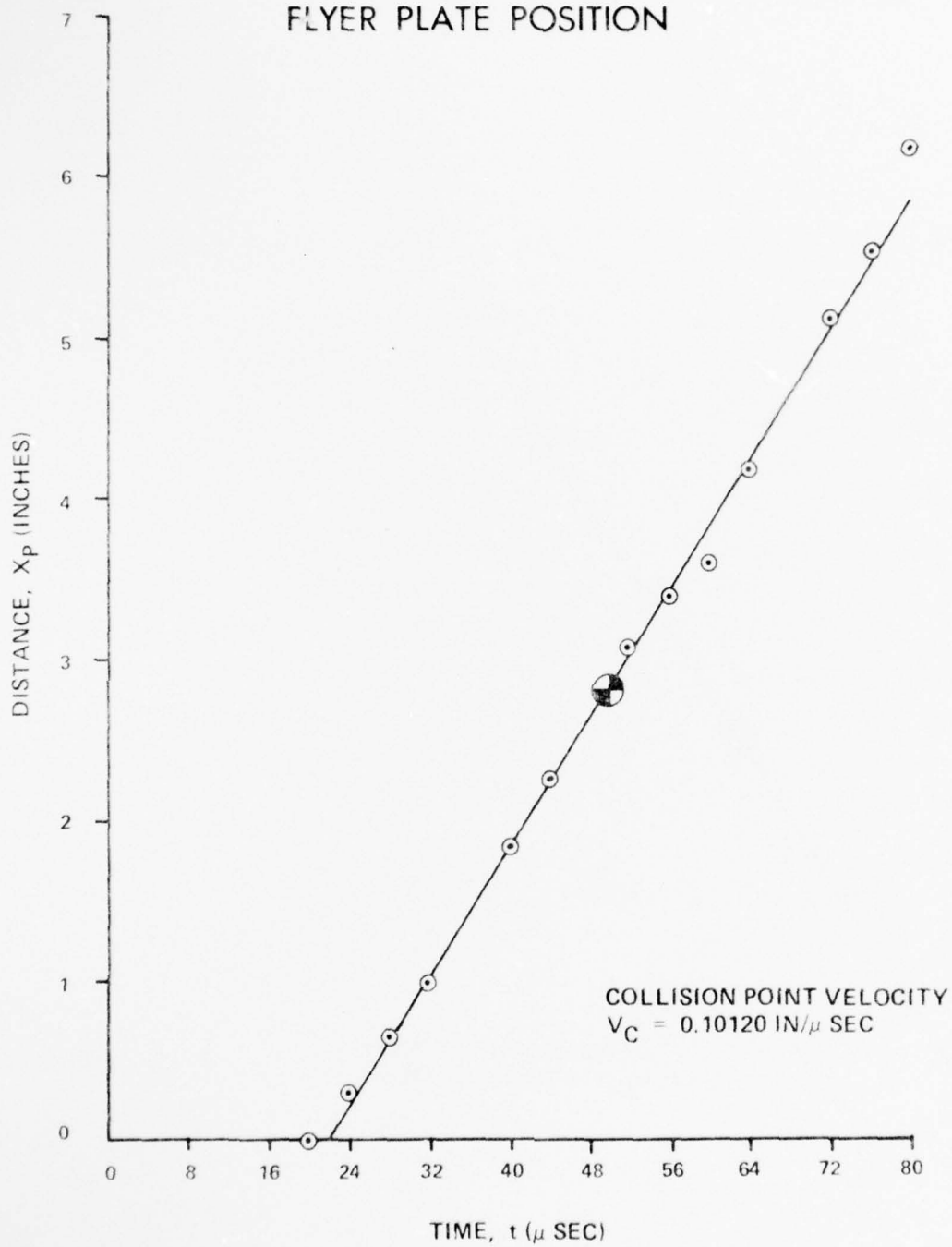


Figure 95

LASL 1277  
FLYER PLATE POSITION



TIME,  $t$  ( $\mu$  SEC)

Figure 96

LASL 1278  
DETONATION POSITION

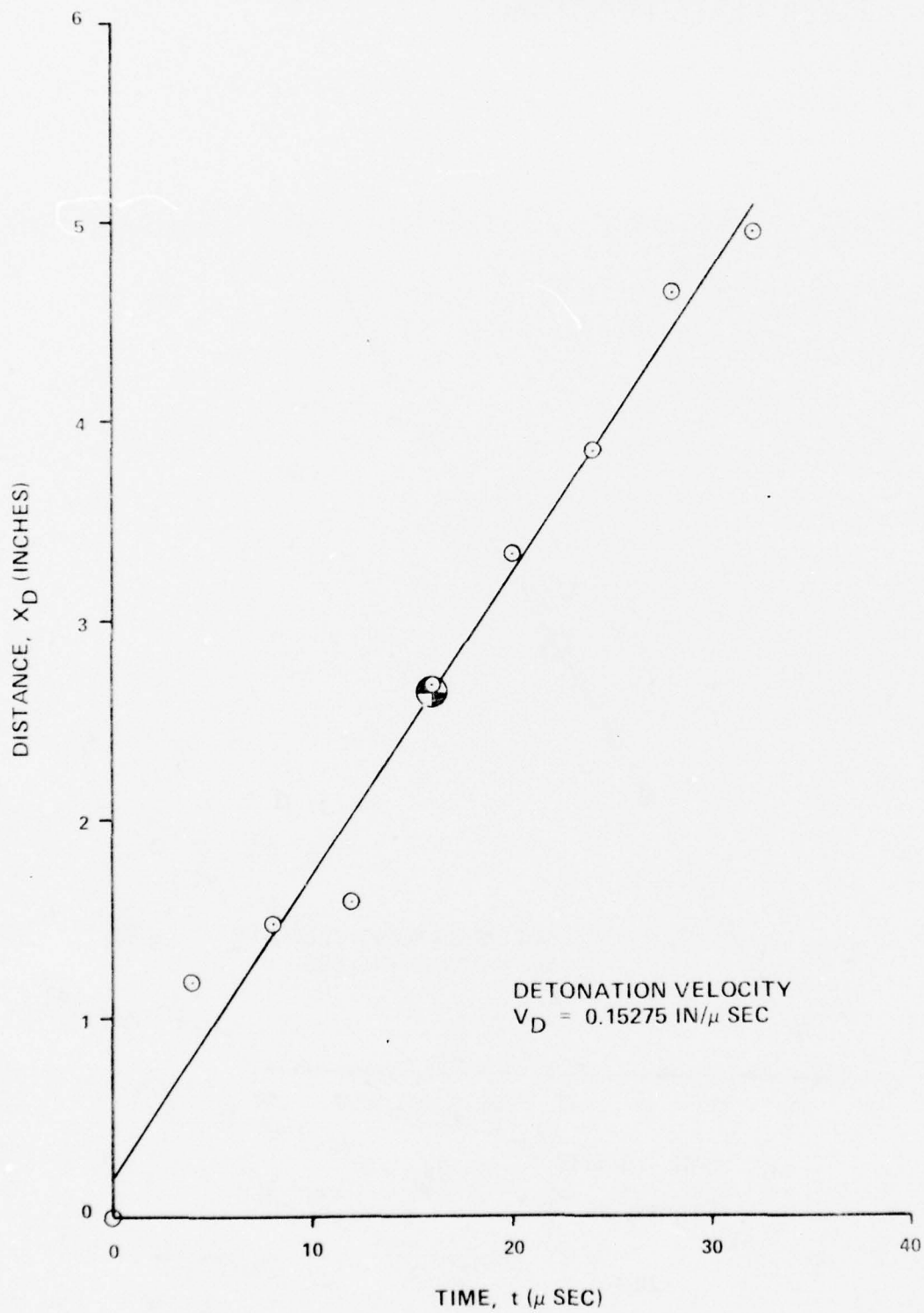


Figure 97

LASL 1278  
FLYER PLATE POSITION

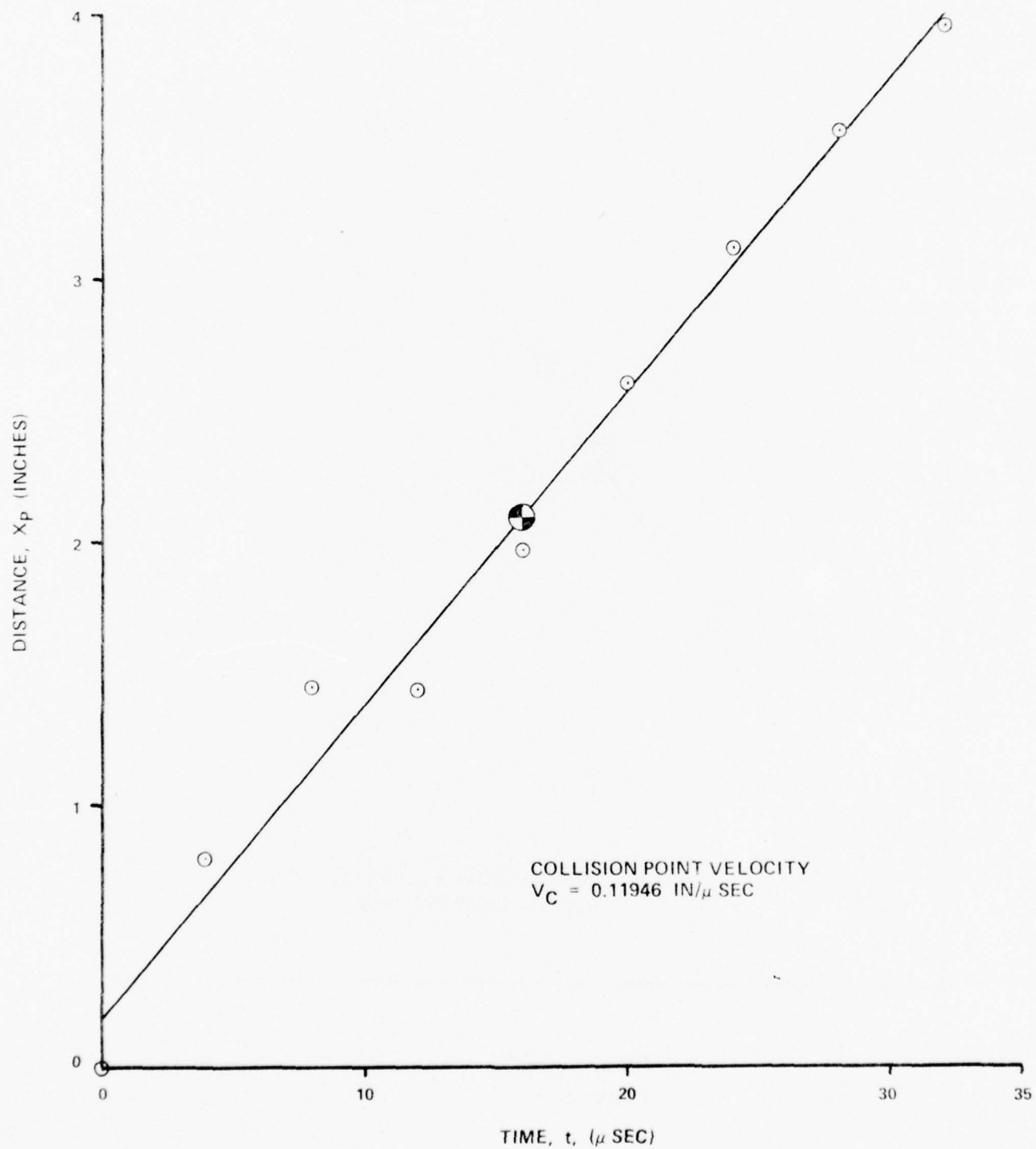


Figure 98

LASL 1279  
DETONATION POSITION

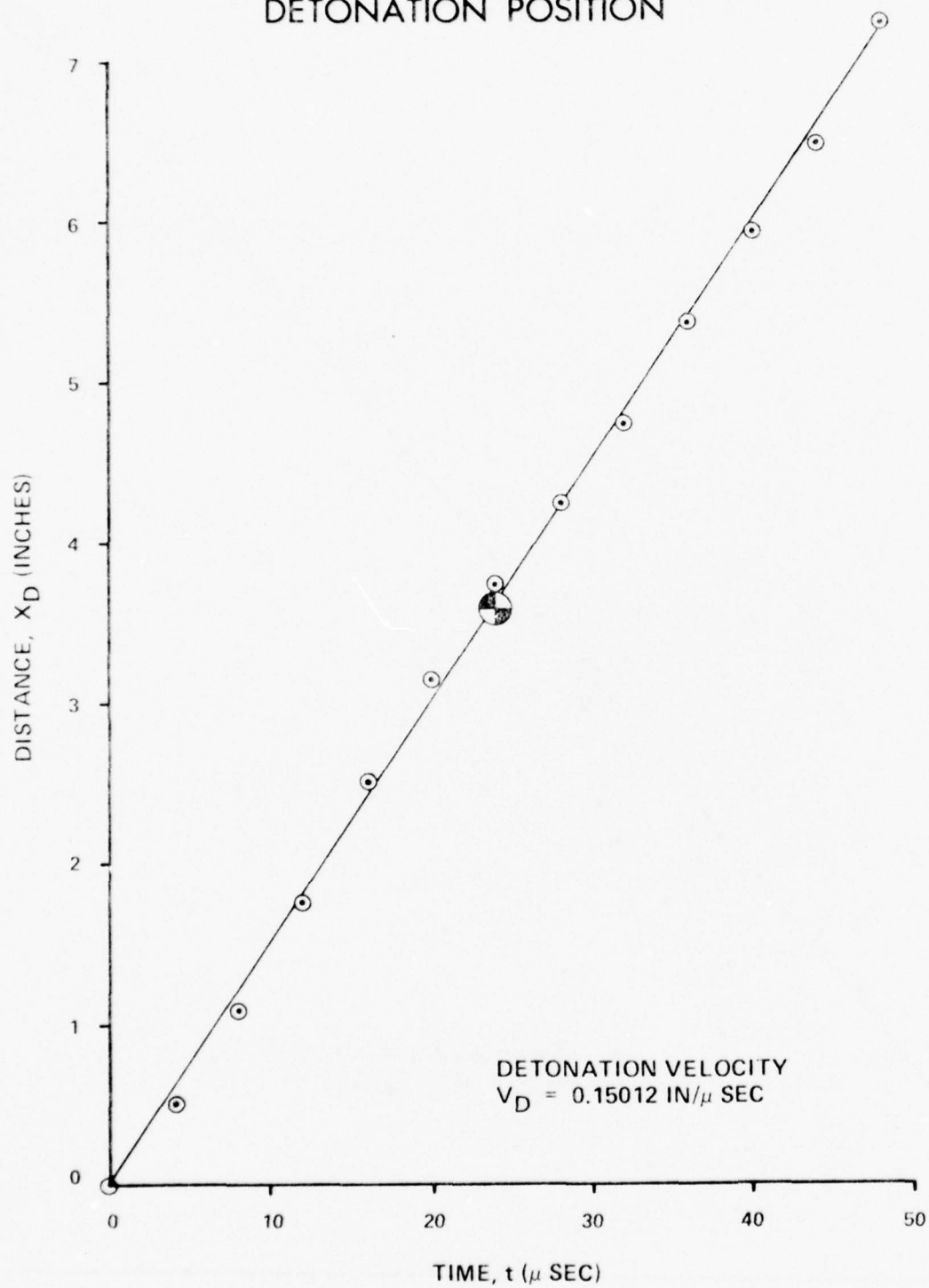


Figure 99



LASL 1279  
FLYER PLATE POSITION

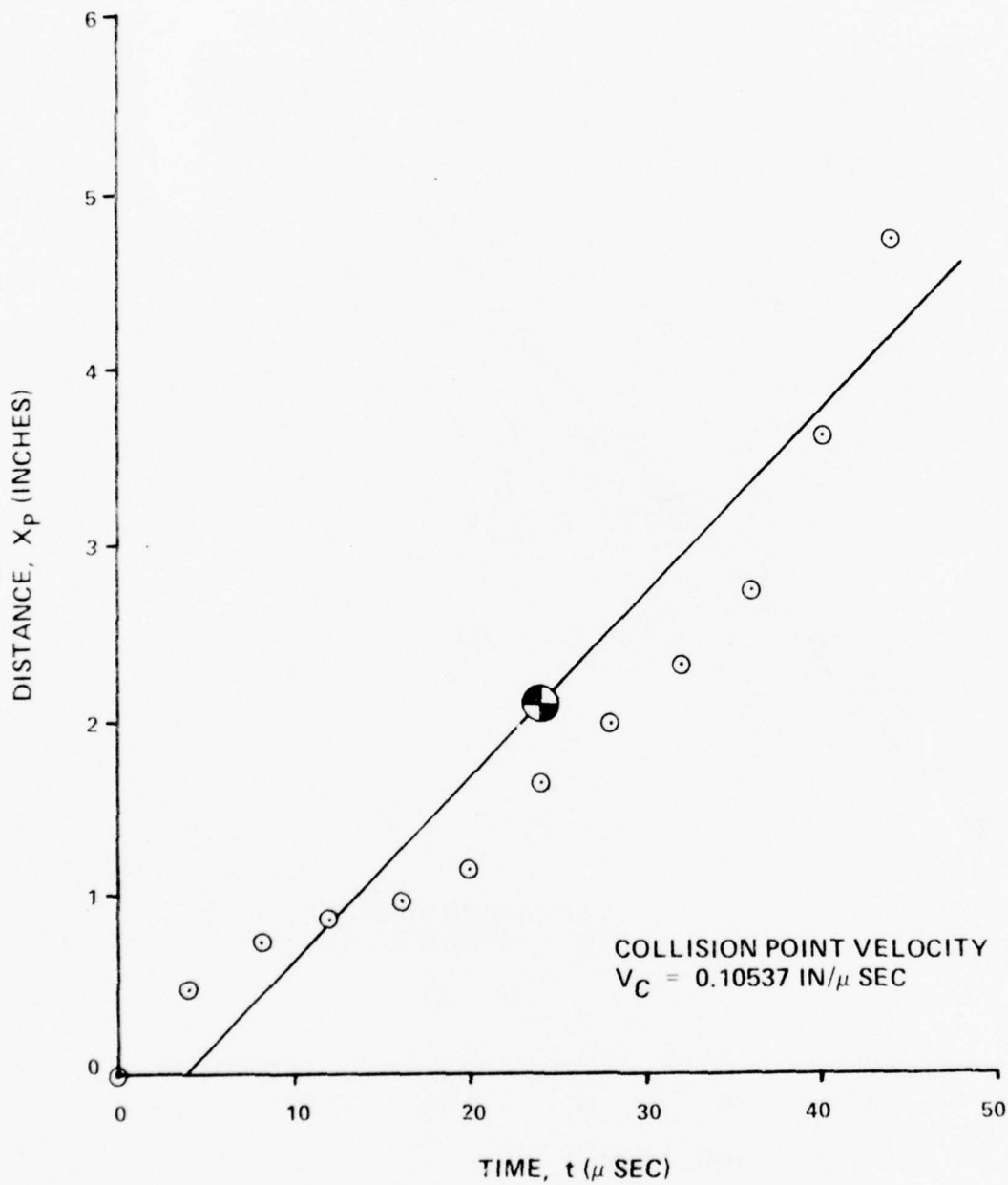


Figure 100

LASL 1280  
DETONATION POSITION

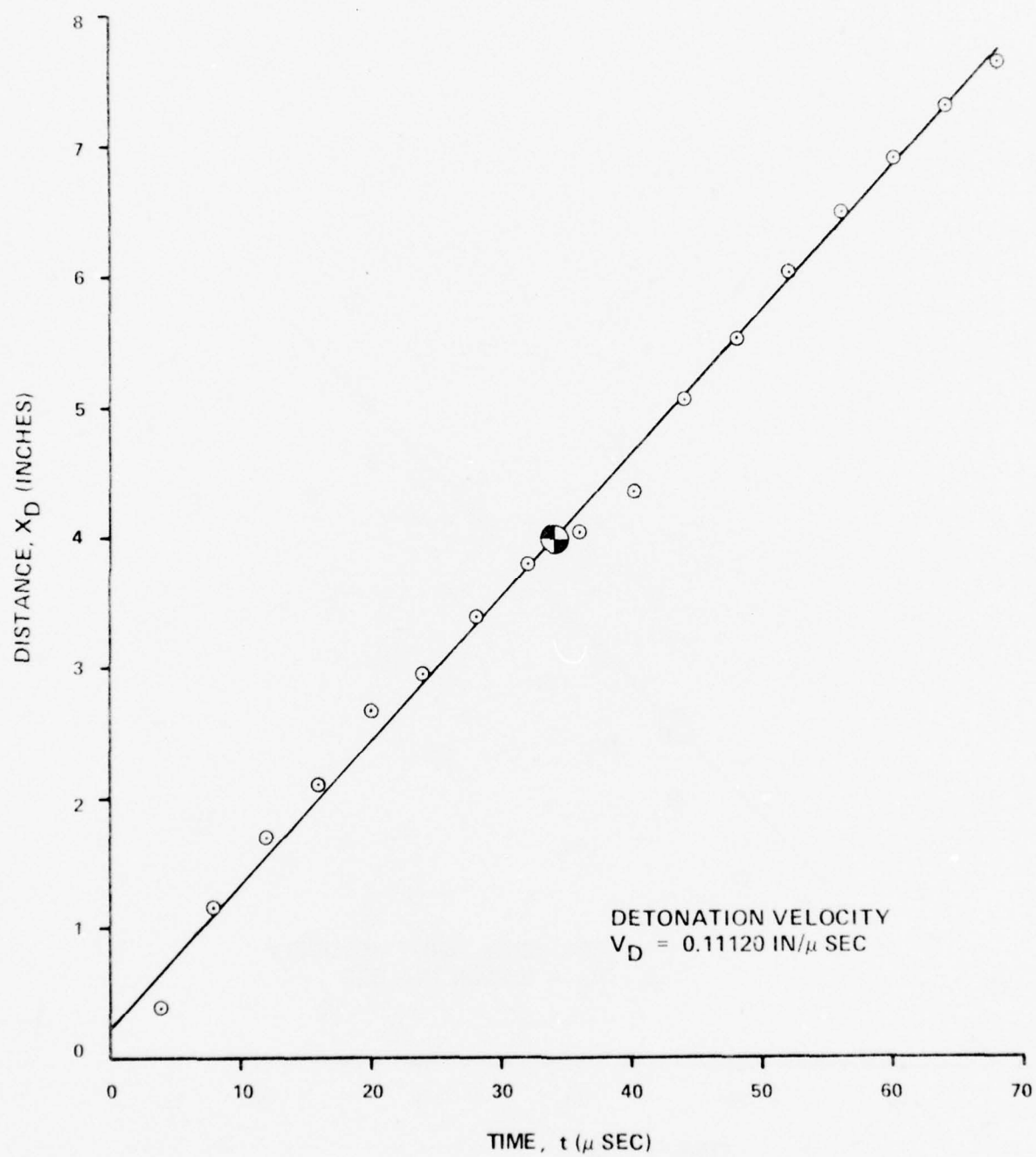


Figure 101

LASL 1280  
FLYER PLATE POSITION

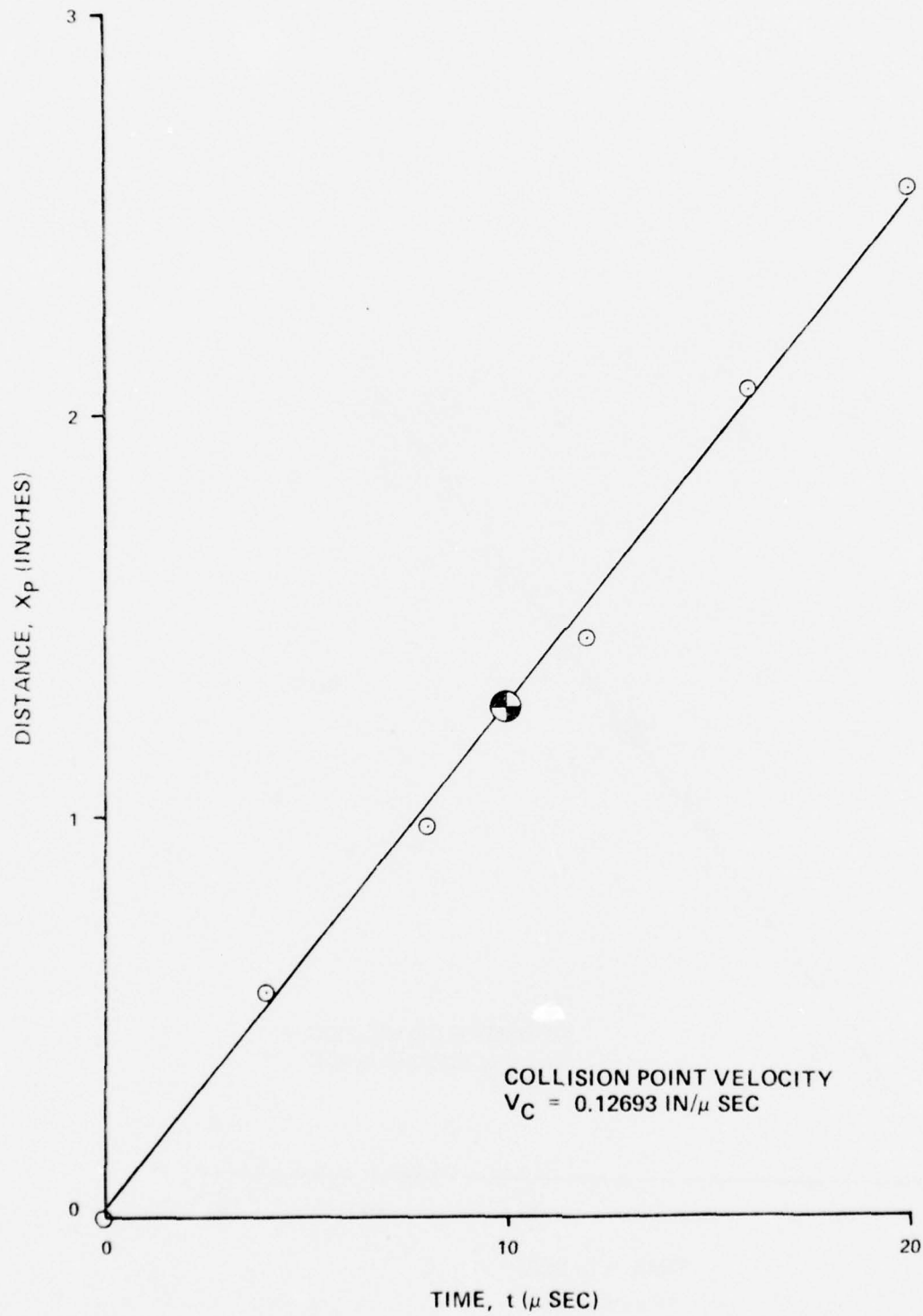


Figure 102

LASL 1281  
DETONATION POSITION

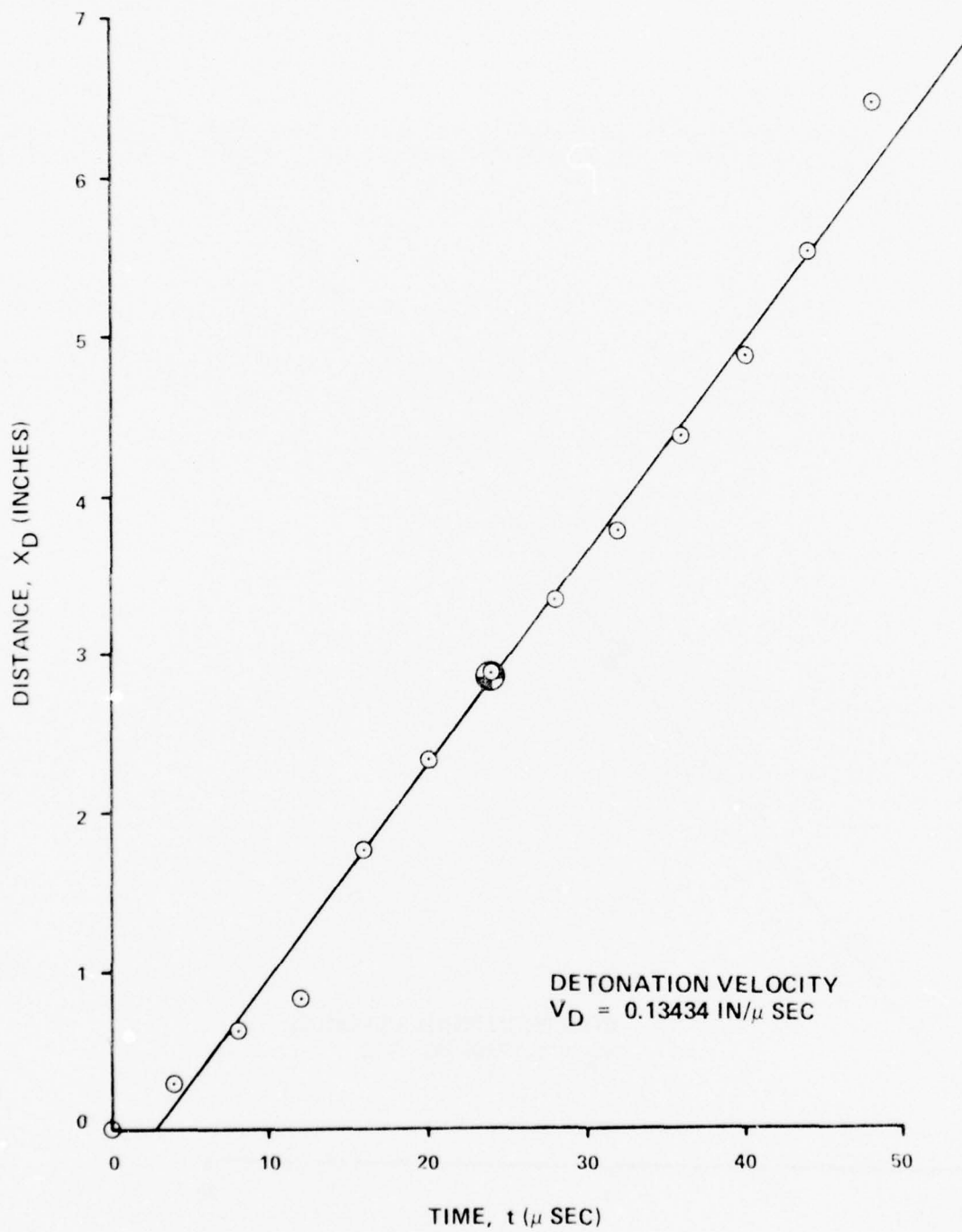


Figure 103

LASL 1281  
FLYER PLATE POSITION

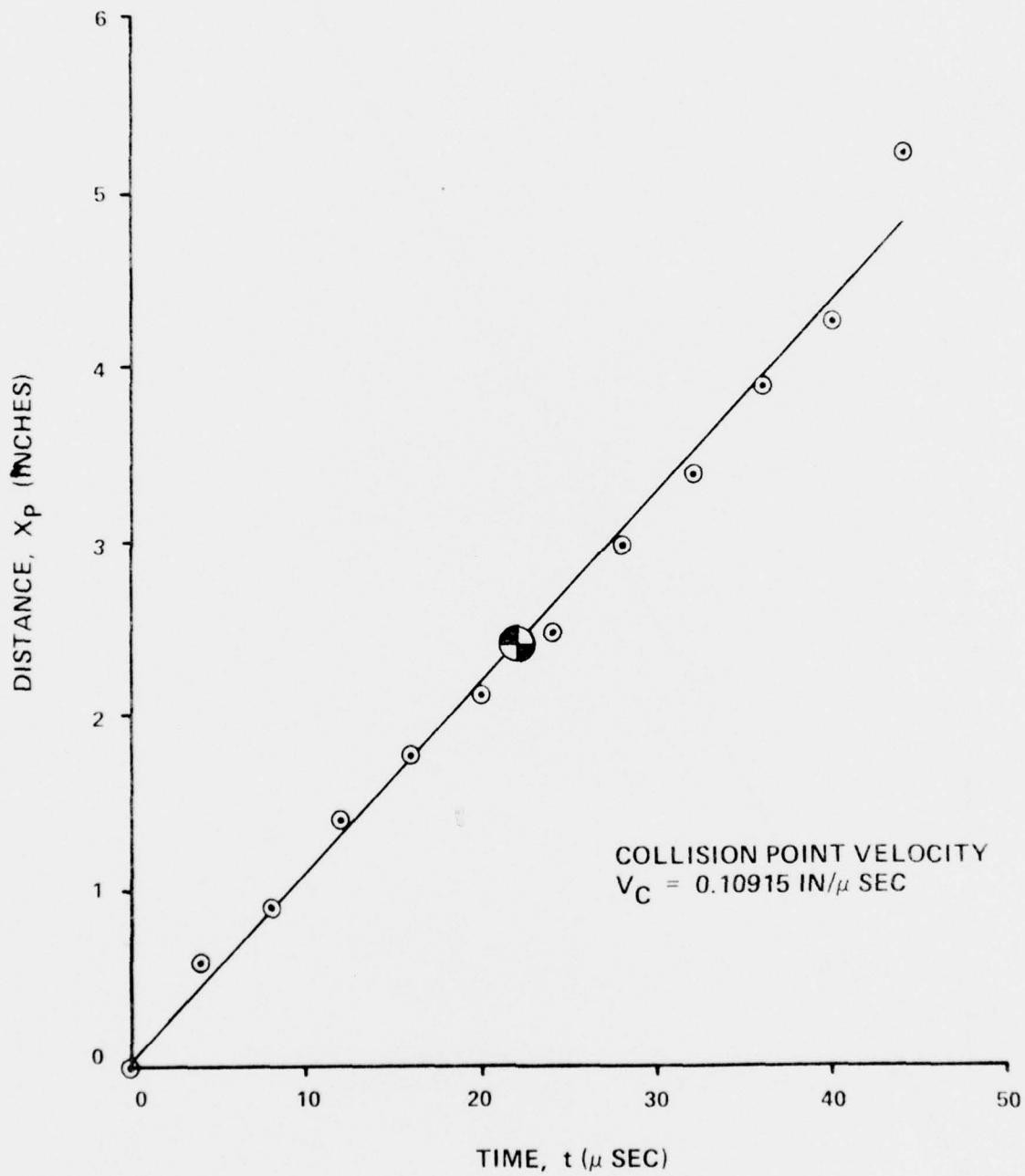
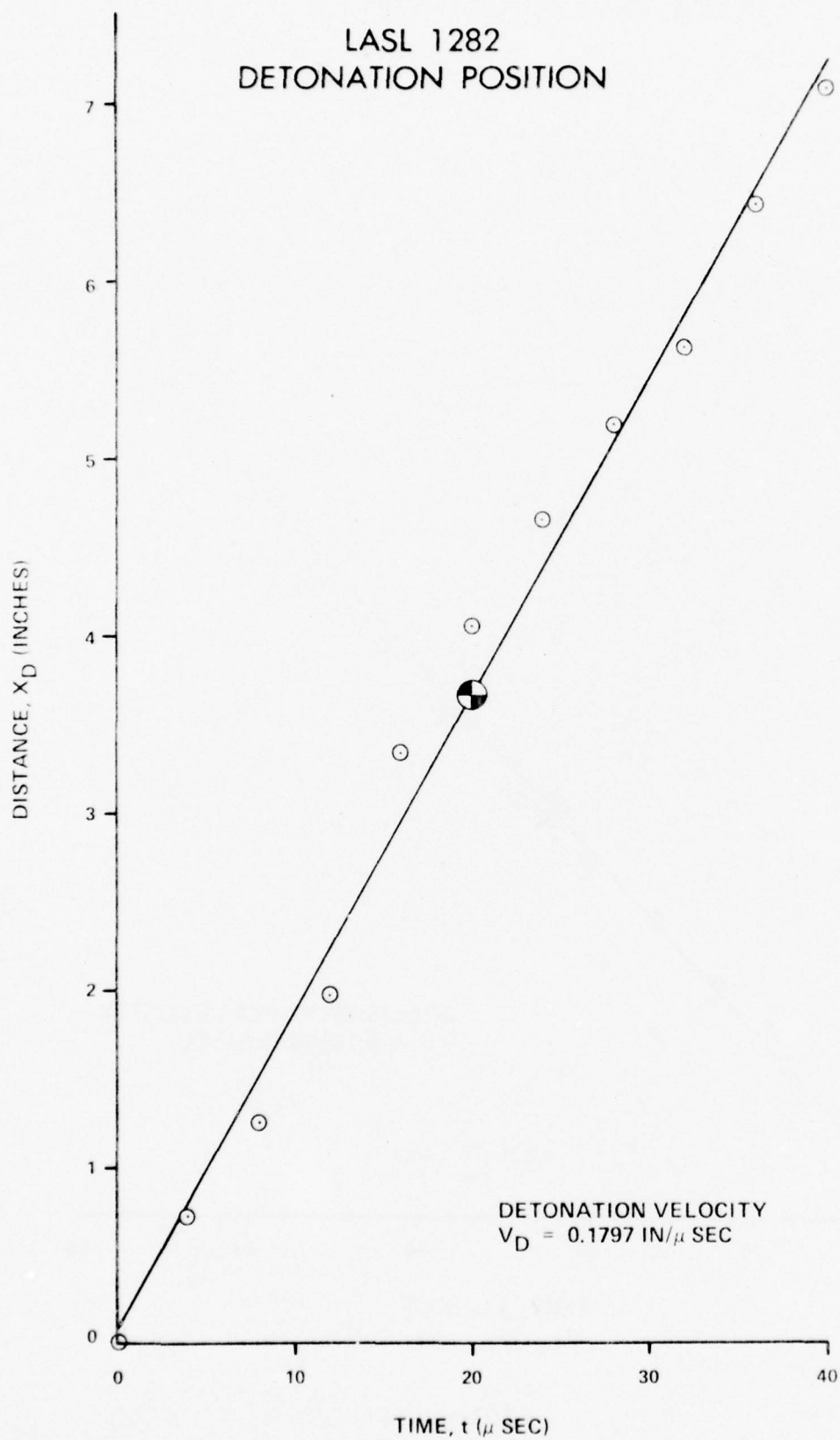


Figure 104



LASL 1282  
DETONATION POSITION



DETONATION VELOCITY  
 $V_D = 0.1797 \text{ IN}/\mu \text{ SEC}$

TIME,  $t$  ( $\mu$  SEC)

Figure 105

LASL 1282  
FLYER PLATE POSITION

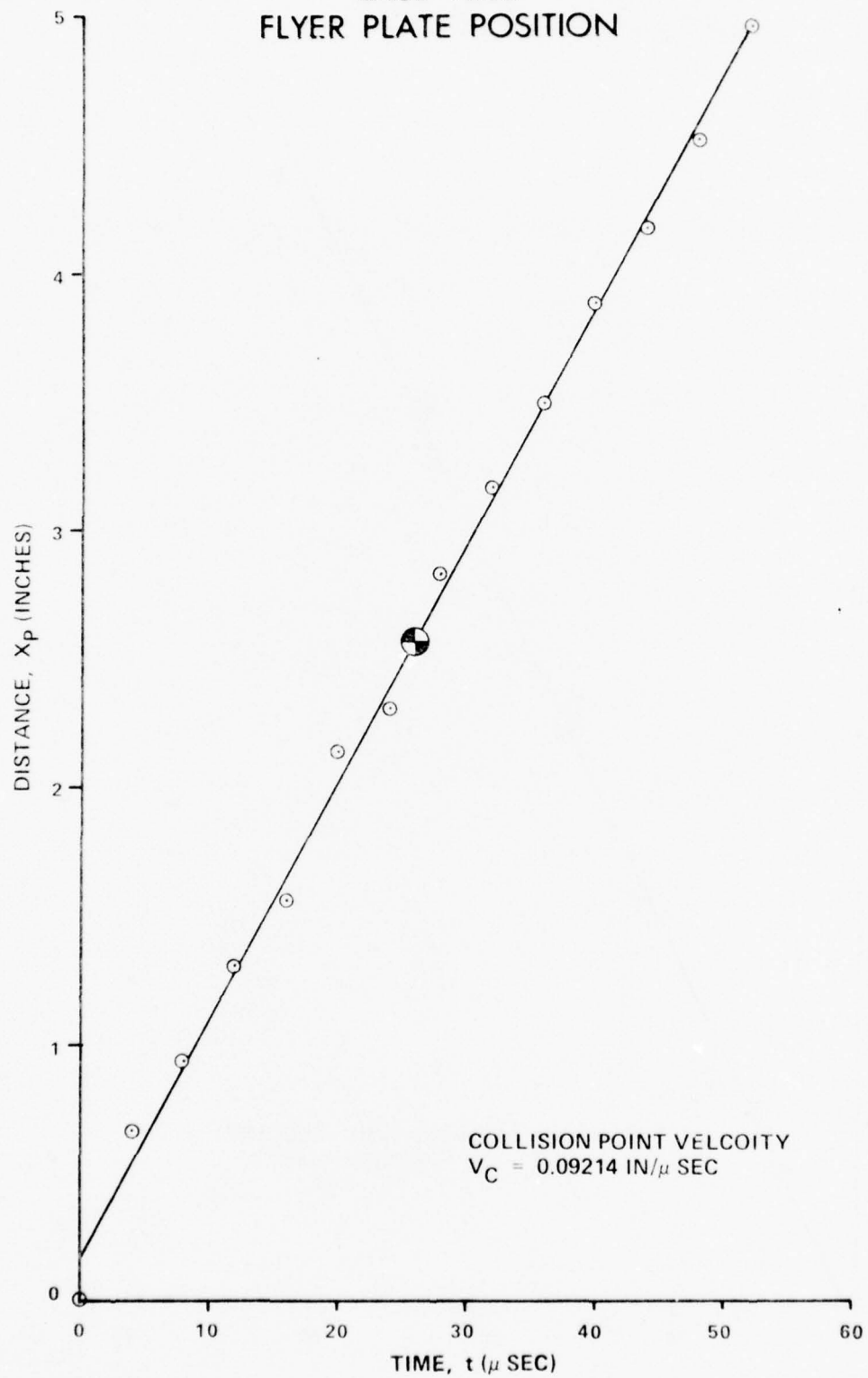
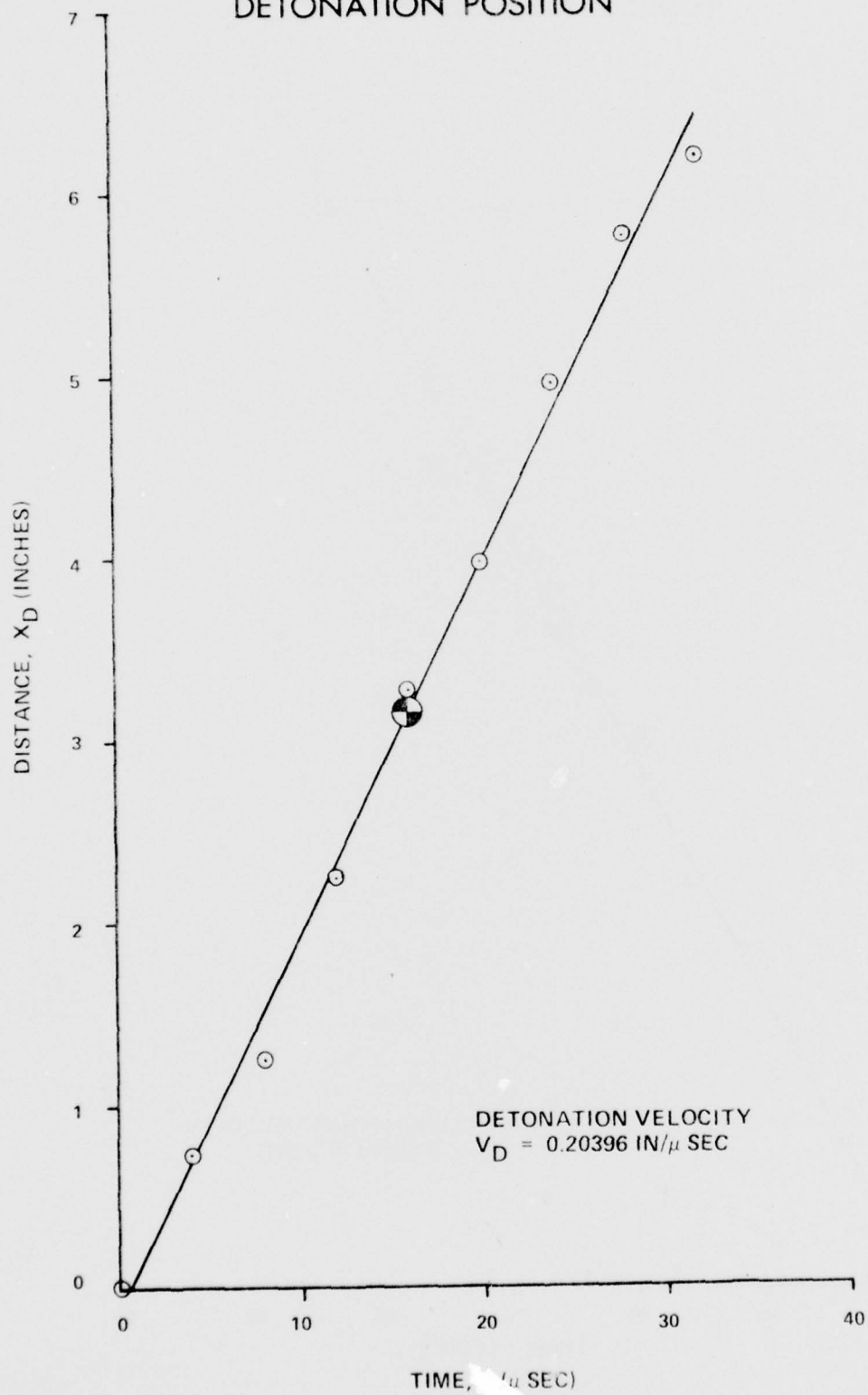


Figure 106

LASL 1283  
DETONATION POSITION



TIME,  $t$  ( $\mu \text{ SEC}$ )

Figure 1.1

LASL 1283  
FLYER PLATE POSITION

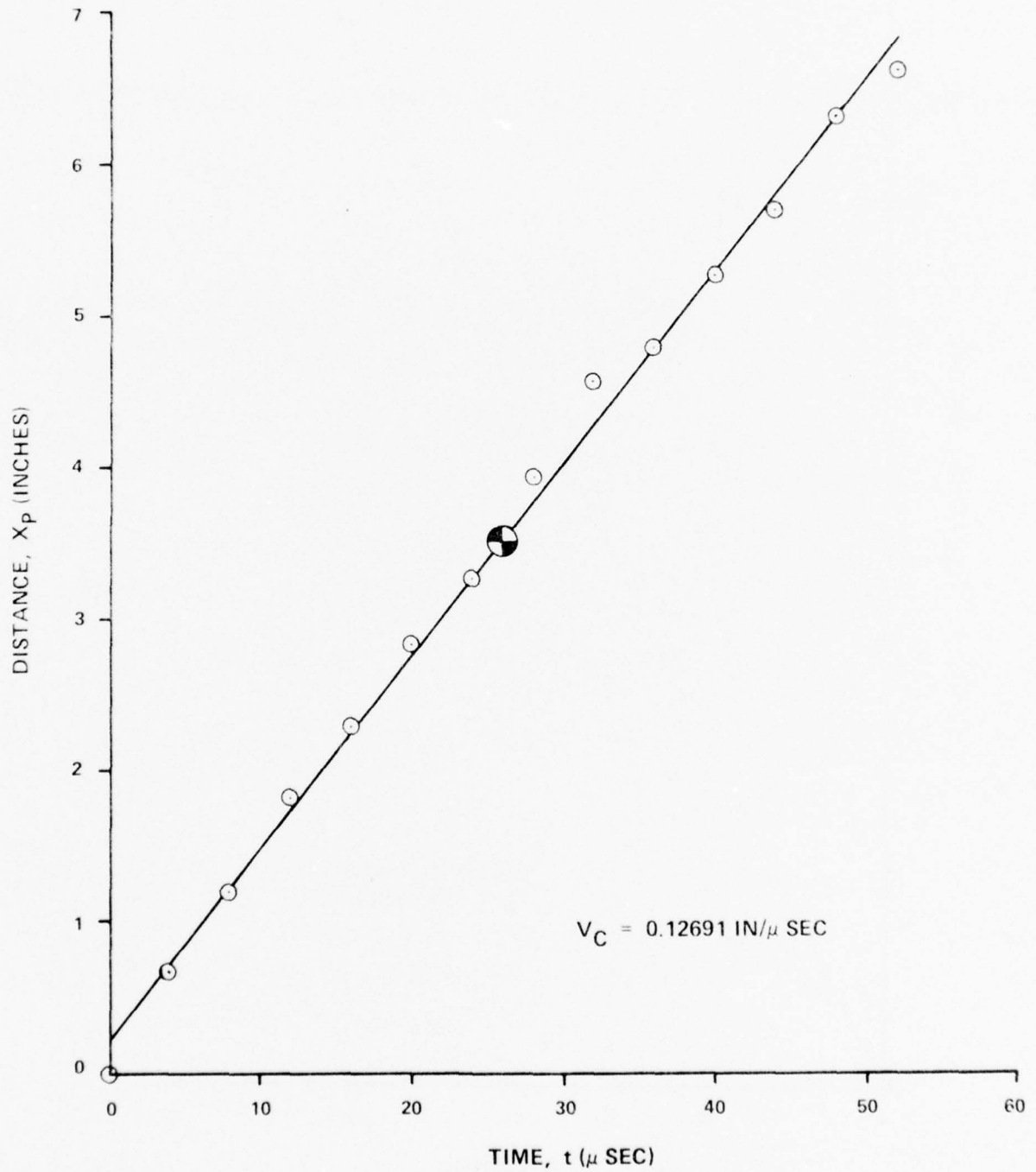


Figure 108

LASL 1284  
DETONATION POSITION

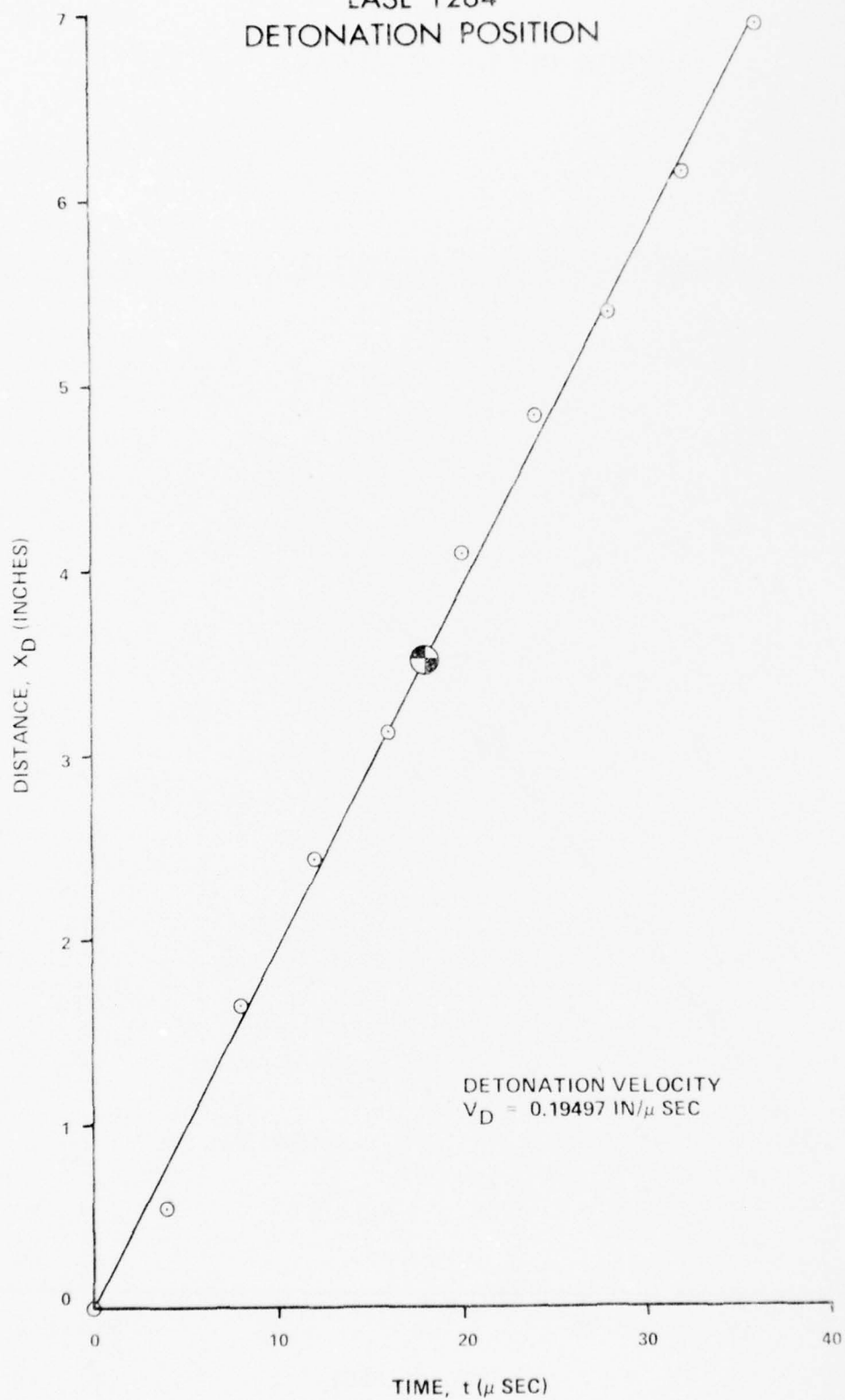


Figure 109



LASL 1284  
FLYER PLATE POSITION

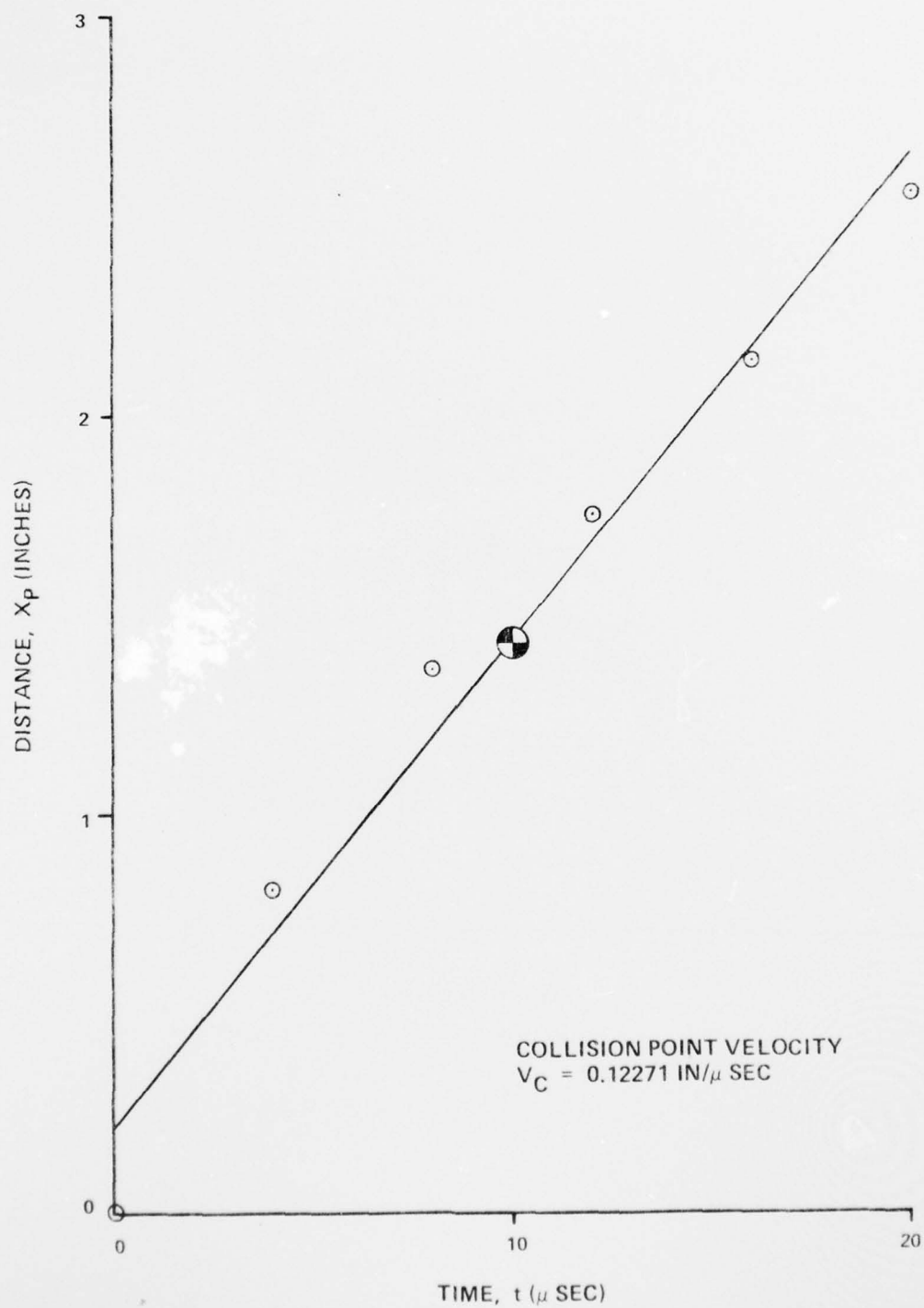


Figure 110

LASL 1285  
DETONATION POSITION

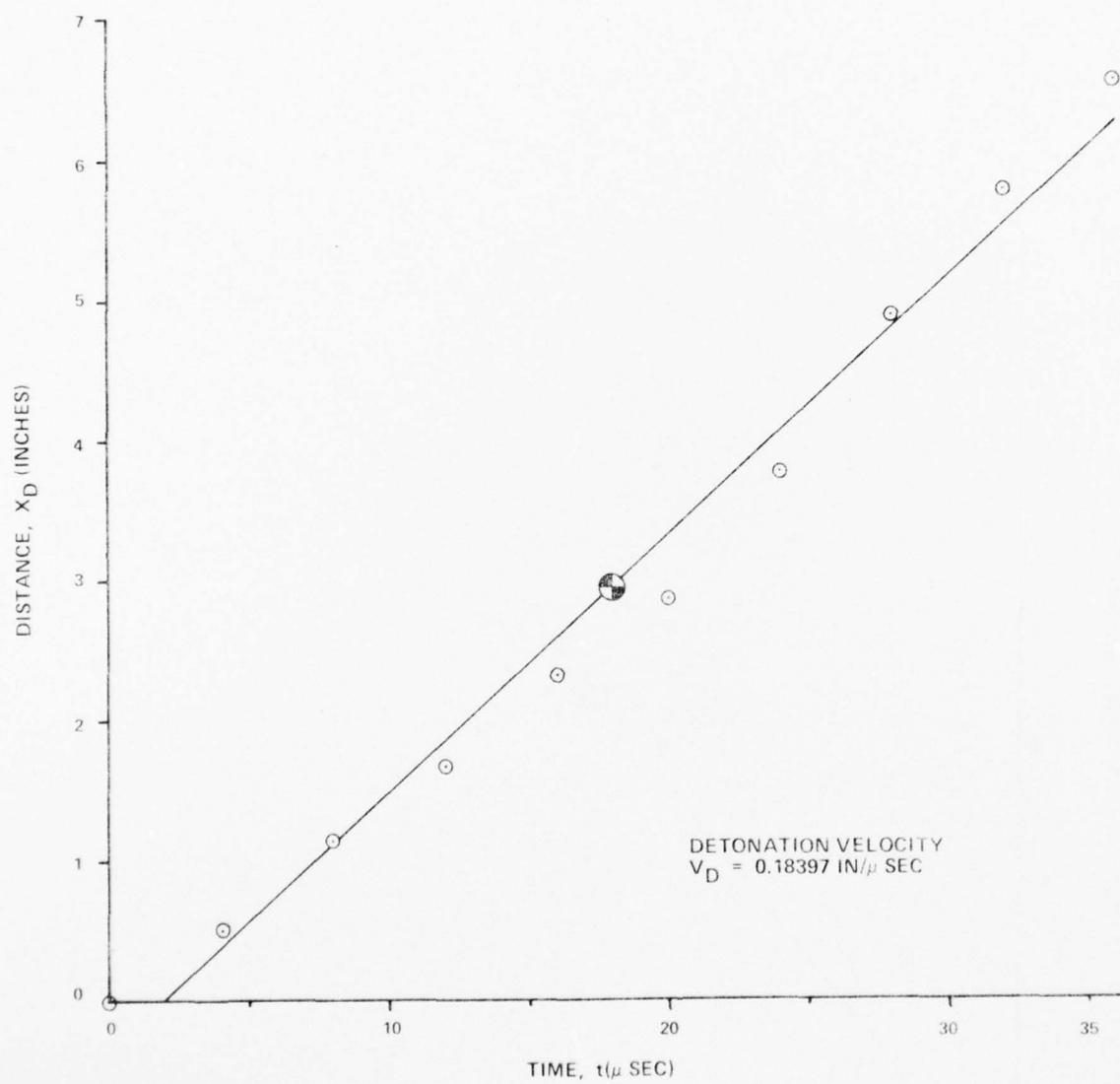


Figure 111

LASL 1285  
FLYER PLATE POSITION

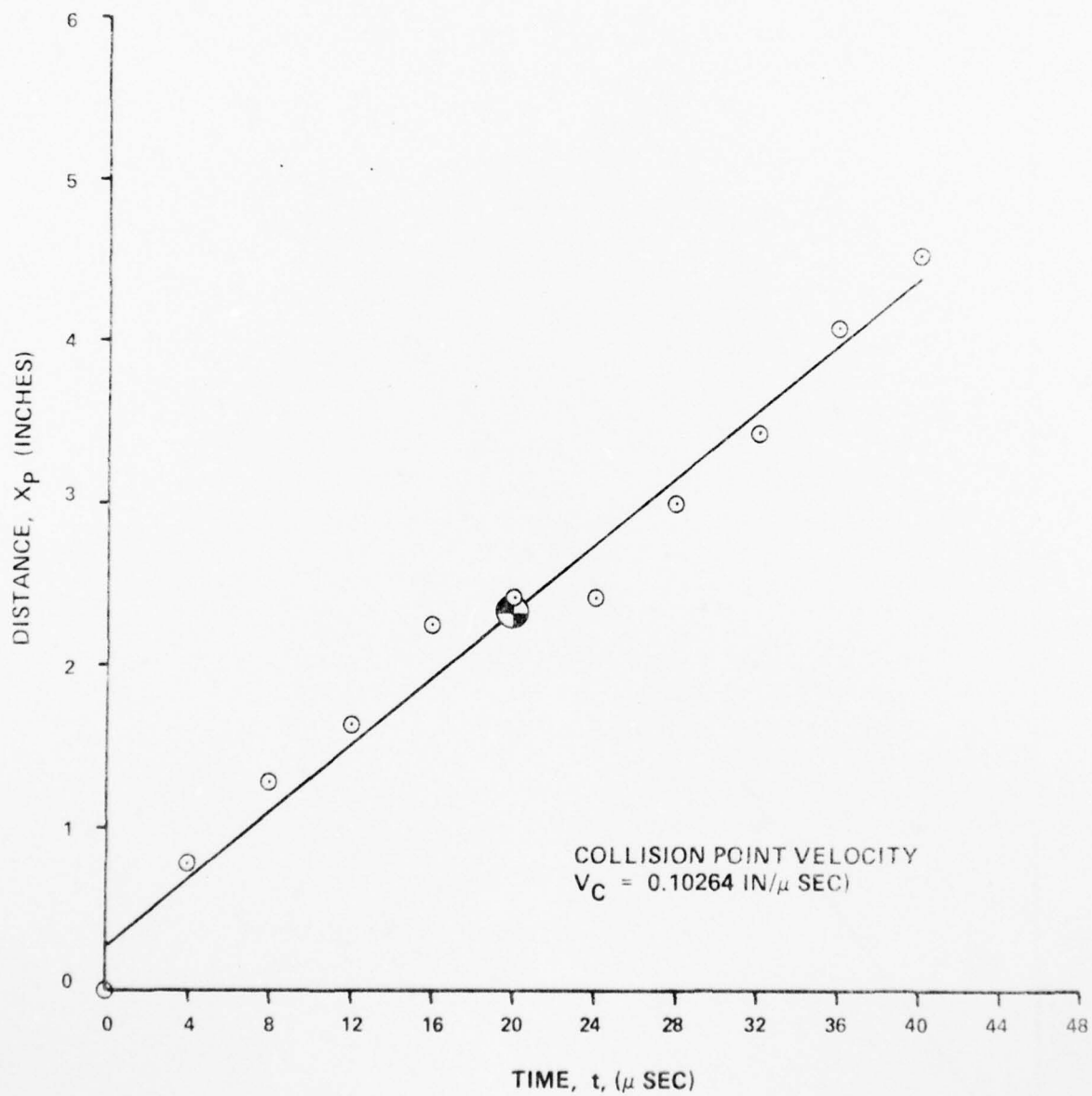


Figure 112

LASL 1286  
DETONATION POSITION

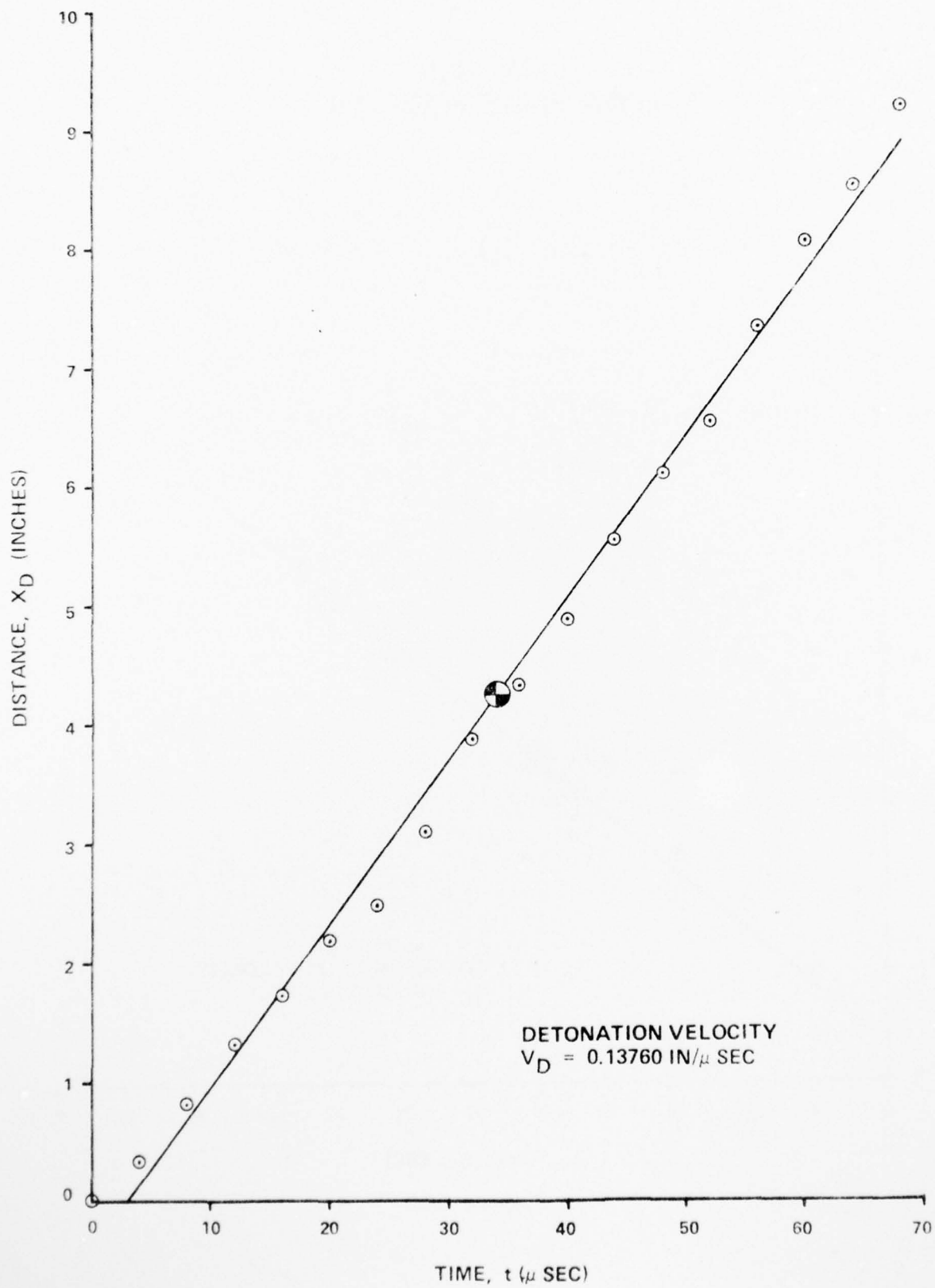


Figure 113

LASL 1286  
FLYER PLATE POSITION

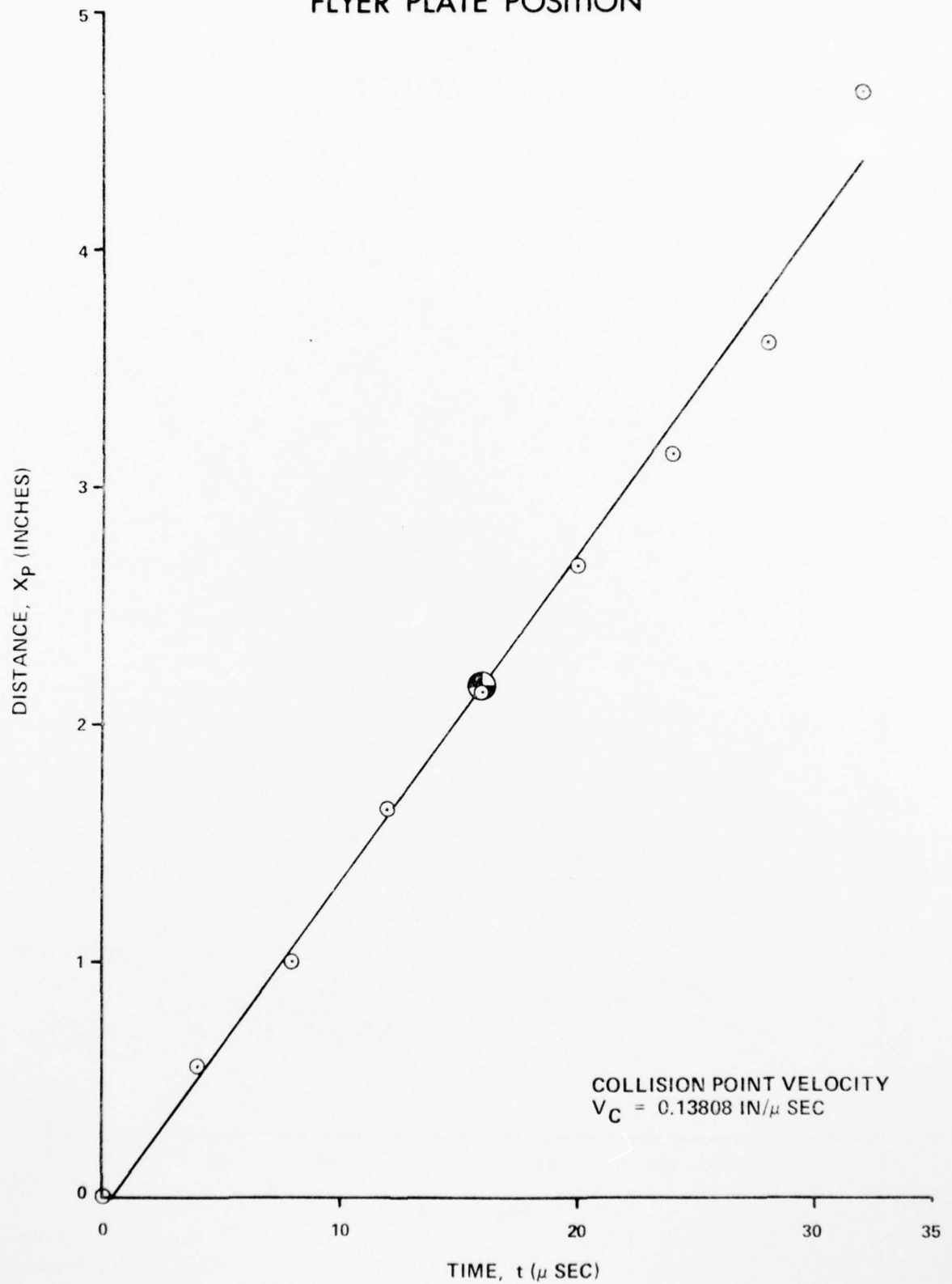


Figure 114



LASL 1312  
DETONATION POSITION

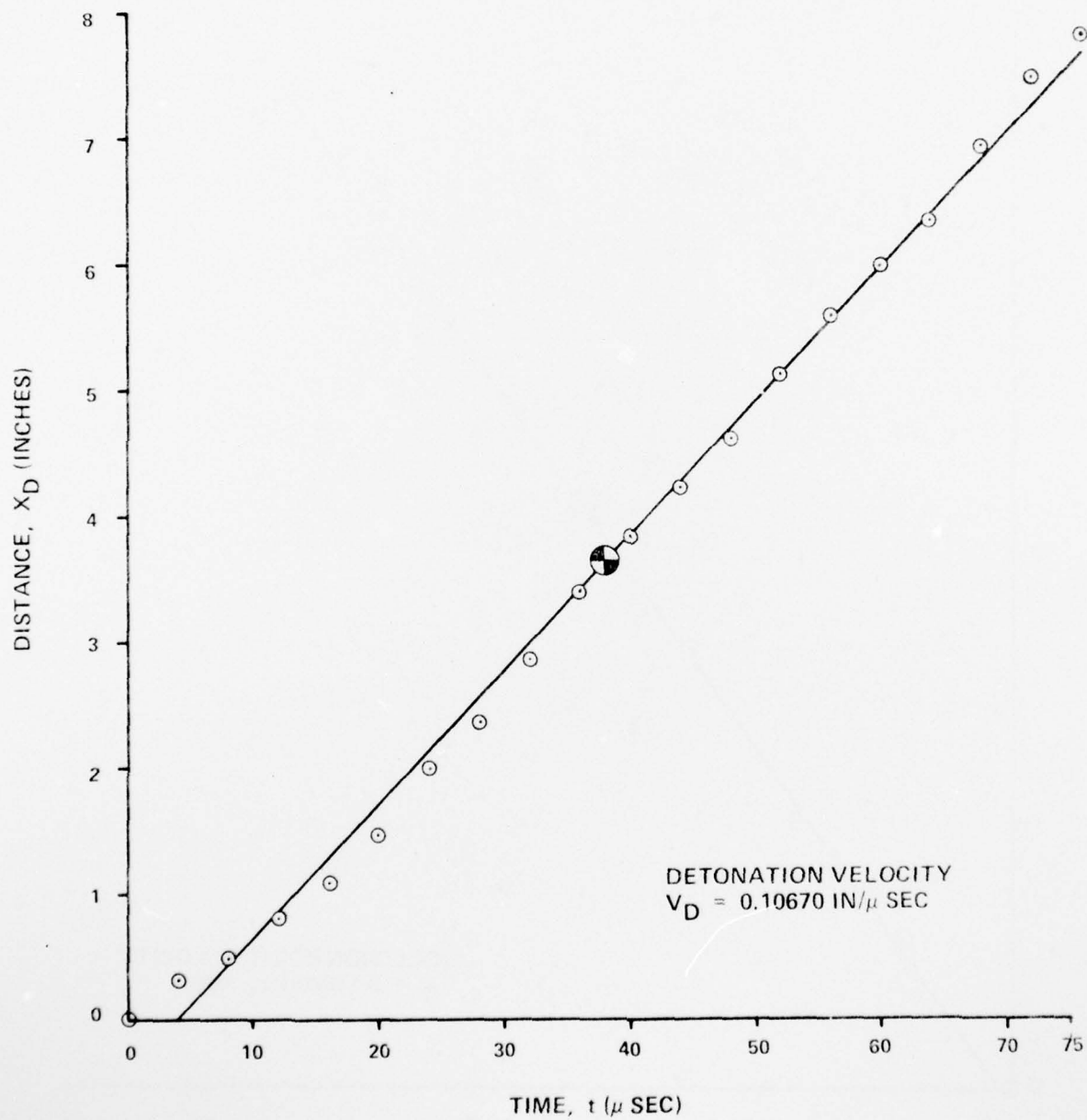


Figure 115

LASL 1312  
FLYER PLATE POSITION

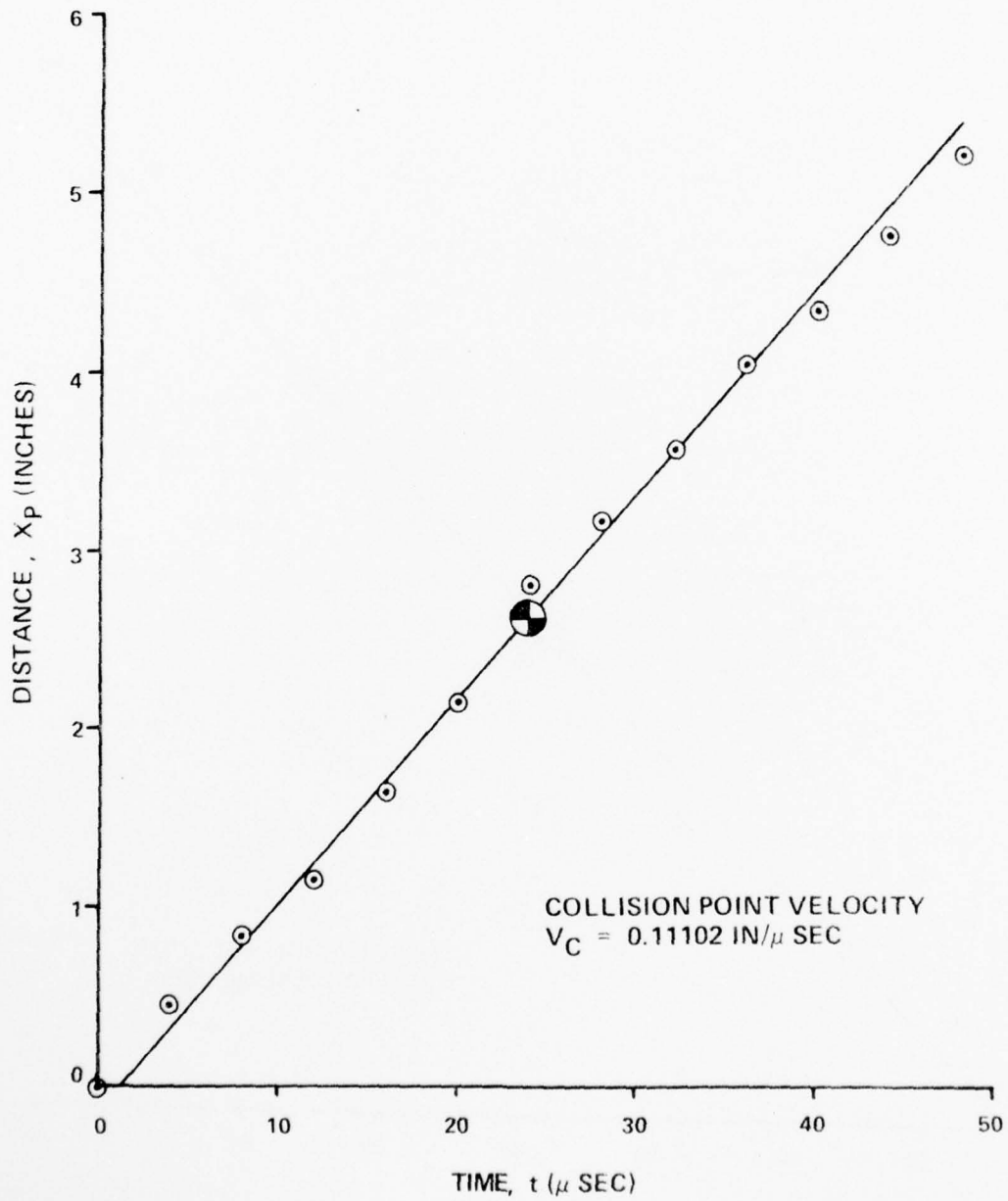


Figure 116

LASL 1317  
DETONATION POSITION

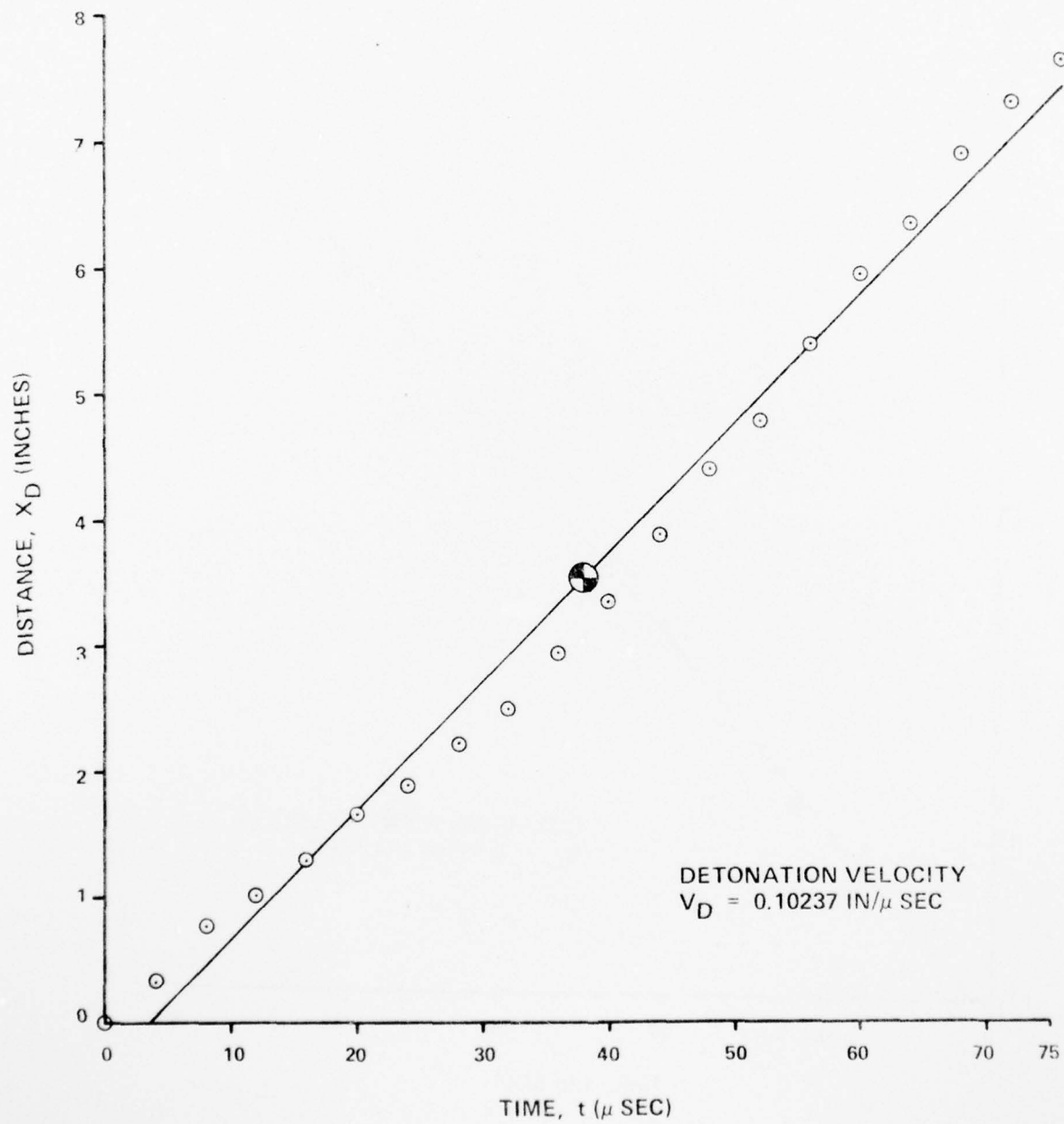


Figure 117

LASL 1317  
FLYER PLATE POSITION

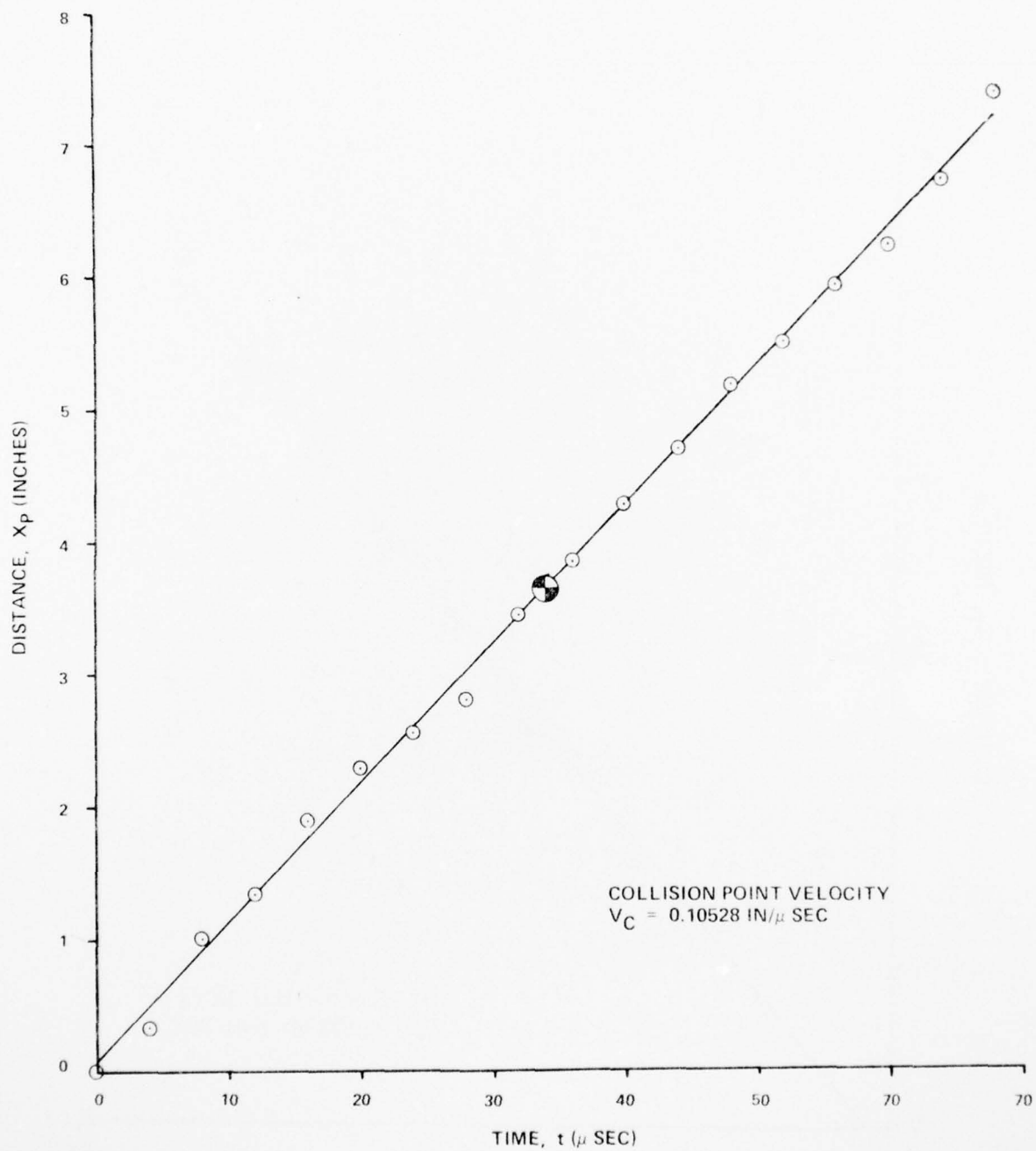


Figure 118

LASL 1320  
DETONATION POSITION

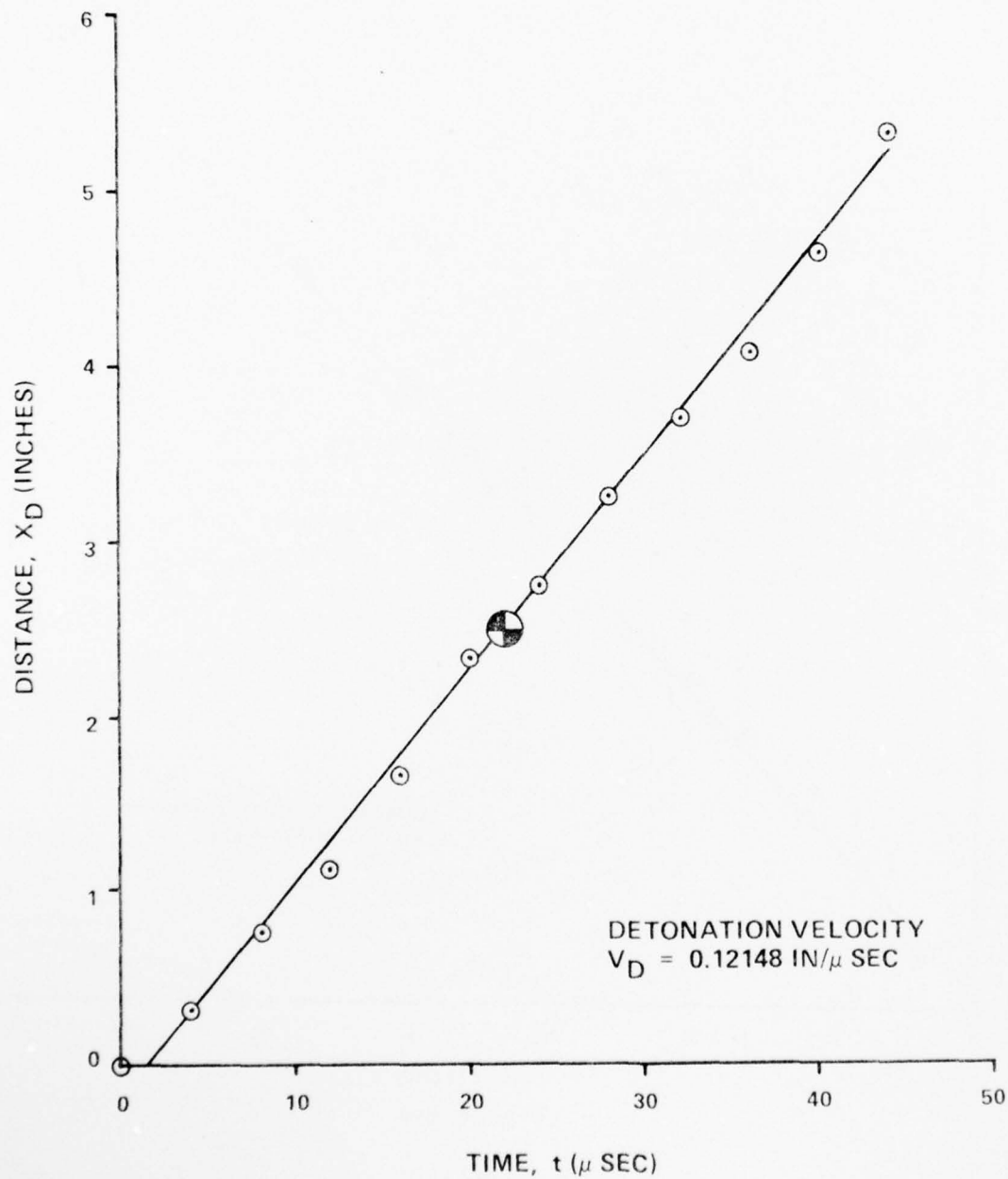


Figure 119



LASL 1320  
FLYER PLATE POSITION

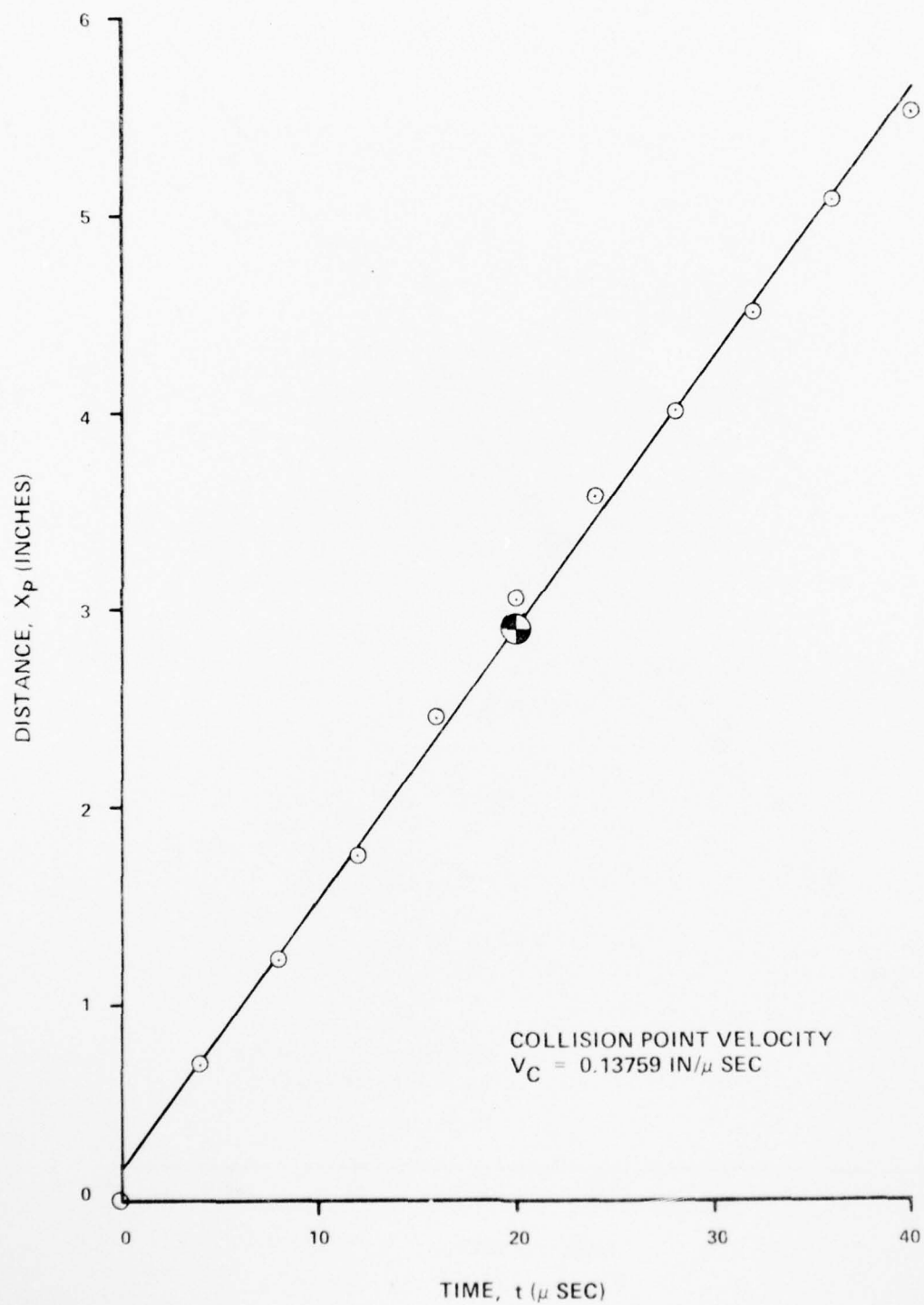


Figure 120

LASL 1321  
DETONATION POSITION

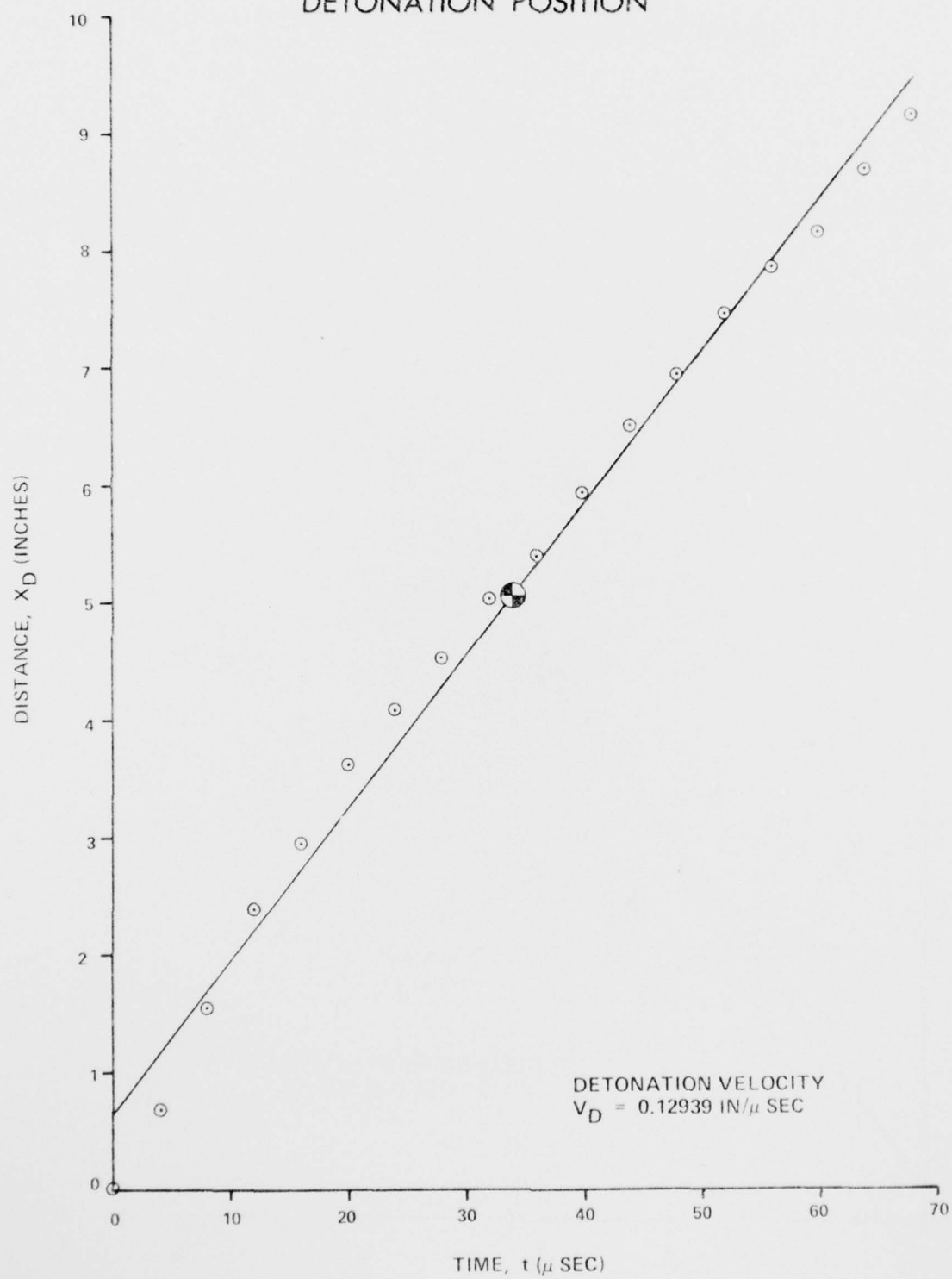


Figure 121

LASL 1321  
FLYER PLATE POSITION

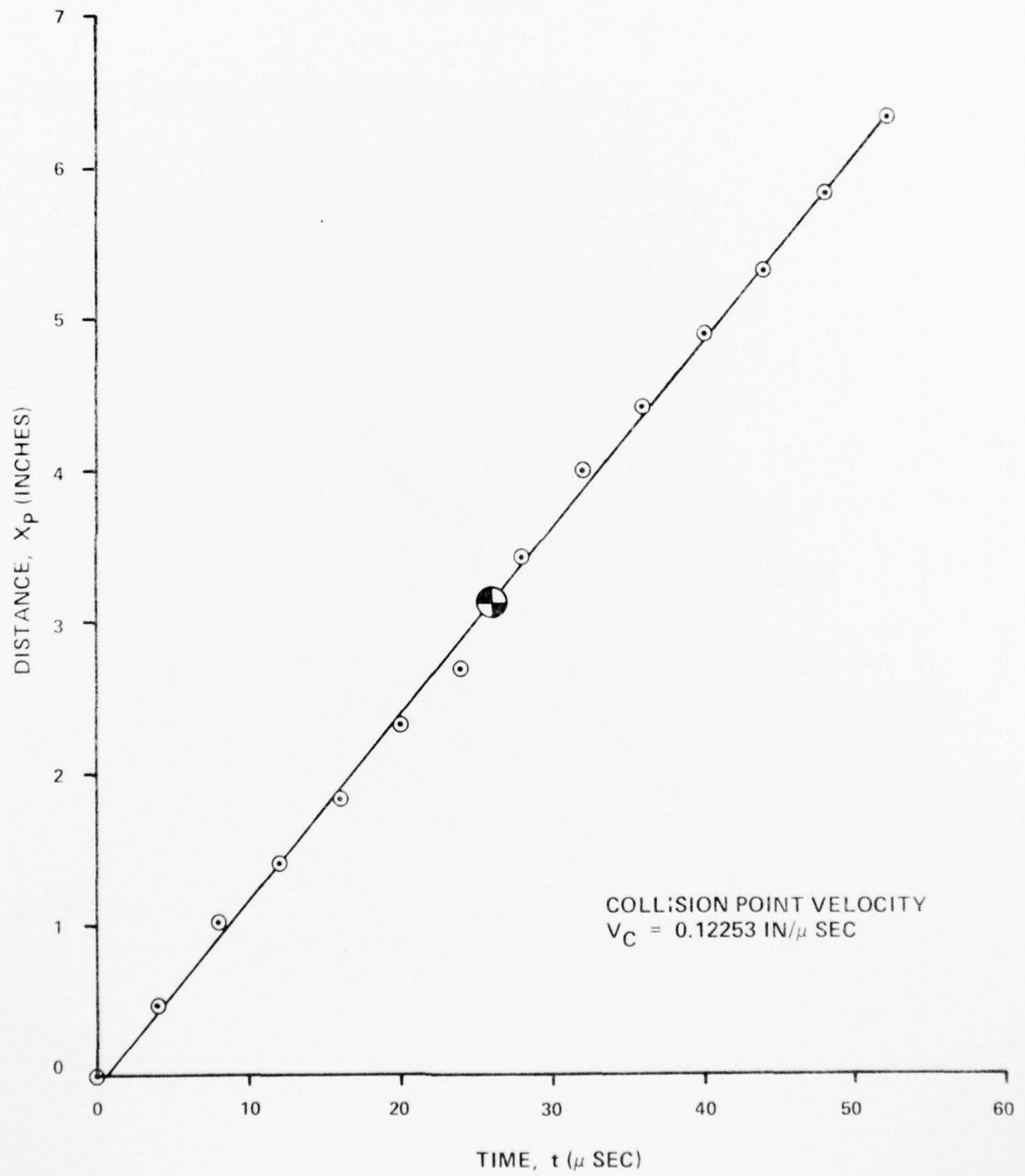


Figure 122

LASL 1322  
DETONATION POSITION

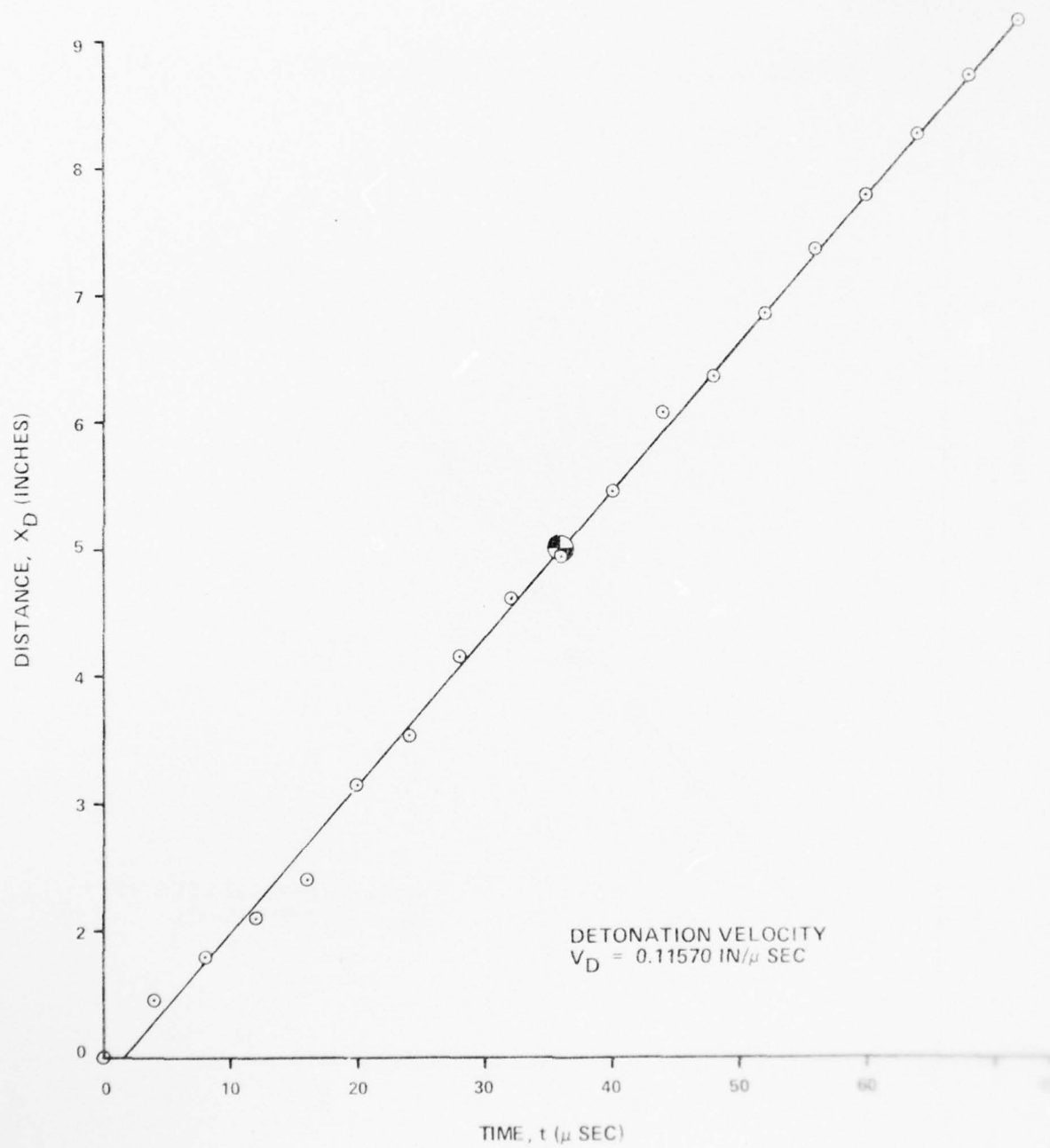


Figure 123

AD-A047 955

FRANK J SEILER RESEARCH LAB UNITED STATES AIR FORCE --ETC F/6 13/8  
EXPLOSIVE IMPULSE WELDING. VOLUME I.(U)

JUL 77 D H MERKLE, G E CANNON

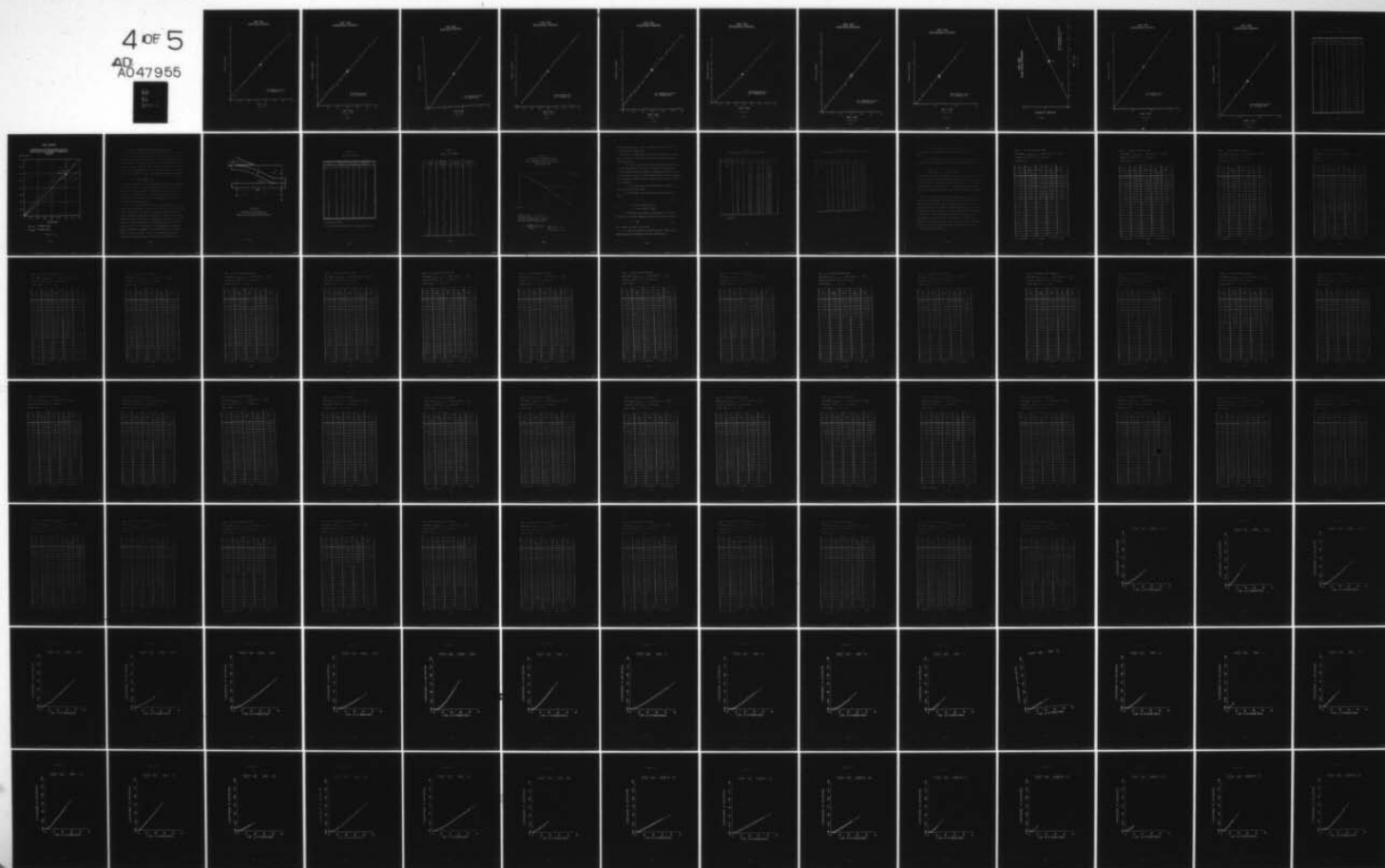
UNCLASSIFIED

FJSRL-TR-77-0012-VOL-1

NL

4 OF 5

AD  
A047955



LASL 1322  
FLYER PLATE POSITION

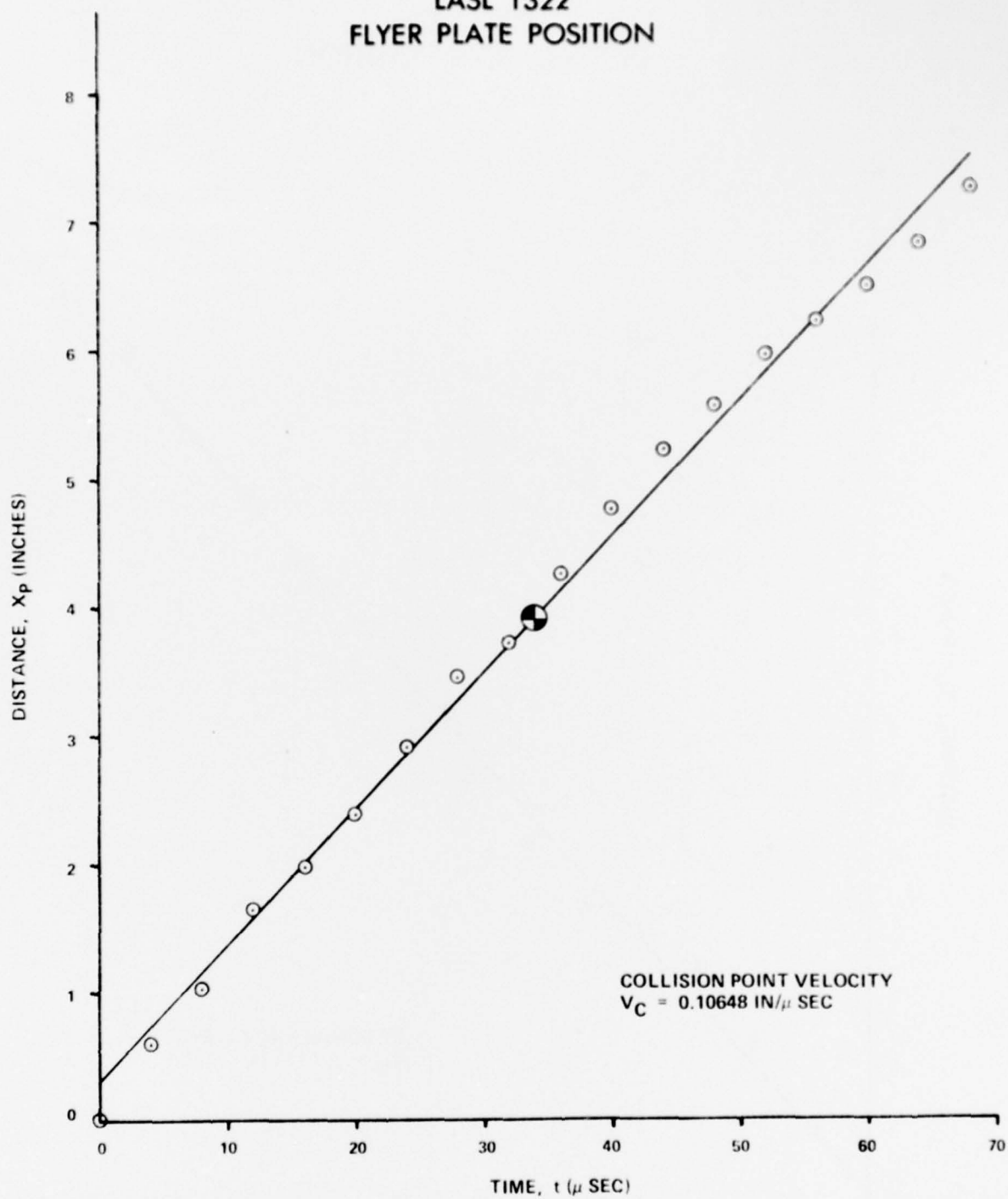


Figure 124



LASL 1323  
DETONATION POSITION

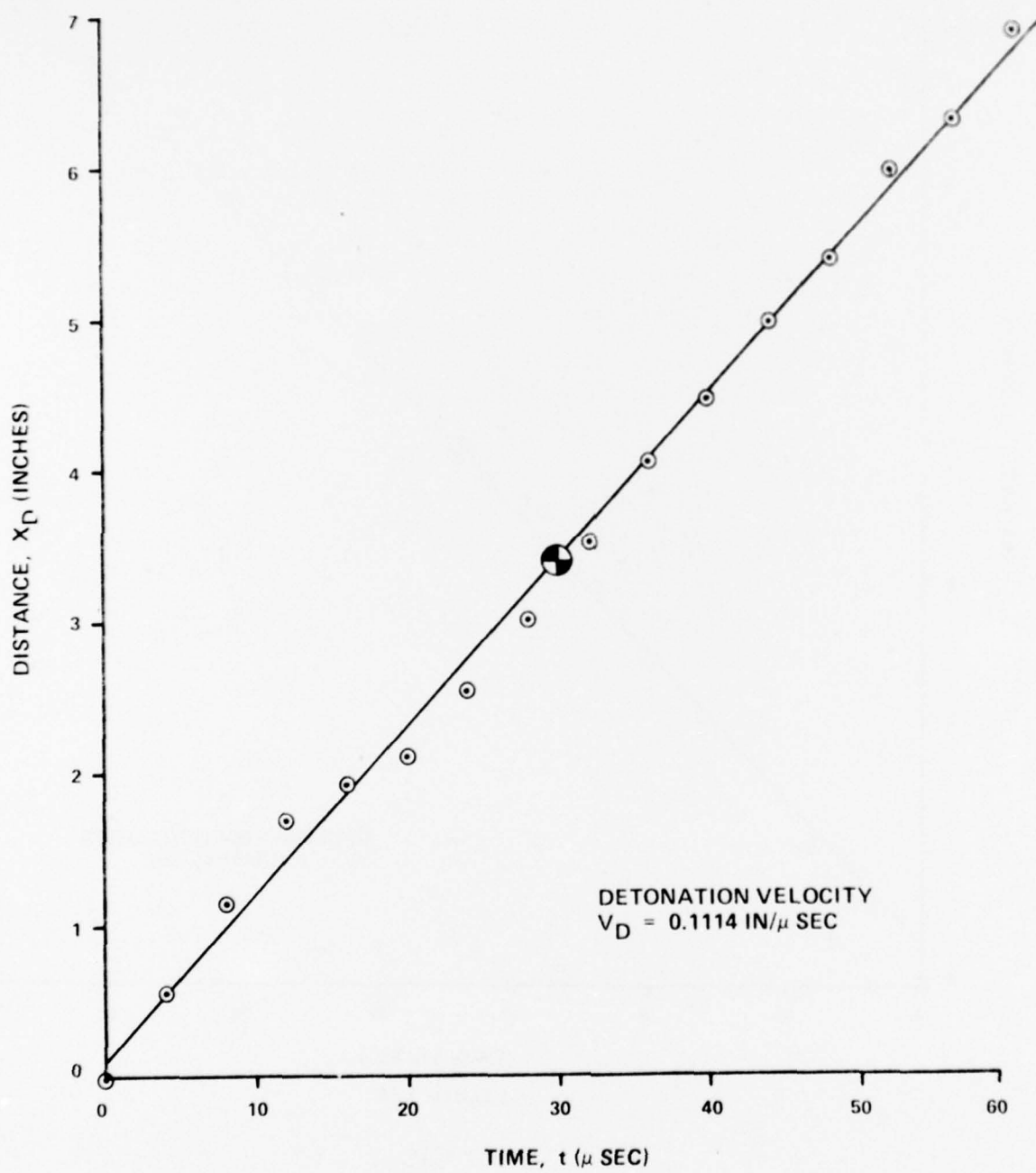
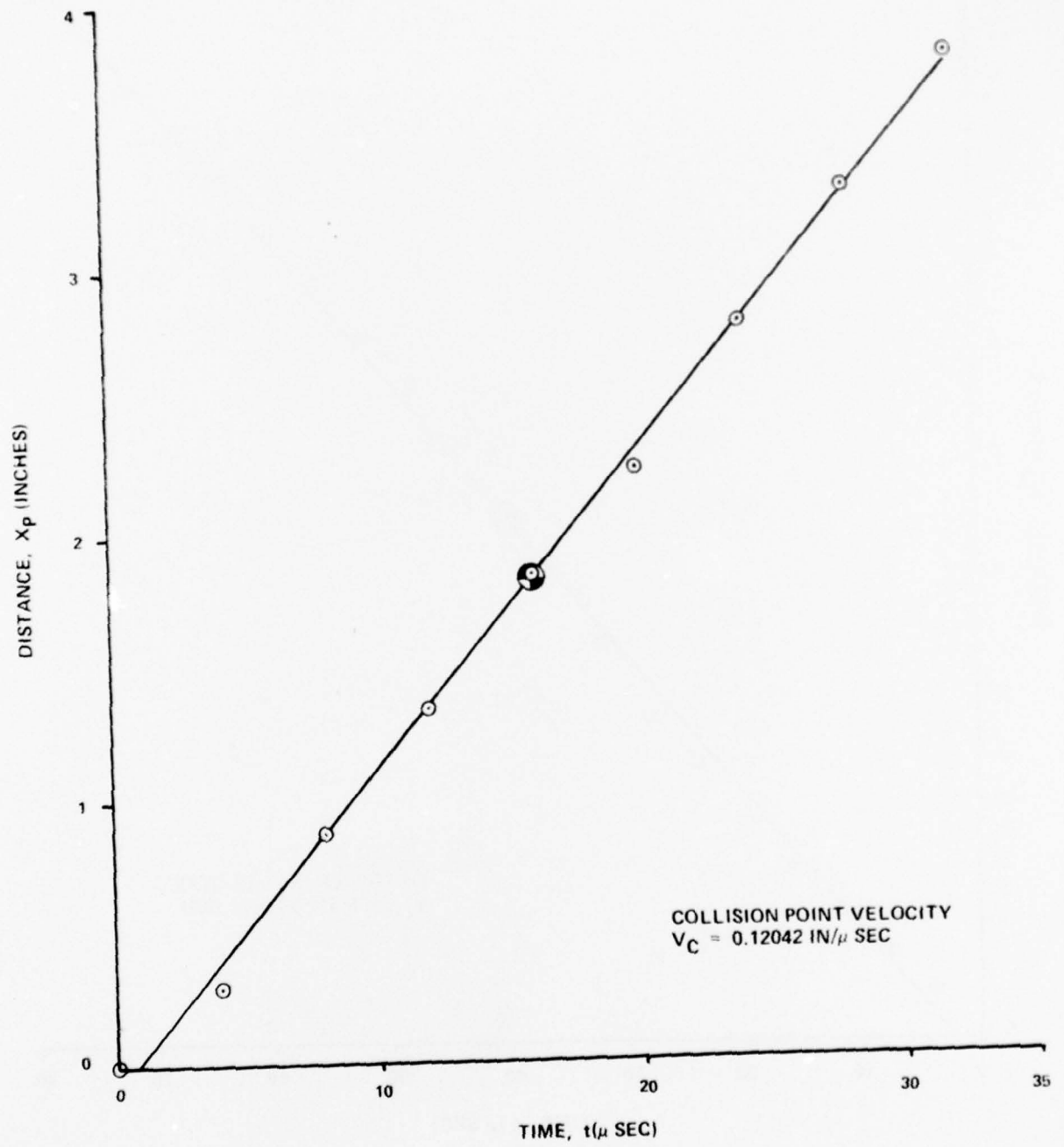


Figure 125

LASL 1323  
FLYER PLATE POSITION



TIME,  $t$  ( $\mu$  SEC)

Figure 126

LASL 1324  
DETONATION POSITION

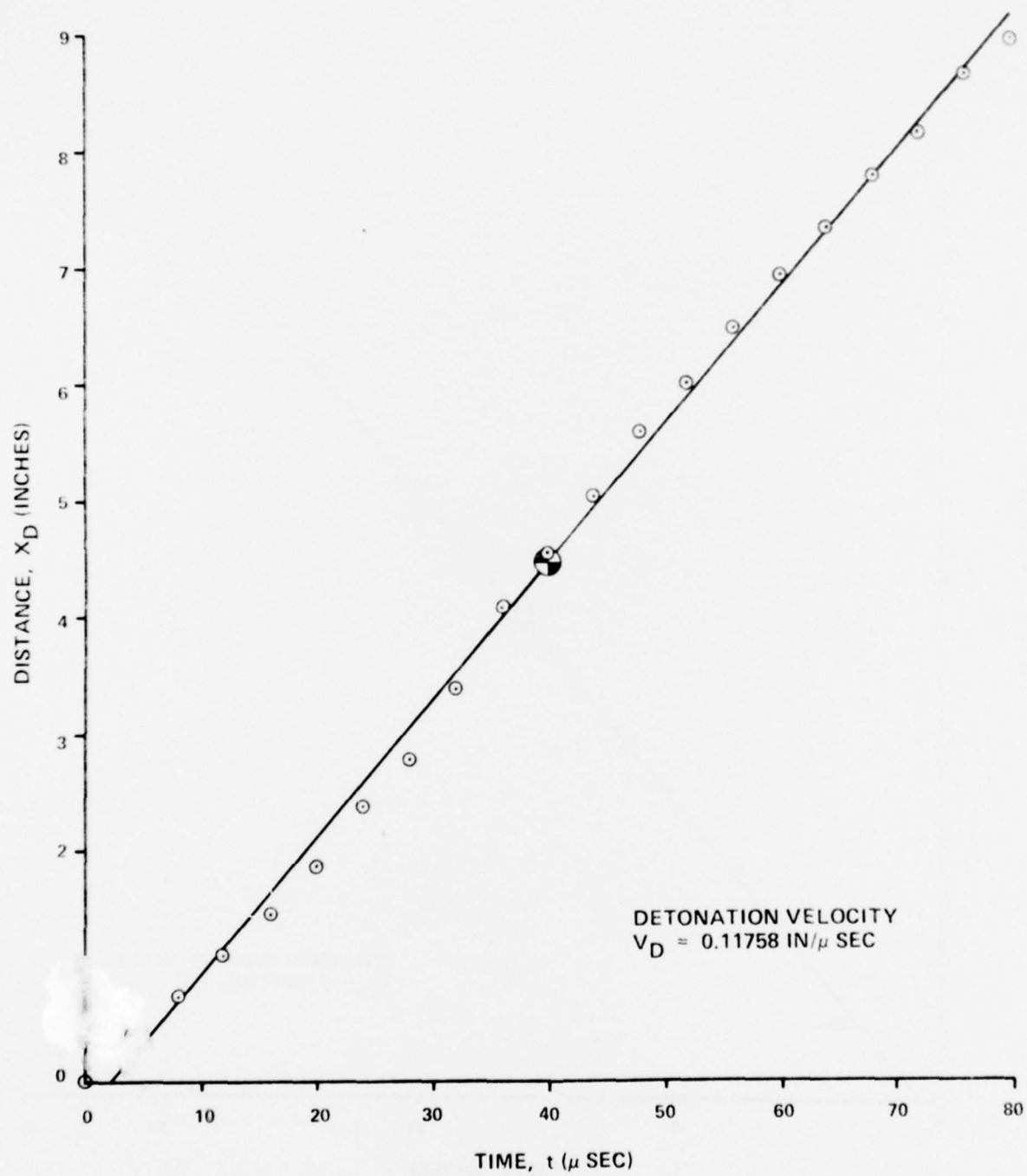


Figure 127

LASL 1324  
FLYER PLATE POSITION

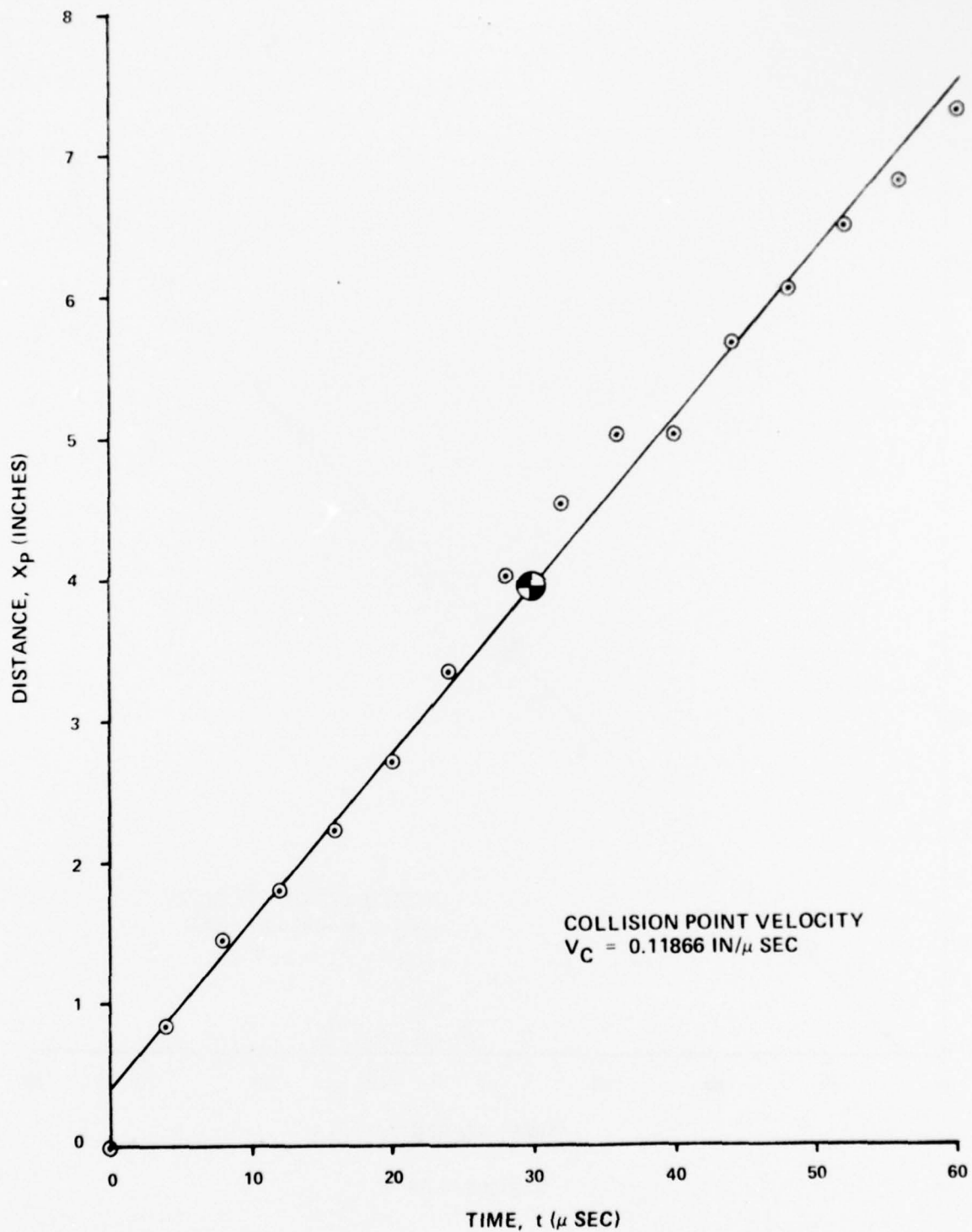


Figure 128

LASL 1325  
DETONATION POSITION

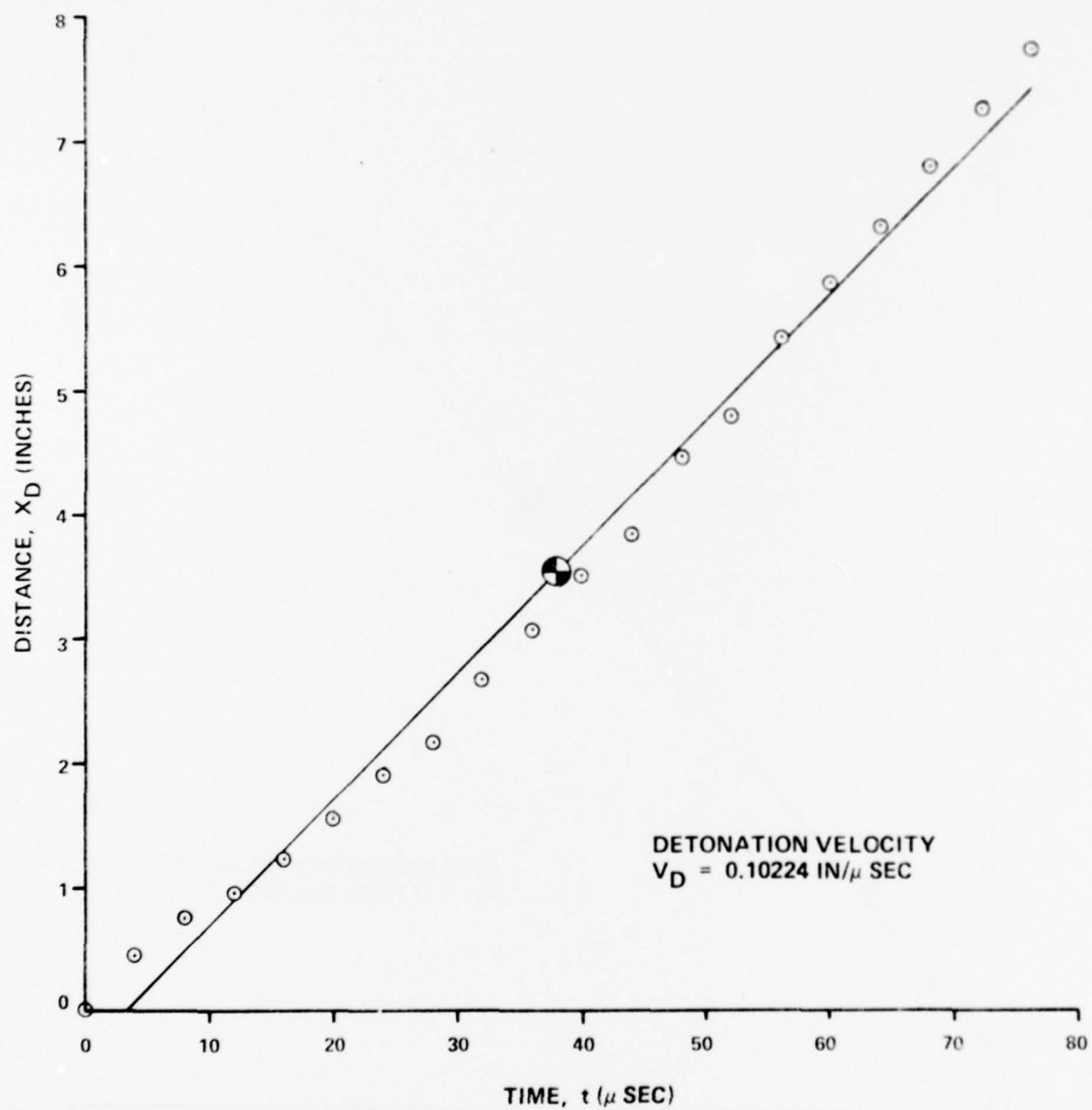


Figure 129

LASL 1325  
FLYER PLATE POSITION

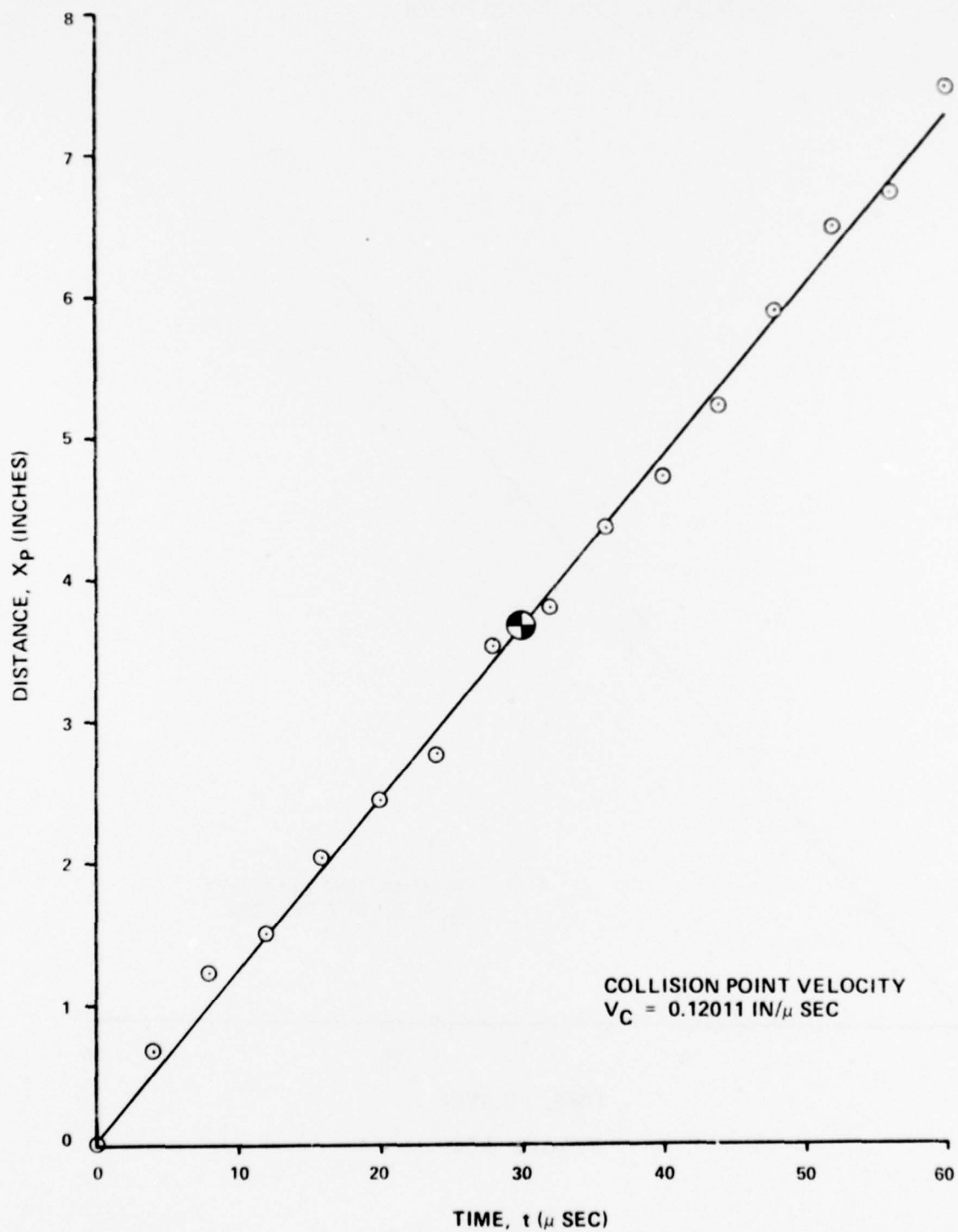


Figure 130



LASL 1328  
DETONATION POSITION

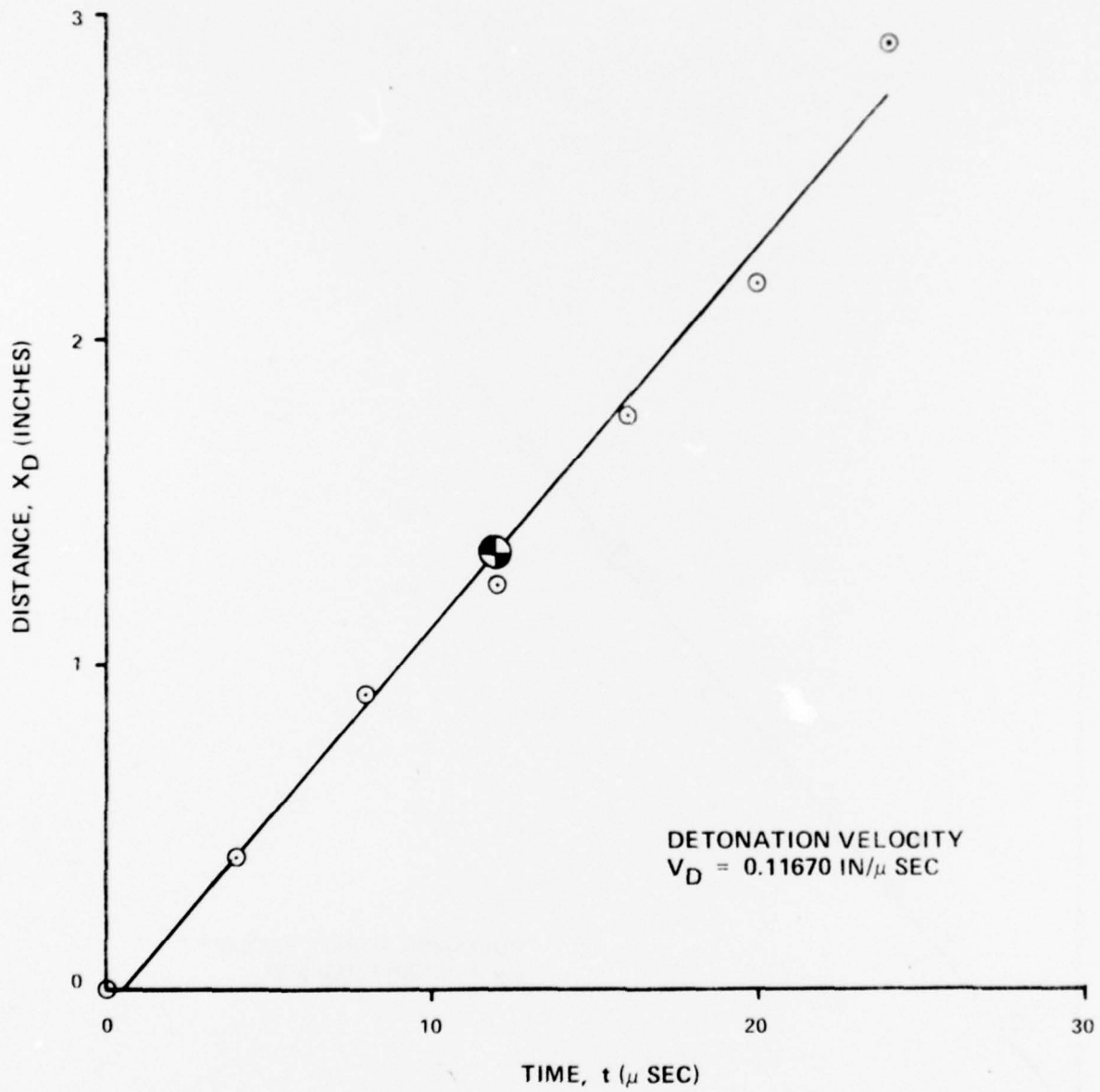


Figure 131

# LASL 1328 FLYER PLATE POSITION

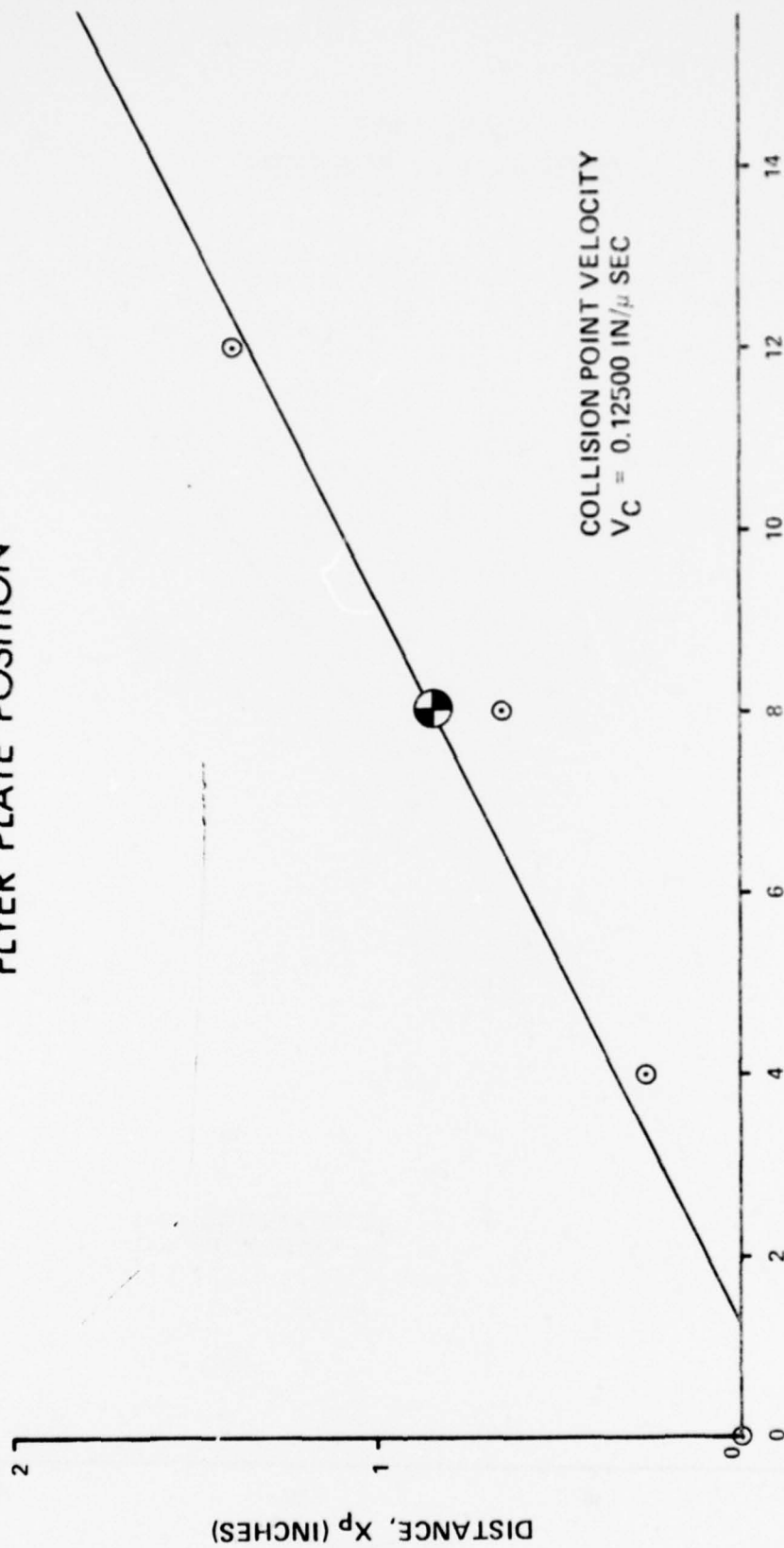


Figure 132

LASL 1362  
DETONATION POSITION

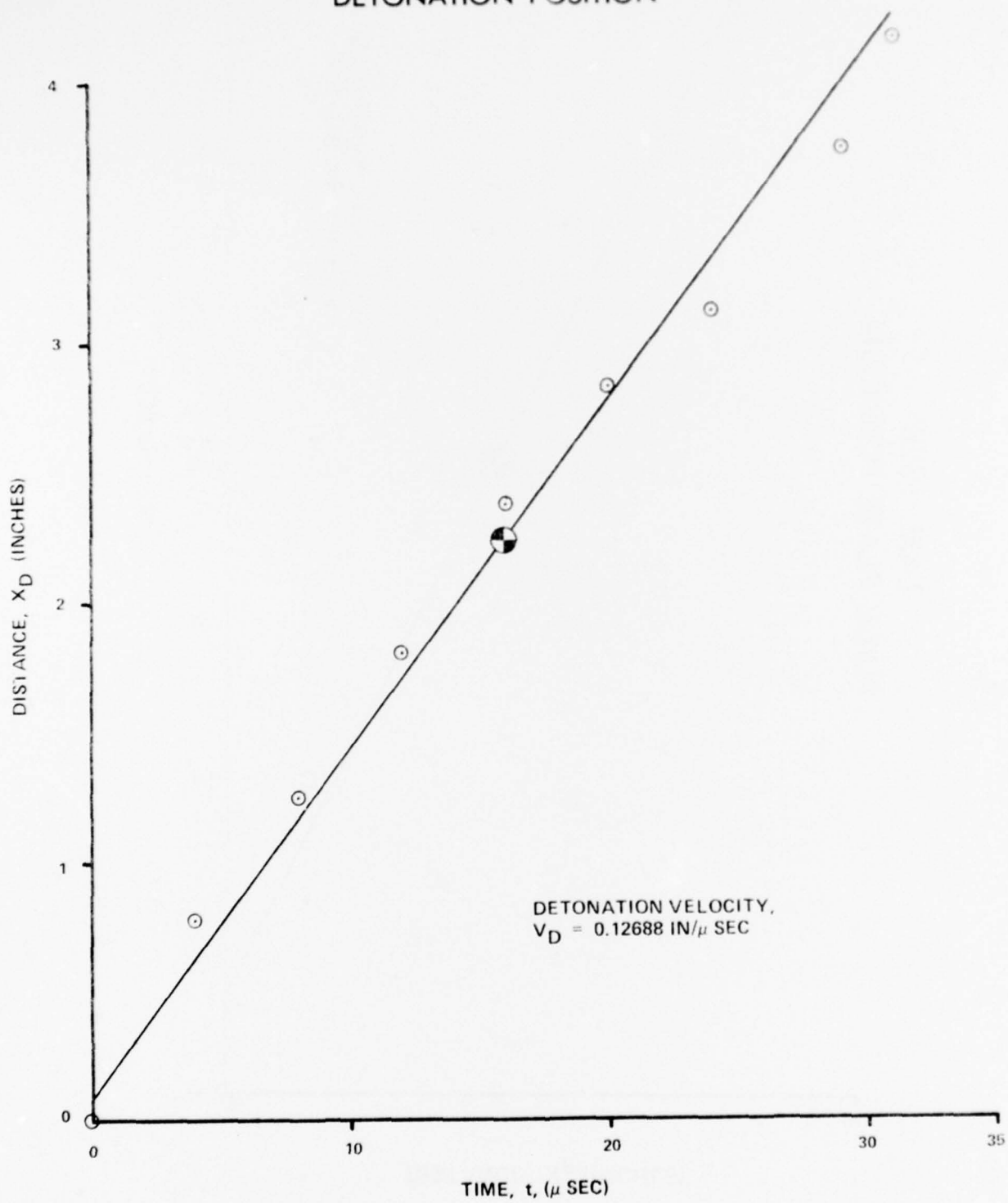


Figure 133

LASL 1362  
FLYER PLATE POSITION

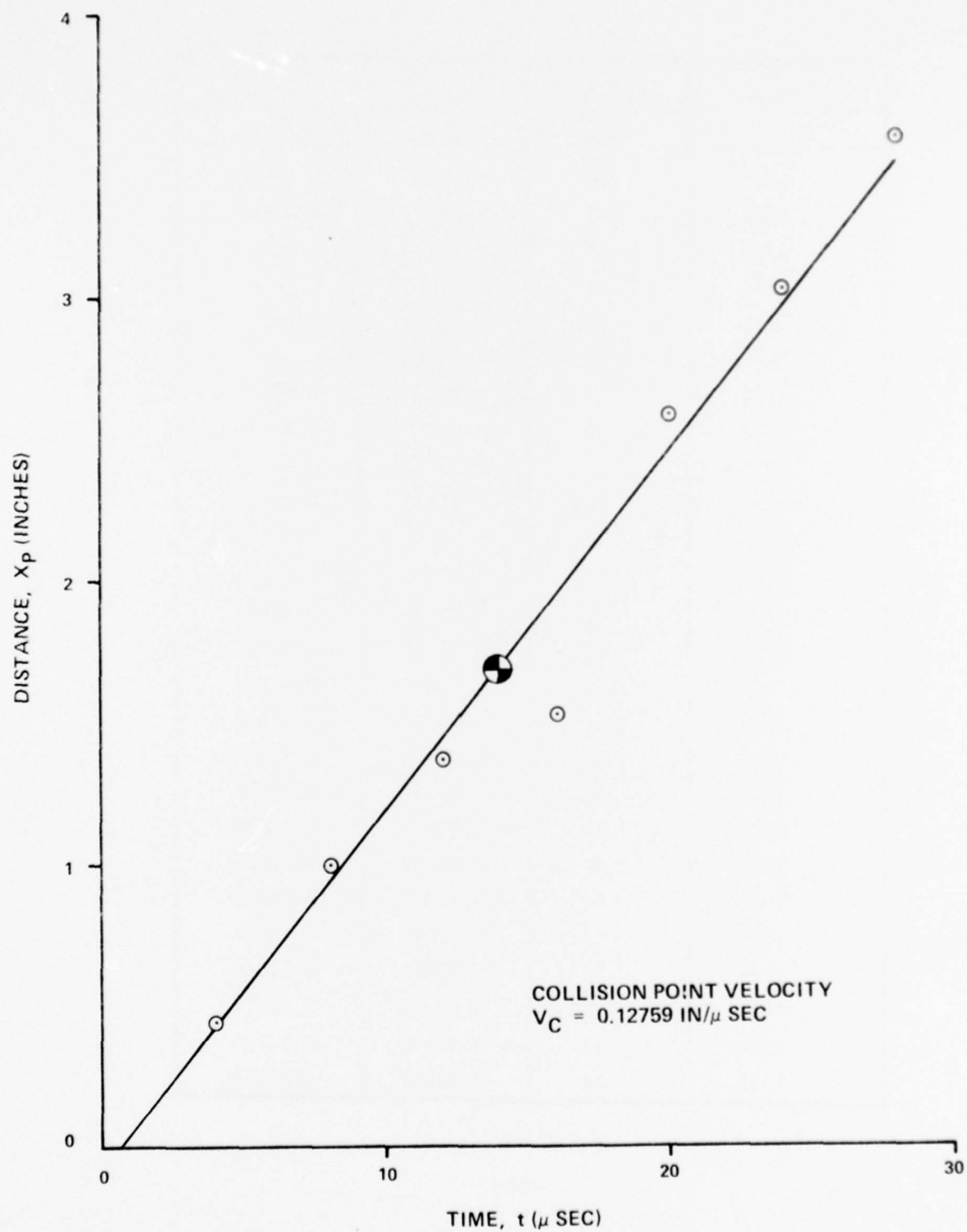


Figure 134

TABLE 68

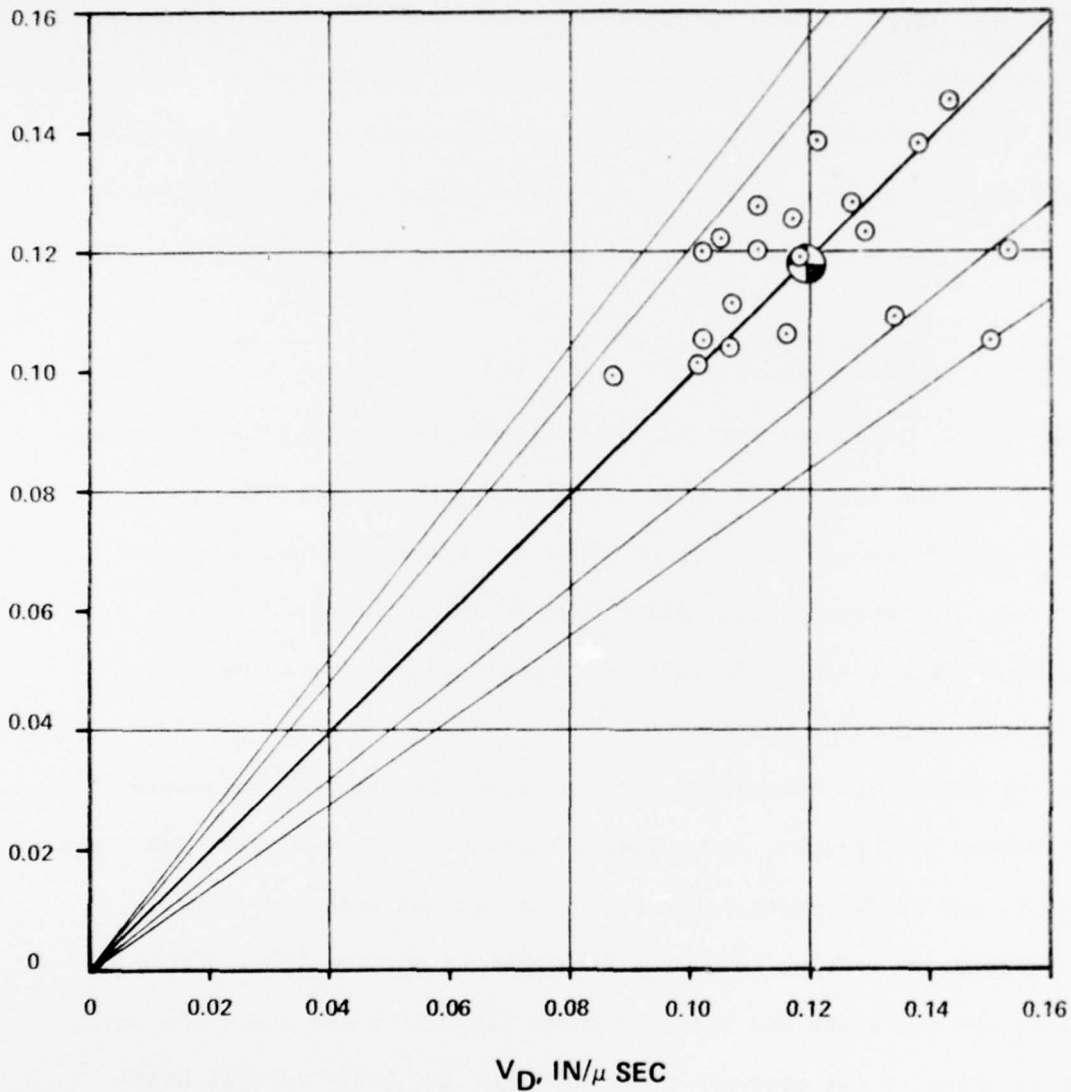
## LASL DETONATION AND COLLISION POINT VELOCITIES

Test Number	Explosive Loading	Detonation Velocity	Collision Velocity
	G/in <sup>2</sup>	in/usec	in/usec
1268	10	0.10465	0.12160
1269	10	0.14275	0.14492
1270	10	0.10070	ND
1271	10	0.10617	0.10449
1273	10	0.08727	0.09890
1274	10	0.09399	ND
1277	10	0.10144	0.10120
1278	10	0.15275	0.11946
1279	10	0.15012	0.10537
1280	10	0.11120	0.12693
1281	10	0.13434	0.10915
1282	10	0.17966	0.09214
1283	14	0.20396	0.12691
1284	8	0.19497	0.12271
1285	14	0.18397	0.10264
1286	14	0.13760	0.13808
1312	10	0.10670	0.11102
1317	10	0.10237	0.10528
1320	12	0.12148	0.13759
1321	14	0.12939	0.12253
1322	10	0.11570	0.10648
1323	14	0.11145	0.12042
1324	10	0.11758	0.11866
1325	14	0.10224	0.12011
1328	12	0.11670	0.12500
1362	12	0.12688	0.12759

## LASL SHOTS

CORRELATION OF DETONATION VELOCITY  
WITH FLYER PLATE APPARENT HORIZONTAL  
VELOCITY

$V_P$ , IN/ $\mu$  SEC



$V_{D, \text{AVG}} = 0.11894$  IN/ $\mu$  SEC

$V_{P, \text{AVG}} = 0.11824$  IN/ $\mu$  SEC

Figure 135



### 3. Analysis of Flash X-Ray Data, LASL, DRI and USAFA

The fact that detonation velocity and collision point velocity are, at least on the average, approximately equal for parallel plate welding configurations suggests that the parallel plate explosive welding process can be viewed as a steady state process. In this case the detonation velocity is assumed constant and the vertical displacement of a point on the flyer plate depends only on how far that point is behind the detonation front, as shown in Fig. 136. The steady state analysis assumes that

$$\underline{y = f(z) = f(V_D t - x)} \quad (1)$$

Equation (1) indicates that an instantaneous flyer plate configuration, such as that shown in a flash X-Ray, should have the same shape except for the X axis scale as a plot of y VERSUS t for a single point in the flyer plate. Therefore a flyer plate position-time curve should be constructable from a single flash X-Ray photograph and the value of the corresponding detonation velocity.

For the LASL shots detonation velocity was obtained from successive framing camera photographs, using linear regression as previously described. For the DRI and USAFA shots detonation velocity was measured directly, using a continuous writing probe, as described in Section IIH. Table 69 summarizes the DRI shots and Table 70 summarizes the USAFA shots for which detonation velocity was measured. The original log books for all USAFA shots were on file in the Department of Civil Engineering, Engineering Mechanics and Materials (DFCEM) at the United States Air Force Academy when this report was written. Fig. 137 illustrates how detonation velocity was calculated from the oscilloscope trace produced by the

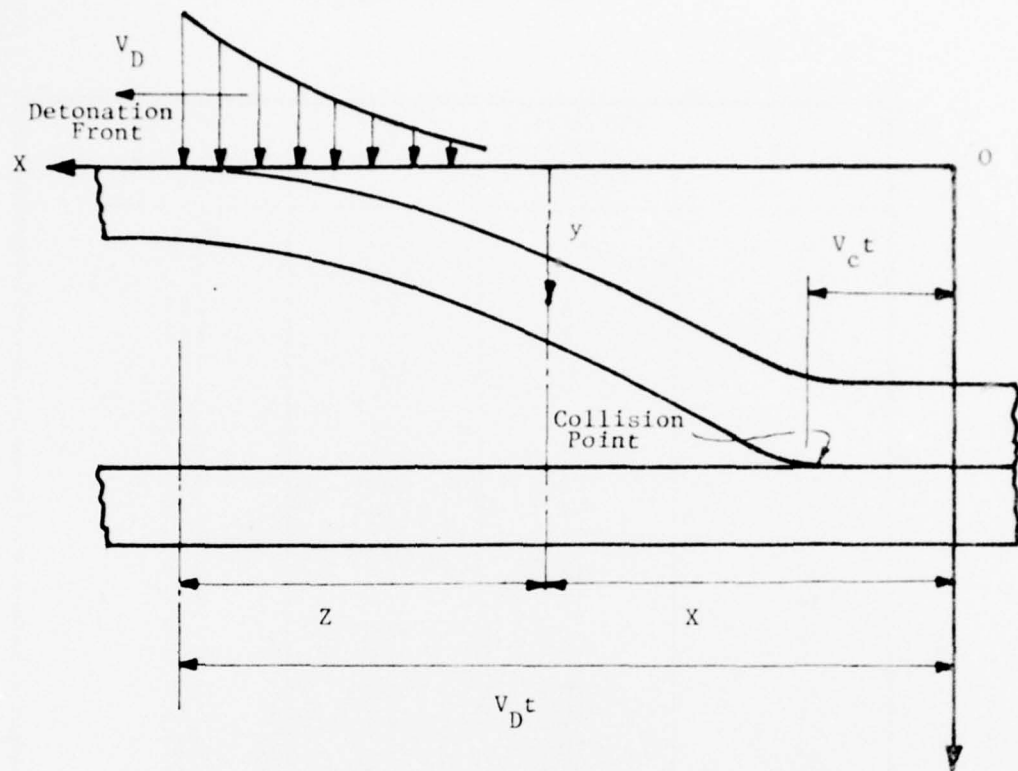


FIGURE 136  
 BASIC STEADY STATE GEOMETRY OF  
 PARALLEL PLATE EXPLOSIVE IMPULSE WELDING

TABLE 69

## DRI SERIES SUMMARY

Test Number	Explosive Loading	Flyer Thickness	Standoff Distance
	G/in <sup>2</sup>	in	in
2	12	1/4	1/8
3	12	1/4	1/2
4	8	1/4	1/2
5	8	1/4	1/2
6	8	1/4	1/4
7	8	1/4	1/8
8	8	1/4	1/8
9	8	1/4	1/4
10	12.8	1/4	1/8
11	12	1/4	1/8
12	12	1/4	1/4
13	12.3	1/4	1/4
14	12	1/4	1/2
15	12	1/4	1/2
16	12	1/4	1/8
17	10	1/2	1/4
18	10	1/2	1/4
19	10	1/2	1/2
20	10	1/2	1/2
22+	14	1/2	1/2
23	10	1/2	1
24*	10	1/2	1/2
25*	14	1/2	1/2
26	14	1/2	1/4
27	10	1/2	1
28	14	1/2	1/4
29	14	1/2	1
30	14	1/2	1

+ There was no shot 21

\* 24 inch long flyer plate with 12 inch long explosive box

TABLE 70  
USAFA SERIES SUMMARY

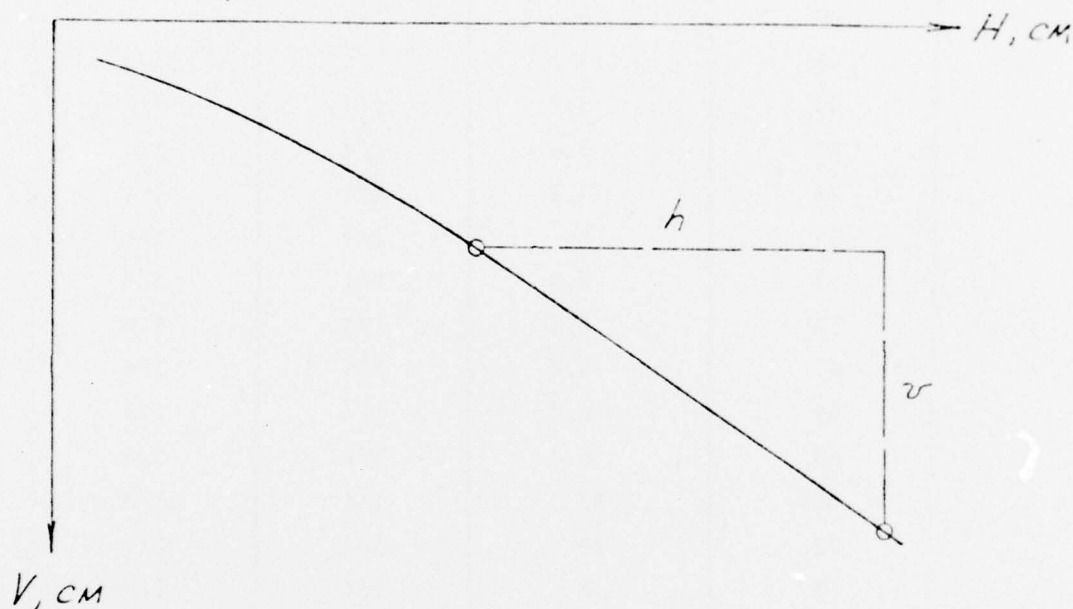
Test Number	Explosive Loading	Flyer Thickness	Standoff Distance
	G/in <sup>2</sup>	in	in
28	10	1/4	1/8
39	3.3	1/4	1/8
40	8	1/4	1/8
45	3.2	1/4	1/2
46	3.2	1/4	1/2
47	3.1	1/4	1/4
48	3.2	1/4	1/4
51	8	1/4	1/8
54	6.4	1/4	1/8
55	6.4	1/4	1/8
57	6.4	1/4	1/4
59	6.4	1/4	1/2
60	6.4	1/4	1/2
62A	12	1/4	1/8
72	14	1/2	1/4
73	6	1/4	1/8
75	8	1/2	1/4
76	8	1/2	1/4
78	14	1/2	1/4
79	12	1/4	1/8
82	8	1/2	1/4
89	7.5	1/2	1/4
94	8	1/2	1/4
98	10	1/4	1
99	12	1/4	1
110	8	1/8	3/4

Figure 137

CALCULATION OF DETONATION VELOCITY

FROM CONTINUOUS WRITING VELOCITY PROBE

OSCILLOSCOPE TRACE



Vertical Scale: 1 cm = 25  $\Omega$   
 Horizontal Scale: 1 cm = 10  $\mu$  sec  
 Velocity Gage Resistance = 86.6  $\Omega$ /ft  
 Detonation Velocity Calculation:

$$V_D = \frac{v \left( \frac{25.0}{86.6} \right) (12.0) (2.54)}{h (10)} = \frac{762}{866} \left( \frac{v}{h} \right) \text{ cm}/\mu\text{sec}$$

continuous writing probe. Table 71 contains detonation velocity data for both the DRI and USAFA shots.

Conversion of an instantaneous flyer plate configuration in a flash X-Ray photograph to a position-time curve was accomplished using the following procedure:

1. The flyer plate configuration was digitized by measuring the vertical displacement at 1cm horizontal intervals on the photograph. The manual digitizer employed allowed the photograph scale factor (ratio of actual standoff distance to scaled standoff distance on the photograph) to be incorporated into the vertical reading (y), but not into the horizontal reading (x).

2. A five column table was constructed, with x entered in column 1 and y entered in column 4.

3. The photograph scale factor,  $\$$ , was calculated from the formula

$$\$ = \frac{s}{s'} \quad (1)$$

s = actual standoff distance

s' = scaled standoff distance

4. Scaled horizontal distance was converted to time (since passage of the explosive detonation pressure front) using the formula

$$t = \frac{x \$}{V_D} \quad (2)$$

and t entered in column 2 of the table.

5. A plot of y VERSUS t was constructed, and a smooth curve drawn through the experimental points with a French curve.



TABLE 71  
 DETONATION VELOCITY FOR DRI AND USAFA SERIES

Series	Test	v	h	V <sub>D</sub>
		cm	cm	cm/usec
DRI	2	2.95	8.60	0.30185
	3	2.85	8.60	0.29160
	4	2.05	8.60	0.20975
	5			0.25000*
	6	2.40	8.60	0.24556
	7	3.00	8.60	0.30694
	8	2.35	8.60	0.24044
	9	2.85	8.60	0.29160
	10	3.30	8.60	0.33764
	11	3.05	8.60	0.31206
	12	2.80	7.80	0.31586
	13	3.20	8.60	0.32741
	14	3.00	8.60	0.30694
	15	3.05	8.60	0.31206
	16	2.90	8.60	0.29671
	17	2.90	8.60	0.29671
	18	3.05	8.60	0.31206
	19	2.85	8.60	0.29160
	20	2.72	8.60	0.27830
	22	3.02	8.60	0.30899
	23	2.57	8.60	0.26295
	24	2.88	8.60	0.29467
	25	3.20	8.60	0.32741
	26	3.30	8.60	0.33764
	27	2.86	8.60	0.29262
	28	3.16	8.60	0.32531
	29	3.11	8.60	0.31820
	30	2.86	8.60	0.29262

\*Estimated

TABLE 71  
 DETONATION VELOCITY FOR DRI AND USAFA SERIES (continued)

Series	Test	v	h	$V_D$
		cm	cm	cm/ $\mu$ sec
USAFA	28	3.30	9.00	0.32263
	39	2.50	7.15	0.30766
	40	3.38	8.95	0.33230
	45	2.40	6.84	0.30874
	46	2.45	7.20	0.29941
	47	2.78	7.45	0.32834
	48	2.71	7.35	0.32443
	51	2.59	6.45	0.35333
	54	2.30	6.10	0.33177
	55	3.00	7.65	0.34506
	57	3.05	7.30	0.36763
	59	3.12	6.69	0.41036
	60	2.85	7.15	0.35073
	62	3.00	6.75	0.39107
	72	3.45	7.22	0.42045
	73	2.80	8.64	0.28516
	75	2.80	7.05	0.34947
	76	2.96	7.21	0.36124
	78	3.25	6.54	0.43726
	79	3.32	6.83	0.42771
	82	3.44	7.75	0.39057
	89	4.40	7.55	0.51279
	94	2.79	6.87	0.35734
	98	1.99	5.16	0.33934
	99	2.61	6.20	0.37041
	110	2.68	6.56	0.35947

6. If required during the drawing of the smooth curve a new time origin,  $t_0$ , was established and  $t-t_0$  entered in column 3 of the table.

7. Using the method of least squares, an  $n^{\text{th}}$  degree hyperbola was fitted to the experimental points. The equation of the fitted curve is

$$\left( \frac{y}{b} + 1 \right)^n = 1 + [a (t-t_0)]^n \quad (3)$$

For mathematical details see Appendices A and B, and for a description of the computer program which was modified slightly for the above curve fitting see [Head (1970)]. Because Equation (3) is nonlinear, the computer program requires initial values of  $a$ ,  $b$  and  $n$ . These were obtained graphically from the plot constructed in Steps 5 and 6 above, as described in Appendix B.

Tables 72 through 114 contain both the digitized data and the fitted curve points and parameters for the eight LASL, fifteen DRI and twenty USAFA shots for which flash X-Ray photographs were obtained. Of the forty-three analyses, ten failed to converge because the computer program convergence criterion could not be satisfied within a predetermined number of iterations. Figures 138 through 180 contain corresponding plots of experimental data and fitted position-time curves. The fitted curve parameters are summarized for all shots in Table 115. Table 116 summarizes the impact velocities and collision angles calculated using Equations (B-16) and (B-17) in Appendix B.

TABLE 72. DIGITIZED FLASH X-RAY DATA

SHOT NUMBER LASL 1311 SCALE FACTOR,  $f = \frac{0.250}{0.430}$

DETONATION VELOCITY,  $V_D = 0.29672 \text{ cm}/\mu\text{sec}$

INITIAL TIME,  $t_0 = 2.29 \text{ } \mu\text{sec}$

[illegible]
$$b = 0.3568 \text{ cm}$$
$$v = 0.1773 \text{ cm}$$
$$h = 7.5700 \text{ } \mu\text{sec}$$

SHOT NUMBER LASL 1312 SCALE FACTOR,  $f = \frac{0.500}{1.220}$

INITIAL TIME,  $t_0 = 4.51 \text{ } \mu\text{sec}$

[illegible]
$$h = 9.5602 \text{ } \mu\text{sec}$$

TABLE 74. DIGITIZED FLASH X-RAY DATA

SHOT NUMBER LASL 1317 SCALE FACTOR,  $f = \frac{0.500}{1.120}$ DETONATION VELOCITY,  $v_D = 0.26002 \text{ cm}/\mu\text{sec}$ INITIAL TIME,  $t_0 = 4.02 \mu\text{sec}$ 

x	t	t - t <sub>0</sub>	y	y'
cm	$\mu\text{sec}$	$\mu\text{sec}$	cm	cm
0.0	0.00		0.000	
1.0	1.72		0.000	
2.0	3.43		0.000	
3.0	5.15	1.13	0.001	0.003
4.0	6.87	2.85	0.013	0.021
5.0	8.58	4.57	0.033	0.053
6.0	10.30	6.28	0.099	0.097
7.0	12.02	8.00	0.162	0.152
8.0	13.74	9.72	0.218	0.213
9.0	15.45	11.43	0.291	0.281
10.0	17.17	13.15	0.358	0.352
11.0	18.89	14.87	0.425	0.426
12.0	20.60	16.59	0.500	0.503
13.0	22.32	18.30	0.570	0.581
14.0	24.04	20.02	0.650	0.661
15.0	25.75	21.74	0.733	0.742
16.0	27.47	23.45	0.825	0.824
17.0	29.19	25.17	0.922	0.906

b = 0.4438 cm

v = 0.1761 cm

h = 8.7032  $\mu\text{sec}$





TABLE 76. DIGITIZED FLASH X-RAY DATA

SHOT NUMBER LASL 1522\* SCALE FACTOR,  $f = \frac{0.250}{0.550}$ DETONATION VELOCITY,  $V_D = 0.29388 \text{ cm}/\mu\text{sec}$ INITIAL TIME,  $t_0 = 1.59 \text{ } \mu\text{sec}$ 

x	t	t - t <sub>0</sub>	y	y'
cm	$\mu\text{sec}$	$\mu\text{sec}$	cm	cm
0.0	0.00		0.002	
1.0	1.55		0.002	
2.0	3.09	1.50	0.009	
3.0	4.64	3.05	0.027	
4.0	6.19	4.60	0.073	
5.0	7.73	6.14	0.118	
6.0	9.28	7.69	0.153	
7.0	10.83	9.24	0.198	
8.0	12.37	10.78	0.240	
9.0	13.92	12.33	0.271	
10.0	15.47	13.88	0.310	
11.0	17.01	15.42	0.358	
12.0	18.56	16.97	0.406	
13.0	20.11	18.52	0.475	
14.0	21.65	20.06	0.514	
15.0	23.20	21.61	0.557	
15.7	24.28	22.69	0.625	

b =            cm            v =            cm            h =             $\mu\text{sec}$   
\*did not converge

TABLE 77. DIGITIZED FLASH X-RAY DATA

SHOT NUMBER LASL 1324 SCALE FACTOR,  $f = \frac{1.000}{1.510}$ DETONATION VELOCITY,  $V_D = 0.29865 \text{ cm}/\mu\text{sec}$ INITIAL TIME,  $t_0 = 4.31 \mu\text{sec}$ 

x	t	t - t <sub>0</sub>	y	y'
cm	$\mu\text{sec}$	$\mu\text{sec}$	cm	cm
0.0	0.00		0.000	
1.0	2.22		0.000	
2.0	4.43	0.13	0.000	0.000
3.0	6.65	2.35	0.026	0.026
4.0	8.87	4.56	0.062	0.068
5.0	11.09	6.78	0.113	0.120
6.0	13.30	9.00	0.175	0.179
7.0	15.52	11.22	0.241	0.244
8.0	17.74	13.43	0.318	0.314
9.0	19.96	15.65	0.401	0.388
10.0	22.17	17.87	0.469	0.466
11.0	24.39	20.09	0.560	0.546
12.0	26.61	22.30	0.631	0.629
13.0	28.83	24.52	0.712	0.715
14.0	31.04	26.74	0.799	0.802
15.0	33.26	28.96	0.875	0.891
16.0	35.48	31.17	0.975	0.982
17.0	37.70	33.39	1.068	1.074
18.0	39.91	35.61	1.172	1.167
19.0	42.13	37.83	1.274	1.262
20.0	44.35	40.04	1.357	1.358

b = 1.5422 cm

v = 0.9493 cm

h = 30.3951  $\mu\text{sec}$

TABLE 78. DIGITIZED FLASH X-RAY DATA

SHOT NUMBER LASL 1325 SCALE FACTOR,  $f = \frac{1.000}{2.370}$ DETONATION VELOCITY,  $V_D = 0.25969$  cm/ $\mu$ secINITIAL TIME,  $t_0 = 6.50$   $\mu$ sec

x	t	t - t <sub>0</sub>	y	y'
cm	$\mu$ sec	$\mu$ sec	cm	cm
0.0	0.00		0.000	
1.0	1.62		0.000	
2.0	3.25		0.000	
3.0	4.87		0.000	
4.0	6.50		0.000	
5.0	8.12	1.62	0.011	0.003
6.0	9.75	3.25	0.018	0.014
7.0	11.37	4.87	0.027	0.033
8.0	13.00	6.50	0.058	0.058
9.0	14.62	8.12	0.094	0.088
10.0	16.25	9.75	0.121	0.124
11.0	17.87	11.37	0.157	0.163
12.0	19.50	13.00	0.204	0.206
13.0	21.12	14.62	0.257	0.251
14.0	22.75	16.25	0.300	0.298
15.0	24.37	17.87	0.346	0.347
16.0	26.00	19.50	0.393	0.397
17.0	27.62	21.12	0.450	0.448
18.0	29.25	22.75	0.504	0.501
19.0	30.87	24.37	0.551	0.554

b = 0.4137 cm

v = 0.1640 cm

h = 11.4155  $\mu$ sec

TABLE 79. DIGITIZED FLASH X-RAY DATA

SHOT NUMBER LASL 1362 SCALE FACTOR,  $f = \frac{0.500}{1.180}$ DETONATION VELOCITY,  $V_D = 0.32228 \text{ cm}/\mu\text{sec}$ INITIAL TIME,  $t_0 = 1.70 \text{ } \mu\text{sec}$ 

x	t	$t - t_0$	y	$y'$
cm	$\mu\text{sec}$	$\mu\text{sec}$	cm	cm
0.0	0.00		0.003	
1.0	1.31		0.003	
2.0	2.63	0.93	0.003	0.001
3.0	3.94	2.25	0.014	0.008
4.0	5.26	3.56	0.021	0.024
5.0	6.57	4.88	0.039	0.050
6.0	7.89	6.19	0.061	0.087
7.0	9.20	7.51	0.134	0.133
8.0	10.52	8.82	0.200	0.189
9.0	11.83	10.14	0.261	0.254
10.0	13.15	11.45	0.335	0.326
11.0	14.46	12.77	0.413	0.405
12.0	15.78	14.08	0.498	0.490
13.0	17.09	15.40	0.574	0.579
14.0	18.41	16.71	0.668	0.673
15.0	19.72	18.03	0.767	0.771
16.0	21.04	19.34	0.865	0.871
17.0	22.35	20.66	0.967	0.975
18.0	23.67	21.97	1.069	1.080
19.3	25.38	23.68	1.240	1.220

 $b = 1.1987 \text{ cm}$  $v = 0.4093 \text{ cm}$  $h = 12.8535 \text{ } \mu\text{sec}$

TABLE 80. DIGITIZED FLASH X-RAY DATA

SHOT NUMBER DRI 3 SCALE FACTOR,  $f = \frac{0.500}{1.400}$

DETONATION VELOCITY,  $V_D = 0.29160 \text{ cm}/\mu\text{sec}$

INITIAL TIME,  $t_0 = 2.88 \mu\text{sec}$

x	t	t - t <sub>0</sub>	y	y'
cm	$\mu\text{sec}$	$\mu\text{sec}$	cm	cm
0.0	0.00		0.002	
1.0	1.22		0.002	
2.0	2.45		0.002	
3.0	3.67	0.79	0.005	0.004
4.0	4.90	2.02	0.024	0.023
5.0	6.12	3.24	0.049	0.054
6.0	7.35	4.47	0.091	0.094
7.0	8.57	5.69	0.142	0.143
8.0	9.80	6.92	0.195	0.199
9.0	11.02	8.14	0.263	0.259
10.0	12.25	9.37	0.327	0.324
11.0	13.47	10.59	0.397	0.392
12.0	14.70	11.82	0.472	0.464
13.0	15.92	13.04	0.535	0.537
14.0	17.15	14.27	0.616	0.612
15.0	18.37	15.49	0.686	0.689
16.0	19.60	16.72	0.766	0.767
17.0	20.82	17.94	0.835	0.846
18.0	22.05	19.17	0.918	0.927
19.0	23.27	20.39	1.008	1.008
20.0	24.50	21.61	1.096	1.089
21.0	25.72	22.84	1.175	1.172
22.0	26.94	24.06	1.256	1.254

b = 0.6212 cm

v = 0.2827 cm

h = 8.5911  $\mu\text{sec}$



TABLE 81. DIGITIZED FLASH X-RAY DATA

SHOT NUMBER DRI 4 SCALE FACTOR,  $f = \frac{0.500}{1.000}$ DETONATION VELOCITY,  $V_D = 0.20975 \text{ cm}/\mu\text{sec}$ INITIAL TIME,  $t_0 = 2.24 \mu\text{sec}$ 

x	t	t - t <sub>0</sub>	y	y'
cm	$\mu\text{sec}$	$\mu\text{sec}$	cm	cm
0.0	0.00		0.002	
1.0	2.38	0.14	0.002	0.000
2.0	4.77	2.53	0.028	0.020
3.0	7.15	4.91	0.059	0.058
4.0	9.54	7.29	0.104	0.108
5.0	11.92	9.68	0.176	0.167
6.0	14.30	12.06	0.232	0.232
7.0	16.69	14.45	0.293	0.303
8.0	19.07	16.83	0.370	0.378
9.0	21.45	19.21	0.462	0.457
10.0	23.84	21.60	0.535	0.538
11.0	26.22	23.98	0.630	0.622
12.0	28.61	26.36	0.710	0.707
13.0	30.99	28.75	0.799	0.794
14.0	33.37	31.13	0.880	0.882
15.0	35.76	33.52	0.963	0.972
16.0	38.14	35.90	1.064	1.063
17.0	40.52	38.28	1.162	1.154
18.0	42.91	40.67	1.247	1.246
18.3	43.62	41.38	1.267	1.273

b = 0.7060 cm

v = 0.3770 cm

h = 16.7785  $\mu\text{sec}$

TABLE 82. DIGITIZED FLASH X-RAY DATA

SHOT NUMBER DRI 5 SCALE FACTOR,  $f = \frac{0.500}{1.380}$ DETONATION VELOCITY,  $V_D = 0.25000 \text{ cm}/\mu\text{sec}$ INITIAL TIME,  $t_0 = 0.00 \text{ } \mu\text{sec}$ 

x	t	t - t <sub>0</sub>	y	y'
cm	μsec	μsec	cm	cm
0.0	0.00		0.002	
1.0	1.45	1.45	0.002	0.000
2.0	2.90	2.90	0.002	0.002
3.0	4.35	4.35	0.007	0.009
4.0	5.80	5.80	0.015	0.024
5.0	7.25	7.25	0.042	0.047
6.0	8.70	8.70	0.070	0.079
7.0	10.14	10.14	0.116	0.119
8.0	11.59	11.59	0.172	0.164
9.0	13.04	13.04	0.229	0.214
10.0	14.49	14.49	0.286	0.268
11.0	15.94	15.94	0.328	0.323
12.0	17.39	17.39	0.374	0.380
13.0	18.84	18.84	0.427	0.438
14.0	20.29	20.29	0.490	0.498
15.0	21.74	21.74	0.554	0.557
16.0	23.19	23.19	0.613	0.618
17.0	24.64	24.64	0.671	0.678
18.0	26.09	26.09	0.728	0.739
19.0	27.54	27.54	0.805	0.800
20.0	28.99	28.99	0.871	0.861
21.0	30.43	30.43	0.931	0.923

b = 0.3907 cm

v = 0.0892 cm

h = 9.1075 μsec

TABLE 83. DIGITIZED FLASH X-RAY DATA

SHOT NUMBER DRI 6 SCALE FACTOR,  $f = \frac{0.250}{0.620}$ DETONATION VELOCITY,  $V_D = 0.24556 \text{ cm}/\mu\text{sec}$ INITIAL TIME,  $t_0 = 4.70 \text{ } \mu\text{sec}$ 

x	t	t - t <sub>0</sub>	y	y'
cm	$\mu\text{sec}$	$\mu\text{sec}$	cm	cm
0.0	0.00		0.001	
1.0	1.64		0.001	
2.0	3.28		0.001	
3.0	4.93	0.22	0.001	0.000
4.0	6.57	1.87	0.017	0.009
5.0	8.21	3.51	0.024	0.027
6.0	9.85	5.16	0.051	0.053
7.0	11.49	6.80	0.087	0.085
8.0	13.14	8.44	0.117	0.124
9.0	14.78	10.08	0.170	0.169
10.0	16.42	11.72	0.217	0.218
11.0	18.06	13.37	0.279	0.274
12.0	19.70	15.01	0.340	0.333
13.0	21.35	16.65	0.396	0.397
14.0	22.99	18.29	0.467	0.465
15.0	24.63	19.93	0.506	0.536
15.6	25.62	20.92	0.602	0.581

b = 3.0610 cm

v = 1.4782 cm

h = 37.4532  $\mu\text{sec}$

SHOT NUMBER DRI 7 SCALE FACTOR,  $f = \frac{0.125}{0.270}$

DETONATION VELOCITY,  $V_D = 0.30694$  cm/ $\mu$ sec

INITIAL TIME,  $t_0 = 0.00 \mu\text{sec}$

$$b = 0.2520 \text{ cm} \quad v = 0.0348 \text{ cm} \quad h = 5.1125 \text{ } \mu\text{sec}$$



TABLE 86. DIGITIZED FLASH X-RAY DATA

SHOT NUMBER DRI 9 SCALE FACTOR,  $f = \frac{0.250}{0.510}$

DETONATION VELOCITY,  $V_D = 0.29160 \text{ cm}/\mu\text{sec}$

INITIAL TIME,  $t_0 \approx 2.45 \text{ } \mu\text{sec}$

[illegible]
$$b = 0.3112 \text{ cm} \quad v = 0.0854 \text{ cm} \quad h = 6.4516 \text{ } \mu\text{sec}$$



1

[illegible]

SHOT NUMBER DRI 13 SCALE FACTOR,  $f = \frac{0.250}{0.580}$

DETONATION VELOCITY,  $V_D = 0.32741 \text{ cm}/\mu\text{sec}$

INITIAL TIME,  $t_0 = 1.32 \text{ } \mu\text{sec}$

[illegible]
$$b = 0.0586 \text{ cm} \quad v = 0.0138 \text{ cm} \quad h = 1.0877 \text{ } \mu\text{sec}$$



SHOT NUMBER DRI 15 SCALE FACTOR,  $f = \frac{0.500}{0.850}$

DETONATION VELOCITY,  $V_D = 0.31206 \text{ cm}/\mu\text{sec}$

INITIAL TIME,  $t_0 = 5.76 \mu\text{sec}$

[illegible]
$$b = 0.1513 \text{ cm} \quad v = 0.0180 \text{ cm} \quad h = 2.4402 \text{ } \mu\text{sec}$$

TABLE 91. DIGITIZED FLASH X-RAY DATA

SHOT NUMBER DRI 16 SCALE FACTOR,  $f = \frac{0.125}{0.280}$

DETONATION VELOCITY,  $V_D = 0.29671 \text{ cm}/\mu\text{sec}$

INITIAL TIME,  $t_0 = 2.96 \text{ } \mu\text{sec}$

[illegible]
$$b = 0.0852 \text{ cm}$$
$$v = 0.0245 \text{ cm}$$
$$h = 2.9300 \text{ } \mu\text{sec}$$

TABLE 92. DIGITIZED FLASH X-RAY DATA

SHOT NUMBER DRI 22 SCALE FACTOR,  $f = \frac{0.500}{0.870}$

DETONATION VELOCITY,  $V_D = 0.30899 \text{ cm}/\mu\text{sec}$

INITIAL TIME,  $t_0 = 1.13 \text{ } \mu\text{sec}$

x	t	t - t <sub>0</sub>	y	y'
cm	$\mu\text{sec}$	$\mu\text{sec}$	cm	cm
0.0	0.00		0.000	
1.0	1.86	0.73	0.001	0.001
2.0	3.72	2.59	0.009	0.014
3.0	5.58	4.45	0.042	0.041
4.0	7.44	6.31	0.078	0.081
5.0	9.30	8.17	0.123	0.132
6.0	11.16	10.03	0.203	0.191
7.0	13.02	11.89	0.264	0.258
8.0	14.88	13.75	0.328	0.330
9.0	16.74	15.61	0.404	0.406
10.0	18.60	17.47	0.482	0.485
11.0	20.46	19.33	0.562	0.567
12.0	22.32	21.19	0.653	0.651
13.0	24.18	23.05	0.745	0.737
14.0	26.04	24.91	0.831	0.824
15.0	27.90	26.77	0.909	0.912
16.0	29.76	28.63	0.994	1.001
17.0	31.62	30.49	1.087	1.091
18.0	33.48	32.35	1.171	1.182
19.0	35.34	34.21	1.287	1.273

b = 0.5748 cm

v = 0.2307 cm

h = 11.1483  $\mu\text{sec}$



TABLE 93. DIGITIZED FLASH X-RAY DATA

SHOT NUMBER DR1 24 SCALE FACTOR,  $f = \frac{0.500}{0.750}$ DETONATION VELOCITY,  $V_D = 0.29467 \text{ cm}/\mu\text{sec}$ INITIAL TIME,  $t_0 = 0.00 \mu\text{sec}$ 

x	t	t - t <sub>0</sub>	y	y'
cm	μsec	μsec	cm	cm
0.0	0.00		0.002	
1.0	2.26	2.26	0.014	0.009
2.0	4.52	4.52	0.038	0.036
3.0	6.79	6.79	0.092	0.079
4.0	9.05	9.05	0.151	0.133
5.0	11.31	11.31	0.184	0.195
6.0	13.57	13.57	0.241	0.264
7.0	15.84	15.84	0.332	0.337
8.0	18.10	18.10	0.412	0.414
9.0	20.36	20.36	0.485	0.493
10.0	22.62	22.62	0.575	0.574
11.0	24.89	24.89	0.655	0.657
12.0	27.15	27.15	0.752	0.740
13.0	29.41	29.41	0.843	0.825
14.0	31.67	31.67	0.921	0.910
15.0	33.94	33.94	1.004	0.996
16.0	36.20	36.20	1.078	1.083
17.0	38.46	38.46	1.156	1.170
18.0	40.72	40.72	1.252	1.257
18.4	41.63	41.63	1.290	1.292

b = 0.4174 cm

v = 0.1711 cm

h = 10.4712 μsec

TABLE 94. DIGITIZED FLASH X-RAY DATA

SHOT NUMBER DRI 28\* SCALE FACTOR,  $f = \frac{0.250}{0.750}$ DETONATION VELOCITY,  $V_D = 0.32331 \text{ cm}/\mu\text{sec}$ INITIAL TIME,  $t_0 = 1.69 \mu\text{sec}$ 

x	t	t - t <sub>0</sub>	y	y'
cm	$\mu\text{sec}$	$\mu\text{sec}$	cm	cm
0.0	0.00		0.000	
1.0	1.03		0.000	
2.0	2.06	0.37	0.002	
3.0	3.09	1.40	0.016	
4.0	4.12	2.43	0.040	
5.0	5.16	3.46	0.075	
6.0	6.19	4.50	0.106	
7.0	7.22	5.53	0.148	
8.0	8.25	6.56	0.187	
9.0	9.28	7.59	0.225	
10.0	10.31	8.62	0.268	
11.0	11.34	9.65	0.287	
12.0	12.37	10.68	0.329	
13.0	13.40	11.71	0.363	
14.0	14.43	12.74	0.400	
15.0	15.47	13.77	0.450	
16.0	16.50	14.81	0.489	
17.0	17.53	15.84	0.537	
18.0	18.56	16.87	0.604	
18.6	19.18	17.49	0.647	

b =            cm            v =            cm            h =             $\mu\text{sec}$ 

\* did not converge

TABLE 95. DIGITIZED FLASH X-RAY DATA

SHOT NUMBER USAFA 45 SCALE FACTOR,  $\xi = \frac{0.500}{1.200}$ DETONATION VELOCITY,  $V_D = 0.30874$  cm/ $\mu$ secINITIAL TIME,  $t_0 = 2.77$   $\mu$ sec

x	t	t - t <sub>0</sub>	y	y'
cm	$\mu$ sec	$\mu$ sec	cm	cm
0.0	0.00		0.000	
1.0	1.35		0.000	
2.0	2.70		0.000	
3.0	4.05	1.28	0.002	0.000
4.0	5.40	2.63	0.013	0.009
5.0	6.75	3.98	0.029	0.035
6.0	8.10	5.33	0.061	0.069
7.0	9.45	6.68	0.114	0.106
8.0	10.80	8.03	0.156	0.144
9.0	12.15	9.38	0.191	0.182
10.0	13.50	10.73	0.216	0.220
11.0	14.85	12.08	0.260	0.258
12.0	16.19	13.43	0.297	0.296
13.0	17.54	14.78	0.337	0.334
14.0	18.89	16.13	0.364	0.372
15.0	20.24	17.48	0.400	0.411
16.0	21.59	18.83	0.442	0.449
17.0	22.94	20.17	0.486	0.487
18.0	24.29	21.52	0.522	0.525
19.0	25.64	22.87	0.557	0.563
20.0	26.99	24.22	0.596	0.602
21.0	28.34	25.57	0.638	0.640
22.0	29.69	26.92	0.688	0.678
23.0	31.04	28.27	0.720	0.716
24.0	32.39	29.62	0.763	0.754

b = 0.0841 cm

v = 0.0139 cm

h = 2.9709  $\mu$ sec

TABLE 96. DIGITIZED FLASH X-RAY DATA

SHOT NUMBER USAFA 46 SCALE FACTOR,  $f = \frac{0.500}{0.850}$ DETONATION VELOCITY,  $V_D = 0.2994 \text{ cm}/\mu\text{sec}$ INITIAL TIME,  $t_0 = 1.97 \mu\text{sec}$ 

x	t	t - t <sub>0</sub>	y	y'
cm	$\mu\text{sec}$	$\mu\text{sec}$	cm	cm
0.0	0.00		0.000	
1.0	1.96		0.000	
2.0	3.93	1.96	0.010	0.012
3.0	5.89	3.92	0.045	0.044
4.0	7.86	5.89	0.086	0.087
5.0	9.82	7.85	0.138	0.136
6.0	11.79	9.82	0.187	0.188
7.0	13.75	11.78	0.239	0.242
8.0	15.72	13.75	0.299	0.297
9.0	17.68	15.71	0.359	0.352
10.0	19.65	17.68	0.404	0.408
11.0	21.61	19.64	0.469	0.465
12.0	23.58	21.61	0.525	0.521
13.0	25.54	23.57	0.573	0.578
14.0	27.51	25.53	0.628	0.635
15.0	29.47	27.50	0.687	0.693
16.0	31.43	29.46	0.752	0.750
17.0	33.40	31.43	0.811	0.807
18.0	35.36	33.39	0.865	0.865
19.0	37.33	35.36	0.925	0.922

b = 0.1293 cm

v = 0.0535 cm

h = 4.3802  $\mu\text{sec}$

TABLE 97. DIGITIZED FLASH X-RAY DATA

SHOT NUMBER USAFA 48 SCALE FACTOR,  $f = \frac{0.250}{0.630}$ DETONATION VELOCITY,  $V_D = 0.32443 \text{ cm}/\mu\text{sec}$ INITIAL TIME,  $t_0 = 0.00 \text{ } \mu\text{sec}$ 

x	t	t - t <sub>0</sub>	y	y'
cm	$\mu\text{sec}$	$\mu\text{sec}$	cm	cm
0.0	0.00		0.000	
1.0	1.22	1.22	0.003	0.001
2.0	2.45	2.45	0.004	0.006
3.0	3.67	3.67	0.008	0.019
4.0	4.89	4.89	0.035	0.042
5.0	6.12	6.12	0.082	0.072
6.0	7.34	7.34	0.111	0.107
7.0	8.56	8.56	0.148	0.144
8.0	9.79	9.79	0.189	0.183
9.0	11.01	11.01	0.225	0.224
10.0	12.23	12.23	0.266	0.265
11.0	13.45	13.45	0.303	0.306
12.0	14.68	14.68	0.349	0.348
13.0	15.90	15.90	0.382	0.390
14.0	17.12	17.12	0.427	0.432
15.0	18.35	18.35	0.463	0.474
16.0	19.57	19.57	0.510	0.517
17.0	20.79	20.79	0.558	0.559
18.0	22.02	22.02	0.607	0.602
18.4	22.51	22.51	0.634	0.619

b = 0.1701 cm

v = 0.0415 cm

h = 4.8638  $\mu\text{sec}$



TABLE 98. DIGITIZED FLASH X-RAY DATA

SHOT NUMBER USAF 51 SCALE FACTOR,  $f = \frac{0.125}{0.280}$

DETONATION VELOCITY,  $V_D = 0.35333 \text{ cm}/\mu\text{sec}$

INITIAL TIME,  $t_0 = 0.00$   $\mu\text{sec}$

[illegible]
$$b = 0.4702 \text{ cm}$$
$$v = 0.0975 \text{ cm}$$
$$h = 6.2267 \text{ } \mu\text{sec}$$



TABLE 99. DIGITIZED FLASH X-RAY DATA

SHOT NUMBER USAEA 54\* SCALE FACTOR,  $f = \frac{0.125}{0.300}$

DETONATION VELOCITY,  $V_D = 0.33177 \text{ cm}/\mu\text{sec}$

INITIAL TIME,  $t_0 =$                        $\mu\text{sec}$

[illegible]

b =            cm            v =            cm            h =             $\mu$ sec

\*did not converge

TABLE 100. DIGITIZED FLASH X-RAY DATA

SHOT NUMBER USAFA 55\* SCALE FACTOR,  $f = \frac{0.125}{0.500}$

DETONATION VELOCITY,  $V_D = 0.34506 \text{ cm}/\mu\text{sec}$

INITIAL TIME,  $t_0 = 1.48 \text{ } \mu\text{sec}$

[illegible]

b =            cm            v =            cm            h =             $\mu$ sec

\* did not converge

SHOT NUMBER USAF 57 SCALE FACTOR,  $\xi = \frac{0.250}{0.540}$

INITIAL TIME,  $t_0 = 3.72 \text{ } \mu\text{sec}$

[illegible]

-322-

TABLE 102 DIGITIZED FLASH X-RAY DATA

SHOT NUMBER USAFA 59 SCALE FACTOR,  $f = \frac{0.500}{1.000}$ DETONATION VELOCITY,  $V_D = 0.41036$  cm/ $\mu$ sec 0.00INITIAL TIME,  $t_0 = 0.00$   $\mu$ sec

x	t	t - t <sub>0</sub>	y	y'
cm	$\mu$ sec	$\mu$ sec	cm	cm
0.0	0.00		0.000	
1.0	1.22	1.22	0.008	0.001
2.0	2.44	2.44	0.007	0.007
3.0	3.66	3.66	0.024	0.019
4.0	4.87	4.87	0.031	0.037
5.0	6.09	6.09	0.054	0.062
6.0	7.31	7.31	0.065	0.095
7.0	8.53	8.53	0.103	0.134
8.0	9.75	9.75	0.163	0.180
9.0	10.97	10.97	0.237	0.232
10.0	12.18	12.18	0.315	0.290
11.0	13.40	13.40	0.397	0.352
12.0	14.62	14.62	0.462	0.419
13.0	15.84	15.84	0.500	0.489
14.0	17.06	17.06	0.559	0.564
15.0	18.28	18.28	0.633	0.640
16.0	19.50	19.50	0.707	0.720
17.0	20.71	20.71	0.774	0.802
18.0	21.93	21.93	0.852	0.886
19.0	23.15	23.15	0.950	0.971
20.0	24.37	24.37	1.045	1.058
21.0	25.59	25.59	1.137	1.146
21.5	26.20	26.20	1.254	1.191

b = 1.1690 cm

v = 0.3920 cm

h = 14.1443  $\mu$ sec

SHOT NUMBER USAFA 60 SCALE FACTOR,  $f = \frac{0.500}{1.150}$

INITIAL TIME,  $t_0 = 2.35 \text{ } \mu\text{sec}$

[illegible]
$$b = 0.0560 \text{ cm}$$
$$v = 0.0157 \text{ cm}$$
$$h = 1.3019 \text{ } \mu\text{sec}$$



TABLE 104. DIGITIZED FLASH X-RAY DATA

SHOT NUMBER USAFA 62A SCALE FACTOR,  $\xi = \frac{0.250}{0.610}$ DETONATION VELOCITY,  $V_D = 0.36928$  cm/ $\mu$ secINITIAL TIME,  $t_0 = 0.00$   $\mu$ sec

x	t	t - t <sub>0</sub>	y	y'
cm	$\mu$ sec	$\mu$ sec	cm	cm
0.0	0.00		0.004	
1.0	1.11	1.11	0.015	0.010
2.0	2.22	2.22	0.029	0.029
3.0	3.33	3.33	0.057	0.054
4.0	4.44	4.44	0.073	0.083
5.0	5.55	5.55	0.116	0.116
6.0	6.66	6.66	0.150	0.151
7.0	7.77	7.77	0.189	0.189
8.0	8.88	8.88	0.235	0.229
9.0	9.99	9.99	0.274	0.271
10.0	11.10	11.10	0.317	0.313
11.0	12.21	12.21	0.357	0.358
12.0	13.32	13.32	0.408	0.403
13.0	14.43	14.43	0.440	0.449
14.0	15.54	15.54	0.494	0.496
15.0	16.65	16.65	0.538	0.544
16.0	17.76	17.76	0.594	0.593
16.3	18.09	18.09	0.614	0.607

b = 0.5816 cm

v = 0.3278 cm

h = 11.4679  $\mu$ sec





TABLE 106. DIGITIZED FLASH X-RAY DATA

SHOT NUMBER USAF 73\* SCALE FACTOR,  $f = \frac{0.125}{0.350}$

DETONATION VELOCITY,  $V_D = 0.28516 \text{ cm}/\mu\text{sec}$

INITIAL TIME,  $t_0 = 1.06 \text{ } \mu\text{sec}$

[illegible]

b =            cm            v =            cm            h =            usec  
\*did not converge

TABLE 107. DIGITIZED FLASH X-RAY DATA

SHOT NUMBER USAF 79\* SCALE FACTOR,  $f = 0.125$

DETONATION VELOCITY,  $V_D = 0.42771 \text{ cm}/\mu\text{sec}$

INITIAL TIME,  $t_0 = 1.07 \text{ } \mu\text{sec}$

[illegible]

b =            cm            v =            cm            h =             $\mu$ sec

\* did not converge

TABLE 108. DIGITIZED FLASH X-RAY DATA

SHOT NUMBER USAFA 82 SCALE FACTOR,  $f = \frac{0.250}{0.550}$ DETONATION VELOCITY,  $V_D = 0.39057 \text{ cm}/\mu\text{sec}$ INITIAL TIME,  $t_0 = 2.75 \mu\text{sec}$ 

x	t	t - t <sub>0</sub>	y	y'
cm	$\mu\text{sec}$	$\mu\text{sec}$	cm	cm
0.0	0.00		0.000	
1.0	1.16		0.000	
2.0	2.33		0.000	
3.0	3.49	0.74	0.002	0.002
4.0	4.66	1.90	0.015	0.012
5.0	5.82	3.07	0.034	0.032
6.0	6.98	4.23	0.058	0.060
7.0	8.15	5.40	0.091	0.092
8.0	9.31	6.56	0.120	0.126
9.0	10.47	7.72	0.167	0.162
10.0	11.64	8.89	0.204	0.200
11.0	12.80	10.05	0.229	0.238
12.0	13.97	11.22	0.282	0.277
13.0	15.13	12.38	0.319	0.316
14.0	16.29	13.54	0.358	0.355
15.0	17.46	14.71	0.392	0.395
16.2	18.85	16.10	0.441	0.443

 $b = 0.1294 \text{ cm}$  $v = 0.0467 \text{ cm}$  $h = 3.6996 \mu\text{sec}$

TABLE 109. DIGITIZED FLASH X-RAY DATA

SHOT NUMBER USAFA 89 SCALE FACTOR,  $f = \frac{0.250}{0.610}$

DETONATION VELOCITY,  $v_D = 0.51279$  cm/ $\mu$ sec

INITIAL TIME,  $t_0 = 0.00$   $\mu$ sec

x	t	t - t <sub>0</sub>	y	y'
cm	$\mu$ sec	$\mu$ sec	cm	cm
0.0	0.00		0.000	
1.0	0.80	0.80	0.001	0.000
2.0	1.60	1.60	0.004	0.002
3.0	2.40	2.40	0.013	0.011
4.0	3.20	3.20	0.029	0.029
5.0	4.00	4.00	0.053	0.056
6.0	4.80	4.80	0.088	0.087
7.0	5.59	5.59	0.123	0.120
8.0	6.39	6.39	0.155	0.154
9.0	7.19	7.19	0.186	0.188
10.0	7.99	7.99	0.227	0.223
11.0	8.79	8.79	0.252	0.258
12.0	9.59	9.59	0.292	0.293
13.0	10.39	10.39	0.330	0.329
14.0	11.19	11.19	0.364	0.364
15.0	11.99	11.99	0.406	0.399
16.0	12.79	12.79	0.440	0.435
17.0	13.59	13.59	0.467	0.470
18.0	14.39	14.39	0.506	0.505
19.0	15.19	15.19	0.540	0.541
20.0	15.98	15.98	0.563	0.576
20.4	16.30	16.30	0.585	0.589

b = 0.1314 cm

v = 0.0231 cm

h = 2.9709  $\mu$ sec



TABLE 110. DIGITIZED FLASH X-RAY DATA

SHOT NUMBER USAEA 94 SCALE FACTOR,  $k = \frac{0.250}{0.500}$ DETONATION VELOCITY,  $V_D = 0.35734 \text{ cm}/\mu\text{sec}$ INITIAL TIME,  $t_0 = 0.00 \text{ } \mu\text{sec}$ 

x	t	t - t <sub>0</sub>	y	y'
cm	$\mu\text{sec}$	$\mu\text{sec}$	cm	cm
0.0	0.00		0.000	
1.0	1.40	1.40	0.0005	0.000
2.0	2.80	2.80	0.001	0.002
3.0	4.20	4.20	0.004	0.006
4.0	5.60	5.60	0.010	0.017
5.0	7.00	7.00	0.025	0.034
6.0	8.40	8.40	0.057	0.058
7.0	9.79	9.79	0.094	0.087
8.0	11.19	11.19	0.126	0.121
9.0	12.59	12.59	0.170	0.157
10.0	13.99	13.99	0.192	0.195
11.0	15.39	15.39	0.235	0.234
12.0	16.79	16.79	0.279	0.274
13.0	18.19	18.19	0.312	0.315
14.0	19.59	19.59	0.345	0.356
15.0	20.99	20.99	0.388	0.397
16.0	22.39	22.39	0.425	0.439
17.0	23.79	23.79	0.468	0.481
18.0	25.19	25.19	0.555	0.523

b = 0.2480 cm

v = 0.0533 cm

h = 8.1433  $\mu\text{sec}$



TABLE 111. DIGITIZED FLASH X-RAY DATA

SHOT NUMBER USAFA 96\* SCALE FACTOR,  $f = \frac{1.000}{1.450}$ DETONATION VELOCITY,  $V_D = 0.33030 \text{ cm}/\mu\text{sec}$ INITIAL TIME,  $t_0 = 2.14 \mu\text{sec}$ 

x	t	$t - t_0$	y	y'
cm	$\mu\text{sec}$	$\mu\text{sec}$	cm	cm
0.0	0.00		0.001	
1.0	2.09		0.001	
2.0	4.18	2.04	0.020	
3.0	6.26	4.13	0.086	
4.0	8.35	6.22	0.215	
5.0	10.44	8.30	0.341	
6.0	12.53	10.39	0.476	
7.0	14.62	12.48	0.600	
8.0	16.70	14.57	0.753	
9.0	18.79	16.66	0.869	
10.0	20.88	18.74	0.989	
11.0	22.97	20.83	1.099	
12.0	25.06	22.92	1.220	
13.0	27.14	25.01	1.351	
14.0	29.23	27.10	1.480	
15.0	31.32	29.18	1.631	
16.0	33.41	31.27	1.802	
17.0	35.50	33.36	1.994	
18.0	37.58	35.45	2.181	
19.0	39.67	37.54	2.358	
20.0	41.76	39.62	2.565	

b =            cm      v =            cm      h =             $\mu\text{sec}$   
\* did not converge

TABLE 112. DIGITIZED FLASH X-RAY DATA

SHOT NUMBER USAFA 97\* SCALE FACTOR,  $f = \frac{0.500}{0.750}$ DETONATION VELOCITY,  $V_D = 0.33620$  cm/ $\mu$ secINITIAL TIME,  $t_0 = 0.00$   $\mu$ sec

x	t	t - t <sub>0</sub>	y	y'
cm	$\mu$ sec	$\mu$ sec	cm	cm
0.0	0.00		0.002	
1.0	1.98	1.98	0.009	
2.0	3.97	3.97	0.029	
3.0	5.95	5.95	0.054	
4.0	7.93	7.93	0.097	
5.0	9.91	9.91	0.143	
6.0	11.90	11.90	0.189	
7.0	13.88	13.88	0.220	
8.0	15.86	15.86	0.261	
9.0	17.85	17.85	0.315	
10.0	19.83	19.83	0.366	
11.0	21.81	21.81	0.425	
12.0	23.80	23.80	0.499	
13.0	25.78	25.78	0.575	
14.0	27.76	27.76	0.653	
15.0	29.74	29.74	0.717	
16.0	31.73	31.73	0.814	
17.0	33.71	33.71	0.897	
18.0	35.69	35.69	0.974	
19.0	37.68	37.68	1.053	
20.0	39.66	39.66	1.144	
21.2	42.04	42.04	1.259	

b =            cm          v =            cm          h =             $\mu$ sec

\* did not converge

TABLE 113 DIGITIZED FLASH X-RAY DATA

SHOT NUMBER USAFA 98 SCALE FACTOR,  $f = \frac{1.000}{1.680}$ DETONATION VELOCITY,  $V_D = 0.33934 \text{ cm}/\mu\text{sec}$ INITIAL TIME,  $t_0 = 1.73 \mu\text{sec}$ 

x	t	t - t <sub>0</sub>	y	y'
cm	$\mu\text{sec}$	$\mu\text{sec}$	cm	cm
0.0	0.00		0.003	
1.0	1.75	0.03	0.003	0.000
2.0	3.51	1.78	0.023	0.026
3.0	5.26	3.54	0.072	0.079
4.0	7.02	5.29	0.143	0.149
5.0	8.77	7.04	0.254	0.232
6.0	10.52	8.80	0.341	0.325
7.0	12.28	10.55	0.433	0.426
8.0	14.03	12.31	0.526	0.534
9.0	15.79	14.06	0.636	0.647
10.0	17.54	15.81	0.749	0.764
11.0	19.30	17.57	0.867	0.884
12.0	21.05	19.32	0.992	1.007
13.0	22.80	21.08	1.124	1.133
14.0	24.56	22.83	1.268	1.261
15.0	26.31	24.58	1.403	1.391
16.0	28.07	26.34	1.546	1.522
17.0	29.82	28.09	1.682	1.655
18.0	31.57	29.85	1.807	1.788
19.0	33.33	31.60	1.923	1.924
20.0	35.08	33.36	2.035	2.059
21.0	36.84	35.11	2.179	2.196
22.0	38.59	36.86	2.317	2.332
23.4	41.05	39.32	2.540	2.526

b = 1.0874 cm

v = 0.5781 cm

h = 12.9870  $\mu\text{sec}$

SHOT NUMBER USAFA 110 SCALE FACTOR,  $f = \frac{0.750}{1.080}$

INITIAL TIME,  $t_0 = 6.42 \text{ } \mu\text{sec}$

[illegible]
$$h = 24.1546 \mu\text{sec}$$

Figure 138

TEST NO. LASL 1311

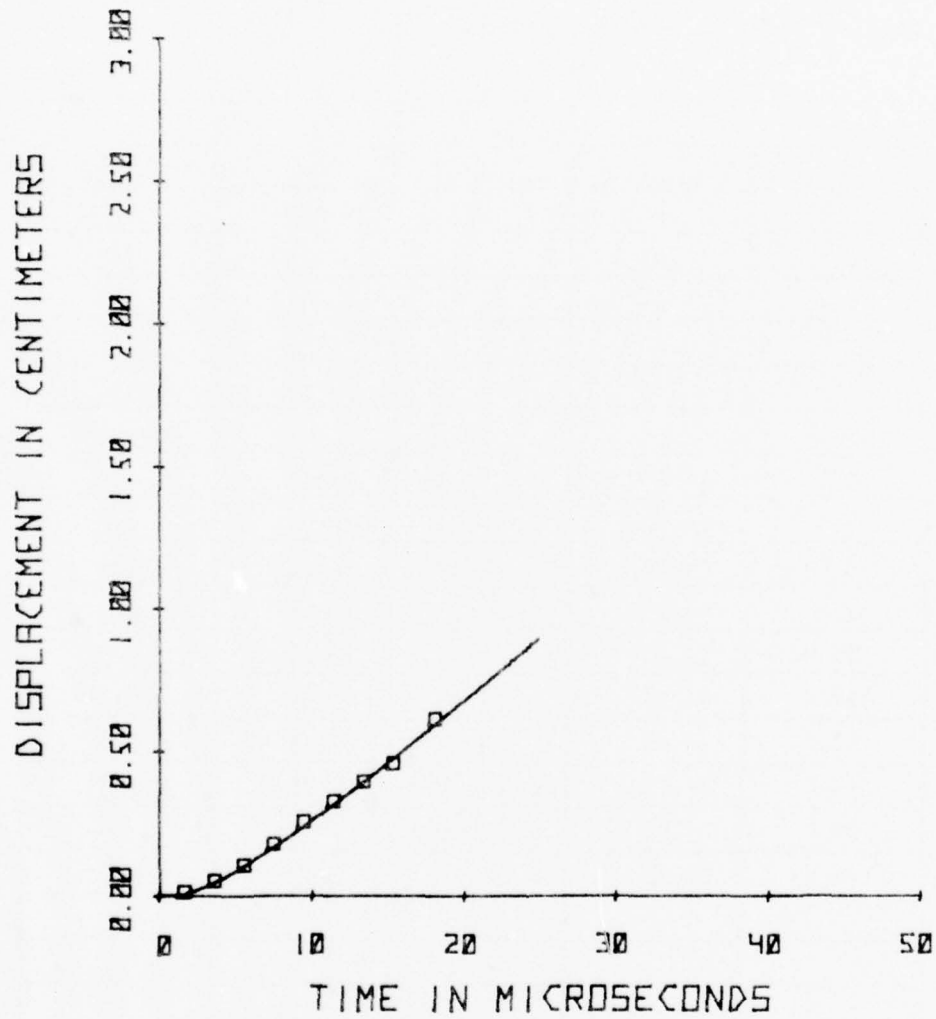




Figure 139

TEST NO. LASL 1312

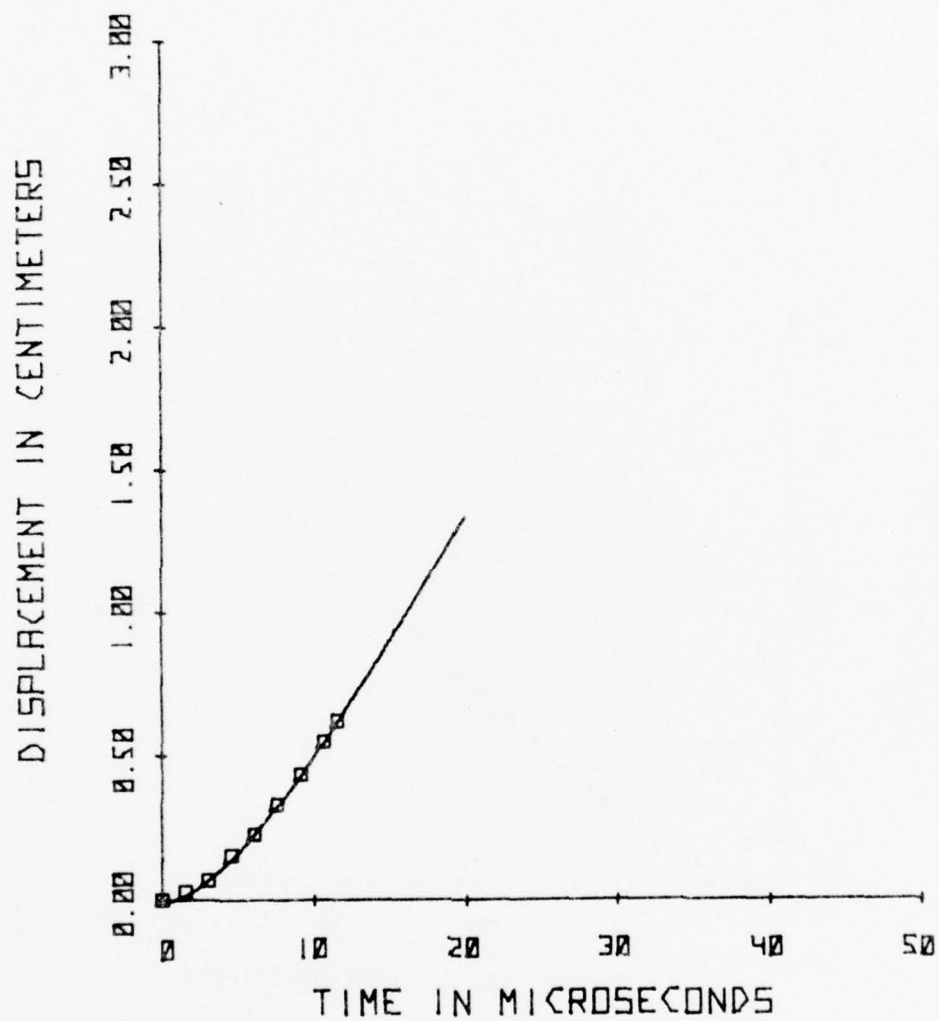




Figure 140

TEST NO. LASL 1317

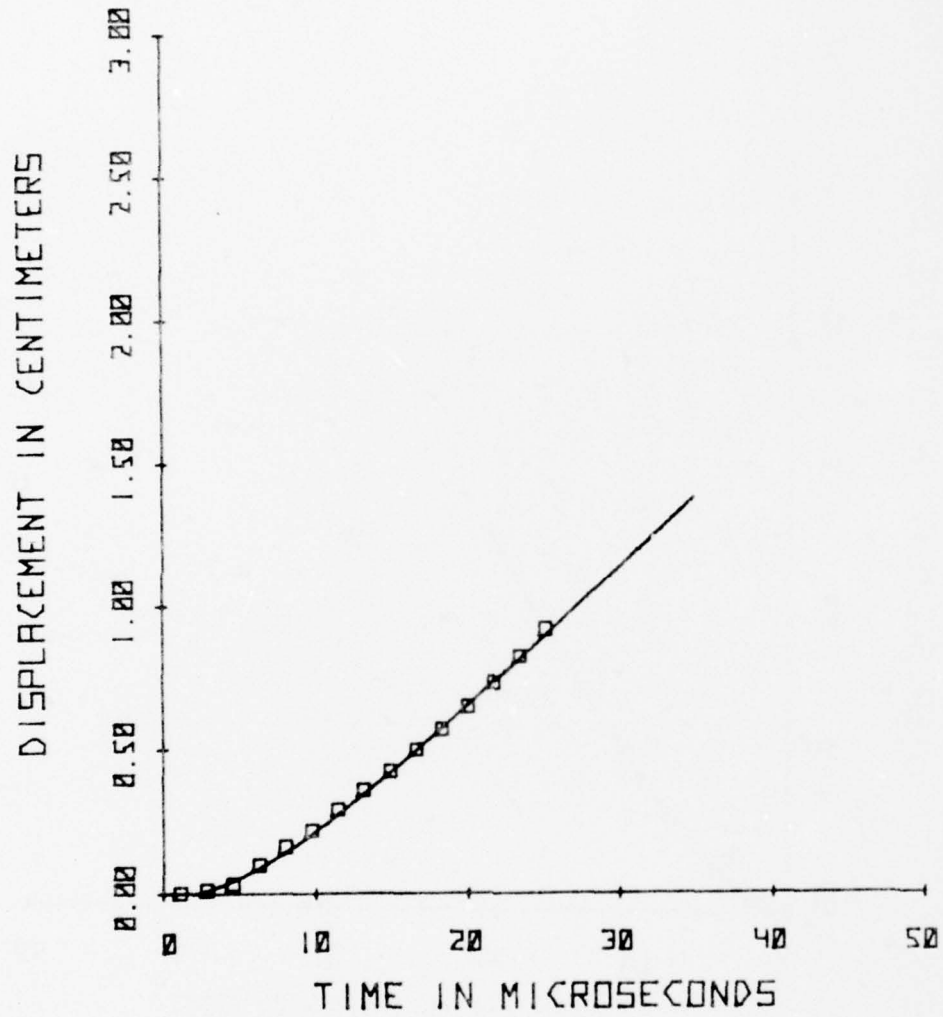


Figure 141

TEST NO. LASL 1321

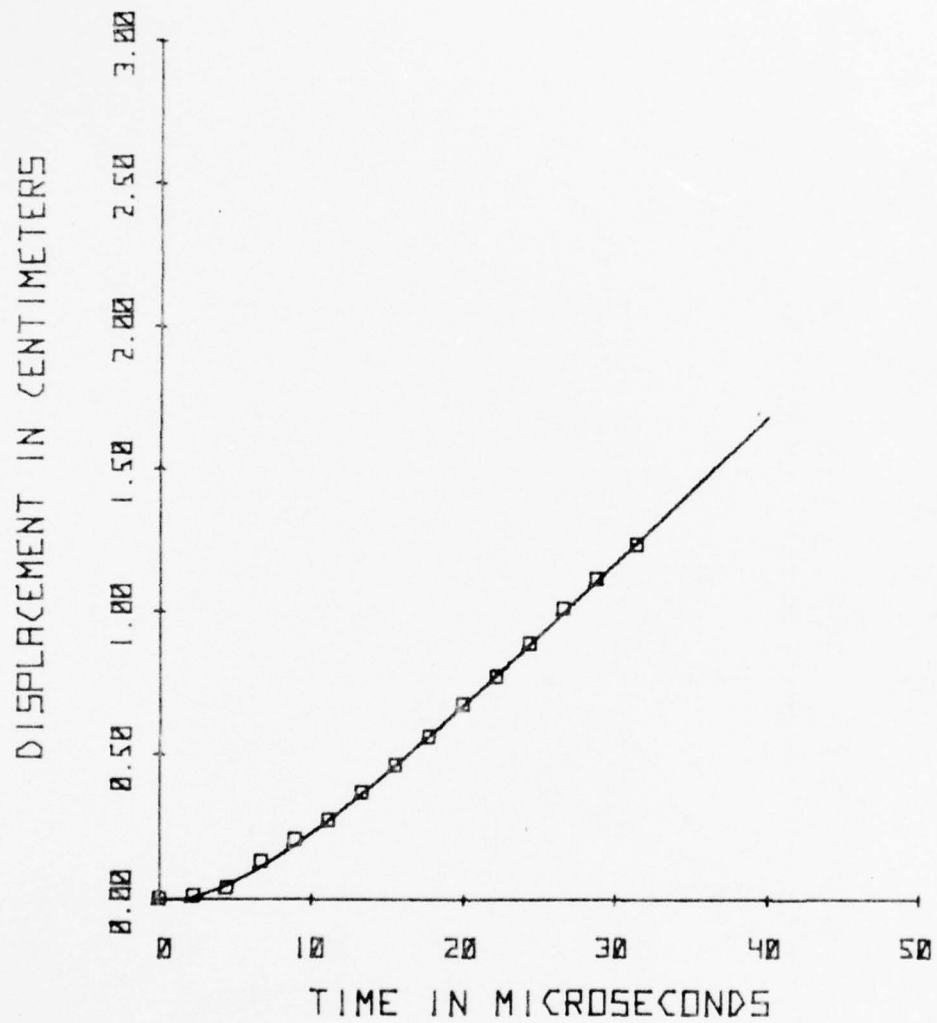


Figure 142

TEST NO. LASL 1322

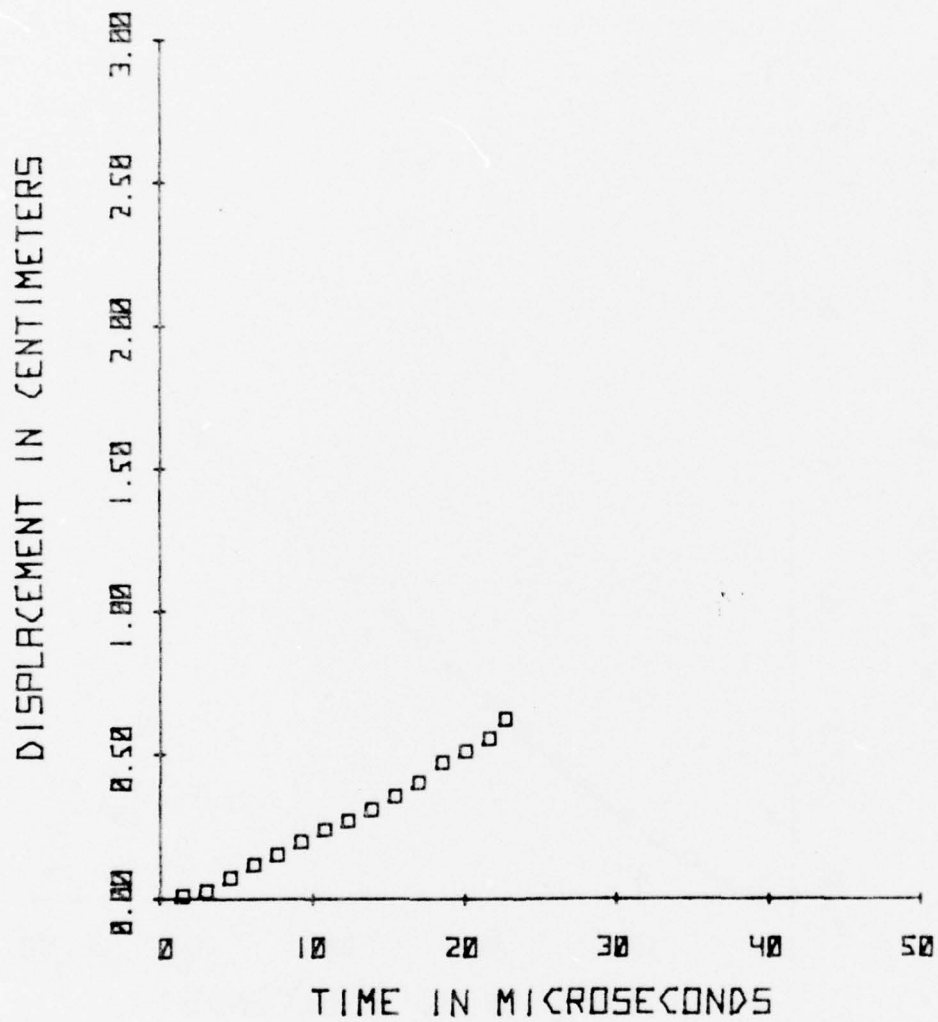


Figure 143

TEST NO. LASL 1324

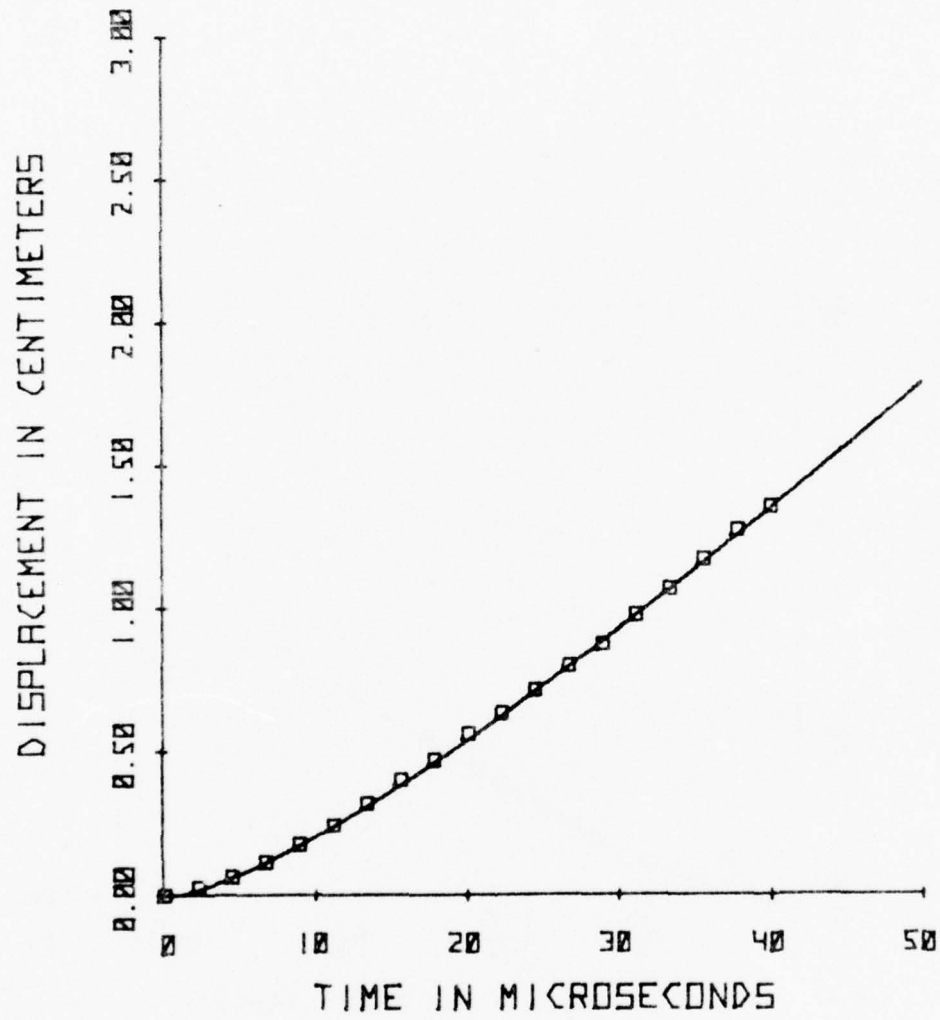


Figure 144

TEST NO. LASL 1325

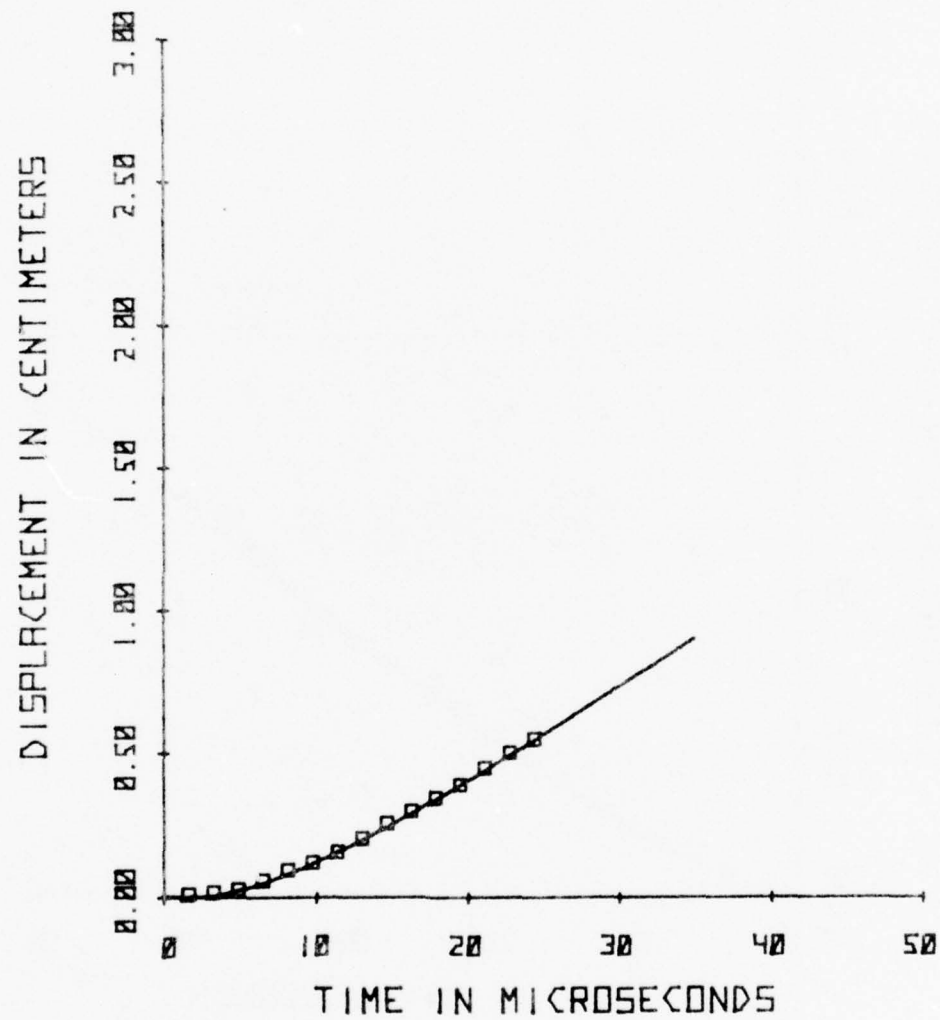


Figure 145

TEST NO. LASL 1362

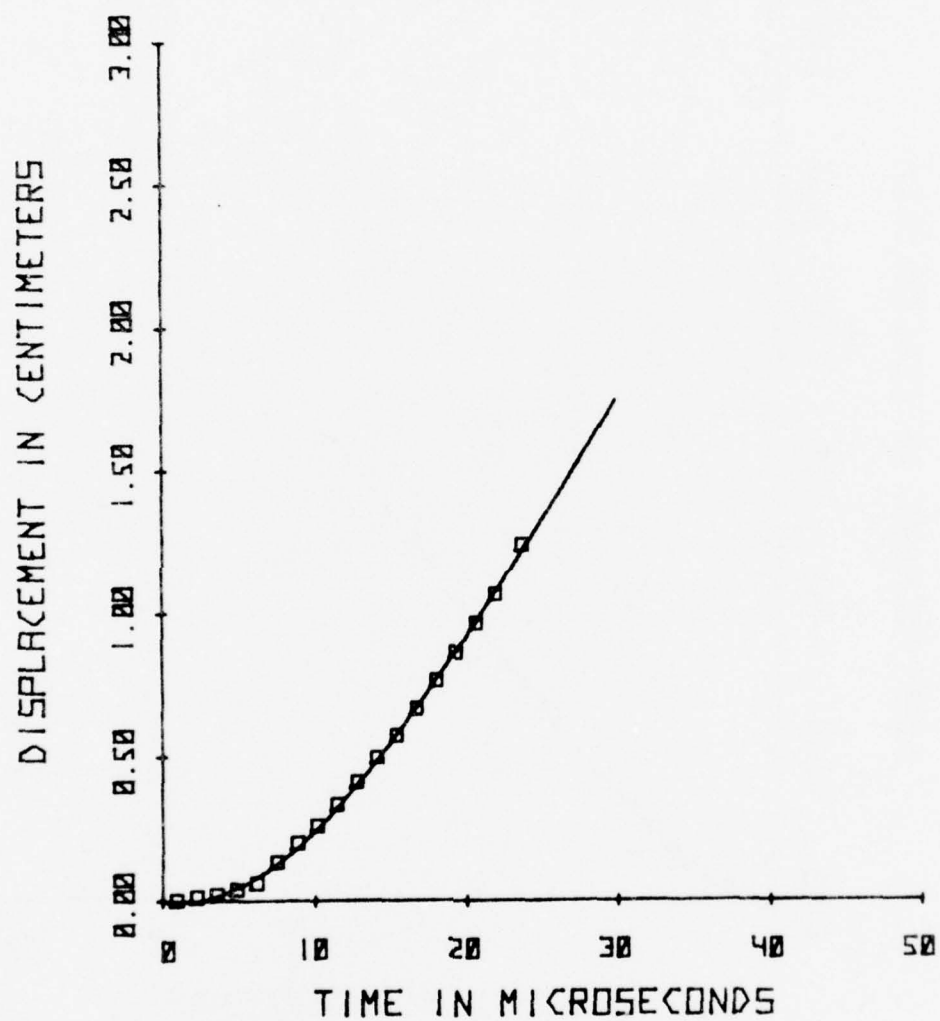




Figure 146

TEST NO. DRI 3

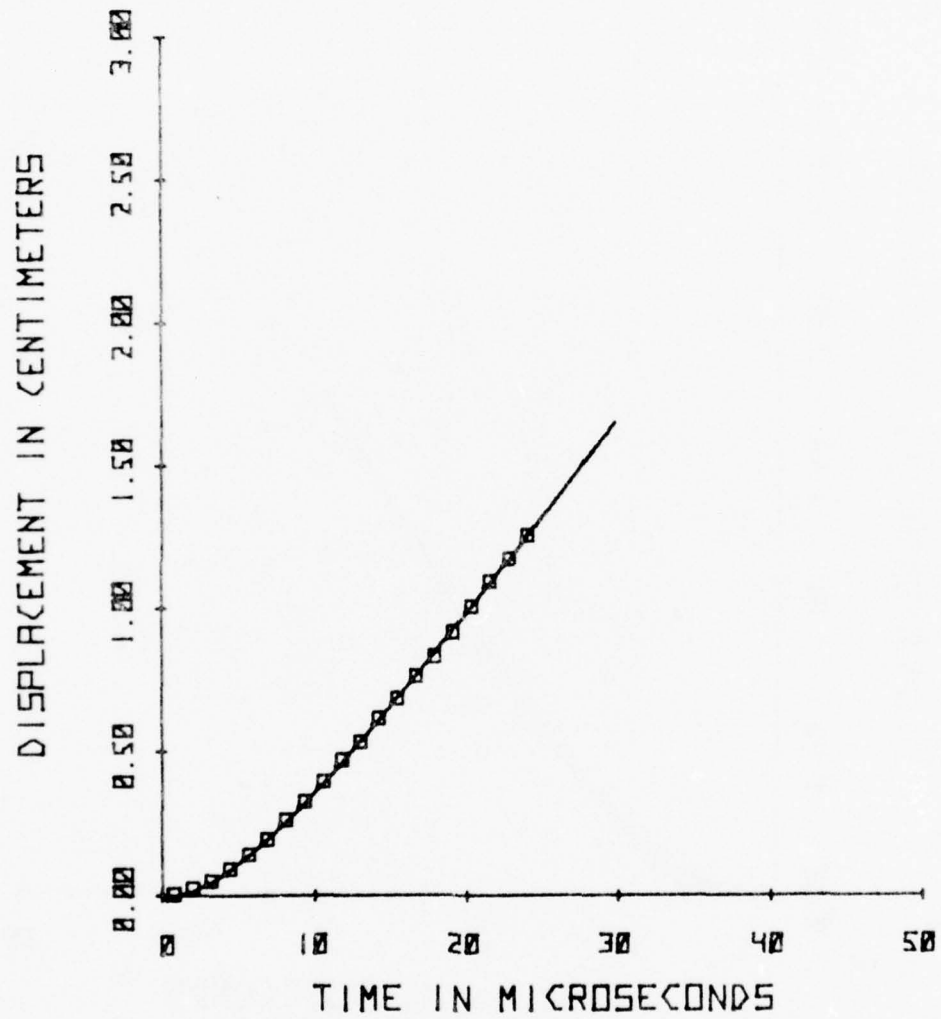


Figure 147

TEST NO. DRI 4

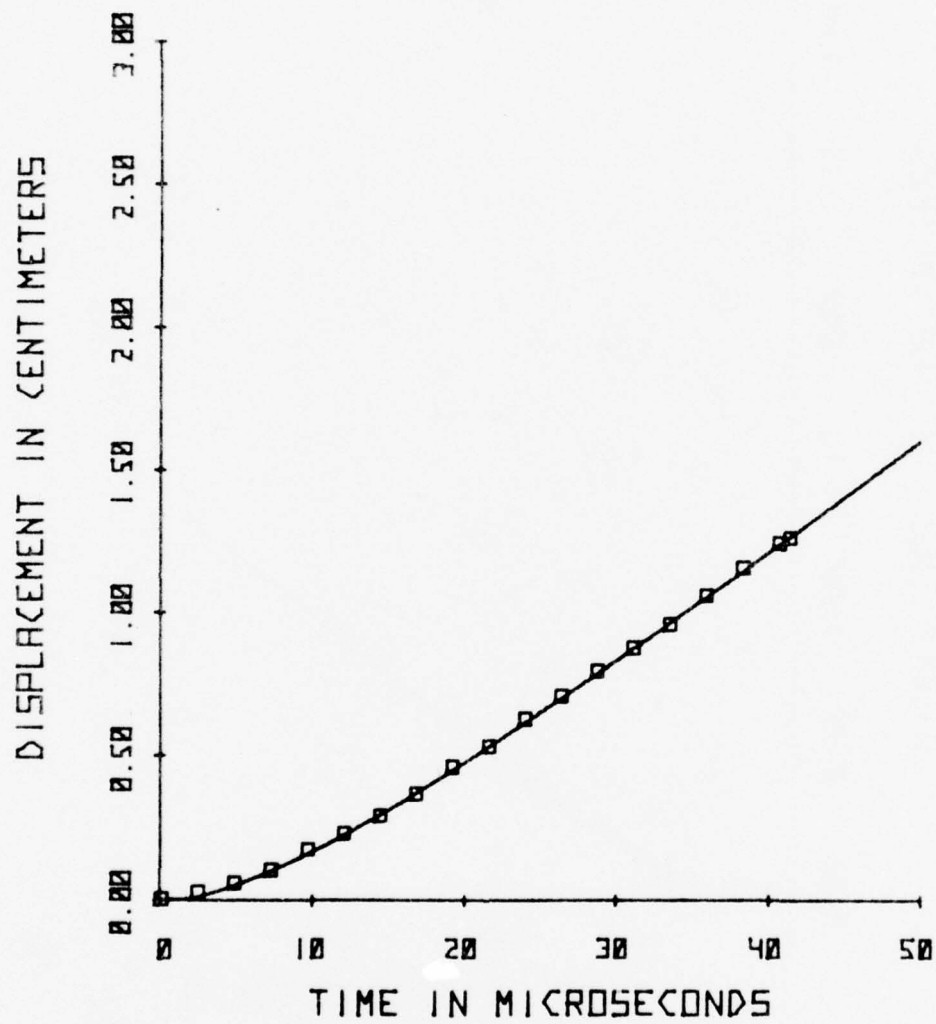


Figure 148

TEST NO. DRI 5

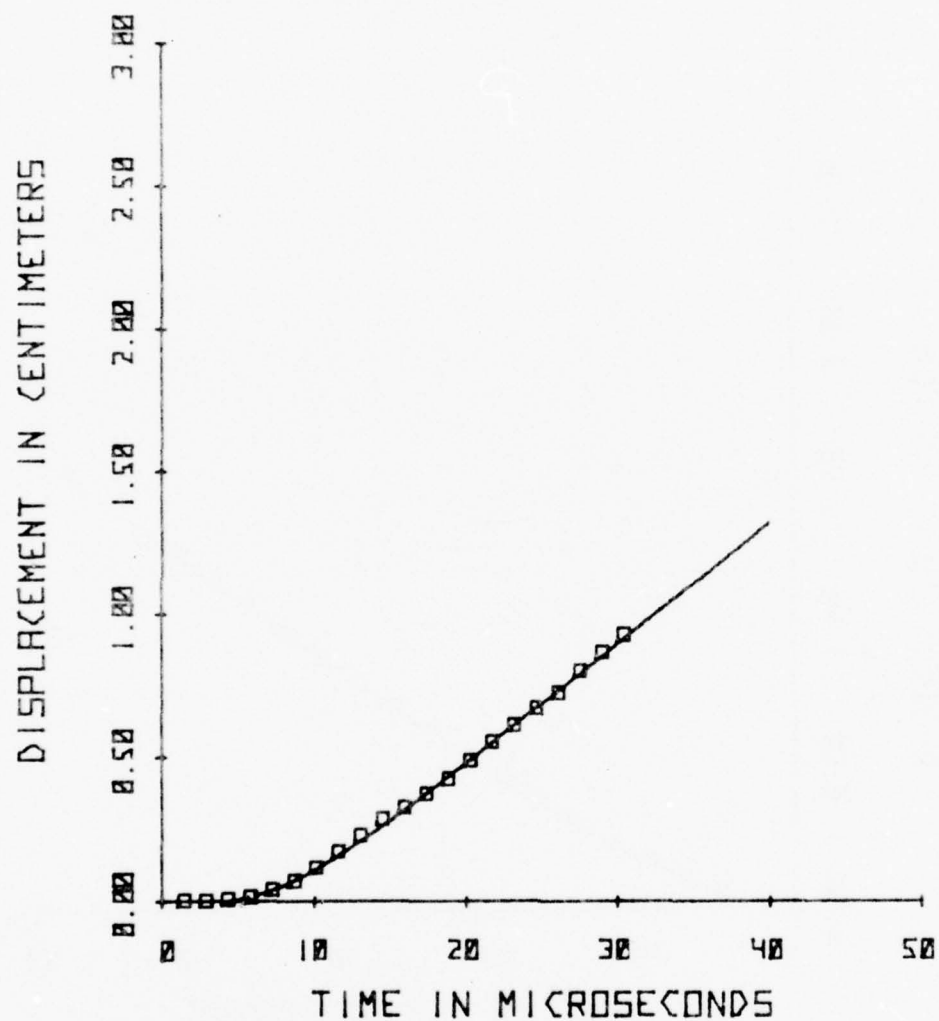


Figure 149

TEST NO. DRI 6

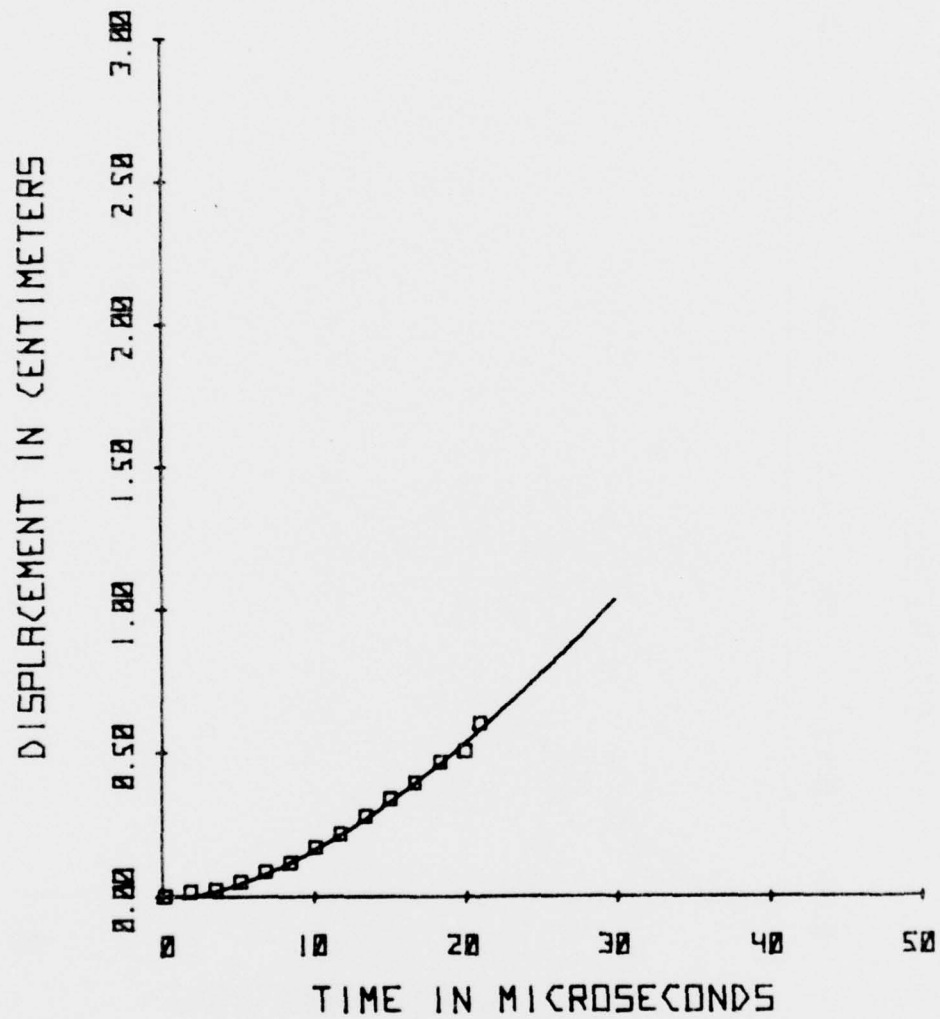


Figure 150

TEST NO. DRI 7

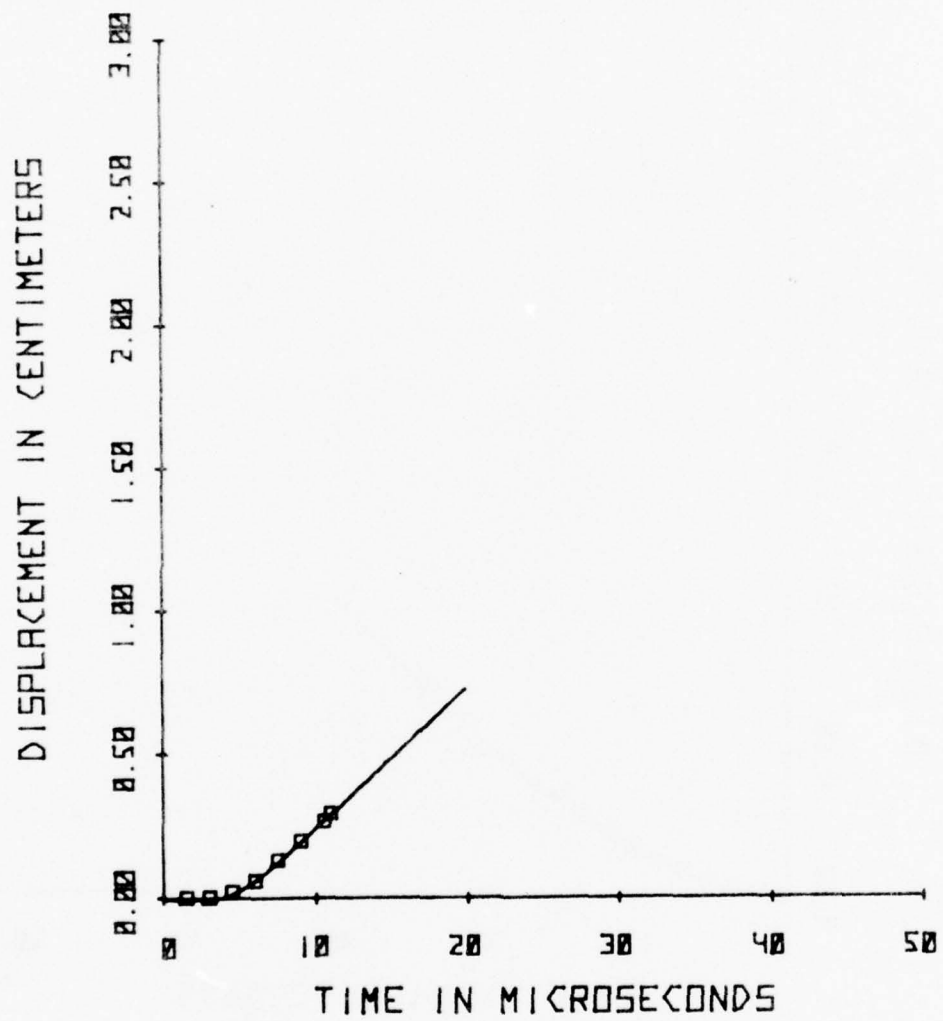


Figure 151

TEST NO. DRI 8

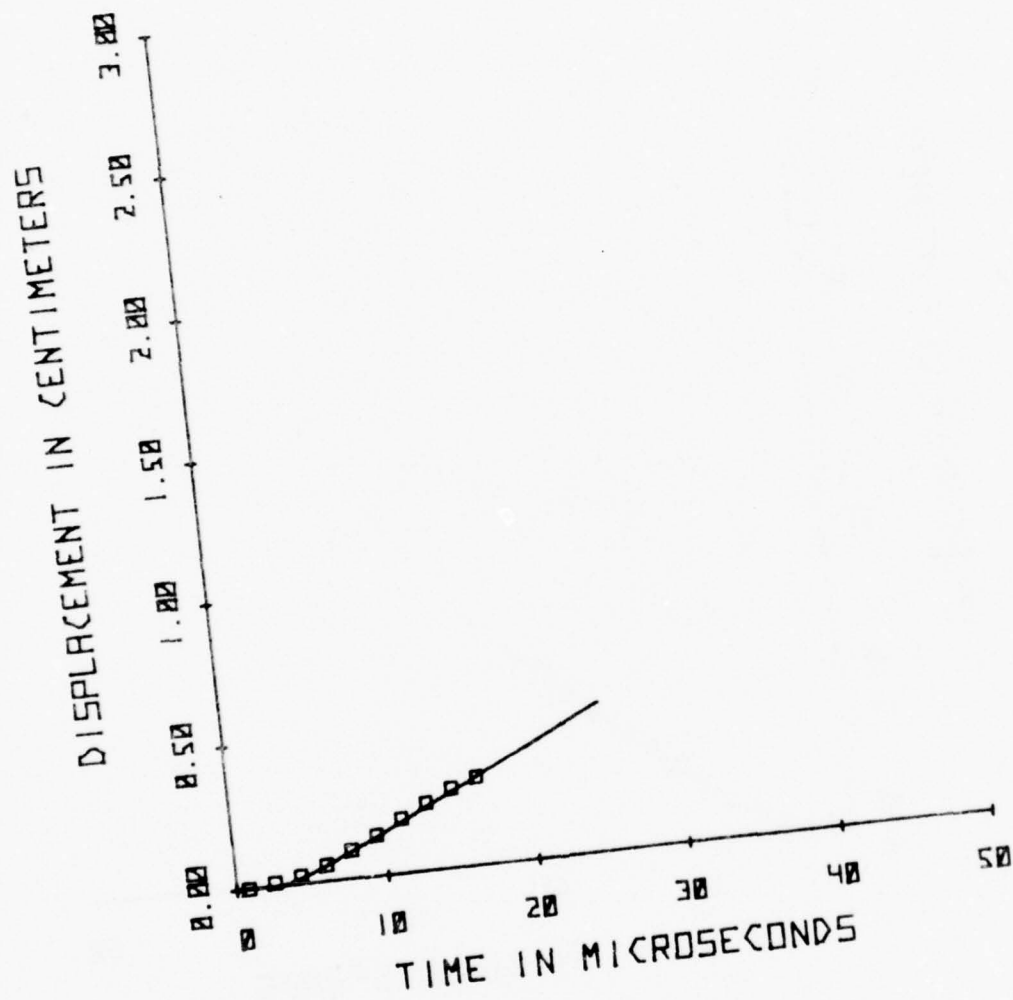




Figure 152

TEST NO. DRI 9

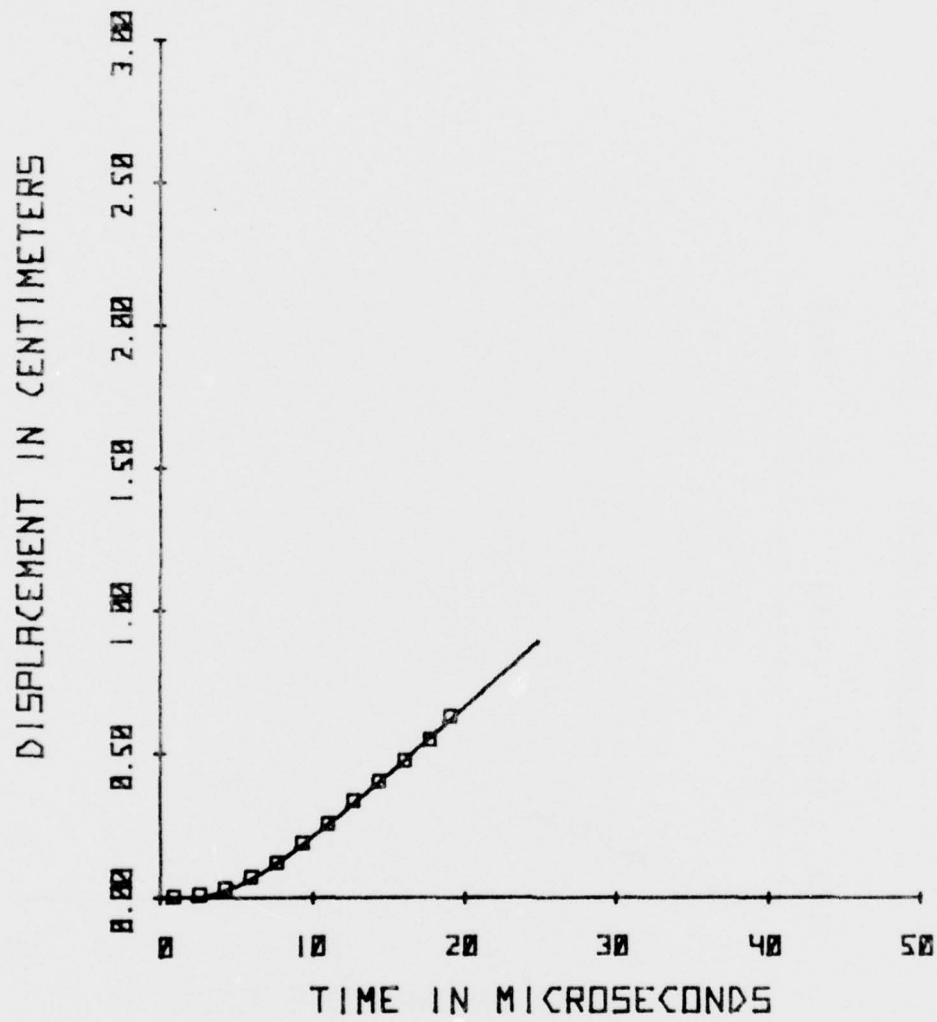


Figure 153

TEST NO. DRI 11

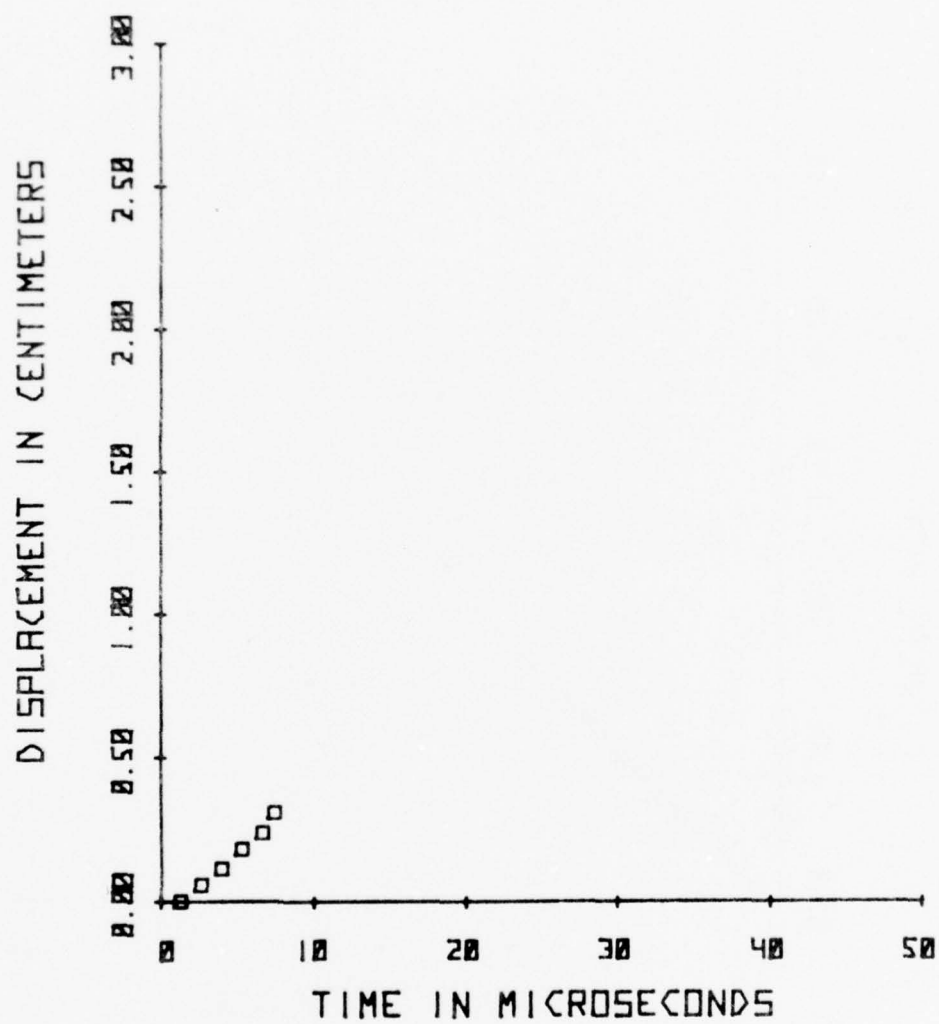


Figure 154

TEST NO. DRI 13

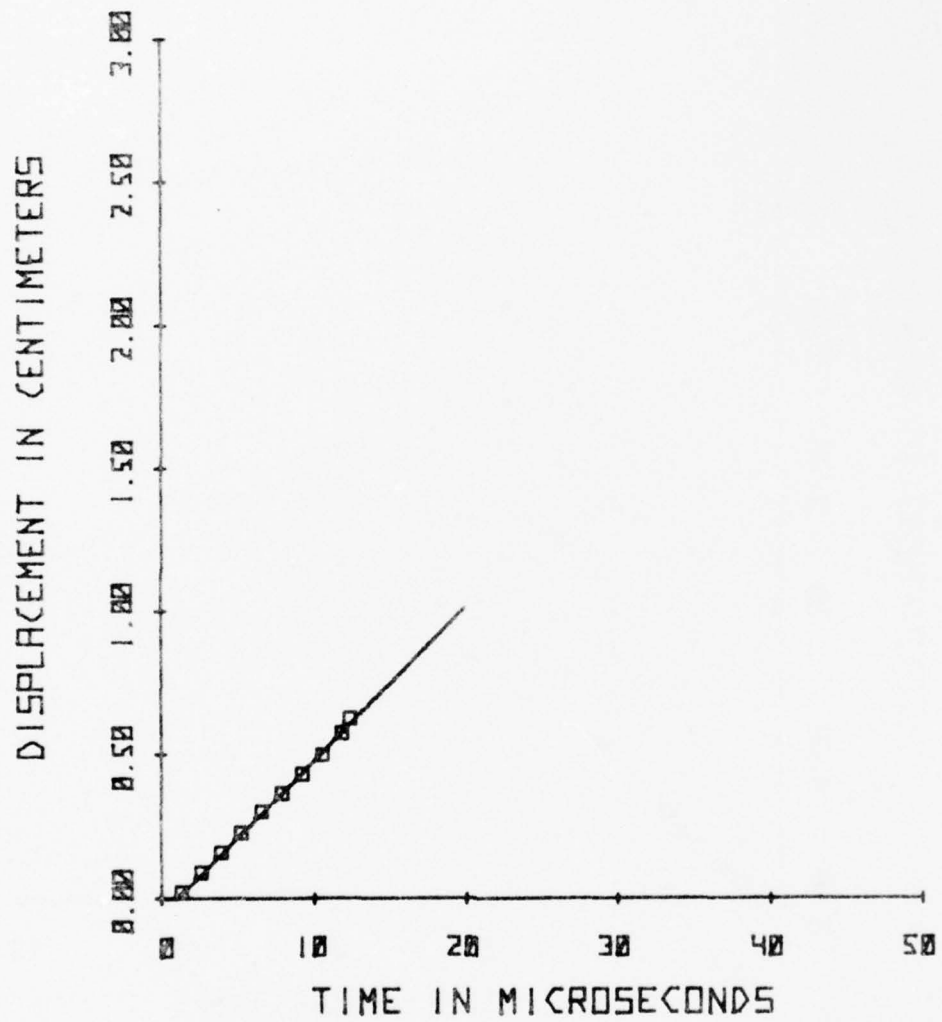


Figure 155

TEST NO. DRI 14

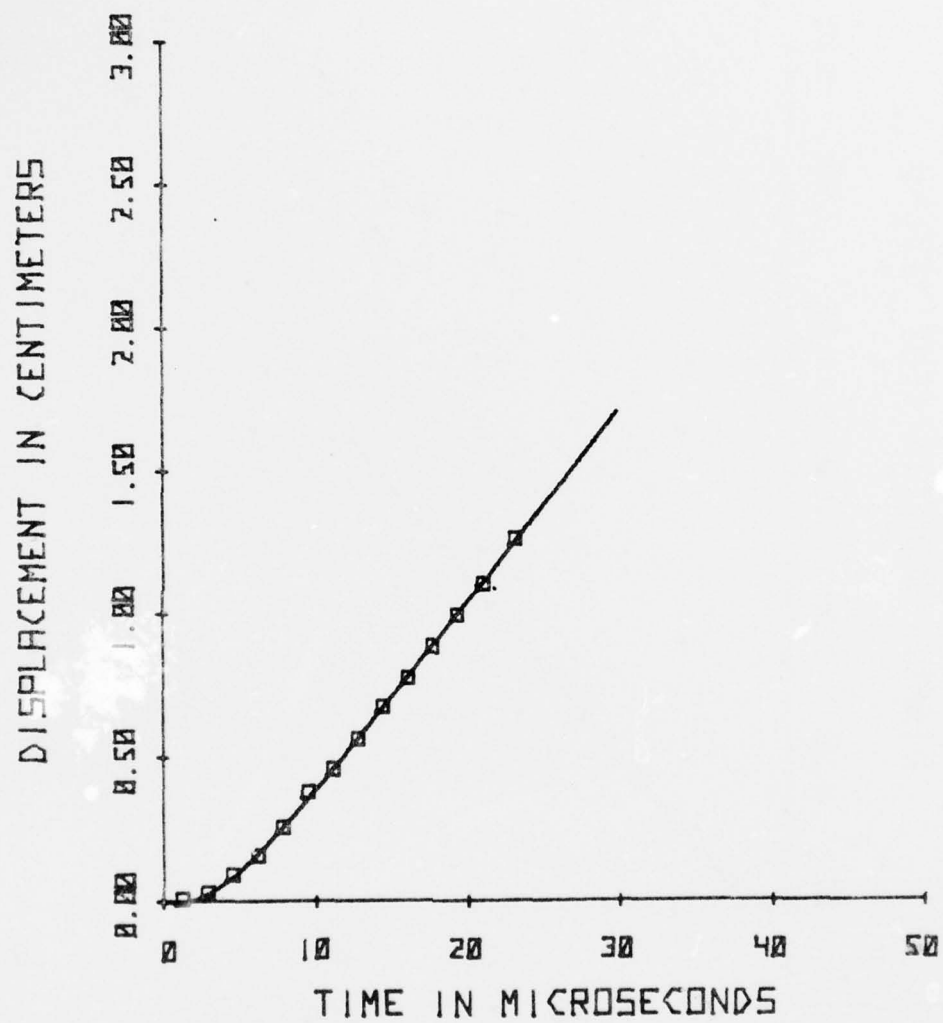


Figure 156

TEST NO. DRI 15

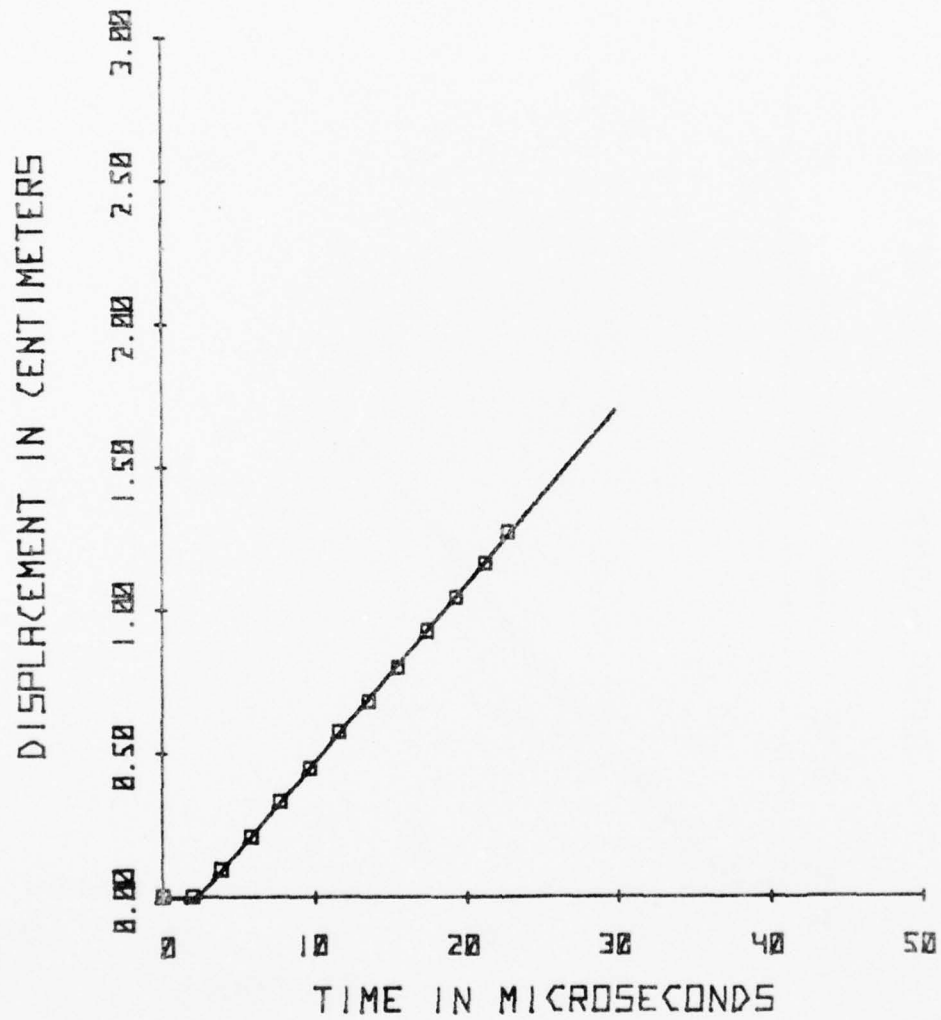


Figure 157

TEST NO. DRI 16

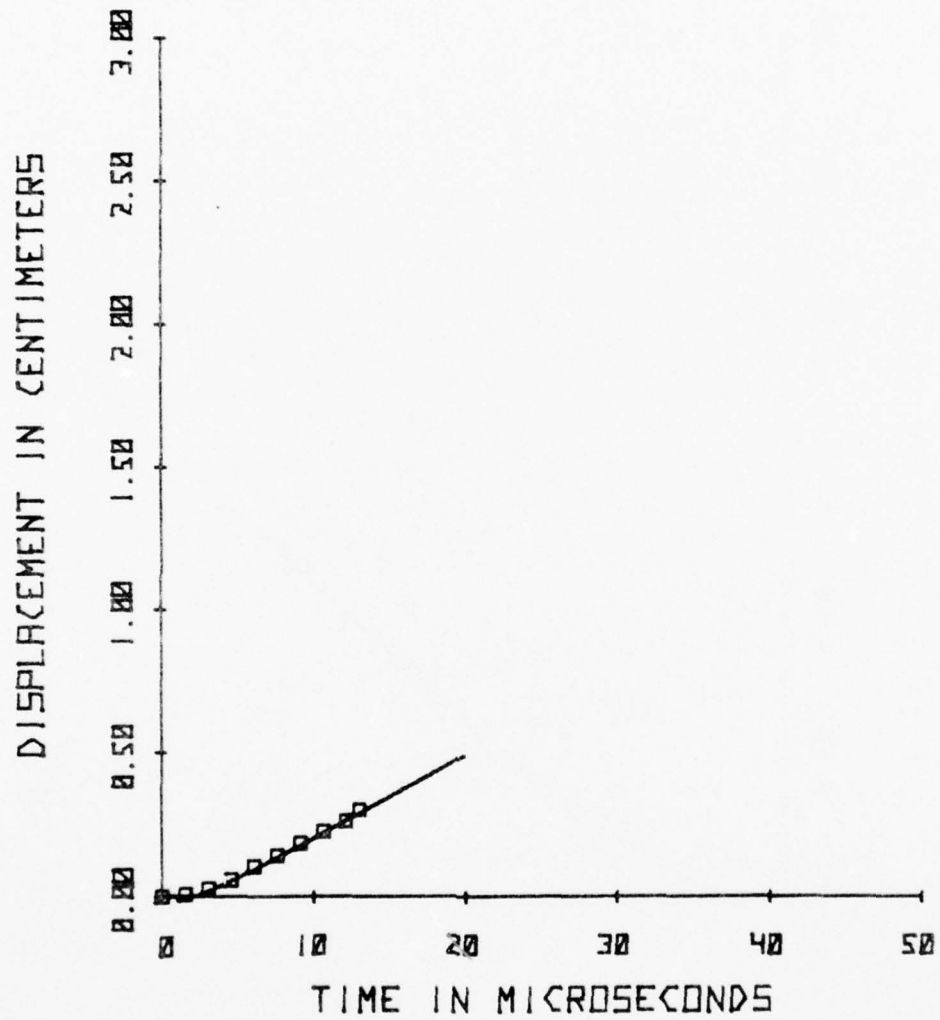




Figure 158

TEST NO. DRI 22

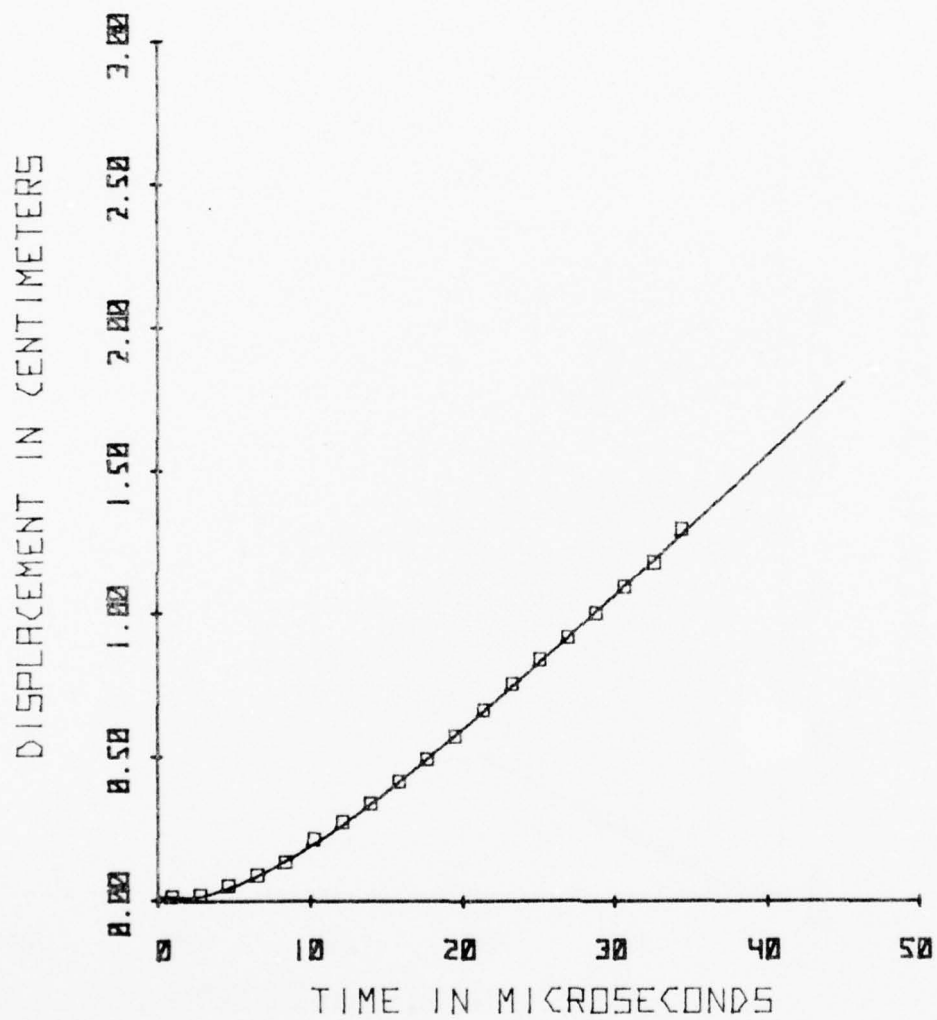


Figure 159

TEST NO. DRI 24

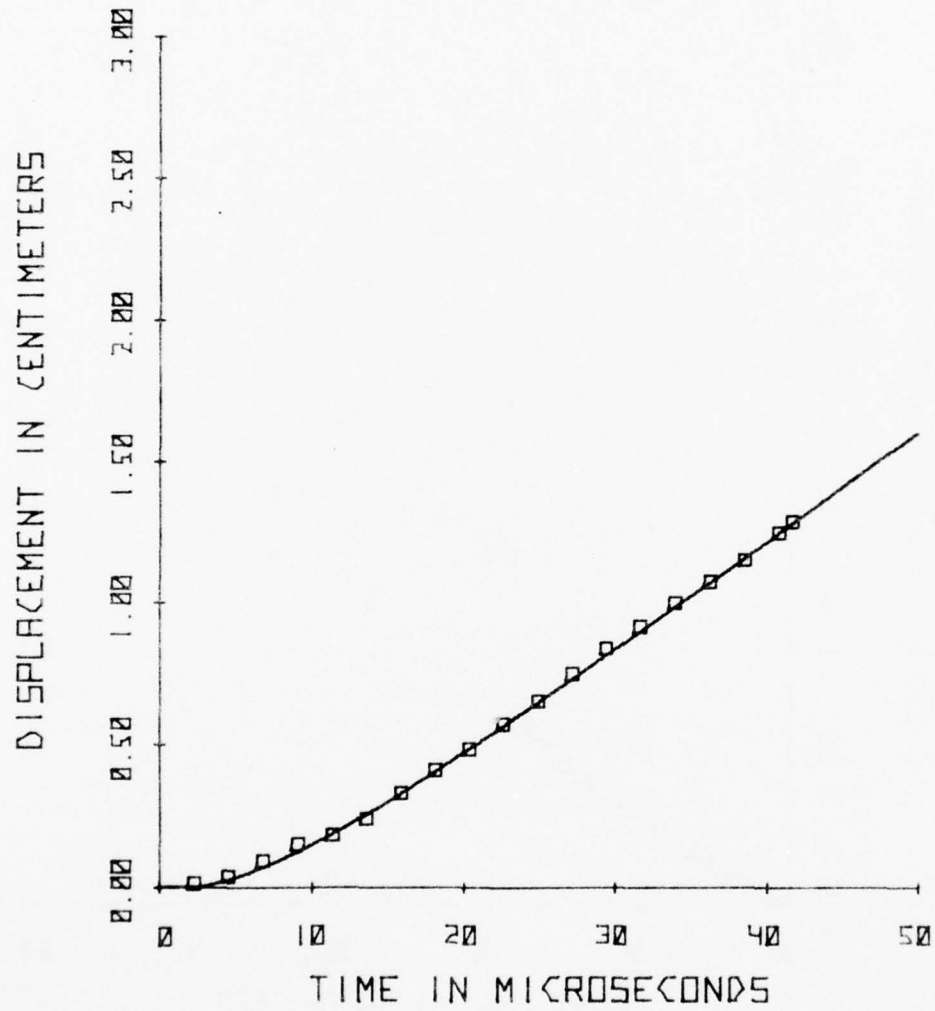


Figure 160

TEST NO. DRI 28

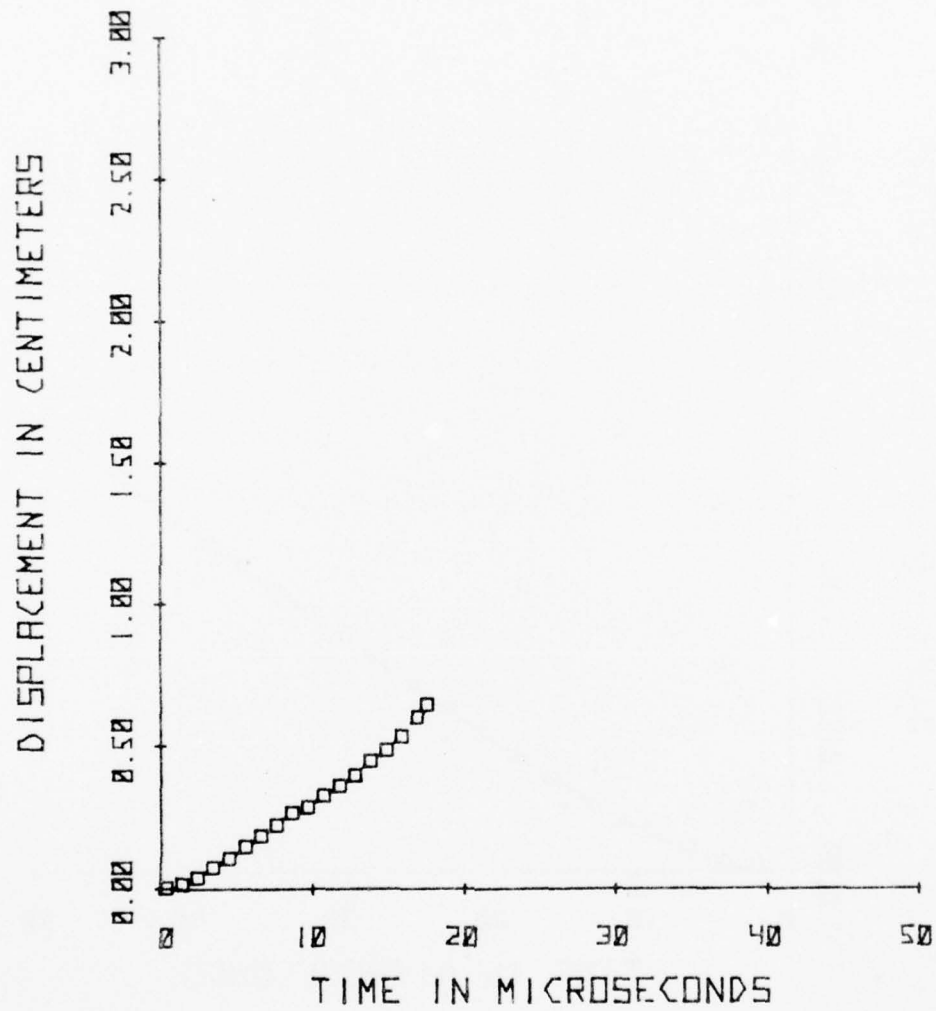


Figure 161

TEST NO. USAFA 45

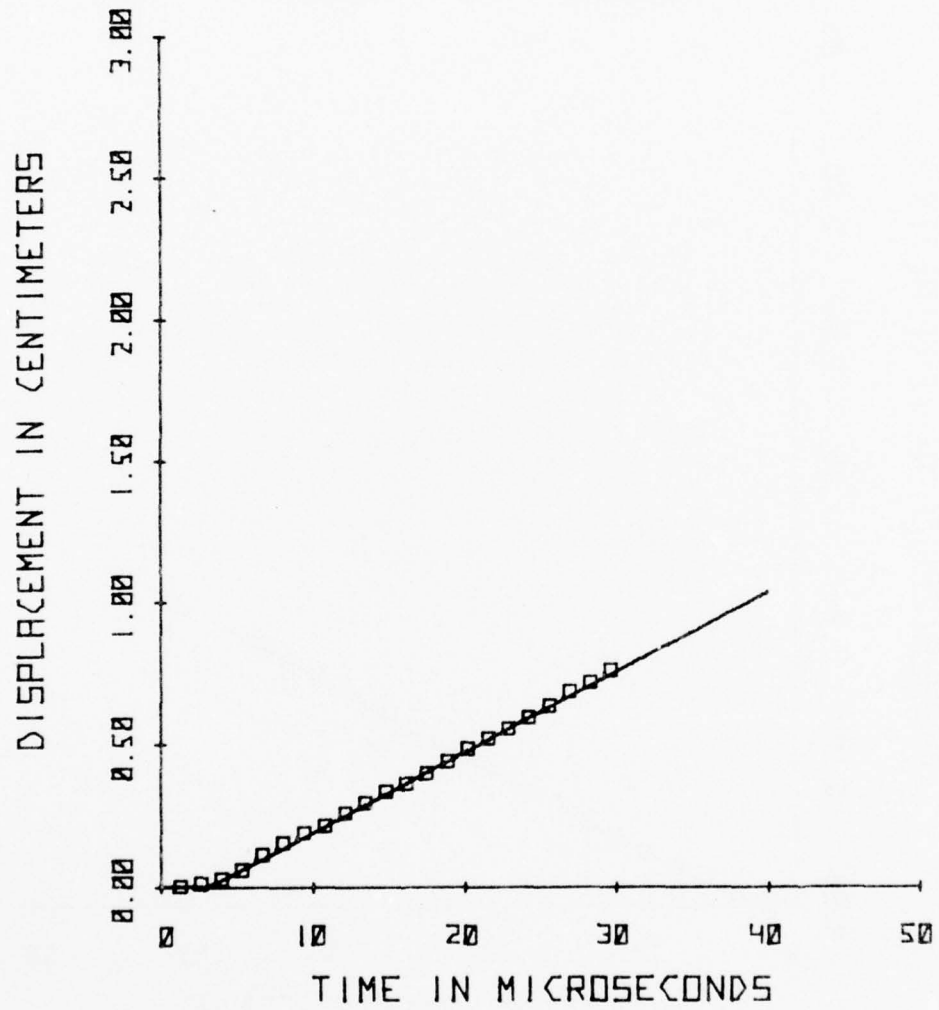


Figure 162

TEST NO. USAFA 46

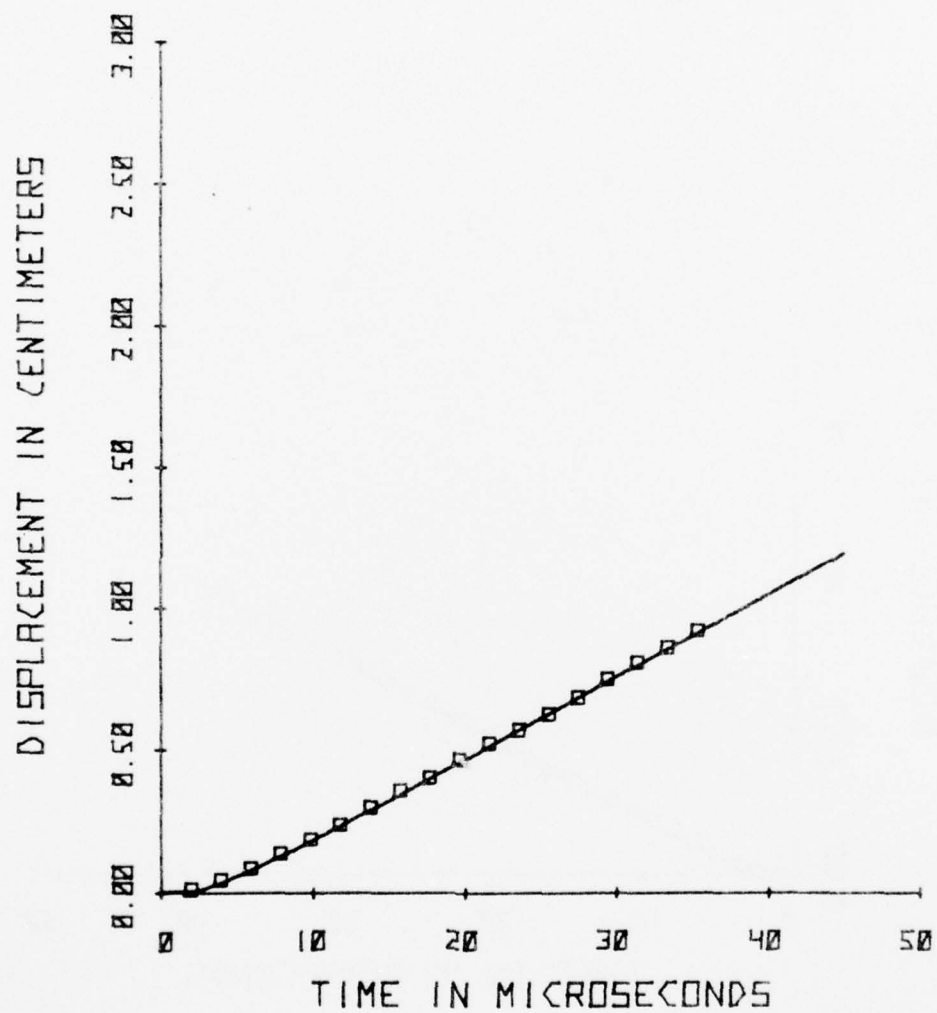


Figure 163

TEST NO. USAFA 48

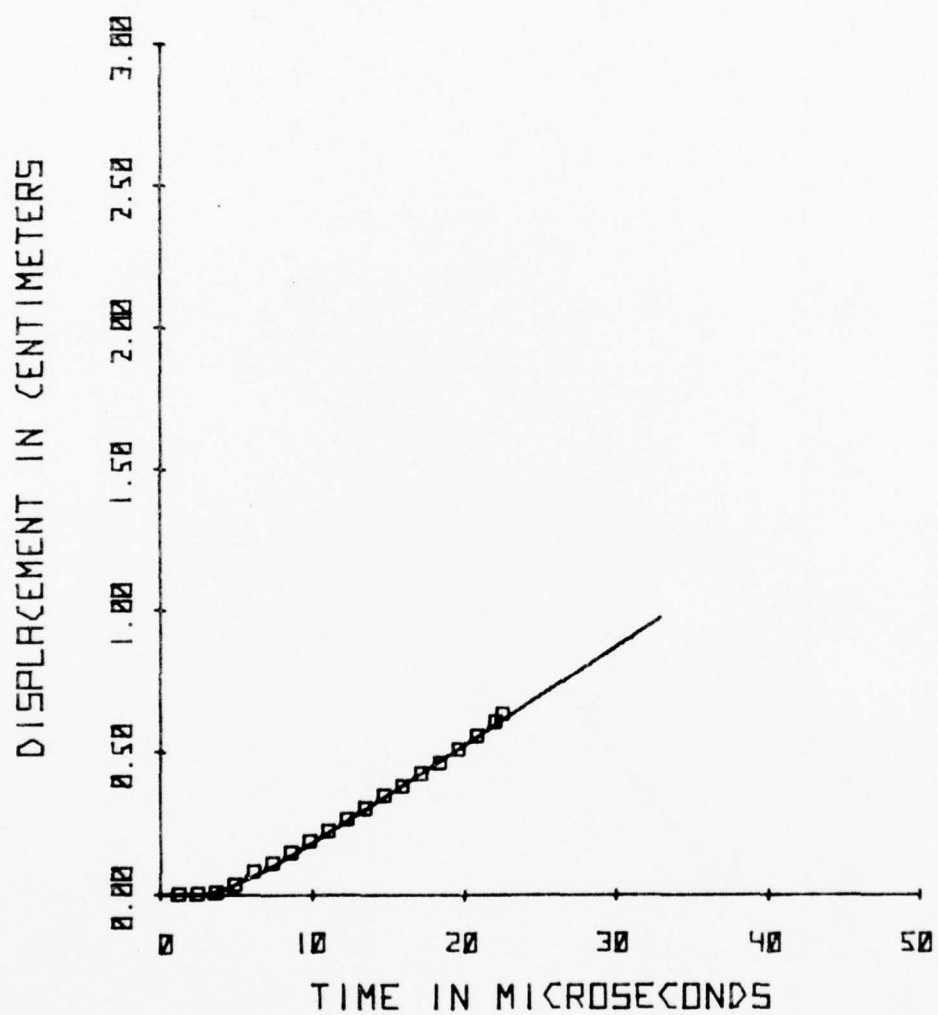




Figure 164

TEST NO. USAFA 51

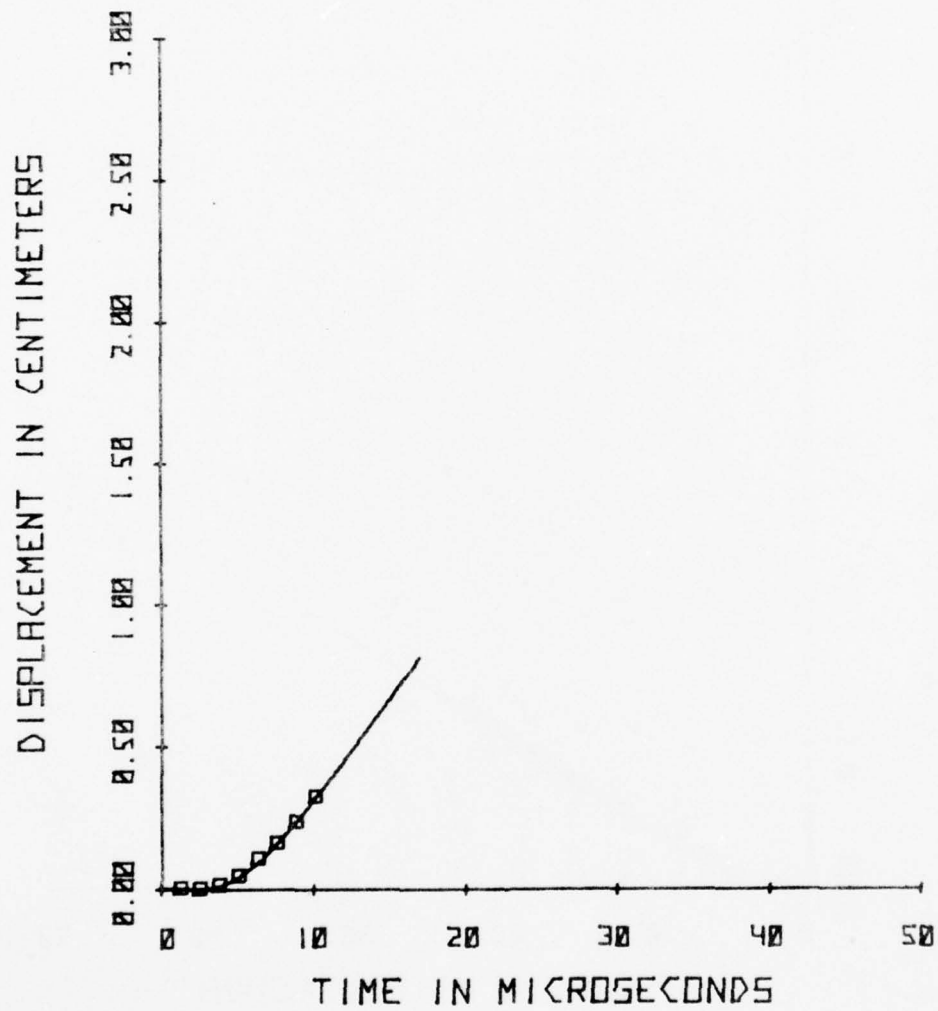


Figure 165

TEST NO. USAFA 54

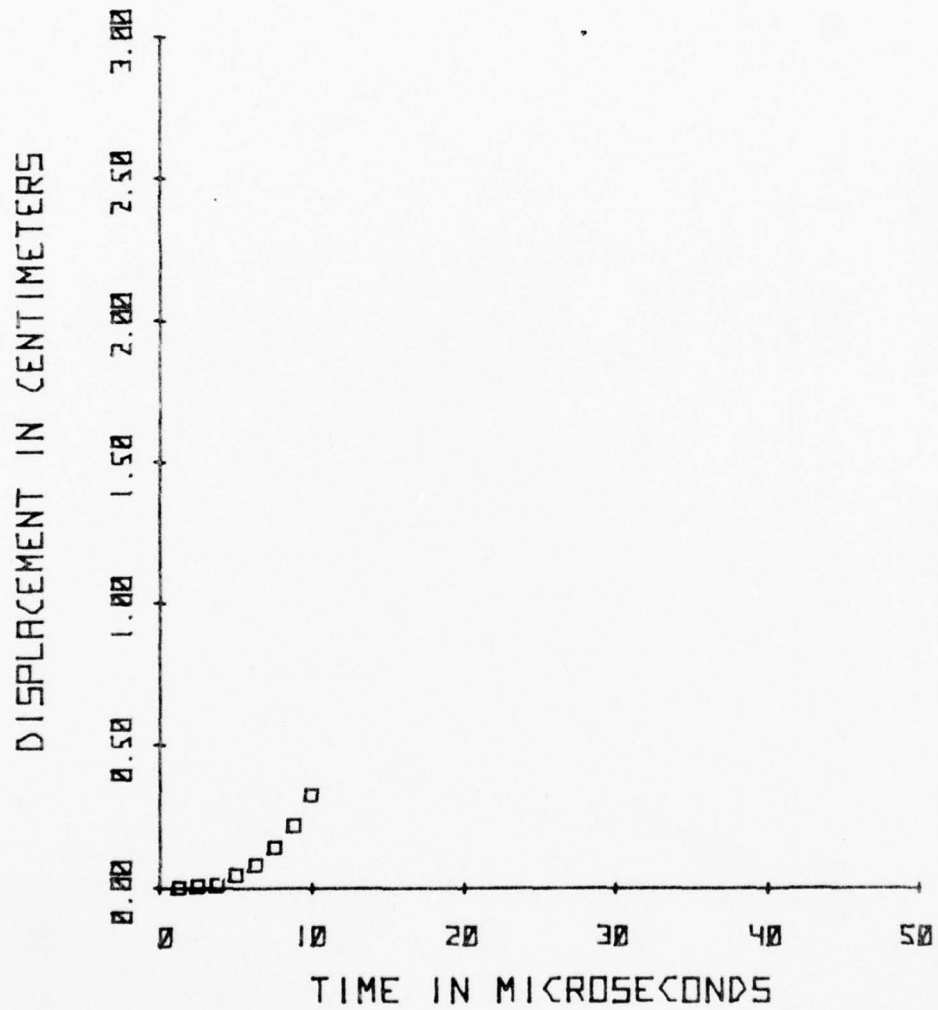


Figure 166

TEST NO. USAFA 55

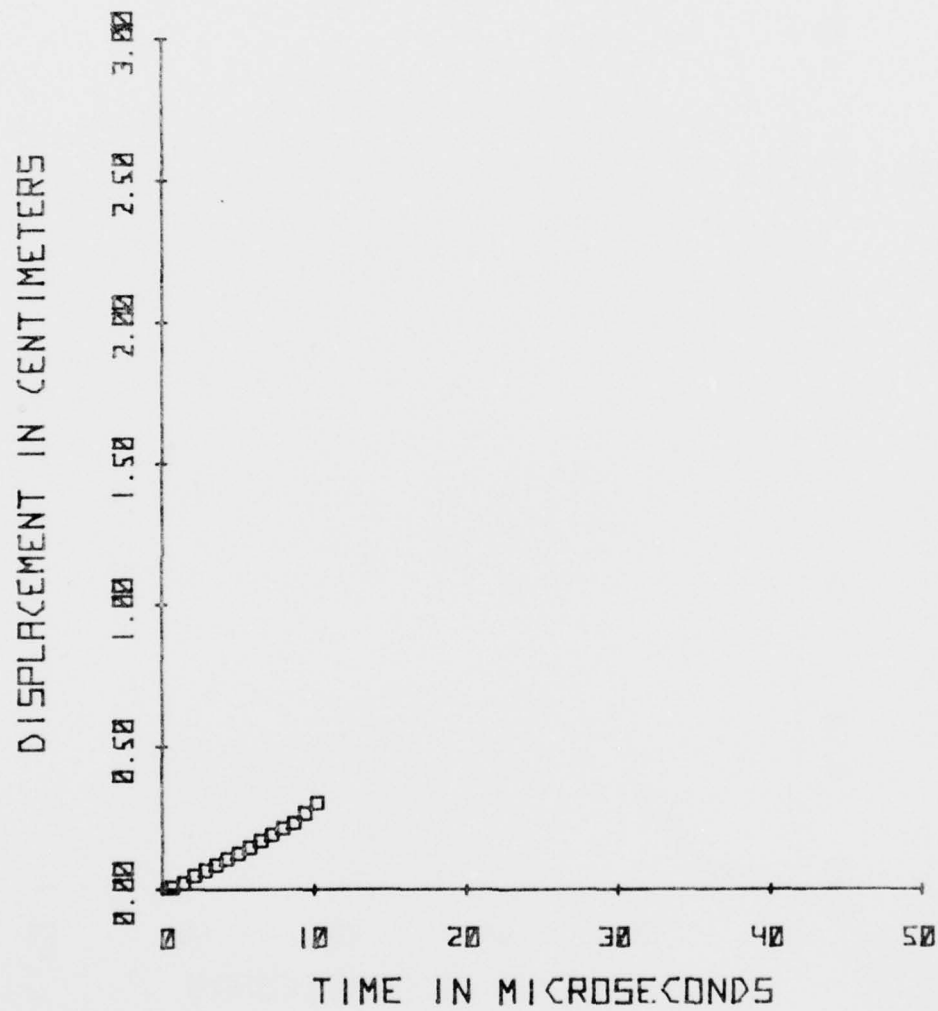


Figure 167

TEST NO. USAFA 57

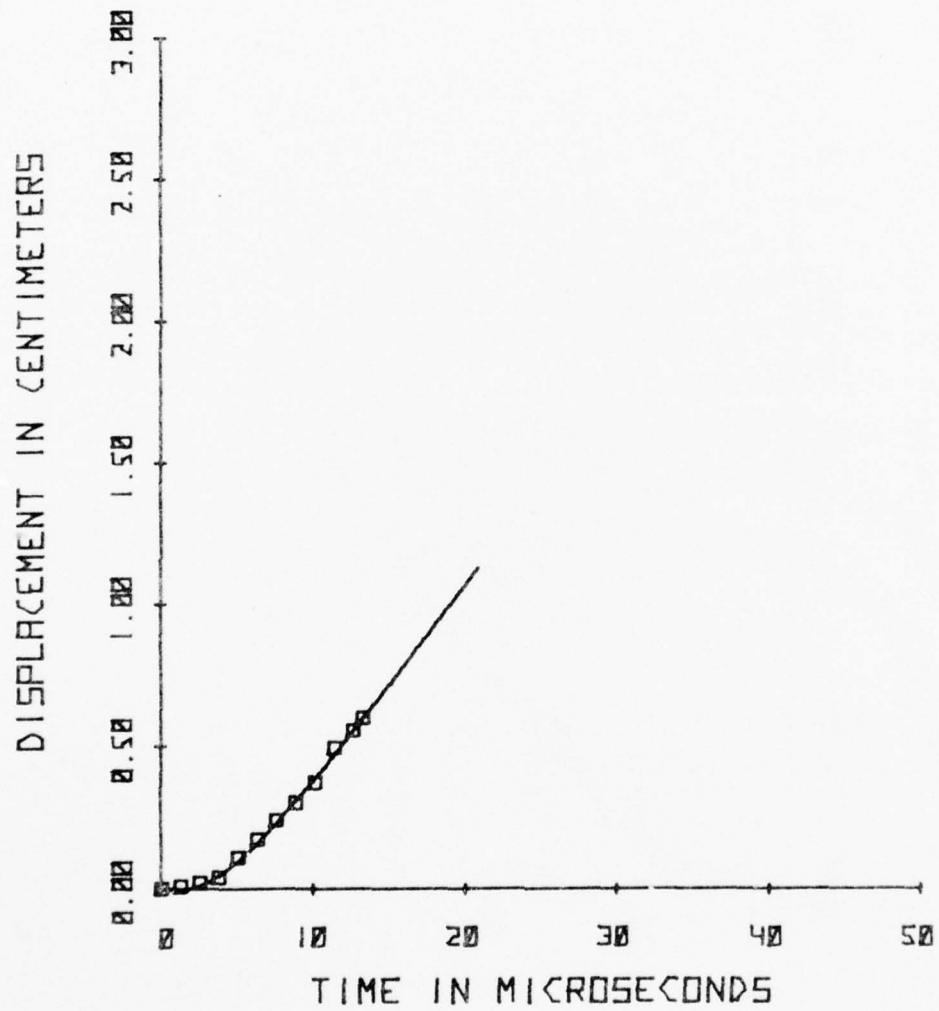
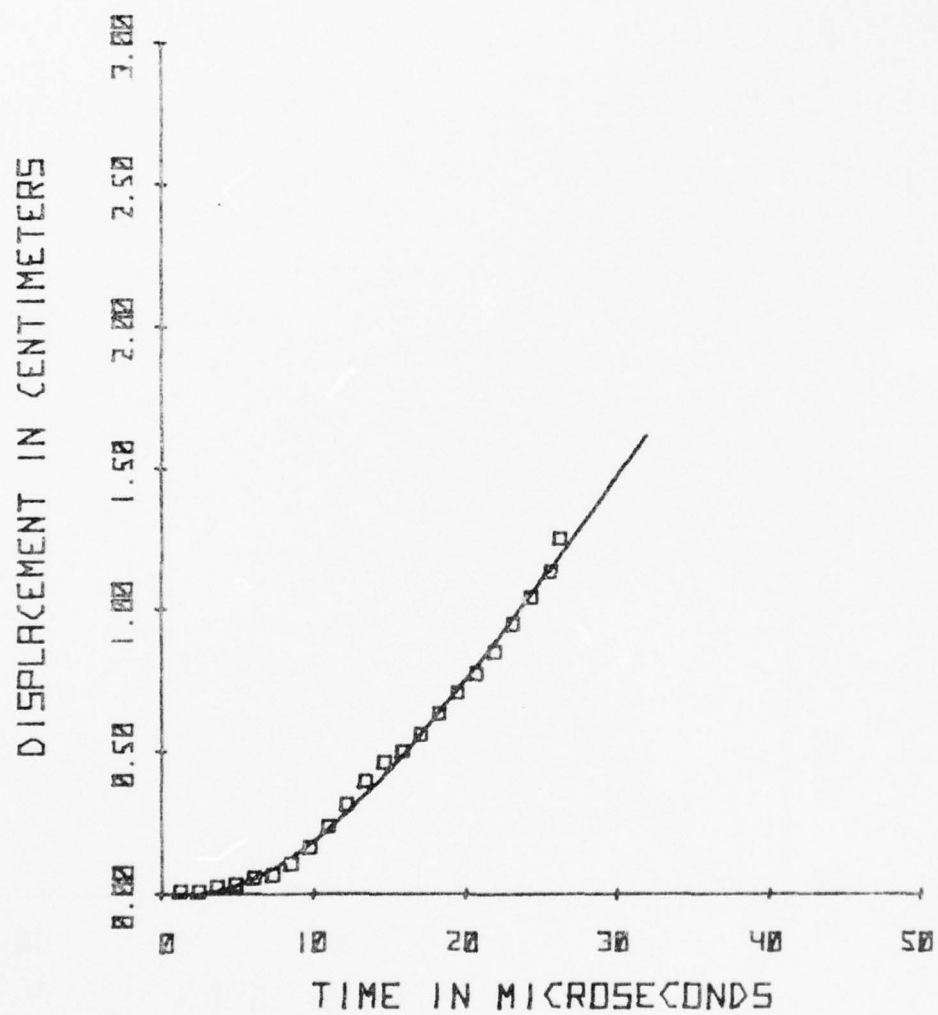


Figure 168

TEST NO. USAFA 59



AD-A047 955

FRANK J SEILER RESEARCH LAB UNITED STATES AIR FORCE --ETC F/O 13/8  
EXPLOSIVE IMPULSE WELDING. VOLUME I.(U)

JUL 77 D H MERKLE, G E CANNON

FJSRL-TR-77-0012-VOL-1

UNCLASSIFIED

NL

5 OF 5

AD  
A047955





Figure 169

TEST NO. USAFA 60

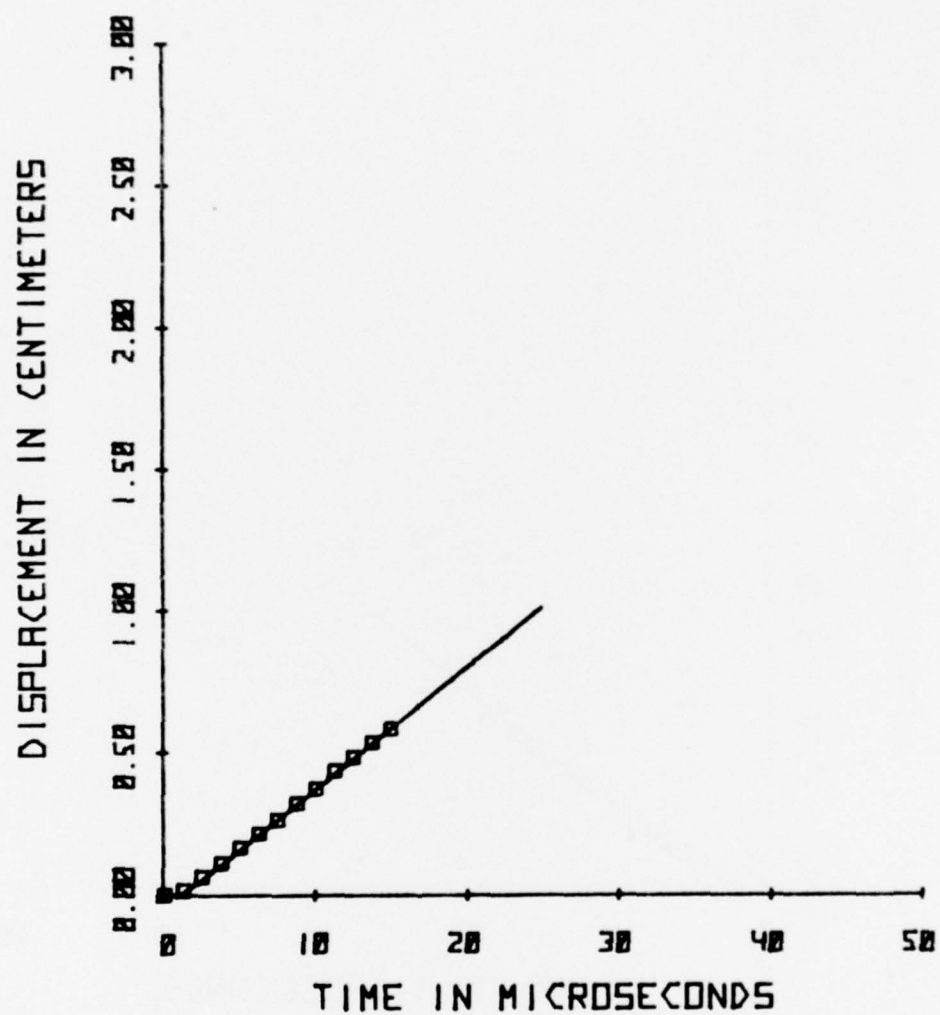


Figure 170

TEST NO. USAFA 62A

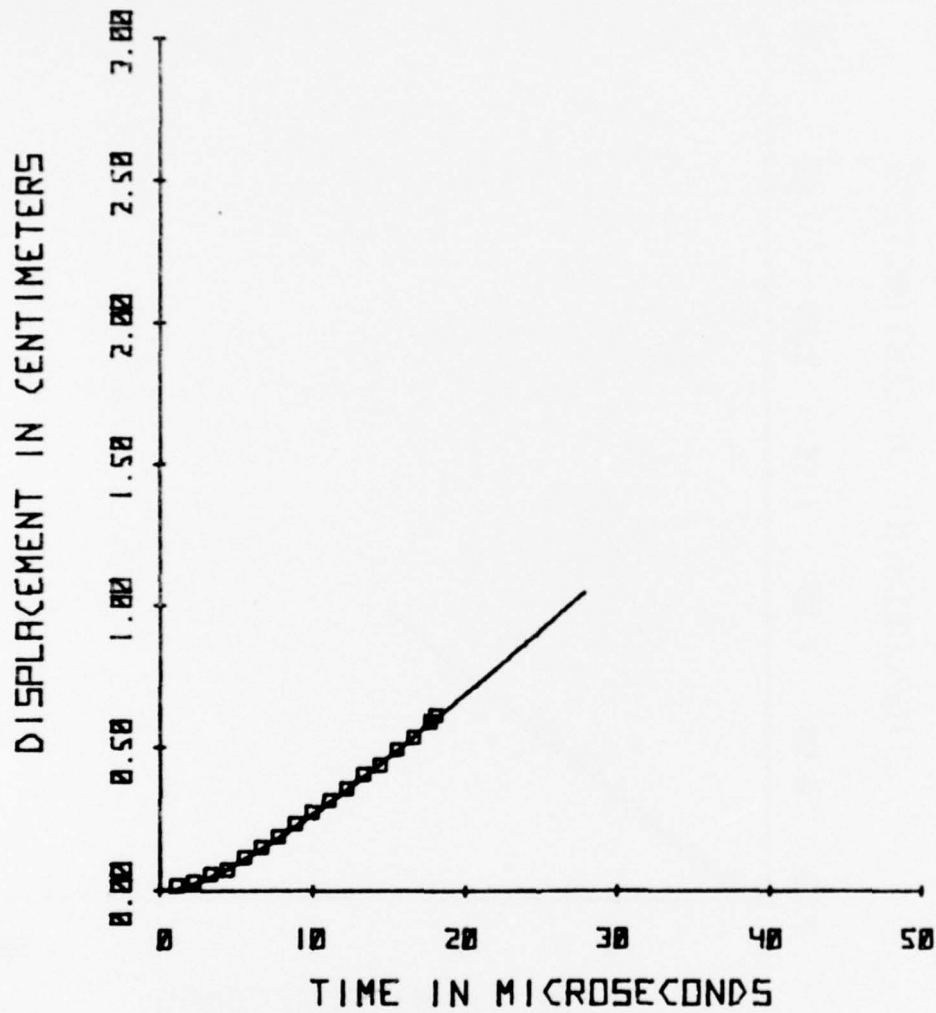


Figure 171

TEST NO. USAFA 72

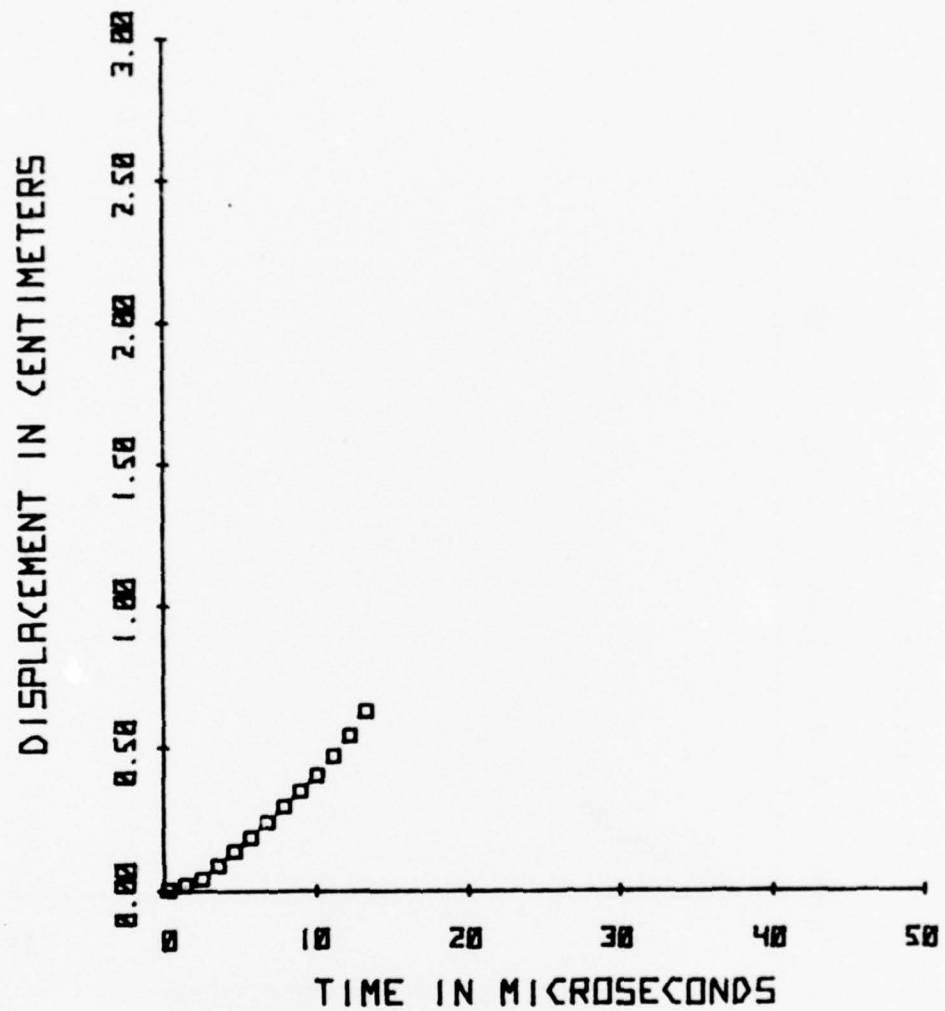


Figure 172

TEST NO. USAFA 73

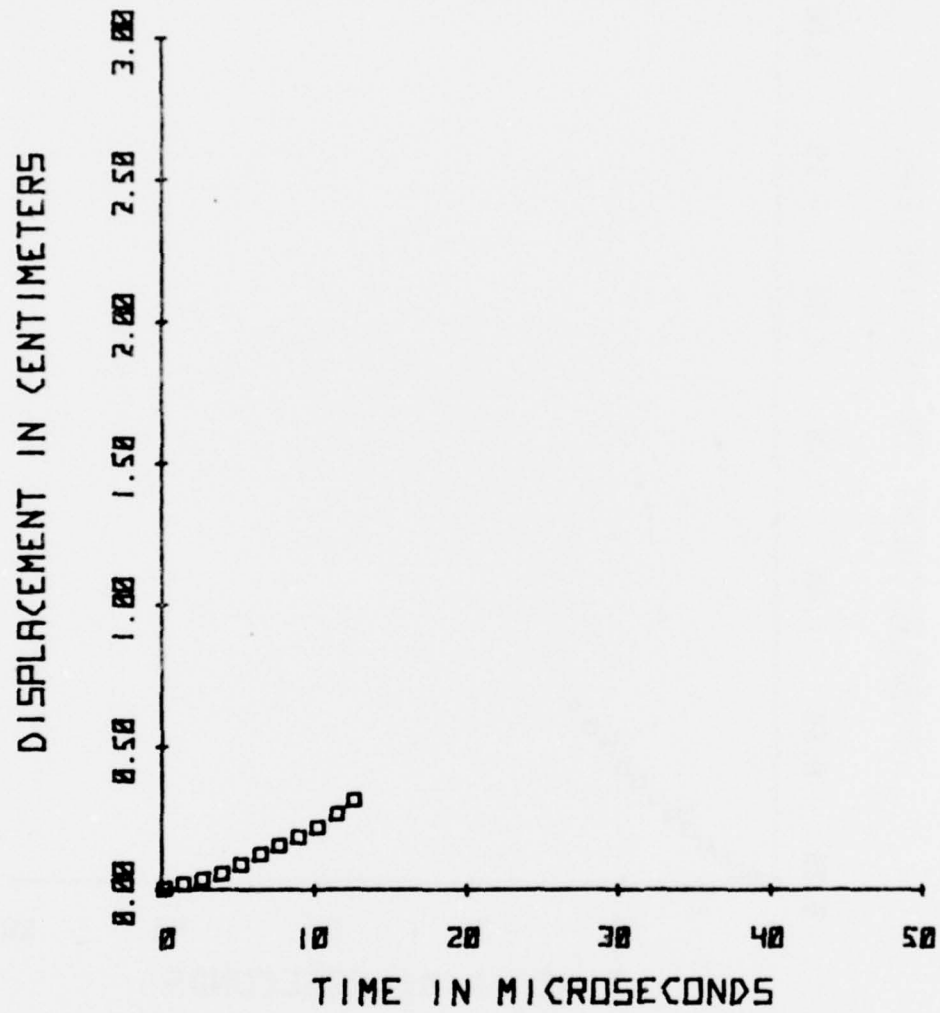


Figure 173

TEST NO. USAFA 79

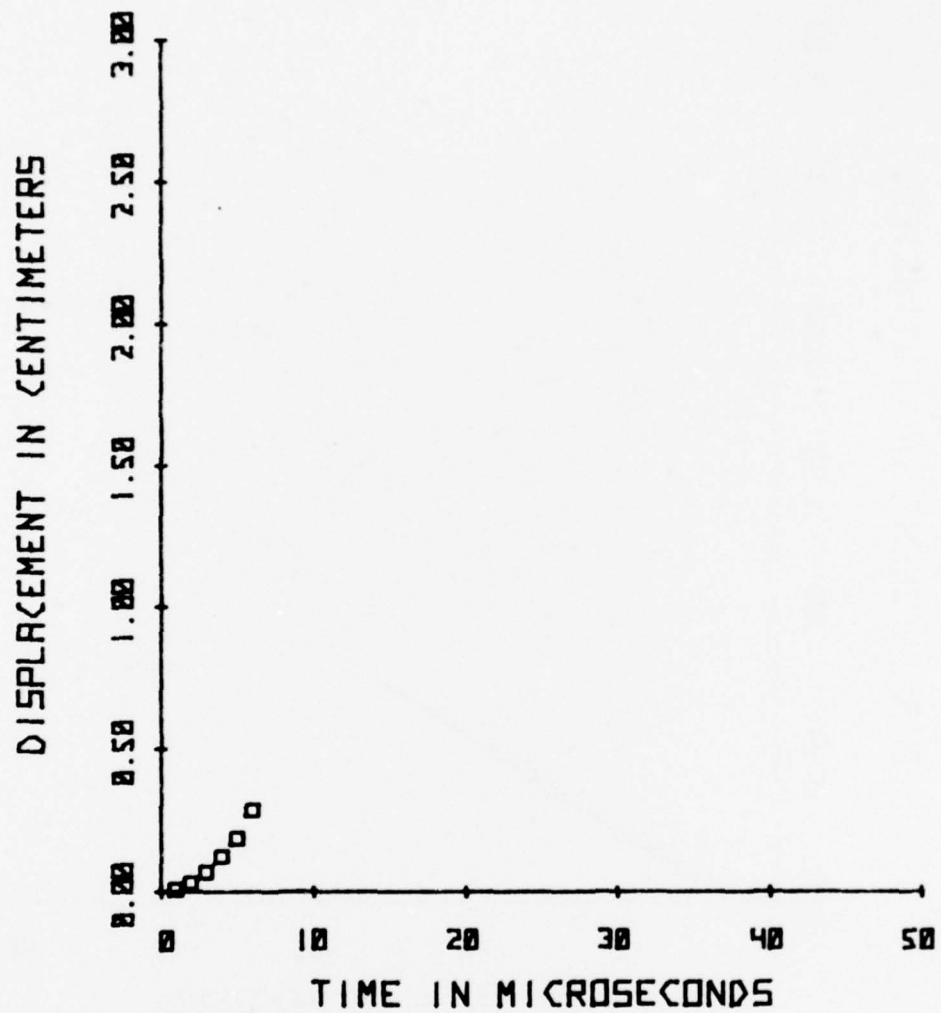


Figure 174

TEST NO. USAFA 82

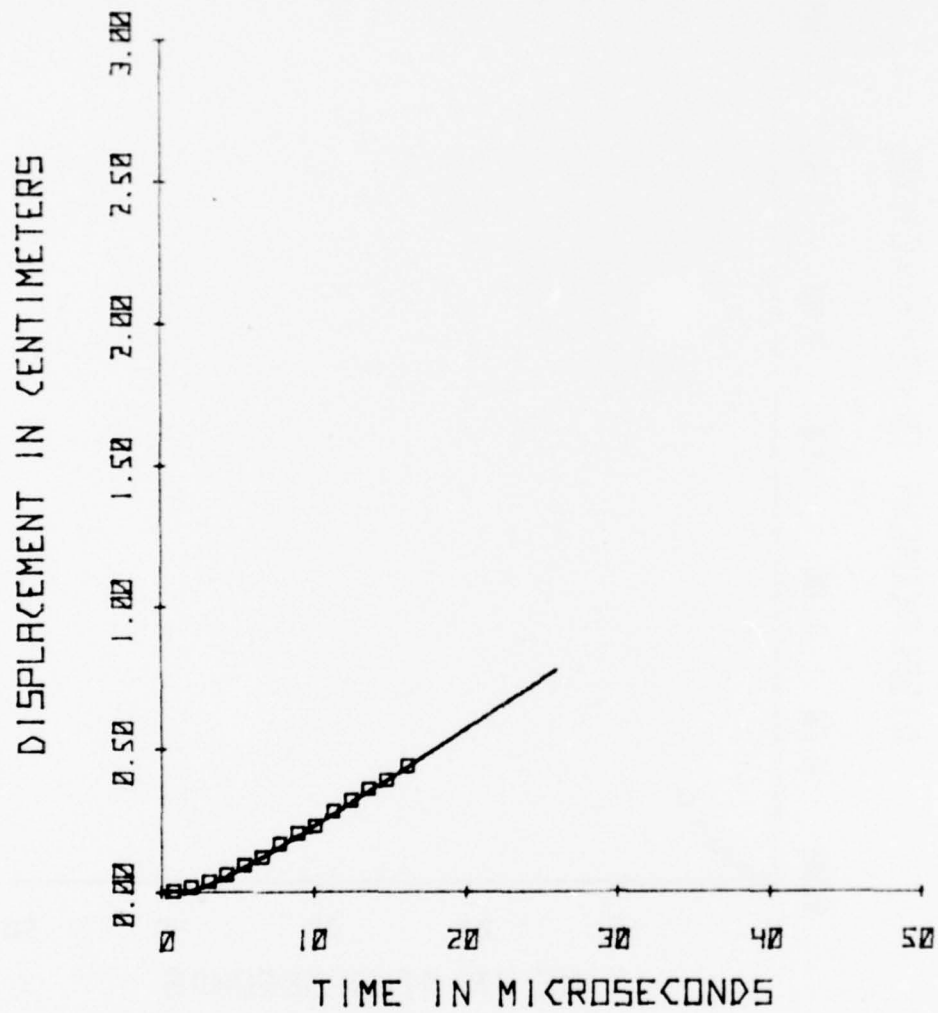




Figure 175

TEST NO. USAFA 89

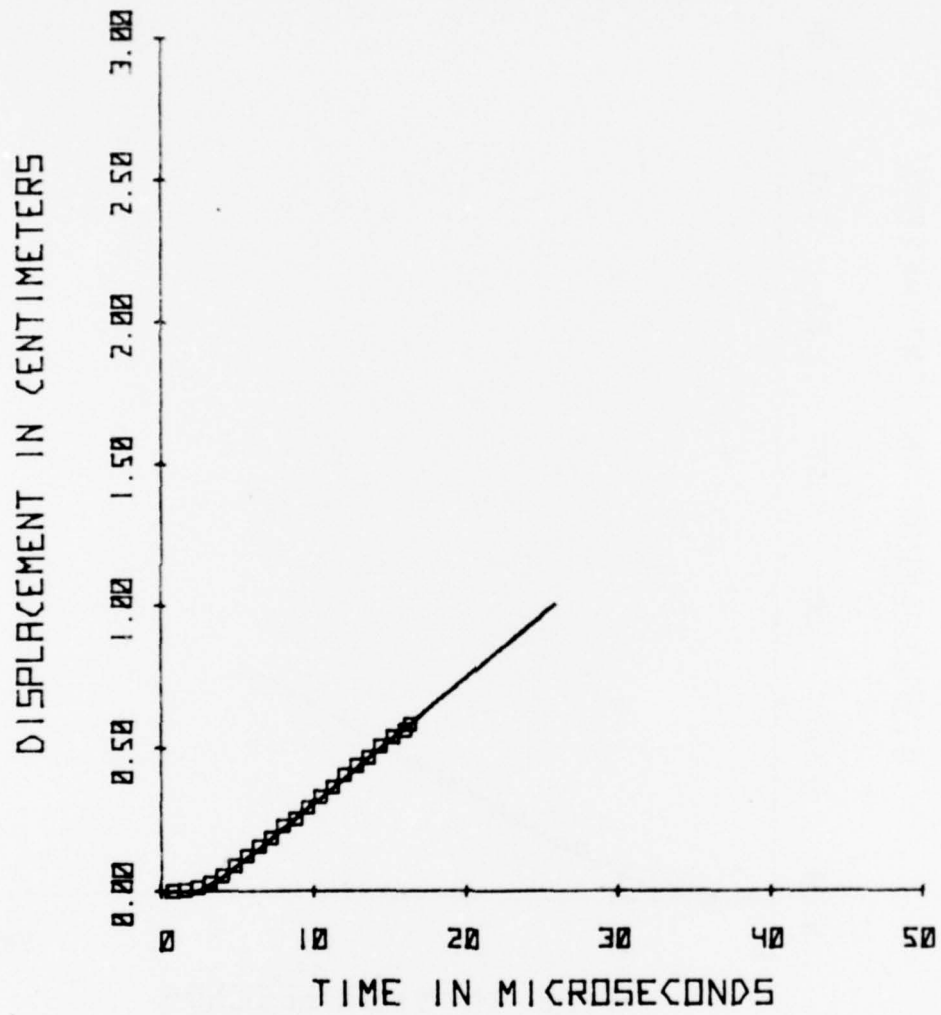


Figure 176

TEST NO. USAFA 94

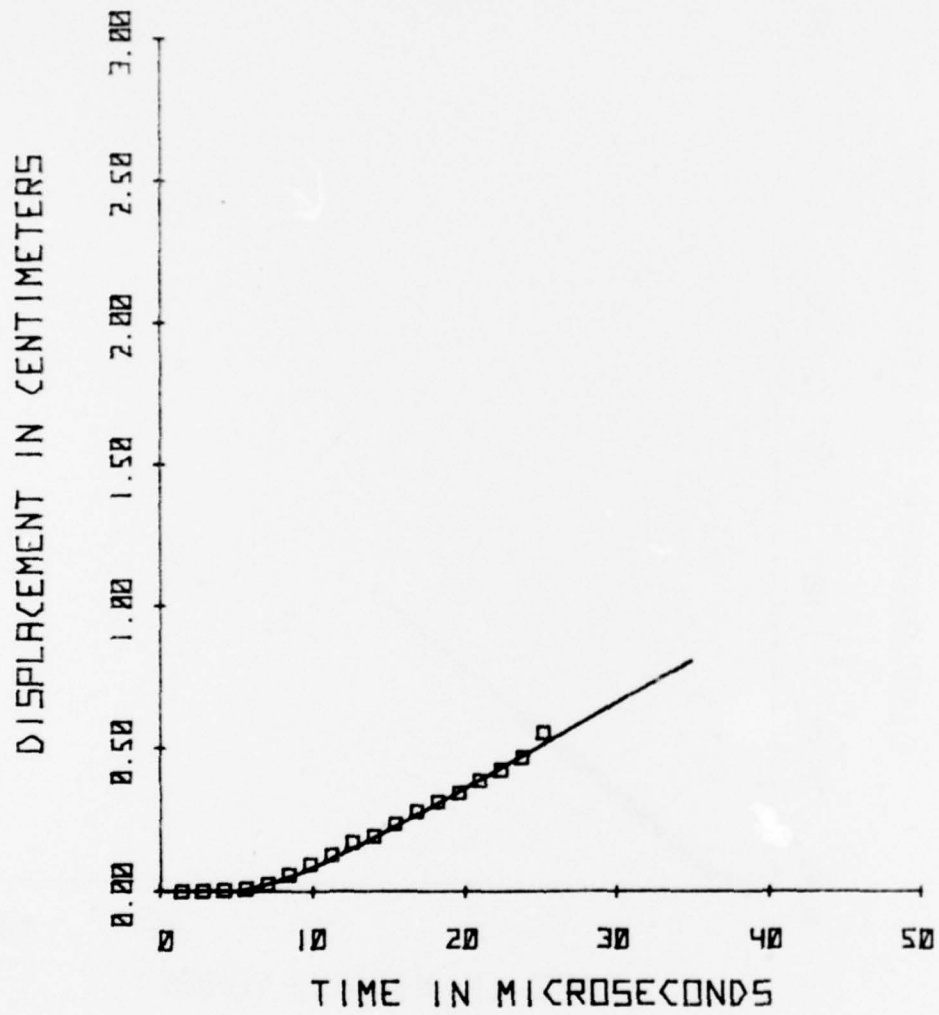


Figure 177

TEST NO. USAFA 96

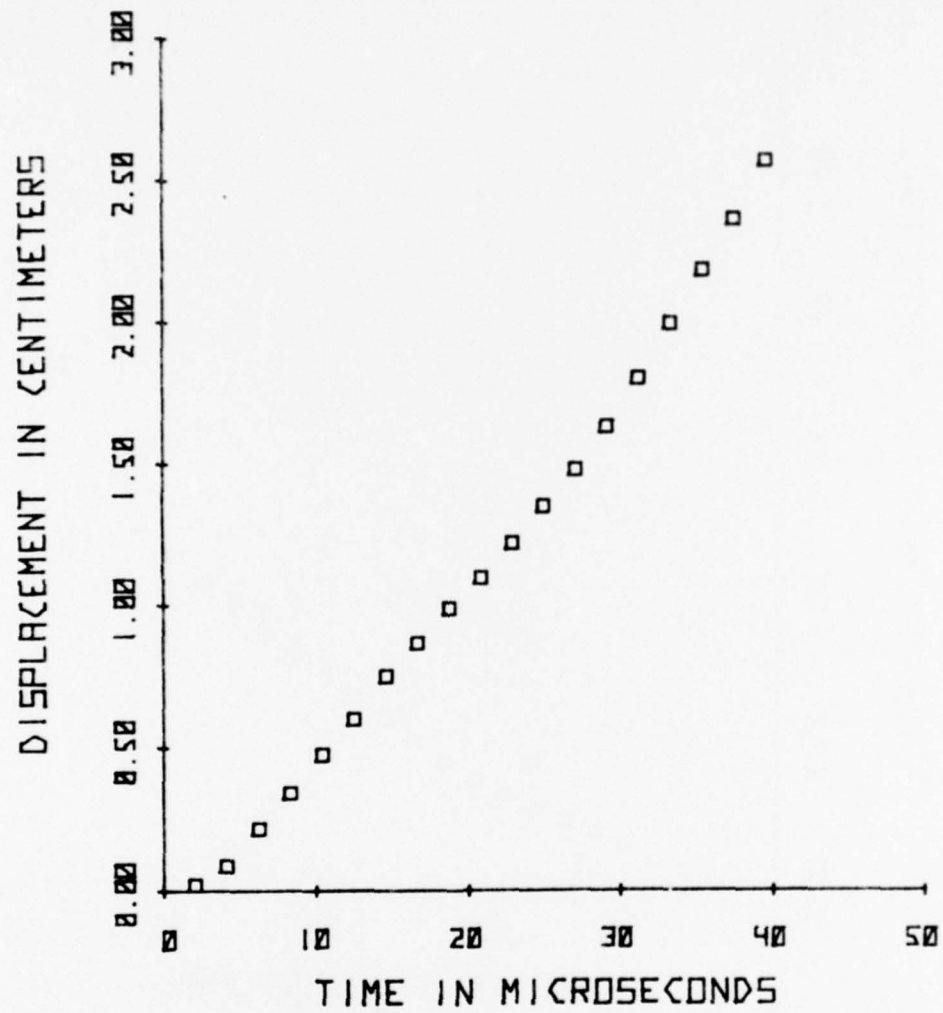


Figure 178

TEST NO. USAFA 97

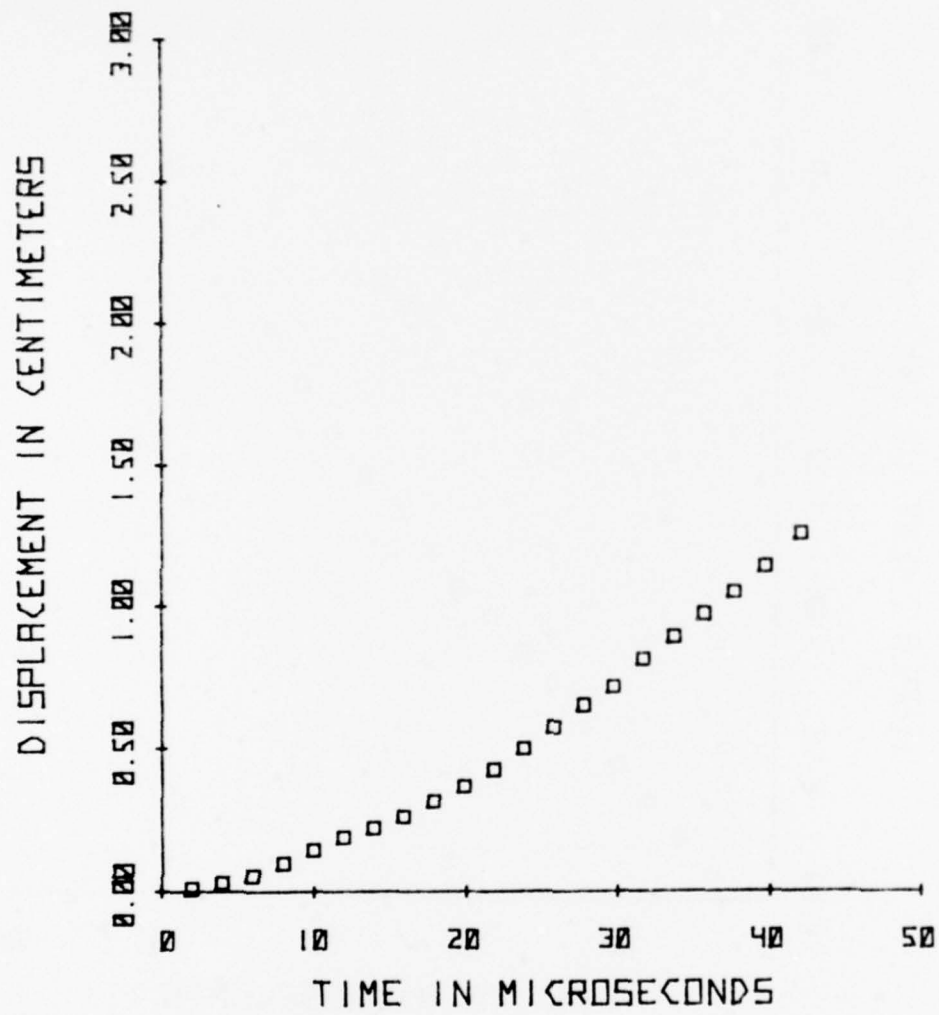


Figure 179

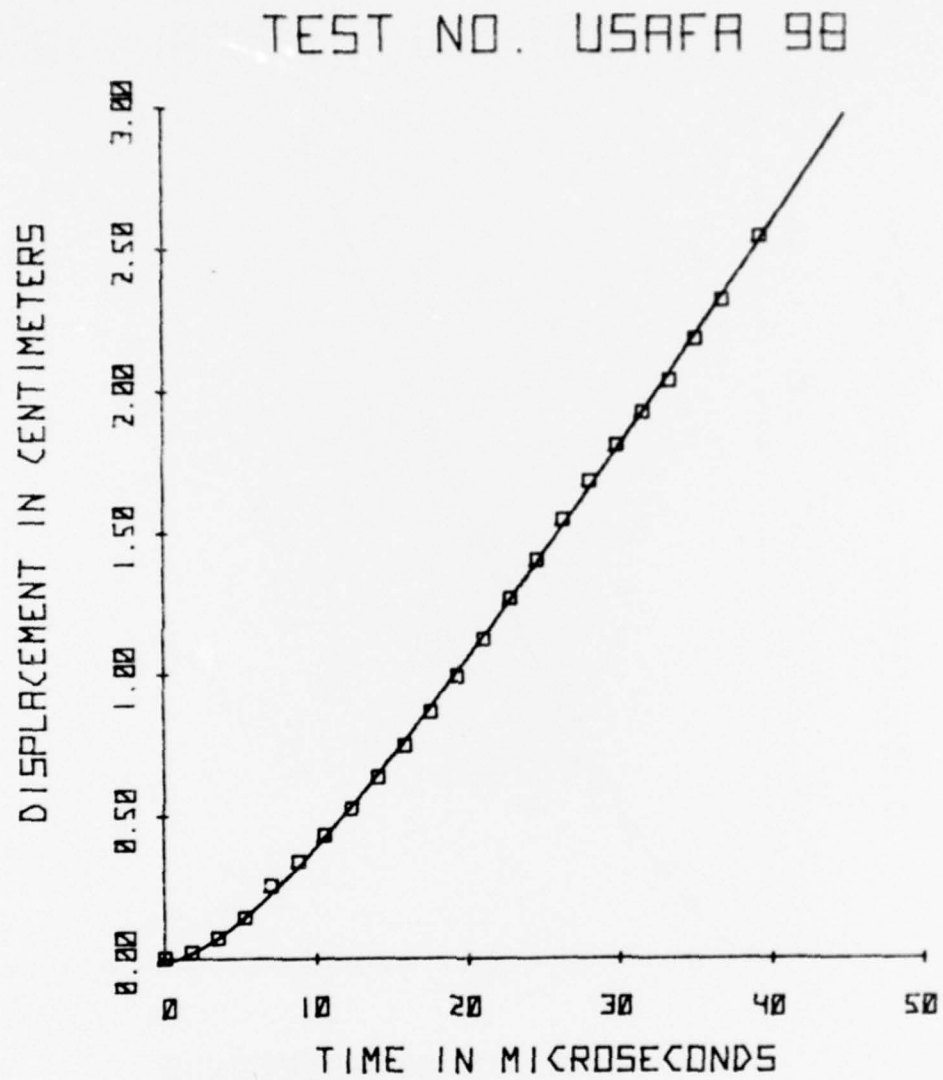


Figure 180

TEST NO. USAFA 110

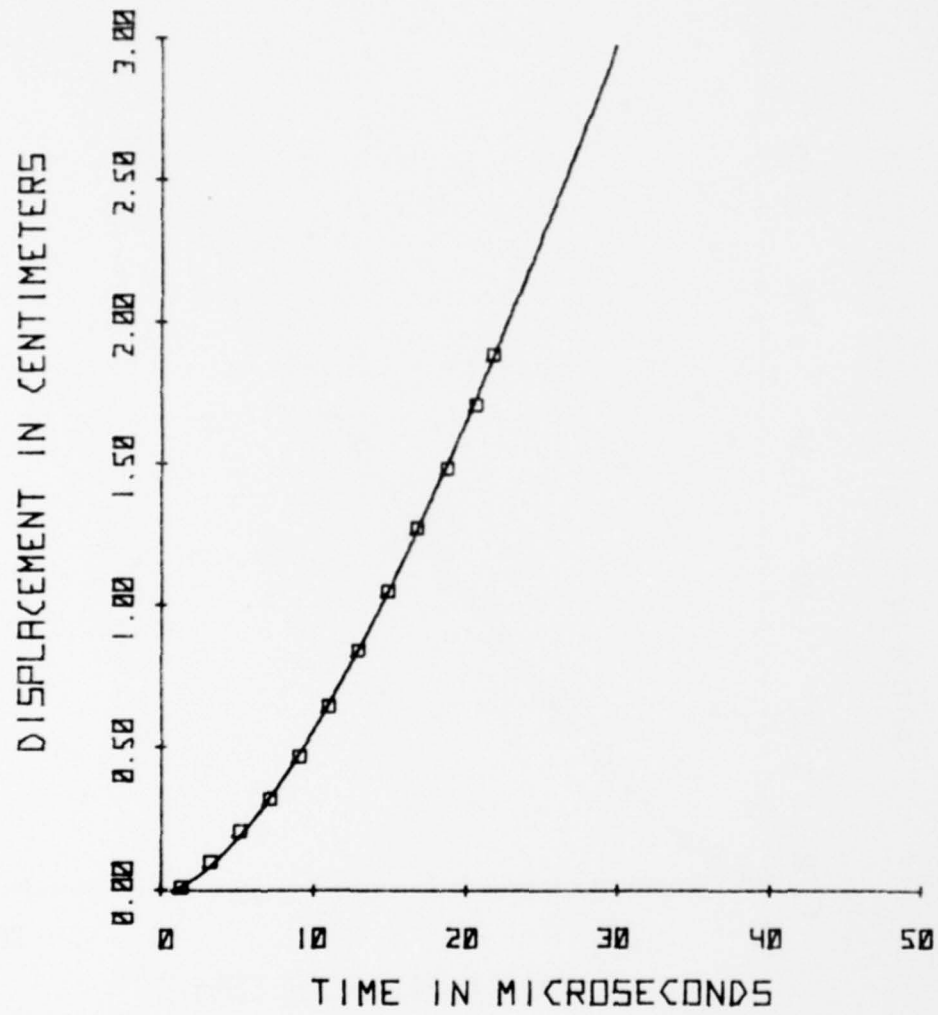




TABLE 115  
FLYER PLATE POSITION-TIME PARAMETERS

Series	Shot	n	a	b	v	h
			$\mu\text{sec}^{-1}$	cm	cm	$\mu\text{sec}$
LASL	1311	1.7180	0.1321	0.3568	0.1773	7.5700
	1312	1.7171	0.1046	0.9476	0.4713	9.5602
	1317	2.0742	0.1149	0.4438	0.1761	8.7032
	1321	1.9015	0.1013	0.5310	0.2336	9.8717
	1322*					
	1324	1.4450	0.0329	1.5422	0.9493	30.3951
	1325	2.0759	0.0876	0.4137	0.1640	11.4155
	1362	2.3595	0.0778	1.1987	0.4093	12.8535
DRI	3	1.8478	0.1164	0.6212	0.2827	8.5911
	4	1.6200	0.0596	0.7060	0.3770	16.7785
	5	3.3695	0.1098	0.3907	0.0892	9.1075
	6	1.7592	0.0267	3.0610	1.4782	37.4532
	7	5.3593	0.1956	0.2520	0.0348	5.1125
	8	3.6717	0.2517	0.1003	0.0208	3.9730
	9	2.8752	0.1550	0.3112	0.0854	6.4516
	11*					
	13	3.2810	0.9194	0.0586	0.0138	1.0877
	14	2.5781	0.2068	0.3282	0.1012	4.8356
	15	6.1553	0.4098	0.1513	0.0180	2.4402
	16	2.7463	0.3413	0.0852	0.0245	2.9300
	22	2.0538	0.0897	0.5748	0.2307	11.1483
	24	2.0179	0.0955	0.4174	0.1711	10.4712
	28*					
USAFA	45	4.5203	0.3366	0.0841	0.0139	2.9709
	46	2.0010	0.2283	0.1293	0.0535	4.3802
	48	3.1738	0.2056	0.1701	0.0415	4.8638
	51	3.6777	0.1606	0.4702	0.0975	6.2267
	54*					
	55*					
	57	2.6894	0.1882	0.3809	0.1120	5.3135
	59	2.3967	0.0707	1.1690	0.3920	14.1443
	60	2.7981	0.7681	0.0560	0.0157	1.3019
	62A	1.5505	0.0872	0.5816	0.3278	11.4679
	72*					
	73*					
	79*					
	82	2.2515	0.2703	0.1294	0.0467	3.6996
	89	4.2740	0.3366	0.1314	0.0231	2.9709
	94	3.5597	0.1228	0.2480	0.0533	8.1433
	96*					
	97*					
* did not converge	98	1.6258	0.0770	1.0874	0.5781	12.9870
	110	1.6572	0.0414	4.1975	2.1799	24.1546

TABLE 116  
FLYER PLATE COLLISION PARAMETERS

Series	Shot	Standoff Distance	Impact Velocity	Collision Angle
		S	V P	$\alpha$
		cm	cm/ $\mu$ sec	DEG
LASL	1311	0.6350	0.04354	8.35
	1312	1.2700	0.08876	18.13
	1317	1.2700	0.04937	10.75
	1321	1.2700	0.05122	8.86
	1324	2.5400	0.04653	8.86
	1325	2.5400	0.03592	7.88
	1362	1.2700	0.08307	14.45
DRI	3	1.2700	0.06791	13.11
	4	1.2700	0.03884	10.49
	5	1.2700	0.04267	9.69
	6	0.6350	0.04735	10.91
	7	0.3175	0.04878	9.03
	8	0.3175	0.02515	5.97
	9	0.6350	0.04692	9.14
	13	0.6350	0.05387	9.34
	14	1.2700	0.06717	12.34
	15	1.2700	0.06200	11.24
	16	0.3175	0.02882	5.55
	22	1.2700	0.04909	9.03
	24	1.2700	0.03864	7.47
USAFA	45	1.2700	0.02831	5.24
	46	1.2700	0.02939	5.61
	48	0.6350	0.03480	6.12
	51	0.3175	0.06709	10.75
	57	0.6350	0.06842	10.54
	59	1.2700	0.07406	10.23
	60	1.2700	0.04301	6.99
	62A	0.3175	0.03940	6.09
	82	0.6350	0.03462	5.07
	89	0.6350	0.04421	4.93
	94	0.6350	0.03022	4.83
	98	2.5400	0.07897	13.10
	110	1.9050	0.12795	12.59

F. The Influence of Collision Parameters on the Strength and Microstructure of an Explosion Welded Aluminum Alloy (by R. H. Wittman)

1. INTRODUCTION

The quantitative understanding of explosion welding has progressed slowly since the inception of the process some 19 years ago. Substantial effort has been devoted to certain features of the explosion welding process, namely the mechanics of wave formation. However, this approach, for the most part, has not contributed substantially to a better technique of explosion welding application or a greater ability to predict the precise conditions that will result in optimum weld quality. In fact, few experiments have been conducted that provide quantitative data to support the hydrodynamic theory of wavy bond zone formation (The author does not doubt the validity of the hydrodynamic argument). As a result, the selection of explosion welding parameters is still strongly influenced by experience gained through trial and error methods, an expensive and often unsatisfactory procedure.

Through careful measurement of collision parameters during a few explosion welding experiments, it has been possible to delineate the range of optimum collision parameters for an aluminum alloy weld. Optimum collision parameters are those which bond tensile strength exceeds parent metal strength. A simple, inexpensive method was used to determine collision point and detonation front distance-time profiles from which collision angle and detonation

velocity can be calculated. Several such experiments, followed by mechanical property and microstructure analyses have proven to be worth hundreds of non-instrumented explosion welds. The above technique is generally applicable to any metals combination and welding geometry.

The results show that weldability increases as the collision point velocity decreases toward a critical flow transition velocity. The range of optimum plate impact velocities can be defined as a function of collision point velocity and collision angle. Four criteria bounding the optimum weld range are described. Such information has been valuable for the designed use of explosion welding in development of certain applications. In particular it is possible to select optimum parallel or preset angle welding parameters in accordance with the detonation velocity of the available explosive. If thorough explosive characterization is available, then accurate explosive loading predictions, to yield the required flyer plate velocity, can be made. Analysis of weld microstructure and mechanical properties, with correlation to known impact conditions, will eventually lead to a more comprehensive understanding of the explosion welding process.

## 2. EXPERIMENTAL DETAILS

This study of explosion weldability was conducted entirely on 6061-T651 aluminum alloy, which has the following normal chemical composition:

	<u>Mg</u>	<u>Si</u>	<u>Cu</u>	<u>Cr</u>	<u>Al</u>
wt. %	1.0	0.6	0.27	0.20	balance

T651 designates the precipitation-hardened condition which is characterized by the following typical mechanical properties:

<u>Strength, ksi (MPa)*</u>		<u>Uniform</u>	<u>Brinell Hardness</u>
<u>Yield</u>	<u>Ultimate</u>	<u>Elongation</u>	<u>(500 Kg, 10 mm Ball)</u>
40(276)	45(310)	12%	95

\* ksi - kilo pounds per square inch

MPa - mega pascals or mega newtons per square meter

Explosion welding was accomplished using both the preset angle and parallel geometries, and a variety of explosives designed to produce the desired range of collision point velocities. An illustration of the general configuration defining important terms is shown in Figure 181.

The use of two pressure-actuated, continuous-writing velocity probes in each experiment made it possible to determine the position of the detonation front and the collision point at the same instant of time. Using this principle it was possible to reconstruct the collision profile along the weld length, and determine the collision angle ( $\alpha$ ), collision point velocity (used interchangeably with flow velocity) ( $V_c$ ), impact velocity ( $V_p$ ) and detonation velocity ( $V_D$ ) at any point.

The velocity probe technique was developed by the U.S. Bureau of Mines Explosives Research Center between 1963 and 1967 and described in the literature in 1968 (Ribovich, 1968). The probe consists of an aluminum tube of 0.058 cm diameter and 0.0038 cm wall thickness, having a skip-insulated resistance wire of 0.0076 cm diameter on the tube axis as shown in Figure 182. A constant, battery-generated, direct current is passed through the tube and wire as shown in the



figure. A pressure wave of relatively small magnitude propagating along the tube collapses the tube onto the wire, shortening the electrical path and decreasing the resistance. The voltage drop across the probe is monitored by an oscilloscope, and is proportional to the uncollapsed distance along the probe. In this way the position-time profile of an advancing pressure front can be recorded.

In these experiments, aluminum flyer and base plates 0.635 cm thick by 15.24 cm wide and 30.48 cm long were explosion welded. The two velocity probes were recessed in grooves, one in the flyer plate to record the position of the detonation point front, and one in the base plate to record the position of the collision point. The probes were carefully located in the same vertical plane. The arrangement of probes in the two plates is illustrated in Figure 183.

The probes were connected to separate power supplies and the voltage drop for each monitored as a function of time using a Tektronix 555 dual-beam oscilloscope. A block circuit diagram is shown in Figure 184. A typical oscilloscope record showing detonation front and collision point distance-time traces is shown in Figure 185.

The 0.635 cm thick aluminum plates were welded using either Detasheet C or TSE 1004 sheet explosive, or 40% Extra dynamite, a granular composition. Typical detonation velocity characteristics for these explosives are shown in Figure 186. The collision point velocity,  $V_c$ , was varied by explosive selection and by use of a preset angle,  $\theta$ , as shown in Figure 1. The impact velocity,  $V_p$ , was changed by adjusting the explosive loading and the standoff,  $S$ . Prior to welding, the aluminum plates were cleaned using a NaOH



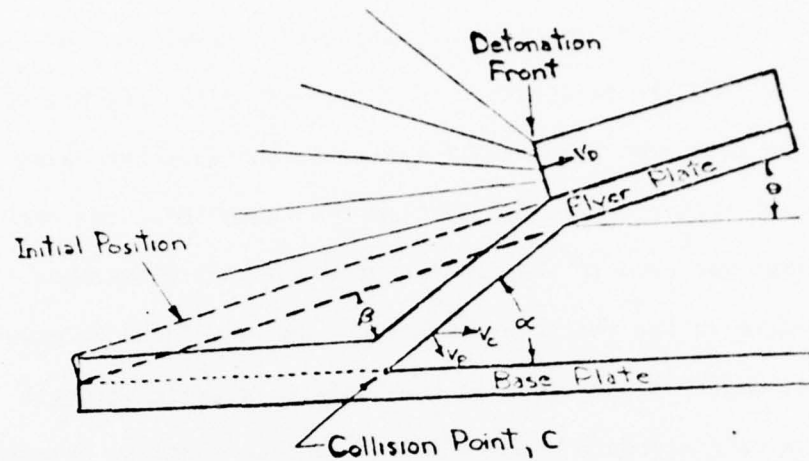


Figure 181. The Generalized Explosion Welding Configuration and Definition of Parameters. Parallel Geometry occurs when  $\theta = 0$ .

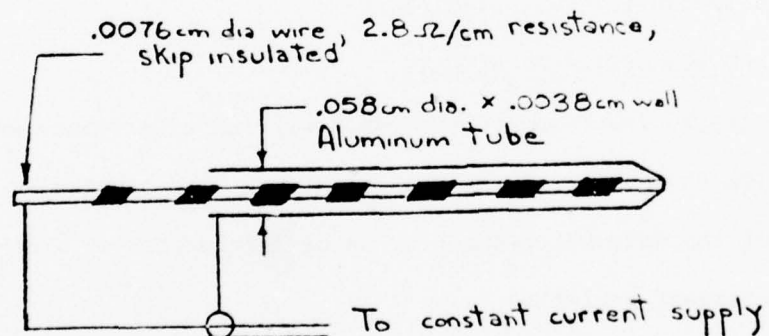


Figure 182. Continuous Writing Velocity Probe

solution, rinsed in warm water and dried, resulting in a bright, metallic lustre.

After welding, mechanical test samples were taken at 7.62, 15.24, and 22.86 cm from the initiation end of the 30.48 cm long welded plates. The weld tensile strength was measured using the "zero gauge length" test specimen illustrated in Figure 187. The same test specimen was used to measure the strength of a homogenous aluminum plate in the thickness direction, and was found to produce fracture strength values equal to the ultimate tensile strength measured using a standard sheet or plate tensile specimen oriented in the rolling direction. When the weld zone was properly located, the test specimen accurately reflected the strength of the weld and immediately adjacent material, since failure was made to occur in that plane. The weld tensile strength was determined by dividing the load at fracture by the initial test area. Samples for metallographic analysis were taken from the spaces remaining in the welded plates between mechanical test samples.

### 3. ANALYSIS AND DISCUSSION OF RESULTS

Approximately 20 instrumented explosion welding experiments were conducted during the course of the investigation. The physical significance of the data was deduced by using a framework of independent and dependent variables.

Four concepts seem to provide the necessary bounding criteria to describe optimum explosion welding characteristics. They are:

- A. The critical collision angle for jet formation,

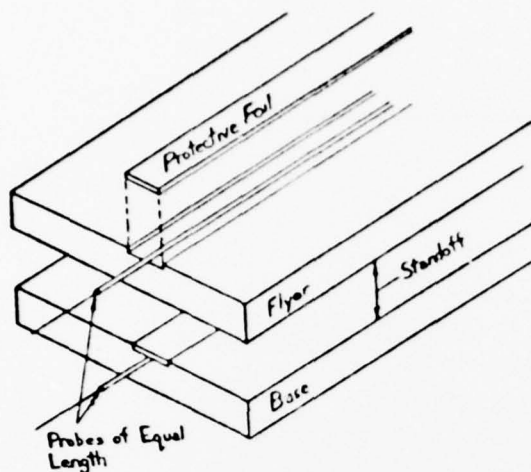


Figure 183. Arrange of Velocity Probes in Flyer and Base Plates of Explosion Welding Experiment.

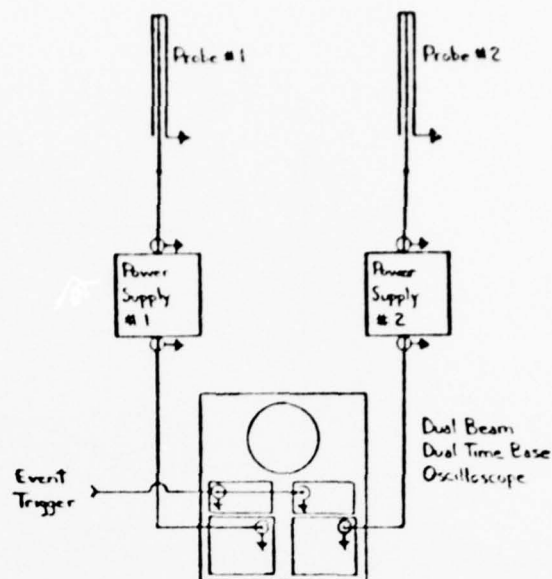


Figure 184. Block Circuit Diagram of Velocity Measuring System.

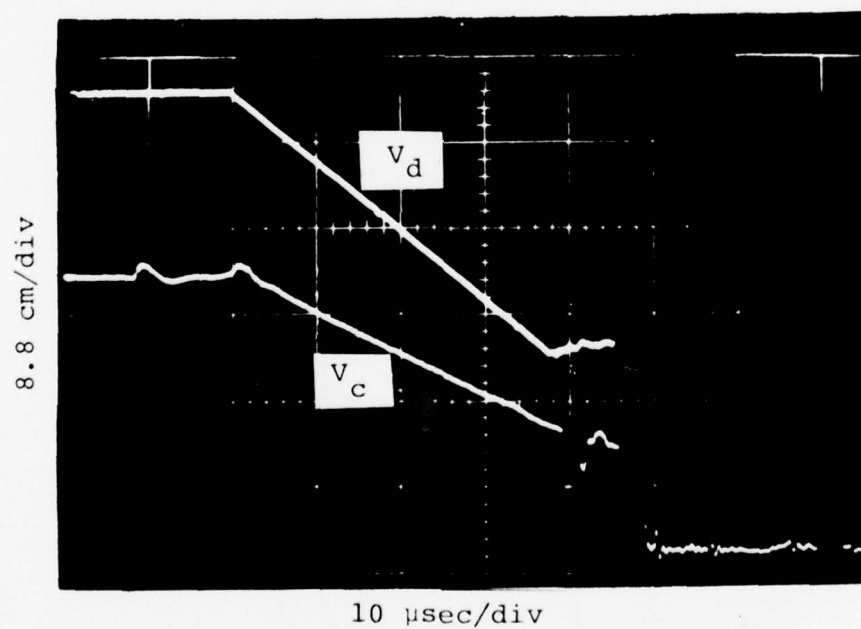


Figure 185. Typical Oscilloscope Record of Detonation Front and Collision Point Distance-Time Profiles.

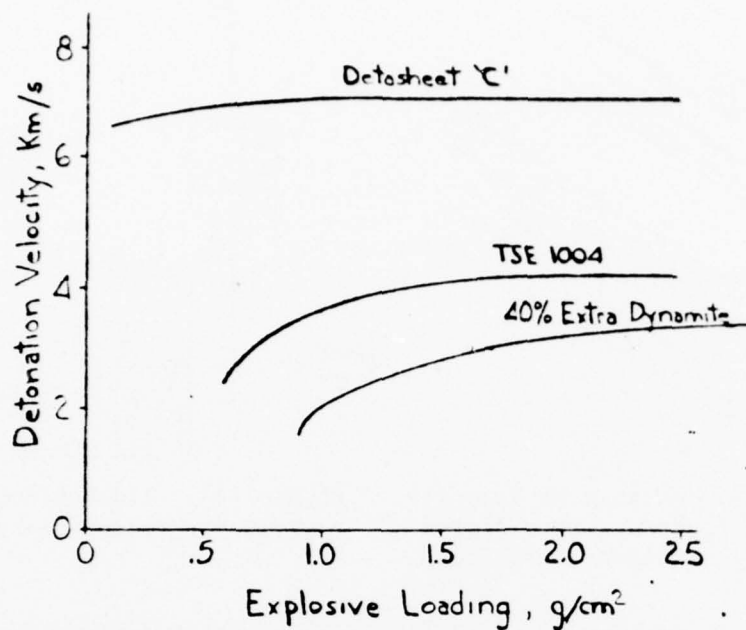


Figure 186. Detonation Velocity as a Function of Explosive Loading.

$\rho$  for Detasheet 'C' = 1.4 g/cm<sup>3</sup>  
 $\rho$  for TSE 1004 = 1.2 g/cm<sup>3</sup>  
 $\rho$  for 40% Extra Dynamite = 1.3 g/cm<sup>3</sup>

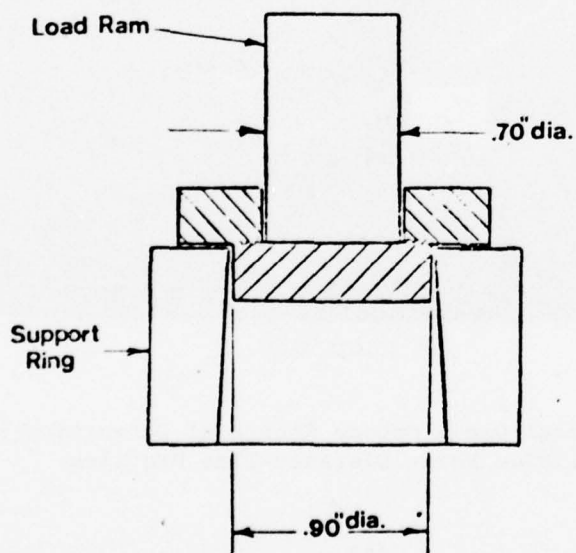


Figure 187. Weld Tensile Test Configuration

- B. The critical impact pressure for jet formation in the subsonic regime,
- C. The critical flow-transition velocity, and
- D. The kinetic energy of the flyer plate and the heat dissipation characteristics of the collision region.

These boundary conditions can be simultaneously represented in a plot of collision angle,  $\alpha$  VERSUS collision point velocity,  $V_c$ , which are related to impact velocity,  $V_p$ , by the equation

$$V_p = 2V_c \sin \frac{\alpha}{2} \quad (1)$$

Equation (1) is obtained by assuming the vector,  $V_p$  in Figure 1 to be perpendicular to the line bisecting the collision angle,  $\alpha$ .

This equation applies to either the preset angle or parallel explosion welding geometry, as it deals only with the collision parameters, not initial or intermediate parameters such as preset angle, dynamic bend angle, or detonation velocity. Figure 188 shows the four bounding criteria, using coordinates  $V_c$  and  $\alpha$ . Experimental data (e.g., microstructure and weld tensile strength) are plotted as a function of the collision parameters  $V_c$  and  $\alpha$  in Figure 189 and 190.

#### a. The Critical Collision Angle for Jet Formation

The concept of a critical collision angle for jet formation has been described by Walsh, et al (1953) and Cowan and Holtzman (1963). It provides an upper flow velocity boundary and the related impact velocity or collision angle. At flow velocities higher than critical, the collision is jetless and presumably no welding occurs. At flow velocities below the boundary, jetting occurs and welding can occur.

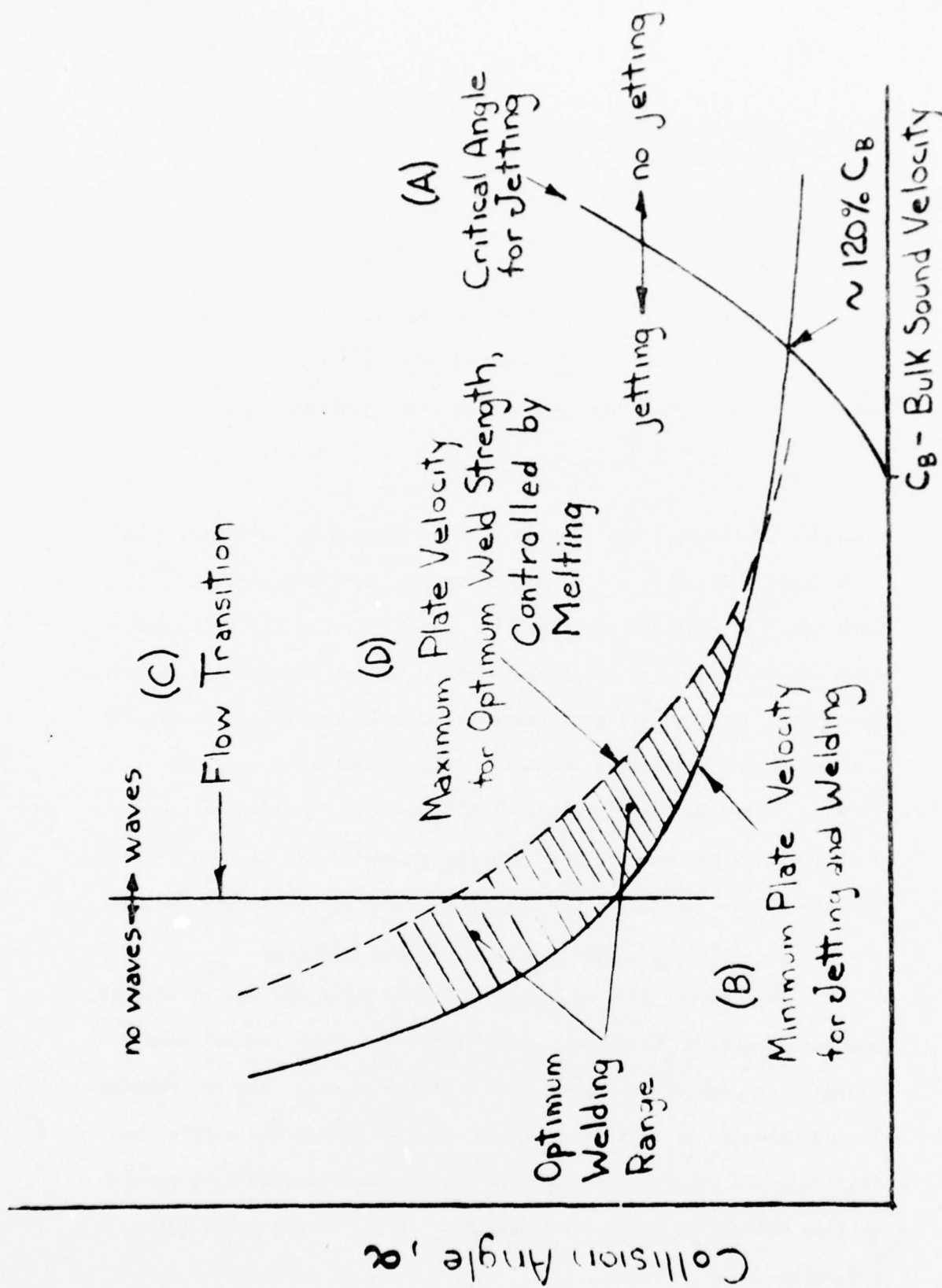


Figure 188. Four Conditions Bounding the Optimum Welding Range Represented Schematically as Functions of  $V_c$  and  $\alpha$ .



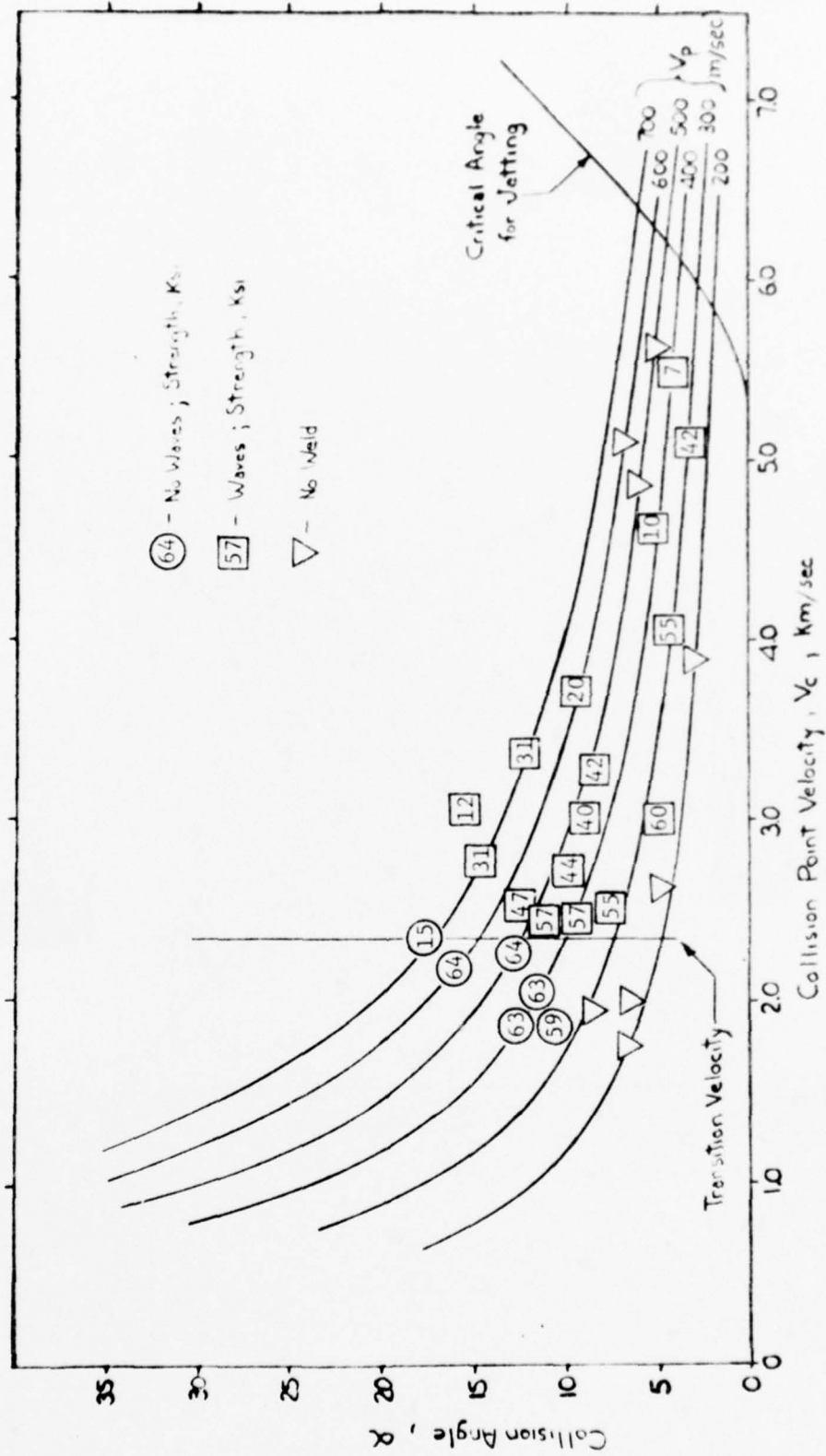


Figure 189. Weld Tensile Strength Data as a Function of  $V_c$  and  $\alpha$ .

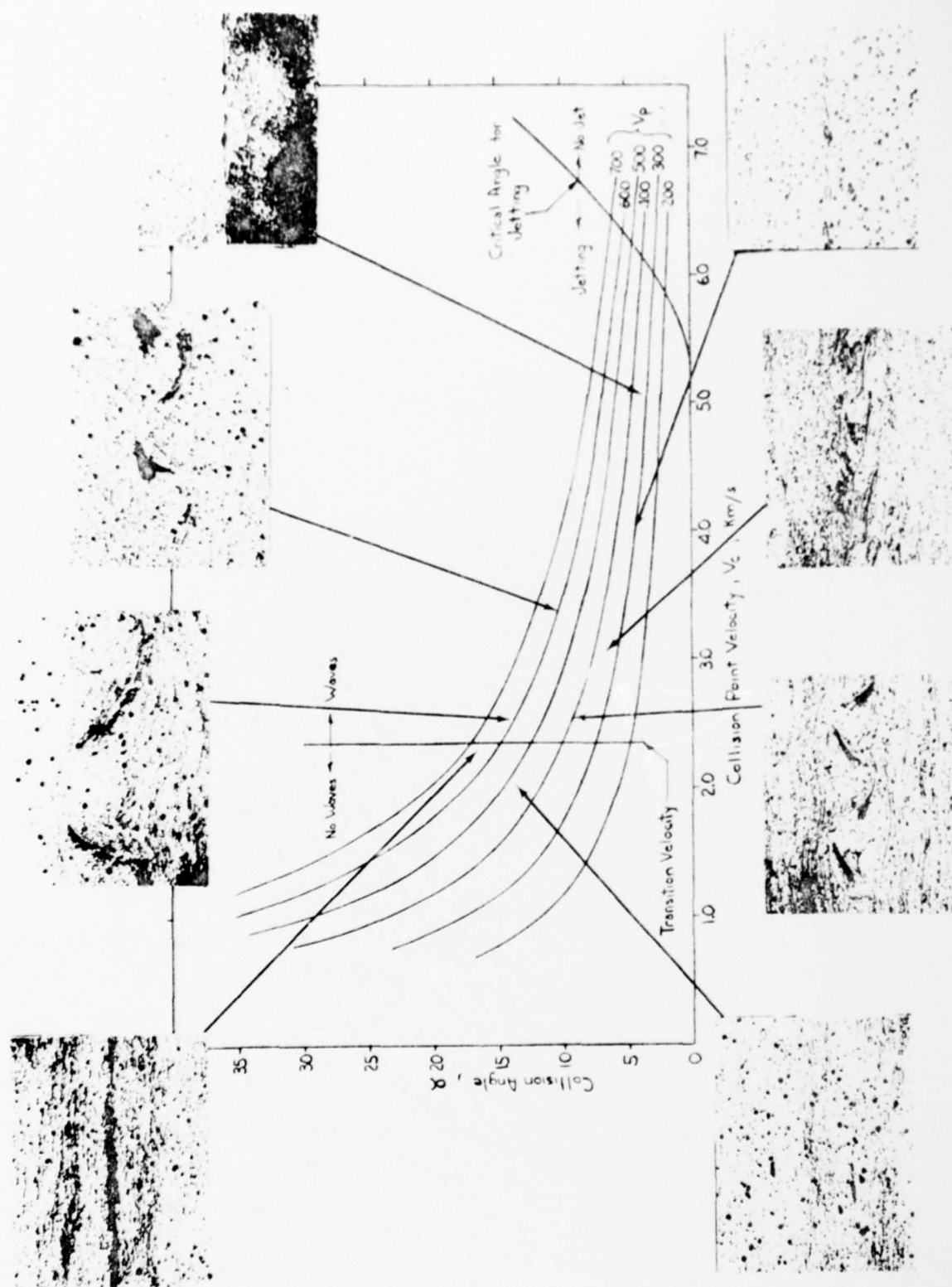


Figure 190. Weld Microstructure as a Function of  $V_c$  and  $\alpha$ .

The critical collision angle for jetting can be calculated as described in (Walsh, 1953). At a  $0^{\circ}$  collision angle the flow velocity boundary begins at the bulk sound velocity for 6061 aluminum (5350 m/s) and increases as the collision angle increases (see Figure 188). The exact slope of this boundary is of little importance since most practical welding activities take place well to the left in the subsonic regime. In fact, verification of this boundary by welding experiments is difficult because of problems encountered in obtaining a weld in that region.

b. The Critical Impact Velocity (or Impact Pressure) in the Subsonic Regime

The description of a critical angle for jetting and its importance to explosion welding gives the impression that jetting and hence welding can occur everywhere in the subsonic regime. Practical experience indicates this is not true, and it can be reasoned that jetting is not likely in the subsonic regime when the impact velocity (or impact pressure) approaches zero. At low impact pressures the metal no longer behaves as a fluid (a necessary behavior in (Walsh, 1953) and (Cowan, 1963)), but rather as an elastic-plastic solid. Clearly in the latter case some non-zero flow stress must be exceeded in order to produce flow and jetting. It is therefore reasonable that some non-zero impact velocity (pressure) must be exceeded for flow and jetting to occur.

The assumed existence of a critical impact pressure at collision point velocities lower than the bulk sound speed has been used as a criteria for welding parameter selection since about 1969 (Wittman,

1972)(Ezra, 1973). Recent experimental work (reported elsewhere in this report) shows that a lower critical impact pressure does indeed exist for aluminum. However, that data was determined for a narrow range of flow velocities and a wide range of flyer-plate thicknesses. The present data extends that conclusion to a wider range of flow velocities. Since impact pressure is related to impact velocity through the pressure-particle velocity equation of state, a lower critical impact velocity must also exist. For 6061-T6 aluminum alloy, data in Figures 189 and 190 and elsewhere in this report, establish this minimum velocity to be about 270 m/s for impact angles below about  $5^\circ$ , corresponding to a pressure of 21 kbar. The minimum velocity appears to increase to at least 350 m/s at higher collision angles in order to maintain a constant normal stress.

At present the minimum flyer plate impact velocity in aluminum and other alloys is estimated by multiplying the Hugoniot elastic limit (HEL) pressure by 5, then determining the corresponding impact velocity using the pressure-particle velocity equation of state. An alternate method used in the absence of HEL data, and which appears to be a good approximation, is to use the purely empirical expression

$$V_{p,min} = \frac{\sigma_{TS}}{\rho}^{1/2} \quad (2)$$

where  $\sigma_{TS}$  is the ultimate tensile strength in  $N/M^2$  and  $\rho$  the density in  $Kg/M^3$ . Using 5.4 kb for the HEL of 6061-T6 aluminum (Lundergan, 1963), a minimum pressure of 27 kb is obtained, corresponding to an impact velocity of 350 m/s. The alternate method predicts a minimum

of 339 m/s. Both values are in fair agreement with the experimentally determined value of 270 m/s.

c. The Critical Flow Transition Velocity

The existence of a critical flow (collision point) velocity for transition to turbulent flow (wavy bond zone) has been noted or discussed by Deribas, et al (Deribas, 1967), Burkhardt, et al (Burkhardt, 1967) and Cowan et al (Cowan, 1971). Cowan et al developed a means for predicting the critical flow velocity that seems both accurate and useful. They used flyer and base plate density ( $\rho_F$  and  $\rho_B$ ) and static hardness ( $Hd_F$  and  $Hd_B$ ) as the yield criteria in an expression defining the Reynolds number,  $R_T$ , at the flow transition velocity,  $V_T$ . Their expression is

$$R_T = \frac{(\rho_F + \rho_B) V_T^2}{2(Hd_F + Hd_B)} \quad (3)$$

and gives values of  $R_T$  ranging from 8.1 to 13.1 for both symmetric and asymmetric cladding configurations, the average  $R_T$  being 10.6.

The author prefers to use the Hugoniot elastic limit (HEL) as the yield criterion instead of static hardness. Using reported HEL data with the collision point velocity at transition,  $V_T$ , in (Cowan, 1971) and equation (3) the value of  $R_T$  becomes 12.6 with a range of static hardness may prove to be entirely satisfactory.

The flow transition velocity reported in (Cowan, 1971) for 6061-T6 aluminum was confirmed by this study. Based on data plotted in Figures 9 and 10 the flow transition velocity is estimated to be 2350 m/s  $\pm$  50 m/s. The value in (Cowan, 1971) is 2300 m/s and the value calculated using an HEL of 5.4 kb and  $R_T$  of 12.6 is 2240 m/s.



d. The Kinetic Energy of the Flyer Plate and the Heat Dissipation Characteristics of the Collision Region

The range of optimum impact velocities,  $V_p$ , beyond the minimum seems to be controlled by the thermo-physical properties and the melting point of the metals being welded. A fraction of the impact kinetic energy of the flyer plate is converted into energy of the jet and remains within the system. Data for copper, nickel and aluminum indicate this fraction can be expressed approximately as

$$f \approx N \frac{V_p^2}{C_B^2} \quad (4)$$

where  $C_B$  is the bulk sound velocity and  $N$  is an empirical coefficient.

The jet energy is converted into heat by flow deformation and friction. The heat is apparently generated within a short distance of the collision point (i.e., one deformation wave length) in a relatively small volume. Because the velocity of deformation is high, adiabatic conditions should exist (i.e.,  $dq = 0$ ), and the generated heat should manifest itself by a rapid rise in temperature. The magnitude of the temperature rise is governed by the thermo-physical properties of the unalloyed mixture of flyer and base plate metals, and the melting point of the two constituents. Presumably little superheating of the melt occurs, limiting the temperature to that of the molten metal at the melting point. As more kinetic energy and subsequently strain-generated heat is added to the collision region, the volume of melt increases. The final weld structure is determined in part by the melt volume, if any, when the free surface reflected tensile wave interacts with the collision



interface. The final weld state properties for aluminum are determined by the number and distribution of flow generated fissures, melt shrinkage voids and hot tears caused by reflected tensile stress. For optimum weld strength to be realized the interface behind the collision point must be sufficiently cooled and free of defects so that tensile wave passage can occur without rupture.

Using the above concept it is possible to determine the set of impact parameters and physical properties of the metal that lead to heat dissipation without melting during tensile wave passage.

The associated heat transfer problem is solved in Carslaw and Jaeger (Carslaw, 1959) Chapter 10, page 269. The problem is that of determining the temperature distribution in a half space  $z \geq 0$ , moving in the  $x$  direction with velocity  $U$  beneath a stationary strip of width  $2b$  in the  $x$  direction, infinitely long in the  $y$  direction and contacting the half space surface  $z = 0$ . Heat is transferred to the half space from the strip at the rate of  $Q$  per unit time per unit area. The mathematical solution is given as

$$T_{X,Z} - T_o = \frac{kQ}{\pi KU} \int_{X-B}^{X+B} e^{uK_o} \left[ (Z^2 + u^2)^{1/2} \right] du \quad (5)$$

where:

$T_{X,Z}$  = temperature in the half space at coordinates  $(X,Z)$  with respect to the strip

$T_o$  = ambient temperature

$k$  = thermal diffusivity =  $\frac{K}{\rho C}$

$K$  = thermal conductivity

$C$  = specific heat

$\rho$  = mass density

with dimensionless parameters

$$X = \frac{Ux}{2k} \quad (6a) \quad Z = \frac{Uz}{2k} \quad (6b) \quad B = \frac{Ub}{2k} \quad (6c)$$

and  $K_0(x)$  is the modified Bessel function of the second kind, zero order.

For large values of  $B$  the maximum temperature rise occurs in the plane  $z = 0$  (i.e. at the surface) near  $x = b$ , and is approximately

$$T_{MAX} - T_o = \frac{Qb}{K(\pi B)^{1/2}} \quad (7)$$

Consider the collision region, i.e., the source of heat, to be moving at a velocity  $U = V_c$  in the collision of like metals. We specify that  $T \leq T_{mp}$  (mp = melting point) at  $x = b$  when the reflected tensile stress just reaches the interface. This will happen provided

$$b = \frac{hV_c}{C_B} \quad (8)$$

where  $h$  is the flyer plate thickness and  $C_B$  is the bulk sound velocity of the flyer plate. Substitution Equation (8) into Equation (6c) for  $B$ , and setting  $U = V_c$ , we have

$$B = \frac{V_c^2 h o C}{2 K C_B} \quad \frac{Ub}{2k} = \frac{V_c}{C_B} \quad \frac{V_c^2 h}{2k C_B} = \frac{V_c^2 \rho h C}{2 K C_B} \quad (9)$$

The total amount of heat deposited per unit area of half space surface is

$$E = Q \left( \frac{2b}{U} \right) \quad (10)$$

In the case of an explosion welding event some fraction  $f$ , given by Equation (4), of the total kinetic energy per unit area of flyer plate is converted to heat.

$$E = f \left( \frac{\rho_h v_p^2}{2} \right) = \left( N \frac{v_c^2}{c_B^2} \right) \left( \frac{\rho_h v_p^2}{2} \right) \frac{N v_p^2 v_c^2 \rho_h}{2 c_B^2} \quad (11)$$

Equating the two expressions for  $E$  given by Equations (10) and (11) yields

$$E = \frac{2Qb}{U} = \frac{N v_p^2 v_c^2 \rho_h}{2 c_B^2}$$

so that, again setting  $U = v_c$ , one obtains

$$Qb = \frac{N v_p^2 v_c^3 \rho_h}{4 c_B^2} \quad (12)$$

Substitution of Equations (12) and (9) into Equation (7) then yields

$$\begin{aligned} T_{mp} - T_o &= \frac{Qb}{K \sqrt{\pi B}} = \frac{N v_p^2 v_c^3 \rho_h}{4 c_B^2 K} \sqrt{\frac{2 K c_B}{\pi v_c^2 \rho_h C}} \\ &= \frac{N v_p^2 v_c^2}{2} \sqrt{\frac{\rho_h}{2 \pi K C c_B^3}} \end{aligned} \quad (13)$$

Solving for the upper limiting value of impact velocity,  $V_{P, MAX}$  one obtains

$$V_{P, MAX}^2 = \frac{2 (T_{mp} - T_o)}{N V_c^2} \frac{2\pi KCC_B^3}{\rho h}$$

so that

$$V_{P, MAX} = \frac{1}{N h^{1/4} V_c} \frac{8\pi KCC_B^3 (T_{mp} - T_o)^{2^{1/4}}}{\rho} \quad (14)$$

Using values of physical constants for 6061-T6 aluminum from Table 117, and assuming that  $T_o = 60^\circ F = 16^\circ C$ , Equation (14) then yields

$$\begin{aligned} V_{P, MAX} &= \frac{1}{N h^{1/4} V_c} \frac{(8\pi)(1.54 \times 10^7)(9.61 \times 10^6)(5.35 \times 10^5)^3(652-16)^{2^{1/4}}}{2.70} \\ &= \frac{3.0393 \times 10^9}{N h^{1/4} V_c} \end{aligned} \quad (15)$$

Test results indicate that for 6061-T6 aluminum,

$$V_{P, MAX} = \frac{11.68 \times 10^9}{h^{1/4} V_c} \quad (16)$$

so that

$$\frac{1}{N} = \frac{11.68}{3.0393}^2 = 14.77 \quad (17)$$

Equation (16) is plotted in Figure 191 along with the other three boundary conditions for 6061-T6 aluminum.

Table 117. Mechanical-Physical Properties of Selected Metals and Alloys and Their Weldability Rating

Metal	$\frac{\text{g}}{\text{cm}^3}$	$\frac{\text{dynes}}{\text{cm}^2}$	$\frac{\text{cm}}{\text{sec}}$	$\frac{^\circ\text{C}}{^\circ\text{C}}$	$\frac{\text{cm}^2\text{sec}^\circ\text{C}}{^\circ\text{C}}$	$\frac{\text{erg}}{\text{g}^\circ\text{C}}$	$\frac{V_{\text{p max}}}{V_{\text{p min}}}$	Silver
Silver (1/2 hard)	10.49	$20 \times 10^8$	$2.8 \times 10^5$	960	$4.18 \times 10^7$	$.234 \times 10^7$	0.848	1
Aluminum 1100-0	2.71	9	5.1	657	2.22	.961	0.777	.92
Copper (1/2 hard)	8.91	31	3.94	1082	3.62	.385	0.697	.82
Columbium (annealed)	8.57	36.5	4.44	2468	.44	.272	0.507	.60
Aluminum (5052-H32)	2.68	22.8	5.3	649	1.38	.96	0.426	.50
AISI 1020 Steel	7.86	45	4.59	1516	.52	.447	0.409	.48
Nickel (annealed)	8.90	48.3	4.82	1422	.59	.439	0.405	.48
Aluminum 6061-T6	2.70	31	5.35	652	1.54	.961	0.376	.44
Titanium 50A	4.50	35	5.22	1704	.16	.52	0.321	.38
304 Stainless Steel	7.90	58	4.57	1454	.16	.50	0.271	.32
Aluminum 7075-T6	2.80	57.3	5.1	635	1.21	.96	0.262	.31
Inconel 600	8.43	62	4.98	1427	.15	.443	0.247	.29
Tl-6Al-4V (annealed)	4.42	95	5.22	1649	.07	.564	0.158	.19

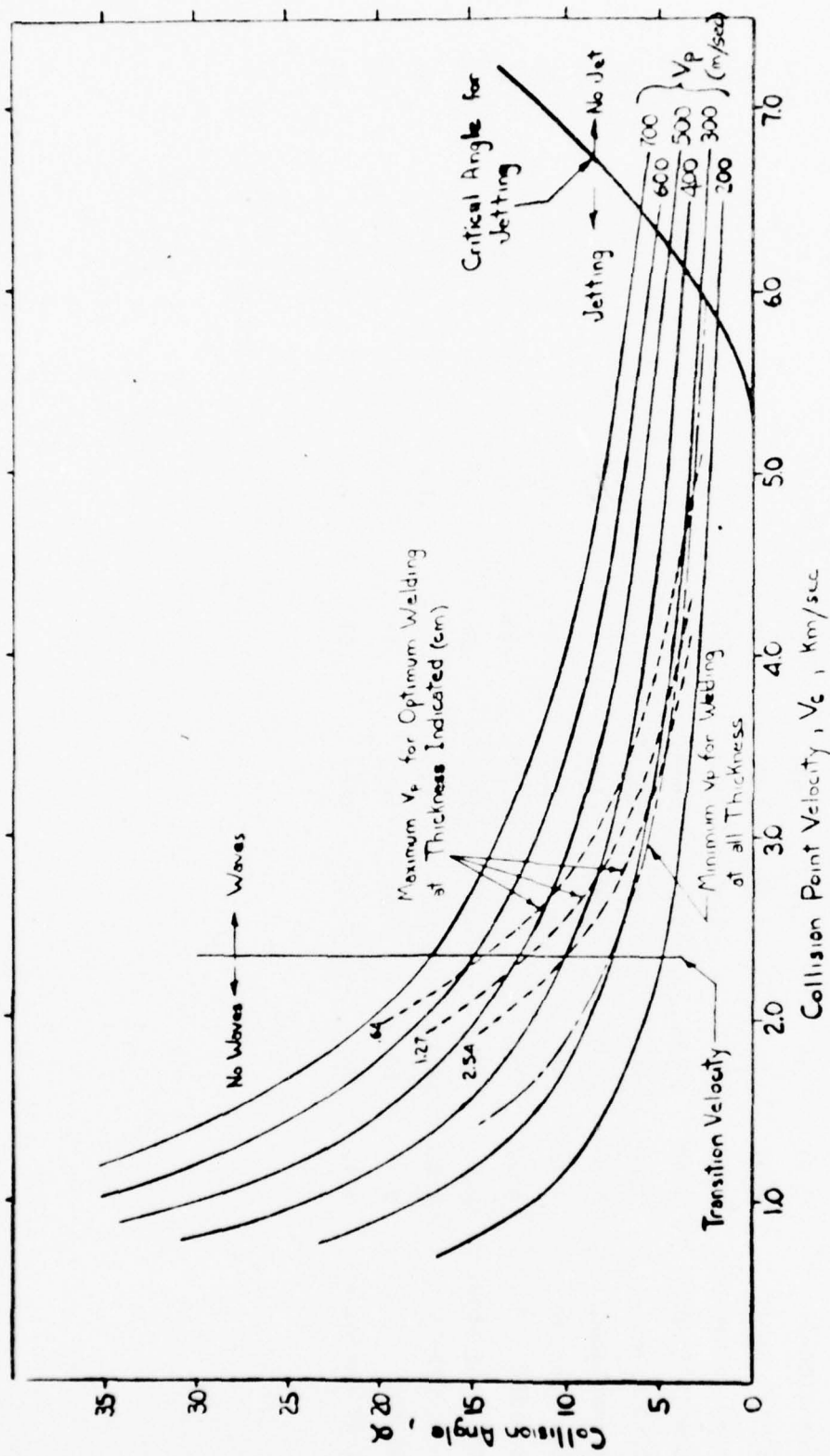


Figure 191. Effect of Flyer Plate Thickness on the Range of Optimum Collision Parameters.



#### 4. EXPLOSION WELDABILITY

Based on the physical property relationship in (14) and a minimum impact velocity or pressure for welding (¶36), an explosion weldability ranking of metals can be made. Explosion weldability is defined to be proportional to the ratio of maximum to minimum flyer plate impact velocities that will result in a parent metal strength weld. The higher the ratio the greater the weldability.

The maximum optimum flyer plate velocity is given by (14). The minimum optimum flyer plate velocity is given approximately by (2). Based on the plate velocity ratio a weldability factor has been calculated for combinations of the same metal or alloy using the expression  $WF = N \sigma_{P, MAX} / \sigma_{P, MIN}$ . For this comparison the flyer plate thickness,  $h$ , was chosen to be 0.635 cm, the collision point velocity was chosen to be 1/2 the bulk sound speed, and the ambient temperature was assumed to be 16°C. These values and other properties in Table I were used to calculate a weldability factor. For 6061-T6 aluminum

$$V_{P, MAX} = \frac{11.68 \times 10^9}{(0.635)^{1/4} \frac{5.35 \times 10^5}{2}} = 48,913 \text{ cm/sec}$$

$$V_{P, MIN} = 33900 \text{ M/sec}$$

so that

$$WF = \frac{1}{14.77} \frac{48,913}{33,900} = 0.376$$

In general, for the purpose of calculating the weldability factor,

$$N V_{P,MAX} = \frac{201.6\pi KC(T_{mp} - 16)^2}{\rho C_B}^{1/4} \quad (18)$$

and since

$$V_{P,MIN} = \frac{\sigma_{TS}}{\rho}^{1/2} \quad (2)$$

we have

$$WF = \frac{N V_{P,MAX}}{V_{P,MIN}} = \frac{201.6\pi KC\rho (T_{mp} - 16)^2}{C_B \sigma_{TS}^2}^{1/4} \quad (19)$$

Pure silver seems to be the most weldable metal. As a result the weldability factor for each metal has been divided by the weldability factor for pure silver to produce a relative weldability index. Whether or not the absolute values in the index are correct is open to question; however, it does appear, based on experience, that the order is approximately correct. Dissimilar metal combinations which can lead to the formation of brittle intermetallic compounds would add another factor further decreasing the weldability. Weldability could also be decreased by surface contaminants and the surface stress state.

It is also seen from (14) that the maximum allowable flyer impact velocity is decreased by increasing collision point velocity and/or flyer plate thickness, thereby decreasing weldability. The data in Figures 189 and 190 support the effect of  $V_c$  on weldability, and other data elsewhere in this report demonstrate the effect of

thickness. The maximum thickness of 6061-T6 aluminum that could be welded to yield near parent metal strength was 3.81 cm. Equation (16) predicts 6.59 cm is the maximum thickness that can be welded at a  $V_c$  of 2700 m/s with a flyer plate velocity,  $V_p$ , greater than the minimum value of 270 m/s.

## 5. CONCLUSIONS

The results of this study show that a minimum flyer plate impact velocity, related to a minimum impact pressure, is necessary to achieve explosion welding of 6061-T6 aluminum. The minimum velocity is near 270 m/s at collision angles less than  $5^\circ$ . The maximum flyer plate velocity to result in a parent metal strength weld is controlled by the kinetic energy of the flyer plate and the heat dissipation characteristics of the aluminum alloy. The maximum velocity increases as the collision point velocity decreases, thus broadening the range of impact velocities for parent metal strength welds. The weldability increases as the collision point approaches the flow transition. The flow transition velocity was found to be 2350 m/s.

The optimum weld state can best be described by four bounding criteria, represented on a graph of collision angle against collision point velocity. The boundary conditions are:

1. The critical collision angle for jet formation,
2. The critical impact pressure for jet formation in the subsonic regime,
3. The critical flow transition velocity, and
4. The kinetic energy of the flyer plate and the heat dissipation characteristics of the collision region.

Explosion welding data available for other metals indicate the four boundary concepts may be generally applicable. If so, estimating the optimum range of collision conditions for explosion welding would be greatly simplified.



#### IV. APPLICATIONS

##### A. Introduction

In an effort to demonstrate the capabilities of EIW to accomplish practical welding tasks, a series of application-oriented welds was conducted as part of the USAFA EIW research program. A major portion of this applications program was the development of a Bomb Damage Repair (BDR) kit for AM-2 aluminum airfield matting. A repair kit was developed and tested successfully, as reported in Technical Report AFWL-TR-70-160 (Lindbergh, 1971). Because the AM-2 repair kit has been explained in detail in that technical report, it will not be reported here. Other possible applications tested included spot welding, welding of tubular specimens such as pipes and structural columns, welding of pipe flanges, and symmetrical welding of structural joints to preclude the need for heavy anvils to absorb blast energy.

##### B. Spot Welding

Because of the extensive nature of the spot welding tests, they are reported in Section IIC as part of the experimental program.

##### C. Explosive Impulse Welding of Tubular Aluminum Joints

Explosive impulse welding could find useful application for the rapid joining of aluminum pipelines and aluminum mechanical tubing for column supports in building towers.

Three types of explosion welded joints appear feasible for the tubular geometry. In the first approach the tubular elements are joined by a welded external collar, necessitating the use of internal support tooling. Depending on the purpose of the structural element to be fabricated, this internal support tooling can be permanent or

removable subsequent to welding. In the second approach the tubular elements are joined by a welded internal collar, requiring the use of an external die to support the tube wall. The third approach uses a flange connection and symmetrical explosive impulses, thus requiring no support tooling for the tube wall. These methods are illustrated in Figures 192 through 197.

It should be emphasized that, although basically successful, neither the EIW technique nor the mandrel design used is considered optimum. Further development would be necessary to finalize the technique and design parameters.

Three external collar welds were made using Detasheet, a high detonation velocity sheet explosive, and three additional welds were made using Trojan SWP-5, a low velocity granular explosive. The first experiment using Detasheet explosive with an integral mandrel was unsuccessful because the explosive loading was too great. Two subsequent experiments using  $3\text{g/in}^2$  of Detasheet, with both integral and extractable mandrels, proved to be generally successful although some shock wave damage to the aluminum was noted. The first attempt to weld an external collar using the Trojan SWP-5 explosive was unsuccessful because the explosive loading was too low. Two subsequent welding trials were successful, both with the extractable and integral mandrels. The lower velocity explosives are better for welding aluminum because of their lower induced shock pressures. Figure 193 is a photograph of the external collar welds made using the integral mandrel and extractable mandrels.

A test of the external collar weld strength was made by subjecting a  $3/4$  inch wide slice from the pipe walls containing the joint to a



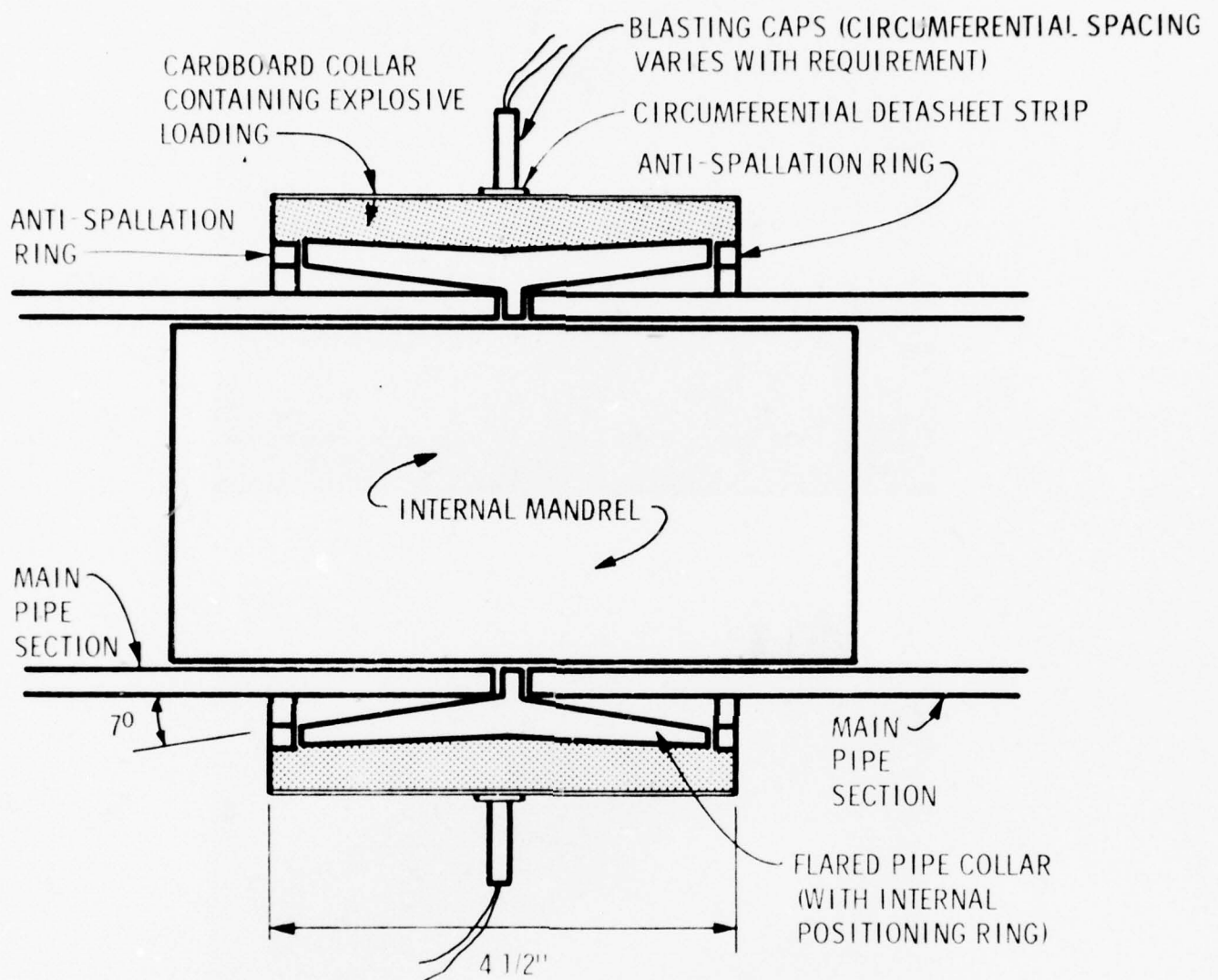


Figure 192 External Collar Welding Configuration

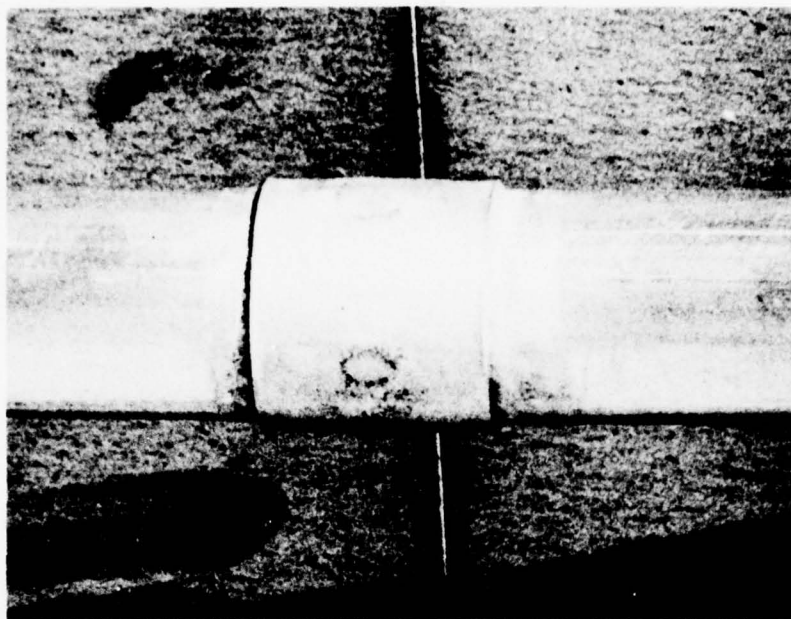


Figure 193 External Collars

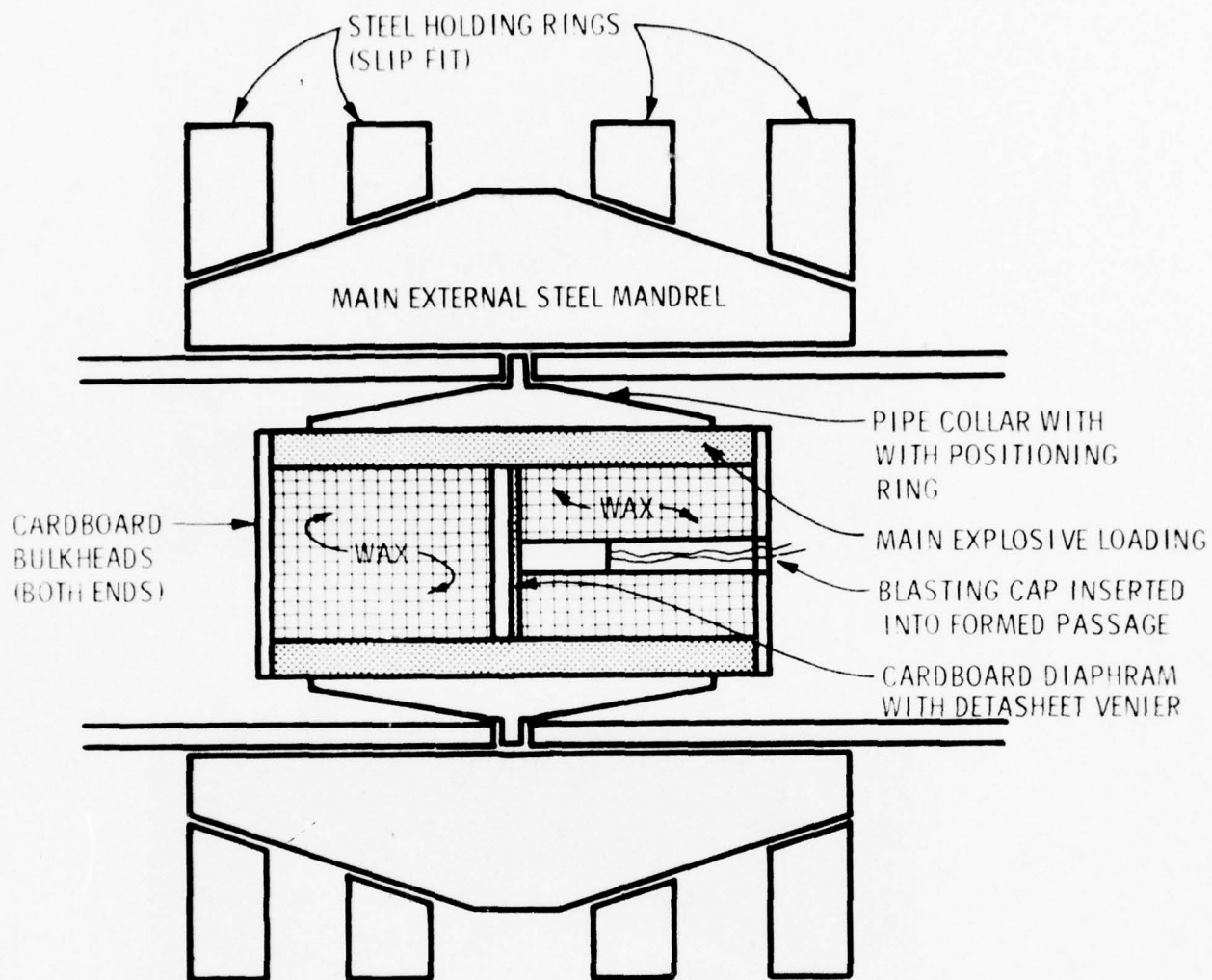


Figure 194 Internal Collar Weld Configuration

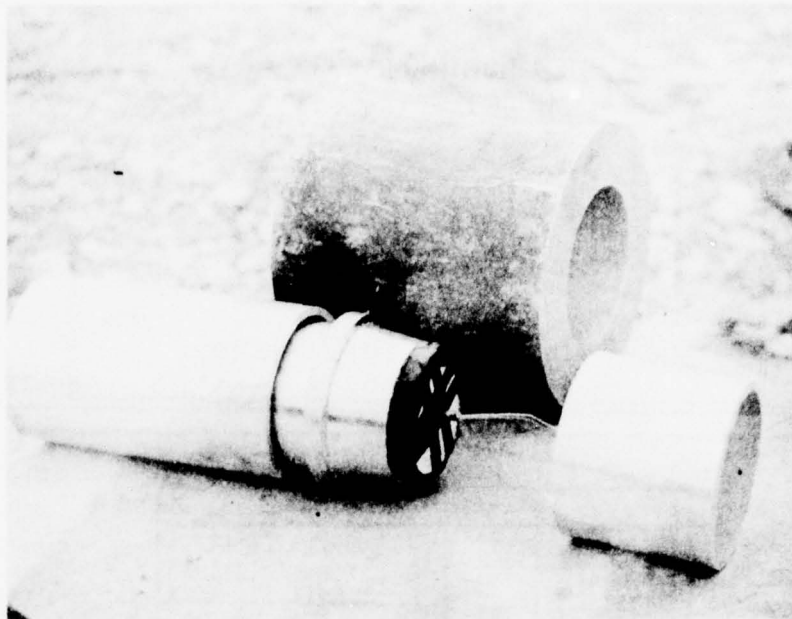


Figure 195 Internal Collar Weld Configuration and Welded Specimen

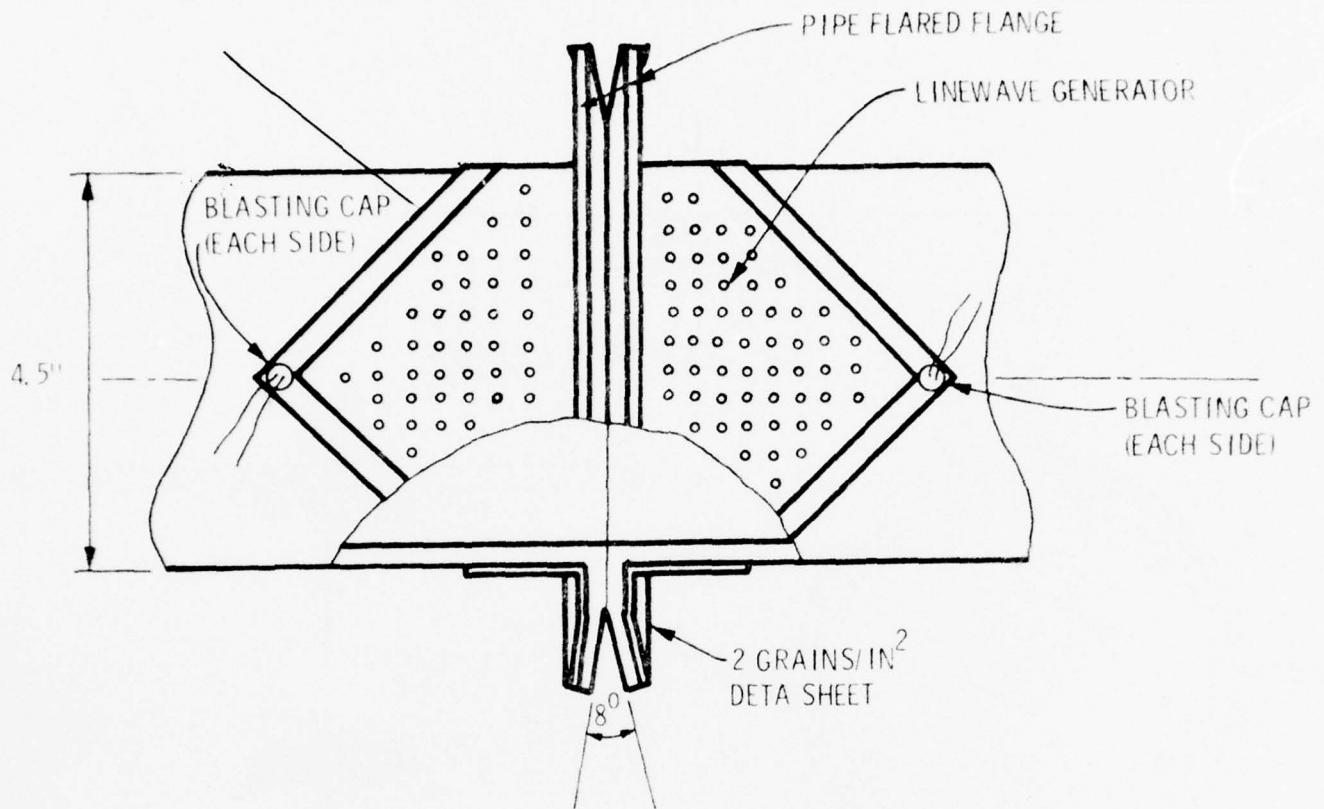


Figure 196 Symmetrical Pipe Flange Joint Configuration

PIPE OR COLUMN RESTRAINING DEVICE

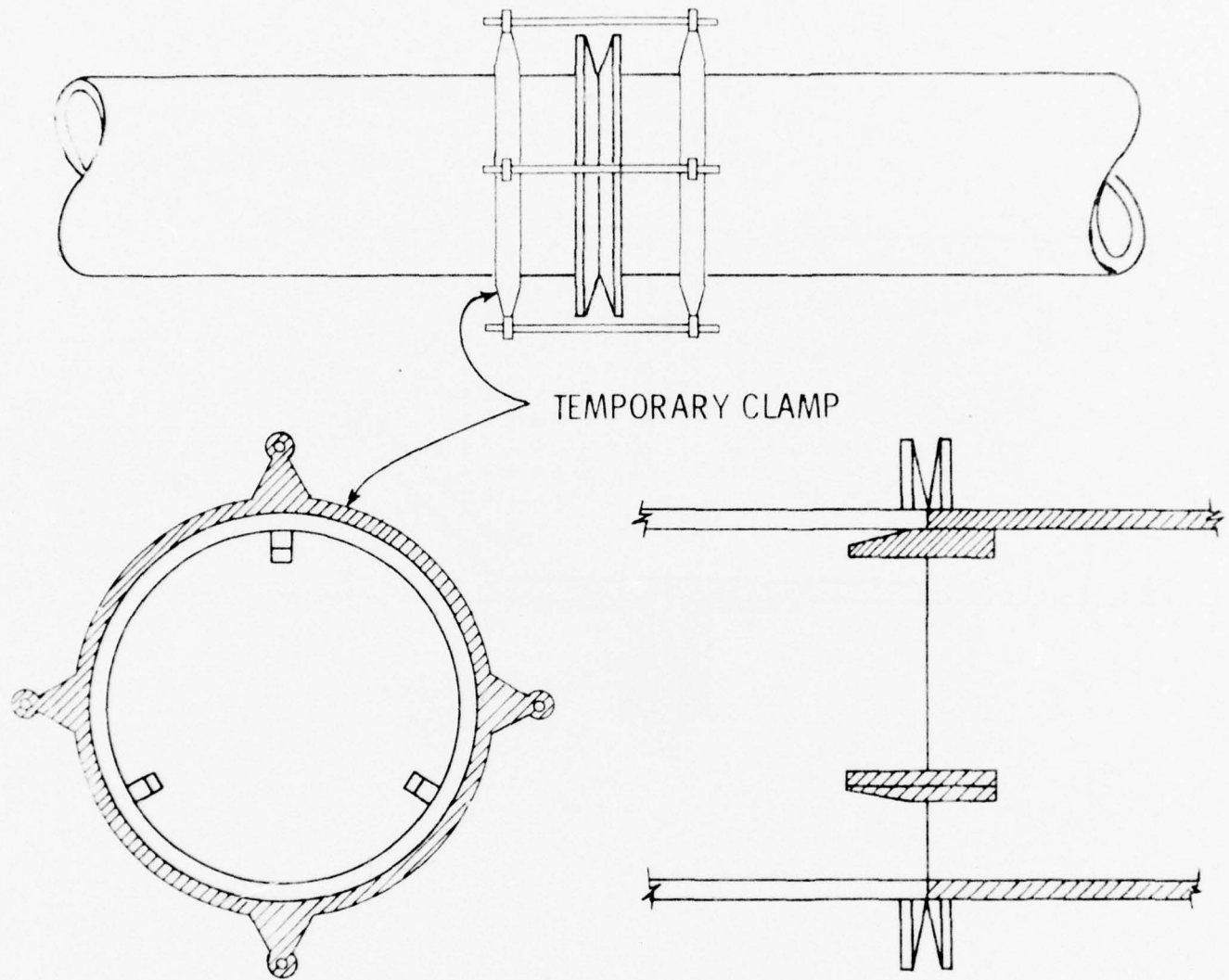


Figure 197 Symmetrical Pipe Flange Joint Test Specimen



tensile load. Failure occurred outside the collar weld area in the parent metal pipe wall. Thus we conclude the tubular joint in this instance was stronger than the pipe. This is to be expected on the basis of relative section thicknesses if the weld is properly made. Additional design safety is obtained due to the length of collar/main pipe overlap.

In an alternate approach it was demonstrated that the collar weld could be made to the inside surface of the pipe as readily as to the external surface. Figure 194 is an illustration of the explosive impulse welding configuration and a supporting external die used in these experiments. The pipe and collar components are 6061-T6 aluminum. Such an external die can be handled by one technician.

The first experiment used an  $8\text{g/in}^2$  explosive loading and the split die design shown in Figure 194. Unfortunately, the explosive loading was too large, and although the collar welded to the pipe, the die was slightly distorted and one of the four supporting rings was fractured.

A second experiment used a smaller explosive loading density,  $6\text{g/in}^2$ , and a shorter charge length. The split die could not be reused without extensive repair, and therefore, a one-piece, thick-walled, extruded steel pipe was used as the support die. The die wall was  $1\frac{3}{4}$  inch thick. The explosive charge proved to be near optimum, and the steel pipe die was not distorted. The appearance of the explosion welded pipe joint was excellent, as shown in the photographs of Figure 195.

The third tubular connection scheme involved the welding of

flanged pipe sections with the use of symmetrical and opposing impulses in lieu of support tooling. Figure 196 shows a related welding specimen with the explosive loading. Explosive charges are placed on opposite sides of the two flanges, and the initiation is timed so that the explosive impulses counteract each other. This method was not highly successful in practice because the initiation is complicated, requiring more explosive than required for the actual weld. One successful connection between 6061-T6 aluminum pipe and flange components was made using a  $2\text{g/in}^2$  Detasheet explosive loading on each side of the 1/4 inch thick flanges. Figure 197 illustrates the specimen setup.

Explosive impulse welding of tubular aluminum assemblies is a feasible connection technique for a variety of joint configurations. The internal collar weld is probably limited from a practical standpoint to pipes less than eight inches in diameter because of the size requirements of the external die. The external collar weld could probably be used on tubular sections of 24 inch or greater diameter. (In another development program at DRI, 12 inch diameter steel pipes have been explosion welded). This technique appears to have the fewest limitations and should be considered the best of the three techniques for fluid distribution lines. The flange connection is possibly the least attractive of the three techniques for pressurized tubular elements. However, the flange joint might prove to be the most attractive for joining large diameter barrel sections or for non-circular geometries.

D. Connections Formed Using Symmetrical Impulse Techniques

One of the more important potential EIW capabilities is that of forming welds using symmetrical impulses in lieu of a massive support anvil. Quite simply, matching explosive loadings and initiation devices are used on both opposing faces of the intended structural connector. As the detonation occurs, the impulses being generated on one side serve as the support for the welding occurring on the other and vice versa. This technique can be used to yield high quality welds without component warpage and with no sophisticated initiation system being required.

The symmetrical impulse technique was first applied to the field fabrication of a simple shear connector. The weld configurations attempted are shown in Figure 198. As shown, the preset angle initial geometry is used since it is more compatible with the fabrication scheme. In actual practice, large flange lengths would be unnecessary. They were used in this situation, however, to provide length-of-weld data. The selected explosive welding parameters were based upon the preliminary results of a preset angle steel parametric welding study not covered in this report. In addition, the three methods of initiation shown in Figure 198 were of interest and included as variables in the test plan. The shear connector components were of AISI 1018 hot-rolled steel. A possible field application is shown in Figure 199. A Saxe connector is used for temporary positioning; the flange angles would be shop welded to the column. The final structural shear connector is made with completion of the explosive impulse welding.

Symmetrical impulse techniques can be most advantageous

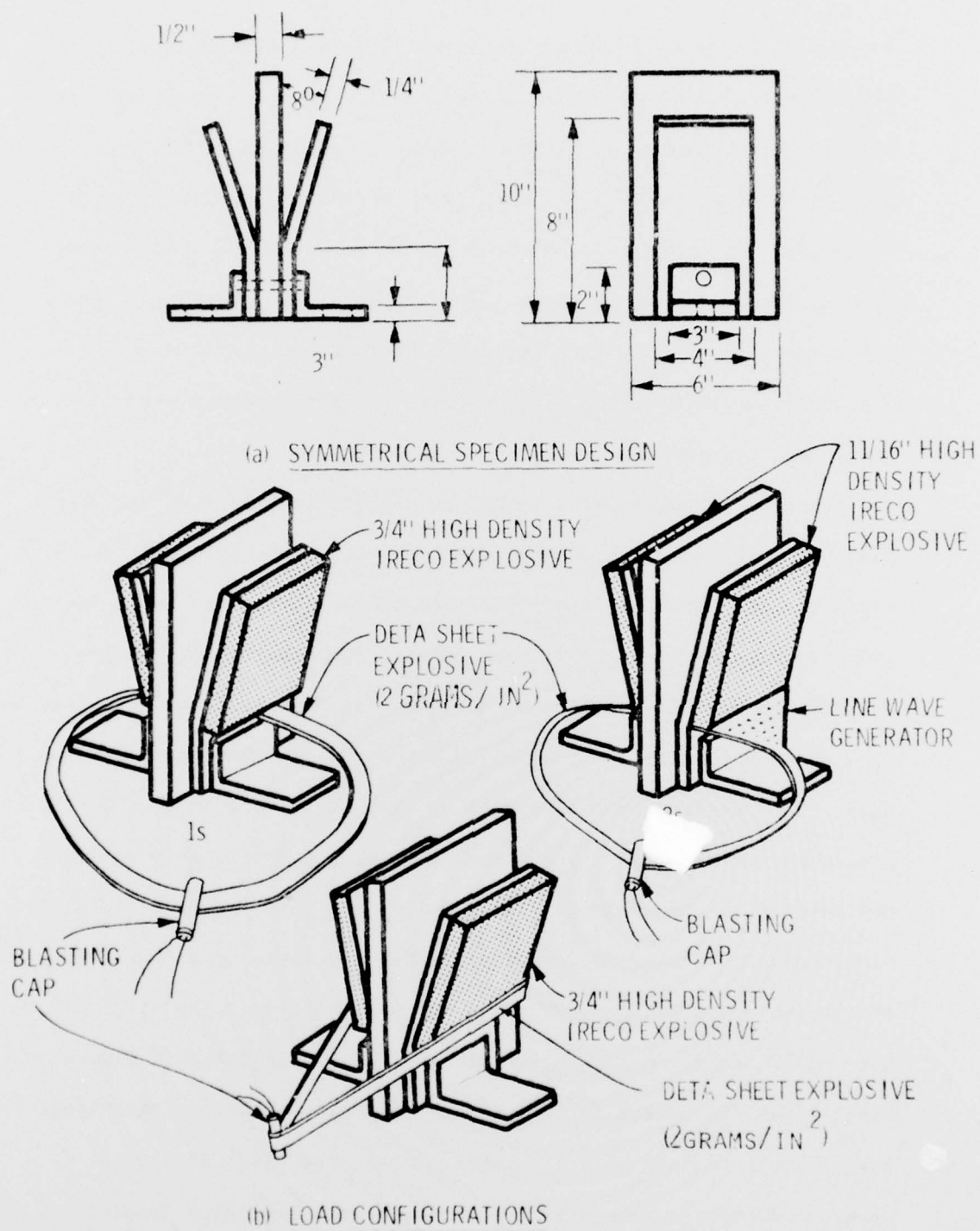


Figure 198 Symmetrical Explosive Load Configurations

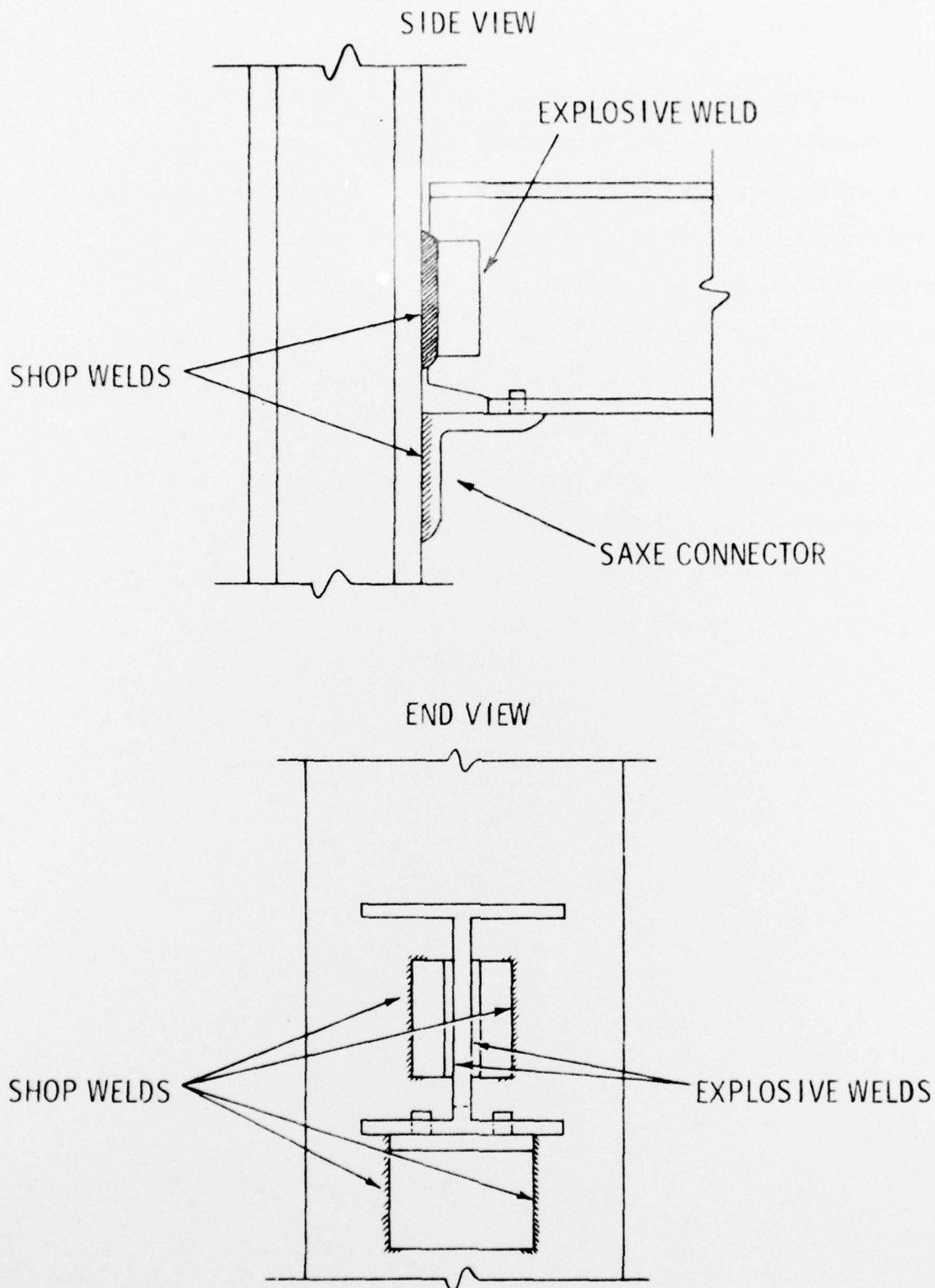


Figure 199 Application of Symmetrical Explosive Impulse Welding Configuration; Shear Connector



in building up flat laminates. This process was demonstrated by welding two external 3/8 inch 6061-T6 aluminum plates to a 1/2 inch 6061-T6 aluminum center plate. The plates were initially positioned vertically with a uniform 1/8 inch standoff. Cardboard boxes on the two outer faces contained the 40% Red Cross Extra dynamite loading (10 grams/in<sup>2</sup>). The resulting symmetrical detonation resulted in the welded composite shown in Figure 200. Note that the element is perfectly flat. Such a means of field cladding could be used, for example, in building up existing structural elements (increasing moment of inertia) in order to increase the structural capacities of existing structures.

Other weld configurations demonstrated in the applications program are shown in Figures 201 and 202.





Figure 200 Flat Laminite Formed Using the Symmetrical  
Impulse Technique

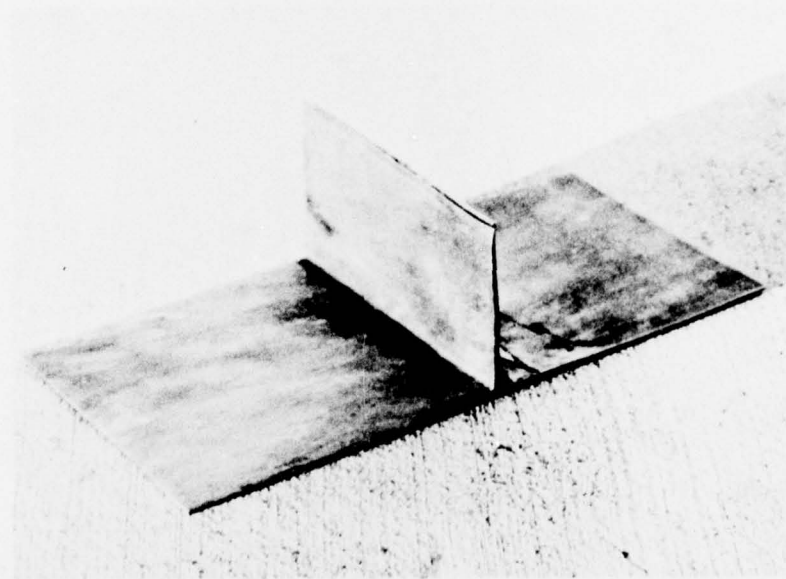
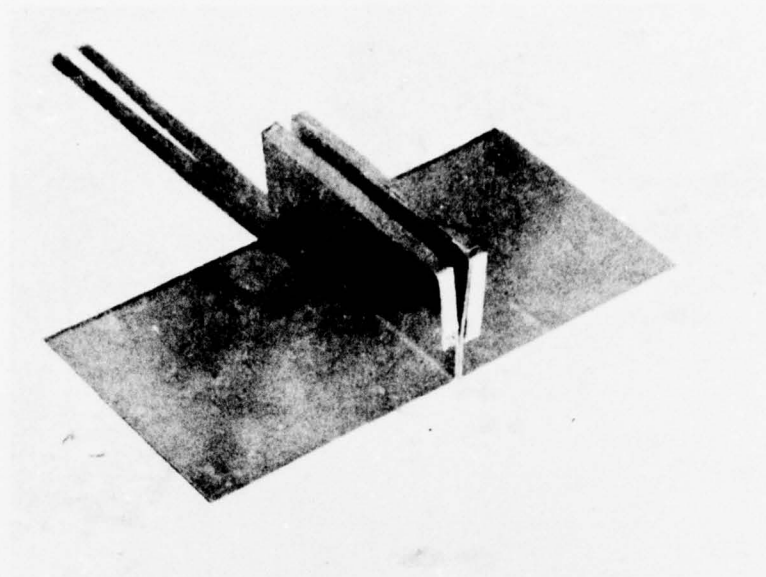


Figure 201 Longitudinal Seam Weld Made Using the Symmetrical Impulse Technique

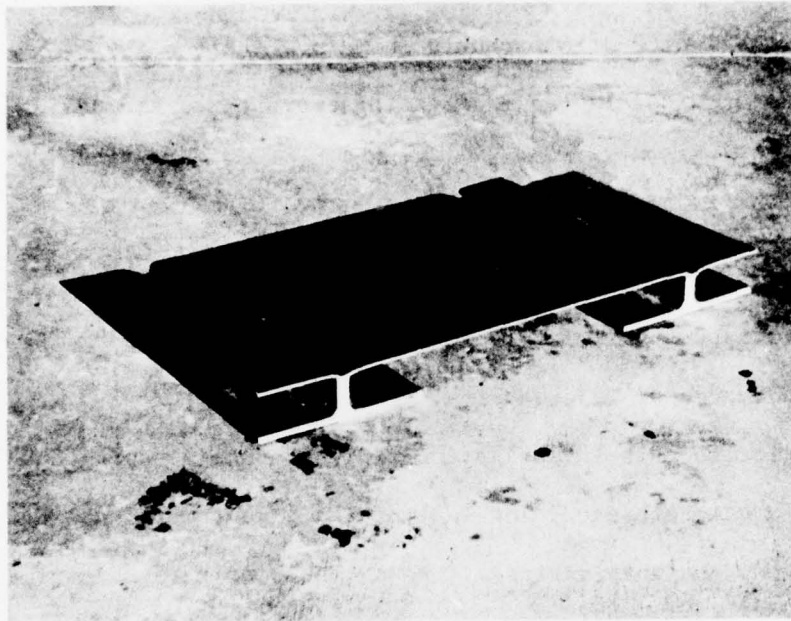


Figure 202 Structural Decking Formed Using the "T" Weld Configuration

## V. CONCLUSIONS AND RECOMMENDATIONS

The primary purpose of this investigation was to identify the parameters which significantly influence the quality of an explosive weld, and to develop an engineering approach to the design of a high quality explosive weld, which minimizes dependence on trial and error.

Throughout the investigation, ultimate tensile strength in the direction perpendicular to the weld plane was taken as the principal indicator of weld quality.

Prior to this investigation explosive welds having an ultimate tensile strength exceeding that of the parent metal had been achieved, but not routinely. As a result of this investigation it became possible to routinely obtain explosive weld tensile strengths in excess of parent metal strength; when optimum welding parameters were employed.

The minimum flyer plate impact velocity required to maximize weld tensile strength was found by Wittman at the Denver Research Institute to be

$$V_{P,MIN} = \frac{\sigma_{TS}}{\rho}$$

where

- |               |   |  |
|---------------|---|--|
| $V_{P,MIN}$   | = | minimum flyer plate impact velocity,<br>METERS/SECOND                  |
| $\sigma_{TS}$ | = | ultimate tensile strength of the<br>parent metal, NEWTONS/SQUARE METER |
| $\rho$        | = | parent metal density, KILOGRAMS/CUBIC<br>METER                         |

The following three parameters were found by Wittman to determine explosive weld quality for a given material:

- a. collision point velocity
- b. collision angle
- c. flyer plate thickness

The above three welding parameters can be optimized to yield weld tensile strengths in excess of the parent metal value, by considering four criteria:

- a. The critical collision angle for jet formation
- b. The critical impact velocity (or pressure) for jet formation in the subsonic regime
- c. The critical collision point transition velocity
- d. The kinetic energy of the flyer plate and the heat dissipation characteristics of the collision region

Weld tensile strength is not uniquely determined by interface deformation wavelength.

Weld shear strength in the plane of the weld appears to be the same in all directions.

A dynamic finite element computer program was written in an initial attempt to model the explosive welding process. The program employed a homogeneous, isotropic, linearly elastic stress-strain relation (Hooke's law) for both flyer and base plate, and predicted surface and interface wave formation in the bond zone. However, the investigation ended before the relative contributions of computational numerical instabilities, and true wave formation mechanisms to the computed wave forms could be determined.



The dynamic finite element computer program yielded calculated stress-time histories qualitatively consistent with experimental results, but significant stress magnitude discrepancies between calculated and measured results were observed which were not resolved. Presumably at least some of these discrepancies were caused by the fact that the computer program, even though quite complex, did not consider many of the material physical processes relevant to explosive welding, e.g., thermodynamic processes and phase changes.

A considerable quantity of experimental data demonstrated the validity of the steady state assumption, that explosive detonation velocity and collision point velocity are, on the average, equal.

Using the steady state assumption, a method was devised for mathematically converting an instantaneous flyer plate configuration to a motion-time history for a typical flyer plate element. Such a mathematical representation for the motion of a flyer plate element can be used to relate explosive parameters to flyer plate impact velocity.

During this investigation work was done by others on explosive characterization and explosive/metal interaction, and prediction of flyer plate impact velocities produced by a given type and amount of explosive.

Future explosive welding investigations should focus on the economic aspects of explosive welding, the performance of explosive materials and the possibility of expanding the presently small number of applications for which explosive welding is the most economical joining technique.



#### REFERENCES

1. Abramson, G. R., "Permanent Periodic Surface Deformations Due to a Traveling Jet", Journal of Applied Mechanics, Dec 1961, pp 519-528.
2. Allen, W. A., J. M. Mapes, and W. G. Wilson, "An Effect Produced by Oblique Impact of a Cylinder on a Thin Target", May 1954.
3. Bahrani, A. S., T. J. Black, and B. Crossland, "The Mechanics of Wave Formation in Explosive Welding", Proceedings of the Royal Society A, Vol. 296, 1967, pp 123-136.
4. Bergmann, O. R., "Explosive Bonding of Metals - Applications and Mechanism", Metals Engineering Quarterly, American Society for Metals, May 1966.
5. Bergmann, O. R., G. R. Cowan, and A. H. Holtzman, "Experimental Evidence of Jet Formation During Explosion Cladding", Trans AIME, Vol. 236, May 1966, pp 646-653.
6. Birkhoff, G., D. P. MacDougall, E. M. Pugh, and G. Taylor, "Explosives with Lined Cavities", Journal of Applied Physics, Vol. 19, June 1948, pp 563-582.
7. Burkhardt, A., E. Hornbogen and K. Keller: Z. Metallk., 1967, Vol. 58, pp 410-415.
8. Carslaw, H. S. and J. C. Jaeger, Conduction of Heat in Solids, 2nd ed., Oxford University Press, 1959.
9. Cowan, G. R., "Flow Configurations in Colliding Plates: Explosive Bonding", Journal of Applied Physics.
10. Cowan, G. R. and A. H. Holtzman, Journal of Applied Physics, Vol. 34, pp 328-339.
11. Cowan, G. R., O. R. Bergmann, and A. H. Holtzman: Met. Trans. Vol. 2, 1971, pp 3145-3155.
12. Crossland, B., A. S. Bahrani, "A Review of Explosive Welding Research Carried Out in the Queen's University of Belfast", Proceedings of the First International Conference of the Center for High Energy Forming, Estes Park, Colorado, June 19-23, 1967.
13. Deribas, A. A., V. M. Kudinov, and F. K. Matveenkov: "Combustion, Explosions and Shock Waves", 1967, Vol. 3, pp 344-348 (English translation).

14. Deribas, A. A., V. M. Kudinov, and F. I. Matveenko, "The Effect of the Initial Parameters Upon the Formation of Waves During Explosive Welding of Metals", Fizika Goreniya i Vzryva (Russian), 1967, No. 4, pp 561-568.
15. Ezra, A. A., Principles and Practice of Explosive Metalworking", Industrial Newspapers Ltd., 1973, Ch. 10, pp 173-228.
16. Hunt, J. N., "Wave Formation in Explosive Welding", Phil. Mag. 17, 1968, page 669.
17. Keller, K., "Investigations of Explosive Cladding - III. Metallographic Investigation and Mechanical Properties of Explosive Clads", Z. Metallkunde (German), Vol. 59, 1968, No. 6, pp 503-514.
18. Kennedy, J. E., "Explosive Output for Driving Metal", Behavior and Utilization of Explosives in Engineering Design. Proceedings of the 12th Annual Symposium, ASME and the University of New Mexico, March 1972, pp 109-124.
19. Lindbergh, Charles, "A Study of Flyer Plate Response as Used in Explosive Impulse Welding", Unpublished Research Study submitted to Air Command and Staff College, Air University, Maxwell Air Force Base, Alabama, May 1973.
20. Lundergan, C. D. and W. Herrman: Journal of Applied Physics, 1963, Vol. 34, pp 2046.
21. Milner, D. R. and G. W. Rowe, "Fundamentals of Solid-Phase Welding", Metallurgical Reviews, Vol. 7, No. 28, 1962, pp 433-480.
22. Otto, H. G., "Aspects Relating to the Welding Mechanisms", Proceedings of the Conference on High Energy Rate Working of Metals, Sandefjord-Lillehammer, Norway, September 14-25, 1964.
23. Ribovich, J., R. W. Watson, and F. C. Gibson: AIAA Journal, 1968, Vol. 6, pp 1260-1263.
24. Rolsten, R. F., A. K. Hopkins, W. A. Dean, and H. H. Hunt, "Effects of Oblique Shocks Produced at Metal Interfaces by Hyper-velocity Particle Impact", Welding Research Supplement, November 1967, pp 517-522.
25. Shribman, V. and B. Crossland, "An Experimental Investigation of the Velocity of the Flyer Plate in Explosive Welding", Second International Conference of the Center for High Energy Forming, Vol. 2, June 23-27, 1969, Estes Park, Colorado.
26. Stone, J. M., "Applications of Explosion-Bonded Clads", Metal Construction, No. 1, January 1969.

27. USAF, Air Force Systems Command, "Maintenance and Repair of Expeditionary and Theater of Operation Airfield Landing Mat Facilities Using Explosive Impulse Welding", Technical Report No. AFWL-TR-70-160, Kirtland AFB, New Mexico: Air Force Weapons Laboratory, January 1971.

28. Walsh, J. M., et. al., Shock Wave Compressions of Twenty-Seven Metals. Equations of State of Metals.

29. Walsh, J. M., R. G. Shreffler, and F. J. Willig: Journal of Applied Physics, 1953, Vol. 24, pp 349-359.

30. Wittman, R. H., "The Explosive Bonding Process", Battelle Technical Review, July 1967.

31. Wittman, R. H. and S. H. Carpenter, "The Theory and Application of Explosion Welding", University of Denver Research Institute Report, 1972.